BOUNDARY LAYER DEVELOPMENT FROM TRANSITION PROVOKING DEVICES.

by

C. J. Fraser, B.Sc. (Mech. Eng.)

Dept. of Mechanical and Industrial Eng.

Dundee College of Technology.

Thesis submitted to C. N. A. A. for the Degree of

Doctor of Philosophy.

Jan. 1979.

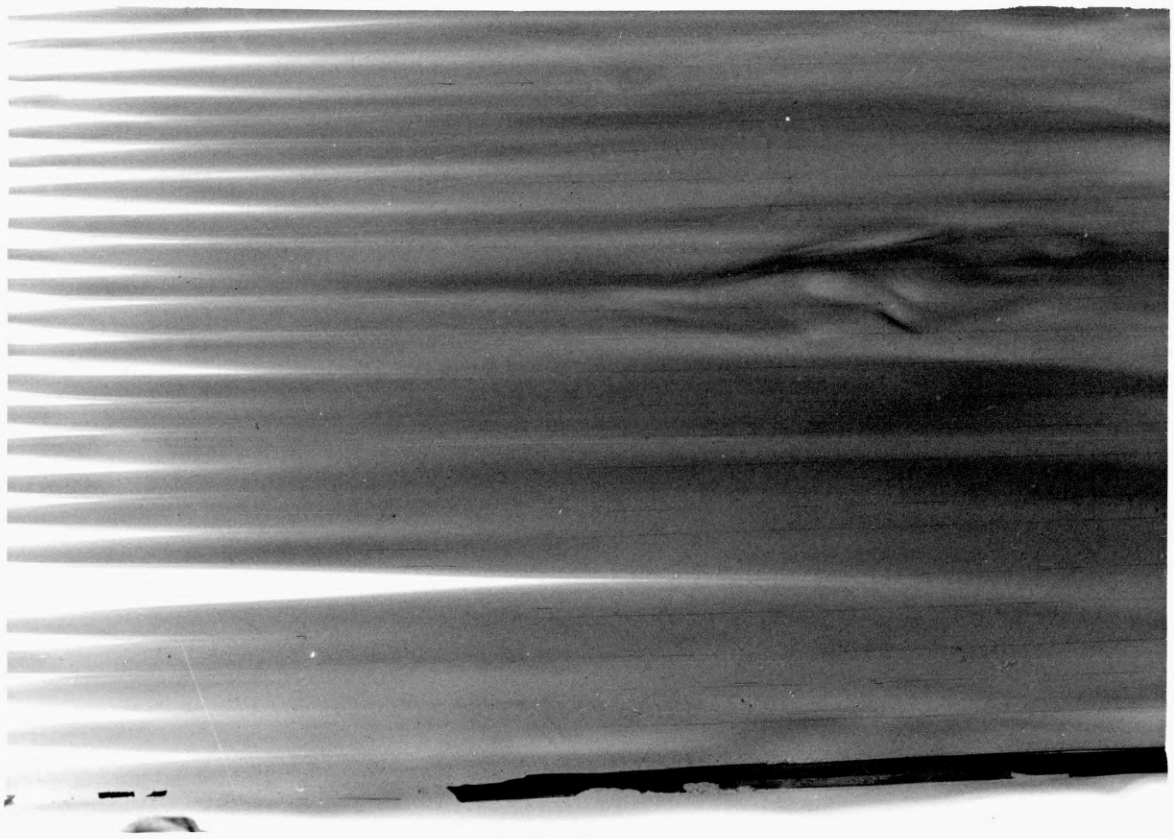

EVOLUTION OF A TURBULENT SPOT ON

A WATER CHANNEL.

(FLOW IS FROM LEFT TO RIGHT.)

DECLARATION.

The following work has been composed by the author, who is not registered for any other award of the C.N.A.A. or of any University.

signed. [redacted]

BOUNDARY LAYER DEVELOPMENT FROM TRANSITION PROVOKING DEVICES.

by C. J. Fraser, B. Sc.

ABSTRACT :-

Data on stream and spanwise variation in four representative transitional boundary layers is presented, the test cases encompassing free transition, transition due to a two-dimensional trip wire, with laminar and with turbulent re-attachment, and transition due to isolated spherical roughness elements.

The concept of statistical similarity in transition regions has been confirmed for the cases of free transition and for transition due to a two-dimensional trip wire, with the streamwise mean intermittency distribution described by the normal distribution function. Significantly, the condition of "transition at the wire" is found to have a very small but well defined intermittency growth region.

Transition due to isolated roughness elements is however seen to have a fundamentally different character. The elements induce large amplitude fluctuations, related to vortex shedding, which degenerate downstream to become random, three-dimensional, turbulent fluctuations in the developing wakes, with only mild recourse to an intermittent type of breakdown.

Spanwise variation in the layer is related to inconsistencies in the turbulent spot source density and occurrence frequency, and can result in substantial non-uniformity of the boundary layer if the transition region is long.

The resulting low Reynolds number turbulent boundary layer exhibits a moderate increase in the additive constant in the law of the wall, and is characterised by a deeper penetration of the transverse intermittency distribution. The choice of transition agent however, has no apparent influence on the rate at which the developing turbulent boundary layer approaches self-preserving conditions.

A general relation, based on local boundary layer parameters, has been developed for the estimation of the transitional skin friction coefficient and has been tested via momentum balance principles.

The skin friction relation has also been employed in a general integral prediction technique for the incompressible transitional boundary layer in two-dimensional, arbitrary pressure gradient flows.

LIST OF COURSES AND CONFERENCES ATTENDED.

Date	Content and location	Comments
24th June, 1976	"Numerical methods for Fluid Flow." Lanchester Polytechnic, Coventry.	Outline of numerical solutions for various field and boundary layer problems.
2-4th May, 1977	"Laminar-Turbulent Transition." Technical University, Lyngby, Denmark.	State of the art conf. on current transition research, sponsored by AGARD.
4-29th July, 1977	"Training in research methods." von Kármán Inst. for Fluid Dynamics, Rhode st. Genese, Belguim.	Valuable experience of research methods at a top level establishment, via a one month supervised research project.
28th March - 1st April , 1977	S.R.C. Summer School, University of Surrey, Guilford, Surrey.	Case studies involving useful experience of group project work.

ACKNOWLEDGEMENTS.

Throughout the duration of this research project, many people have been actively involved in its development and progress and I feel quite sure that the exchange of opinions and ideas have mutually contributed towards a better understanding of the problems encountered.

I would like to express thanks to the technical staff of Dundee College of Technology for their helpful suggestions on the design and construction of the wind tunnel facility, particularly Len Crighton, Sid Donegan, John Black and Andy Collins. Also to Bill Harper for his experienced knowledge of electronic circuitry.

My gratitude extends to my supervisors, John Milne and Dr. David Cockrell, for their guidance throughout and for all they have taught me in this field.

I must also thank the Science Research Council without whose financial support the work would not be possible.

Lastly my gratitude to all the many other people whose names are not included who have helped me in my research work over the last three years.

NOMENCLATURE:-

Symbol	Function	Connotation	Units
x		streamwise coordinate	mm.
y		transverse coordinate	mm.
z		spanwise coordinate	mm.
$\overline{u}$		local mean velocity	m/s.
U_∞		freestream velocity	m/s.
u'	$(\sqrt{\overline{u'^2}}/U_\infty)\times 100$	streamwise component of fluctuating velocity	%
δ	y at $\overline{u} = 0.995U_\infty$	edge of the boundary layer	mm.
δ^*	$\int_0^\infty (1-\frac{\overline{u}}{U_\infty})dy$	displacement thickness	mm.
Θ	$\int_0^\infty \frac{\overline{u}}{U_\infty}(1-\frac{\overline{u}}{U_\infty})dy$	momentum thickness	mm.
δ^{**}	$\int_0^\infty \frac{\overline{u}}{U_\infty}(1-(\frac{\overline{u}}{U_\infty})^2)dy$	energy thickness	mm.
H_{12}, H	δ^*/Θ	shape factor	-
H_{32}	δ^{**}/Θ	shape factor	-
R_Θ	$U_\infty\Theta/\nu$	mom. th. Reynolds N°	-
R_{δ^*}	$U_\infty\delta^*/\nu$	disp. th. Reynolds N°	-
$Cf._{1,2,3,4}$		local skin friction coeff.	-
τ_o	$\frac{1}{2}\rho U_\infty^2\, Cf.$	wall shear stress	N/m^2
U_τ	$\sqrt{\tau_o/\rho}$	wall friction velocity	m/s.
Π		wake parameter	-
$\Delta U/U_\tau$		wake strength parameter	-
y^+	$y.U_\tau/\nu$	dimensionless y coordinate	-
u^+	$\overline{u}/U_\tau$	dimensionless velocity	-
$\frac{U_\infty-\overline{u}}{U_\tau}$		velocity defect	-

Symbol	Function	Connotation	Units
F	$d(\delta - \delta^*)/dx$	entrainment rate	-
γ		local intermittency	%
$\overline{\gamma}$		mean intermittency near the wall.	%
x_{tr}		location of the start of transition.	mm.
$\overline{x}$		location of the 50% intermittency point	mm.
Λ	$x_{\overline{\gamma}=0.75} - x_{\overline{\gamma}=0.25}$	transition length parameter	mm.
∇		mean standard deviation of the intermittency distribution.	mm.
R_Λ		transition length Reynolds number	-
R_∇		transition length Reynolds number	-
ξ	$\frac{x - x_{tr}}{\Lambda}$	normalised transition length.	-
ζ	$(x - \overline{x})/\nabla$ $y\sqrt{U_\infty/\nu x}$	normalised transition length. also denotes the Blasius coordinate	-
k		roughness height, also used to denote von Kármán's constant in the law of the wall.	mm.
C		additive constant in the law of the wall.	
R_k	$U_\infty . k/\nu$	wire Reynolds number	-
R_{xk}	$U_\infty . x_k/\nu$	wire location Reynolds number.	-
u_k		velocity at the trip wire height in the undisturbed boundary layer.	m/s.

Symbol	Function	Connotation	Units
$R_{k_{crit}}$	$u_k.k/\nu$	wire Reynolds number	-
$R_{x_{tr}}$	$U_\infty.x_{tr}/\nu$	axial transition Reynolds number	-
$R_{\theta_{tr}}$	$U_\infty.\theta_{tr}/\nu$	momentum thickness Reynolds number at transition	-
PL.	$\frac{U_\infty^2.\theta}{(U_\infty^2.\theta)_i} - 1 + \frac{1}{2}\int_{x_i}^{x} \frac{\delta^*}{\theta_i} d\left[\frac{U_\infty}{U_{\infty_i}}\right]^2$	L.H.S. of momentum balance eqn.	-
PR.	$\int_{x_i}^{x} \left[\frac{u_\tau}{U_{\infty_i}}\right]^2 d(x/\theta_i)$	R.H.S. of monentum balance eqn.	-
ν		kinematic viscosity	$m^2/s.$
μ		dynamic viscosity	kg./m.s.
ρ		air density	$kg./m^3$

SUBSCRIPTS.

T - turbulent

L - laminar

t - transitional

k - relating to trip wire or roughness element.

tr- at the transition point.

i - denoting initial conditions.

subscripts 1,2,3 and 4 for the skin friction coefficient denotes :-

C_{f_1} - from the velocity profile.

C_{f_2} - from eqn. 3.25

C_{f_3} - from the 1.105mm. O.D. Preston tube.

C_{f_4} - from the 1.410mm. O.D. Preston tube.

All other, less used, symbols are defined within the relevant sections.

CONTENTS :- Page N°.

Frontispiece - Evolution of a turbulent spot on a water channel I

Declaration II

Abstract III

List of courses and conferences attended IV

Acknowledgements V

Nomenclature VI

Contents IX

List of figures in the main text XIII

List of figures in Appendix 6. XVI

Objectives of the current research 1

Chapter 1. - Historical development and Introduction 2 - 18

1.1 The initial experiments 3

1.2 Stability considerations 4

1.3 The semi-empirical approach 5

1.4 Experimental evidence of a stability mechanism 6

1.5 Turbulent spots 7

1.6 The intermediate transition process 8

1.7 Developments in the stability theory 9

1.8 Provoked transition 9

1.9 Transition mechanisms due to roughness 12

1.10 Centrifugal instability and transition 12

1.11 The prediction of transition 13

1.12 The present investigation 15

Chapter 2. - Experimental facilities, instrumentation and measurements 19 - 64

2.1 Wind tunnel facility 20

2.2 Measurement of fluid properties 20

2.3 Power unit and speed controller 21

2.4 Turbulence damping screens 21

2.5 Inlet contraction section 22

2.6 The working section 23

2.7 The boundary layer plate 24

2.8 Tunnel instrumentation carriage 25

2.9 Tunnel performance- preliminary testing 27

2.10 Hot wire and associated instrumentation 28

2.11 Mean velocity profile measurements 30

2.12 The pressure gradient 32

2.13 The measurement of intermittency 32

2.14 Measurement of surface skin friction coefficient 35

2.15 Flow two-dimensionality by the "two-pin" test 37

2.16 Tunnel modifications and commissioning 38

2.17 Future tunnel modifications 41

Chapter 3. Data reduction and theoretical considerations. 65 - 88

3.1 Data reduction, laminar mean velocity profiles 66

3.2 Data reduction, turbulent mean velocity profiles 67

3.3 Turbulent skin friction coefficients 72

3.4 Wall proximity effects 73

3.5 Transitional mean velocity profiles 74

3.6 Low Reynolds number effects 77

3.7 Equilibrium and self-preserving boundary layers 79

3.8 Flow two-dimensionality by the "momentum balance" test 82

3.9 Estimation of the entrainment rate 83

Chapter 4. - Details of experiments conducted and discussion of results. 89 - 127

4.1 Experimental test boundary layers 90

4.2 Transition Reynolds numbers downstream of a two-dimensional trip wire 93

4.3 Statistical similarity of transition regions 94

4.4 Transitional mean and fluctuating velocity profile similarity 96

4.5 Transitional local skin friction coefficient similarity 98

4.6 Description of the transition region 98

4.7 Correlations of transition length Reynolds number 99

4.8 Flow visualisation studies 101

4.9 Intermittency profiles through transition 101

4.10 Spanwise variation in the boundary layer 102

4.11 Entrainment rates 106

4.12 Turbulent boundary layer development 106

Chapter 5. Calculation of transitional boundary layers 128 - 141

5.1 Introduction 129

5.2 Transition model A. 130

5.3 Transition model B. 134

5.4 Comparison of models A and B. 135

Conclusions 142

Suggestions for further work 146

References 148

Appendix 1. - Experimental apparatus 1.1 - 1.3

Appendix 2. - Experimental uncertainty in integral thicknesses 2.1 - 2.3

Appendix 3. - Computer programs and flow charts 3.1 - 3.22

Appendix 4. - Development of a general relationship for estimating the transitional boundary layer skin friction coefficient 4.1 - 4.7

Appendix 5. - Integral prediction methods for laminar and turbulent boundary layers. 5.1 - 5.9

Appendix 6. - Experimental data 6.1 - 6.133

LIST OF FIGURES IN THE MAIN TEXT.

FIG. N°.	Title	Page N°
1.1	Pictorial representation of natural transition on a flat plate	18
2.1.1	Schematic diagram of wind tunnel	42
2.4.1.	Turbulence damping screens	43
2.5.1.	Inlet contraction section	44
2.6.1.	Detail of roof adjustment	45
2.6.2.	Wind tunnel working section	46
2.7.1.	Detail of leading edge configuration	46
2.8.1.	Calibration of sweep drive unit	47
2.8.2.	Detail of traversing mechanism	48
2.10.1.	Hot wire instrumentation	48
2.10.2.	Instrumentation layout	49
2.10.3.	Relationship between probe voltage and fluid velocity	50
2.10.4.	Probe linearisation	51
2.11.1.	Measurement of u' turbulence component	52
2.11.2.	Distribution of streamwise component of turbulence in the freestream	53
2.12.1.	Velocity distribution near the leading edge	54
2.13.1.	Measurement of intermittency	55
2.13.2.	Laminar/turbulent discriminating signal q	56
2.13.3.	Intermittency distribution in a fully developed turbulent boundary layer	57
2.14.1.	Details of Preston and total head tubes	58

2.15.1.	Two-pin test for flow two-dimensionality	59
2.15.2.	Two-pin wake traverse	60
2.16.1.	Wind tunnel test boundary layer (1)	61
2.16.2.	Wind tunnel test boundary layer (2)	62
2.16.3.	Two-pin wake traverse (final condition)	63
2.16.4.	Spanwise variation of local skin friction coefficient	64
3.1.1.	Analysis of laminar velocity profiles	86
3.2.2.	Analysis of turbulent velocity profiles	88
4.1.1.	Plot of R_{l_k} vs. R_{xk} for transition at a two-dimensional trip wire, from Hall (1968)	110
4.1.2.	Plot of $R\Theta_{tr}$ against $(\sqrt{\overline{u'^2}}/U_\infty)\times 100\%$ for natural transition	111
4.1.3.	Plot of $R_{x_{tr}}$ vs. $R_{l_{crit}}$ for transition immediately behind a spherical roughness element; from Tani et. al. (1962)	112
4.2.1.	Correlations of transition Reynolds number downstream of a two-dimensional trip wire	113
4.3.1.	Normalised intermittency distribution	114
4.3.2.	Normalised intermittency distribution	115
4.3.3.	Streamwise fluctuations behind spherical roughness elements	116
4.3.4.	Oscillation induced behind spherical roughness elements	117
4.4.1.	Similarity of transitional mean velocity profiles	118
4.4.2.	Transition similarity profiles of $(\overline{u}/U_\infty)$	119
4.4.3.	Similarity of u' fluctuating velocity profiles (1)	120
4.4.4.	Similarity of u' fluctuating velocity profiles (2)	121

4.4.5.	Transition similarity profiles of $(\sqrt{\overline{u'^2}}/U_\infty)\%$	122
4.5.1.	Similarity of local skin friction coefficient through transition.	123
4.6.1.	Instantaneous velocity, $(\overline{u} + u')$ in a transitional boundary layer.	124
4.7.1.	Correlations of transition length Reynolds numbers	125
4.10.1.	Spanwise variation in local skin friction coefficient for free transition and for abrupt transition at a trip wire.	126
4.10.2.	Plan of wake development behind spheres.	127
5.2.1.	Approximating polynomials used in transition model A.	137
5.4.1.	Comparison of transition models against the data of Schubauer and Klebanoff (1956)	139
5.4.2.	Comparison of transition models against the present data, (FLOW 2, z = -50mm.)	140
5.4.3.	Comparison between measured and modelled transitional mean velocity profiles.	141

LIST OF FIGURES IN APPENDIX 6.

FIG N°	Title	Page N°
FLOW 1.		
1.1	Distribution of dynamic pressure about the mean	6.4
1.2-1.4	Mean velocity profiles	6.5
1.5-1.10	Semi-logarithmic and velocity-defect profiles	6.8
1.11-1.25	Streamwise turbulence component profiles	6.14
1.26	Profiles at wire position with the wire removed	6.29
1.27-1.32	Intermittency profiles	6.30
1.33-1.35	Tabulated secondary data	6.36
1.36-1.41	Streamwise development of integral parameters and skin friction coefficient	6.39
1.42-1.44	Streamwise entrainment rate	6.45
1.45-1.47	Streamwise development of mean intermittency	6.48
1.48	Two-pin wake traverse	6.51
1.49-1.50	Momentum balance results	6.52
1.51	Side wall boundary layer profiles at x = 1132mm.	6.54
1.52	Development of wake and wake strength parameters	6.55
1.53	Spanwise variation in momentum and energy thicknesses	6.56
1.54-1.60	Spanwise boundary layer profiles	6.57
FLOW 2.		
2.1	Distribution of dynamic pressure about the mean	6.64
2.2	Mean velocity profiles	6.65
2.3	Comparison with Blasius profile	6.66
2.4-2.5	Semi-logarithmic and velocity-defect profiles	6.67

2.6-2.7	Streamwise turbulence component profiles	6.69
2.8-2.9	Intermittency profiles	6.71
2.10	Tabulated secondary data	6.73
2.11-2.12	Streamwise development of integral parameters and skin friction coefficient	6.74
2.13	Streamwise entrainment rate	6.76
2.14	Streamwise development of mean intermittency	6.77
2.15	Momentum balance results	6.78
2.16	Development of wake and wake strength parameters	6.79
2.17	Spanwise boundary layer profiles at x = 200mm.	6.80
FLOW 3.		
3.1	Distribution of dynamic pressure about the mean	6.81
3.2	Mean velocity and streamwise component of turbulence profiles	6.82
3.3	Semi-logarithmic and velocity-defect profiles	6.83
3.4-3.6	Streamwise turbulence component profiles	6.84
3.7-3.8	Intermittency profiles	6.87
3.9	Tabulated secondary data and the development of wake and wake strength parameters	6.89
3.10-3.11	Streamwise development of integral parameters and skin friction coefficient	6.90
3.12	Streamwise entrainment rate and momentum balance results	6.92
3.13	Streamwise development of mean intermittency and mean velocity profiles in the recovery zone	6.93

3.14	Spanwise boundary layer profiles at x = 400mm. and spanwise variation in skin friction coefficient at x = 400mm. and x = 1800mm.	6.94
FLOW 4.		
4.1	Distribution of dynamic pressure about the mean	6.95
4.2-4.6	Mean velocity profiles	6.96
4.7-4.10	Semi-logarithmic and velocity-defect profiles	6.101
4.11-4.16	Streamwise turbulence component profiles	6.105
4.17-4.25	Intermittency profiles	6.111
4.26-4.27	Tabulated secondary data	6.120
4.28-4.29	Streamwise development of integral parameters and skin friction coefficient	6.122
4.30	Momentum balance results	6.124
4.31	Streamwise and spanwise entrainment rates	6.125
4.32	Spanwise variation in momentum and energy thicknesses	6.126
4.33-4.35	Development of wakes behind roughness elements	6.127
4.36-4.38	Spanwise variation in skin friction coefficient	6.130
4.39	Spanwise boundary layer profiles at x = 1000mm and at x = 1500mm.	6.133

OBJECTIVES OF THE CURRENT RESEARCH.

1. To review the relevant literature regarding transition phenomena in the boundary layer.

2. To develop suitable experimental facilities and reliable measuring techniques for the study of transitional boundary layer behaviour.

3. To confirm, or otherwise, the concept of statistical similarity in transition regions by the observation of four significantly different transitional boundary layer flows, and to investigate various methods of representing the similarity, if it exists.

4. To develop a general relationship, in terms of $(R\theta, H12, \bar{\delta})$, for the local mean skin friction coefficient in transition regions.

5. To investigate various correlations of transition onset and transition length.

6. To investigate the extent of spanwise variation in the boundary layer, due to the various transition provoking agents.

7. To investigate the merits and limitations of the transition device with respect to the resulting turbulent boundary layer development towards self-preserving conditions.

8. To investigate the mean intermittency as a definitive criterion for the state of flow in the boundary layer.

9. To develop a "general" integral prediction technique, based on an idealised model of an alternate switching process between laminar and turbulent flow states, for the transitional boundary layer growth in arbitrary pressure gradient, two-dimensional incompressible flows.

BOUNDARY LAYER DEVELOPMENT FROM TRANSITION PROVOKING DEVICES.

CHAPTER 1.

HISTORICAL DEVELOPMENT AND INTRODUCTION.

The progress in understanding of the phenomenon of boundary layer transition, (free and forced), is traced from its early development through to modern concepts, in particular relation to the present investigation.

BOUNDARY LAYER DEVELOPMENT FROM TRANSITION PROVOKING DEVICES.

HISTORICAL DEVELOPMENT AND INTRODUCTION.

1.1 The initial experiments.

The boundary layer theory originated from the intuition of Ludwig Prandtl (1904) who introduced his classic paper "On Fluid Motion at Very Small Viscosity." and one is certainly justified in regarding this as the moment in which modern fluid mechanics was born. The first tentative steps of transition analysis were however laid down even before Prandtl and the boundary layer equations were known. Osborne Reynolds (1883) performed the first fundamental experiments on transition by observing a liquid dye filament as it flowed through a straight uniform pipe. He thereby discovered the principle of similarity which bears his name and asserts that transition is governed by the Reynolds number, ($R = U.L/\nu$), the ratio of inertial to viscous forces. About this same time, Lord Rayleigh (1880) was also concerned with the physical causes of transition and both he and Reynolds formulated the hypothesis that transition can be traced to an instability in the basic laminar flow. All subsequent theoretical investigations of the process of transition are based on this, the Reynolds/Rayleigh hypothesis.

In 1914, Prandtl carried out his famous experiments with spheres and succeeded in showing that the flow in the boundary layer may also be either laminar or turbulent and furthermore, that the problem of flow separation and the estimation of drag are

dependent on transition. These particular experiments also mark the first documented use of trip wires as a means of artificially provoking transition in a boundary layer. Prandtl thus supplied the impetus for continued research into the phenomenon of boundary layer transition.

1.2 Stability considerations.

The starting point for all boundary layer stability analyses is the so-called Orr-Sommerfeld equation, independently derived by Orr (1907) and Sommerfeld (1908) in the form:-

$$(U - c)(v'' - \alpha^2 v) - U''v + \frac{i\nu}{\alpha}(v'''' - 2\alpha^2 v'' + \alpha^4 v) = 0 \qquad 1.1$$

(v denoting the disturbance amplitude,

U the basic flow,

α the wave number,

c the wave propagation speed,

the prime denoting differentiation with respect to y.)

The equation is derived from a small disturbance analysis of the Navier-Stokes and Continiuty equations; a full description of which is given by White (1974) and other standard texts. The eigenvalues of the equation then determine the stability of the parallel flow. In its frictionless form:-

$$(v'' - (\frac{U''}{U - c} + \alpha^2)v = 0) \qquad 1.2$$

the equation had been solved by Rayleigh in 1913. Rayleigh succeeded in deriving several important theorems concerning the stability of laminar velocity profiles; among them the "point of inflection criterion", where the said constitutes a necessary condition for

the occurrence of frictionless instability. These earlier analyses however created the dogma that the flat plate laminar boundary layer was completely stable with respect to small disturbances. Prandtl however was convinced of a small disturbance mechanism, a belief inspired from flow visualisation studies where he had observed the formation of small eddies in the vicinity of the wall of his water channel. On reporting his qualitative findings, Prandtl (1921) laconically added:-

"We then addressed ourselves to the theoretical study of transition."

The theoretical investigations into the origins of turbulence were carried on by Prandtl's students, Tietjens (1922), Heisenberg (1924) and Tollmien (1929) who finally obtained a solution, success being hard won only after ten years of sustained effort. Tollmien's results were the first solutions of the theory of small disturbances which led to the evaluation of a critical Reynolds number with the same order of magnitude as that measured experimentally.

1.3 The semi-empirical approach.

Some time before the first successes of the stability theory had been achieved, experimental investigations had led to a semi-empirical theory of transition. Schiller (1934) and notably Taylor (1936) further developed the empirical approach, based on the premise that transition was due to finite disturbances originating from a pipe inlet, or in the case of a boundary layer, from the external

freestream. These disturbances induced local pressure gradients and tended to promote local boundary layer separation thereby prompting transition. Taylor, in fact, was reasonably successful in correlating the Reynolds number for the critical drag coefficient of a sphere with the freestream turbulence in terms of intensity and scale. He showed that generally:-

$$(Rx)_{tr} = f\left\{\left(u'/U\right)\left(x/l\right)^{1/5}\right\} \qquad 1.3$$

where $(Rx)_{tr}$ is the transition Reynolds number,

(u'/U) the freestream turbulence level as a percentage,

x the distance downstream of the turbulence generator ie. (a grid)

and l a turbulence length scale related to the grid mesh size.

The conflict of opinions as regards the transition mechanism was however not to be reconciled for a further decade.

1.4 Experimental evidence of a stability mechanism.

During the early years of the Second World War, H. Dryden and his collaborators, working in the National Bureau of Standards in Washington, U.S.A., undertook a very thorough and careful investigation of the phenomenon of boundary layer transition. Results initially were inconclusive, however in 1942, under the direction of Dryden, Schubauer and Skramstad (1942) were investigating the effect of freestream turbulence on the location of the transition point on a flat plate. The study required unusually low turbulence levels, ie. (about $u'/U = 0.02\%$), to determine the boundary layer

behaviour when it was as little disturbed as possible. The discovery of the boundary layer oscillations is reported by Schubauer and Skramstad as follows:-

"With greatly reduced stream turbulence, it was expected that the slow irregular fluctuations would be correspondingly reduced. Such fluctuations were, in fact, almost nonexistant; but as the (hot) wire was moved downstream through the boundary layer, a regular oscillation appeared, weak at first but with increasing amplitude as the distance downstream increased."

Schubauer and Skramstad's work was indeed experimental confirmation of the mathematical theory of stability; published as a wartime report, it was not until 1947 that German researchers became aware at last that the theory for which they had been largely responsible had been verified experimentally. The now respectable stability theory has since continued to be developed by many workers. The experiment also partly reconciles the Tollmien-Schlichting and Taylor theories by the evidence of the critical nature that free-stream turbulence has on transition, with the Tollmien-Schlichting mode being operative in low turbulence flows and the Taylor or other modes applicable in highly turbulent flows.

1.5 Turbulent spots.

Harvard University was to be the scene of the next great experimental breakthrough in transition research. Emmons and Bryson (1950) were concerned with a water table analogy to supersonic flow, where in addition to the modelled "supersonic" phenomena, Emmons

noticed strange bursts of turbulence occuring on the table and had the foresight to recognise this as the breakdown of laminar flow. The turbulent bursts, or spots, as witnessed by Emmons, were seen to appear randomly with time and position on the surface of the table, to grow as they propagated downstream and to culminate in fully developed turbulence. It is interesting to note that Schubauer and Skramstad (1942) had also observed turbulent bursts, (see figs. 11 and 12 of their report.). The then more startling presence of the regular two-dimensional fluctuations had however drawn the attention away from the three-dimensional aspects of the problem. The three-dimensional and intermittent nature of turbulent spots were studied by Schubauer and Klebanoff (1956). Using the technique developed by Mitchner (1954), they generated artificial turbulent spots by causing a spark to jump the gap between an electrode and the experimental plate and thus established some quantitative data on the growth and physical dimensions of turbulent spots. They further intimated that the spot growth and coalesence process was statistically similar in zero pressure gradient transitional boundary layers, regardless of how the transition was initiated. (see also section 1.12)

1.6 The intermediate transition processes.

The transitory process between two-dimensional boundary layer oscillations, or Tollmien-Schlichting waves as they became to be known, and turbulent spot evolution was essentially clarified by Klebanoff et al. (1962). Using the vibrating ribbon technique developed by Schubauer and Skramstad (1942), they were able to show

that a shear layer in the unstable region has a strong ability to amplify any slight three-dimensionality, which certainly must be present in any natural disturbance spectrum. There then followed the rapid development of spanwise peaks and valleys in the intensity of the streamwise velocity fluctuation. Vortex breakdown occurred at regions of high localised shear, followed by the emergence of fully three-dimensional fluctuations, and turbulent spots would ultimately manifest themselves from the local regions of intense fluctuations. This is basically the present conceptual picture we have of the transition region today and is shown in the idealised pictorial representation of FIG. 1.1, taken from White (1974).

1.7 Developments in the stability theory.

The advances in the understanding of the transition process has been mirrored to a certain extent in the development of stability analyses, which by the end of the 1960's had reached a fairly high level of sophistication. Non-linear theories had appeared eg.(Stuart (1958), Meksyn and Stuart (1951) and Benney (1961),(1964)) and were moderately successful in predicting the three-dimensional amplification. None however have found universal application and this topic is still in a state of development and modification.

1.8 Provoked transition.

Artificial fixing of transition, as distinct from the process of natural transition, has significant practical importance. Transition provoking agents are necessary in small scale model testing to fully simulate flight Reynolds numbers, ie. (to reproduce

the same relative transition point of the prototype on the model). The generation of a turbulent boundary layer can also be effective in reducing drag, such as in the case of dimpled golf balls, where the dimples promote a turbulent boundary layer flow around the ball. The increased skin friction coefficient associated with the turbulent boundary layer results in a delayed separation point on the ball and consequently a reduction in the form drag. The drag due to skin friction is of course increased, but is much less significant than the decrease in form , or profile drag.

Since Prandtl first used a trip wire to produce turbulent boundary layers in 1914, the effectiveness of trip wires and other transition provoking devices have been the topic of many research programs. Primary studies were ultimately of an empirical nature, aimed at determining critical roughness heights in terms of a Reynolds number, to satisfy a variety of limiting conditions. eg:- (Smith and Clutter (1959), Tani and Sato (1956), Gregory and Walker (1951), Mochizuki (1961), Tani and Hama (1953), Goldstein (1936), Dobbinga (1965), Gibbings (1958), Tani et al. (1954), "Wings" data sheet (1953), Preston (1958), Potter (1957), Tani et al. (1962) and Dryden (1953)).

Typical criteria are:-

(i) For immediate transition at a two-dimensional trip wire:-

$$R_k = \frac{U_\infty k}{\nu} = 826 \qquad \text{Gibbings (1958)}$$

(ii) For no effect on transition:-

two-dimensional trip wire $\quad 40 \leqslant {}^{R_k}{}_{crit} \leqslant 260$ Smith and Clutter (1959)

where U_∞ is the freestream velocity,

k is the roughness height above the plate

and $R_{k_{crit}} = u_k.k/\nu$, with u_k the velocity in the undisturbed laminar boundary layer at the wire height k.

Dryden (1953), on reviewing the available published data, found that when transition was induced abruptly at a two-dimensional trip wire , the transition Reynolds number, R_{xtr}, correlated well against the ratio of the roughness height to the undisturbed boundary layer displacement thickness, (k/δ^*_k). He also obtained good correlation between the ratio of the provoked and natural transition Reynolds numbers against the parameter (k/δ^*_k).

For isolated roughness elements, a relation between R_{xtr} and $R_{k_{crit}}$ was given by Tani et al. (1962), for the limiting case of abrupt transition behind the element:-

$$\text{ie.} \quad R_{xtr} = 2.08(x_k/k)^{4/3} . (R_{k_{crit}})^{2/3} \qquad 1.4$$

Over the years a substantial bank of data has been accumulated with many similar correlations to those above and Tani and Sato (1956) adequately expressed the prevailing view at the time:-

"Thus the steps seem to have been reached in that the transition due to roughness can be predicted sufficiently accurately for most practical purposes. Much is left however to be explained concerning the fundamental mechanism of this type of transition."

1.9 Transition mechanisms due to roughness

Klebanoff et al. (1955) had pointed out the differences between the effects of two and three-dimensional roughness elements, where the isolated three-dimensional protuberance introduced a localised three-dimensional disturbance and the flow downstream appeared as a continuous wake-like wedge of turbulence. Klebanoff (1966) and Klebanoff and Tidstrom (1972) then clarified the mechanism by which a two-dimensional roughness element induced transition. They observed the same basic processes involved as in a natural transition, the behaviour being characterised by wave-like disturbances rather than discrete vortex filaments which had been inferred from previous studies utilising flow visualisation techniques. Although Klebanoff reported a similar process to natural transition, he also emphasised significant departures from Tollmien-Schlichting theory. Disturbances which should have been stable according to theory were seen to grow and decay. Klebanoff also noted higher frequencies and much larger increases in amplification, all lying outside the zone of amplification of Tollmien-Schlichting theory.

1.10 Centrifugal instability and transition.

While the discussion so far has been solely concerned with parallel flows, it is prudent to digress slightly to mention centrifugal instability as this can have some bearing when the boundary layer in question flows over a concave surface. Taylor (1923) performed the pioneering work by observing the flow between two concentric cylinders, (Couette flow), and establishing the existence

of "Taylor Vortices". Görtler (1940) pointed out the existence of a similar longitudinal vortex instability in the boundary layer on a concave wall. It is sufficient to state that the "Taylor-Görtler" mode of instability may take precedence over the "Tollmien-Schlichting " mode in such flows.

1.11 The prediction of transition.

With the state of knowledge of transition mechanisms thus far advanced, it is worthwhile to review how this knowledge has influenced practical transition prediction techniques. Early prediction methods consisted of empirical relationships correlated from available experimental data. The method of Michel (1951) is probably the simplest, comprising only one relationship between the momentum thickness Reynolds number and the axial length Reynolds number at transition. A curve-fit, given by Cebeci and Smith (1974) is:-

$$R\theta_{tr} = 1.174\left[1 + (22400/R_{xtr})\right] R_{xtr}^{0.46} \qquad 1.5$$

When the corresponding flow Reynolds numbers coincide with Michel's curve, eqn. 1.5, then transition is "predicted". Granville (1953) proposed a more plausible method which at least recognised the importance of the stability theory and the physical reality that transition occured over a region and not at a singular point. He expressed the distance between the point of instability and the point of transition ie. (fully developed turbulent boundary layer), as a function of mean Pohlhausen parameter in a tentative attempt to account for the disturbance growth processes, etc. Although only

moderately successful, Granville's method still finds application today. Other methods of the time, eg. (Crabtree (1957), Smith and Gamberoni (1956) and van Ingen (1956)), were in the same mould in that a heavy dependence on limited experimental data tended to restrict their range of application. The methods of Smith and Gamberoni and of van Ingen are however rather interesting as both, employing extensive stability calculations, independently observed that the transition point in many cases corresponded to about the same total amplification of Tollmien-Schlichting waves. Both subsequently using the fact in developing their respective prediction techniques.

The method of van Driest and Blumer (1963), a development of Taylor's hypothesis, gives a correlation between the transition Reynolds number and the freestream turbulence level. Their method is particularly good in zero pressure gradient flows but less convincing in pressure gradients.

More recent transition prediction techniques are of increased complexity. The method of Jaffe et. al.(1970) resorts directly to stability analysis and is an extension of the earlier method due to Smith and Gamberoni. Jaffe's method consists of the numerical determination of the velocity profile at each calculation step. Stability calculations then give the total amplification of a select band of frequencies and a total amplification criterion is applied to predict transition. Jaffe et. al. quote an accuracy of transition location to within 20% of chord length .

1.12 The present investigation.

If the transition point is defined as that point where turbulent spot evolution is imminent, then downstream of the point the boundary layer undergoes the transformation from being characteristically laminar to being characteristically turbulent. Most, but not all, of the transition prediction techniques previously discussed are concerned with the location of this point, the start of transition.

The present study is however almost solely concerned with the development of the transitional boundary layer from spot evolution to the completion of laminar breakdown. The disturbance environment and the mechanism leading to the local seeding of turbulent spots is also considered within the limitations of the particular measurements made.

Emmons and Bryson (1950) analysed the transition region by assuming the existence of a function, $g(x,z,t)$, of position and time which specified the rate of spot production per unit area. Using a statistical analysis, they deduced a relation for the downstream turbulence probability in the form :-

$$f(x) = 1 - e^{-\alpha g x^3 / 3U_\infty} \qquad 1.6$$

where g is a spot production rate function,

x is the streamwise coordinate

and α is a dimensionless propagation parameter of the turbulent spot.

The propagation parameter α, has the form:-

$$\alpha = \varepsilon^2 \eta / \xi' \qquad 1.7$$

where ε = TAN(1/2 the spot propagation angle).

ξ' = velocity of the spot centre/freestream velocity.

η = area of the spot/square of 1/2 its width.

Using the very limited experimental data available at the time, Emmons proposed that $\alpha = 0.1$, but did not attempt to specify a functional relationship for g. He did however show that if the numerical value of g were to increase, ie. (denoting more spots per unit area), then the overall length of the transition region would be correspondingly reduced.

Schubauer and Klebanoff (1956) showed that the transition regions in a number of different flows were statistically similar. They found that the streamwise development of intermittency, ie. (the fraction of time spent in turbulent motion) was well represented by the statistical normal distribution function, irrespective of how the transition was initiated. Dhawan and Narasimha (1958) corroborated the concept and proposed an empirical function, developed from Emmons's argument, for the streamwise development of intermittency in the form:-

$$\bar{\gamma} = 1 - e^{-0.412\xi^2} \qquad 1.8$$

Where $\xi = (x - x_{tr})/\lambda$, a normalised streamwise coordinate with x_{tr} the start of transition, ie. (denoted by the first appearance of turbulent bursts) and λ is a measure of the intermittency spread, given by:-

$$\lambda = \left[(x \text{ at } \overline{\gamma} = 0.75) - (x \text{ at } \overline{\gamma} = 0.25)\right] \qquad 1.9$$

In the present work the concept of statistical similarity in transition regions is further tested and the best representation for the intermittency distribution is determined. The loosely used term "transition-point" is clarified in terms of the intermittency, as this provides the means to classify the various regimes numerically.

Dhawan and Narasimha proposed that for the case of a flat plate, the transition region could be adequately described as a region of alternate laminar and turbulent flow. With a known intermittency distribution, they then assumed that the transitional mean velocity profiles could be expressed as the intermittency weighted average of the Blasius and "wall-wake" turbulent profiles, thus allowing the gross flat plate transitional boundary layer parameters to be estimated. The conditionally sampled data of Arnal et al. (1977), showing velocity profiles in and out of turbulent spots, would appear to vindicate, at least in principle, Dhawan and Narasimha's assumptions. In the present investigation, therefore, the earlier model is extended, so as to be capable of transitional boundary layer prediction in pressure gradients.

By its very nature, the present study generates data related to the initial growth of the subsequent turbulent boundary layer. This data is therefore viewed with due regard to low Reynolds number effects and non-equilibrium development.

FIG. 1.1

PICTORIAL REPRESENTATION OF NATURAL TRANSITION ON A FLAT PLATE FROM WHITE (1974)

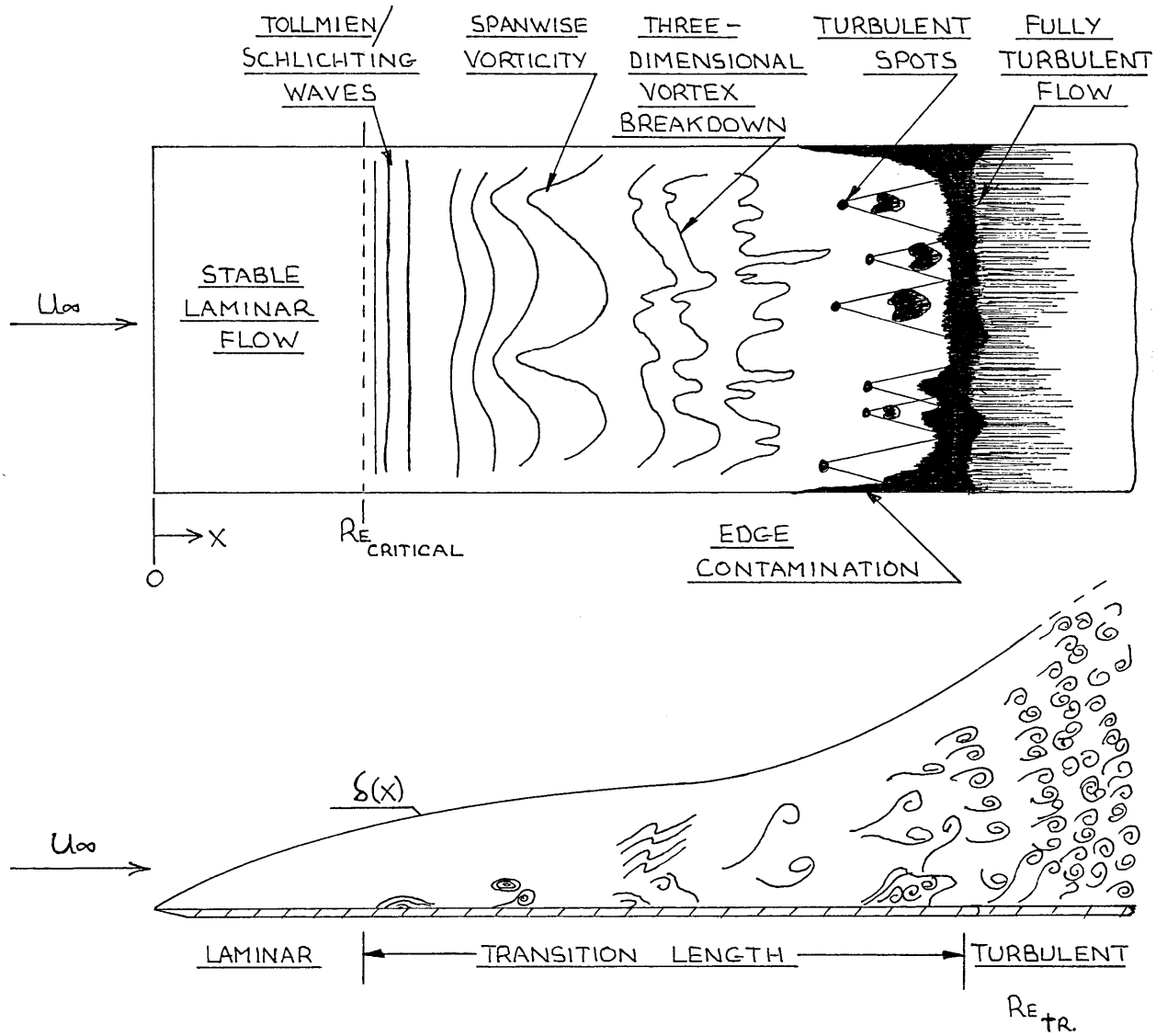

CHAPTER 2.

EXPERIMENTAL FACILITIES, INSTRUMENTATION AND MEASUREMENTS.

The design, construction and commissioning of a low speed, medium performance, boundary layer wind tunnel, for the study of transition phenomena is described. The development of instrumentation and measuring techniques is outlined and a specification of the tunnel performance with proposals for future modifications included.

BOUNDARY LAYER DEVELOPMENT FROM TRANSITION PROVOKING DEVICES.

EXPERIMENTAL FACILITIES, INSTRUMENTATION AND MEASUREMENTS.

2.1 Wind tunnel facility.

A special purpose, open-return wind tunnel facility was designed and constructed, utilising an existing diffuser and propeller-fan and motor.

The inlet and working section, turbulence damping system and instrumentation mounting arrangement were designed from basics to suit the content of the present investigation. A schematic diagram of the complete assembly is shown in FIG. 2.1.1. and a detailed description follows.

2.2 Measurement of fluid properties.

An empirical relation was given by Kinghorn et al. (1972) for the dynamic viscosity of air, in the form:-

$$\mu = (1.725 + 0.004375 \times T)/10^5 \quad \text{kg/m.s.} \qquad 2.1$$

where T is is the air temperature in degrees Centigrade. The equation was adopted and used throughout.

The air density was given by the relation:-

$$\rho = (0.46535 \times Z)/(T + 273) \quad \text{kg/m}^3 \qquad 2.2$$

where Z is the barometric pressure in mm. of mercury, and the kinematic viscosity thus follows from:-

$$\nu = \mu/\rho \quad \text{m}^2/\text{s.} \qquad 2.3$$

2.3 Power unit and speed controller.

The power unit is an Airscrew Weyroc, type N° 4/B/20, incorporating a 0.75hp., D.C. motor driving a four blade propeller-fan at 1500 maximum rev/min. Speed control is effected via feedback of the armature voltage to a thyratron valve control unit, (Watford Controls, type N° SCA-6400-1H). By maintaining a constant armature voltage under varying load conditions, a pre-selected fan speed is stabilised and held.

2.4 Turbulence damping screens.

The reduction of the turbulence level in the tunnel working section was partly achieved by the inclusion of three wire mesh damping screens, arranged in series at the entry to the inlet contraction. The screens effectively remove the large scale eddies from the flow but introduce smaller eddies immediately downstream. These smaller scale eddies however decay more rapidly, such that the overall turbulence intensity is reduced further downstream. The screens used, were flush mounted in collapsible rectangular box sections, FIG. 2.4.1., and were specified to the following design requirements:-

(i) The open area ratio, defined as $\beta = (1-\frac{d}{l})^2$, where d is the screen wire diameter and l is the mesh spacing, was to be greater than 0.57. East (1972), has shown that screens with open area ratios of less than 0.57 can cause a flow instability resulting in a significant spanwise variation in the boundary layer parameters.

(ii) The screen Reynolds number, defined as $R_s = U_s d/\nu$, where U_s is the velocity through the screen, was to be less than 40, to minimise the self-generation of turbulence by the screens. The criterion is based on the observation that regular vortex shedding from a cylinder is suppressed at Reynolds numbers, based on cylinder diameter, below 40, see Pankhurst and Holder (1956).

(iii) The axial screen spacing should be in excess of about 500 screen wire diameters. Bradshaw and Pankhurst (1964), have shown that this spacing will suffice, in most instances, to enable the screen generated turbulence to decay.

The actual screen specifications are listed along with the sketch in FIG. 2.4.1.

2.5 Inlet contraction section.

The inlet contraction has the triple purpose of further reducing the turbulence level, accelerating the flow to the entry of the working section and minimising spatial non-uniformity of the mean flow. It can be shown, eg. Pope and Harper (1966), that the variation in mean velocity across any section, varies inversely as the square of the contraction ratio. It is therefore desirable to have as large a contraction ratio as is practically feasible. Whilst a two-dimensional inlet contraction was prefered, space limitations at present necessitated a three-dimensional option. The contraction

had a rectangular cross-section with a constant aspect ratio of 2/1 and an area reduction ratio of 9/1 over 1.5m. total length.

An important design requirement is that the contour shape should be such that local adverse pressure gradients and possible separation points are avoided at the contour walls. Cohen and Ritchie (1962), proposed a design procedure for an octagonal section contraction; however, acknowledging the absence of design criteria for rectangular section contractions, it was elected to form the the present inlet section along simple elliptical profiles, FIG.2.5.1., and to adjust accordingly if local separation proved troublesome.

2.6 The working section.

In a zero pressure gradient flow, with a freestream turbulence level of about 0.3%, the method of van Driest and Blumer (1963), predicts the start of natural transition at an axial length Reynolds number of about 1.5×10^6. If the freestream velocity is say 15 m/s., then transition may be expected to start at about 1.5 m. from the leading edge. It was deemed necessary that the length of the test section should be able to accommodate the complete transition region under the above conditions. Using the observation of Keir (1971), that the ratio of the lengths from the leading edge to the end and to the start of transition are approximately constant, ie. ($^{x}etr/x_{str} = 1.5$); the end of transition might then be expected to occur at about 2.25 m. from the leading edge. The test section was thus chosen as 2.5 m. on the basis of the preceeding argument.

Entry to the working section was matched to the contraction

outlet and an infinitely variable height roof enables control of the pressure gradient and can allow the aspect ratio to be varied from 2/1 at the entry to 1/1 at the exit. The roof adjustment assembly is shown in FIG. 2.6.1. and the distribution of adjusters shown in FIG. 2.1.1.

Access to the test section is provided through four hinged doors on the front wall, the tunnel is illuminated from the rear wall and a flexible coupling joins the tunnel exit to the diffuser. The tunnel is also equipped with a fixed Pitot-static tube, coupled to an inclined water manometer, constantly monitoring the reference approach velocity to the leading edge of the plate, U_o. FIG 2.6.2. (photograph), shows the essential details of the complete tunnel working section.

2.7 The boundary layer plate.

The flat plate on which the boundary layer growth was to be measured, consists of a rectangular, 6mm. thick aluminium sheet, 8 ft., (2.44 m.) long and completely spanning the tunnel working section. The plate is fixed to two underside rails which are bolted through the tunnel floor on to the main supporting framework. The assembly allows the capability of setting the plate at small angles of positive or negative incidence to the oncoming flow. For the present studies, the plate was set at 0° of incidence and 50mm. above the tunnel floor. By so doing it was intended to minimise interference at the leading edge due to the boundary layer development through the inlet section.

To ensure a stagnation point on the upper surface of the plate, the leading edge was shaped and bent slightly down, see FIG. 2.7.1. (photograph), thereby presenting a convex surface to the oncoming flow. Following Klebanoff and Tidstrom (1972), a small blockage was also introduced on the upper surface at the trailing edge to create a minimally favourable pressure gradient over the whole length of plate.

The plate was equipped with static pressure tappings along the centre line at 50mm. pitch and the upper surface was polished to a mirrorlike finish. Some surface undulations were evident with varying degrees of severity, the worst of which constituted a peak to valley amplitude of 0.008 ins.,(0.203mm.) over a wavelength of 9 ins.,(229mm.). This waviness however compares favourably with that quoted by Schubauer and Skramstad (1942), for their experimental plate, ie. (0.010 to 0.020 ins. over 1 to 2 ft.).

2.8 Tunnel instrumentation carriage.

To provide three-dimensional flexibility for the hot-wire probe sensor positioning, an overhead carriage was designed to allow probe movement in the three cartesian axes. The carrier runs on two rails fixed to the tunnel side walls at a constant height above the plate. A cross-slide, to which all the neccessary measuring equipment and vertical traversing gear can be attached, provides for, slightly limited, spanwise traversing. The spanwise position is in fact restricted to the range, $+145 \gg z \gg -100$mm., relative to the tunnel centre-line. Probe positioning in the x and z directions is

performed manually, with an accuracy of ±0.5mm. The vertical traverse is carried out remotely, with the added facility of arbitrary step lengths, using DISA equipment. The DISA sweep drive unit, (type 52B01), is used in conjunction with an external stepper motor, (type 52C01), which drives, through reduction gearing, a rack and pinion. The rack is ultimately fixed to the probe sensing head, thus transmitting the required motion to the probe. The accuracy of the vertical positioning, relative to some datum, is ±0.02mm. Calibration of the sweep drive unit, FIG. 2.8.1., gives the linear relationship between voltage and displacement:-

$$y = y_o + K(V - V_o) \qquad 2.4$$

where y is the vertical displacement in mm., corresponding to V, the displacement voltage. The suffix "o", denotes datum values, and K is a constant equal to about 10. The calibration gave K = 10.04 for the earlier experimental work. This value later became 9.96, after an overhaul of the sweep drive unit.

The stepper motor, reduction gearing and the rack and pinion are assembled as a unit and fixed to the cross-slide of the instrumentation carriage, see FIG. 2.8.2. (photograph).

The y_o,V_o datum is determined by lowering the probe towards the plate and then bringing the probe back up to y_o at 0.5mm, determined by viewing the probe through a Cathetometer and comparing the position of the probe against a graduated setting block. Having fixed the datum, the probe traverse is continued invariably upwards when making measurements, to eliminate errors due to backlash.

2.9 Tunnel performance - preliminary testing.

Flow visualisation studies were carried out using smoke in order to check for flow separation in the inlet contraction. As there was no evidence of any flow reversal along any of the contour walls, it was concluded that separation did not occur in the inlet section. A smoke plume introduced in the freestream of the working section gave no indications of swirl but did exhibit a strong tendency to drift towards the rear side wall, thereby suggesting a lack of two-dimensionality. No attempt was made to correct the flow at this stage as more quantitative tests were to be carried out, regarding flow two-dimensionality, later in the testing program.

Coupling a hot-wire output to a loudspeaker results in an effective transition detection device, analogous to a stethoscope. With the hot-wire signal being made audible, one can easily distinguish between laminar, intermittently turbulent and fully turbulent flow regimes. The above device was used to assess the extent of the transition region on the test plate at a freestream velocity of 12 m/s. Disappointingly, the first indications of turbulent bursts occured at a distance of only 200mm. from the leading edge. Under these conditions, it was expected that the flow would remain laminar up to about 2.0 metres. After some considerable experimental effort it was discovered that negative incidence of the plate to the oncoming flow, still in a zero pressure gradient, greatly improved the transition characteristics and indicated that the early transition was due to a leading edge effect.

Unfortunately however, the tunnel dimensional restraints restrict the amount of incidence which can be imposed and an alternative was sought. The tunnel was therefore modified to allow variable suction rates through a slot partly spanning the tunnel floor and just ahead of the leading edge, see FIG. 2.7.1. The suction pressure was controlled by a variable speed D.C. motor/blower, with the tunnel slot connected to the low pressure side of the blower. The arrangement was found to have the desired effect with the transition location considerably delayed, although still occurring rather prematurely. The modification also resulted in the considerable advantage of being able to control the location of the transition region. Varying the suction motor speed from zero to maximum, could fix the approximate location of the start of transition within a range of 300 - 400mm, depending on the flow conditions. Considering the objectives of the current research to be more concerned with the transition region as opposed to the location of the start of transition, no further attempts were made to improve the transition characteristics.

2.10 Hot-wire and associated instrumentation.

DISA hot wire equipment has been consistently used throughout the project for the measurement of mean velocity and the r.m.s. of the fluctuating velocity. The instrumentation bank is shown in FIG. 2.10.1. (photograph), and a schematic layout is shown in FIG. 2.10.2. Hot wire sensors, (type 55P15), were coupled to a standard anemometer bridge, (type 55M10), operating in the constant

temperature mode. The usual square-wave test was carried out to ensure bridge stability, with the "Q" and "L" functions adjusted to obtain an acceptable oscillation-free signal and an upper operating cut-off frequency well in excess of the low-pass filter setting. A spectral analysis of the freestream turbulence shows that most of the turbulent energy is contained below a frequency of around 1kHz. The hot wire signal was therefore filtered at a -3db. cut-off frequency of 2kHz.

The anemometer was invariably used in conjunction with a DISA lineariser, (type 55M25), and a DISA true integrator, (type 52B30), for the advantages of improved accuracy in the measurement of highly turbulent flows and for the convenience of manual "on-site" calibration and adjustment. The lineariser is in essence an analogue computer, which, through exponential and square root functions, imposes a linear relationship between the probe voltage and the fluid velocity. A pictorial comparison between a non-linearised and a linearised relationship is shown in FIG.2.10.3. and a typical linearised probe calibration in FIG. 2.10.4. The true integrator, using the $\frac{1}{T}\int_0^T f(t)dt.$ function, where f(t) is the input, provides the extremely useful facility for making true time-averaged measurements over a wide choice of selected integration times. A brief specification of the various units is given in Appendix 1. and for a more detailed description, the reader is referred to the DISA specification and instruction manuals.

2.11 Mean velocity profile measurements.

The fundamental measurements made in the present work are those of mean and fluctuating velocity, however, before any boundary layer velocity profiles were measured, the hot wire output was firstly linearised. The linearisation was carried out against a Pitot-static tube, coupled to a micromanometer, (Furness Controls, type MDC), with both, well in the freestream. The linearisation procedure briefly consists of setting the "gain high" control of the lineariser such that the hot wire output voltage corresponds to $^1/_{10}$th. of the velocity, at the maximum velocity. The minimum velocity is then checked and adjusted, if necessary, by the "exponent factor" control to again give a voltage corresponding to $^1/_{10}$th. of the velocity. The air speed is then returned to the maximum and the procedure repeated until consistent agreement is obtained at both the high and low ends of the velocity range.

In a personal discussion with a representative at the DISA main factory in Copenhagen, the said jokingly suggested that a probe linearisation should be checked every two minutes. Whilst this would involve the operator in perpetual linearisation checks, it is however obvious that the linearisation should be checked as frequently as is practicable. In the present work, the probe linearity was calibrated, in the freestream, before and after every boundary layer velocity profile was measured. By measuring a set of velocities against a Pitot-static, in the range of interest, it was usually found that while the two end velocities were in good

agreement, mid-range velocities developed an increasing error from the two end points. The maximum mid-range error could be between $^1/_2$% and 2%, positive or negative, depending on the lineariser settings. If the maximum error was found to be in excess of ±2%, then the data was discarded and the boundary layer profiles re-measured. For maximum errors up to ±2%, a local velocity correction was applied, based on the known error distribution.

It was found during the course of the project that new probes had good stability characteristics and required only nominal re-adjustment. After some use however, the probes deteriorated, eventually developing significant drift in their calibration to the point where they became unusable.

Integration of the linearised probe voltage over a period of time and then dividing by the integration time, ie. electronically, results in true time-averaged measurements. In the present work, an integration time of 5 secs. was normally employed for both laminar and fully turbulent flow regions. For transitional regions, the integration time was doubled to 10 secs. and the mean value, if necessary, extracted from a number of readings.

The streamwise component of fluctuating velocity was measured both in the freestream and in the boundary layer. A DISA auxiliary filter unit, (type 55D25), with the low-pass filter set at 2kHz. was fed with the linearised output voltage. This signal was then passed to an r.m.s. voltmeter, ultimately yielding the streamwise turbulence component:-

$$\frac{\sqrt{\overline{u'^2}}}{U_\infty} 100\% \qquad 2.5$$

The freestream turbulence level, for the three screen configuration, is shown as functions of velocity and of streamwise position in FIG. 2.11.1. and FIG. 2.11.2. respectively.

2.12 The pressure gradient.

All of the boundary layer flows studied in the present work are flows under the condition of zero pressure gradient. The condition was initially set up crudely by adjusting the variable height roof to give a constant static pressure distribution along the tunnel length. The static pressure was measured from the plate tappings to an inclined multi-tube manometer. Fine adjustment was implemented by measuring, with a hot wire, the freestream velocity distribution through the tunnel and adjusting the roof height accordingly. The resulting pressure distributions are represented indirectly by the percentage variation in the dynamic pressure, ie. $(\frac{1}{2}\rho U_\infty^2)$, from the mean value along the tunnel length, see FIGS. 1.1,2.1,3.1,and 4.1 of App. 6. The variation could be controlled to within $\pm 1/2\%$ of the mean for most of the length, with the exception of the leading edge, where the velocity distribution is as shown in FIG.2.12.1.

2.13 The measurement of intermittency.

It became quite apparent early on in the investigation that one of the most fundamental characteristics of laminar breakdown is the so-called intermittency, defined as the ratio or percentage of time spent in turbulent motion. Its measurement therefore became an essential feature of the proposed studies.

Klebanoff (1955), used the flatness factor method to determine the intermittency distribution in a turbulent boundary layer, where the flatness factor for u' is given as:-

$$\overline{u'^4}/(\overline{u'^2})^2 \qquad 2.6$$

As the probability distribution of the interface between turbulent and non-turbulent fluid is approximately Gaussian, then near the wall, where the intermittency is equal to 1, the flatness factor corresponds closely to the Gaussian value of 3. The intermittency, described as an on/off process, may then be defined by:-

$$\gamma = 3 \Big/ \frac{\overline{u'^4}}{(\overline{u'^2})^2} \qquad 2.7$$

Klebanoff showed that the intermittency as obtained by the flatness factor method compared favourably with the intermittency gleaned from a visual analysis of oscilloscope records of u' and of $\partial(u')/\partial(t)$, at least up to $y/\delta = 0.9$. Sandborn (1959), also used the flatness factor method; for the present investigation however, an intermittency measuring system was designed along the lines of that outlined by Corrsin and Kistler (1954). The choice of method, sometimes referred to as the on/off method, was strongly influenced by the fact that an amplitude comparator, DISA type 52B10, was available and also because the on/off method is much more direct. The amplitude comparator is capable of measuring the percentage of time a given input signal spends above a given threshold level. The output is in terms of a voltage from 0 - 5V corresponding to probabilities from 0 - 1. This function, in fact, constitutes a

large number of the basic elements required in an intermittency measuring circuit and needs only a suitable input signal to be complete. The input signal, by necessity, must have a significantly different character in laminar and in turbulent regions to enable accurate discrimination between the two flow regimes. The instantaneous streamwise fluctuating velocity, u', in itself is unsuitable, but can be modified electronically, or rather the fluctuating voltage representing u' can be modified, to produce the required discriminating signal. A suitable circuit was designed, see FIG. 2.13.1., and basically converts the instantaneous time-dependent voltage, corresponding to velocity, into a random pulse train, where the pulses are generated by the higher valued u' in the turbulent regions. The circuit performance consists of the three fundamental operations of:-

(i) removal of the D.C. component, leaving only a time-dependent voltage corresponding to u'.

(ii) the residual A.C. voltage is then amplified by 1000/1 to enable full-wave rectification through a diode bridge. The amplifier, Radio Spares N° 741, is driven by a regulated ±15V D.C. supply, see Radio Spares (1977).

(iii) removal of the zeros and smoothing, resulting in an approximate square pulse.

The 1.1μF. capacitor across the output was chosen on a trial and error basis, balancing effective zero removal against long discharge times, in an attempt to obtain optimum, undistorted pulse shapes.

Some typical signals are shown in FIG. 2.13.2., where the discriminating signal "q", is compared with u', the traces being taken simultaneously. The ragged tops of the pulses, while undesirable, present no serious drawbacks as the signal, although crude, has all the discriminatory characteristics required and can be analysed quite adequately with the amplitude comparator.

A schematic layout of the intermittency measuring system is shown in FIG. 2.13.1. The signal q is fed to the comparator, which indirectly determines the percentage of time that q spends above a selected threshold level, ie. the intermittency. The threshold voltage is set with a Farnell stabilised D.C. supply which is reduced by a factor of 1/100 to give a suitable range of voltages. A threshold level of 15 -20mV. was found to be most suitable for the present investigation and was subsequently used throughout.

As a basis for comparison, typical measured intermittency distributions in a fully developed turbulent boundary layer are shown in FIG. 2.13.3. and are compared with the relationship given by Klebanoff (1955), based on a Gaussian integral distribution, with the mean value, ie. $\gamma = 0.50$, at $y = 0.78\delta$ and standard deviation $= 0.14\delta$.

$$\text{ie. } \gamma = {}^{1}/_{2}\left(1 - \text{erf.}5\left({}^{y}/_{\delta} - 0.78\right)\right) \qquad 2.8$$

The lack of agreement close to the wall is possibly an indication of a low Reynolds number effect, where the intermittency would appear to have a deeper penetration into the boundary layer.

2.14 Measurement of surface skin friction coefficient.

The Preston tube technique was used for the measurement of

the wall shear stress and hence the local skin friction coefficient in the turbulent flow regions. Two circular total head and static tube pairs were designed, see FIG. 2.14.1., where each was to be used as an independent check against the other. When the mean value of skin friction coefficient was within ±1.5% of the two readings, then the mean value was accepted as being accurate. The Preston tubes could be mounted on the traversing mechanism allowing the same positional flexibility as for velocity profile measurements.

To check the validity of measurements made with the tube pairs, a comparison was made with measurements from an independent total head tube, with the static pressure being obtained from the experimental plate tappings. Consistent agreement was observed over a large range of measurements.

The differential pressure measured with the two tubes in contact with the surface of the plate, was converted to wall shear stress and skin friction coefficients via the calibration due to Patel (1965).

ie. $$y^* = 0.8287 - 0.1381x^* + 0.1437x^{*2} - 0.0060x^{*3} \qquad 2.9$$

for $1.5 < y^* < 3.5$

or $$y^* = 0.5x^* + 0.037 \qquad 2.10$$

for $y^* < 1.5$

where $$x^* = \log_{10}\left[\frac{\Delta p_p . d^2}{4\rho\nu^2}\right] \quad \text{and} \quad y^* = \log_{10}\left[\frac{\tau_o . d^2}{4\rho\nu^2}\right]$$

Δp_p being the Preston tube differential pressure in N/m^2 and d the tube external diameter.

The local skin friction coefficient is then:-

$$C_{f.} = \frac{2.\tau_o}{\rho.u_\infty^2} \qquad 2.11$$

The accuracy, quoted by Patel, for the calibration is ±1.5% of τ_o. The computer program CFPT., see Appendix 3, carries out the Preston tube data analysis.

2.15 Flow two-dimensionality by the "two-pin" test.

Two experimental techniques were adopted to test for flow two-dimensionality, the first of which gives a good qualitative indication of the dimensional uniformity and is referred to as the two-pin test. The test procedure consists of fixing two pins or needles, (1.42mm diameter), equidistant from the tunnel centre-line, (±75mm. in this case), and perpendicular to the plate surface at an upstream location, (x = 100mm.). By traversing a linearised hot wire probe across the tunnel span at several downstream locations, the velocity defect in the pin generated wakes can be easily detected, see FIG. 2.15.1. Deviation of the wakes from their pin centre-lines is then indicative of a departure from two-dimensional conditions, in the form of spanwise drift, see FIG. 2.15.2. The method currently employed is to traverse the probe automatically using the DISA sweep drive unit and external stepper motor described in section 2.8. The linearised probe voltage was fed to the Y-potentiometer of an X-Y recorder and the displacement voltage to the X-potentiometer. Using the tunnel centre-line as a datum, the spanwise axis can be quickly established, thereby providing a convenient means of measuring the spanwise variation in velocity. The actual numerical values of the velocity need not even be considered, although this is

possible, as the test is purely qualitative, being only concerned with the location of the pin generated wakes relative to their original centre-line.

The second method, the momentum balance test, is described in the following chapter.

2.16 Tunnel modifications and commissioning.

In section 2.9, a brief reference is made to the effect that the earliest tunnel measurements indicated a lack of two-dimensionality. The first two-pin test, FIG. 2.15.2., confirmed the earlier suspicions as a large lateral drift was observed, although seemingly restricted to the near, or door side of the tunnel. After many attempts, the dominant cause was traced to inefficient roof sealing near the entry to the working section. With an improved sealing arrangement, the pin wake traverses were as shown in the lower set of three traces in FIG. 2.15.2., which are as far as can be determined by the two-pin test, the indications of a two-dimensional flow. A trip wire was then selected to satisfy and exceed Gibbings (1958) criterion, see section 1.8., with the wire located at x = 200mm. The resulting turbulent boundary layer growth was measured from x = 400mm., along the spanwise location, z = +25mm. The two sides of the momentum balance equation were then computed and compared with that for the data from Wieghardt's flow ,(see Coles and Hirst (1968), FLOW1400). The results, see FIG. 2.16.1., show that the test boundary layer is comparable with Wieghardt's flow, as regards two-dimensionality, at least up to x = 1600mm. A significant flow divergence was however in

evidence beyond this point. The factors promoting three-dimensionality were to remain elusive for some considerable time, however the contradictory evidence of the two-pin test, ie. good two-dimensionality was indicated up to and beyond x = 1745mm., eventually pointed to the prime cause.

The two-pin tests were invariably carried out with the boundary layer traversing mechanism removed from the tunnel. The lack of two-dimensionality as evidenced by the momentum balance test, (derived from measurements made with the traversing mechanism in the tunnel), leads to the conclusion that the traversing mechanism, due to its blockage effect, promotes three-dimensionality. The effect becoming prominent only when the underlying boundary layer has grown sufficiently large. On reflection this seems rather obvious, it was initially thought however that at 150mm. upstream, the measured boundary layer was sufficiently remote from such influences. A Pitot-static traverse of the freestream ahead of the traversing mechanism, confirmed the above and the probe mounting arrangement was subsequently altered such that the hot wire was fixed at 300mm. upstream of the blockage effect due to the traversing mechanism. The modified arrangement however introduced the new problem of probe vibration.

It can be shown that if a hot wire probe oscillates vertically in a velocity gradient, say the linear region of a Blasius velocity profile, with a peak to peak amplitude of only 0.025mm., (ie. 0.001 ins.), there results an apparent velocity fluctuation which could have a

peak to peak amplitude of 1% of the freestream velocity, depending on the Reynolds number. More significantly, with the probe moving downstream at a fixed height in a Blasius boundary layer, the probe oscillation could conceivably be mis-interpreted as a damped boundary layer oscillation. In consequence it became of paramount importance to eradicate the probe oscillation completely. To this end a remotely operated cable brake assembly was designed and incorporated into the probe traversing mechanism, see FIG. 2.8.2., (photograph). The vee-clamp component of the brake assembly was in fact found to be redundant, as probe oscillation was effectively eliminated by the closely toleranced fit of the sliding rod in its bush.

Having thus modified the profile measuring facility, the boundary layer development was again measured from x = 900mm. to the end of the plate, with a satisfactory momentum balance being obtained, see FIG. 2.16.2. A final two-pin test, FIG. 2.16.3., confirmed flow two-dimensionality. With a reasonably two-dimensional flow established, the spanwise variation in local skin friction coefficient was measured by Preston tubes at x = 1800mm. The accuracy of the Preston tube calibration is, according to Patel (1965), $\pm 1.5\%$ of τ_o, such that a spanwise variation of about $\pm 2\%$ of the mean would indicate a reasonable spanwise uniformity. The measured variation is shown in FIG. 2.16.4. which would appear to indicate an acceptable spanwise uniformity and suggests that the "screen-generated" instability referred to by East (1972), is not apparent in the present

facility. The wind tunnel at this stage, was considered to be fully commissioned and ready to enable the proposed experimental study to be carried out.

2.17 Future tunnel modifications.

Recognising the limitations of the present facility, steps were taken for its future improvement in that a completely new motor/fan and speed controller were ordered. The new power unit is rated at 3hp. and drives a six bladed, 780mm. fan. This in itself will enable higher Reynolds numbers to be set up in the working section. A longer square-round diffuser has also been specified and these are, in fact, now available. The present author would also like to propose the following modifications for the tunnel improvement. With a zero pressure gradient set up in the present configuration, the working section outlet to diffuser inlet constitutes a sudden enlargement with all the attendant inefficiency. An additional adjustable diffusing section could be incorporated into the tunnel layout to enable a more gradual enlargement to the new square-round diffuser.

The early transition which occurs with the present facility, could probably be delayed substantially by lowering the boundary layer plate to the tunnel floor and extending the present suction slot across the full tunnel span. The present tunnel freestream turbulence characteristics could also be improved by the addition of a rectangular settling length between the screen arrangement and the inlet contraction.

SCHEMATIC DIAGRAM OF WIND TUNNEL

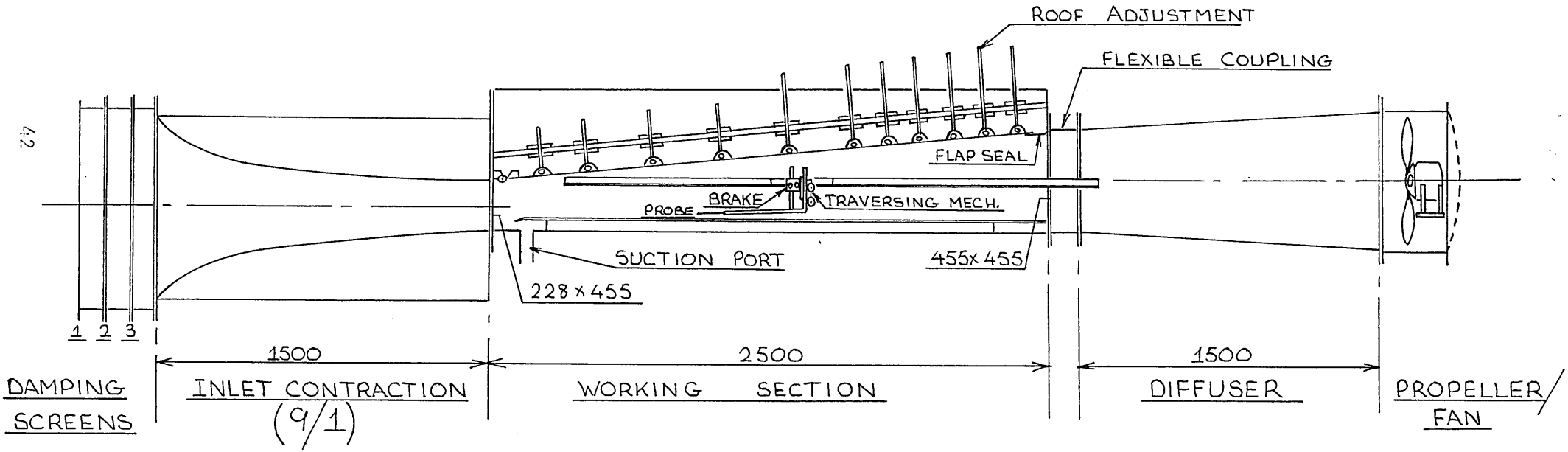

BOUNDARY LAYER PLATE— 1/4" POLISHED ALUMINIUM, 455x 2438 MM. WITH SHAPED LEADING EDGE

FIG. 2.1.1.

FIG. 2.4.1.

TURBULENCE DAMPING SCREENS

INTERNAL SIZES :- 786 x 1472 MM

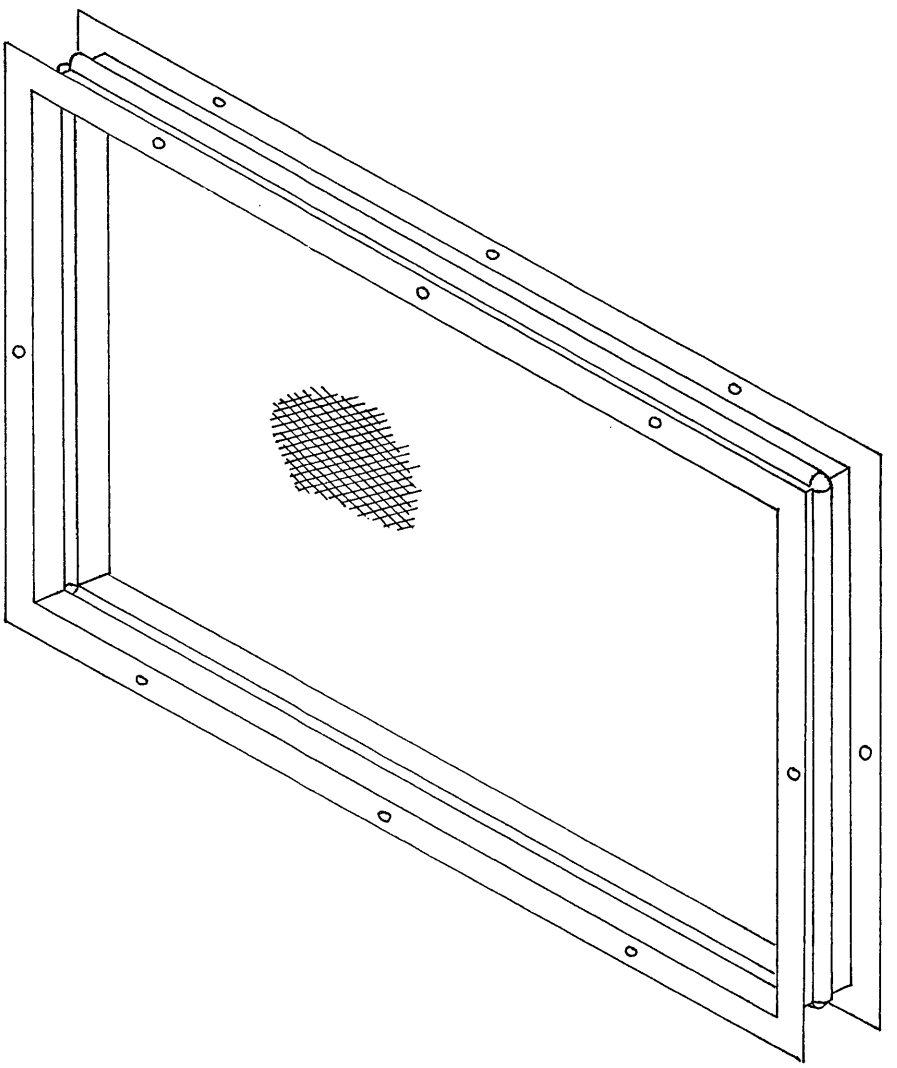

	SCREENS 1 AND 2	SCREEN 3
OPEN AREA RATIO	= 0.645	= 0.583
SCREEN REYNOLDS Nº (BASED ON Us = 2 M/S.)	= 33	= 27
WIRE DIAMETER	= 0.25 MM.	= 0.20 MM.
MESH SIZE	= 20 x 20	= 30 x 30

SPACING BETWEEN 1 AND 2 = 125 MM OR 500 WIRE DIA'S.

SPACING BETWEEN 2 AND 3 = 160 MM OR 640 WIRE DIA'S.

FIG. 2.5.1.

INLET CONTRACTION SECTION

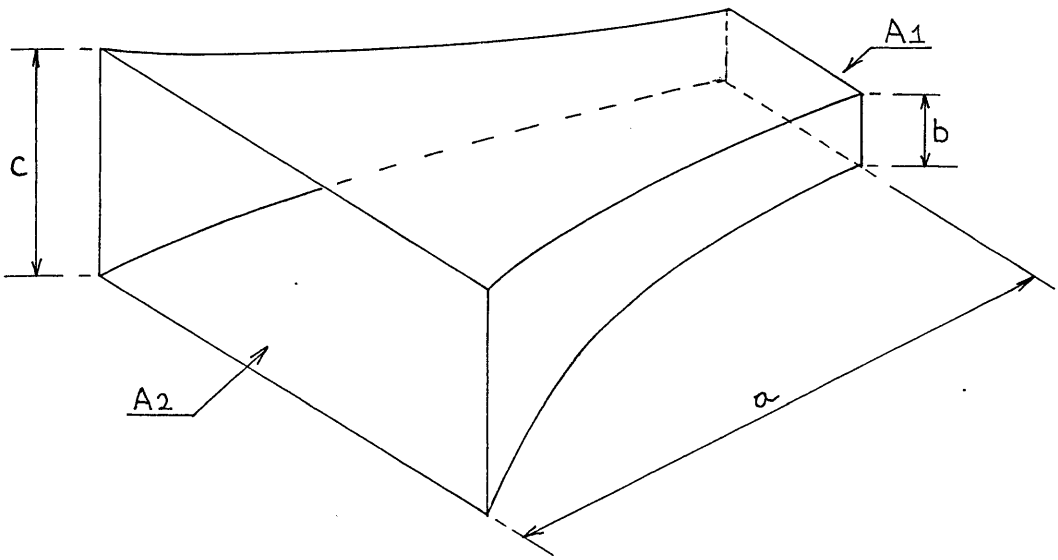

ASPECT RATIO = 2/1, CONSTANT

HENCE $A1 = 2b^2$

CONTRACTION RATIO = 9/1

HENCE $A2 = 18b^2$ AND $c = 3b$

CONTOUR PROFILE FOR TOP AND BOTTOM

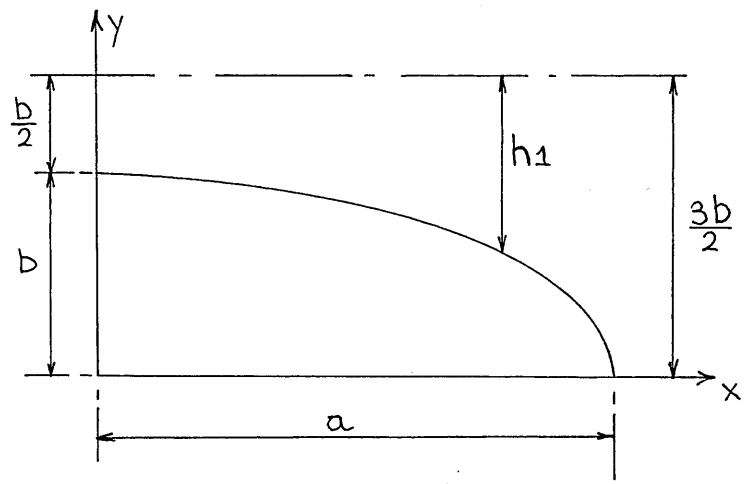

EQN. OF CURVE IS :-

$$\frac{x^2}{a^2} + \frac{y^2}{b^2} = 1$$

$$\therefore y = b\sqrt{1-\left(\frac{x}{a}\right)^2}$$

$$\therefore h_1 = b\left[\frac{3}{2} - \sqrt{1-\left(\frac{x}{a}\right)^2}\right]$$

SIMILARLY FOR THE SIDE WALLS :-

$$h_2 = b\left[3 - 2\sqrt{1-\left(\frac{x}{a}\right)^2}\right] = 2h_1$$

FIG. 2.6.1.

DETAIL OF ROOF ADJUSTMENT

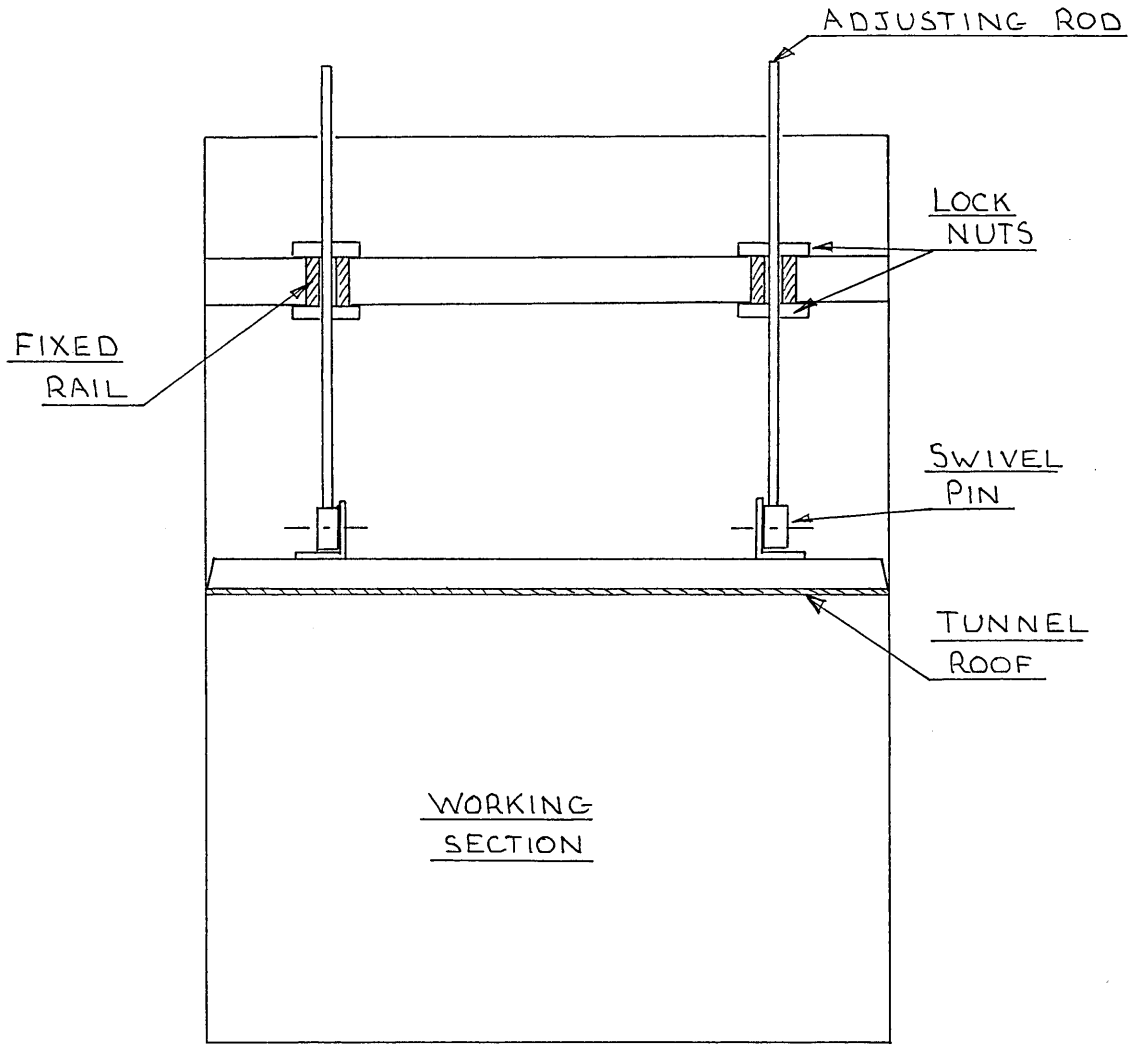

FIG. 2.6.2.

WIND TUNNEL WORKING SECTION.

FIG. 2.7.1.

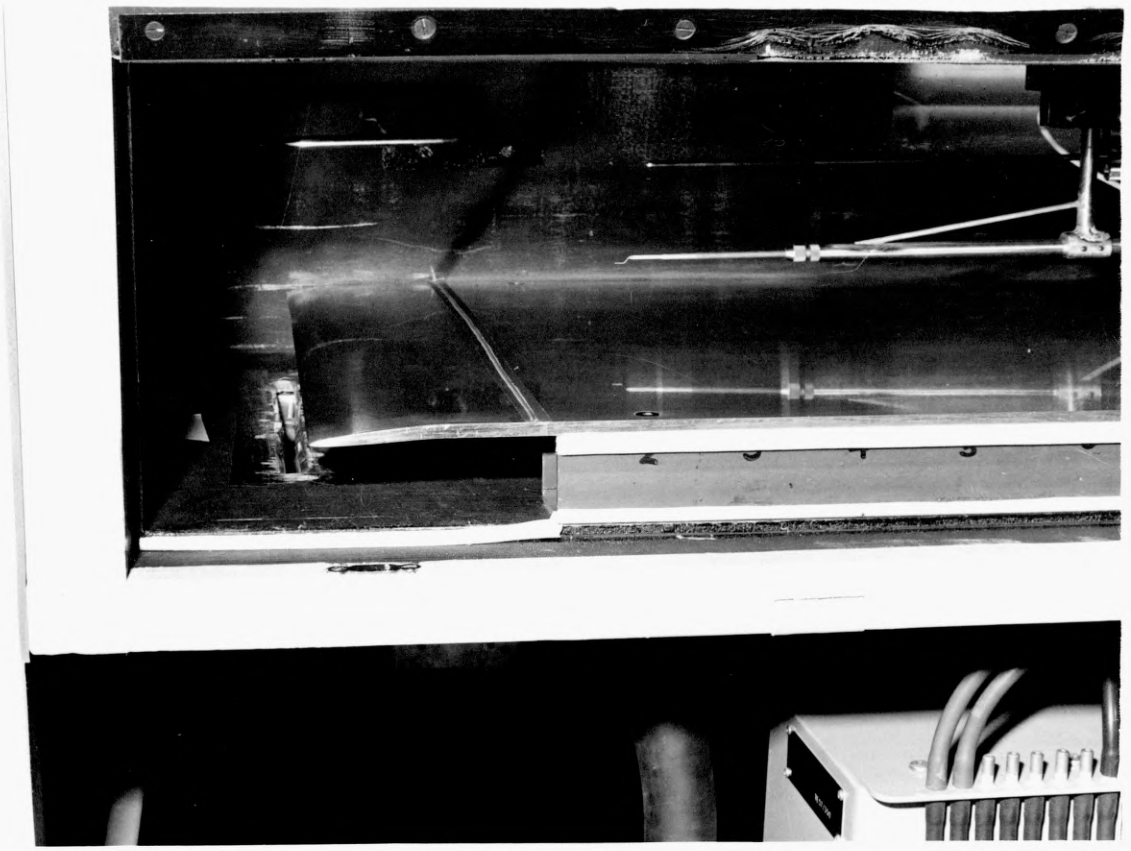

DETAIL OF LEADING EDGE CONFIGURATION.

CALIBRATION OF SWEEP DRIVE UNIT

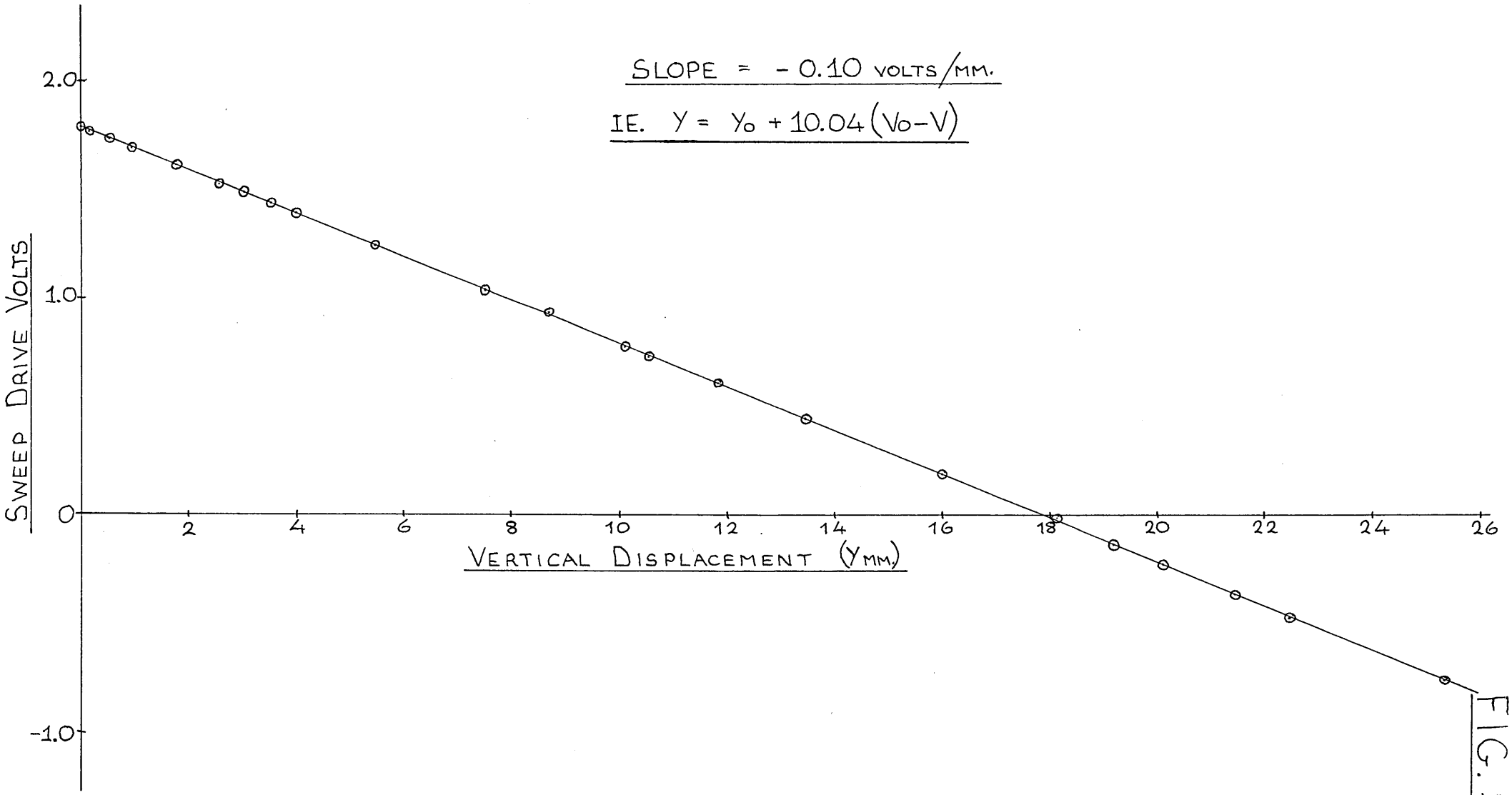

FIG. 2.8.1.

FIG. 2.10.1.

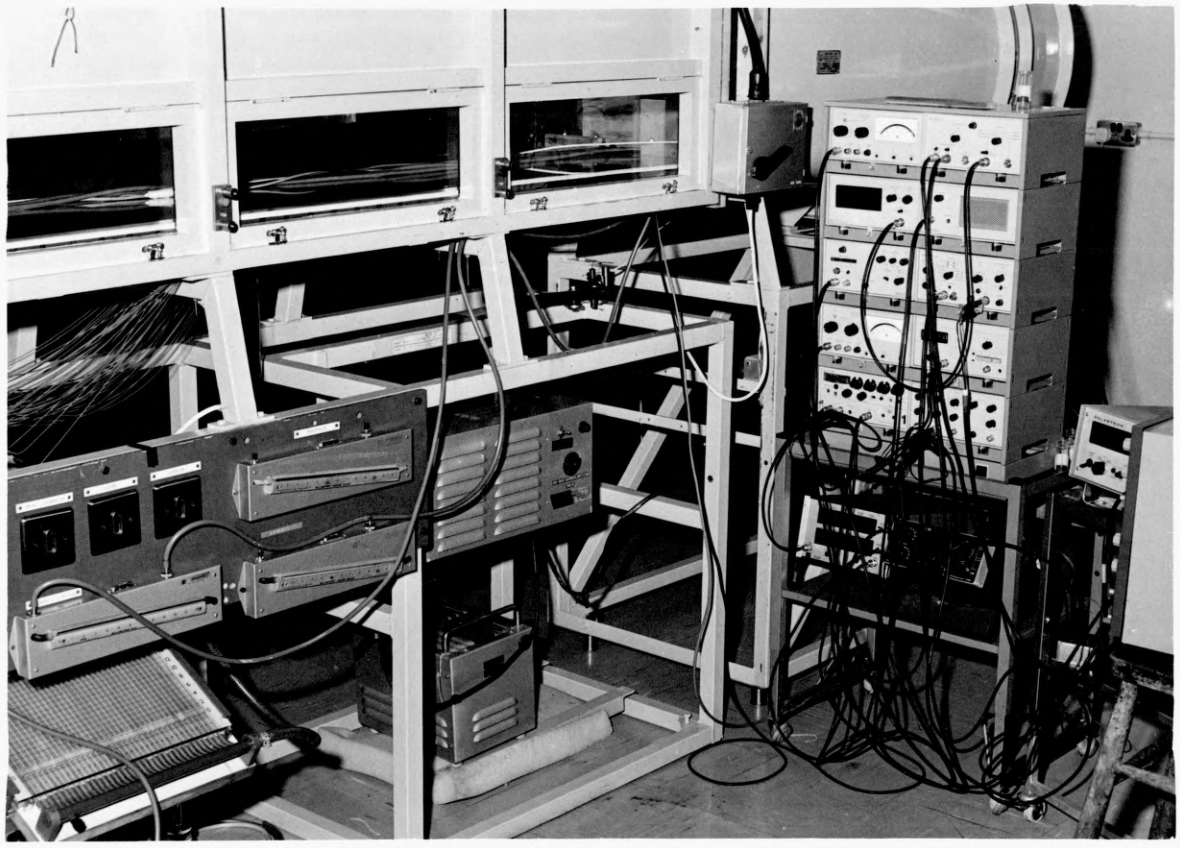

HOT WIRE INSTRUMENTATION.

FIG. 2.8.2.

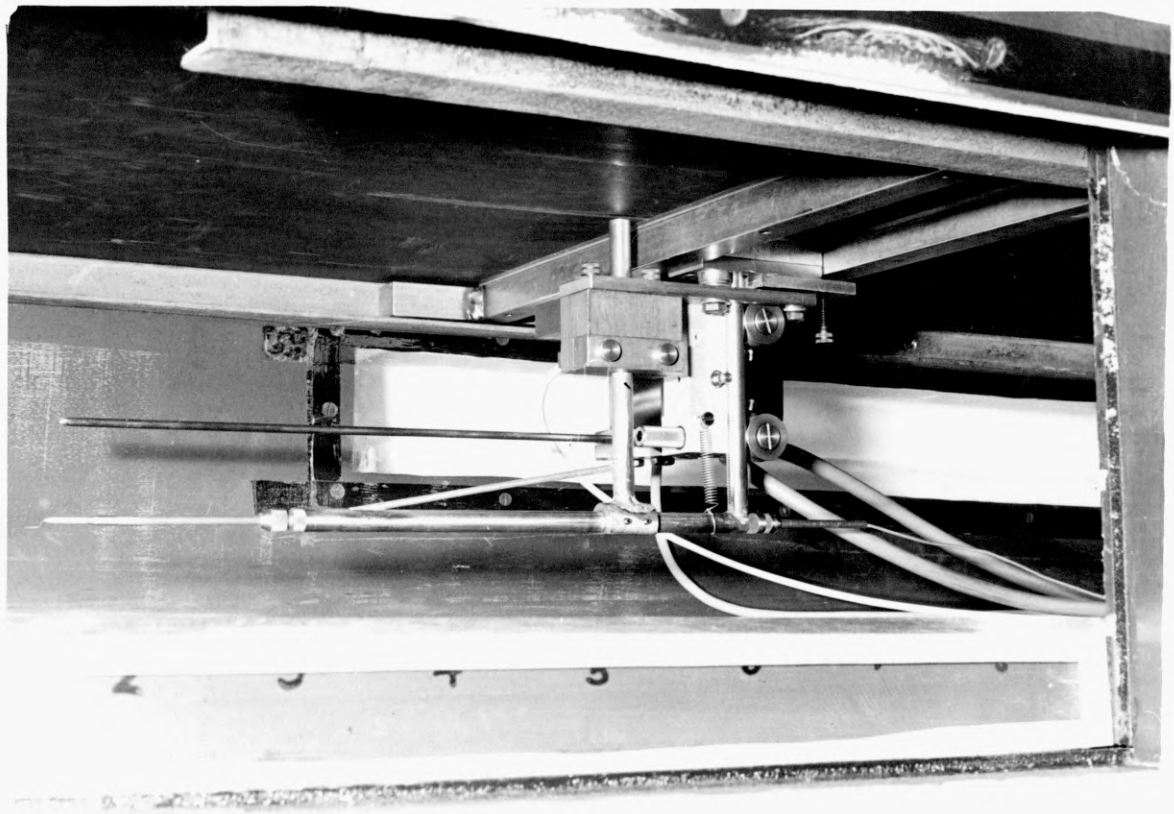

DETAIL OF TRAVERSING MECHANISM.

FIG. 2.10.2.

INSTRUMENTATION LAYOUT

SCHEMATIC DIAGRAM :-

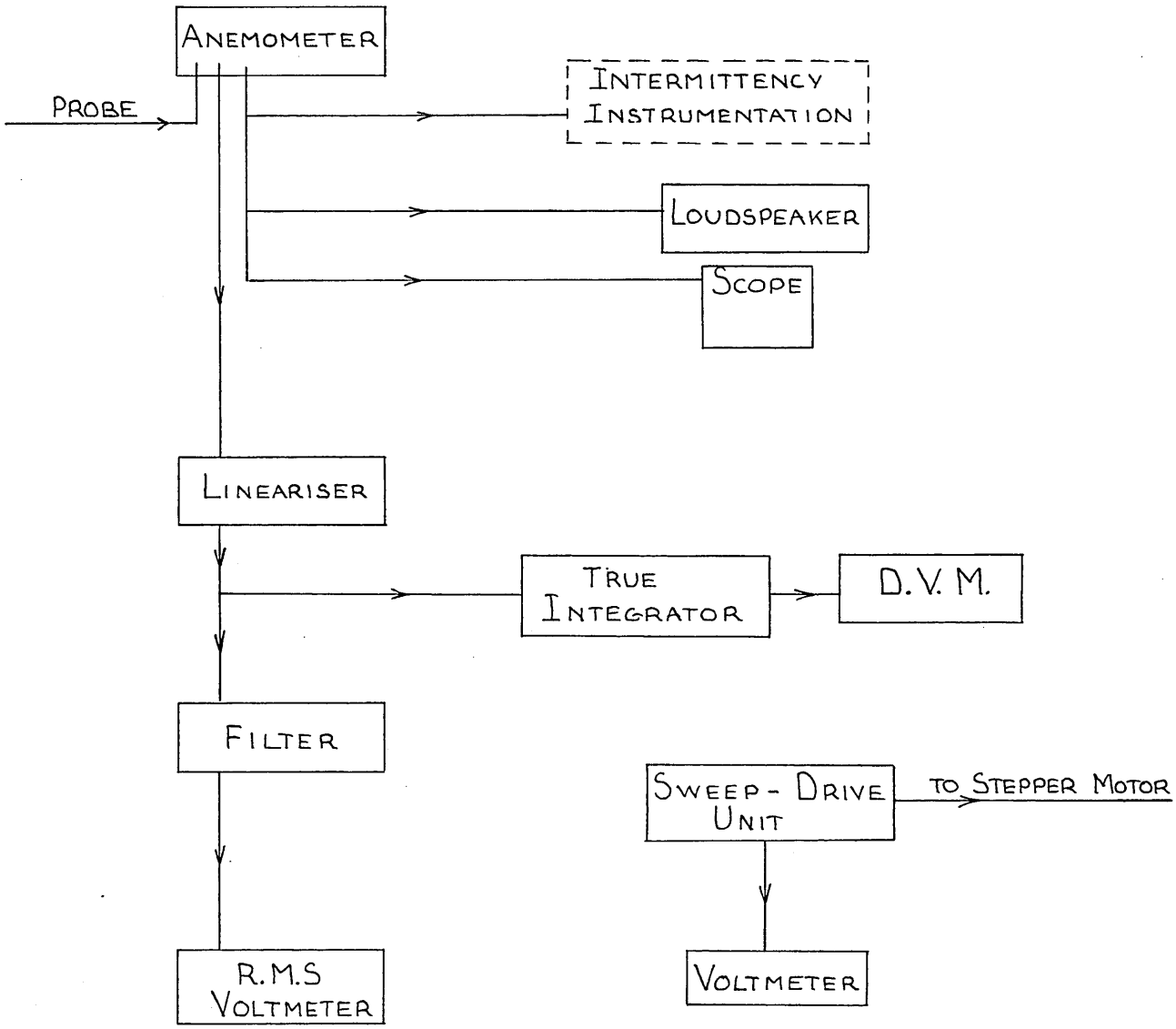

FIG. 2.10.3.

RELATIONSHIP BETWEEN PROBE VOLTAGE AND FLUID VELOCITY

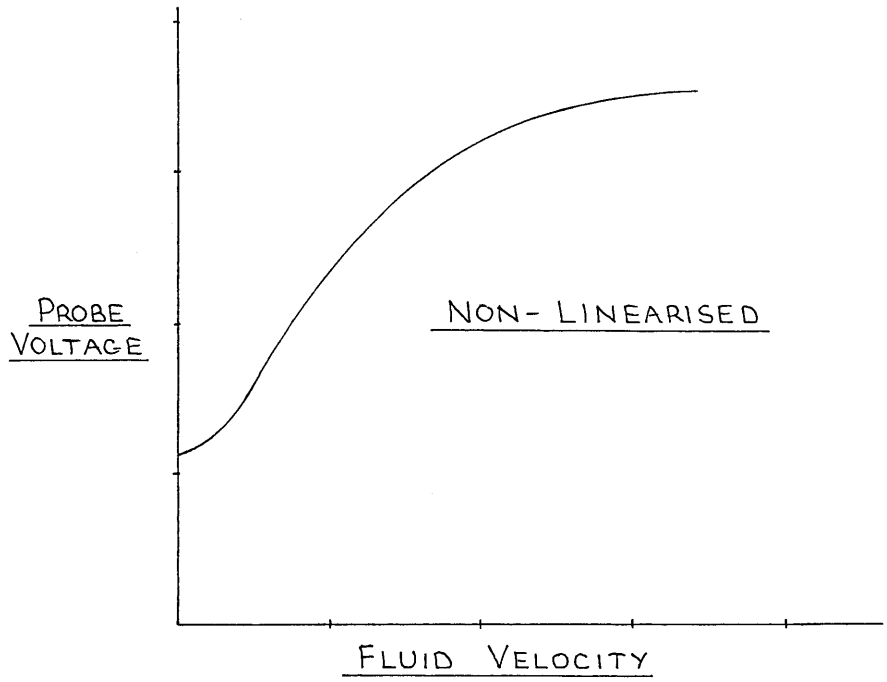

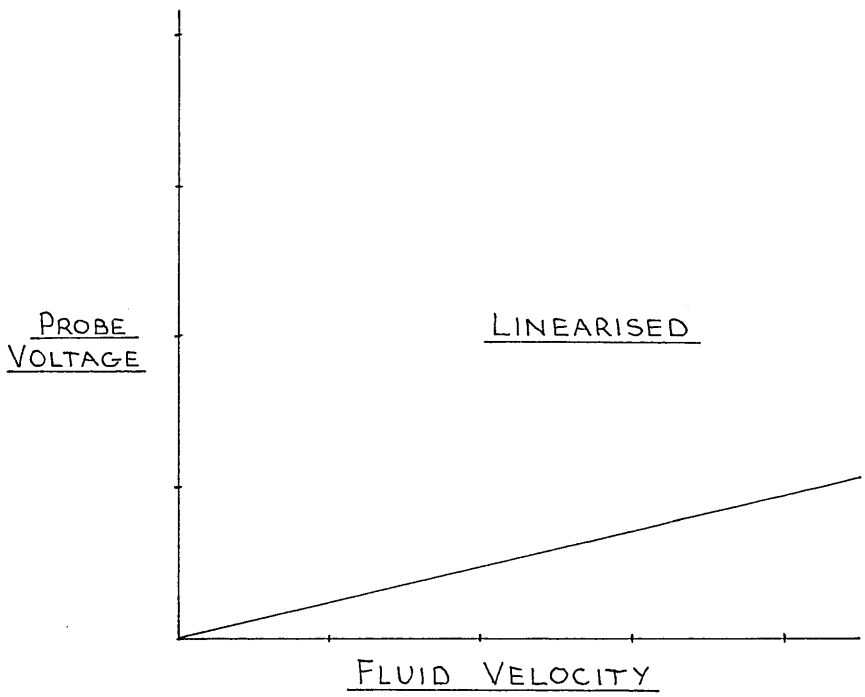

FIG. 2.10.4.

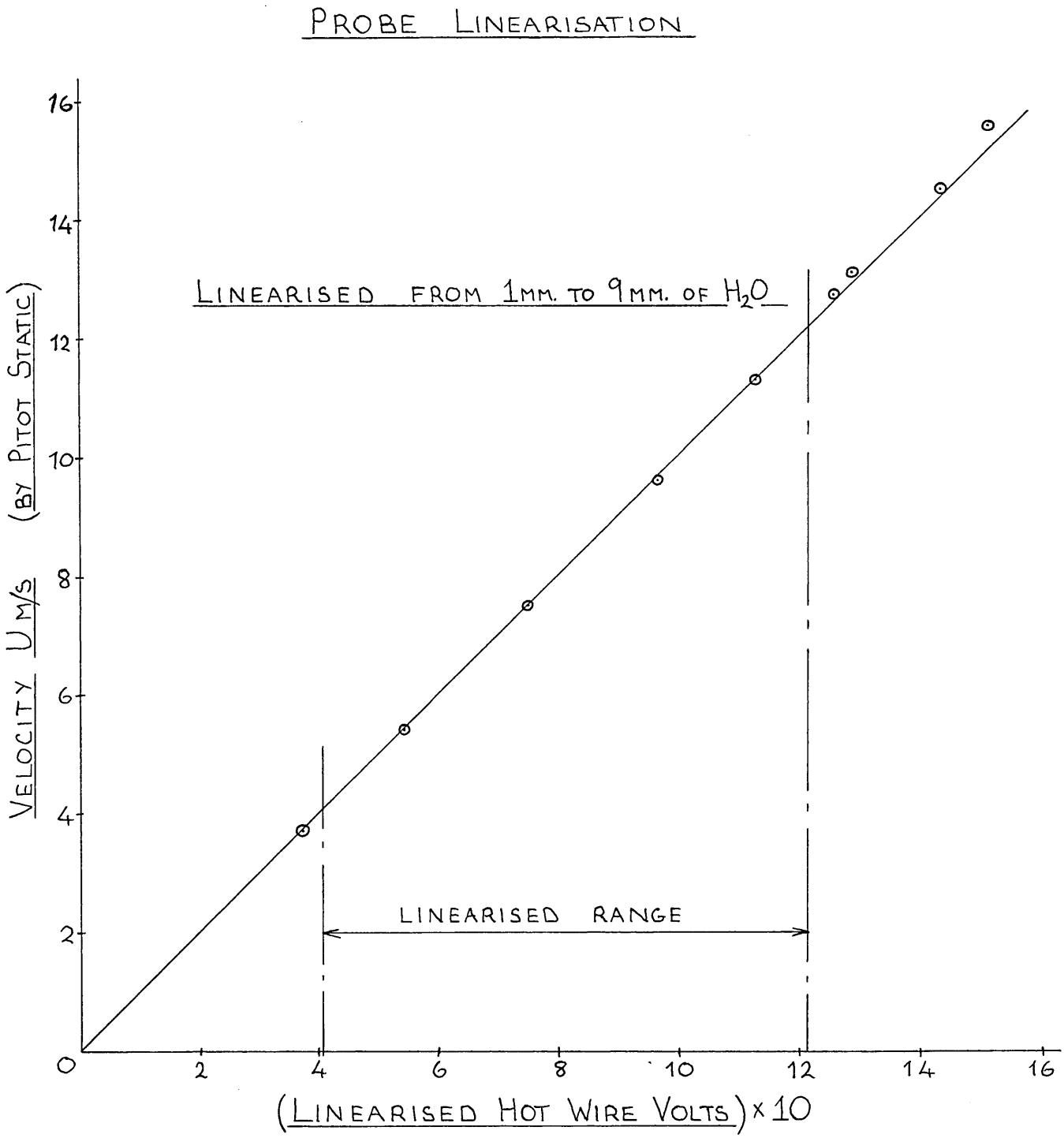
PROBE LINEARISATION
LINEARISED FROM 1MM. TO 9MM. OF H_2O
LINEARISED RANGE
VELOCITY U M/S (BY PITOT STATIC)
(LINEARISED HOT WIRE VOLTS) × 10
0
2
4
6
8
10
12
14
16

MEASUREMENT OF u' TURBULENCE COMPONENT

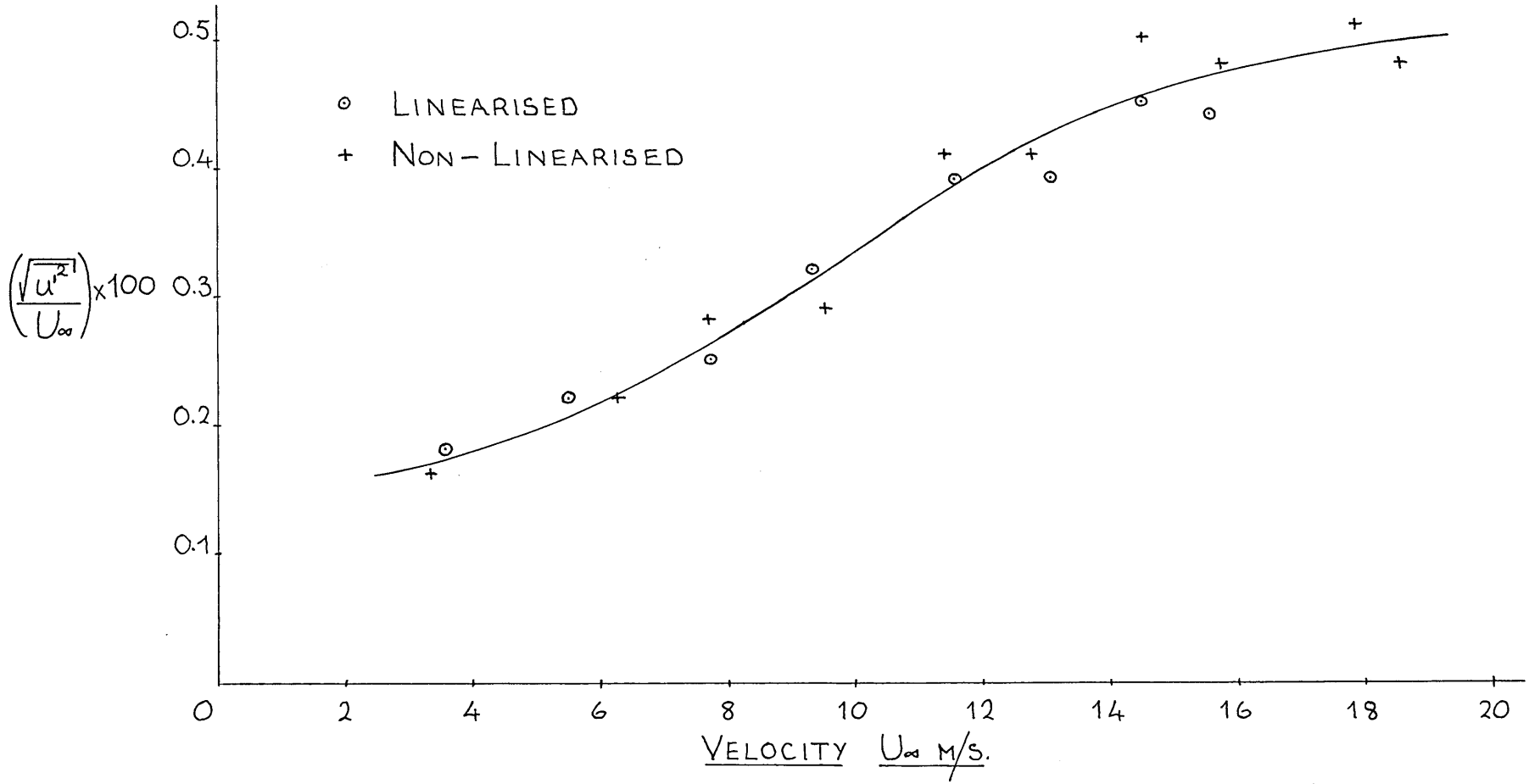

FIG. 2.11.1.

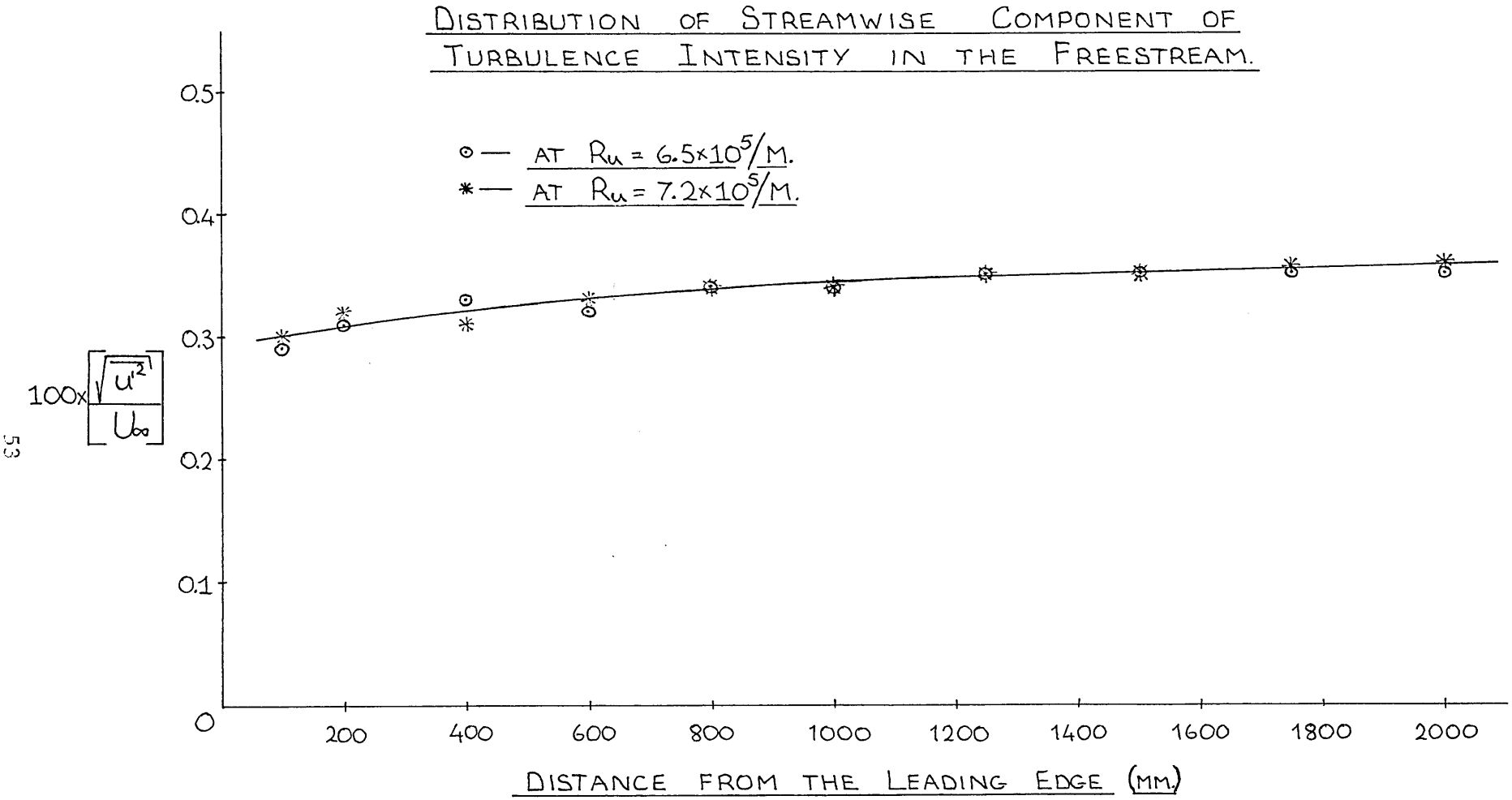
DISTRIBUTION OF STREAMWISE COMPONENT OF TURBULENCE INTENSITY IN THE FREESTREAM.
⊙ — AT $R_u = 6.5\times10^5/M$.
* — AT $R_u = 7.2\times10^5/M$.
$100\times\frac{\sqrt{\overline{u'^2}}}{U_\infty}$
0.5
0.4
0.3
0.2
0.1
0
200
400
600
800
1000
1200
1400
1600
1800
2000
DISTANCE FROM THE LEADING EDGE (MM.)

FIG 2.11.2.

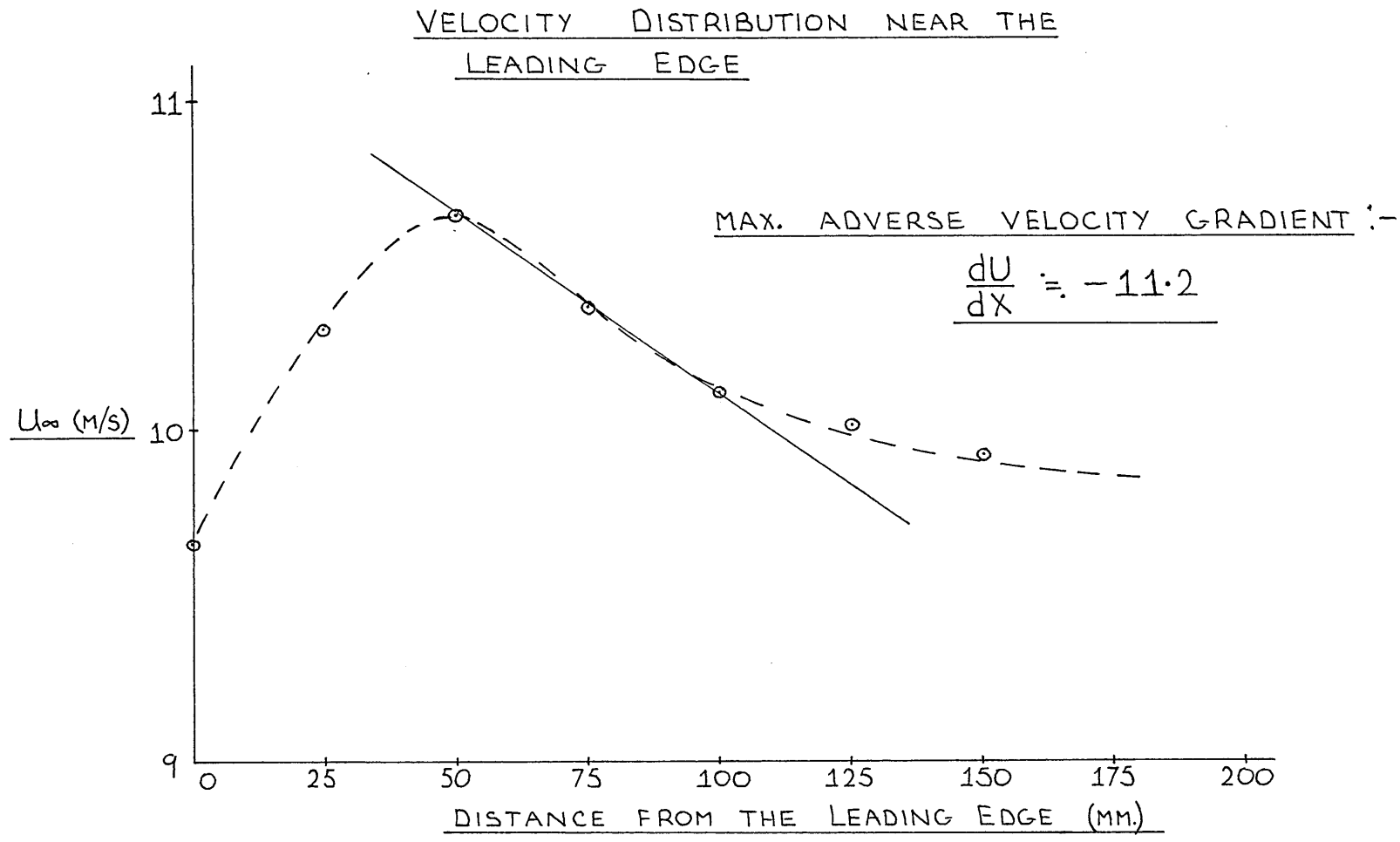
VELOCITY DISTRIBUTION NEAR THE LEADING EDGE
MAX. ADVERSE VELOCITY GRADIENT :-
dU/dX ≒ −11·2
U∞ (M/S)
11
10
9
0
25
50
75
100
125
150
175
200
DISTANCE FROM THE LEADING EDGE (MM.)

FIG. 2.12.1.

MEASUREMENT OF INTERMITTENCY

SIGNAL PROCESSOR :-

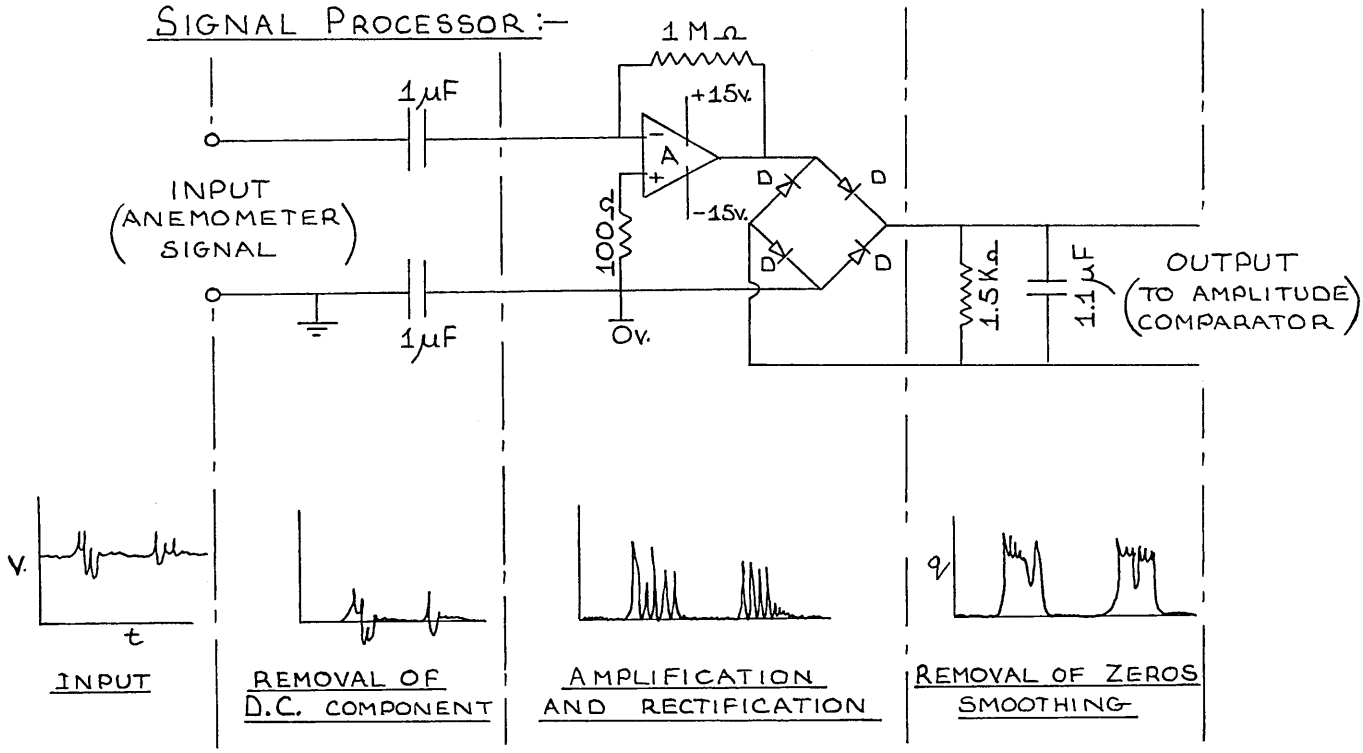

SCHEMATIC LAYOUT :-

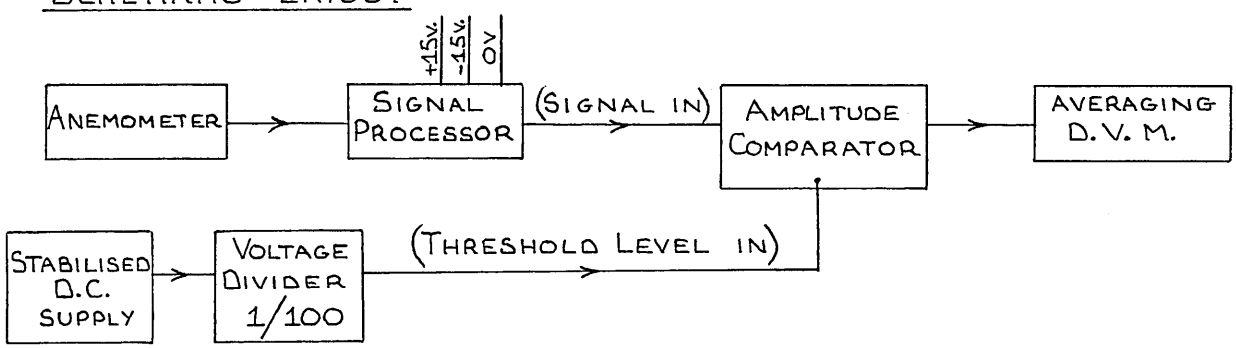

MEASUREMENT OF INTERMITTENCY :-

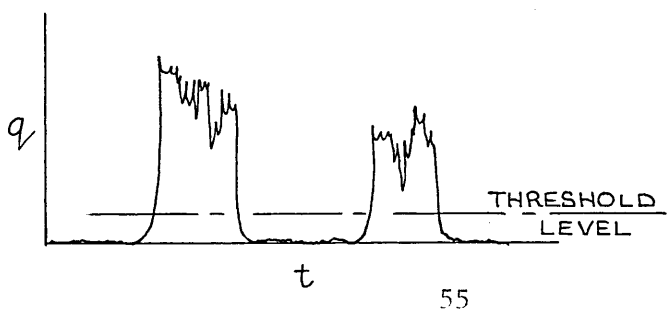

Amplitude Comparator measures the percentage of time spent above the selected threshold level.

Output is in terms of a voltage, with 5v. indicating 100% (ie. γ = 1) and 0v. indicating 0% (ie. γ = 0)

FIG. 2.13.2.

LAMINAR/TURBULENT DISCRIMINATING SIGNAL q

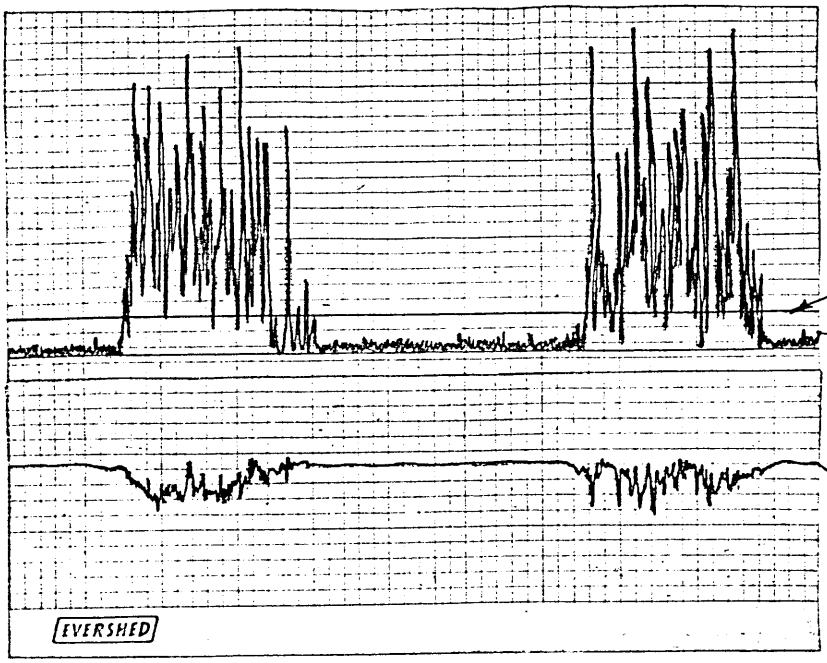

ARTIFICIAL TURBULENT BURSTS IN THE FREESTREAM

THRESHOLD LEVEL = 15 mV.

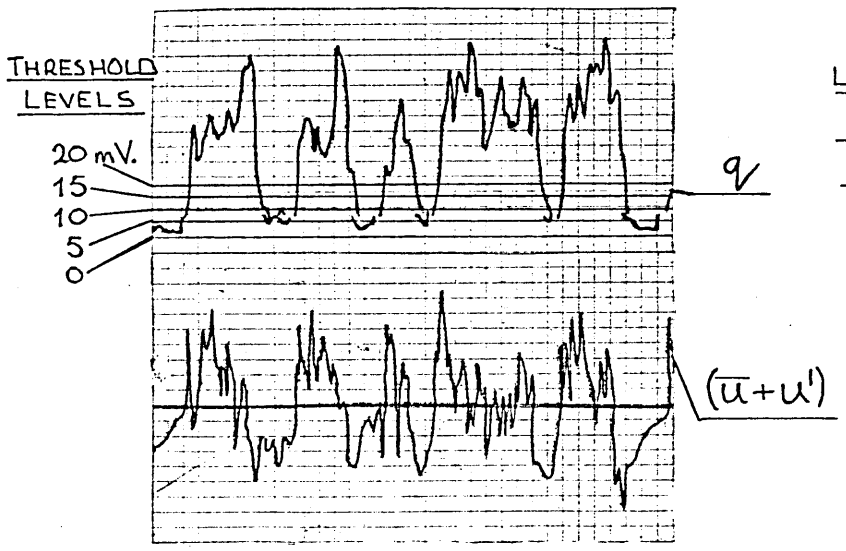

LAMINAR/TURBULENT INTERMITTENCY IN A TRANSITIONAL BOUNDARY LAYER.

$\bar{\gamma} = 0.66$

FIG. 2.13.3.

INTERMITTENCY DISTRIBUTION IN A FULLY DEVELOPED TURBULENT BOUNDARY LAYER

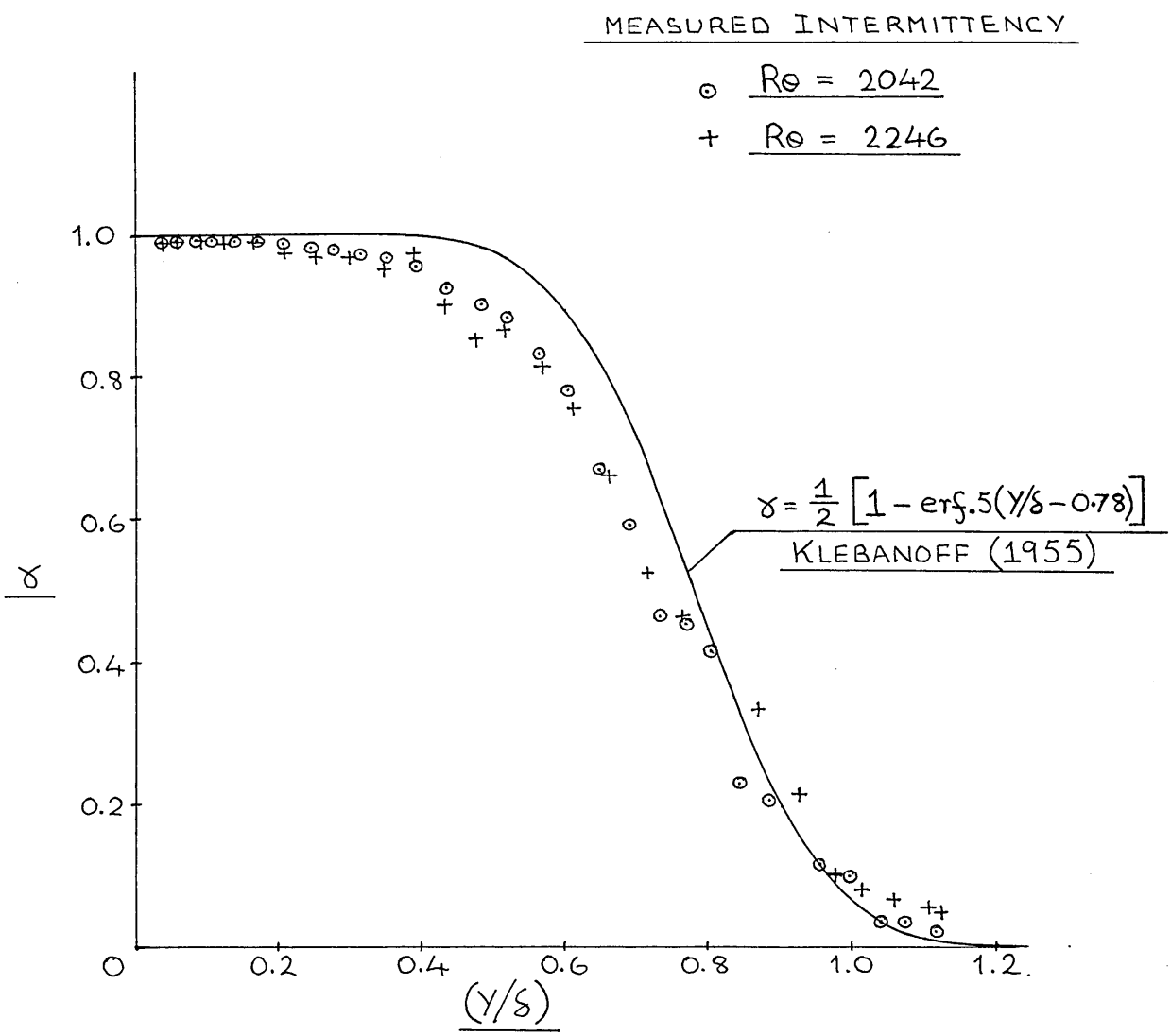

FIG. 2.14.1.

DETAILS OF PRESTON & TOTAL HEAD TUBES

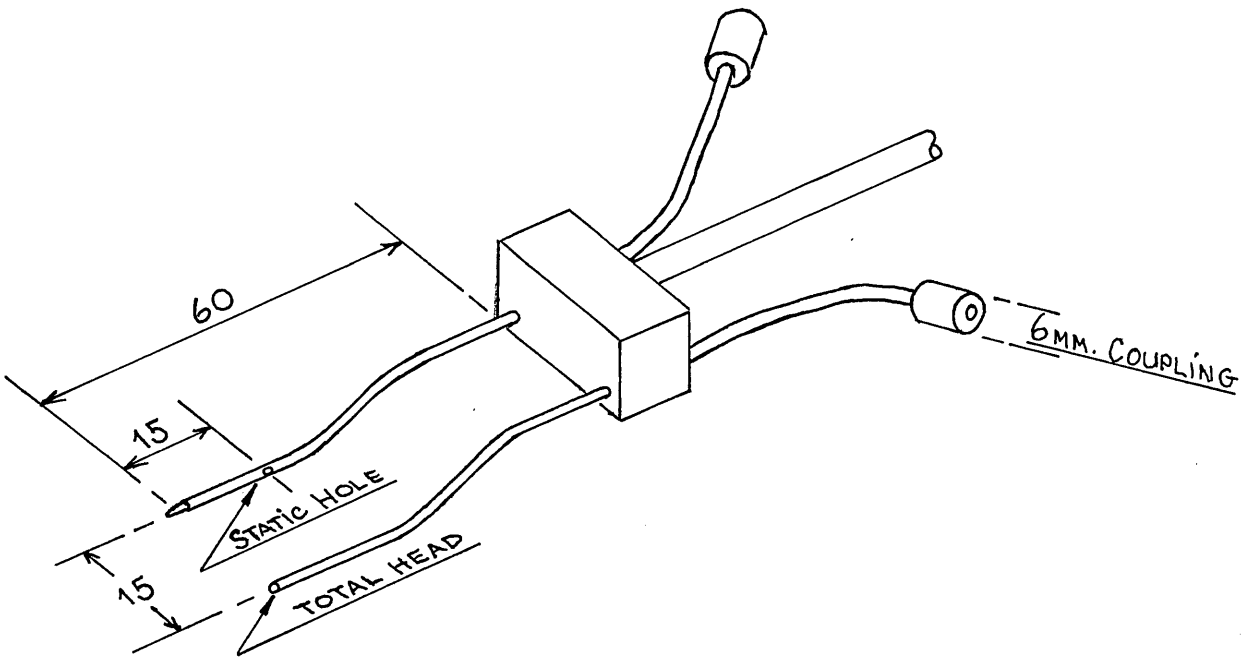

STATIC TUBE O.D. = 1.410 MM.

TOTAL HEAD TUBES 1 - O.D. = 1.410 MM.
2 - O.D. = 1.105 MM.

FIG. 2.15.1.

TWO PIN TEST FOR FLOW TWO-DIMENSIONALITY

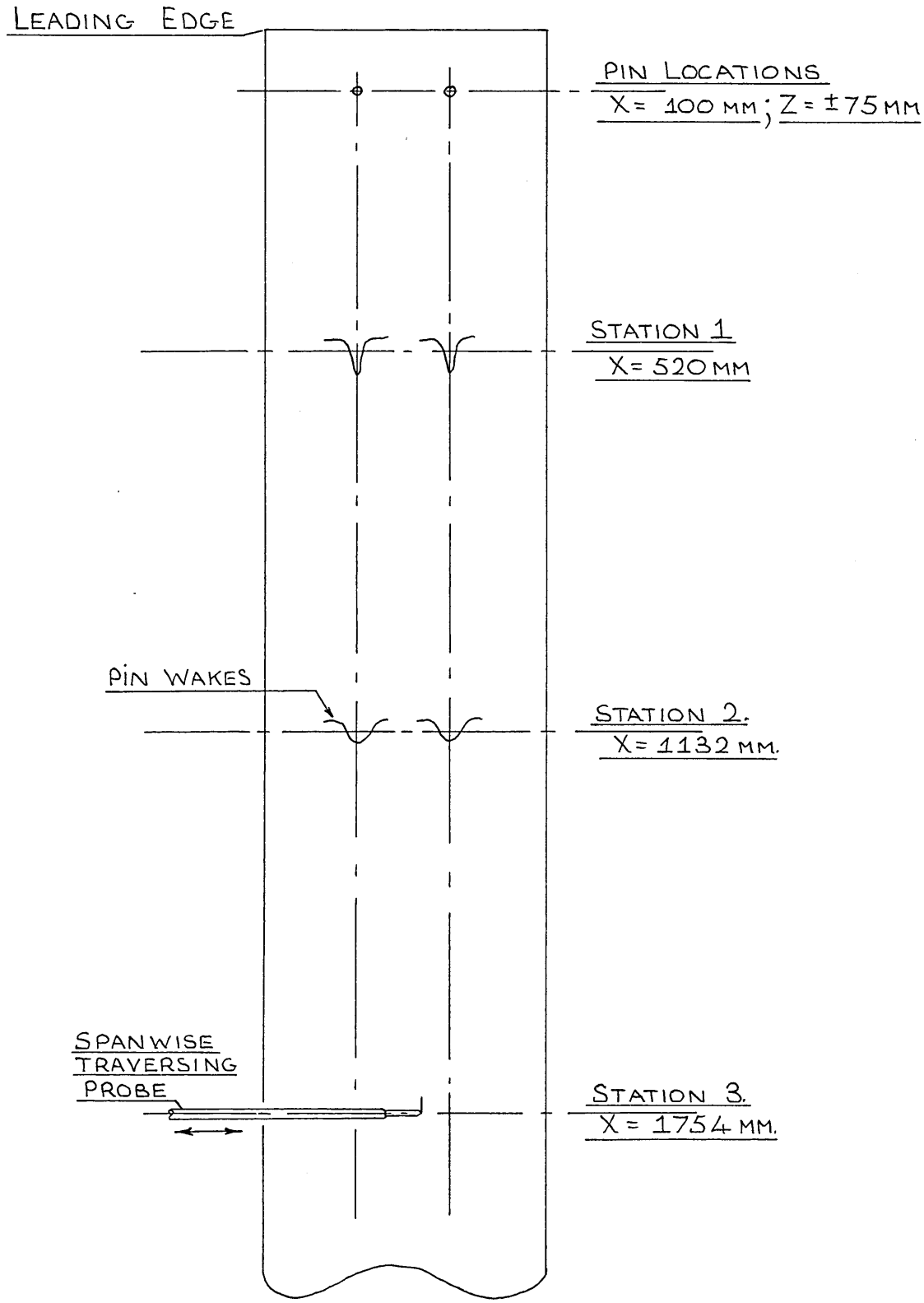

FIG. 2.15.2.

TWO PIN WAKE TRAVERSE (INITIAL TEST)

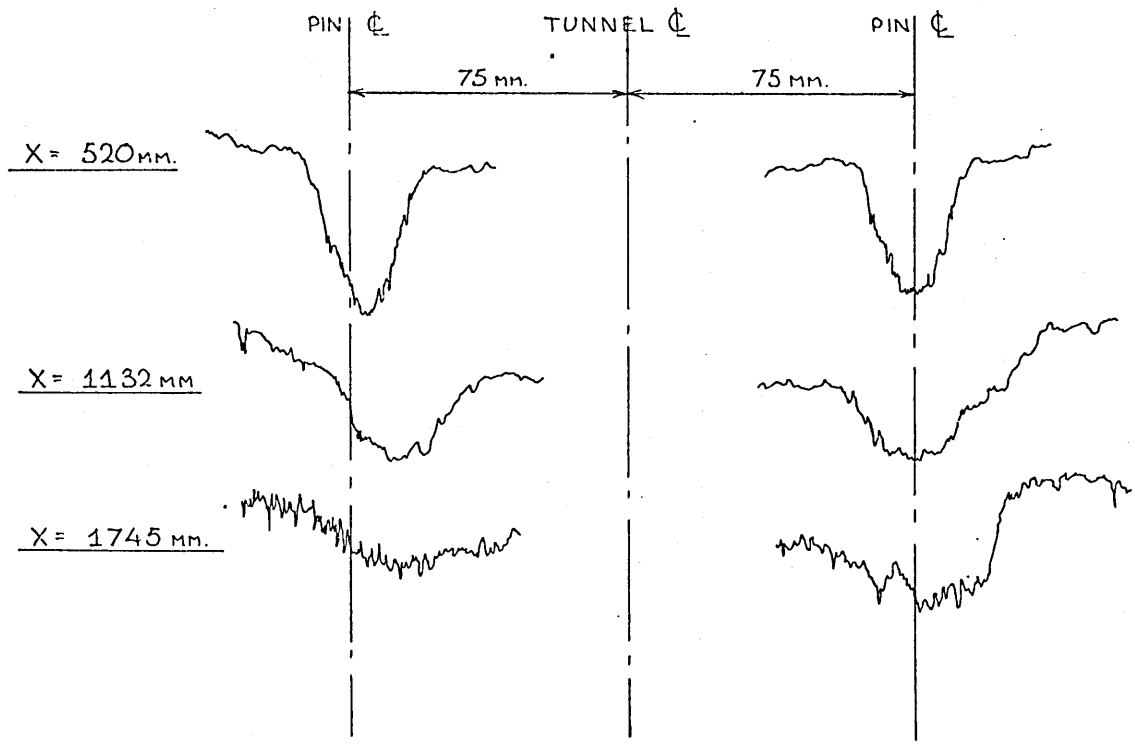

FIG.

TWO PIN WAKE TRAVERSE (IMPROVED TUNNEL SEALING)

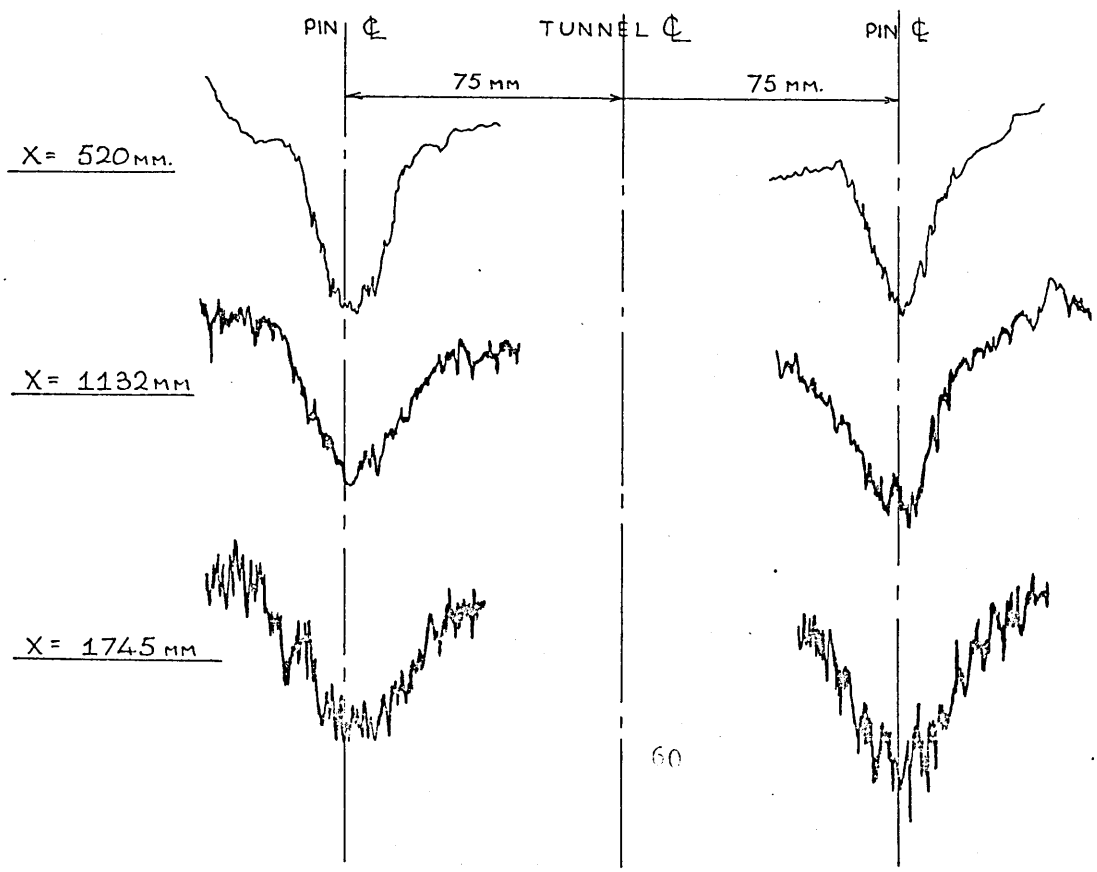

FIG.

FIG. 2.16.1.

WIND TUNNEL TEST BOUNDARY LAYER (1)

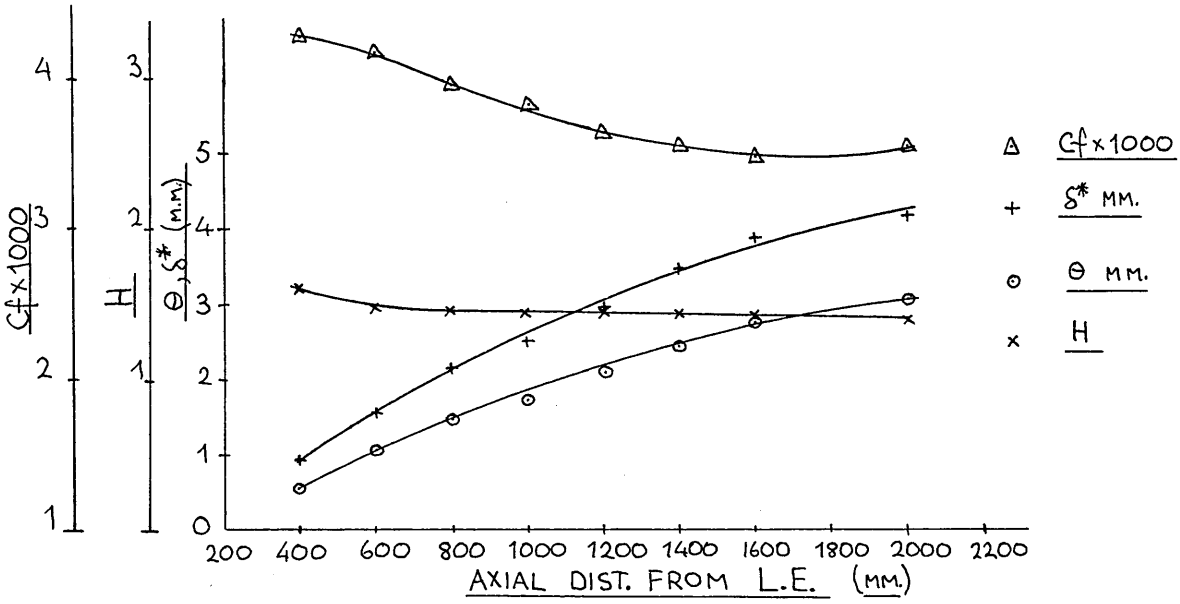

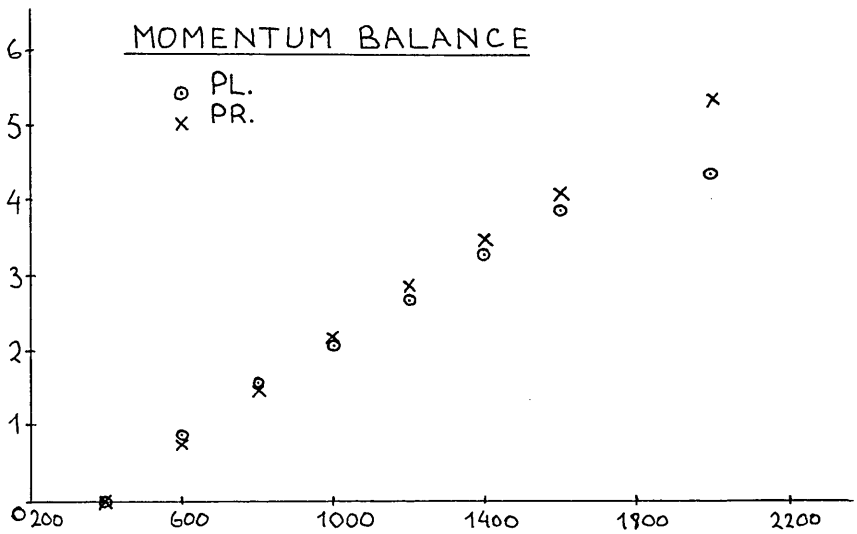

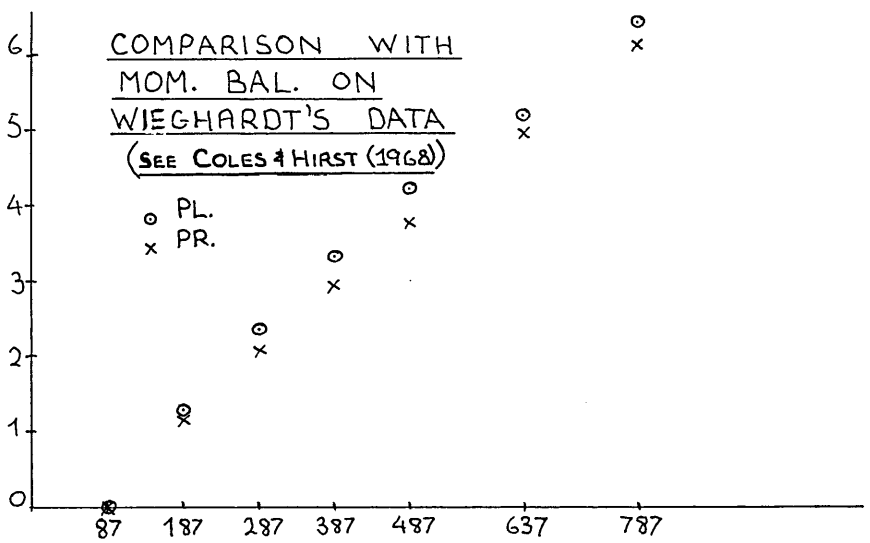

FIG. 2.16.2.

WIND TUNNEL TEST BOUNDARY LAYER (2)

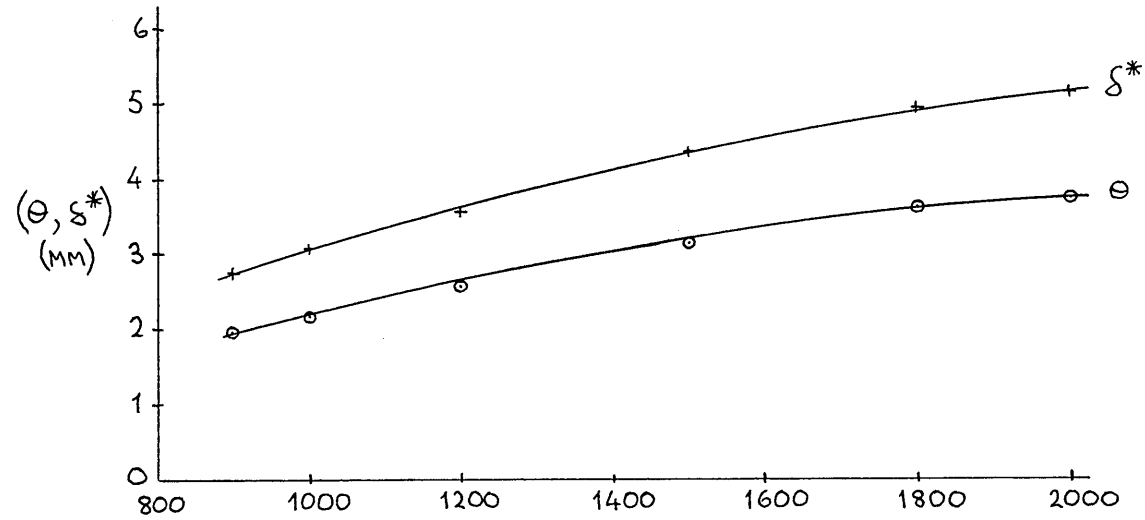

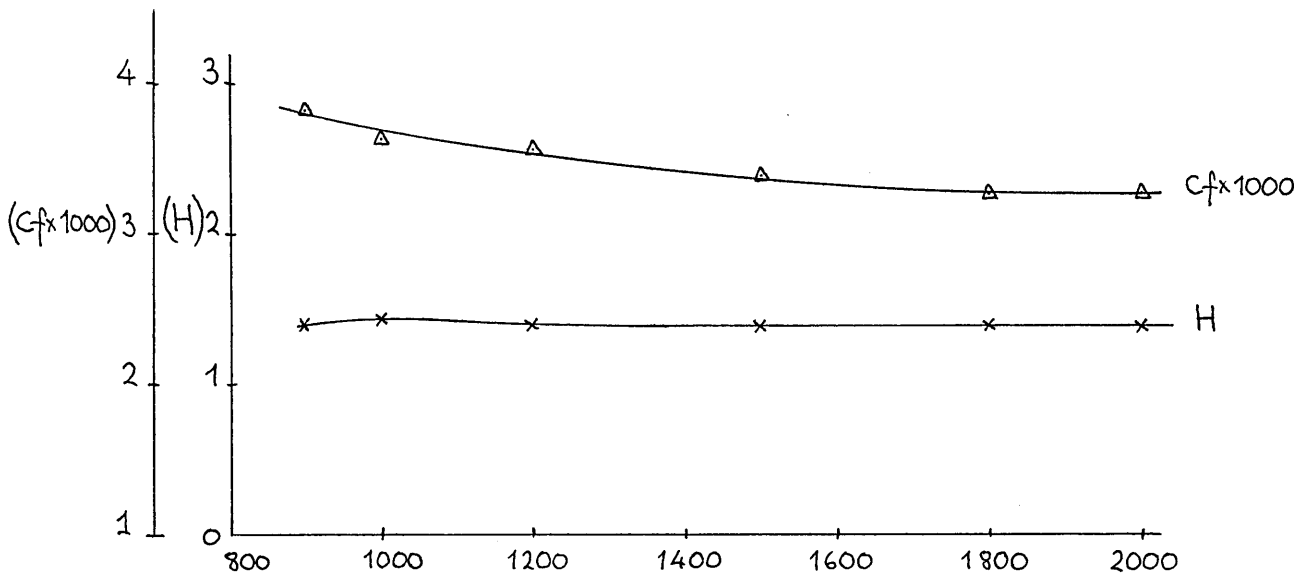

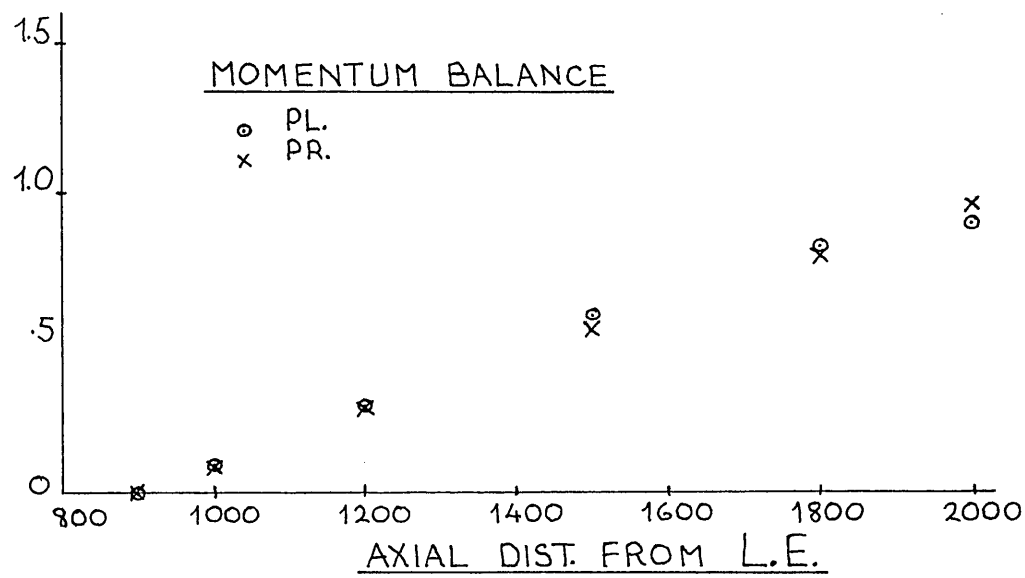

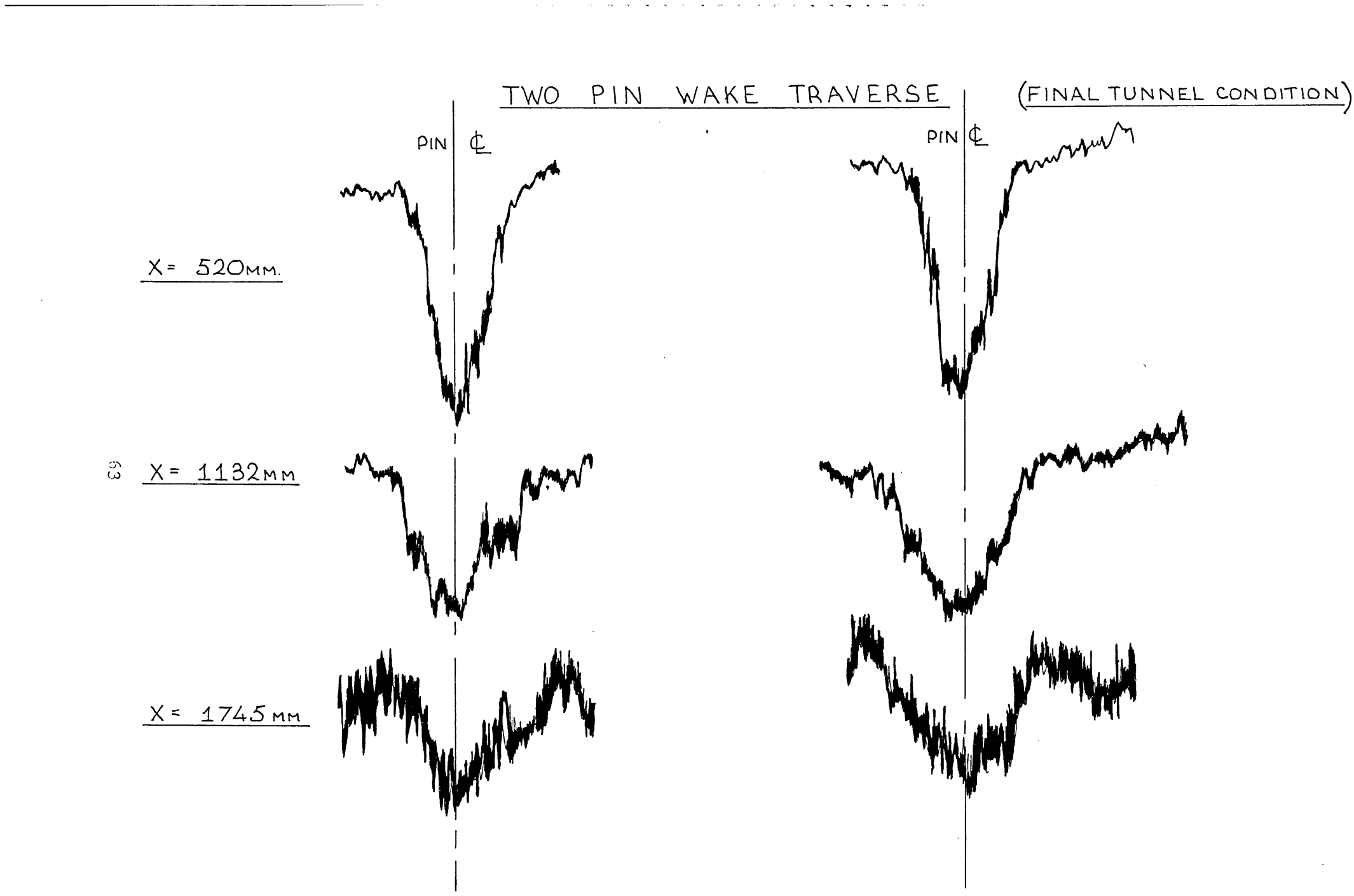
TWO PIN WAKE TRAVERSE
(FINAL TUNNEL CONDITION)
PIN ℄
PIN ℄
X = 520MM.
X = 1132MM
X = 1745 MM

FIG. 2.16.3.

SPANWISE VARIATION OF LOCAL SKIN FRICTION COEFFICIENT

MEASUREMENTS MADE BY PRESTON TUBE AT X = 1800MM. AND U_∞ = 11.96 M/S

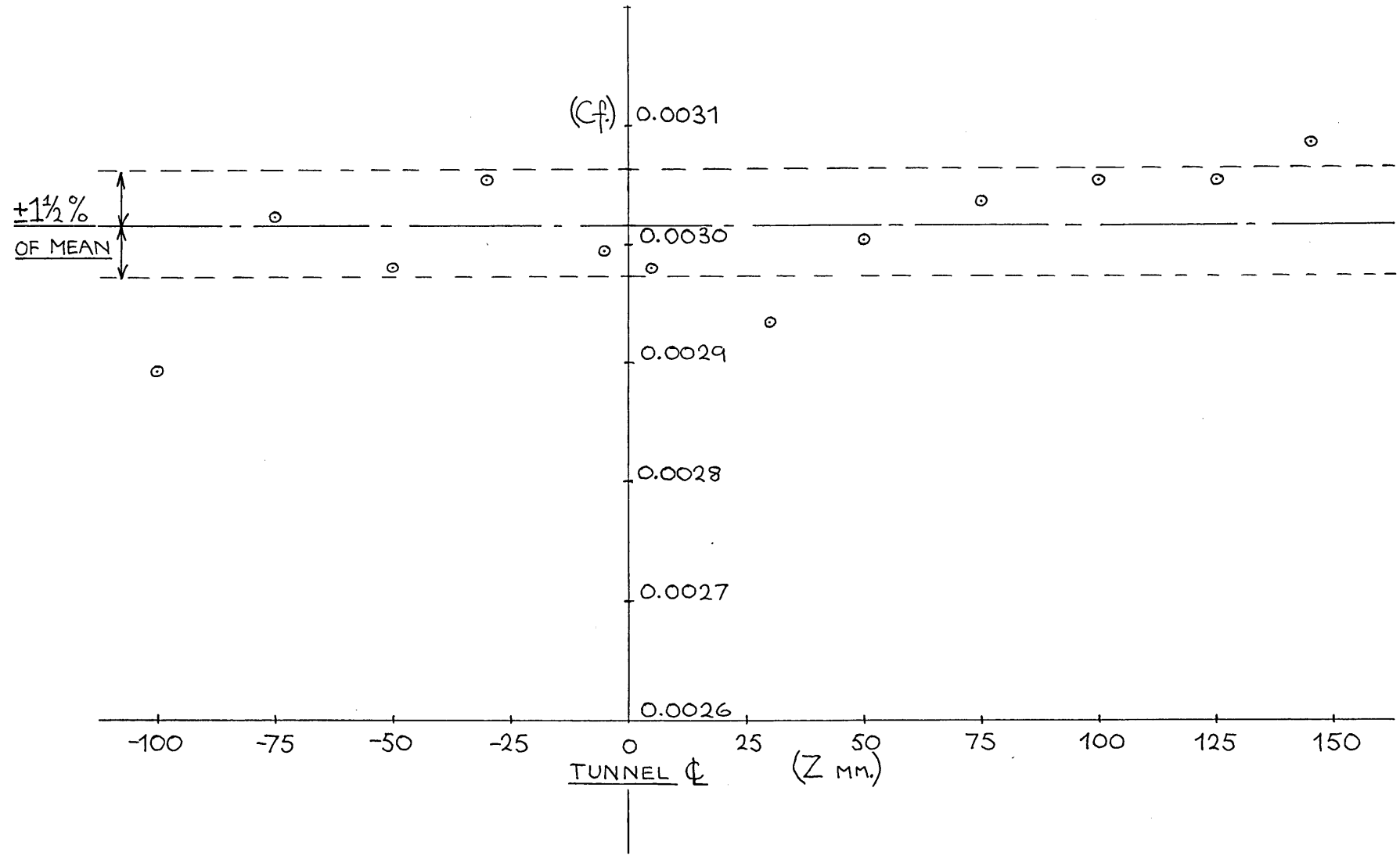

FIG. 2.16.4.

CHAPTER 3.

DATA REDUCTION AND THEORETICAL CONSIDERATIONS.

The methods of data reduction adopted for the analysis of laminar, turbulent and transitional mean velocity profiles are described with an estimate of the errors involved and the limitations of use. Modifications to the turbulent analysis for low Reynolds number effects are included and the turbulent boundary layer data is considered with regard to non-equilibrium development.

The momentum balance method, as a criterion for flow two-dimensionality, is discussed and the method adopted for the estimation of the entrainment rate is outlined.

BOUNDARY LAYER DEVELOPMENT FROM TRANSITION PROVOKING DEVICES.

DATA REDUCTION AND THEORETICAL CONSIDERATIONS.

3.1 Data reduction, laminar mean velocity profiles.

The Pohlhausen (1921) solution for laminar boundary layers, makes use of the assumption that the laminar velocity profiles can be represented by fourth order polynomials and the idea is extended here to the analysis of experimental data. The method of least squares is employed to optimise the fit of a fourth order polynomial through all the data points of $(\overline{u}/U_\infty)$ against (ymm.).

ie. $$\overline{u}/U_\infty = Ay + By^2 + Cy^3 + Dy^4 \qquad 3.1$$

With the constants known, the integral parameters δ^*, Θ and δ^{**} and the shape factors H_{12} and H_{32} immediately follow upon integration of the respective functions.

The wall shear stress, given as :-

$$\tau_0 = \mu \partial\overline{u}/\partial y \qquad 3.2$$

is determined via the average slope, $d\overline{u}/dy$, of all the data points in the range, $0 \leqslant (\overline{u}/U_\infty) \leqslant 0.45$, and the edge of the boundary layer, defined as the y value corresponding to $\overline{u}/U_\infty = 0.995$, is determined independently by the method of "Aitken interpolation." A typical profile analysis is given in TABLE 3.1. and shown graphically in FIG. 3.1.1. As the data was obtained in a zero pressure gradient, a comparison with the Blasius profile is also shown. Additionally, the integral thicknesses, δ^* and Θ , as obtained from the profile

analysis, are compared with that obtained from a planimeter measurement of the plotted functions. The agreement of 1.3% and 1.4% between displacement and momentum thicknesses respectively, indicates the basic soundness of the numerical technique. The relevant computer program, CFLBL, and associated subroutines, PLYINT and AITKEN, are included in Appendix 3., along with flow diagrams.

3.2 Data reduction, turbulent mean velocity profiles.

Turbulent velocity profiles were analysed by the method outlined by Coles and Hirst (1968), where the profile outside the viscous sublayer is considered to be composed of two separate wall and wake functions, which form the composite velocity profile, see FIG. 3.2.1.

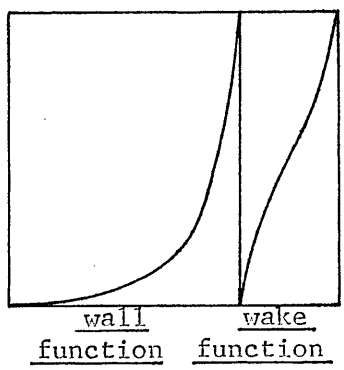

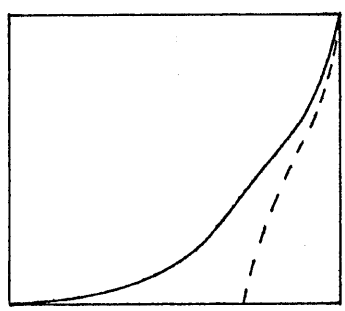

composite profile.

FIG. 3.2.1.

In the laminar, or viscous sublayer, the viscous forces dominate and the velocity profile can be approximated to :-

$$\overline{u}/u_\tau = y.u_\tau/\nu \qquad 3.3$$

where $u_\tau = \sqrt{\tau_0/\rho}$, the wall friction velocity.

The wall function follows either from Prandtl's mixing length concept, ie. ($l = ky$), and the assumption that the wall shearing stress, ie. ($\tau = \rho l^2 (\frac{d\overline{u}}{dy})^2$) remains constant, or can be deduced from a

dimensional analysis argument. It has the form :-

$$\overline{u}/_{u_\tau} = 1/_k \ln.\left[\frac{y.u_\tau}{\nu}\right] + C \qquad 3.4$$

or

$$u^+ = 1/_k \ln.[y^+] + C \qquad 3.5$$

where the constants k and C are wholly empirical. Coles quotes the values as:- k = 0.41 and C = 5.0. The additive constant was later changed to 5.2 for the present studies, see section 3.6.

Coles (1956), related the mean velocity profile in the outer part of the boundary layer to the inner part, by defining a convenient empirical wake function, which represented the deviation from the logarithmic wall law.

ie.

$$W(y/\delta) = 2\sin^2(\pi/2 . y/\delta) \qquad 3.6$$

The composite turbulent velocity profile outside the viscous sublayer, ie. ($\frac{y.u_\tau}{\nu} > 50$), is then :-

$$\overline{u}/_{u_\tau} = f\left[\frac{y.u_\tau}{\nu}\right] + \mathcal{K}/_k . W(y/\delta) \qquad 3.7$$

or fully expanded :-

$$\overline{u}/_{u_\tau} = 1/_k \ln.\left[\frac{y.u_\tau}{\nu}\right] + C + 2\mathcal{K}/_k . \sin^2(\pi/2 . y/\delta) \qquad 3.8$$

where $\mathcal{K}$, is a wake parameter, related to the strength of the wake function.

At $y = \delta$, the strength of the wake component, $\Delta\overline{u}/_{u_\tau}$, defined by Coles as the maximum deviation , or residual, of the velocity profile from eqn. 3.4., is given by :-

$$\Delta\overline{u}/_{u_\tau} = \overline{u}/_{u_\tau} - (1/_k \ln.(y^+) + C) = 2\mathcal{K}/_k \qquad 3.9$$

On setting $\overline{u} = U_\infty$ at $y = \delta$, eqn 3.8. becomes :-

$$U_\infty/_{u_\tau} = 1/_k \ln.\left[\frac{\delta.u_\tau}{\nu}\right] + C + 2\mathcal{K}/_k \qquad 3.10$$

which can be regarded as a local friction law. With k, C, ν and

U_∞ all known, eqn. 3.10 can be used to determine any one of the remaining three parameters, u_τ, δ or Π, provided the other two are also known.

Integration of the various functional relationships containing eqn. 3.8. leads to simple expressions for the boundary layer integral thicknesses.

$$\text{ie.} \quad \delta^*/\delta = \left[\frac{1 + \Pi}{k}\right] u_\tau/U_\infty \quad , \qquad 3.11$$

$$\theta/\delta = \delta^*/\delta - \left[\frac{2 + 3.179\Pi + 1.5\Pi^2}{k^2}\right]\left[u_\tau/U_\infty\right]^2 \qquad 3.12$$

$$\text{and} \quad \delta^{**}/\delta \simeq \theta/\delta + \left[u_\tau/U_\infty\right]^2 . 1/k^2\left[6 + 11.14\Pi + 8.5\Pi^2 + 2.56\Pi^3\right] \qquad 3.13$$

One final relationship results from the subtraction of eqn. 3.8 from eqn.3.10. and is an approximate expression for the velocity-defect profile :-

$$\text{ie.} \quad \frac{U_\infty - \bar{u}}{u_\tau} = -1/k \ln.(y/\delta) + 2\Pi/k\left[1 - \sin^2\left\{\pi/2 . y/\delta\right\}\right] \qquad 3.14$$

or in functional notation,

$$\frac{U_\infty - \bar{u}}{u_\tau} = f\left[y/\delta, \Pi\right] \qquad 3.15$$

Following Coles, the profile analysis proceeds by assuming the universal validity of the law of the wall, ie. eqn. 3.4., in the region given by :-

$$100 \leqslant \frac{y.u_\tau}{\nu} \leqslant 300 \qquad 3.16$$

For the present studies, the region was in fact re-defined to suit the analysis of very low Reynolds number data, see section 3.6.

For each data point in the above region, the parameter u_τ is determined iteratively to give optimum agreement with eqn. 3.4. The average value of u_τ in the fitting region, is then taken as the representative wall friction velocity for the particular velocity profile. The edge of the boundary layer is determined independently, by the same Aitken interpolation method as used for the laminar profile analysis. Substitution of u_τ and δ into eqn. 3.10. then yields the wake parameter Π.

Integral parameters are evaluated using Coles's standard integrals for the viscous sublayer.

ie.
$$\int_0^{50}\left[\frac{\bar{u}}{u_\tau}\right] d\left[\frac{y.u_\tau}{\nu}\right] = 540.6 \qquad 3.17$$

$$\int_0^{50}\left[\frac{\bar{u}}{u_\tau}\right]^2 d\left[\frac{y.u_\tau}{\nu}\right] = 6546 \qquad 3.18$$

$$\int_0^{50}\left[\frac{\bar{u}}{u_\tau}\right]^3 d\left[\frac{y.u_\tau}{\nu}\right] = 82770 \qquad 3.19$$

Equation 3.4. is then assumed in order to continue the integrations from $y^+ = 50$ to $y^+ = y^+(3)$, the third data point. In most instances, this region constitutes a minute portion of the velocity profile and in some cases $y^+(3)$ was less than 50, in which case the first data points were deleted and the remainder re-analysed. Integration of the rest of the profile from the third data point was carried out using the parabolic fitting technique, also described by Coles and Hirst (1968). The technique, a modified Simpsons rule, involves the fitting of a parabola through three successive data points and obtaining the two integral segments from the algebraic equation of the parabola. The central point is then moved one point

outwards and the process repeated, with overlapping integral segments being averaged. Addition to the suitably converted inner integrals, ultimately yield the integral functions :-

$$\int_0^{y_\infty}(\overline{u}/U_\infty)dy, \int_0^{y_\infty}(1 - (\overline{u}/U_\infty))dy, \int_0^{y_\infty}(\overline{u}/U_\infty)^2 dy \text{ and } \int_0^{y_\infty}(\overline{u}/U_\infty)^3 dy$$

from which all the relevant integral thicknesses and shape factors can be obtained.

The analysis is performed by the computer program CFTBL and associated subroutines LOGLAW, PARINT, and AITKEN, all of which are included in Appendix 3., along with the respective flow diagrams. A typical profile analysis is given in TABLE 3.2. and in graphical form in FIG. 3.2.2. A comparison between the computed integral thicknesses, δ^* and Θ, and those obtained by planimeter measurements, shows the agreement to be within 0.7% and 0.1% respectively and indicates the reliability of the integration procedure. FIG. 3.2.1. also shows the profile, plotted semi-logarithmically in terms of the inner variables, showing the strength of the wake component, $\Delta\overline{u}/u_\tau$ and the logarithmic fitting region.

The error analysis in Appendix 2., shows that for a constant error of -2% in the velocity measurements, the corresponding errors in momentum and displacement thicknesses, for a power law profile, are both +14%. The velocity error in practice however, is more likely to be randomly positive and negative, such that the actual error in integral thicknesses is expected to be considerably less. The accuracy of "turbulent" integral thicknesses are therefore in the region of about ± 5 - $\pm 6\%$, and slightly better for the laminar counterparts.

Coles (1962), suggested that for an uncertainty of only ±1% in the velocity measurements, the accuracy with which the parameter $\Delta^{\overline{u}}/_{u_\tau}$ can be determined, is no better than about ±5 - ±10%. Considerable scatter in $\Delta^{\overline{u}}/_{u_\tau}$ and also Π is then, only to be expected.

3.3 Turbulent skin friction coefficients.

The profile analysis of the previous section yields the wall friction velocity, from which the wall shear stress immediately follows :-

$$\text{ie.} \qquad \tau_o = \rho . u_\tau^2 \qquad 3.20$$

The local skin friction coefficient is then given by eqn. 2.11. The profile analysis also gives the shape factor H12 and the momentum thickness Reynolds number, which can then be substituted into any number of skin friction correlations of the form :-

$$C_f = f(R_\theta, H12) \qquad 3.21$$

Two such correlations are presently employed, which are due to Ludwieg and Tillman (1950), and a curve-fit due to White (1974) for the skin friction relation given indirectly by eqns. 3.10, 3.11, and 3.12.

$$\text{ie. (White)} \quad C_f = \frac{0.3\, e^{(-1.33H12)}}{(\log_{10}R_\theta)^{(1.74 + 0.31.H12)}} \qquad 3.22$$

$$\text{(Lud-Till)} \quad C_f = \frac{0.246\, e^{(-1.561.H12)}}{(R_\theta)^{0.268}} \qquad 3.23$$

The skin friction coefficient as determined by Preston tubes, section 2.14., serves as an additional independent check and a comparison of the five values are included in TABLE 3.2. The local skin friction coefficients, as measured by the two Preston tubes, are within ±0.8% of their mean value. If this mean value is then taken

as a reference, then the skin friction coefficient as determined by the other methods have the following deviations :-

Log-plot, ie. eqn. 3.4.	+3.69%
Ludwieg/Tillman	+0.26%
White	-3.16%

3.4 Wall proximity effects.

As a hot wire moves through a fluid stream and approaches a solid boundary, there is a tendency for the wire to increasingly lose more heat to the solid wall, as opposed to the surrounding fluid. As the voltage applied to the wire, operating in the constant temperature mode, is a measure of the convective heat loss from the wire, hence the fluid velocity, then wall proximity effects are manifested as an apparently higher velocity than is actually present.

For the case of a fully turbulent boundary layer, Oka et al. (1972), has shown that wall effects are prominent, only when the dimensionless height, $\frac{y.u_\tau}{\nu}$, becomes less than about 5. In the present studies, the minimum values of $\frac{y.u_\tau}{\nu}$ are not expected to be much less than about 20. It was therefore concluded that no wall correction factors need be introduced for the measured turbulent boundary layer mean velocity profiles.

For laminar profiles, Wills (1962), gives a velocity correction, $\Delta\overline{u}$, for varying values of $^{2y}/_{d}$, where y is the height above the plate, and d is the hot wire sensor diameter. In physical terms however, $\Delta\overline{u}$ becomes necessary only when the y-height is less

than about 0.25mm. It was thus apparent that no wall correction factors are required for either the turbulent or the laminar mean velocity profiles.

A "still" air test, in fact, confirmed the above statement, as no effects were observed right down to y = 0.25mm. This would be indicated by the probe voltage increasing from zero. The minimum y-height subsequently adopted for the test program was taken as y = 0.5mm.

3.5 Transitional mean velocity profiles.

The transitional boundary layer is characterised by the intermittency function, which determines the relative duration times of the laminar and turbulent regimes. A time-averaged mean velocity profile is therefore the intermittency weighted average of the two separate laminar and turbulent contributions and to a certain extent, neither a laminar nor a turbulent profile analysis is really applicable. For near-wall intermittency values below 0.5 however, the velocity profile is dominantly laminar and similarly for near-wall intermittency values greater than 0.5, the velocity profile is dominantly turbulent. The laminar analysis, section 3.1., is also a purely numerical procedure, optimising the fit of a fourth order polynomial through the data. The resulting integral thicknesses are therefore true transitional values. The estimation of the local skin friction coefficient is however suspect, as eqn. 3.2 is assumed valid and cannot account for the substantially larger contribution from the turbulent regime to the overall skin friction

coefficient. The local C_f's will, in fact, be underestimated. The turbulent analysis, section 3.2., also uses a purely numerical technique, at least for the bulk of the outer profile, and integral thicknesses can again be assumed to be representative transitional values. In like manner however, the skin friction coefficient from a turbulent analysis of a transitional velocity profile is subject to error. The C_f's in this case ARE overestimated.

In the present context, the laminar analysis was adopted for the data reduction of transitional velocity profiles, when the near-wall intermittency was less than 0.5. The turbulent analysis was of course used otherwise. It is of interest to note that the laminar analysis would fail to output a value for C_f if the intermittency was in excess of 0.5. and the turbulent analysis would similarly fail when used outside its range of application.

In an attempt to give a better account of the transitional local skin friction coefficients, an empirical relation was derived in the form :-

$$C_{f_t} = f(R\theta, H12, \overline{\gamma}) \qquad 3.24$$

using the measured transitional values of $R\theta$ and H12. The derivation of eqn 3.24. and the assumptions made are outlined fully in Appendix 4.

For a zero pressure gradient eqn. 3.24 has the form :-

$$C_{f_t} = (1-\overline{\gamma})\frac{0.44}{R\theta} + 2\overline{\gamma}\left[\frac{R\theta(K)^{\frac{2}{H-1}}}{100} \times \frac{H(H+1)}{(H-1)}\right]^{\frac{2(H-1)}{(H+1)}} \qquad 3.25$$

An important subtlety, regarding the measurement of the mean velocity profile in the transition region, was pointed out by Dhawan and Narasimha (1958). They showed that the mean velocity profile, as measured by a Pitot tube, is not the same as the true mean velocity profile. The reason being that the Pitot measurement is proportional to $\overline{u}^2$ as opposed to $\overline{u}$. The mean velocity profile, from a Pitot traverse is given by :-

$$\overline{u}_{p_t}(y) = \left[(1 - \overline{\gamma})\overline{u}_L^2(y) + \overline{\gamma}\overline{u}_T^2(y)\right]^{1/2} \qquad 3.26$$

where subscripts t, L and T refer to transitional, laminar and turbulent regions respectively.

In comparison, the true mean velocity profile is given by:-

$$\overline{u}_t(y) = (1 - \overline{\gamma})\overline{u}_L(y) + \overline{\gamma}\overline{u}_T(y) \qquad 3.27$$

The difficulty also extends to similar measurements made with a non-linearised hot wire anemometer.

In order to obtain the true mean velocity profile from the Pitot measured profile, it becomes necessary to make some assumptions about the distributions of $\overline{u}_L(y)$ and $\overline{u}_T(y)$. Dhawan and Narasimha assumed that $\overline{u}_L(y)$ was the Blasius and that $\overline{u}_T(y)$ was a logarithmic turbulent velocity profile. They then computed the equivalent "Pitot" profile and observed good agreement with the actual Pitot measurements, thereby concluding that $\overline{u}_L(y)$ and $\overline{u}_T(y)$ were properly specified. This then allows $\overline{u}_t(y)$ to be described.

The method however, has one serious drawback in that an almost infinite combination of profiles of $\overline{u}_L(y)$ and $\overline{u}_T(y)$ can be chosen to satisfy eqn. 3.26., which then results in an infinite

set of profiles of $\overline{u}_t(y)$.

The problem can be circumvented however, if the velocity sensor has a linear response to velocity changes. This in fact, is achieved by using a linearised hot wire anemometer, where the probe sensor voltage is directly proportional to the fluid velocity. The linearised system thus allows the direct measurement of $\overline{u}_t(y)$ and dispenses with the need for rather limiting assumptions in order to implement the conversion from a measured to a true velocity profile in transition regions.

3.6 Low Reynolds number effects.

The present study, while mainly concerned with the transitional boundary layer, is also related to the early development of the resulting turbulent boundary layer. In consequence, the turbulent data is subject to low Reynolds number effects, which are associated with the approach to equilibrium of the developing turbulent boundary layer in a zero pressure gradient. Simpson (1970), suggested that the von Kármán constant, k, and the additive constant, C, in the law of the wall, ie. eqn. 3.4., were unique functions of the momentum thickness Reynolds number. Coles (1962), on the other hand, found that the velocity-defect formula, ie. eqn. 3.15., in the outer part of the boundary layer, was dependent on the Reynolds number and expressed the dependency through the variation of the wake parameter $\mathfrak{C}$, or $^1/_2 k \Delta\overline{u}/_{u_\tau}$, with Reynolds number. The variation is conveniently correlated by Cebeci and Smith (1974) as :-

$$\mathfrak{C} = 0.55 \times \left[1 - \exp\left(-0.243Z^{0.5} - 0.298Z\right)\right] \qquad 3.28$$

where $Z = (R\theta/425 - 1)$.

The contradiction was resolved by Huffman and Bradshaw (1972), who showed that the von Kármán constant was consistent and that the additive constant was only mildly Reynolds number dependent. The effect being associated with the turbulent/irrotational interface, which influences the shear stress distribution in the viscous sublayer and so modifies the damping constant, A^+, which in turn modifies the constant C. The damping constant A^+ being related to a constant defined by van Driest (1956), which was introduced to account for the mixing length, based on local equilibrium assumptions, attaining non-equilibrium values in the viscous sublayer near the wall. The smoke photographs due to Fiedler and Head (1966), showing a turbulent boundary layer at both high and low Reynolds numbers, would appear to provide qualitative support to Huffman and Bradshaws conclusions, which in effect vindicate the Coles interpretation of the low Reynolds number effect.

Huffman and Bradshaw do however concede that the additive constant may vary, in fact increase, if the non-dimensional shear stress gradient, ie. $\frac{\nu}{\rho u_\tau^3} \cdot \frac{\partial \tau}{\partial y}$, in the viscous sublayer, becomes numerically greater than 10^{-3}. In terms of Reynolds number this corresponds to about $R\theta < 1000$. In the present context, these low Reynolds numbers are fully expected and following Murlis (1975), the additive constant was taken as C = 5.2 as opposed to 5.0.

One of the earliest observations in the present study, was that the logarithmic region specified by Coles and Hirst (1968),

ie. eqn. 3.16. , was somewhat unsuitable at very low Reynolds numbers. The turbulent velocity profiles, when plotted in terms of u^+ and y^+, showed significant wake influence inside the upper bound of the specified region. The logarithmic law region was therefore re-defined for the present studies as :-

$$60 \leqslant \frac{y.u_\tau}{\nu} \leqslant 220 \qquad 3.29$$

3.7 Equilibrium and self-preserving boundary layers.

The boundary layer velocity profile is governed by the shear stresses which exist through the layer and in laminar flows, the shear stresses are simply related to the local strain rates, ie. eqn. 3.2. In turbulent flows however, the shear stresses cannot be so conveniently related and one has to resort to semi-empirical turbulence models such as the concepts of mixing length and eddy viscosity. Townsend (1976), defines the equilibrium turbulent boundary layer as one in which the classical turbulent energy terms of production and dissipation are dominant and are locally balanced. In such a boundary layer, the shear stresses can be related to the local flow properties, ie. eqn. 3.4. In contrast, self-preserving boundary layers are those where at given y/δ, outside the viscous sublayer, the flow differs only in the velocity and length scales. The condition for a flow to be self-preserving is therefore that the equations for the mean velocity and the turbulent energy and the boundary conditions, can be represented approximately by self-preserving mean velocity and Reynolds stress, etc. distributions.

Clauser (1954), showed that a boundary layer with variable

pressure gradient, but with a constant value to the parameter β,

ie. $$\beta = \frac{\delta'}{\tau_o} \cdot \frac{dp}{dx} \qquad 3.30$$

is in turbulent equilibrium and is approximately self-preserving. The parameter was introduced by Clauser in order to specify the history effects, ie. the response time to changing boundary layer forces, of the developing layer. The pressure gradient acts across some effective frontal area, δ', per unit width and as the only other gross boundary layer force is the wall shear, τ_o, then a boundary layer with the term, $(\delta'/\tau_o)/(dp/dx)$, invarient with x, will have a constant history. Clauser (1956), later showed, with considerable effort, that the correct choice of boundary layer thickness is, in fact δ^*, the displacement thickness.

The inner region of a turbulent velocity profile, described by eqn. 3.4., is in approximate local equilibrium, as local mean velocities are related to local shear stresses. The inner profile may not however be self-preserving, as this necessitates $(\frac{U_\infty - \overline{u}}{u_\tau})$ equal to $f(y/\delta)$ which is invariant with x.

The outer region, expressed as a velocity-defect profile, is a consequence of the shear stress at the wall, τ_o, and depends on the distance to which the effects of τ_o have diffused. It is also a function of the pressure gradient, and has the form :-

$$\frac{U_\infty - \overline{u}}{u_\tau} = g(y/\delta \ , \ \frac{\delta^*}{\tau_o} \cdot \frac{dp}{dx}) \qquad 3.31$$

On comparison with the Coles formulation, ie. eqn. 3.15., it is seen that Π and β must be related and consequently that Π and $\Delta\frac{\overline{u}}{u_\tau}$ as well as β must be constant in a self-preserving turbulent boundary

layer. An empirical formula, relating Π to β, was given by White (1974), in the form :-

$$\Pi = 0.8(\beta + 0.5)^{0.75} \qquad 3.32$$

It should be stated however, that the wake function, ie. eqn. 3.6., is merely an empirical fit and does not imply any universal similarity.

Clauser also determined that the most relevant thickness parameter for self-preserving flow was the defect thickness, defined as :-

$$\Delta = \int_0^\infty \frac{U_\infty - \bar{u}}{u_\tau}\, dy. = \delta^*/\sqrt{C_f/2} \qquad 3.33$$

and that self-preserving velocity profiles could be scaled with y/Δ and a shape factor, G, which would remain constant in a self-preserving boundary layer.

ie. $$G = {}^1/_\Delta \int_0^\infty \left[\frac{U_\infty - \bar{u}}{u_\tau}\right]^2 dy \qquad 3.34$$

The Kármán shape factor is related to G through the relation :-

$$H_{12} = \left(1 - G\sqrt{\frac{C_f}{2}}\right)^{-1} \qquad 3.35$$

It follows from eqn. 3.35, that H_{12} will be constant only when G and C_f are both effectively constant.

In the present context, the approach of the developing turbulent boundary layers towards self-preservation are judged on the values of Π and ${}^{\bar{u}}/_{u_\tau}$ and also on comparison of the velocity-defect profile, with an approximate self-preserving distribution. The self-preserving, or more frequently termed, equilibrium values of Π and ${}^{\bar{u}}/_{u_\tau}$ are 0.55 and 2.68 respectively and the self-preserving velocity-defect profile is given by eqn. 3.14., with $\Pi = 0.55$.

3.8 Flow two-dimensionality by the "momentum balance" test.

The two-pin test for flow two-dimensionality, section 2.15., was supplemented by the following method, also outlined by Coles and Hirst (1968). The method, referred to as the momentum balance test, is much more quantitative and consists of integrating, with respect to x, the von Kármán momentum equation. The momentum eqn. can be re-arranged in the form :-

$$\frac{d(U_\infty^2\Theta)}{dx} + \delta^*/_2 \cdot \frac{d(U_\infty^2)}{dx} = \tau_0/\rho \qquad 3.36$$

Normalising by dividing through by initial values, U_{∞_i} and Θ_i and then integrating with respect to x, from $x = x_i$ to $x = x$, results in :-

$$\frac{U_\infty^2 \cdot \Theta}{(U_\infty^2 \cdot \Theta)_i} - 1 + 1/_2 \int_{x_i}^{x} \frac{\delta^*}{\Theta_i} \cdot d\left[\frac{U_\infty}{U_{\infty_i}}\right]^2 = \int_{x_i}^{x} \left[\frac{u_\tau}{U_{\infty_i}}\right]^2 d(^x/_{\Theta_i}) \qquad 3.37$$

For the special case of a zero pressure gradient, eqn. 3.37 reduces to :-

$$2(\Theta - \Theta_i) = \int_{x_i}^{x} C_f \cdot dx \qquad 3.38$$

The left and right hand sides of eqn. 3.37 are denoted by PL. and PR. respectively. Following Clauser (1954), and neglecting the effect of absent Reynolds stress terms, any lack of agreement between PL and PR implies a departure from two-dimensionality of the flow. Flow divergence is represented by PR being greater than PL, as due to lateral outflow and boundary layer thinning, Θ is underestimated in comparison with the two-dimensional relationship. Conversely, the flow must be converging if PR is less

than PL. Paradoxically however, these last two statements are applicable only if the C_f or u_τ values are confidently known to be accurate.

The computer program MOBAL and subroutine MOINT, listed in Appendix 3, performs the integration of the two sides of eqn.3.37. from the input data of $x, \theta, \delta^*, U_\infty$ and u_τ and outputs the left and right hand sides, PL and PR, at each step. The integral terms are obtained using a similar parabolic fitting and averaging technique as that outlined in section 3.2., for the integration of the outer region of the turbulent boundary layer mean velocity profile.

3.9. Estimation of the entrainment rate .

Entrainment as defined by Head (1958), is the interaction between turbulent and irrotational or non-turbulent flow regions, where the turbulence spreads with time into the neighbouring fluid which due to turbulent mixing, partakes of the general motion of the turbulent flow. Head defined the quantity flow per unit time into the boundary layer as :-

$$Q = \int_0^\delta \bar{u}.dy = U_\infty(\delta - \delta^*) \qquad 3.39$$

hence

$$dQ/dx = d/dx\left[\bar{U}_\infty(\delta - \delta^*)\right] \qquad 3.40$$

or non-dimensionally :-

$$1/U_\infty . dQ/dx = F \qquad 3.41$$

For the case of a zero pressure gradient, eqn. 3.41 becomes :-

$$d/dx\,(\delta - \delta^*) = F \qquad 3.42$$

Green (1968), correlated the entrainment parameter F against

the shape factor H12 in the form :-

$$F = 0.025H12 - 0.022 \qquad 3.43$$

basing the correlation on Head's argument that the velocity-defect at the centre of a wake exerts a controlling influence on the rate of entrainment. This leads to the suggestion that the velocity distribution in the boundary layer and particularly the velocity-defect in the outer region, (indicated approximately by the shape factor H12), is related to the entrainment rate and hence the correlation of eqn.3.43.

In the present study, the entrainment is illustrated by plots of $(\delta - \delta^*)$ against x. It is obvious however, that the approximate nature of the method of determining δ , plus its arbitrary definition and also the subsequent differentiation of the function $(\delta - \delta^*)$, graphical or otherwise, will lead to considerable scatter in the estimated values of the entrainment parameter F.

TABLE. 3.1.

ANALYSIS OF LAMINAR VELOCITY PROFILES.

Air Temperature = 23.2°C.

Atmospheric Pressure = 770.0mm. of Hg.

Freestream Velocity = 10.86 m/s.

Distance from the Leading Edge = 300mm.

Spanwise Location = 50mm.

X-distance Reynolds N° = 215783

y-dist (mm).	y/delta	zeta	u/Uinf	(1-u/Uinf)	u/Uinf(1-u/Uinf)
0.50	0.142	0.77	0.229	0.771	0.177
0.69	0.196	1.07	0.308	0.692	0.213
0.91	0.259	1.41	0.426	0.574	0.245
1.15	0.328	1.78	0.541	0.459	0.248
1.44	0.411	2.23	0.686	0.314	0.215
1.71	0.488	2.65	0.784	0.216	0.169
1.99	0.565	3.08	0.856	0.144	0.123
2.30	0.653	3.56	0.907	0.093	0.084
2.63	0.747	4.07	0.943	0.057	0.054
2.93	0.833	4.54	0.967	0.033	0.032
3.23	0.919	5.00	0.985	0.015	0.015
3.56	1.013	5.51	0.996	0.004	0.004
3.81	1.084	5.90	0.997	0.003	0.003
4.12	1.173	6.58	1.000	0.000	0.000

Approximate edge of the Boundary Layer = 3.52mm. (ie. 0.995Uinf)
NB. zeta is the Blasius co-ordinate $=y\sqrt{U/\nu x}$.

Boundary Layer Parameters :-

Displacement thickness = 1.176mm. (1.161mm. by Planimeter)
Momentum thickness = 0.437mm. (0.431mm. by Planimeter)
Energy thickness = 0.685mm.
Shape factor H12 = 2.693
Shape factor H32 = 1.569
Rtheta = 314
Rdstar = 846
Cf. = 0.001271 (average du/dy)
Wall shear stress = 0.0907 N/m^2

Comparison with Blasius values :-

Edge of Boundary Layer = 3.23mm.
Displacement thickness = 1.111mm.
Momentum thickness = 0.429mm.
Cf. = 0.001429

ANALYSIS OF LAMINAR VELOCITY PROFILES

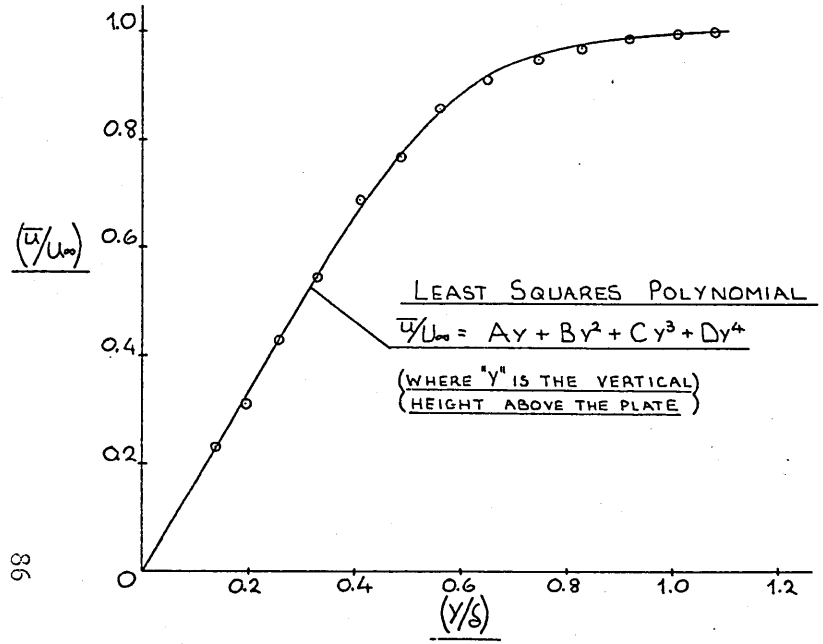

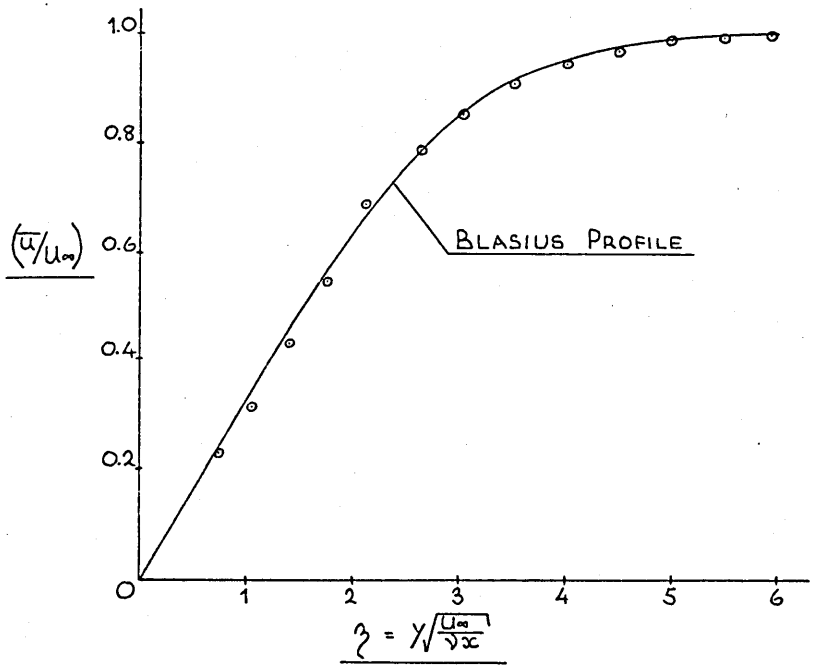

ANALYSIS OF LAMINAR VELOCITY PROFILES

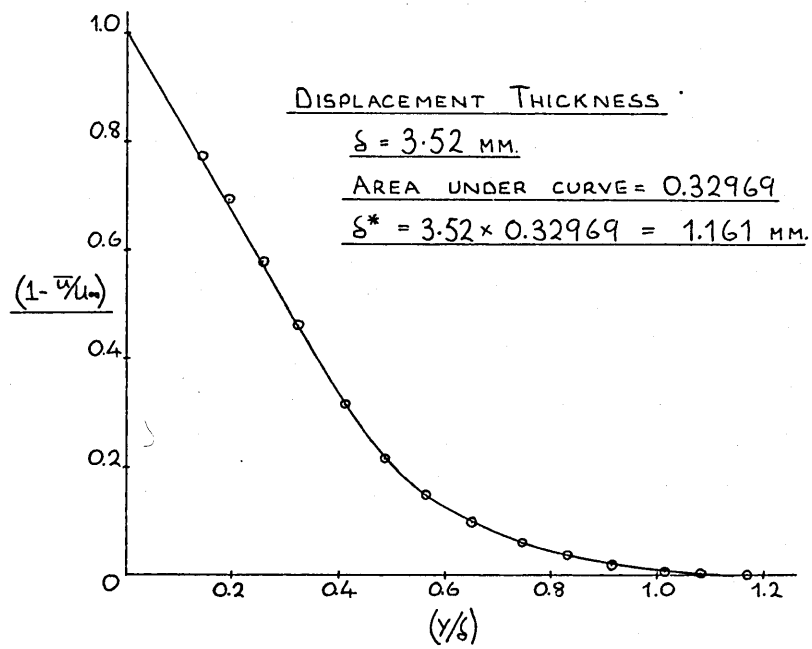

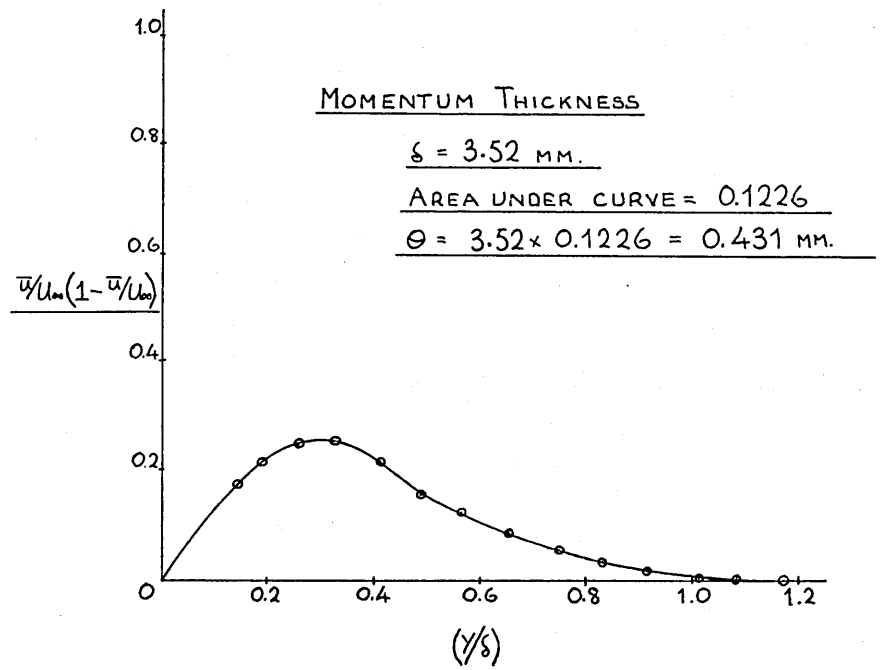

FIG. 3.1.1.

ANALYSIS OF TURBULENT VELOCITY PROFILES.

Air Temperature = 21°C.

Atmospheric Pressure = 742.75mm. of Hg.

Freestream Velocity = 11.19 m/s.

Distance from the Leading Edge = 1200mm.

Spanwise Location = 0mm.

X-distance Reynolds N° = 868883

y-dist (mm)	y/delta	u/Uinf	(1-u/Uinf)	u/Uinf(1-u/Uinf)
0.98	0.039	0.5907	0.409	0.242
1.49	0.059	0.6443	0.356	0.229
2.01	0.080	0.6667	0.333	0.222
2.52	0.100	0.6908	0.309	0.214
3.02	0.120	0.7194	0.281	0.202
3.51	0.140	0.7292	0.271	0.197
4.01	0.160	0.7480	0.252	0.188
4.51	0.180	0.7748	0.225	0.174
5.01	0.199	0.7721	0.228	0.176
5.50	0.219	0.7873	0.213	0.167
7.01	0.279	0.8132	0.187	0.152
8.02	0.319	0.8141	0.186	0.151
9.02	0.359	0.8508	0.149	0.127
10.04	0.399	0.8579	0.142	0.122
11.07	0.440	0.8838	0.116	0.103
12.05	0.480	0.9097	0.090	0.082
13.08	0.520	0.9214	0.079	0.072
14.08	0.560	0.9231	0.077	0.071
15.09	0.600	0.9357	0.064	0.060
16.08	0.640	0.9500	0.050	0.048
17.09	0.680	0.9500	0.050	0.048
18.10	0.720	0.9714	0.029	0.028
19.10	0.760	0.9866	0.013	0.013
20.11	0.800	0.9830	0.017	0.017
21.12	0.840	0.9911	0.009	0.009
23.14	0.921	0.9902	0.010	0.010
24.15	0.961	0.9920	0.008	0.008
25.16	1.001	0.9982	0.002	0.002
26.17	1.041	1.0000	0.000	0.000

Approximate edge of the Boundary Layer = 25.14mm. (ie. 0.995Uinf.)

ANALYSIS OF TURBULENT VELOCITY PROFILES

yplus	uplus	residual	velocity defect
31.18	13.44	-0.1457	9.32
47.47	14.66	0.0494	8.09
64.08	15.17	-0.1739	7.59
80.05	15.72	-0.1675	7.04
96.02	16.37	0.0396	6.39
111.67	16.60	-0.1050	6.16
127.64	17.02	-0.0039	5.74
143.61	17.63	0.3188	5.13
159.27	17.57	0.0054	5.19
174.92	17.92	0.1226	4.84
223.15	18.51	0.1184	4.25
255.09	18.53	-0.1875	4.23
287.03	19.36	0.3586	3.40
319.30	19.53	0.2615	3.23
352.20	20.11	0.6122	2.64
383.50	20.70	0.9943	2.05
416.08	20.97	1.0598	1.79
448.02	21.01	0.9201	1.75
479.96	21.29	1.0369	1.46
511.59	21.62	1.2067	1.14
543.85	21.62	1.0575	1.14
575.79	22.11	1.4064	0.65
607.73	22.45	1.6205 ***	0.31
639.67	22.37	1.4142	0.39
671.93	22.56	1.4773	0.20
736.14	22.54	1.2343	0.22
768.40	22.58	1.1704	0.18

Boundary Layer Parameters:-

Displacement thickness = 3.3914mm. (3.368mm. by Planimeter)
Momentum thickness = 2.4214mm. (2.419mm. by Planimeter)
Energy thickness = 4.2909mm.
Shape factor H12 = 1.4006
Shape factor H32 = 1.7720
Mom. th. Reynolds N° = 1753
Disp. th. Reynolds N° = 2456
Wall Friction Velocity = 0.4917 m/s. (from Log-Plot)
Cf. = 0.003733 (Ludweig-Tillman)
Cf. = 0.003861 (Log-Plot)
Cf. = 0.003606 (Coles formula)
Cf. = 0.003753 (Preston tube 1.41mm. O.D.)
Cf. = 0.003694 (Preston tube 1.105mm. O.D.)
Wall shear stress = 0.275 N/m^2
Wake Parameter Π = 0.2575
Wake Strength Parameter $\Delta(u/u_\tau)$ = 1.6205

TABLE. 3.2.

ANALYSIS OF TURBULENT VELOCITY PROFILES

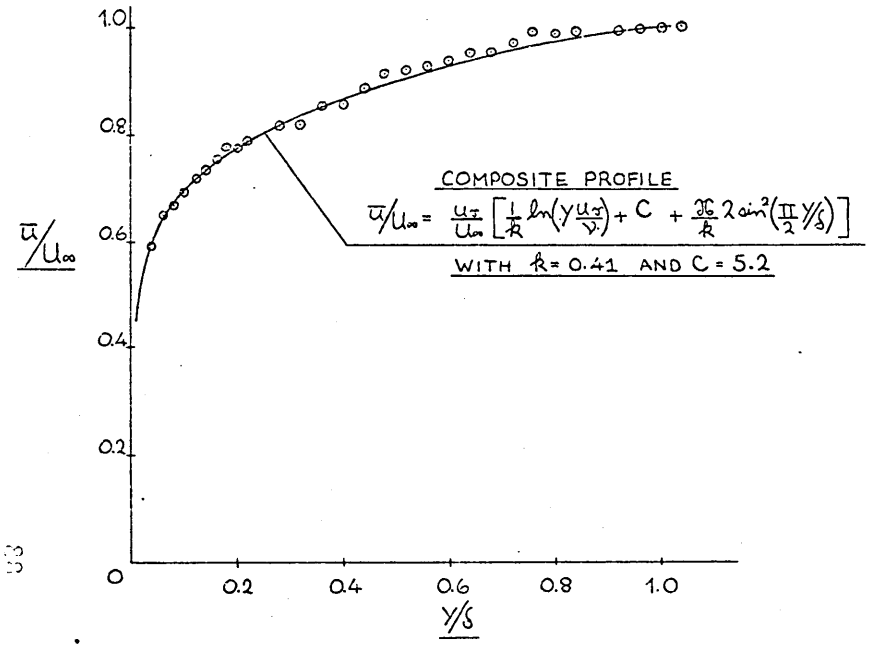

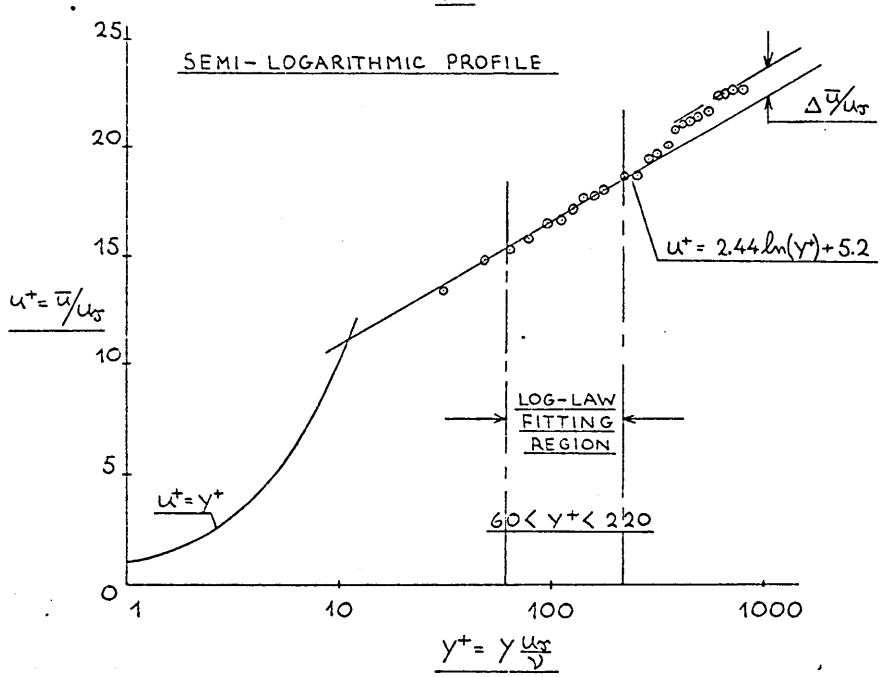

ANALYSIS OF TURBULENT VELOCITY PROFILES

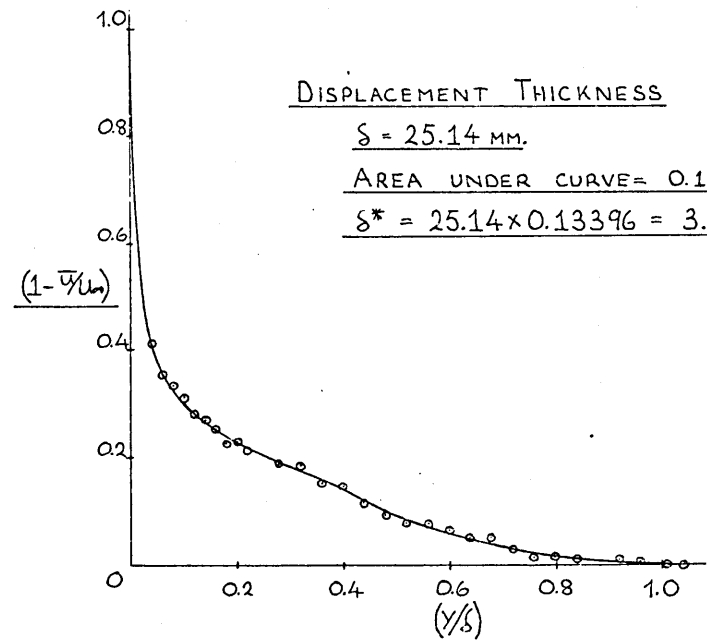

DISPLACEMENT THICKNESS

$\delta = 25.14$ MM.

AREA UNDER CURVE = 0.13396

$\delta^* = 25.14 \times 0.13396 = 3.368$ MM.

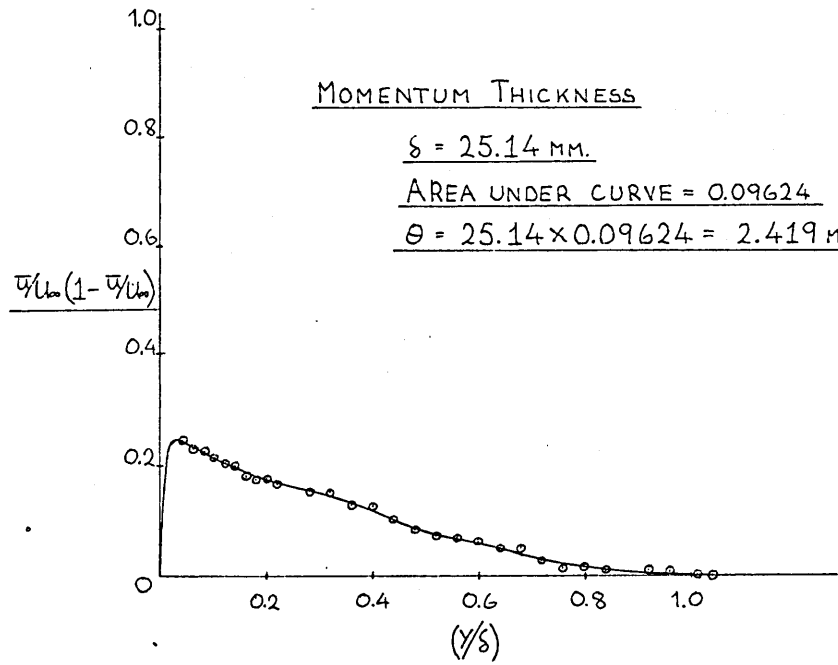

MOMENTUM THICKNESS

$\delta = 25.14$ MM.

AREA UNDER CURVE = 0.09624

$\theta = 25.14 \times 0.09624 = 2.419$ MM.

FIG. 3.2.2.

CHAPTER 4.

DETAILS OF EXPERIMENTS CONDUCTED AND DISCUSSION OF RESULTS.

The experimental conditions investigated are described and the present data are reviewed and compared with that of other workers.

BOUNDARY LAYER DEVELOPMENT FROM TRANSITION PROVOKING DEVICES

DETAILS OF EXPERIMENTS CONDUCTED AND DISCUSSION OF RESULTS.

4.1 Experimental test boundary layers.

In relation to the stated objectives, four experimental test conditions were investigated, all in a zero pressure gradient. The test program necessitated the measurements to be carried out over reasonably long periods of time and to maintain dynamical similarity, in varying ambient conditions, the unit Reynolds number, defined as $R_u = U_\infty/\nu$, was kept constant for each test. This was implemented by adjustment of the freestream velocity on a daily basis. The adjustment, fortunately however, had no noticable effect on the streamwise pressure gradient. To ensure a similar transition location and region, the suction pressure at the leading edge was also adjusted to give a mean value of intermittency of 0.5 at the same (x,z) location on the plate surface.

Many of the figures referred to in this chapter are contained in Appendix 6. and are identified by a double number suffix, other figures, relating to derived data, are given a treble number suffix and these are included at the end of the chapter.

The test conditions investigated were :-

FLOW 1. - Transition due to a two-dimensional trip wire with laminar re-attachment.

Hall (1968), showed that when transition occurs abruptly at a two-dimensional trip wire, the wire Reynolds number, R_k, is a

function of the location Reynolds number, R_{xk}, when the wire is fixed near the leading edge, ie. $R_{xk} < 10^6$. For transition to occur downstream of the wire, R_k should be less than that quoted by Hall.

In FLOW 1, transition occurs some way downstream of the wire. The wire was located at x = 100mm. and the unit Reynolds number for this flow was $R_u = 6.5 \times 10^5/m$. such that $R_{xk} = 6.5 \times 10^4$. The wire diameter was 0.52mm. and subsequently, $R_k = 340$. From Hall's correlation, see FIG 4.1.1, it is seen that the experimental data point does, in fact, lie slightly below the curve. Additionally, Rk_{crit} for FLOW 1 has the value of 107 which is suitably below the range of values, ie. $200 < R_{k_{crit}} < 300$, suggested by Klebanoff et al. (1955) for this form of Reynolds number correlation for transition at the wire.

FLOW 2. - Free transition.

The transitional boundary layer characteristics in the absence of obvious provoking agents was investigated at a unit Reynolds number of $R_u = 7.2 \times 10^5/m$. The higher value being adopted to contain the transition region within a suitable area of the plate. The start of transition at two spanwise locations, along which measurements were made, is shown in comparison with a correlation due to van Driest and Blumer (1963), in the form $R\theta_{tr}$ vs. $(\sqrt{\overline{u'^2}}/U_\infty)\%$, for natural transition in a zero pressure gradient, see FIG 4.1.2. The lack of agreement between the present data and the correlation necessitates FLOW 1 to be referred to as "free" transition in preference to natural transition, where natural transition is that due to the amplification of small disturbances. The velocity distribution at the leading edge, see

FIG 2.12.1, and leading edge disturbances are thought to be the major contributing factors promoting the early transition.

FLOW 3. - Transition due to a two-dimensional trip wire with turbulent re-attachment.

The condition, often referred to as transition at the wire, was induced with a trip wire located at x = 200mm. and the unit Reynolds number at $R_u = 7.2 \times 10^5$/m. The location Reynolds number is then $R_{xk} = 1.44 \times 10^5$ and with a wire diameter of 1.2mm., the wire Reynolds number is $R_k = 864$. Referring to FIG 4.1.1, it is seen that the wire Reynolds number is in excess even of the asymptotic value for transition at the wire. This was however a deliberate choice to provide a severe test for the concept of statistical similarity in transition regions.

FLOW 4. - Transition due to isolated spherical roughness elements.

Two spherical elements were located at x = 100mm. from the leading edge and at ±75mm. equidistant from the tunnel centre-line. For transition to occur immediately behind an isolated roughness element, Tani et al. (1962), give a relation, ie. eqn. 1.4, between R_{xtr} and $R_{k_{crit}}$. With a sphere diameter of 1.59mm. and the unit Reynolds number at $R_u = 6.5 \times 10^5$, the condition is achieved in the present configuration. The corresponding value of $R_{k_{crit}}$ is 910. The location and transition Reynolds number is $R_{xk} = R_{xtr} = 6.5 \times 10^4$ and the point is plotted in relation to eqn. 1.4 in FIG 4.1.3. It can be seen that the sphere diameter is slightly greater than that required to induce immediate transition, but not excessively so.

4.2 Transition Reynolds numbers downstream of a two-dimensional trip wire.

Dryden (1953), showed that when transition occurs downstream of a two-dimensional trip wire, the ratio of provoked to free transition Reynolds numbers correlated well against the parameter k/δ^*_k. In the present studies, the undisturbed displacement thickness at the wire position was determined from measured velocity profiles rather than assuming Blasius distributions. The data from FLOWS 1 and 2, provide two suitable points for comparison with Dryden's curve, see FIG 4.2.1, where it is seen that the present data is slightly high. The early transition which occurs in the free transition condition of FLOW 2, see FIG 4.1.2, means that $(R_{xtr})_o$ is unusually low and that the ratio of provoked to free transition Reynolds numbers will be higher than might be expected. The deviation from the curve however, is not much worse than some of the original data on which the correlation was based.

An alternative method of correlating the transition Reynolds number downstream of a two-dimensional trip wire is due to Potter (1957), in the form :-

$$R_{xtr}\cdot\left(\frac{k}{x_k}\right)\cdot\left(\frac{x_k}{x_{tr}}\right)^{0.5} = 780 \qquad 4.1$$

The six data points from FLOW 1, are plotted to compare with the above relation, see FIG 4.2.1, where the agreement is seen to be satisfactory. NB. (two sets of points are coincident.).

4.3 Statistical similarity of transition regions.

The concept of statistically similar transition regions is a development from the observations of Emmons and Bryson (1950), who concluded that the length of the laminar breakdown region was related to the density of turbulent spot sources. Dhawan and Narasimha (1958), showed that the spot sources were confined to a narrow, localised region and that the resulting downstream turbulence probability, or intermittency, was defined by a unique relation, ie. eqn. 1.8. Schubauer and Klebanoff (1956), also gave support to the concept of statistical similarity, although in contrast to Dhawan and Narasimha, they normalised the streamwise intermittency distribution to the Gaussian integral curve, or normal distribution function.

In the present study the procedure adopted for determining the standard deviation of the intermittency distribution, was to firstly obtain $\overline{x}$, the location of the 50% intermittency point, from a plot of $\overline{\gamma}$ vs. x, see FIGS. 1.45-1.47, 2.14 and 3.13. These plots also locate the start of transition, x_{tr}, and the transition length parameter, λ. For each point in the distribution, the value of the standard deviation, ∇_L, which normalises the point on to the Gaussian integral curve, can be determined. The average value of ∇ is then taken to be the representative standard deviation of the complete distribution. The data was then re-plotted against the normalised coordinate $(x-\overline{x})/\nabla$ and compared with the normal distribution function. The results for FLOWS 1,2 and 3 are shown in FIGS 4.3.1. and 4.3.2, where it can be seen that the distributions are especially well described

by the normal distribution function. The empirical relation due to Dhawan and Narasimha also compares favourably, although the present data does exhibit a slight tendency to lie below the curve.

It is particularly significant that the measured intermittency distribution of FLOW 3 is in good agreement with the normal distribution function. The apparent lack of agreement between the data from FLOW 3 and Dhawan and Narasimha's curve stems from their use of x_{tr}. as a datum length, whereas $\overline{x}$, used in the normal distribution, is much more readily defined. The lack of agreement should not be viewed too critically however, as FLOW 3 is a particularly severe test case. The transition region in this flow consists of a short length, 30mm., where the mean intermittency increases from 0 immediately behind the wire, to 1.0 downstream. Transition is therefore complete before the separated layer re-attaches, see FIG 3.13. The mean velocity profiles in this transition region are subsequently of an inflectional form, however, the intermittency profiles remain relatively undistorted, see FIGS 3. 7 and 3. 8. This indicates that the intermittency distribution is little affected by the mean velocity profile shape. The intermittency data from FLOWS 1,2 and 3 therefore corroborate the concept of statistical similarity of transition regions and support Emmon's and Dhawan and Narasimha's overall picture of the laminar breakdown process.

The transition region behind isolated roughness elements, with transition at the element, is however, distinctly different. The hot wire signal behind an element is shown in FIG 4.3.3, where a periodic

fluctuation is observed with an initial r.m.s. amplitude of 3.4% of U_∞ . This oscillation gradually degenerates to a more familiar "turbulent-like" signal 40mm. downstream from the element. While an intermittent character is mildly in evidence at x = 125 and 140mm, with two distinctive mean voltage levels indicated, the fluctuations in the "laminar" regions are so large that they are registered as turbulent regions when discriminated with the present intermittency measuring circuitry. The more usual type of intermittent signal obtained in a transition region is also shown for comparison. It is seen that the laminar region to the left of the photograph has a noticable absence of large amplitude fluctuations. It would appear then that when transition is induced immediately behind an isolated, three-dimensional roughness element, the intermittency growth process is less dominant and that this condition is as near as possible to an instantaneous transition. This result does not however imply that the intermittency growth process will be absent when transition occurs downstream of an isolated roughness element. The smoke photographs of Mochizuki (1961), in fact, show strong evidence of an intermittency growth process under these conditions. The oscillation frequency induced by the element also has a nearly linear relationship with the freestream velocity, see FIG 4.3.4. The measurements, obtained from a frequency scan with a wave analyser, suggest that the induced oscillation is a consequence of vortex shedding from the element.

4.4 Transitional mean and fluctuating velocity profile similarity.

Following Dhawan and Narasimha, the velocity ratio $(\overline{u}/U_\infty)$, at a constant height (y/Θ) was plotted against the normalised transition coordinate $\zeta = \frac{x-\overline{x}}{\nabla}$. The ζ coordinate was used here in favour of Dhawan and Narasimha's coordinate $\xi = \frac{x-x_{tr}}{\lambda}$. The data from FLOWS 1 and 2 are shown in FIG 4.4.1, and a set of unique curves are apparent for each value of (y/Θ). This implies that the transition mean velocity profiles are approximately similar when plotted in terms of $(\overline{u}/U_\infty)$ vs. (y/Θ) and a set of similarity transition mean velocity profiles can be cross-plotted from FIG. 4.4.1. These are shown in FIG. 4.4.2.

In a consistent manner, the u' profiles were likewise tested for similarity through transition. FIGS 4.4.3. and 4.4.4. show the results for FLOWS 1 and 2, where unique curves are obtained although the experimental scatter is more pronounced. It can be readily seen however, that the intensity of fluctuation reaches a peak at approximately $\zeta = 0.5$, corresponding to $\overline{\gamma} = 0.70$, for all values of (y/Θ). The complete u'- intensity profile therefore grows in magnitude up to the point where the mean intermittency becomes 0.70, and then diminishes to become the characteristic "turbulent" shape described by the broken line shown on FIG 4.4.5. The other similar u'-profiles, at particular mean intermittencies, are also shown on the FIG. It should be noted that some of the u' intensity is attributable to the intermittency. The mean velocity alternates between two distinctive levels in transition regions and is therefore registered as an apparent velocity fluctuation. The alternating character of transition regions is further discussed in section 4.6.

4.5 Transitional local skin friction coefficient similarity

Having observed the existence of approximate similarity in the mean and fluctuating velocity profiles, the local skin friction coefficient was tested for similarity through transition. Following Dhawan and Narasimha, the increase in local skin friction coefficient was determined from the start, through to the end of transition. By relating the increase in C_{f_t} to the local value at the start of transition, the plots are effectively rendered independent of Reynolds number. The data from FLOWS 1 and 2 are plotted in FIG. 4.5.1. and a consistent trend is apparent, although the experimental scatter is considerable.

4.6 Description of the transition region.

A number of workers, eg. Schubauer and Klebanoff (1956), Arnal et al. (1977) and Feliss et al. (1978), have observed the transition region to be an alternation between laminar and turbulent flow states. While the separate laminar and turbulent components were not measured in this work, the instantaneous velocity, $(\overline{u} + u')$, recordings provides strong support to the physical model. The instantaneous velocity signals near the wall and in the outer layer are shown for a low and high intermittency transition region in FIG 4.6.1. In both cases, the signal near the wall shows an increase in the mean level as a turbulent region is encountered. Further away from the wall, the signal appears inverted and is associated with a lower mean velocity in the turbulent region. The interpretation of the signals is consistent with the sketch shown on the FIG., where

at $y < y_c$, the turbulent component of mean velocity is greater than the laminar component and vice-versa at $y > y_c$. The implications are that the component laminar and turbulent profiles, which make up the transitional mean velocity profile, are qualitatively similar to those shown on the FIG.

The conditionally sampled data of Arnal et. al. (1977), in fact, confirms the physical model by explicit measurements of the component profiles.

It is noted also that if the velocity trace is recorded at $y = y_c$, then there will be no apparent mean velocity jump between laminar and turbulent regions. This coincidently would appear to be the case in the last oscilloscope photograph shown in FIG. 4.3.3.

4.7 Correlations of transition length Reynolds number.

Various direct or indirect correlations of transition length have been published in the literature, eg. Forest (1977) and Dhawan and Narasimha (1958). These are highly empirical however, and none seem to be significantly superior. The simplest correlation, due to Dhawan and Narasimha, has the form :-

$$R_\lambda = 5(R_{xtr})^{0.8} \qquad 4.2$$

The present data is compared with eqn. 4.2 in FIG 4.7.1., where the scatter is typical. The log-log plot however, disguises the fact that deviations of 100% are not uncommon. It was thought that some improvement might be obtained if a local boundary layer thickness Reynolds number was used to correlate the transition length Reynolds number. As λ and ∇ are both a measure of the same effect, they

can be related. The present data suggests :-

$$\lambda = 1.4\,\nabla \qquad 4.3$$

Using the Blasius relation between R_x and R_θ and eqn. 4.3, eqn. 4.2 converts to :-

$$R_\nabla = 6.89(R_{\theta_{tr}})^{1.6} \qquad 4.4$$

On re-plotting the present data for comparison with eqn. 4.4, it is seen that the improvement, if indeed any, is only marginal. The data point due to Hall (1968) shown on the plot, is an approximation, and is not determined from a known intermittency distribution. Hall quoted the start and end of transition as the points of minimum and maximum total head pressure respectively; measured by a total head tube in contact with the wall. It was assumed here, that these points corresponded to the mean intermittency values of 0.01 and 0.99 respectively and that the 50% intermittency point was mid-way between these two points. These assumptions enable ∇ to be estimated and hence R_∇. The artifice however, provides the approximate means of determining R_∇ for a large amount of existing data where the intermittency distributions are unknown.

The degree of scatter in the plots shown in FIG 4.7.1, indicate that the length of transition is dependent, but not solely dependent, on the transition Reynolds number, The length is, in fact, a consequence of the turbulent spot source density and occurrence frequency and any correlation should be based on the relevant influencing factors. On reviewing the present data, it was observed that the maximum value of $(\sqrt{\overline{u'^2}}/U_\infty)\%$ at transition showed only a nominal

increase with the transition Reynolds number and hence transition length. It would therefore seem that the spot density is not increased simply by larger amplitude streamwise disturbances in the boundary layer. The possible factors which influence the rate of seeding of turbulent spots is further discussed in the following section.

4.8 Flow visualisation studies.

In a tentative attempt to gain some insight of the laminar breakdown process, a water channel was built with a series of dye ports positioned across the span, near the leading edge. When water flows along the channel, the dye filaments trace out the flow pattern. The investigation was moderately successful in that an increase in flow velocity noticeably increased the spot source density and moved the transition location upstream.

In addition, turbulent spot evolution could be anticipated by a significant local darkening of the dye sheet, see frontispiece, and in many cases, spot bursting was preceeded by a visible lateral oscillation. The observation suggests that turbulent spots are more likely seeded by lateral as opposed to longitudinal influencing factors.

4.9 Intermittency profiles through transition.

In all the flows studied, the intermittency profiles have a consistent shape variation through transition, and in the early development of the turbulent boundary layer, see FIGS 1.27-1.32, 2.8-2.9 and 3.7-3.8. The transition intermittency profiles are of a similar form to that shown by Corrsin and Kistler (1954). If the

transverse intermittency distribution due to Klebanoff (1955), ie. eqn. 2.8, is regarded as a reference, then the intermittency in the latter stages of transition is greater, away from the wall. During the initial development of the turbulent boundary layer however, the intermittency diminishes, and has a deeper penetration into the layer at low values of momentum thickness Reynolds number.

4.10 Spanwise variation in the boundary layer.

Much of the data measured in the present study relates to spanwise variation in the laminar, transitional and turbulent boundary layer. A comparison is made between the spanwise variation in local skin friction coefficient for the cases of free transition and transition at a two-dimensional trip wire, see FIG 4.10.1. The measurements were taken, in both cases, at x = 1800mm. in a region of turbulent flow. The superior spanwise uniformity in the case of transition at the wire indicates that optimum spanwise uniformity is obtained with the shortest transition length.

When transition occurs downstream of a two-dimensional trip wire, as in FLOW 1, the initial laminar boundary layer growth is relatively uniform as indicated by the spanwise plots of momentum and energy thickness, see FIG 1.53, and the similarity of the mean and fluctuating velocity profiles across the span, see FIG 1.54. Transition is however, initiated at particular spanwise locations and further boundary layer growth sees the onset of large lateral non-uniformity. There is also no evidence in the present data of any tendency for the non-uniformity to diminish further downstream.

With such extensive spanwise variation across the layer, the question of flow two-dimensionality arises. A two-pin test at the flow Reynolds number indicates that the flow remains essentially two-dimensional up to about x = 600mm., see FIG 1.48. Beyond this point however, an apparent divergence is indicated. The momentum balance analysis, along six spanwise stations, confirms a flow divergence from the region of the approximate tunnel centre-line, see FIGS. 1.49-1.50., and that the nett outflow from the approximate centre to the door side of the tunnel is greater than the outflow to the back wall. These results are consistent with the plots of momentum and energy thickness variation across the span, where the divergence would appear to be centred nearer z = -50mm. The present data relating to the two-dimensionality of FLOW 1 indicates that the results of a momentum balance analysis should be interpreted with some care. Along a single spanwise location, a momentum balance might indicate a divergence or convergence where, in fact, the flow is subject to a gross lateral cross-flow component. Coupled with a two-pin test however, the momentum balance analysis provides a good qualitative indication of the flow behaviour. It should be noted also, that the results of the momentum balance analysis are subject to the accuracy of the estimated local skin friction coefficient. In FLOW 1, the analysis is carried through the transition region where the estimated skin friction coefficients are slightly less accurate. The uncertainty in C_{f_t} therefore has some bearing on the seemingly excessive deviation from the left and right hand sides of the momentum

balance equation in some of the plots.

For the case of free transition, ie. FLOW 2, the initial laminar boundary layer growth is uniform, indicated by the similarity of the mean and the fluctuating velocity profiles, see FIG 2.17, across the span. In this case, as in FLOW 1, particular transition locations generate downstream non-uniformity and ultimately induce flow divergence from the central region of the plate. The effect is evident from the two momentum balance tests along z = ±50mm., see FIG 2.15.

Optimum spanwise uniformity is obtained when transition is initiated at a two-dimensional trip wire, as in FLOW 3. The variation in local skin friction coefficient is within $\pm\frac{1}{2}\%$ at x = 400mm. and within ±1% at x = 1800mm., see FIG 3.14. The mean velocity profiles at x = 400mm. also describe a single curve, confirming spanwise similarity. In addition, the momentum balance along z = -50mm., see FIG 3.12, indicates reasonable agreement between left and right hand sides.

When transition is induced immediately behind an isolated roughness element, turbulence appears in a laterally spreading turbulent wedge. In FLOW 4, two such elements were placed upstream near the leading edge and equidistant from the tunnel centre-line. A plan view of the developing turbulent wakes is mapped out from measured intermittencies, see FIG 4.10.2. The asymptotic spread half-angles are about 4.6° for the inner, fully turbulent core and about 9.1° for the outer edge of the intermittent region. The

fully turbulent cores eventually merge at about x = 800mm. The spread angles are reasonably close to those quoted by Schubauer and Klebanoff (1956), which are 6.4° and 10.6° respectively. The present values are lower because the wakes have not quite reached the asymptotic spread rate.

A surprising result, considering the persistent spanwise variation in FLOW 1, is the degree of boundary layer uniformity across the span after a mean value of intermittency of 1.0 is established over the entire plate. This effect is shown in the plots of spanwise variation in momentum and energy thickness, see FIG 4.32., and also in FIGS 4.36-4.38, which illustrate the spanwise variation in local skin friction coefficient at several downstream locations. At x = 750mm., ie. just before the merge point of the turbulent cores, a near-symmetrical irregularity exists in the spanwise variation of C_f, see FIG 4.37. On the same FIG, the variation in C_f at x = 1000mm. is almost negligible. FIGS 4.32-4.35 show the development of the turbulent wakes, in terms of constant spanwise intermittency contours at several downstream positions. It is again seen that a significant non-uniformity rapidly decreases after the fully turbulent cores have merged. The spanwise uniformity is also confirmed by the plots of the mean and fluctuating velocity profiles across the span at x = 1000mm. and at x = 1500mm., see FIG 4.39.

The momentum balance analysis, FIG. 4.30, applied along the wake centre-lines, indicate quite correctly that the flow in the wakes is highly divergent. It would be surprising, in fact, if this was not the case.

4.11 Entrainment rates.

In all the flows examined, see FIGS 1.42-1.44, 2.13, 3.12 and 4.31, the entrainment rate, denoted by the slope of the mean line shown in the plots of $(\delta - \delta^*)$ vs. x, reaches a near constant value in the fully turbulent regions, ranging from F = 0.023 to 0.011. In FIG 4.31, the spanwise entrainment rate associated with the lateral spread of the turbulent wakes is also shown. The larger spanwise entrainment rate, indicated by the plots, is consistent with the observation that the lateral growth rate of the turbulent wedge, greatly exceeds the transverse growth rate.

4.12 Turbulent boundary layer development.

The approach to self-preserving conditions of the developing turbulent boundary layer is gauged on comparison of the development of the wake parameter Π and the wake strength parameter $\Delta\overline{u}/u_J$, see FIGS 1.52, 2.16 and 3.9. The data, from FLOWS 1, 2 and 3, show that there is no significant difference due to the choice of transition agent in this respect. The wake strength parameter would appear however, to be in closer agreement with the "theoretical" distributions for a flat plate, given by eqn. 3.28 and the relation between Π and $\Delta\overline{u}/u_J$.

The approach to equilibrium is also indicated in the plots of $(\overline{u'}^2/u_J^2)$ vs. (y/δ), see FIGS 1.23-1.25 and 3.2. These serve as an indicator of the turbulence structure and it can be seen that the profile undergoes a rapid change during the initial development of the turbulent boundary layer. The experimental scatter however, masks any subtle change as the boundary layer further proceeds towards

equilibrium. The mean line shown on the plots is purely for convenience and is not intended to represent any typical self-preserving distribution.

Comparison of the velocity-defect profile against the approximate equilibrium form, ie. eqn.3.14, provides another means of estimating the deviation from self-preserving conditions, see FIGS. 1.5-1.10, 2.4-2.5 and 3.3. The FIGS just quoted also show the turbulent velocity profiles plotted in terms of inner variables, u^+ and y^+. It is seen that a recognisable linear, inner region exists only when the mean intermittency reaches a value of unity. This observation therefore constitutes a necessary condition for the existence of a characteristic turbulent boundary layer, because the fluctuating velocity profile also requires $\overline{\gamma} = 1.0$ before it takes on a typical turbulent shape, see section 4.4. One exception to the above rule is observed in FLOW 3, where the mean intermittency reaches a value of unity before the mean velocity profile acquires a linear inner region. The disparity is due however, to the inflectional nature of the mean velocity profile, which is in a region of separated flow and is not, strictly speaking, a breakdown of the criterion.

Using the intermittency criterion for the existence of a turbulent boundary layer, it would seem that the minimum corresponding Reynolds number in FLOW 3 is $R_\theta = 408$, which is in reasonable agreement with the accepted value of $R_\theta = 425$, (NB. Preston (1958) quotes $R_{\theta_{min}} = 320$). This minimum Reynolds number criterion should however, be regarded with a reasonable degree of caution as the

turbulent boundary layer at these Reynolds numbers are almost always a consequence of some severe tripping agent. In FLOW 3, the minimum axial length at which the turbulent velocity profile appears to have recovered from the distortion effects of the trip wire, is at x = 300mm., see FIG 3.2. The corresponding Reynolds number at this location is R_θ = 540, which is regarded by the present author as a more realistic minimum Reynolds number. The axial length where the mean velocity profile becomes distortion free, corresponds to a distance of about 85 wire diameters downstream of the wire. The axial length Reynolds number at this location is $R_x = 2.16 \times 10^5$, which is in qualitative agreement with the observations of Graham (1968).

The graphs showing the streamwise development of integral parameters and local skin friction coefficient, see FIGS 1.36-1.41, 2.11-2.12, 3.10-3.11 and 4.28-4.29, indicate that the most prominent low Reynolds number effect is manifested in the uncertainty in the estimation of C_f. The C_f as obtained by the log-law method, is invariably higher than that obtained by Preston tube measurements. The present data however, suggests that the two methods of estimating C_f are in reasonable agreement when $R_\theta > 2400$. The disparity at lower Reynolds numbers must however, be partly related to the assumptions regarding the particular form of the law of the wall, ie. eqn. 3.4. Both the Preston tube and the log-law methods, although physically different, rely on the validity of the law of the wall for their accuracy. The Preston tube measurements however, are based on an empirical correlation over a wide range of Reynolds numbers and

are quoted as being accurate to ±1.5%. Thinness of the boundary layer and a deep intermittency penetration at low R_θ may however influence the accuracy.

The value of the constant C, in the law of the wall was taken as 5.2, in preference to 5.0 for the reduction of low Reynolds number turbulent velocity profile data, see section 3.6. The choice of 5.2, ultimately results in a lower estimate, about -2%, for C_f as determined by the log-law method, at Reynolds numbers of the order R_θ = 1000. To be in agreement with the Preston tube C_f's however, the constant would have to be taken as 6.0, with the von Kármán constant, k, remaining fixed at 0.41. This is slightly excessive to the point where it begins to contradict the conclusions of Huffman and Bradshaw (1972), who suggested that the constant C was only very mildly Reynolds number dependent, see section 3.6. It would seem most likely therefore that the local skin friction, in fact, lies somewhere between the Preston tube and log-law estimates, with the error in the Preston tube measurements attributable to the thinness of the boundary layer at low Reynolds number. The difference between the values of the present data is of the order of 6 - 7%, for $R_\theta < 2400$. If the correct local skin friction coefficient lies exactly mid-way between the two estimates, then the maximum value of C is of the order of 5.4 - 5.5, which is more in keeping with Huffman and Bradshaws conclusions.

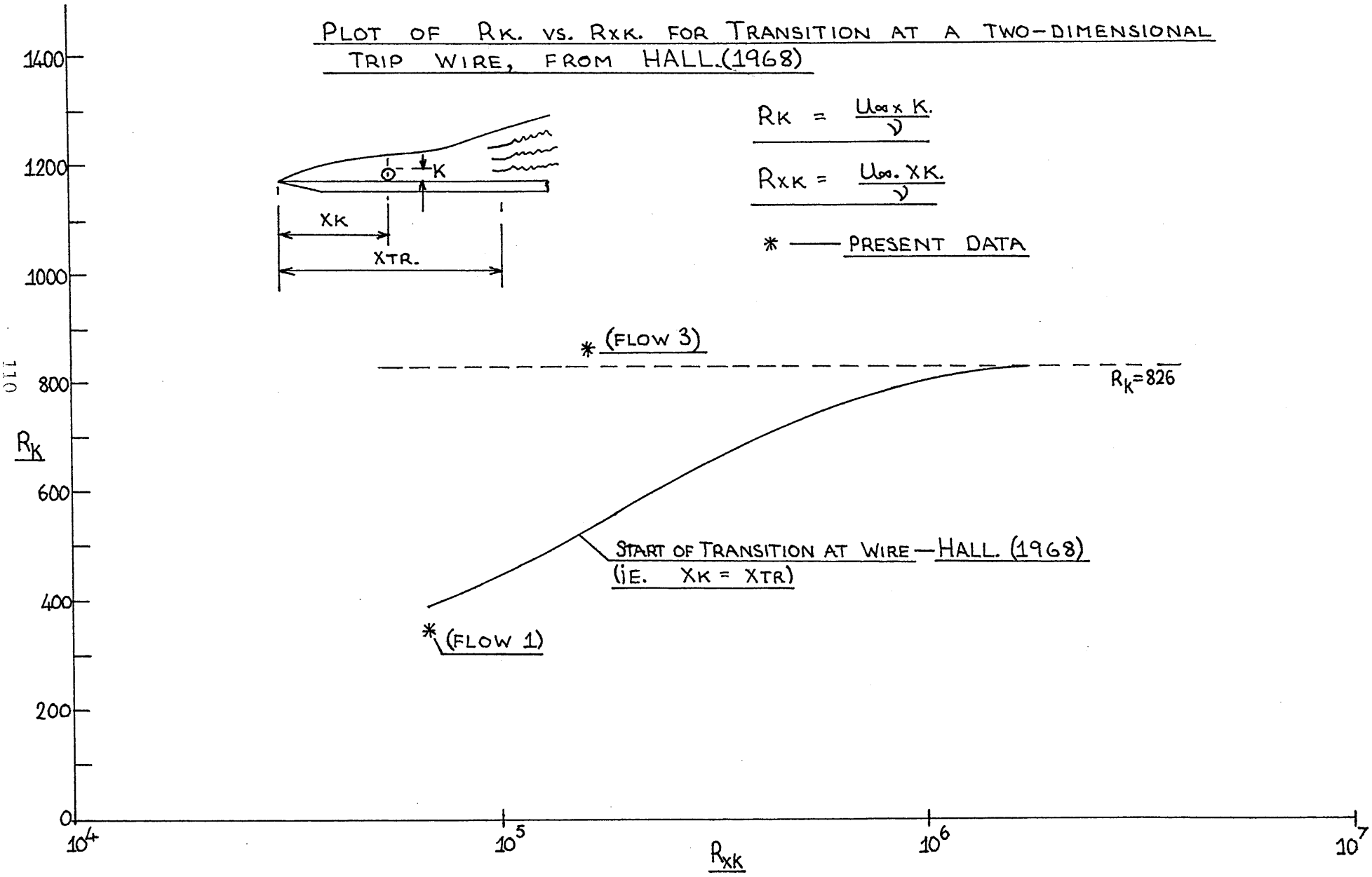
PLOT OF RK. VS. RXK. FOR TRANSITION AT A TWO-DIMENSIONAL TRIP WIRE, FROM HALL.(1968)
RK = U∞ x K. / ν
RXK = U∞. XK. / ν
* —— PRESENT DATA
K
XK
XTR.
* (FLOW 3)
RK=826
START OF TRANSITION AT WIRE — HALL. (1968)
(IE. XK = XTR)
* (FLOW 1)
RK
RXK
1400
1200
1000
800
600
400
200
0
10^4
10^5
10^6
10^7

FIG. 4.1.1.

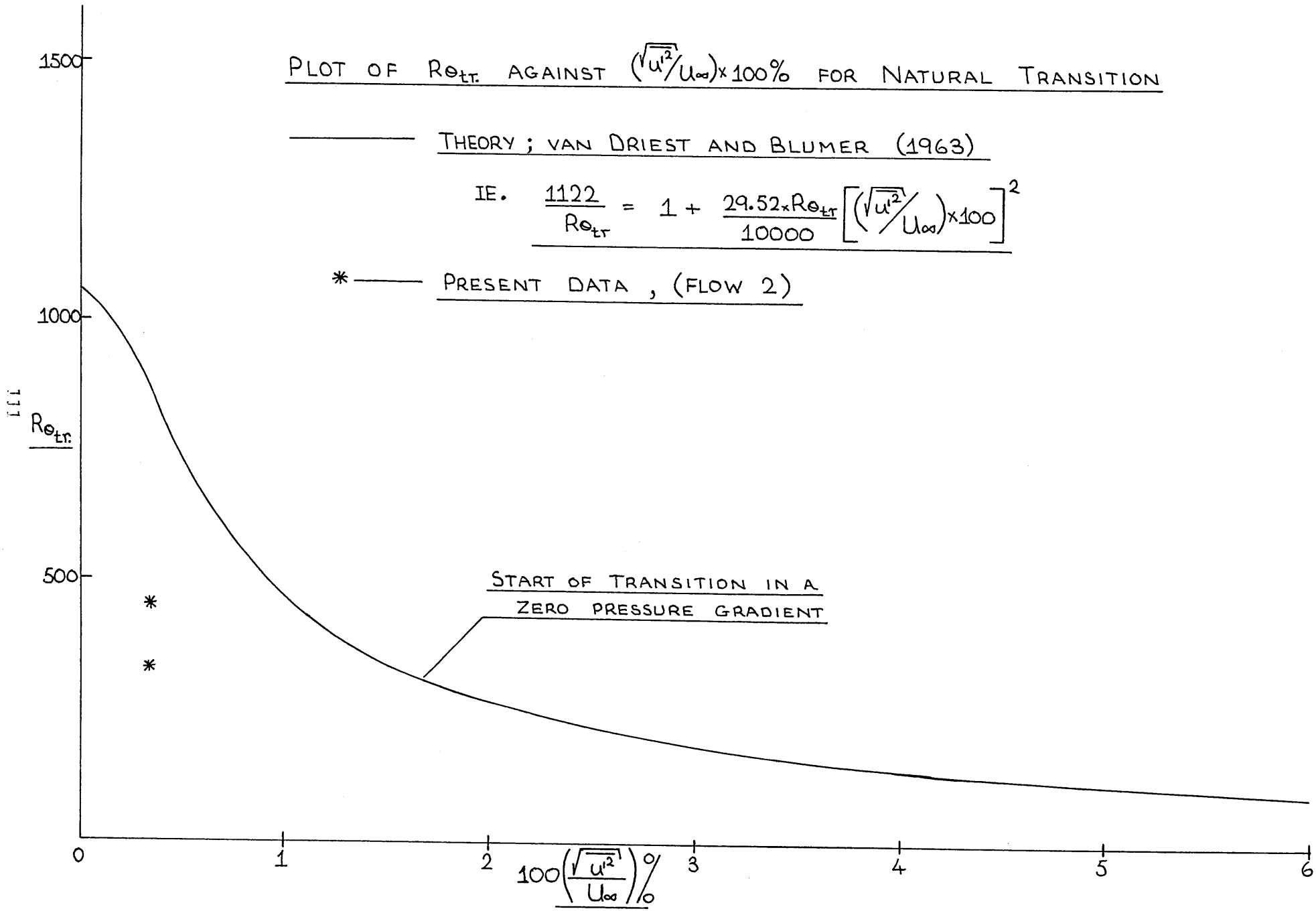
PLOT OF $R\theta_{tr.}$ AGAINST $(\sqrt{\overline{u'^2}}/U_\infty)\times 100\%$ FOR NATURAL TRANSITION
THEORY ; VAN DRIEST AND BLUMER (1963)
IE. $\frac{1122}{R\theta_{tr}} = 1 + \frac{29.52\times R\theta_{tr}}{10000}\left[\left(\sqrt{\overline{u'^2}}/U_\infty\right)\times 100\right]^2$
PRESENT DATA , (FLOW 2)
START OF TRANSITION IN A ZERO PRESSURE GRADIENT
$R\theta_{tr.}$
1500
1000
500
0
1
2
3
4
5
6
$100\left(\frac{\sqrt{\overline{u'^2}}}{U_\infty}\right)\%$

FIG. 4.1.2.

FIG. 4.1.3.

PLOT OF $R_{XTR.}$ VS. $R_{K_{CRIT.}}$ FOR TRANSITION IMMEDIATELY BEHIND A SPHERICAL ROUGHNESS ELEMENT; FROM TANI ET. AL. (1962)

$$R_{XTR} = \frac{U_\infty . X_{TR.}}{\nu}$$

$$R_{K_{CRIT}} = \frac{\bar{u}_K . K}{\nu}$$

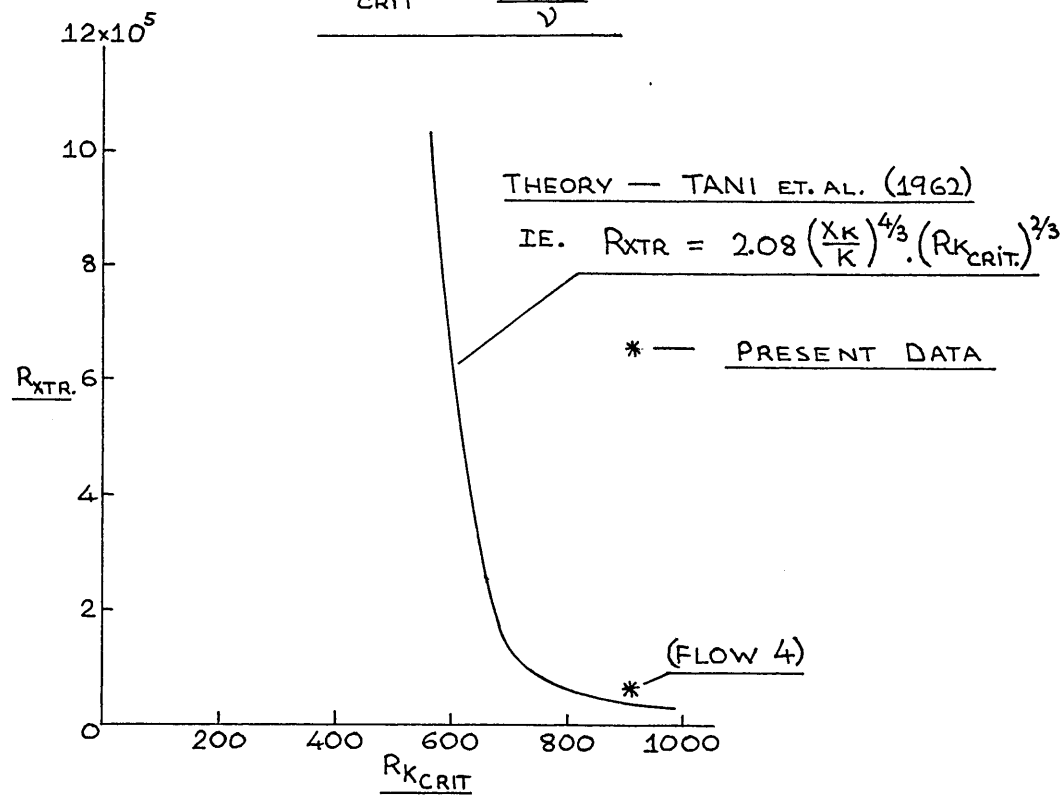

CORRELATIONS OF TRANSITION REYNOLDS NUMBER DOWNSTREAM OF A TWO-DIMENSIONAL TRIP WIRE

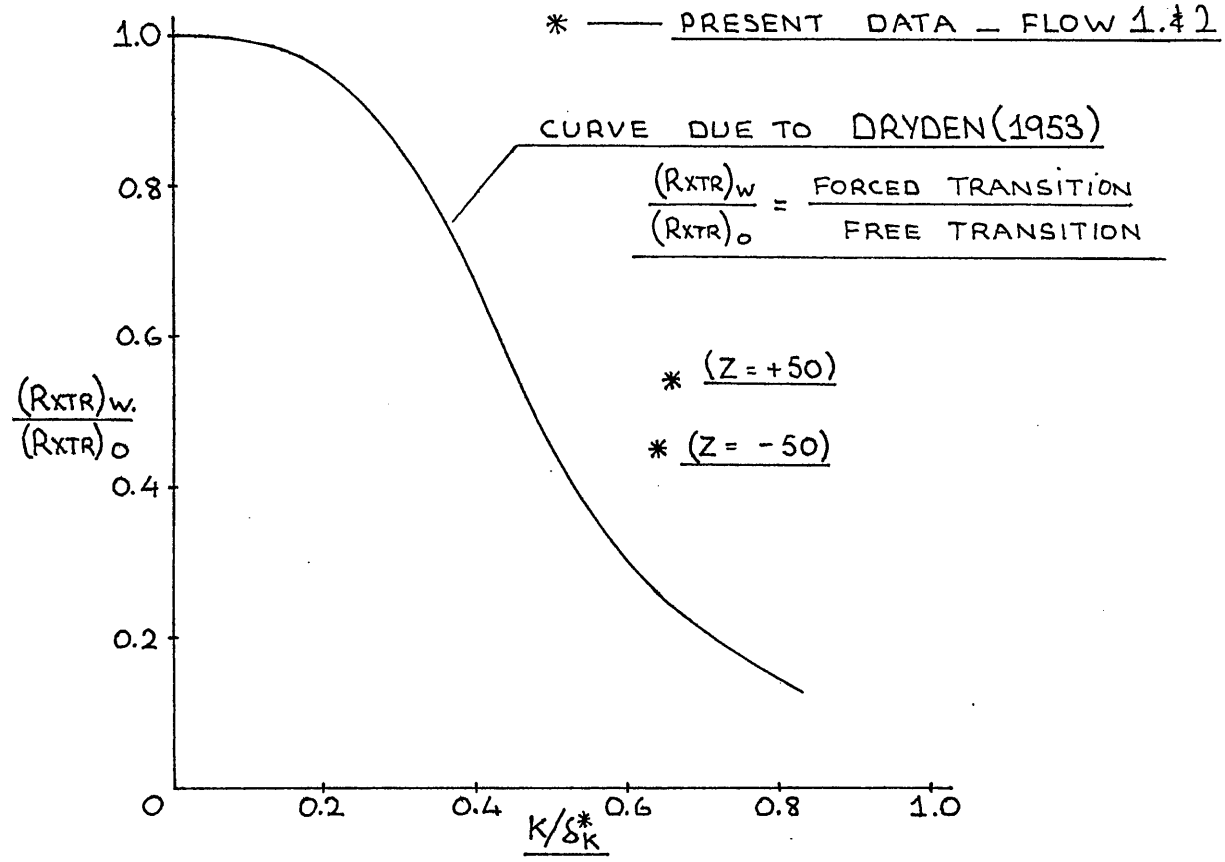

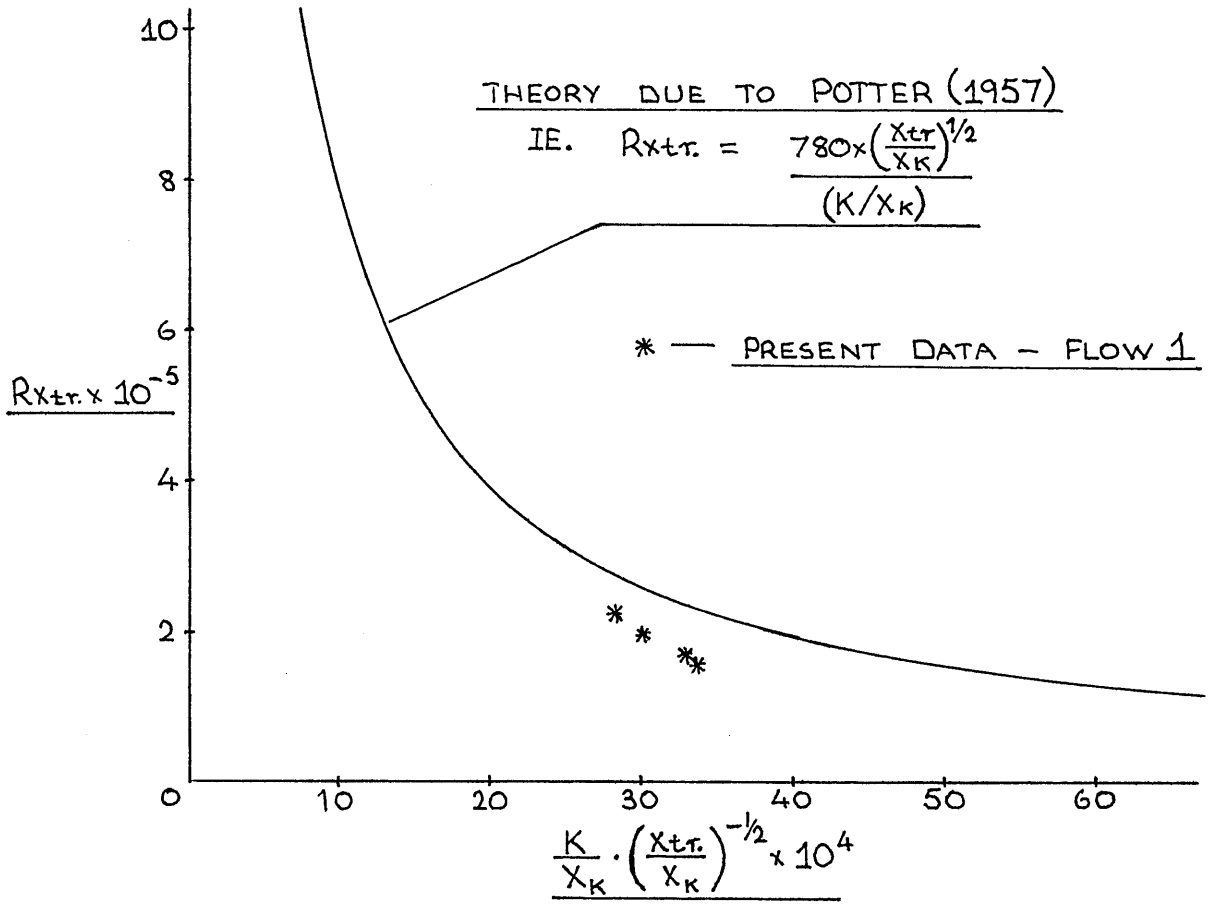

INTERMITTENCY DEVELOPMENT WITH NORMALISED STREAMWISE CO-ORDINATE

DATA POINTS — FLOW 1

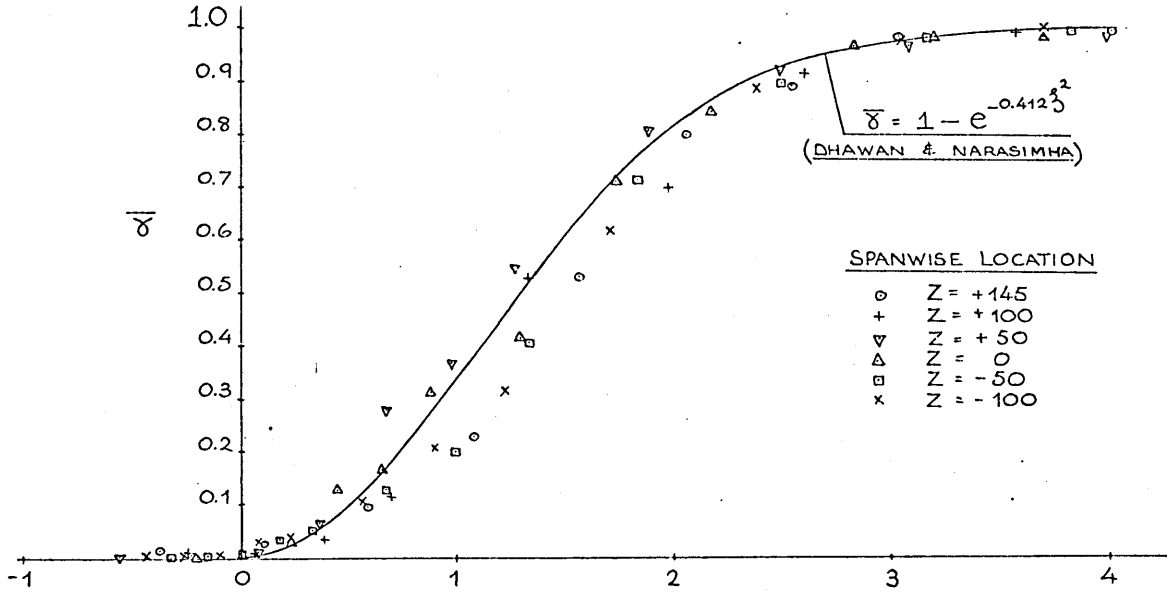

$$\xi = \left(\frac{x - x_t}{\lambda}\right)$$

INTERMITTENCY DEVELOPMENT FITTED TO NORMAL DISTRIBUTION FUNCTION

DATA POINTS — FLOW 1

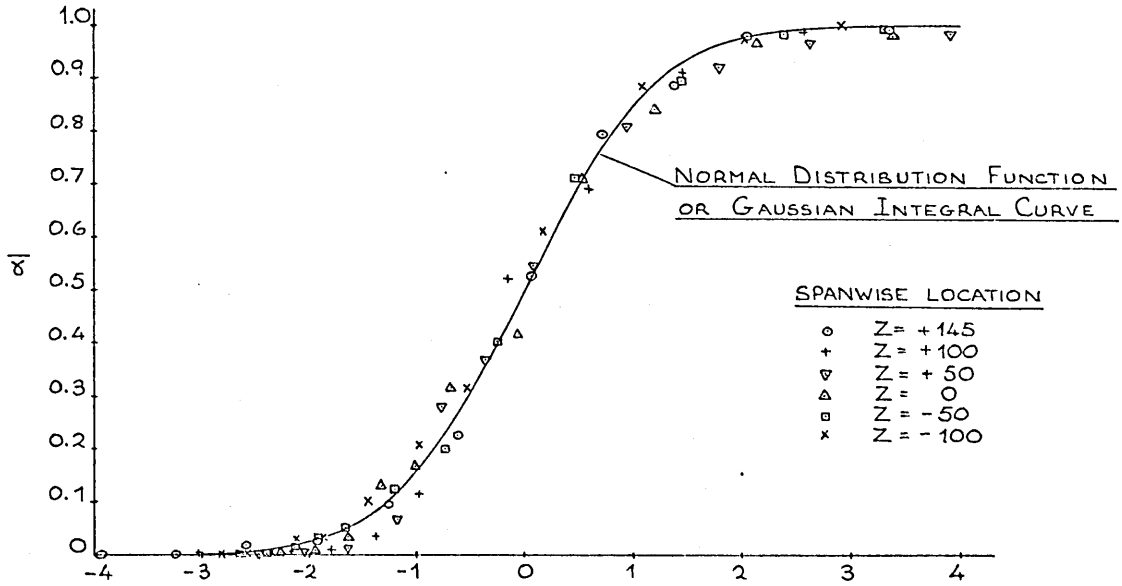

$$\xi = \left(\frac{x - \bar{x}}{\sigma}\right)$$

INTERMITTENCY DEVELOPMENT FITTED TO NORMAL DISTRIBUTION FUNCTION

DATA POINTS — FLOW 2 & 3

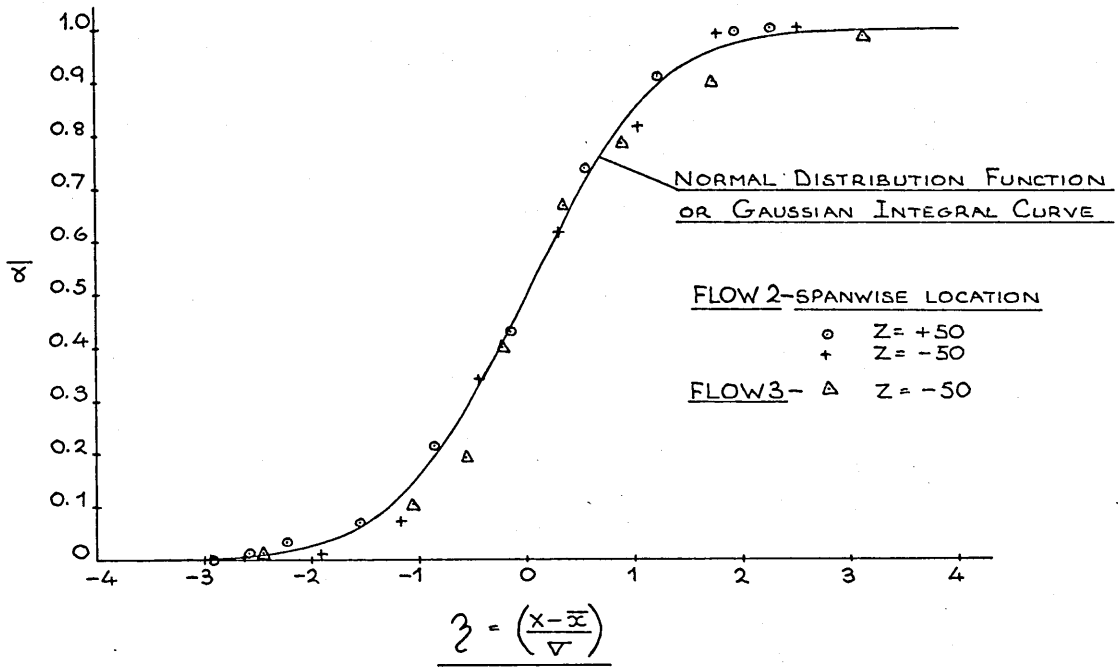

$$\zeta = \left(\frac{x-\bar{x}}{\sigma}\right)$$

FIG.

INTERMITTENCY DEVELOPMENT WITH NORMALISED STREAMWISE CO-ORDINATE

DATA POINTS — FLOW 2 & 3

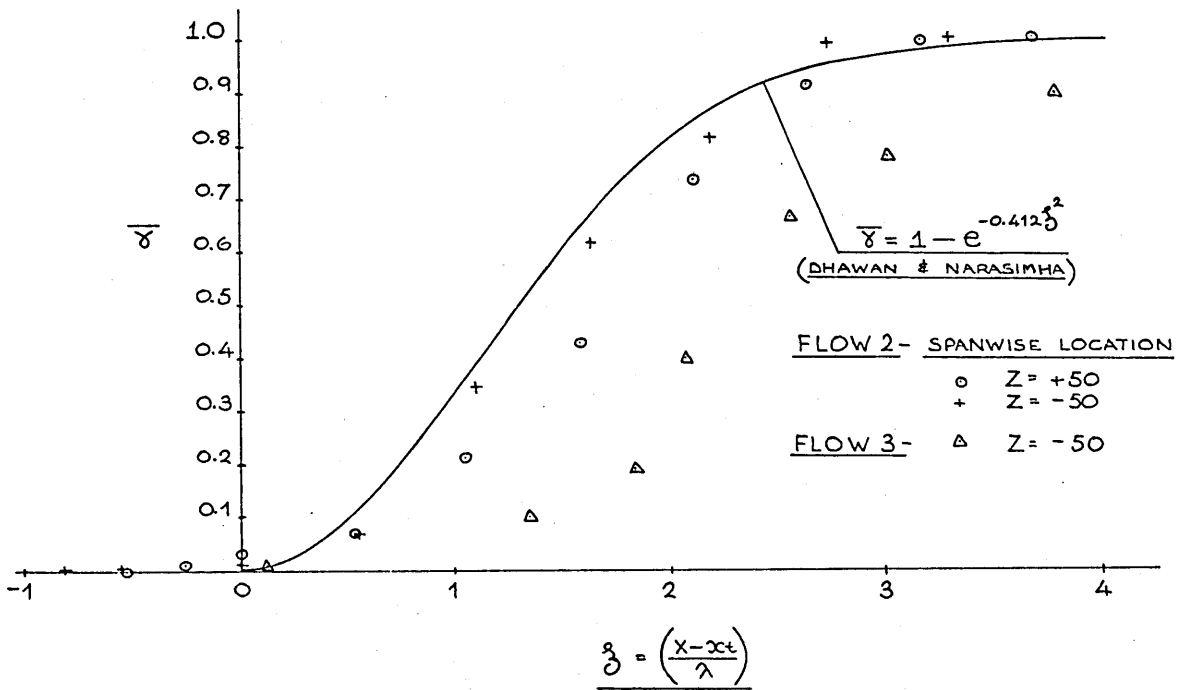

$$\zeta = \left(\frac{x-x_t}{\lambda}\right)$$

FIG.

FLOW 4 - Streamwise Fluctuations behind Isolated Roughness Elements.

Roughness elements located at X = 100mm.
Y-scale, constant at 0.1 volts/cm., or 1.0m/s./cm.
All measurements made at Y = 0.5mm. above the plate.

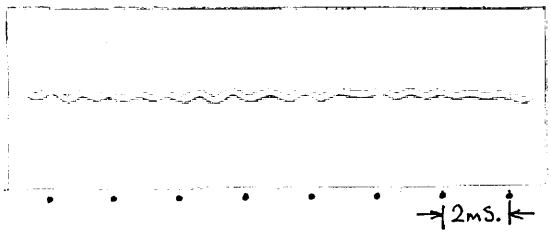

X = 105mm.
Time scale = 2mSecs./DIV.
Intensity, $(u'/Uinf.)_x 100\% = 3.37$
Oscillation frequency = 1500Hz. (approx.)

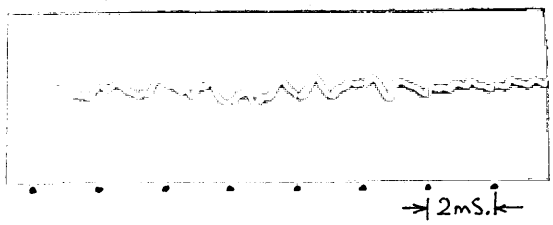

X = 115mm.
Time scale = 2mSecs./DIV.
Intensity, $(u'/Uinf.)_x 100\% = 5.50$

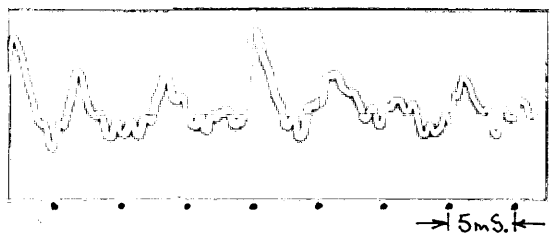

X = 125mm.
Time scale = 5mSecs./DIV.
Intensity, $(u'/Uinf.)_x 100\% = 9.30$

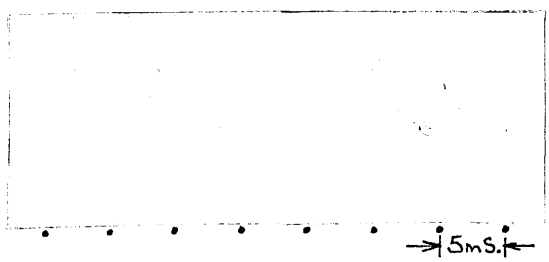

X = 140mm.
Time scale = 5mSecs./DIV.
Intensity, $(u'/Uinf.)_x 100\% = 13.6$

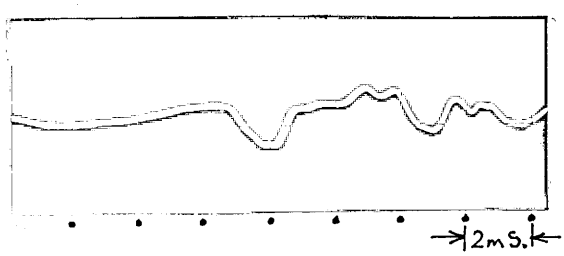

Intermittent character of transition developing behind a two-dimensional trip wire.
Note the absence of large amplitude fluctuations in the laminar region to the left.

FIG. 4.3.4.

FLOW 4 — OSCILLATION INDUCED BEHIND SPHERICAL ROUGHNESS ELEMENTS

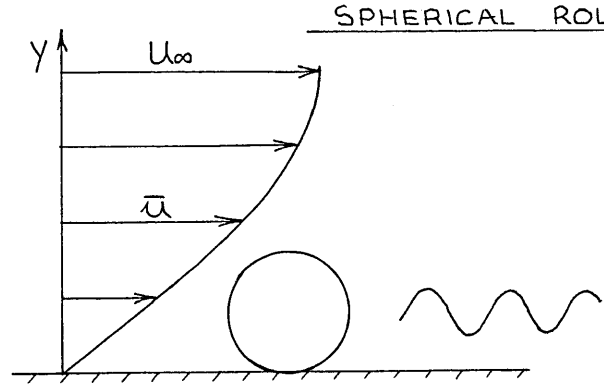

OSCILLATION FREQUENCY (Hz.)

2400
2200
2000
1800
1600
1400
1200
1000
800
600
400

5 6 7 8 9 10 11 12

U_∞ (M/S.)

FLOW 1 — SIMILARITY OF TRANSITIONAL MEAN VELOCITY PROFILES

SPANWISE LOCATION :-
- ○ Z = +145
- \+ Z = +100
- △ Z = +50
- ▽ Z = 0
- □ Z = -50
- ◇ Z = -100

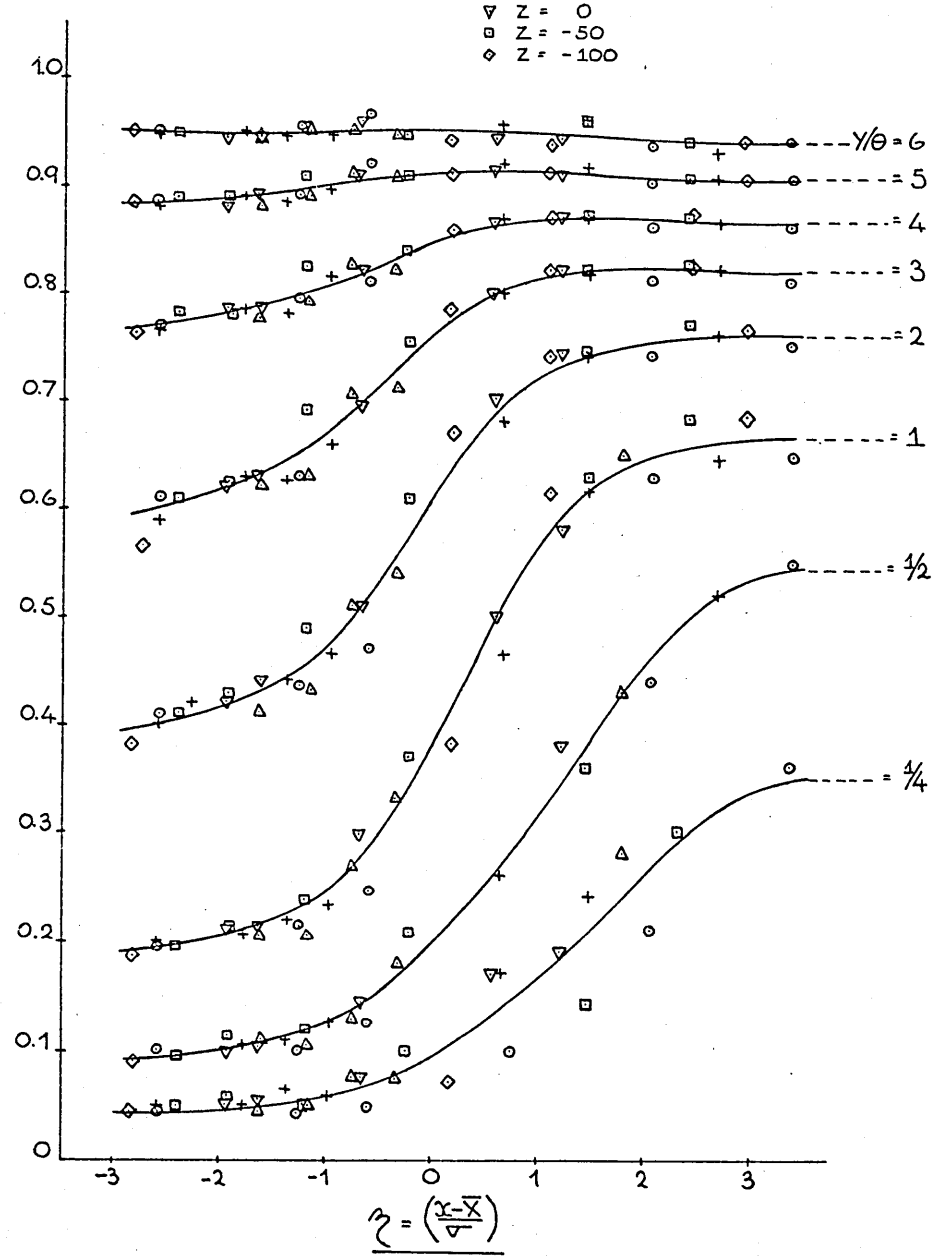

FLOW 2 — SIMILARITY OF TRANSITIONAL MEAN VELOCITY PROFILES

SPANWISE LOCATION :-
- ○ Z = +50
- \+ Z = -50

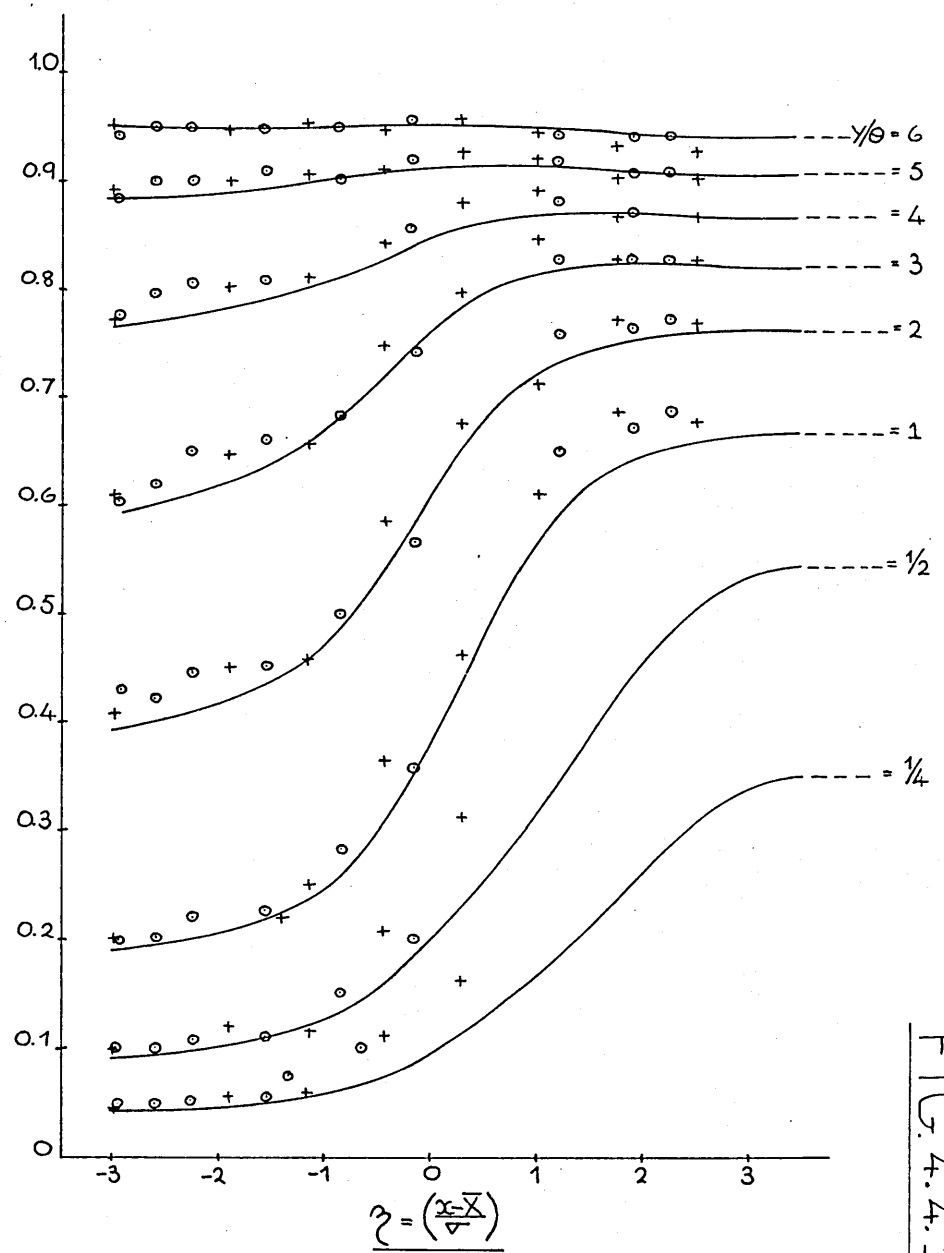

FIG. 4.4.1.

FLOW 1 — TRANSITION SIMILARITY PROFILES OF $(\overline{u}/u_\infty)$

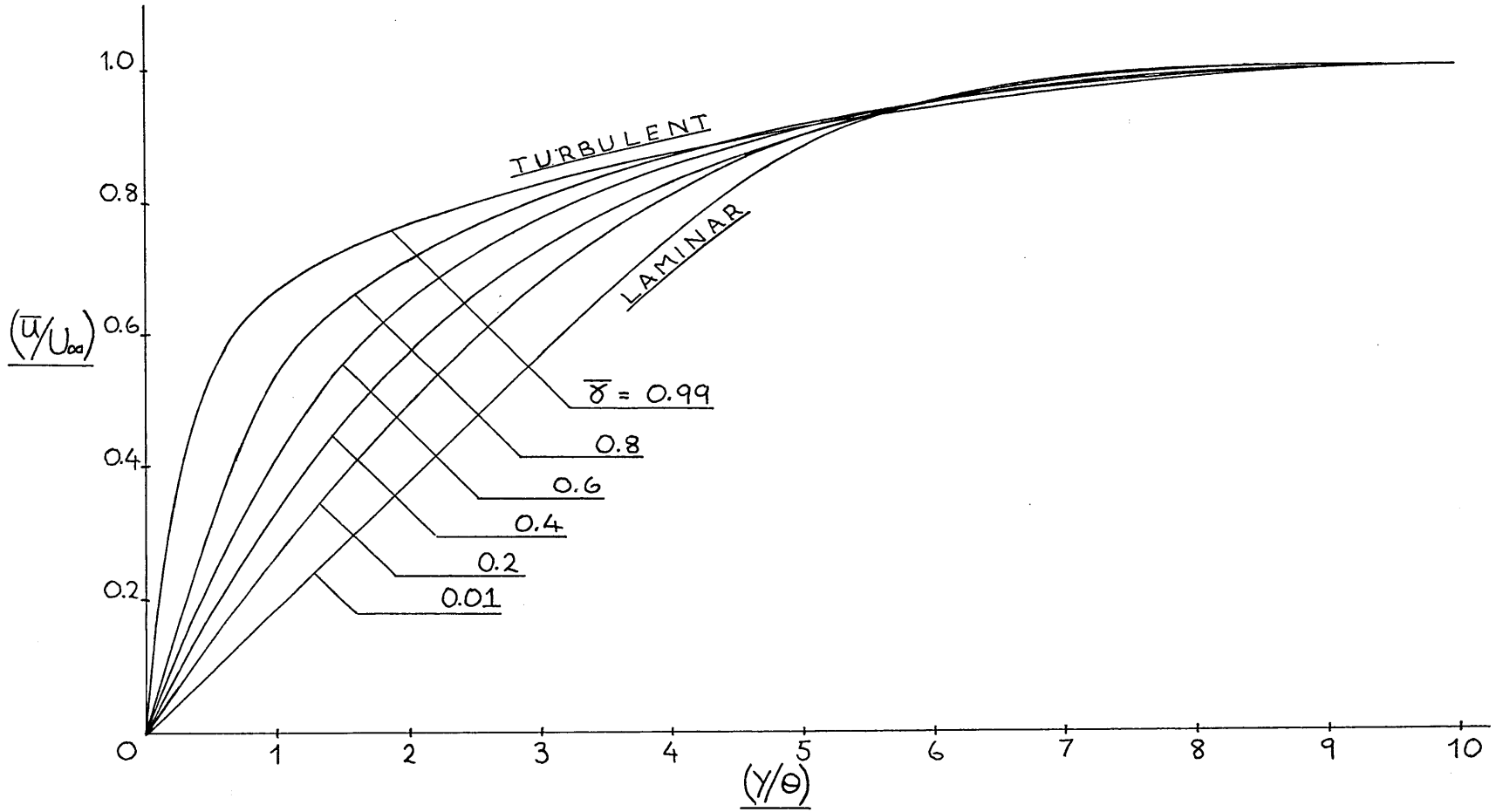

FIG. 4.4.2.

SIMILARITY OF TRANSITIONAL u' FLUCTUATING VELOCITY PROFILES (1)

DATA — FLOWS 1 & 2

FLOW 1		FLOW 2	
⊙	Z = 145	*	Z = 50
+	100	×	-50
▽	50		
△	0		
⊡	-50		
◇	-100		

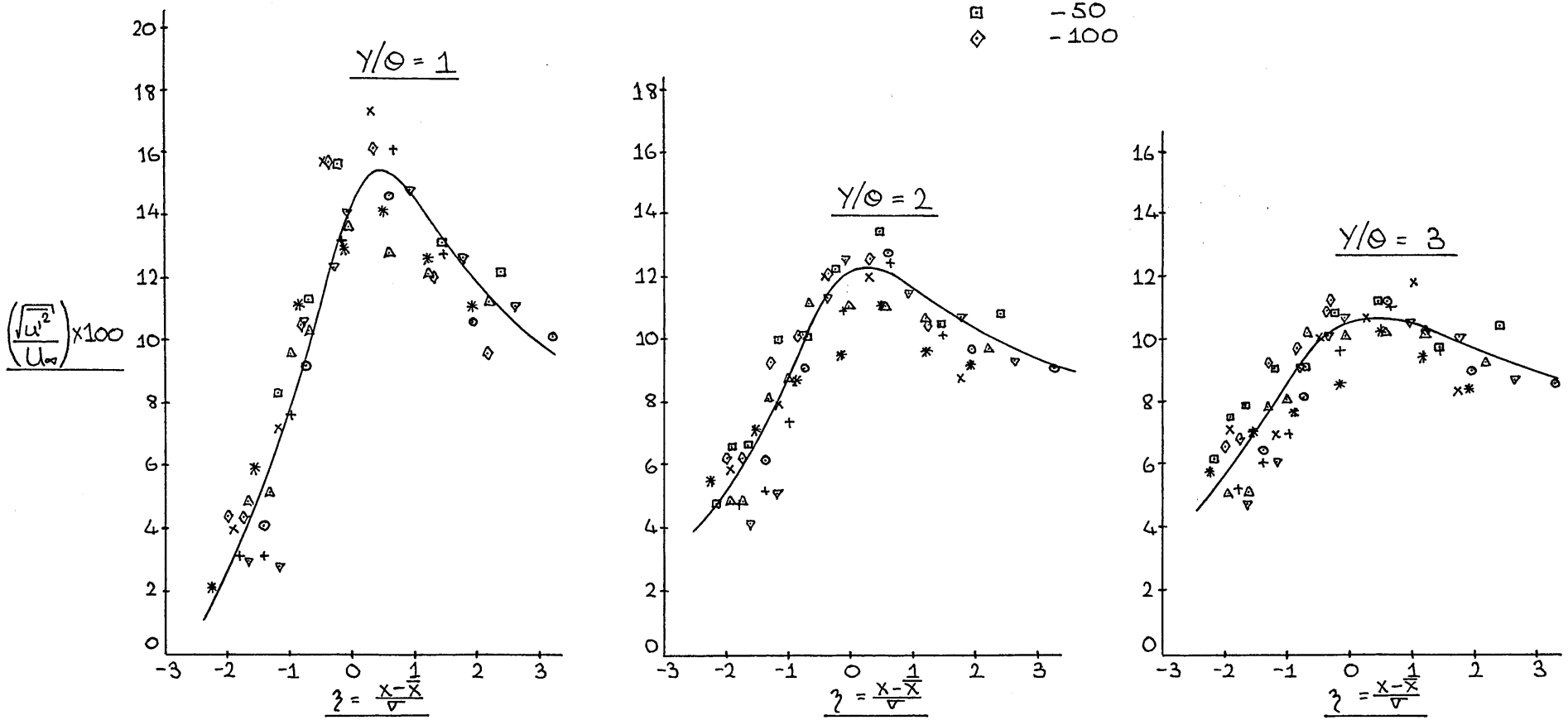

FIG. 4.4.3

SIMILARITY OF TRANSITIONAL u' FLUCTUATING VELOCITY PROFILES (2)

DATA — FLOWS 1 & 2

FLOW 1		FLOW 2	
○	Z = 145	✱	Z = 50
+	100	×	-50
▽	50		
△	0		
□	-50		
◇	-100		

$\left(\frac{\sqrt{\overline{u'^2}}}{U_\infty}\right) \times 100$

Y/θ = 4

Y/θ = 5

Y/θ = 7

Y/θ = 9

Y/θ = 11

$\zeta = \frac{x-\bar{x}}{\nabla}$

FIG. 4.4.4.

FIG. 4.4.5.

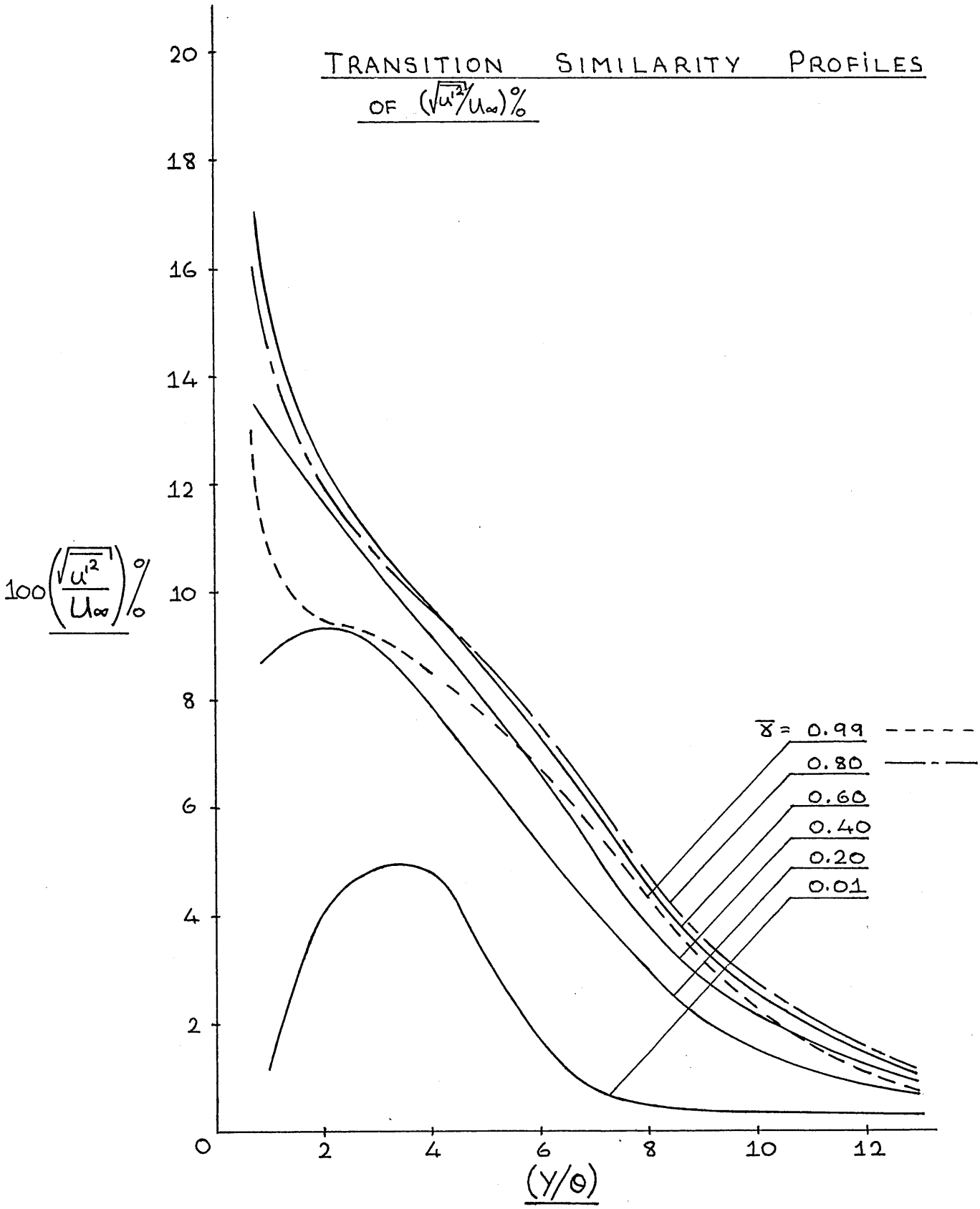
TRANSITION SIMILARITY PROFILES
OF $(\sqrt{u'^2}/U_\infty)\%$
$100\left(\frac{\sqrt{u'^2}}{U_\infty}\right)\%$
20
18
16
14
12
10
8
6
4
2
0
2
4
6
8
10
12
(Y/θ)
$\overline{\gamma}$ = 0.99
0.80
0.60
0.40
0.20
0.01

SIMILARITY OF LOCAL SKIN FRICTION COEFFICIENT THROUGH TRANSITION

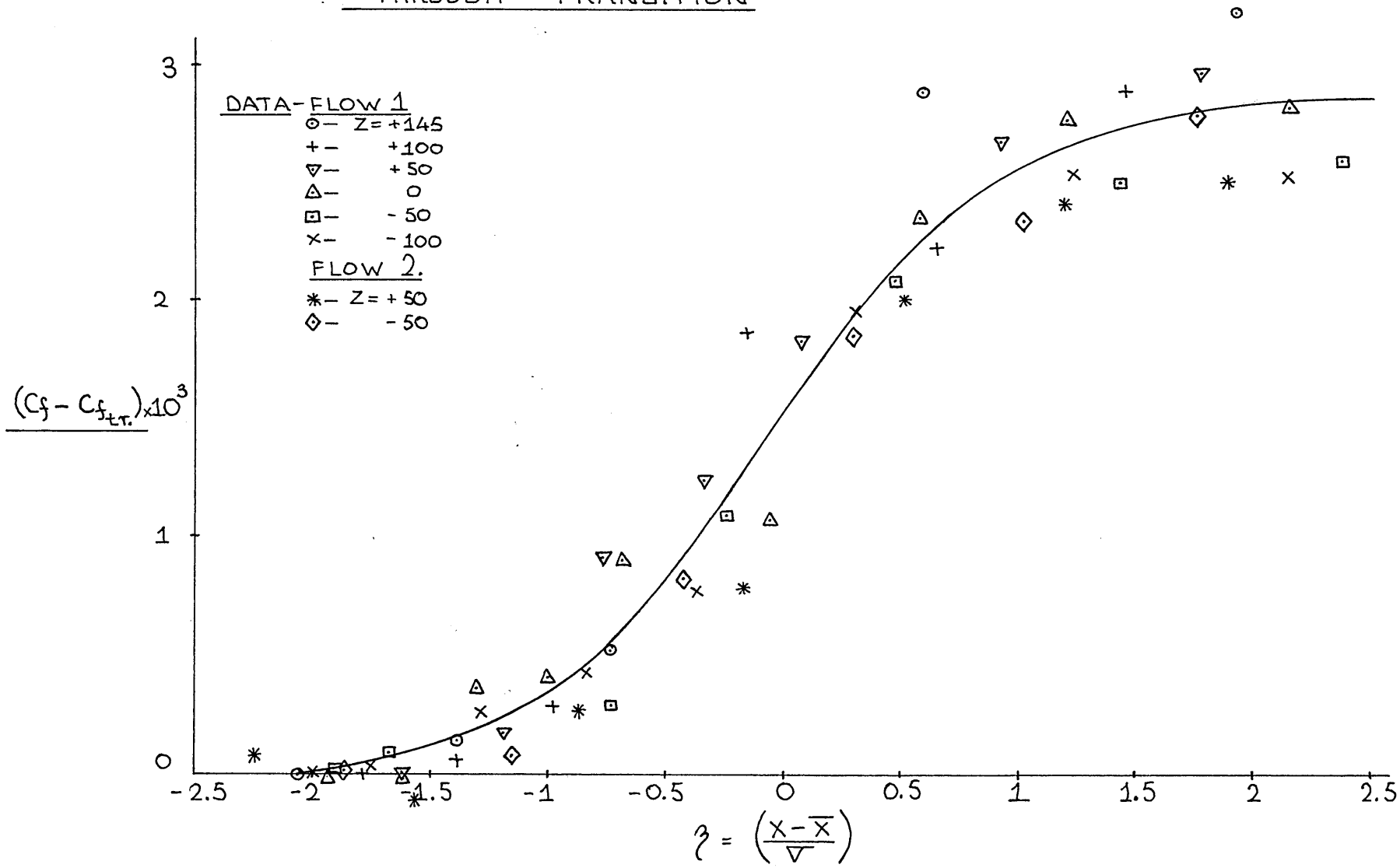

FIG. 4.5.1.

FIG. 4.6.1.

INSTANTANEOUS VELOCITY, $(\bar{u}+u')$ IN A TRANSITIONAL BOUNDARY LAYER

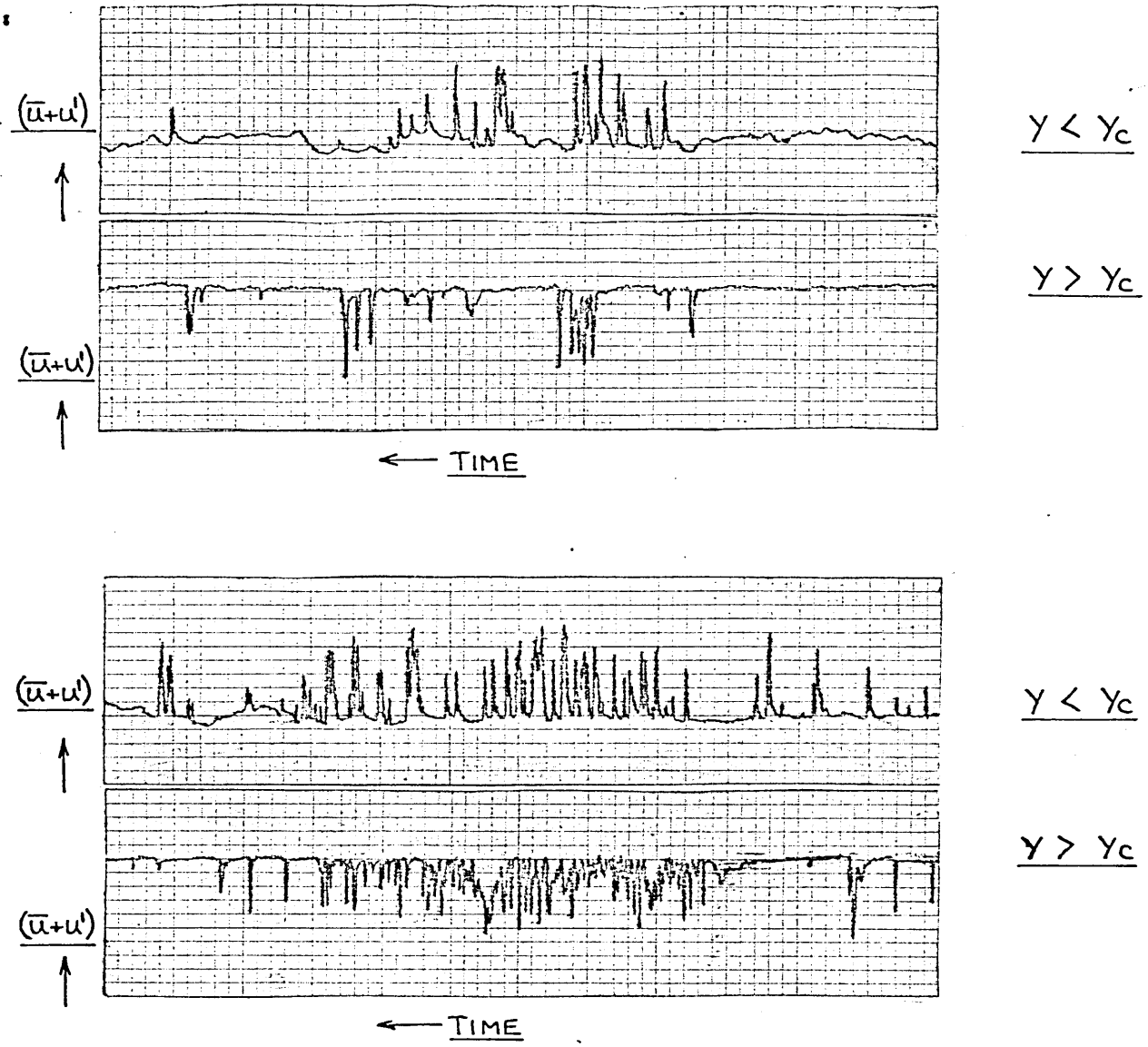

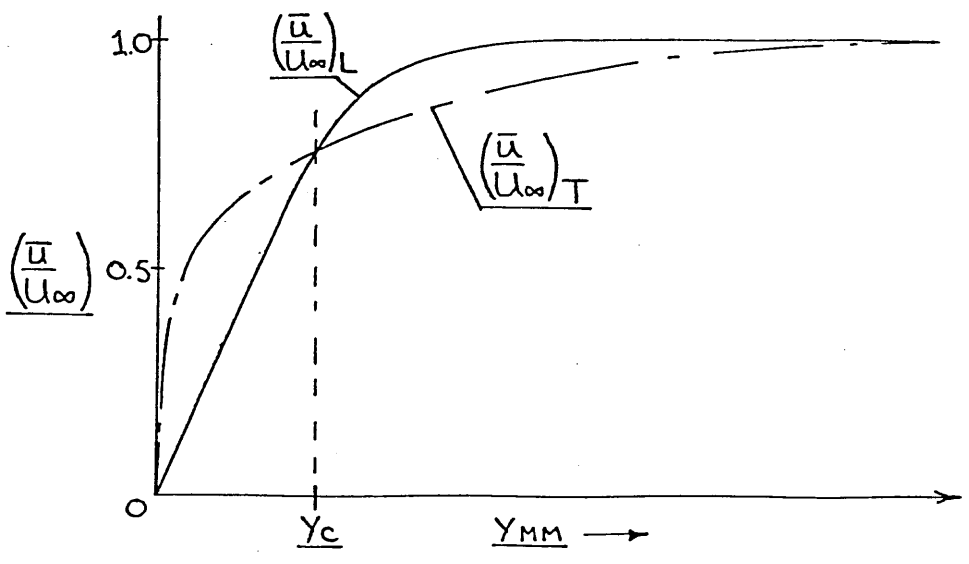

CORRELATIONS OF TRANSITION LENGTH REYNOLDS NUMBERS

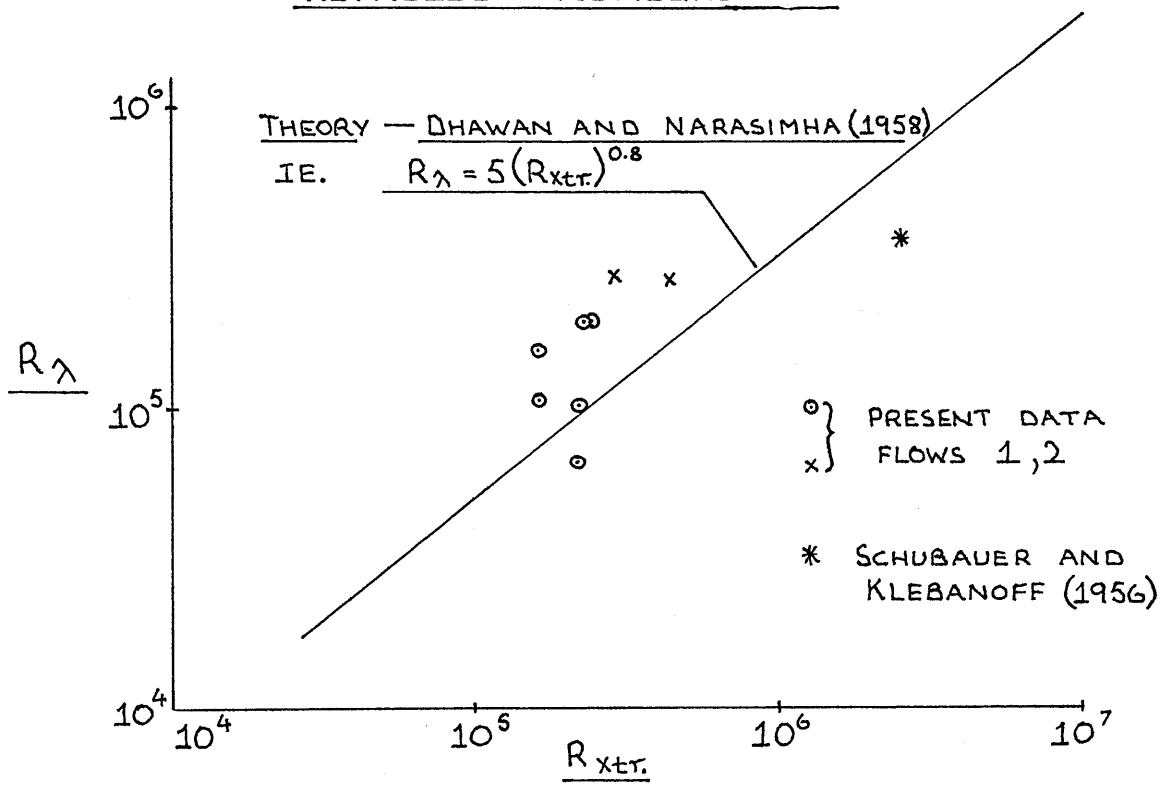

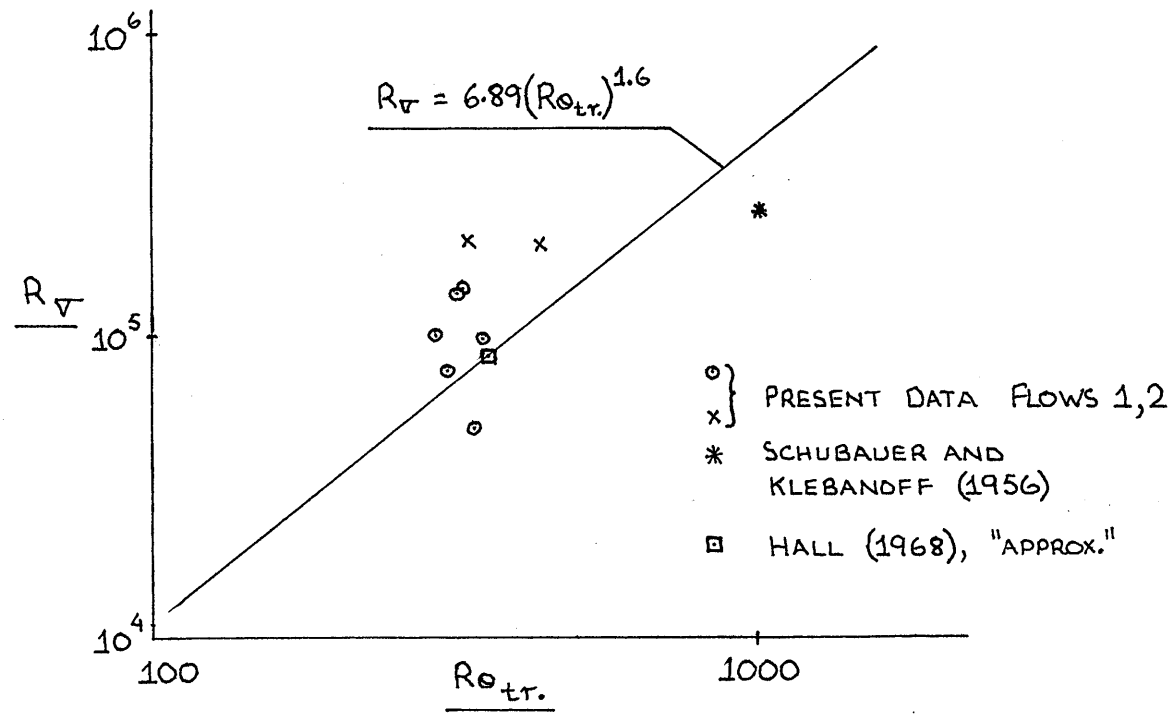

FIG. 4.10.1

SPANWISE VARIATION IN LOCAL SKIN FRICTION COEFFICIENT, FOR FREE TRANSITION AND FOR ABRUPT TRANSITION AT A TRIP WIRE

(MEASUREMENTS MADE BY PRESTON TUBE AT X = 1800 MM.)

Δ% – REPRESENTS THE PERCENTAGE VARIATION FROM THE MEAN VALUE

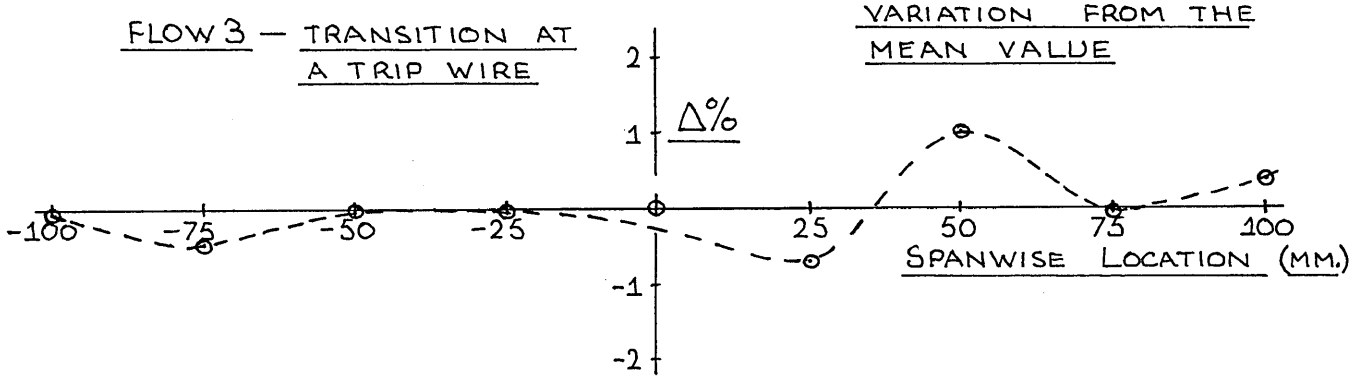

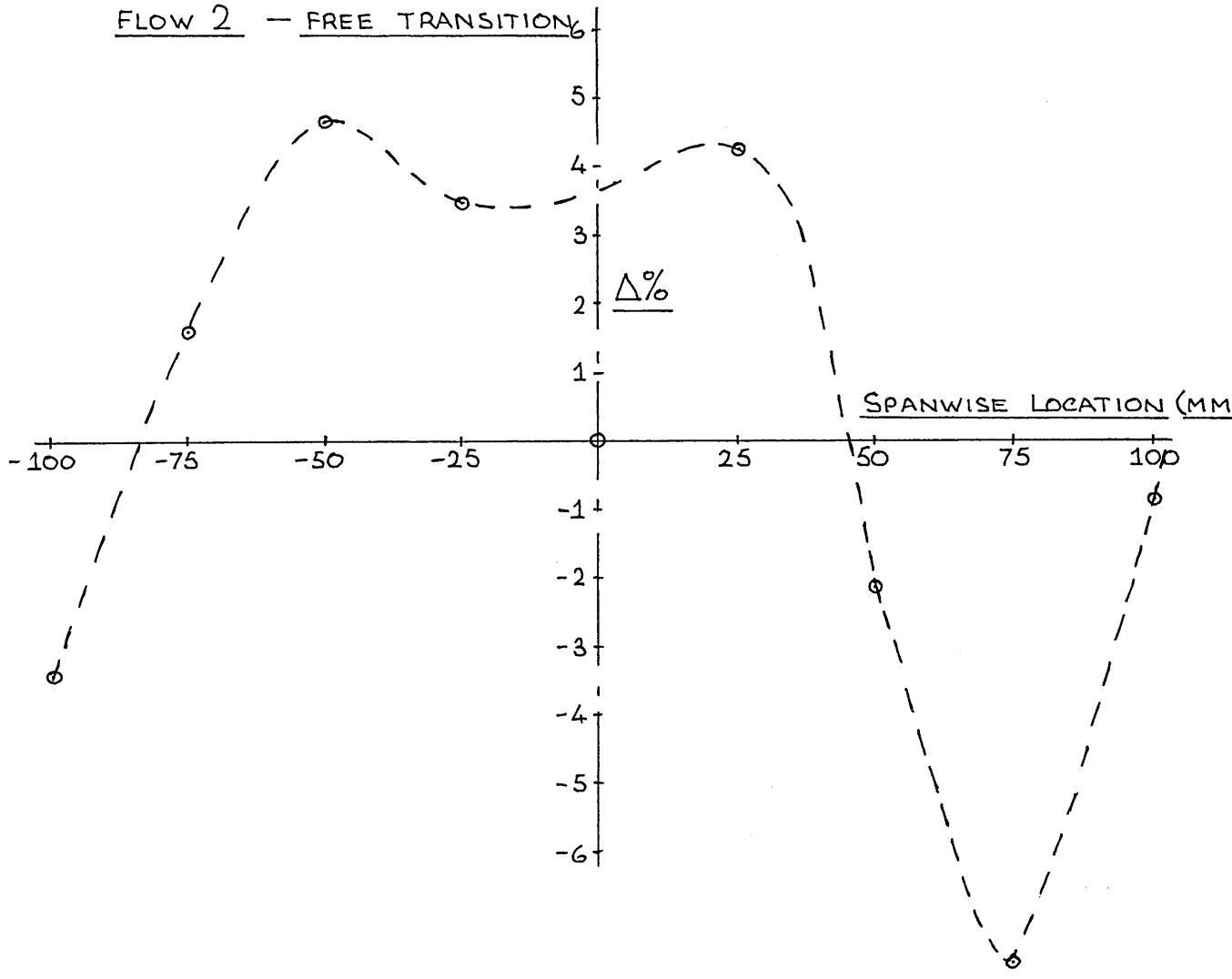

FLOW 4 – PLAN OF WAKE DEVELOPMENT BEHIND SPHERES

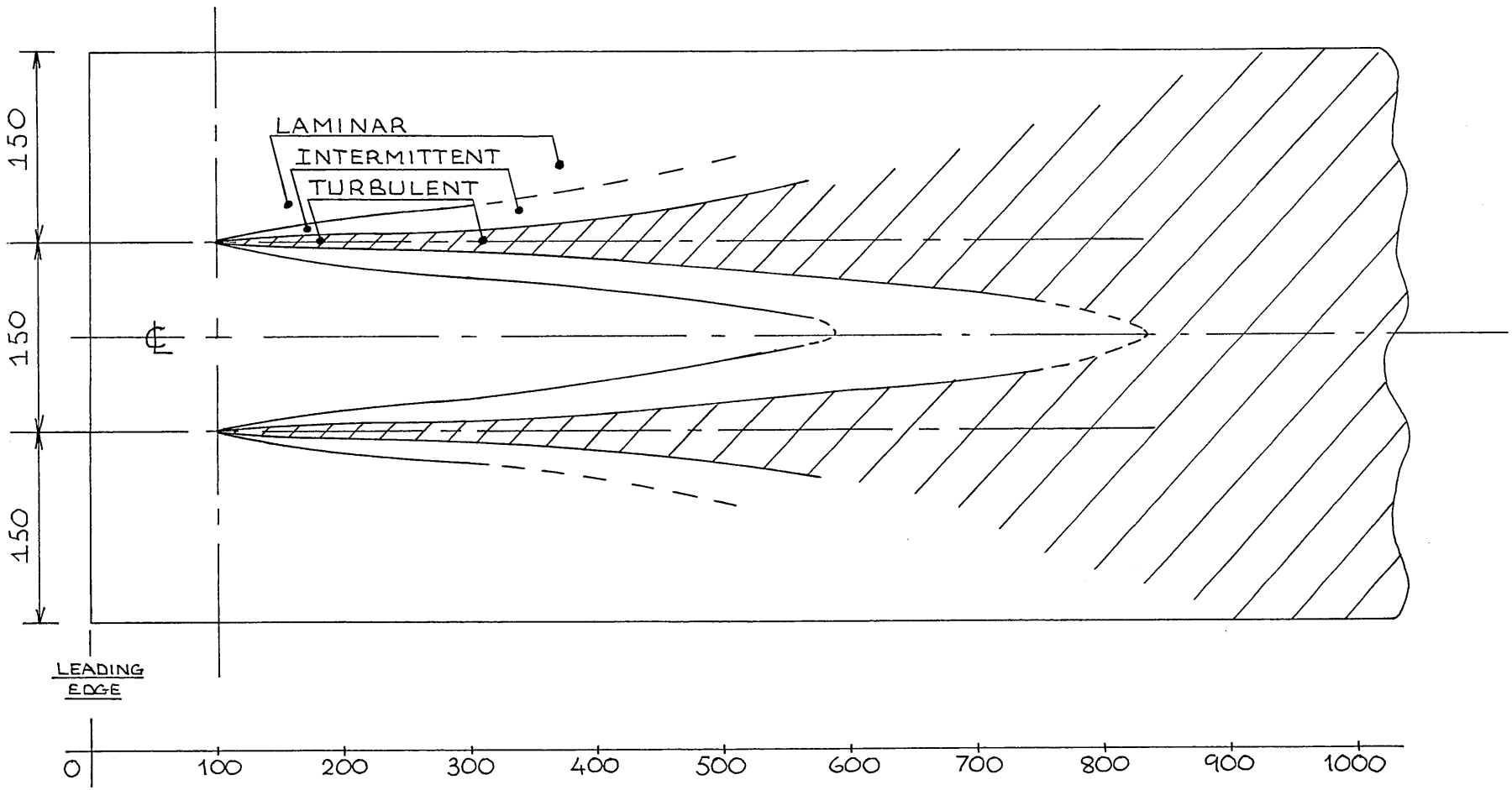

FIG. 4.10.2.

CHAPTER 5.

CALCULATION OF TRANSITIONAL BOUNDARY LAYERS.

A method of calculating the transitional boundary layer in arbitrary pressure gradient flows is developed using existing, well established integral prediction techniques. Transition is modelled on the observation that the region is made up of an alternation between laminar and turbulent flow states, with the relative duration times of each state being determined by the present intermittency function. A simpler "point" transition model is also considered.

BOUNDARY LAYER DEVELOPMENT FROM TRANSITION PROVOKING DEVICES.

CALCULATION OF TRANSITIONAL BOUNDARY LAYERS.

5.1 Introduction.

While prediction techniques for laminar and turbulent boundary layers are in abundance, calculation methods for the transition region between the two flow states are still relatively uncommon. A popular ploy, used in the past, (see Rotta (1962) and Thompson (1967)), is to assume that transition occurs at a point, which is an instantaneous switching station from laminar to turbulent flow. If integral prediction methods are utilised, then the momentum and energy thicknesses are assumed to be continuous at this "transition-point". The initial shape factor, H12, to start the turbulent calculation can be determined from say Garner's criterion, (see Chang (1970)). The assumption of an instantaneous transition point however, leads to discontinuities in the predicted integral parameter and skin friction coefficient distributions. The simple model can therefore result in substantial errors, especially at lower Reynolds numbers.

By modelling the transition region with an intermittency, or related function, a significant improvement can be achieved. The simple transition models of Emmons and Bryson (1950) and Dhawan and Narasimha (1958) are perhaps the first such attempts to calculate the transitional boundary layer. They are both however,

restricted to the zero pressure gradient case. Other, more recent, methods eg. (McDonald and Fish (1973), Forest (1977) and Mari and Mathieu (1977)), are generally applicable in arbitrary pressure gradients. The newer methods, quoted above, are all however differential methods, with the solution of the basic partial differential equations ultimately resulting in "predicted" mean velocity profiles. The profiles are then integrated numerically to give the boundary layer parameters.

The present study is concerned with the development of a general "integral" technique for the calculation of arbitrary pressure gradient , transitional boundary layers in two-dimensional sub-sonic flows. The integral approach is adopted here because the transition region can be modelled more simply, the required input data is considerable less and the computation is less extensive. Two transition models are considered, where model A utilises an approximated intermittency distribution to describe the transition region and model B is based on an assumed instantaneous transition point.

5.2 Transition model A.

The method due to Thwaites (1949), is used for the laminar calculation and the lag-entrainment method due to Green et al. (1977) is used for the turbulent calculation. These respective prediction methods are described in Appendix 5.

The transition region is defined by an intermittency distribution in the form of an approximate Gaussian integral curve.

For computing convenience, a polynomial approximation to the curve is used in the form :-

$$\overline{\gamma} = \frac{1}{2}\left[1 + \frac{\zeta}{|\zeta|}(0.8273\,|\zeta| - 0.094\,|\zeta|^2 - 0.073\,|\zeta|^3 + 0.0165\,|\zeta|^4)\right] \qquad 5.1$$

where $\zeta = \dfrac{(x - \overline{x})}{\sigma}$

$\overline{x}$ = x at $\overline{\gamma} = 0.50$

and σ = the standard deviation of the axial intermittency spread.

The approximating polynomial, eqn. 5.1, is shown in comparison to the Gaussian integral curve in FIG. 5.2.1. The start of transition is defined when $\overline{\gamma} = 0.01$, ie. $\zeta = -2.25$, and the transition region is defined by the range :-

$$0.01 \leq \overline{\gamma} \leq 0.99 \qquad 5.2$$

ie.
$$-2.25 \leq \zeta \leq 2.25 \qquad 5.3$$

For the moment, the start of transition, x_{tr}, and the standard deviation, σ, of the intermittency distribution are simply read in as input data. In an arbitrary boundary layer, where x_{tr} and σ would not be known, the method of Michel (1951) or of van Driest and Blumer (1963) or others, see section 1.11, could be used to determine the start of transition. A correlation of the type discussed in section 4.7 could then be used to establish the length of the transition region.

If the mean transition velocity profile is assumed to have the form given by eqn. 3.27, then it can be shown that the transition integral parameters are given by the following relations, (see also

Dhawan and Narasimha (1958)):-

$$\delta^*_t = (1 - \overline{\gamma})\,\delta^*_L + \overline{\gamma}\,\delta^*_T \qquad 5.4$$

$$\Theta_t = (1 - \overline{\gamma}).\Theta_L\left[(1 - \overline{\gamma}) - \overline{\gamma}H_L\right] + \overline{\gamma}\Theta_T\left[\overline{\gamma} - (1 - \overline{\gamma})H_T\right] + 2\overline{\gamma}(1 - \overline{\gamma})\,Q(\delta_t) \qquad 5.5$$

where $$Q(\delta_t) = \int_0^{\delta_t}(1 - (\overline{u}/U_\infty)_L.(\overline{u}/U_\infty)_T)\,dy. \qquad 5.6$$

and δ_t is the thickness of the transitional boundary layer, taken as $\delta_t = \delta_L$ or $\delta_t = \delta_T$, whichever is the larger. The suffixes t,L and T denoting transitional, laminar and turbulent respectively.

The function $Q(\delta_t)$ necessitates a modelling of the laminar and turbulent mean velocity profiles to enable the integral to be evaluated. The laminar velocity profile is assumed to be represented by a Pohlhausen type, fourth order polynomial :-

ie. $$(\overline{u}/U_\infty)_L = \left[2(y/\delta_L) - 2(y/\delta_L)^3 + (y/\delta_L)^4\right] + \lambda/_6\left[(y/\delta_L) - 3(y/\delta_L)^2 + 3(y/\delta_L)^3 - (y/\delta_L)^4\right] \qquad 5.7$$

where λ is the Pohlhausen pressure gradient parameter given by :-

$$\lambda = \frac{\delta_L^2}{\nu}.\frac{dU_\infty}{dx} \qquad 5.8$$

The laminar calculation however, is performed by Thwaites' method which outputs the parameters Θ_L, H_L, C_{f_L} and M. In the present method, λ was related to M by curve-fitted functions :-

ie. $$\lambda = 10.M.\left[M^2(543 + 6600\,M) - (7 - 31\,M)\right] \quad \{\text{for } M < 0\} \qquad 5.9$$

and $$\lambda = -M.\left[73 - 109\,M + 790\,M^2\right] \quad \{\text{for } M \geqslant 0\} \qquad 5.10$$

The functions are shown in FIG. 5.2.1. and compared with

the relation $M = f(\lambda)$ using the Pohlhausen function for $(\Theta/\delta)_L$. The edge of the laminar boundary layer is obtained by averaging the two Pohlhausen relations for the displacement and momentum thickness.

ie. $$\delta_L = \frac{1}{2}\cdot\Theta_L\cdot\left[\frac{H_L}{0.3 + \frac{\lambda}{120}} + \frac{63}{7.4 - \frac{\lambda}{15} - \frac{\lambda^2}{144}}\right] \qquad 5.11$$

The turbulent velocity profile was modelled on the Coles and Hirst (1968) , wall-wake composite profile, ie. eqn. 3.7., written in the form :-

$$\left(\bar{u}/U_\infty\right)_T = \frac{u_\tau}{U_\infty}\left[\frac{1}{k}.\ \ln.(y^+) + C + \frac{2\mathfrak{C}}{k}\sin^2\left(\pi/2\ .\ y/\delta_T\right)\right] \qquad 5.12$$

The turbulent calculation is performed by Green's lag-entrainment method, with the output parameters, Θ_T, H_T, C_{f_T} and F. Using the wake integrations, ie. eqns. 3.11 and 3.12, to eliminate δ_T, it can be shown that :-

$$\mathfrak{C} = \left[(P - 2.119) + \sqrt{(P - 2.119)^2 + 4(P - 1.333)}\right]/2 \qquad 5.13$$

where $$P = \frac{k(H_T - 1)}{1.5\ H_T}\left(\frac{C_{f_T}}{2}\right)^{-0.5} \qquad 5.14$$

Having thus obtained $\mathfrak{C}$, δ_T is then given via eqn. 3.11 :-

ie. $$\delta_T = \frac{\delta^*_T \times k}{(1 - \mathfrak{C})}\left(\frac{C_{f_T}}{2}\right)^{-0.5} \qquad 5.15$$

Expressing C_{f_T} in terms of the wall friction velocity, u_τ, allows the turbulent velocity profile to be specified. The integral function $Q(\delta_t)$ can then be determined and also, the transitional mean velocity profile, eqn. 3.27, can be described. Equations 5.4 and 5.5 give the transitional integral thicknesses δ^*_t and Θ_t and the velocity profile shape factor is then :-

$$H_t = \delta^*_t/\Theta_t \qquad 5.16$$

The transitional local skin friction coefficient is determined from eqn. A. 4.13, see Appendix 4, which completes the analysis.

It was found that the turbulent calculation by the lag-entrainment method could not be started at the origin, taken to be the start of transition, as this necessitates $\Theta_{T_o} = 0$. This then causes R_Θ to be zero and results in numerical difficulties in the skin friction relations. To overcome the problem, the turbulent momentum thickness at the origin of the turbulent boundary layer was assumed to be given by :-

$$\Theta_{T_o} = \Theta_L/5 \qquad 5.17$$

and the initial shape factor H_T was assumed to be equal to 1.7. These arbitrary assumptions were then maintained until $\overline{\gamma} = 0.10$, ie. $\zeta = -1.25$, where the turbulent calculation was continued by the lag-entrainment method.

The computer program LTBL and subroutines THWAIT, RUNGE, TCF and TRAN perform the calculation of the transitional boundary layer and these are listed in Appendix 3. along with the corresponding flow diagrams.

5.3 Transition model B.

The simpler model of an assumed transition "point" was also considered in order to assess the limitations of such a model. The transition point is defined, for the purpose of analysis, as the axial length where the mean value of intermittency near the wall

is 0.50. The laminar calculation was continued up to this point and the momentum thickness was assumed to be continuous.

ie. $$(\theta_L)_{xtr} = (\theta_T)_{xtr}$$

To determine the initial value of the turbulent shape factor, Garner's criterion, (see Chang (1970)), was employed. If the transition is at, or downstream, of the point of maximum velocity, then Garner's criterion gives :-

$$H_{T_o} = 1.4 - \frac{\theta_{tr}}{U_\infty}.\frac{dU_\infty}{dx}\Big/0.0135 \qquad 5.18$$

For a zero pressure gradient, the criterion then suggests that H_{T_o} invariably equals 1.4 at transition.

With the necessary input parameters thus obtained, the turbulent calculation can then proceed.

The computer program HEAD, see Appendix 3, which is the entrainment method due to Green (1968), carries out the turbulent analysis and Thwaites' method was again used for the laminar analysis.

5.4 Comparison of models A and B.

The predictions of the transitional boundary layers, according to models A and B, are shown plotted against the data of Schubauer and Klebanoff (1956) and against the present data, see FIGS. 5.4.1. and 5.4.2. The numerical values for the prediction of Schubauer and Klebanoff's flow are also included in TABLE 5.4. It is seen that the simple model B, in fact, gives a good account of the development of the momentum thickness, but the assumed instantaneous transition point is not representative of the local skin friction or shape factor distributions through transition.

Transition model A however, results in a very reasonable distribution for all the boundary layer parameters. The predicted displacement and momentum thicknesses near the end of transition against Schubauer and Klebanoff's data however, appears to be slightly low. It is not known if the original velocity profiles, from which the data was obtained , were corrected to true mean velocity profiles, see section 3.5, and so the "error" would not seem to be too significant.

Model A, in addition, predicts the transitional mean velocity profiles and these are compared against the measured profiles from FLOW 2, A The agreement is seen to be quite good at lower intermittencies, but less so as the intermittency approaches 1.0. The deviation is partly due to delaying the turbulent calculation in the initial stages of transition, but also due to the assumed velocity distribution for $(\overline{u}/u)_T$ and the approximate manner in which the profile parameters α and δ_T are obtained.

SEE FIG 5.4.3.

The computer simulations do however show that, with some further development, the integral technique can give a reasonable estimate of the transitional boundary layer parameters. The method is also capable of application to transitional boundary layer prediction in pressure gradient flows, although its performance in such flows has not yet been tested. The effect of a pressure gradient on the intermittency distribution also remains to be established.

APPROXIMATING POLYNOMIAL TO GAUSSIAN DISTRIBUTION FUNCTION

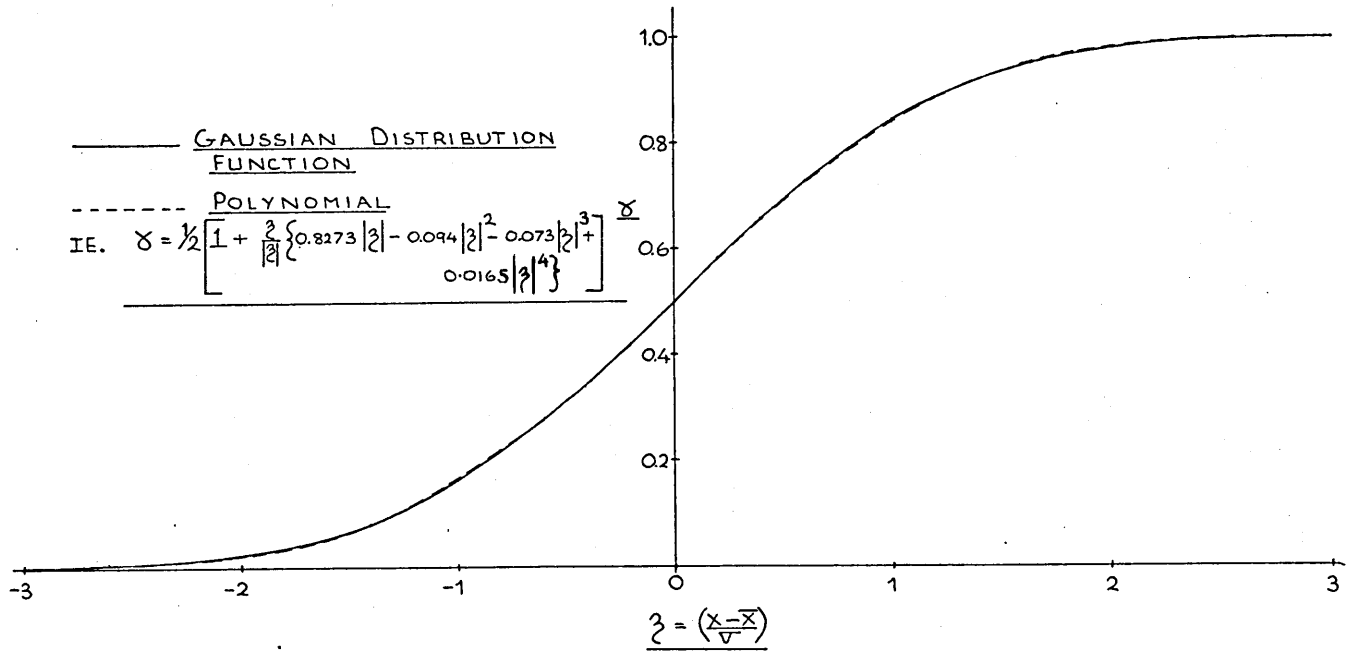

POLYNOMIAL RELATIONSHIPS BETWEEN PRESSURE GRADIENT PARAMETERS

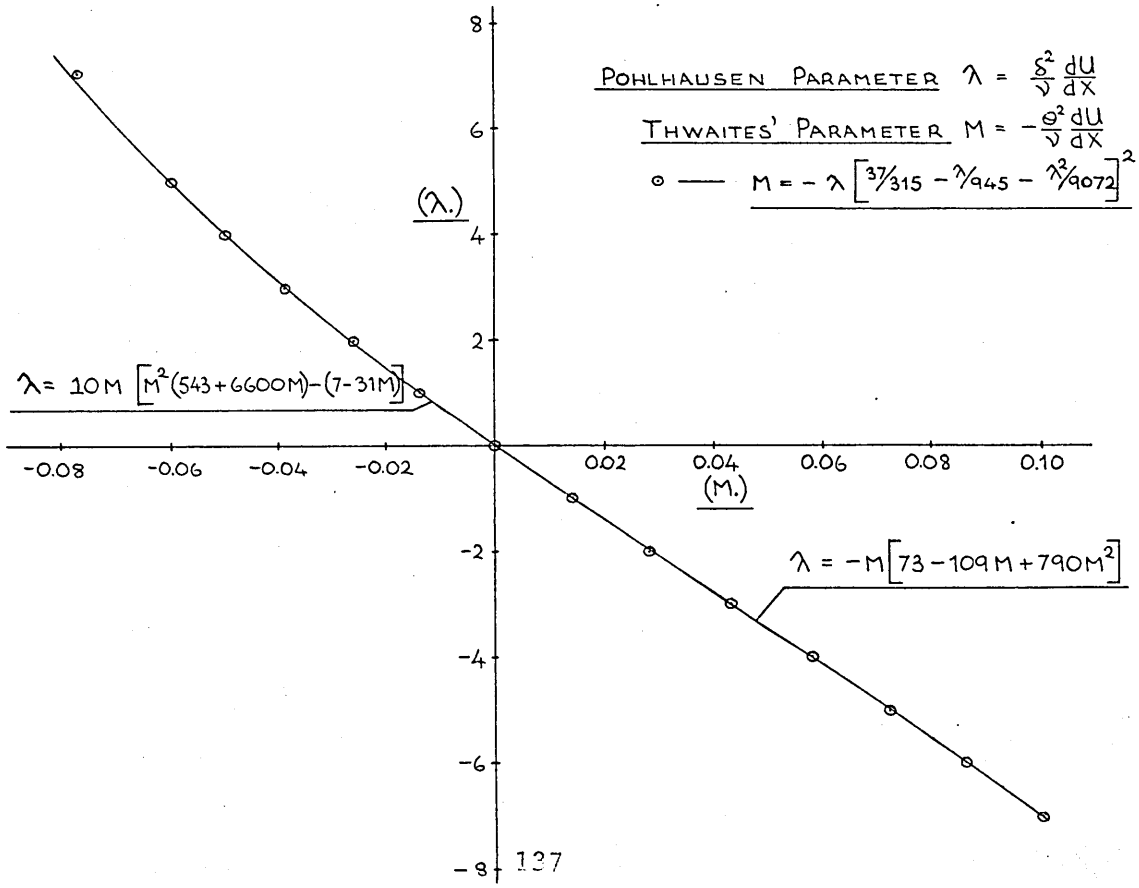

TABLES 5.4

COMPUTER PREDICTIONS OF SCHUBAUER AND KLEBANOFF'S (1956), TRANSITIONAL BOUNDARY LAYER

MODEL A.

```
RUN LTBL
      LAMINAR/TURBULENT BOUNDARY LAYER GROWTH
      BY THWAITES AND LAG ENTRAINMENT METHOD

      AIR TEMP. IN DEG.C= 20
      ATMOS.PRESS.IN MM HG= 760
      FREESTREAM VELOCITY DISTRIBUTION:
      U/UO=E(Q)**P+A+B(Q)+C(Q)**2+D(Q)**3
      WHERE Q=X/XMAX
            E= 0
            P= 0
            A= 1
            B= 0
            C= 0
            D= 0
            UO IN M/S= 24.4

      STARTING POINT IN MM= 1500
      STEP LENGTH IN MM= 10
      LENGTH OF PLATE IN MM= 2600
      INITIAL MOMENTUM THICKNESS IN MM= 0.638
      START OF TRANSITION= 1600
      STANDARD DEVIATION FOR TRANSITION
            INTERMITTENCY DISTRIBUTION= 150
```

X (MM)	DSTR (MM)	THETA (MM)	H(12)	CF
1500.0	1.665	0.638	2.61	0.000424
1550.0	1.693	0.649	2.61	0.000417
1600.0	1.704	0.661	2.58	0.000431
1650.0	1.709	0.674	2.54	0.000450
1700.0	1.689	0.688	2.45	0.000501
1750.0	1.633	0.702	2.33	0.000606
1800.0	1.576	0.703	2.24	0.000776
1850.0	1.507	0.710	2.12	0.001023
1900.0	1.439	0.726	1.98	0.001354
1950.0	1.384	0.757	1.83	0.001770
2000.0	1.362	0.806	1.69	0.002207
2050.0	1.380	0.874	1.58	0.002609
2100.0	1.433	0.954	1.50	0.002941
2150.0	1.514	1.044	1.45	0.003268
2200.0	1.615	1.139	1.42	0.003485
2250.0	1.728	1.233	1.40	0.003569
2300.0	1.845	1.324	1.39	0.003588
2350.0	1.962	1.413	1.39	0.003544
2400.0	2.077	1.502	1.38	0.003504
2450.0	2.191	1.589	1.38	0.003467
2500.0	2.304	1.675	1.38	0.003431
2550.0	2.415	1.760	1.37	0.003398
2600.0	2.526	1.845	1.37	0.003366

```
STOP

END OF EXECUTION
CPU TIME: 6.16  ELAPSED TIME: 2:24.60
EXIT
```

MODEL B.

```
      LAMINAR/TURBULENT BOUNDARY LAYER GROWTH
      BY THWAITES AND ENTRAINMENT METHOD. WITH
      AN ASSUMED TRANSITION "POINT".
      TRANSITION AT X = 1910mm.
```

X (MM)	DSTR (MM)	THETA (MM)	H(12)	CF
1500.0	1.665	0.638	2.61	0.000424
1550.0	1.693	0.649	2.61	0.000417
1600.0	1.721	0.659	2.61	0.000411
1650.0	1.748	0.670	2.61	0.000404
1700.0	1.775	0.680	2.61	0.000398
1750.0	1.801	0.690	2.61	0.000392
1800.0	1.827	0.700	2.61	0.000387
1850.0	1.853	0.710	2.61	0.000381
1900.0	1.878	0.720	2.61	0.000376

```
STOP
```

TRANSITION POINT

1910	1.010	0.720	1.40	0.004162

HEAD/GREEN METHOD FOR TUBULENT BOUNDARY LAYERS

X-MM	TH-MM	DSTR-MM	H	CF
1950.00	0.822	1.155	1.406	0.00398
2000.00	0.920	1.294	1.408	0.00385
2050.00	1.015	1.428	1.407	0.00376
2100.00	1.108	1.557	1.406	0.00368
2150.00	1.199	1.683	1.404	0.00361
2200.00	1.288	1.806	1.402	0.00355
2250.00	1.376	1.927	1.400	0.00350
2300.00	1.463	2.045	1.398	0.00346
2350.00	1.549	2.162	1.396	0.00341
2400.00	1.634	2.277	1.394	0.00338
2450.00	1.718	2.390	1.392	0.00334
2500.00	1.801	2.503	1.390	0.00331
2550.00	1.883	2.613	1.388	0.00328
2600.00	1.965	2.723	1.386	0.00325
2650.00	2.046	2.832	1.384	0.00323

FIG 5.4.1

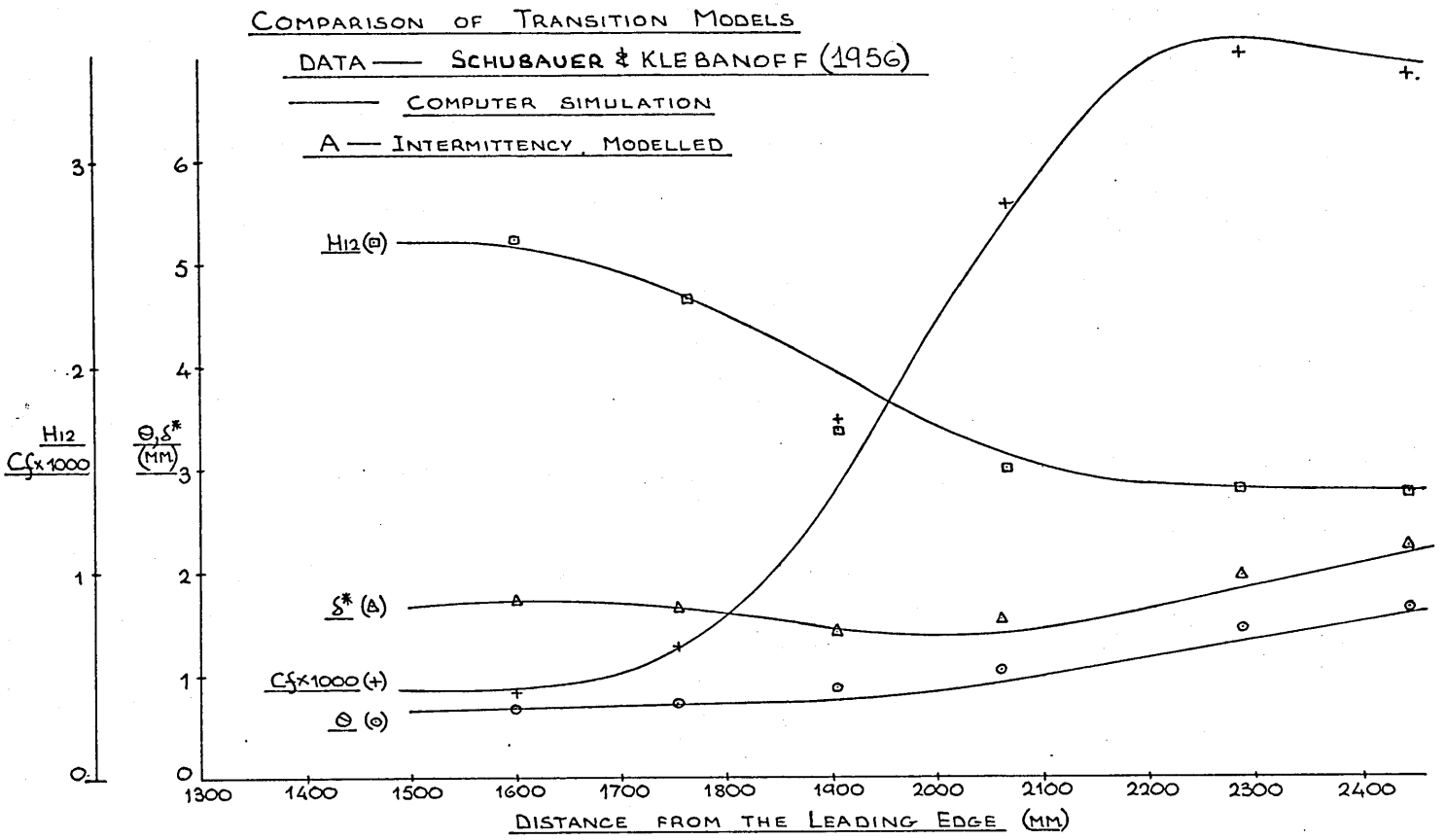
COMPARISON OF TRANSITION MODELS
DATA — SCHUBAUER & KLEBANOFF (1956)
——— COMPUTER SIMULATION
A — INTERMITTENCY, MODELLED
H12 (□)
δ* (Δ)
Cfx1000 (+)
Θ (○)
H12 / Cfx1000
Θ, δ* (MM)
DISTANCE FROM THE LEADING EDGE (MM)

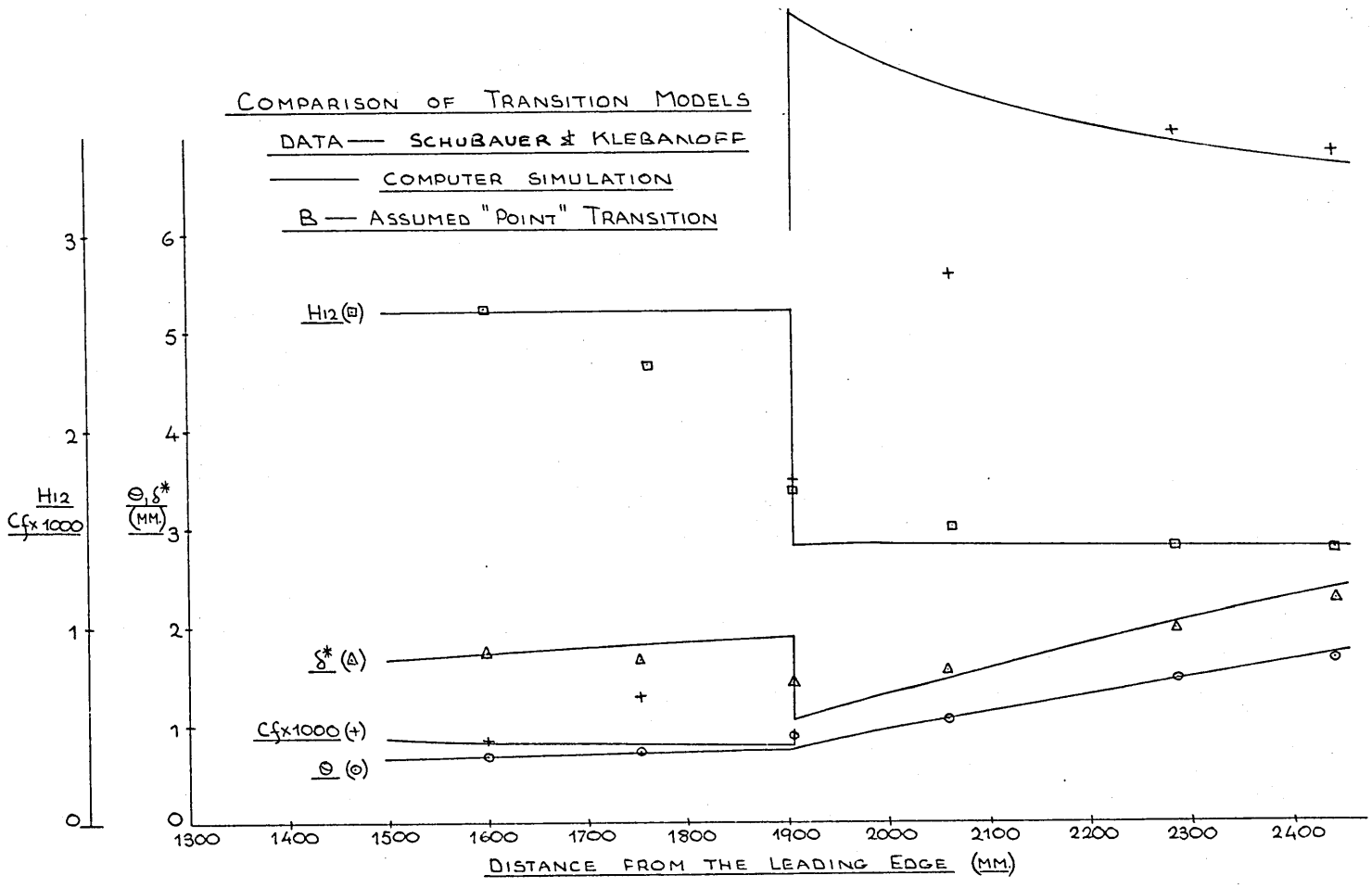
COMPARISON OF TRANSITION MODELS
DATA — SCHUBAUER & KLEBANOFF
——— COMPUTER SIMULATION
B — ASSUMED "POINT" TRANSITION
H12 (□)
δ* (Δ)
Cfx1000 (+)
Θ (○)
H12 / Cfx1000
Θ, δ* (MM)
DISTANCE FROM THE LEADING EDGE (MM)

FIG 5.4.2.

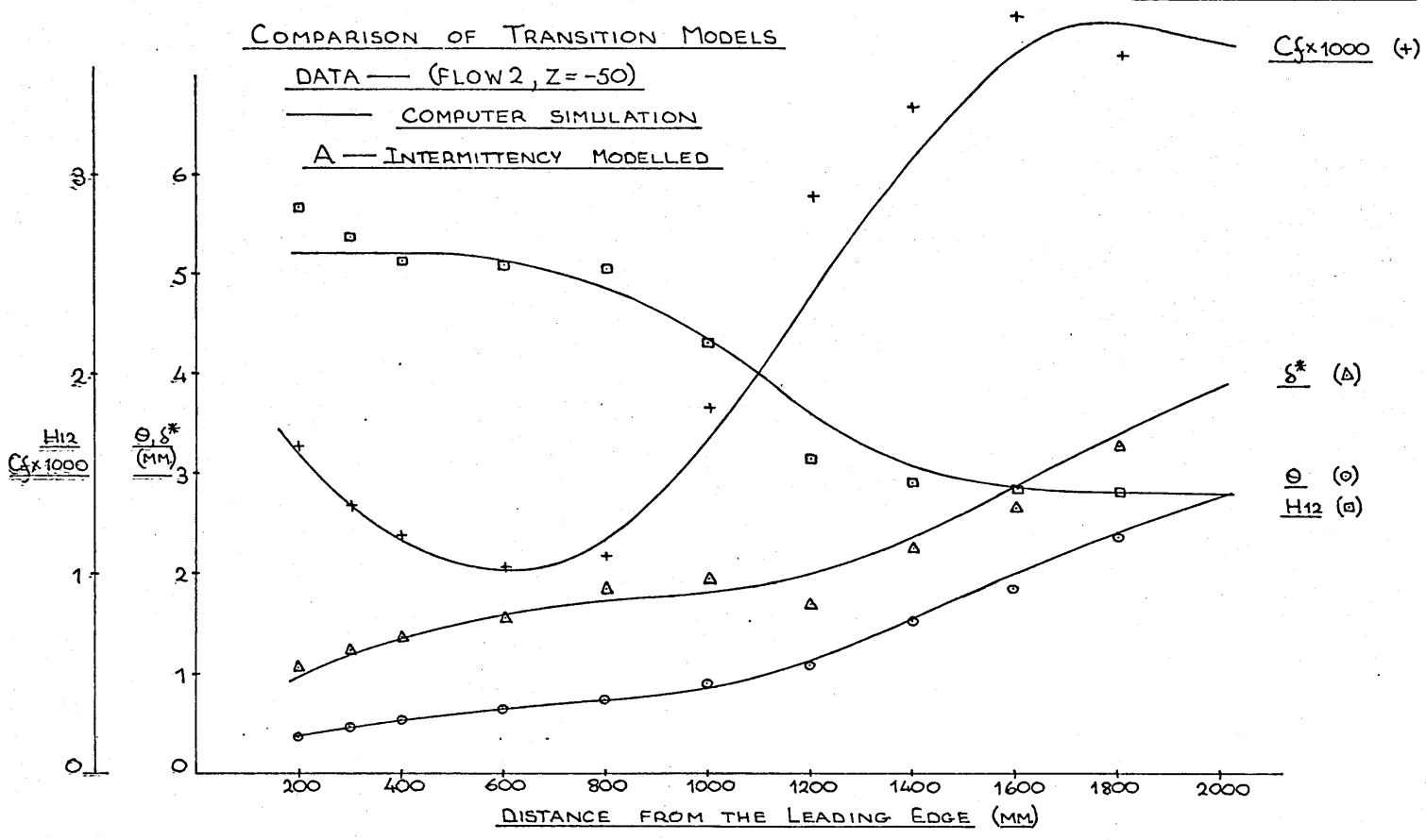
COMPARISON OF TRANSITION MODELS
DATA — (FLOW 2, Z = -50)
——— COMPUTER SIMULATION
A — INTERMITTENCY MODELLED
Cfx1000 (+)
δ* (Δ)
θ (○)
H12 (□)
H12 / Cfx1000
θ, δ* (MM)
DISTANCE FROM THE LEADING EDGE (MM)

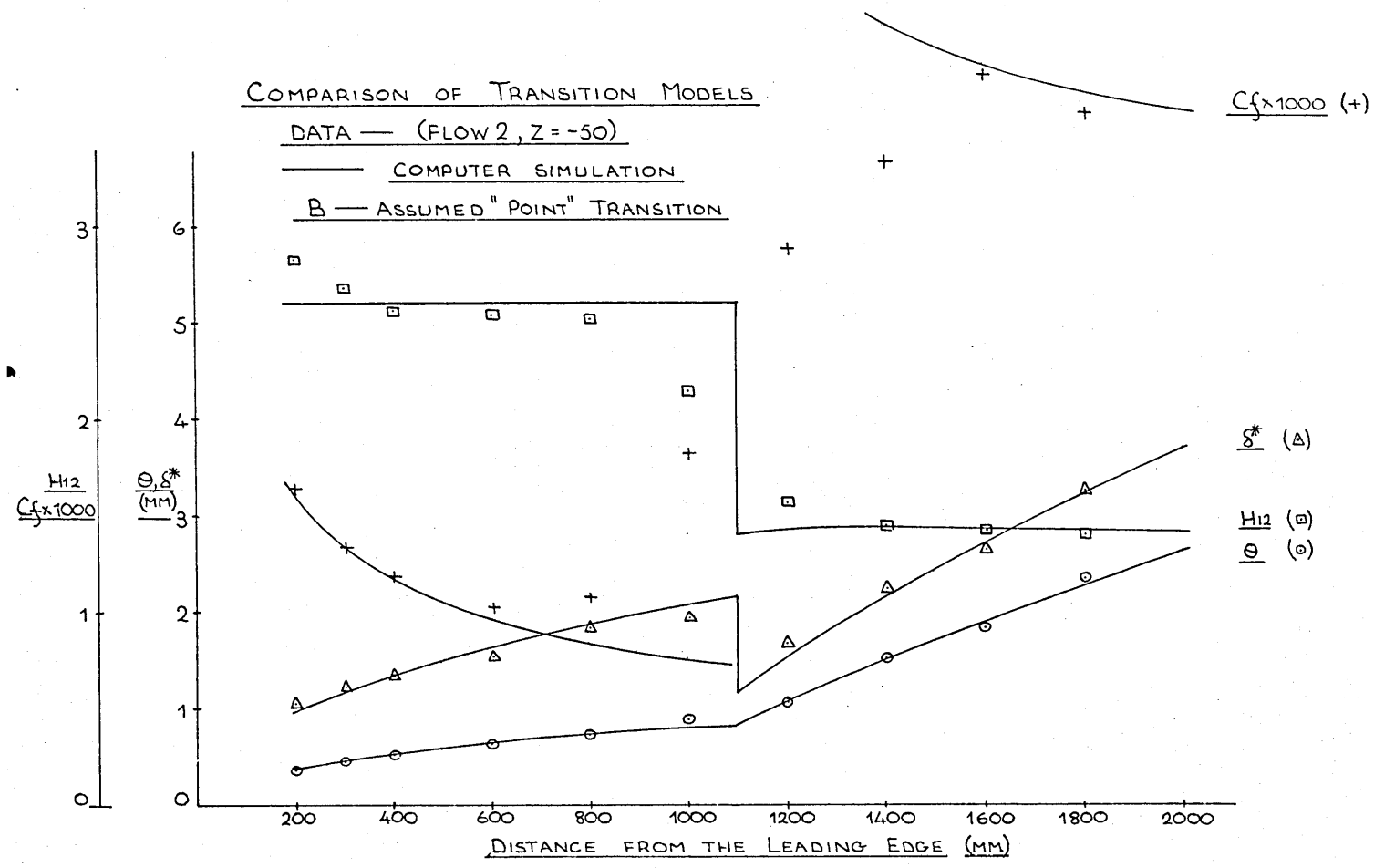
COMPARISON OF TRANSITION MODELS
DATA — (FLOW 2, Z = -50)
——— COMPUTER SIMULATION
B — ASSUMED "POINT" TRANSITION
Cfx1000 (+)
δ* (Δ)
H12 (□)
θ (○)
H12 / Cfx1000
θ, δ* (MM)
DISTANCE FROM THE LEADING EDGE (MM)

FIG 5.4.3.

COMPARISON BETWEEN MEASURED AND MODELLED TRANSITIONAL MEAN VELOCITY PROFILES

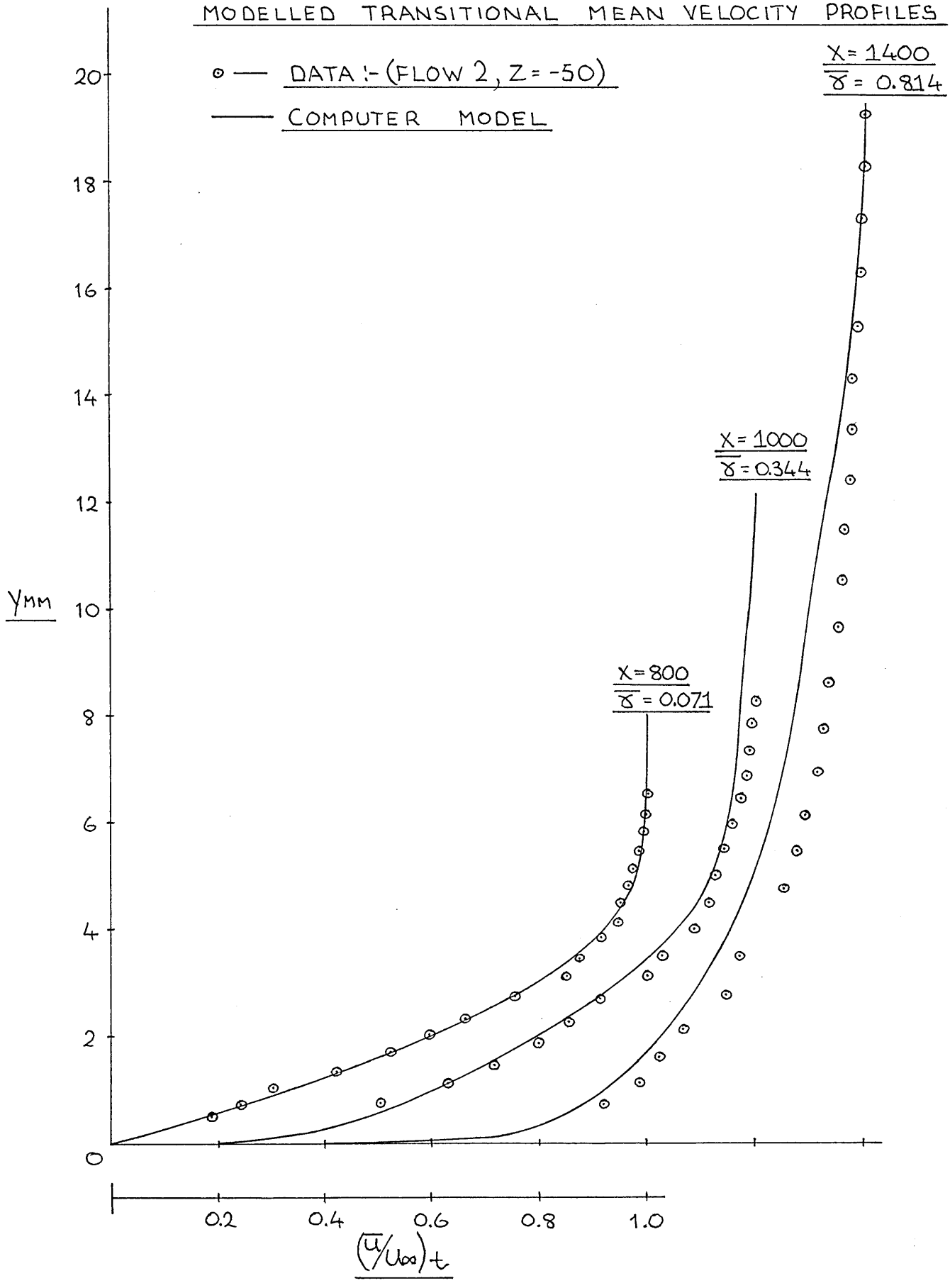

CONCLUSIONS.

1. The results show that the concept of statistical similarity in transition regions, remains intact for freely developing transition and for transition due to a two-dimensional trip wire. The universal character of the developing intermittency, see FIGS 4.3.1. and 4.3.2., and flow visualisation observations, indicate that the statistical similarity is a consequence of the turbulent spot source density and occurrence frequency. The transition mechanism, free or forced, ultimately influences the density and rate of spot sources at a narrow, localised downstream position. The spots then grow in accordance with the observations of Emmons (1950), Dhawan and Narasimha (1958) and Schubauer and Klebanoff (1956).

2. The present data suggests that the normal distribution function, curve-fitted by eqn. 5.1., provides the better method of representation of the mean intermittency development in transition regions.

3. There is at least one exception to the above general rules, and occurs when transition is induced immediately behind an isolated roughness element. In this case, the transition region is dominated by a periodic velocity fluctuation which is associated with vortex shedding from the element. The fluctuation rapidly degenerates to a random disturbance turbulent character a short distance from the element with a mild recourse to an intermittent type of breakdown.

4. The general boundary layer is well qualified by the mean intermittency value near the wall. At intermittencies below $\overline{\gamma} = 0.01$, the mean velocity profile in a zero pressure gradient, is reasonably accurately

described by the Blasius distribution, see FIG 2.3. A laminar boundary layer is therefore defined by the criterion, $\overline{\gamma} \leqslant 0.01$.

In addition, the mean intermittency value of $\overline{\gamma} \geqslant 0.99$ appears to be the only requirement to specify a fully developed turbulent boundary layer, although the turbulent boundary layer may still be remote from self-preserving conditions.

5. The mean velocity profiles and the streamwise component of fluctuating velocity profiles both exhibit approximate similarity in transition regions, when plotted against the coordinate (y/θ), see FIGS 4.4.1.-4.4.5. The local transitional skin friction coefficient also shows approximate similarity through transition, see FIG 4.5.1.

6. The early transition, which occurs in FLOW 2, illustrates the danger of unrecognised by-pass routes to transition. In this flow, transition is accelerated partly by the adverse pressure gradient at the leading edge of the plate. Application of Stratford's criterion, (see White (1974)), however, indicates that there is no separation.

7. The present data appears to be in reasonable agreement with contemporary transition Reynolds number correlations for transition downstream of a two-dimensional trip wire, see FIG 4.2.1.

8. Flow visualisation studies indicate that a turbulent spot is preceded by a significant lateral oscillation in the boundary layer. The streamwise velocity fluctuation, u', at transition however, would seem to have little influence on the transition length and hence the spot seeding process. The evidence therefore suggests that the generation of turbulent spots is more sensitively related to lateral

as opposed to longitudinal flow properties.

9. The idealised transition model of an alternate switching process between laminar and turbulent flow states is corroborated in a qualitative manner by the observations of the instantaneous velocity at particular heights in the transitional boundary layer, see FIG 4.6.1.

10. The choice of transition provoking agent has no apparent influence on the rate at which the resulting turbulent boundary layer will approach self-preserving conditions. The transition device need only then be selected to satisfy the particular transition location requirements.

11. If transition is induced abruptly at a two-dimensional trip wire, allowance must be made for the boundary layer to recover from the distortion effects of the wire. A recovery length of 85 wire diameters would appear to be a reasonable approximate criterion. In the same context, a minimum Reynolds number for undistorted turbulent boundary layers is quoted at $R_{\theta_{min.}} = 540$.

12. Optimum downstream spanwise uniformity is achieved with the shortest transition length. Long transition regions are however, intrinsically subject to spanwise variation, which appears to be a consequence of a variation in the local spot source density or spot occurrence frequency.

When transition is induced behind isolated roughness elements however, the boundary layer rapidly becomes regular after a mean intermittency value of unity is established across the entire span.

13. The effect of low Reynolds number on the turbulent boundary layer

is manifested as a moderate increase in the additive constant, C, in the law of the wall, ie. eqn. 3.4. The non-dimensional shear stress gradient in the viscous sublayer, must therefore be in excess of the numerical limit, $(\frac{-\nu}{\rho.u_\tau^3}.\frac{\partial \tau}{\partial y} > 10^{-3})$, suggested by Huffman and Bradshaw (1972). Uncertainty in the local skin friction coefficients at these Reynolds numbers however, prevent the use of the present data to develop anything but a speculative Reynolds number correlation for the "constant" C.

14. A general relationship for the transitional skin friction coefficient , ie. eqn. A. 4.13., developed for the present investigation, has been tested and seen to give reasonable estimates. The present relation for the turbulent C_f. component is however limited to Reynolds numbers below R_θ = 1600. For $R_\theta > 1600$, any other standard existing relations can be recommended.

15. A general integral prediction method for incompressible, transitional boundary layers in two-dimensional, arbitrary pressure gradient flows has been developed using existing integral techniques. The transition model, based on the findings of the present research, is seen to give good agreement against the present data and that of Schubauer and Klebanoff (1956).

SUGGESTIONS FOR FURTHER WORK.

The two most outstanding questions remaining unanswered relate to additional external influences on the laminar breakdown region. These are the pressure gradient and the freestream turbulence level. The effect of pressure gradient, was suggested by Dhawan and Narasimha to influence only the initial spot growth region and that when turbulent spots are established, they then grow in a self-consistent manner, irrespective of the pressure gradient. The assumptions however, require experimental verification and it is not known, with any certainty, how the pressure gradient affects the spot source density and hence the transition length. Measurements of transitional boundary layers in pressure gradient, would also make the use of a linearised hot wire system almost essential, for the reasons outlined in section 3.5.

The effect of the freestream turbulence level on the breakdown process is also important. In the present study, the turbulence level in the freestream was nominally 0.35%, based on u'. The data obtained, relating to the spot growth process, compares favourably with that of Schubauer and Klebanoff (1956), which was under the condition of 0.01 - 0.02% turbulence in the freestream. Higher freestream turbulence levels, ie. greater than 1%, may however, influence the transitional intermittency in a similar manner to the way it affects the intermittent outer region of a fully developed turbulent boundary layer; where the latter effectively dis/appears when the freestream turbulence level exceeds a nominated value.

While empirical correlations exist for the start and end of transition in the influence of freestream turbulence, see Hall and Gibbings (1972), little, if indeed any, data exists on the spot growth characteristics under such influences.

There is still however, a strong argument for continued research on the breakdown process in low turbulence, zero pressure gradient flows. The amount of scatter in the correlations of transition length Reynolds number, see FIG 4.7.1, reflects the ignorance of the basic mechanism resulting in the seeding of turbulent spots. The present studies have suggested that spot evolution may be preceeded by lateral disturbances. An experimental study of the lateral flow properties in relation to spot source density, occurrence frequency and the resulting transition length, would therefore seem appropriate. Such a study might then also account for the spanwise variation, which appears to be inherent in long transition regions.

The present transitional boundary layer prediction scheme may be further optimised or extended to application in axi-symmetric and/or compressible flows, assuming that the intermittency relation, ie. eqn. 5.1., still holds in such flows. The accuracy might also be further improved by performing the laminar and turbulent calculations with existing "dissipation integral" methods.

REFERENCES : - [square brackets denote page numbers]

Arnal, D., Juillen,J.C. and Michel,R. (1977) Analyse Expérimentale et calcul de l'apparition et du développement de la transition de la couche limite., AGARD conf. Proc. N° 224., Laminar-Turbulent Transition, paper N° 13, 1977. [7,98]

Benney, D.J. (1961) A non-linear theory for oscillations in a parallel flow., Jour. Fluid. Mech., vol. 10, (1961) [9]

Benney, D.J. (1964) Finite amplitude effects in an unstable boundary layer., Phy. of Fluids., vol. 7, N° 3, (1964) [9]

Bradshaw, P., Ferris, D.H. and Atwell, N.P. (1967) Calculation of turbulent boundary layer development using the turbulent energy equation., Jour. Fluid Mech., vol. 28, (1967) [5.5]

Bradshaw, P. and Pankhurst, R.C. (1964) The design of low speed wind tunnels.,Progress in Aero. Sc., 5, (1964) [2.2]

Cebeci, T. and Bradshaw, P. (1977) Momentum transfer in boundary layers., McGraw-Hill (1977) [4.3,5.3]

Cebeci, T. and Smith, A.M.O. (1974) Analysis of turbulent boundary layers., Academic Press (1974) [3,7]

Chang, P.K. (1970) Advanced topics in science and engineering., vol. 3. - Separation of Flow., Pergamon Press., (1970). [129,135]

Clauser, F.H. (1954) [79,80,81,82] Turbulent boundary layers in adverse pressure gradients., Jour. Aero. Sc., 21, (1954)

Clauser, F.H. (1956) [80] The turbulent boundary layer., Advances in App. Mechs, vol. 4, (1956)

Cohen, M.J. and Ritchie, N.J.B. (1962) [23] Low speed three-dimensional contraction design., Jour. Roy. Aero. Soc., vol. 66, 1962)

Coles, D.E. (1956) [63] The law of the wake in the turbulent boundary layer., Jour. Fluid. Mech., vol. 1, 1956.

Coles, D.E. (1962) [72,77,80] The turbulent boundary layer in a compressible fluid., Rand Rept., R-403-PR., Appendix A - A manual of experimental boundary layer practice for low speed flow. 1962.

Coles, D.E. and Hirst, E.A. (1968) [38,67,69,70,78, 82,133,4.6] Proc. Computation of turbulent boundary layers., AFOSR- IFP, Stanford Conf. 1968.

Corrsin, S. and Kistler, A. (1954) [33,101] The freestream boundaries of turbulent flows., N.A.C.A., Rep. N° 1244, 1954.

Crabtree, L.F. (1957) [14] Prediction of transition in the boundary layer of an aerofoil., R.A.E., T.N. AERO 2491, 1957.

Dhawan, S. and Narasimha, R. (1958) [16,17,76,94,95, 97,98,99,129, 132, 142,146,4.2] Some properties of boundary layer flow during the transition from laminar to

turbulent motion., Jour. Fluid. Mech., vol. 3, 1958.

Dobbinga, E. (1965) [10] Boundary layer disturbance by isolated protuberances of variable height on a cylinder nose.,AGARDograph 97, Part 1. Recent developments in boundary layer research. 1965.

Dryden, H.L. (1953) [10,11,93] Review of published data on the effect of roughness on transition from laminar to turbulent flow., Jour. Aero. Sc., vol. 20, N° 7, 1953.

East, L.F. (1972) [21,40] Spatial variations of the boundary layer of a large low speed wind tunnel., Aero. Jour., 76, 1972.

Emmons, H. and Bryson, A.E. (1950) [7,15,16,94,95 129,142,4.2] The laminar-turbulent transition in a boundary layer - Part 1., Jour. Aero. Sc., 18, 1951.

Feliss, N.A., Potter, M.C. and Smith, M.C. (1978) [98] An experimental investigation of incompressible channel flow near transition., (to be published)

Fiedler, H. and Head, M.R. (1966) [78] Intermittency measurements in the turbulent boundary layer., Jour. Fluid. Mech. vol. 25, part 4, 1959.

Forest, A.E. (1977) [99,130] Engineering predictions of transitional boundary layers., AGARD. conf. Proc. N° 224, Laminar-turbulent transition., paper N°24., 1977

Gibbings, J.C. (1958) [10,38] On boundary layer transition wires., Aero Res. Coun., current paper N° 462, 1958.

Goldstein, S. (1936) [10] A note on roughness., Aero. Res. Coun. R&M. 1763, 1936.

Görtler, H. (1940) [13] Über eine dreidimensionale instabilität laminarer grenzschichten an konkaven. Wänden. Nachr. Wiss. ges. Göttingen, Math. Phy. Klasse, Neue Fogle 2, N° 1, 1940

Graham, J.M.R. (1968) [108] The structure of the turbulent boundary layer artificially produced by roughness. Ph. D. thesis, London Univ., 1968.

Granville, P.S. (1953) [13] The calculations of viscous drag on bodies of revolution., Navy Dept., The David Taylor model basin, Rept. 849, 1953.

Green, J.E. (1968) [83,135,5.3,5.4] The prediction of turbulent boundary layer development in compressible flow. Jour. Fluid. Mech., vol. 31, part 4, 1968.

Green, J.E., Weeks, D.J. and Brooman, B.G. (1977) [130,4.6, 5.4,5.5, 5.6,5.7] Prediction of turbulent boundary layers and wakes in compressible flow by a lag entrainment method., Aero. Res. Coun., R&M. N° 3791, 1977.

Gregory, N. and Walker, W.S. (1951) [10] The effect on transition of isolated surface excrescences in the boundary layer., R.A.E., R&M. N° 2779, 1951.

Hall, D.J. (1968) [90,91,100] Boundary layer transition. Ph. D. thesis, Liverpool Univ., 1968.

Hall, D.J. and Gibbings, J.C. (1972) [147] Influence of stream turbulence and pressure gradient upon boundary layer transition., Jour. Mech. Eng. Sc., vol. 14, N° 2, 1972.

Head, M.R. (1958) [83] Entrainment in the turbulent boundary layer. Aero. Res. Coun. R&M. 3152, 1958.

Heisenberg, W. (1924) [5] Ueber stabilität und turbulenz von flüssigkeitsstromen. Ann. d. Physik, 24, 1924.

Huffman, G.D. and Bradshaw, P. (1972) [78,109,145] A note on von Karman's constant in low Reynolds number turbulent flows., Jour. Fluid. Mech., vol. 53, part 1, 1972.

Jaffe, N.A., Okamura, T.T. and Smith, A.M.O. (1970) [14] Determination of spatial amplification factors and their application to predicting transition. A.I.A.A., vol. 1, 1963.

Keir, G.G.H. (1971) [23] An experimental investigation of the influence of pressure gradient and freestream turbulence on transition in the boundary layer on a flat plate., M. Sc. thesis, Dundee Univ., 1971.

Kinghorn, F.C., McHugh,A. and Duncan, W. (1972) [20] Accuracy of airflow measurements using Pitot traverses and Orifice plates., N.E.L. Rept. N° 518, 1972.

Klebanoff, P.S. (1955) [3,3,5] Characteristics of turbulence in a boundary layer with zero pressure gradient., N.A.C.A., Tech. note 3178, 1955.

Klebanoff, P.S. (1966) [1,2] The effect of a two-dimensional roughness element on boundary layer transition., Proc. 11th Int. cong. of App. Mech., 1966.

Klebanoff, P.S., Schubauer, G.B. and Tidstrom, K.D. (1955) [1,2,9] Measurements of the effect of two-dimensional and three-dimensional roughness elements on boundary layer transition., Jour. Aero. Sc., vol. 22, N° 11, 1955.

Klebanoff, P.S., Tidstrom, K.D. and Sargent, L.M. (1962) [8] The three-dimensional nature of boundary layer instability. Jour. Fluid. Mech., vol. 12, part 1, 1962.

Klebanoff, P.S. and Tidstrom, K.D. (1972) [1,2,25] Mechanism by which a two-dimensional roughness element induces boundary layer transition.,Phy. of Fluids., vol 15, N° 7, 1972.

Lord Rayleigh (1880) [3,4] Sci. Papers 1, 474, 1880; 3,17,1887; 4,197, 1913. see also: On the stability of certain fluid motions., Proc. London Math. Soc., 2, 57, 1880, and 19, 67, 1887., Sci. Papers 1, 474 and 3,17. see also: Sci. Papers 4, 203,1895 and 6. 197, 1913.

Ludwieg, H. and Tillman, W. (1950) Investigation of the wall shearing
[72,73,5.4] stress in turbulent boundary layers.,
N.A.C.A., Tech. memo. 1285, 1950

Mari, C. and Mathieu, J. (1977) Méthode de prédiction de la couche
[130] limite., AGARD conf. proc. N° 224.,
Laminar-Turbulent Transition., paper N° 24, 1977

McDonald, H. and Fish, R.W. (1973) Practical calculations of transitional
[130] boundary layers., Int. Jour. Heat & Mass
Transfer, vol. 16, N° 9, 1973.

Meksyn, D. and Stuart, J.D. (1951) Stability of viscous motion between
[9] parallel planes for finite disturbances.,
Proc. Roy. Soc. pt. A 208., 1951.

Michel, R. (1951) Etūde de la transition sur le profiles d'aile;
[13,131] établissement d'un critére de determination
du point de transition et calcul de la trainée
de propil en incompressible., ONERA.
rapport 1/1578A., 1951.

Mitchner, M. (1954) Propagation of turbulence from an instantaneous
[8] point disturbance., Readers Forum, Jour. Aero.
Sc., vol. 21, N° 5, 1954

Mochizuki, M. (1961) Smoke observations on boundary layer transition
[10,96] caused by spherical roughness element.,
Jour. of Phy. Soc. of Japan., vol. 16, N° 5, 1961.

Murlis, J. (1975) The structure of turbulent boundary layers at
[78] low Reynolds number., Ph. D. thesis, Imperial
College, London., 1975.

Oka, S. and Kostic, Z. (1972) Influence of wall proximity on hot-wire
[73] velocity measurements., DISA. Information
N° 13, Measurement and analysis., 1972

Orr, W.M.F. (1907) The stability or instability of the steady
[4] motions of a perfect fluid and of a viscous
liquid. Part 1: A perfect fluid; Part 2 A
viscous liquid. Proc. Roy. Irish Acad. 27,
1907.

Pankhurst, R.C. and Holder, D.W. (1956) Wind tunnel techniques.
[22] Pitman, 1956.

Patel, V.C. (1965) Calibration of the Preston tube and
[36,37,40] limitations on its use in pressure gradients.
Jour. Fluid. Mech., vol. 23, part 1, 1965.

Pohlhausen, K. (1921) Zur näherungsweisen integration der
[66,132,133] differentialgleichung der laminaren
reibungsschicht., Zeit. für ang. Math & Mech. 1
1921.

Pope, A. and Harap, J.J. (1966) Low speed wind tunnel testing., Wiley, 1966.
[22]

Potter, J.L. (1957) Subsonic boundary layer transition caused by
[10,93] single roughness elements., Jour. Aero. Sc.,
vol. 24, N° 2, 1957.

Prandtl, L. (1904) On fluid motion at very small viscosity.,
[3] Proc. 3rd Int. Math. Cong., (Heidelberg)

Prandtl, L. (1914) Der luftwiderstand von kugeln., Ges. Wiss.
[3,10] Göttingen, Math. Phy. Klasse., 1914.

Prandtl, L. (1921) [5] Bemerkungen über die entstehung der turbulenz Zeit. für ang. Math. & Mech. 11, 1931.

Preston, J.H. (1958) [10,107] The minimum Reynolds number for a turbulent boundary layer and the selection of a transition device., Jour. Fluid. Mech., vol. 3, part 4, 1958.

Radio Spares (1977) [34] Dual monolithic voltage regulator., R.S. applications sheet R/2040., 1977.

Reynolds, O. (1883) [3] Phil. Trans. Roy. Soc. 1883, or Collected Papers 2, 51, see also Sci. Papers 2, 1883, see also On the dynamic theory of incompressible viscous fluids and the determination of the criterion., Phil. Trans. Roy. Soc. 1895.

Rotta, J.C. (1962) [129] Turbulent boundary layers in incompressible flow: Progress in Aero.Sc. vol 2., editors:- Ferri, A., Küchemann, D. and Sterne, L.H.G., Pergamon Press, 1962.

Sandborn, V.A. (1959) [33] Measurements of intermittency of turbulent motion in a boundary layer., Jour. Fluid. Mech., vol 6, 1959.

Schiller, L. (1934) [5] Neue quantitative versuche zur turbulenz-entstehung., Zeit für ang. Math. & Mech. 14, 1934.

Schubauer, G.B. and Klebanoff, P.S. (1956) [8,16,94,98,105, 135,136,142,145, 146,4.7] Contributions on the mechanics of boundary layer transition.,N.A.C.A. rept.

1289. and N.A.C.A. T.N. 3489, 1956

Schubauer, G.B. and Skramstad, H.K. (1942) Laminar boundary layer
[6,8,25] oscillations and stability of laminar flow., Nat. Bur. St., Res. Rept. 1772, 1943; see also N.A.C.A. Rept. 909, 1948.

Simpson, R.L. (1970) Characteristics of the turbulent boundary
[7] layer., Jour. Fluid. Mech., vol. 42, 1970.

Smith, A.M.O. and Clutter, D.W. (1959) The smallest height of roughness
[10] capable of affecting boundary layer transition., Jour. Aero/Space., 1959.

Smith, A.M.O. and Gamberoni, N. (1956) Transition, pressure gradient and
[14] stability theory., Proc. 9th Int. cong. App. Mech., 1956.

Sommerfeld, A. (1908) Ein beitrag zur hydrodynamischen erklärung
[4] der turbulenten flüssig-keitsbeivegungen., Atti del 4, Cong. Int. dei Mat., vol. 3, 1908.

Stuart, J.T. (1958) On the non-linear mechanics of hydrodynamic
[9] stability., Jour. Fluid. Mech., vol 4, 1958.

Tani, I. and Hama, F.R. (1953) Some experiments on the effect of a single
[10] roughness element on boundary layer transition., Jour. Aero. Sc. 1953.

Tani, I., Komoda, H., Komatsu, Y. and Iuchi, M. (1962) Boundary layer
[10,11,92] transition by isolated roughness., Aero. Res. Inst., Univ. of Tokyo.,Rept. N° 375, vol. 28, N° 7, 1962.

Tani, I., Hama, F.R. and Mituisi, S. (1954) On the effect of a single
[10] roughness element on boundary layer transition., Repts. of Inst. of Sc. & Tech., Tokyo Univ., vol. 8, 1954.

Tani, I. and Sato, H. (1956) Boundary layer transition by roughness
[10,11] element., Jour. of Phy. Soc. of Japan., vol. 11, N° 12, 1956.

Taylor, G.I. (1923) Stability of a viscous fluid contained between
[12] two rotating cylinders., Phil. Trans. A 223; see also Proc. Roy. Soc. A151 and 565, 1936.

Taylor, G.I. (1936) Statistical theory of turbulence, 5. Effect
[5] of turbulence on boundary layer., Proc. Roy. Soc., London A 156, 1936; see also: Some recent developments on the study of turbulence., Proc. 5th Int. cong. App. Mech., New York, 1938.

Thompson, B.G.J. (1967) A critical review of existing methods of
[129] calculating the turbulent boundary layer., Aero. Res. Coun. R & M N° 3447, 1967.

Thwaites, B. (1949) Approximate calculation of the laminar boundary
[130,132,135,4.3,5.2,5.3] layer., Aero. Quarterly Jour. vol. 1, 1949.

Tietjens, O. (1922) Beiträge zur entstehung der turbulenz., Thesis,
[5] Göttingen, 1922, and Zeit. fur ang. Math. & Mech., 5, 1922.

Tollmien, W. (1929) Ueber die entstehung der turbulenz. 1. Mitteilung
[5] Nachr. Ges. Wiss. Göttingen, Math. Phy. Klasse, see also N.A.C.A., T.M. 1265, 1950.

Townsend, A.A. (1976) [79] The structure of turbulent shear flow., 2nd edition, Cambridge Univ. Press, 1976.

van Driest, E.R. (1956) [78] On turbulent flow near a wall., Jour. Aero. Sc., vol. 23, 1956.

van Driest,E.R. and Blumer, C.B. (1963) [14,23,91,131] Boundary layer transition: free stream turbulence and pressure gradient effects., A.I.A.A., vol. 1, 1963.

van Ingen, J.L. (1956) [14] A suggested semi-empirical method for the calculation of the boundary layer transition region., Rept. V.T.H. 74, Dept. Aero. & Eng., Inst. of Tech., Delft, Holland, 1956.

White, F.M. (1974) [4,9,72,73,81,143] Viscous fluid flow., McGraw-Hill, 1974.

Wills, J. (1962) [73] The correction of hot wire readings for proximity to a solid boundary., Jour. Fluid. Mech., vol. 12, part 3, 1962.

Wings- data sheet (1953) [10] Limit of grain size for laminar flow over wings or bodies., sheet 02.04.09., Roy. Aero. Soc., issue 3, 1953.

Winter, K.G. (1975) [4.4] An outline of the techniques available for the measurement of skin friction in turbulent boundary layers., R.A.E., tech. memo. AERO 1656, 1975.

APPENDIX 1.

Experimental apparatus.

A brief specification of the main instrumentation is outlined along with an indication of the accuracy and the operating limits.

Experimental instrumentation.

Description	Maker	Model	Function
Hot wire Anemometer	DISA	55M10	Standard bridge operating in the constant temperature mode.
Lineariser	DISA	55M25	Linearisation of anemometer voltage over flow velocity ranges of 2.5 decades. Accuracy of ±0.05% of max. velocity and ±0.5% of reading
True integrator	DISA	52B30	Integration of input over selected time periods from:- 0.5,1,2,5,10,30 and 100 secs. max. output of ±5V in the $\frac{1}{T}\int_0^T f(t)dt$. mode.
Amplitude comparator	DISA	52B10	Input amplitude limit of ±5V. Output volts of 0 - 5V., corresponding to probabilities 0 - 1. with an accuracy of ±0.0002, plus frequency dependent errors:- ±1% at 10kHz. ; ±5% at 20kHz.

Description	Maker	Model	Function
Micromanometer	Furness Controls	MDC.	Reading in mm. of H_2O. from 0.05mm. to 1000mm., with an accuracy of ±1% in all ranges.
Sweep Drive Unit + external stepper motor.	DISA DISA	52B01 52C01	Automatic or manual sweep, with arbitrary step lengths available on manual. Accuracy of "y" displacement ±0.02mm. relative to a reference datum.
Aux. Filter Unit	DISA	55D25	High or Low pass filters available. Operated with low pass filter at 2kHz. and high pass filter out.

APPENDIX 2.

Experimental uncertainty in integral thicknesses

An error analysis is given for the estimated displacement and momentum thicknesses, where the primary error is due to uncertainty in the velocity measurements. Errors due to uncertainty in the y-datum are also considered.

Experimental uncertainty in integral thicknesses.

1. Errors due to uncertainty in local velocity measurements.

The local momentum and displacement thicknesses can be written respectively as:-

$$\overline{\Theta} = \int_0^1 \overline{U}(1-\overline{U})\,d\overline{Y} \quad , \quad \overline{\delta^*} = \int_0^1 (1-\overline{U})\,d\overline{Y}$$

where $\overline{U}, \overline{Y}, \overline{\Theta}$ and $\overline{\delta^*}$ are the non-dimensional expressions u/U_∞, y/δ, Θ/δ and δ^*/δ respectively.

If a relative error of ε, which can be either positive or negative, is introduced in the local velocity measurements.

ie. $\overline{U}' = \overline{U} + \varepsilon\overline{U}$.

Then the error introduced in the momentum and displacement thicknesses are respectively:-

$$\overline{\Theta}' = \int_0^1 (\overline{U}+\varepsilon\overline{U})(1-(\overline{U}+\varepsilon\overline{U}))\,d\overline{Y} \text{ and } \overline{\delta^*}' = \int_0^1 (1-(\overline{U}+\varepsilon\overline{U})\,d\overline{Y}$$

Expanding the terms and neglecting smaller orders of magnitude yields:-

$$\overline{\Theta}' = \overline{\Theta} + \varepsilon\int_0^1 \overline{U}(1-2\overline{U})\,d\overline{Y} \quad \text{and} \quad \overline{\delta^*}' = \overline{\delta^*} - \varepsilon\int_0^1 \overline{U}\,d\overline{Y}$$

or $\Delta\overline{\Theta} = (\overline{\Theta}' - \overline{\Theta}) = \varepsilon\int_0^1 \overline{U}(1-2\overline{U})\,d\overline{Y}$ and $\Delta\overline{\delta^*} = (\overline{\delta^*}' - \overline{\delta^*}) = -\varepsilon\int_0^1 \overline{U}\,d\overline{Y}$.

Hence $\dfrac{\Delta\overline{\Theta}}{\overline{\Theta}} = \dfrac{\varepsilon\int_0^1 \overline{U}(1-2\overline{U})\,d\overline{Y}}{\int_0^1 \overline{U}(1-\overline{U})\,d\overline{Y}}$ and $\dfrac{\Delta\overline{\delta^*}}{\overline{\delta^*}} = \dfrac{-\varepsilon\int_0^1 \overline{U}\,d\overline{Y}}{\int_0^1 (1-\overline{U})\,d\overline{Y}}$

(i) If the velocity profile is assumed to be parabolic

ie. $\overline{U} = 2\overline{Y} - \overline{Y}^2$

Then substitution gives the errors in momentum and displ. thickness as $\dfrac{\Delta\overline{\Theta}}{\overline{\Theta}} = -3\varepsilon$ and $\dfrac{\Delta\overline{\delta^*}}{\overline{\delta^*}} = -2\varepsilon$ respectively.

(ii) If the velocity profile is now assumed to be a 1/7 power law.

ie. $\bar{U} = (\bar{Y})^{1/7}$

Then similarly, $\frac{\Delta\bar{\theta}}{\bar{\theta}} = -7\varepsilon$ and $\frac{\Delta\bar{\delta}^*}{\bar{\delta}^*} = -7\varepsilon$.

If the error in velocity measurement is consistently under, ie. $\varepsilon = -2\%$, then the errors in momentum and displacement thickness are +14% and +14% respectively for the power law profile and +6% and +4% for the parabolic law.

The signifigance of the sign indicates that if the velocity is underestimated then the integral thicknesses are overestimated. and vice-versa.

2. Errors due to uncertainty in the y-datum.

The integral functions of momentum and displacement thickness are as shown below:-

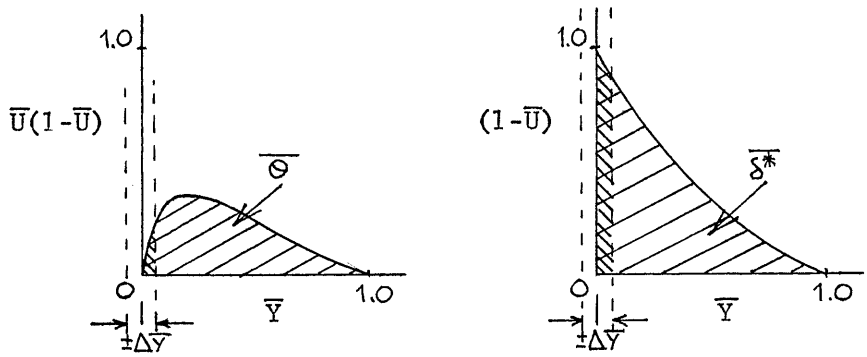

The y-datum can be set with an accuracy of ±0.2mm. at the very worst. If the boundary layer thickness is relatively small then this error may constitute a non-negligible error in the integral parameters.

As shown in the sketched functions, the displacement thickness is the more susceptible of the two to this kind of error. The relative error however tends to diminish as the boundary layer thickens.

APPENDIX 3.

Computer programs and flow charts.

Programs are included for laminar and turbulent velocity profile data reduction, momentum balance analysis and the reduction of Preston tube data.

Also included are theoretical prediction programs for turbulent boundary layers by the Head/Green entrainment method, by Green's lag entrainment method and a simple model of the transitional boundary layer incorporating Thwaites method for the laminar layer and the lag entrainment method for the turbulent layer.

Flow charts accompany the more complex programs.

CALCULATION OF TRANSITIONAL BOUNDARY LAYER

TY LTBL.FOR

```
      COMMON X,XMAX,DX,E,P,A,B,C,D,ANU,RHO,UO
      WRITE(5,10)
10    FORMAT(//'       LAMINAR/TURBULENT BOUNDARY LAYER GROWTH
     2',///'        BY THWAITES AND LAG ENTRAINMENT METHOD')
      WRITE(5,20)
20    FORMAT(///'       AIR TEMP. IN DEG.C= ',$)
      READ(5,210)T
      WRITE(5,30)
30    FORMAT(/'         ATMOS.PRESS.IN MM HG= ',$)
      READ(5,210)Z
      WRITE(5,40)
40    FORMAT(/'         FREESTREAM VELOCITY DISTRIBUTION:')
      WRITE(5,50)
50    FORMAT(//'        U/UO=E(Q)**P+A+B(Q)+C(Q)**2+D(Q)**3'/
     2'          WHERE Q=X/XMAX')
      WRITE(5,60)
60    FORMAT(/'                 E= ',$)
      READ(5,210)E
      WRITE(5,70)
70    FORMAT(/'                 P= ',$)
      READ(5,210)P
      WRITE(5,80)
80    FORMAT(/'                 A= ',$)
      READ(5,210)A
      WRITE(5,90)
90    FORMAT(/'                 B= ',$)
      READ(5,210)B
      WRITE(5,100)
100   FORMAT(/'                 C= ',$)
      READ(5,210)C
      WRITE(5,110)
110   FORMAT(/'                 D= ',$)
      READ(5,210)D
      WRITE(5,120)
120   FORMAT(/'                 UO IN M/S= ',$)
      READ(5,210)UO
      WRITE(5,130)
130   FORMAT(///'       STARTING POINT IN MM= ',$)
      READ(5,210)XO
      WRITE(5,140)
140   FORMAT(/'         STEP LENGTH IN MM= ',$)
      READ(5,210)DX
      WRITE(5,150)
150   FORMAT(/'         LENGTH OF PLATE IN MM= ',$)
      READ(5,210)XMAX
      WRITE(5,170)
170   FORMAT(/'         INITIAL MOMENTUM THICKNESS IN MM= ',$)
      READ(5,210)THETA
      WRITE(5,180)
180   FORMAT(/'         START OF TRANSITION= ',$)
      READ(5,210)XTR
      WRITE(5,190)
190   FORMAT(/'         STANDARD DEVIATION FOR TRANSITION',//'
     2          INTERMITTENCY DISTRIBUTION= ',$)
      READ(5,210)ASD
210   FORMAT(F)
220   FORMAT(I)
      RHO=(0.46535*Z)/(T+273)
      VISC=(1.725+0.004375*T)/10.0**5.0
      ANU=VISC/RHO
      XBAR=XTR+2.25*ASD
      X=XO
      Q=XO/XMAX
      U=UO*(E*(Q)**P+A+B*Q+C*Q*Q+D*Q*Q*Q)
      DUDX1=UO*1000.0/XMAX
      DUDX2=(P*E*(Q**(P-1.0)))+B+2.0*C*Q+3.0*D*Q*Q
      DUDX=DUDX1*DUDX2
      AM=-(THETA*THETA*DUDX/(ANU*10.0**6.0))
      IF (AM.LE.0.0) GOTO 230
      AL=0.22-1.402*AM-0.018*AM/(0.107-AM)
      H=2.61+3.75*AM+5.24*AM*AM
      GOTO 240
230   AL=0.22-1.57*AM-1.8*AM*AM
      H=2.088+0.0731/(0.14-AM)
240   CF=2000.0*AL*ANU/(THETA*U)
      DSTR=THETA*H
      UT5=THETA*THETA*U**6.0/(450000.0*ANU)
      WRITE(5,250)
250   FORMAT(////'          X        DSTR       THETA     H(12)
     2'//'          (MM)       (MM)       (MM)')
      WRITE(5,260)X,DSTR,THETA,H,CF
260   FORMAT(6X,F6.1,4X,F6.3,4X,F6.3,4X,F5.2,4X,F9.6)
      AJ=0.0
270   X=X+DX
      XPR=(X-XO)/50.0
      IF (X.GT.XMAX) GOTO 400
      R=(X-XBAR)/ASD
      IF (R.LT.-2.25) GOTO 280
      IF (R.LE.2.25.AND.R.GE.-2.25) GOTO 300
      IF (R.GT.2.25) GOTO 340
280   CALL THWAIT(UT5,UT5NX,HL,THL,CFL,AM)
      H=HL
      THETA=THL
      CF=CFL
      UT5=UT5NX
      DSTR=THETA*H
      IF(AM.GT.0.09) GOTO 360
      IF(XPR.NE.INT(XPR)) GOTO 290
      WRITE(5,260)X,DSTR,THETA,H,CF
290   GOTO 270
300   CALL THWAIT(UT5,UT5NX,HL,THL,CFL,AM)
      UT5=UT5NX
      IF (R.LT.-1.25)GOTO 302
      AJ=AJ+1.0
302   IF (AJ.GT.1.0) GOTO 310
      HNX=1.7
      THNX=THL/5
      FNX=0.025*HNX-0.022
      CALL TRAN(THL,HL,AM,HNX,THNX,R,H,THETA,CF,DSTR)
      IF(XPR.NE.INT(XPR)) GOTO 305
      WRITE(5,260)X,DSTR,THETA,H,CF
305      GOTO 270
310   HT=HNX
      THT=THNX
```

```
      FT=FNX
      X=X-DX
      CALL RUNGE(FT,HT,THT,FNX,HNX,THNX)
      CALL TRAN(THL,HL,AM,HNX,THNX,R,H,THETA,CF,DSTR)
      IF(XPR.NE.INT(XPR)) GOTO 320
      WRITE(5,260)X,DSTR,THETA,H,CF
320   GOTO 270
340   HT=H
      THT=THETA
      FT=FNX
      X=X-DX
      CALL RUNGE(FT,HT,THT,FNX,HNX,THNX)
      CALL TCF(HNX,THNX,CFNX)
      H=HNX
      THETA=THNX
      CF=CFNX
      Q=X/XMAX
      U=UO*(E*(Q)**P+A+B*Q+C*Q*Q+D*Q*Q*Q)
      TO=RHO*CF*U*U/2.0
      DSTR=H*THETA
      IF(TO.LE.0.000001) GOTO 380
      IF(XPR.NE.INT(XPR)) GOTO 350
      WRITE(5,260)X,DSTR,THETA,H,CF
350   GOTO 270
360   WRITE(5,370)
370   FORMAT(/'            LAMINAR SEPARATION ')
      GOTO 400
380   WRITE(5,390)
390   FORMAT(/'            TURBULENT SEPARATION ')
400   STOP
      END
```


TY THWAIT.FOR

```
      SUBROUTINE THWAIT(UT5,UT5NX,HL,THL,CFL,AM)
      COMMON X,XMAX,DX,E,P,A,B,C,D,ANU,RHO,UO
      DIMENSION Z(12),U5(12)
      ASUM=0.0
      Q=X/XMAX
      U=UO*((E*(Q)**P)+A+B*Q+C*Q*Q+D*Q*Q*Q)
      DUDX=(UO*1000.0/XMAX)*
     2      ((P*E*(Q**(P-1.0)))+B+2.0*C*Q+3.0*D*Q*Q)
      N=11
      STEP=DX/10.0
      XI=X-(DX+STEP)
      DO 10 K=1,N
      XI=XI+STEP
      Z(K)=XI/XMAX
      U5(K)=(UO*(E*Z(K)**P+A+B*Z(K)+C*Z(K)**2.0+D*Z(K)**3))**5.0
10    CONTINUE
      ASUM=ASUM+U5(1)+U5(11)
      N1=N-1
      DO 20 K=2,N1,2
      ASUM=ASUM+4.0*U5(K)
20    CONTINUE
      N2=N-2
      DO 30 K=3,N2,2
      ASUM=ASUM+2.0*U5(K)
30    CONTINUE
      APLUS=STEP*ASUM/3000.0
      UT5NX=UT5+APLUS
      THL=((0.45*ANU*UT5NX/(U**6))**0.5)*1000.0
      AM=-(THL*THL*DUDX/(ANU*1000000.0))
      IF (AM.LE.0.0) GOTO 40
      HL=2.61+3.75*AM+5.24*AM*AM
      AL=0.22-1.402*AM-0.018*AM/(0.107-AM)
      GOTO 50
40    HL=2.088+0.0731/(0.14-AM)
      AL=0.22-1.57*AM-1.8*AM*AM
50    CFL=2000.0*AL*ANU/(THL*U)
      RETURN
      END
```

```
TY RUNGE.FOR
      SUBROUTINE RUNGE(F,H,THETA,FNX,HNX,THNX)
      COMMON X,XMAX,DX,E,P,A,B,C,D,ANU,RHO,UO
      KSUM=0
      FR=F
      HR=H
      THR=THETA
10    Q=X/XMAX
      U=UO*((E*(Q)**P)+A+B*Q+C*Q*Q+D*Q*Q*Q)
      DUDX=(UO*1000.0/XMAX)*
     2     ((P*E*(Q**(P-1.0)))+B+2.0*C*Q+3.0*D*Q*Q)
      RTH=U*THR/(ANU*1000.0)
      CFO=0.01013/(0.43429*(ALOG(RTH))-1.02)-0.00075
      IF(RTH.LE.1200.0) GOTO 12
      CF=CFO*(0.9/(HR*(1.0-6.55*((CFO/2.0)**0.5))-
     2        0.4)-0.5)
      GOTO 13
12    B1=HR*(HR+1.0)/(HR-1.0)
      AP1=2.0/(HR-1.0)
      AP2=2.0*(HR-1.0)/(HR+1.0)
      B2=16.432**AP1
      B3=RTH*B2*B1/100.0
      CF1=2.0/(B3**AP2)
      CFF=0.01013/(0.43429*(ALOG(RTH))-1.02)-0.00075
      CF2=CFF*(0.9/(HR*(1.0-6.55*((CFF/2.0)**0.5))-
     2         0.4)-0.5)
      IF(CF1.LE.CF2) GOTO 14
      CF=CF1
      GOTO 13
14    CF=CF2
13    KSUM=KSUM+1
      FUNC1=(CF/2.0)-(HR+2.0)*THR*DUDX/(U*1000.0)
      FUNC2=(CF/2.0)-(HR+1.0)*THR*DUDX/(U*1000.0)
      FUNC3=3.15+1.72/(HR-1.0)-0.01*(HR-1.0)**2.0
      FUNC4=1.72/((HR-1.0)**2.0)+0.02*(HR-1.0)
      FUNC5=(FUNC3*FUNC2-FR)*1000.0/(THR*FUNC4)
      FUNC6=(FR*(FR+0.02)+0.2667*CFO)/(FR+0.01)
      FUNC7=1.25*((CF/2.0)-((HR-1.0)/
     2            (6.432*HR))**2.0)/HR
      FUNC9=FUNC3*((CF/2.0)-(HR+1.0)*FUNC7)
      ALAM=1.0
      ALSQ=ALAM*ALAM
      ZED=(0.024*FUNC9+1.2*FUNC9*FUNC9+0.32*CFO)/
     2    (1.2*ALSQ)-0.2667*CFO
      FUNC10=((0.0001+ZED)**0.5)-0.01
      FUNC11=(HR+FUNC3)*(CF/2.0-FUNC10/FUNC3)/(HR+1.0)
      FUNC12=(0.32*CFO+0.024*FUNC9+1.2*FUNC9*FUNC9)**0.5
      FUNC13=ALAM*(0.32*CFO+0.024*FR+1.2*FR*FR)**0.5
      FUNC14=(HR+FUNC3)*THR*DUDX/(U*1000.0)
      FUNC15=(FUNC6*(2.8*(FUNC12-FUNC13)+FUNC11-FUNC14))*
     2       1000.0/(THR*(FUNC3+HR))
      IF(KSUM.EQ.1) GOTO 20
      IF(KSUM.EQ.2) GOTO 30
      IF(KSUM.EQ.3) GOTO 40
      IF(KSUM.EQ.4) GOTO 50
20    AK1=DX*FUNC1/1000.0
      AL1=DX*FUNC5/1000.0
      AM1=DX*FUNC15/1000.0
      X=X+DX/2.0
      THR=THETA+500.0*AK1
      HR=H+AL1/2.0
      FR=F+AM1/2.0
      GOTO 10
30    AK2=DX*FUNC1/1000.0
      AL2=DX*FUNC5/1000.0
      AM2=DX*FUNC15/1000.0
      THR=THETA+500.0*AK2
      HR=H+AL2/2.0
      FR=F+AM2/2.0
      GOTO 10
40    AK3=DX*FUNC1/1000.0
      AL3=DX*FUNC5/1000.0
      AM3=DX*FUNC15/1000.0
      X=X+DX/2.0
      THR=THETA+1000.0*AK3
      HR=H+AL3
      FR=F+AM3
      GOTO 10
50    AK4=DX*FUNC1/1000.0
      AL4=DX*FUNC5/1000.0
      AM4=DX*FUNC15/1000.0
      THNX=THETA+(AK1+2.0*(AK2+AK3)+AK4)*500.0/3.0
      HNX=H+(AL1+2.0*(AL2+AL3)+AL4)/6.0
      FNX=F+(AM1+2.0*(AM2+AM3)+AM4)/6.0
      RETURN
      END
```

```
TY TCF.FOR
      SUBROUTINE TCF(HNX,THNX,CFNX)
      COMMON X,XMAX,DX,E,P,A,B,C,D,ANU,RHO,UO
      Q=X/XMAX
      U=UO*((E*(Q)**P)+A+B*Q+C*Q*Q+D*Q*Q*Q)
      RTHETA=U*THNX/(ANU*1000.0)
      DSTR=THNX*HNX
      CFO=0.01013/(0.43429*(ALOG(RTHETA))-1.02)-0.00075
      IF (RTHETA.LE.1200) GOTO 10
      CF2=CFO*(0.9/(HNX*(1.0-6.55*((CFO/2.0)**0.5))-0.4)-0.5)
      GOTO 20
10    B1=HNX*(HNX+1.0)/(HNX-1.0)
      AP1=2.0/(HNX-1.0)
      AP2=2.0*(HNX-1.0)/(HNX+1.0)
      B2=16.432**AP1
      B3=RTHETA*B2*B1/100.0
      CF1=2.0/(B3**AP2)
      CFO=0.01013/(0.43429*(ALOG(RTHETA))-1.02)-0.00075
      CF2=CFO*(0.9/(HNX*(1.0-6.55*((CFO/2.0)**0.5))-0.4)-0.5)
      IF (CF1.LE.CF2) GOTO 20
      CFNX=CF1
      GOTO 30
20    CFNX=CF2
30    RETURN
      END
```

```
TY TRAN.FOR
      SUBROUTINE TRAN(D2L,HL,AM,HT,D2T,R,H,THETA,
     2 CF,DSTR)
      COMMON X,XMAX,DX,E,P,A,B,C,D,ANU,RHO,UO
      DIMENSION UNL(22),UNT(22),AINT(22)
      IF (AM.LE.0.0) GOTO 10
      ALAM=-73.0*AM+109.0*AM*AM-790.0*AM*AM*AM
      GOTO 20
10    ALAM=-70.0*AM+310.0*AM*AM+5430.0*AM*AM*AM+
     2 66000.0*AM*AM*AM*AM
20    IF(R.LE.0.0) GOTO 22
      Z=R
      GOTO 23
22    Z=-1.0*R
23    G=0.8273*Z-0.094*Z*Z-0.073*Z*Z*Z+0.0165*Z*Z*Z*Z
      IF (R.LE.0.0) GOTO 30
      GAMA=0.5*(1.0+G)
      GOTO 40
30    GAMA=0.5*(1.0-G)
40    DSTR=D2L*(1.0-GAMA)*HL+GAMA*D2T*HT
      AN=2.0/(HT-1.0)
      DT=D2T*HT*(HT+1.0)/(HT-1.0)
      AT1=(0.30-ALAM/120.0)
      AT2=(7.40-ALAM/15.0-ALAM*ALAM/144.0)/63.0
      DL=0.5*(HL/AT1+1.0/AT2)*D2L
      IF (DL.GT.DT) GOTO 50
      DEL=DT
      GOTO 60
50    DEL=DL
60    N=21
      DY=DEL/20.0
      Y=0.0
      DO 110 K=2,N
      Y=Y+DY
      IF (Y.GE.DL)GOTO 70
      UNL(K)=(2.0*Y/DL-2.0*(Y/DL)**3+(Y/DL)**4)+
     2       ALAM*((Y/DL)-3.0*(Y/DL)**2+3.0*(Y/DL)**3-
     3       (Y/DL)**4)/6.0
      GOTO 80
70    UNL(K)=1.0
80    IF (Y.GT.DT) GOTO 90
      UNT(K)=(Y/DT)**(1.0/AN)
      GOTO 100
90    UNT(K)=1.0
100   AINT(K)=(1.0-UNL(K)*UNT(K))
110   CONTINUE
      ASUM=0.0
      ASUM=ASUM+1.0+AINT(21)
      N1=N-1
      DO 120 K=2,N1,2
      ASUM=ASUM+4.0*AINT(K)
120   CONTINUE
      N2=N-2
      DO 130 K=3,N2,2
      ASUM=ASUM+2.0*AINT(K)
130   CONTINUE
      AQ=DY*ASUM/3
      THETA=(1.0-GAMA)*((1.0-GAMA)*D2L-GAMA*D2L*HL)+
     2      GAMA*(GAMA*D2T-(1.0-GAMA)*D2T*HT)+
     3      2.0*GAMA*(1.0-GAMA)*AQ
      H=DSTR/THETA
      Q=X/XMAX
      U=UO*((E*(Q)**P)+A+B*Q+C*Q*Q+D*Q*Q*Q)
      IF (AM.LE.0.0) GOTO 135
      AL=0.22-1.402*AM-0.018*AM/(0.107-AM)
      GOTO 140
135   AL=0.22-1.57*AM-1.8*AM*AM
140   CFCL=2000.0*AL*ANU/(THETA*U)
      RTH=U*THETA/(ANU*1000.0)
      B1=H*(H+1.0)/(H-1.0)
      AP1=2.0/(H-1.0)
      AP2=2.0*(H-1.0)/(H+1.0)
      B2=16.432**AP1
      B3=RTH*B2*B1/100.0
      CFT1=2.0/(B3**AP2)
      CFO=0.01013/(0.43429*(ALOG(RTH))-1.02)-0.00075
      CFT2=CFO*(0.9/(H*(1.0-6.55*((CFO/2.0)**0.5))-
     2          0.4)-0.5)
      IF (CFT1.LE.CFT2) GOTO 150
      CFCT=CFT1
      GOTO 160
150   CFCT=CFT2
160   CF=CFCL*(1.0-GAMA)+GAMA*CFCT
      RETURN
      END
```

* MODIFIED SUB-ROUTINE:- TURBULENT POWER LAW REPLACED BY A "WALL-WAKE" PROFILE

```
TY TRAN.FOR
      SUBROUTINE TRAN(D2L,HL,AM,HT,D2T,R,H,THETA,
     2 CF,DSTR)
      COMMON X,XMAX,DX,E,P,A,B,C,D,ANU,RHO,UO
      DIMENSION UNL(22),UNT(22),AINT(22)
      Q=X/XMAX
      U=UO*((E*(Q)**P)+A+B*Q+C*Q*Q+D*Q*Q*Q)
      IF (AM.LE.0.0) GOTO 10
      ALAM=-73.0*AM+109.0*AM*AM-790.0*AM*AM*AM
      GOTO 20
10    ALAM=-70.0*AM+310.0*AM*AM+5430.0*AM*AM*AM+
     2 66000.0*AM*AM*AM*AM
20    IF(R.LE.0.0) GOTO 22
      Z=R
      GOTO 23
22    Z=-1.0*R
23    G=0.8273*Z-0.094*Z*Z-0.073*Z*Z*Z+0.0165*Z*Z*Z*Z
      IF (R.LE.0.0) GOTO 30
      GAMA=0.5*(1.0+G)
      GOTO 40
30    GAMA=0.5*(1.0-G)
40    DSTR=D2L*(1.0-GAMA)*HL+GAMA*D2T*HT
      ARTH=U*D2T/(ANU*1000.0)
      ACFO=0.01013/(0.43429*(ALOG(ARTH))-1.02)-0.00075
      C1=HT*(HT+1.0)/(HT-1.0)
      C2=2.0/(HT-1.0)
      C3=2.0*(HT-1.0)/(HT+1.0)
      C4=16.432**C2
      C5=ARTH*C4*C1/100.0
      ACF1=2.0/(C5**C3)
      ACF2=ACFO*(0.9/(HT*(1.0-6.55*((ACFO/2.0)**0.5))-
     2           0.4)-0.5)
      IF (ACF1.LE.ACF2) GOTO 42
      ACF=ACF1
      GOTO 43
42    ACF=ACF2
43    ZT=(2.0/ACF)**0.5
      UT=1.0/ZT
      AA=0.2733*ZT*(HT-1.0)/HT
      API=((AA-2.119)+((AA-2.119)*(AA-2.119)+
     2    4.0*(AA-1.3333))**0.5)/2.0
      DT=HT*D2T*0.41*ZT/(1.0+API)
      AT1=(0.30-ALAM/120.0)
      AT2=(7.40-ALAM/15.0-ALAM*ALAM/144.0)/63.0
      DL=0.5*(HL/AT1+1.0/AT2)*D2L
      IF (DL.GT.DT) GOTO 50
      DEL=DT
      GOTO 60
50    DEL=DL
60    N=21
      DY=DEL/20.0
      Y=0.0
      DO 110 K=2,N
      Y=Y+DY
      IF (Y.GE.DL)GOTO 70
      UNL(K)=(2.0*Y/DL-2.0*(Y/DL)**3+(Y/DL)**4)+
     2       ALAM*((Y/DL)-3.0*(Y/DL)**2+3.0*(Y/DL)**3-
     3       (Y/DL)**4)/6.0
      GOTO 80
70    UNL(K)=1.0
80    IF (Y.GT.DT) GOTO 90
      UNT(K)=UT*(ALOG(Y*UT*U/(ANU*1000.0))/0.41+5.2+
     2      4.878*API*(SIN(1.5708*Y/DT))**2.0)
      GOTO 100
90    UNT(K)=1.0
100   AINT(K)=(1.0-UNL(K)*UNT(K))
110   CONTINUE
      ASUM=0.0
      ASUM=ASUM+1.0+AINT(21)
      N1=N-1
      DO 120 K=2,N1,2
      ASUM=ASUM+4.0*AINT(K)
120   CONTINUE
      N2=N-2
      DO 130 K=3,N2,2
      ASUM=ASUM+2.0*AINT(K)
130   CONTINUE
      AQ=DY*ASUM/3
      THETA=(1.0-GAMA)*((1.0-GAMA)*D2L-GAMA*D2L*HL)+
     2      GAMA*(GAMA*D2T-(1.0-GAMA)*D2T*HT)+
     3      2.0*GAMA*(1.0-GAMA)*AQ
      H=DSTR/THETA
      IF (AM.LE.0.0) GOTO 135
      AL=0.22-1.402*AM-0.018*AM/(0.107-AM)
      GOTO 140
135   AL=0.22-1.57*AM-1.8*AM*AM
140   CFCL=2000.0*AL*ANU/(THETA*U)
      RTH=U*THETA/(ANU*1000.0)
      B1=H*(H+1.0)/(H-1.0)
      AP1=2.0/(H-1.0)
      AP2=2.0*(H-1.0)/(H+1.0)
      B2=16.432**AP1
      B3=RTH*B2*B1/100.0
      CFT1=2.0/(B3**AP2)
      CFO=0.01013/(0.43429*(ALOG(RTH))-1.02)-0.00075
      CFT2=CFO*(0.9/(H*(1.0-6.55*((CFO/2.0)**0.5))-
     2          0.4)-0.5)
      IF (CFT1.LE.CFT2) GOTO 150
      CFCT=CFT1
      GOTO 160
150   CFCT=CFT2
160   CF=CFCL*(1.0-GAMA)+GAMA*CFCT
      RETURN
      END
^Z
```

CALCULATION OF TURBULENT BOUNDARY LAYER

TY HEAD.FOR

```
      WRITE(5,10)
10    FORMAT(/' HEAD/GREEN METHOD FOR TURBULENT
     2 BOUNDARY LAYER COMPUTATION'//
     3' THE MAINSTREAM FLOW FOR NON-DIMENSIONAL U(=U/U0) AND
     4 X(=X/L)'/' IS IN THE FORM:'/
     5' U=A+B*X+C*X^2+D*X^3'//
     6' WHERE:'/
     7' CHARACTERISTIC LENGTH L IN MM= ',$)
      READ(5,120)CL
      WRITE(5,15)
15    FORMAT(/' A= ',$)
      READ(5,120)A
      WRITE(5,20)
20    FORMAT(/' B= ',$)
      READ(5,120)B
      WRITE(5,30)
30    FORMAT(/' C= ',$)
      READ(5,120)C
      WRITE(5,40)
40    FORMAT(/' D= ',$)
      READ(5,120)D
      WRITE(5,50)
50    FORMAT(//' INITIAL X VALUE IN MM= ',$)
      READ(5,120)X
      X=X/CL
      WRITE(5,60)
60    FORMAT(/' INITIAL MOMENTUM THICKNESS IN MM= ',$)
      READ(5,120)TH
      TH=TH/CL
      WRITE(5,70)
70    FORMAT(/' INITIAL SHAPE FACTOR H= ',$)
      READ(5,120)H
      WRITE(5,80)
80    FORMAT(/' REYNOLDS NUMBER OF THE FLOW(U0*L/NU)= ',$)
      READ(5,120)RE
      WRITE(5,90)
90    FORMAT(/' STEP LENGTH IN X-MM FOR INTEGRATION= ',$)
      READ(5,120)DX
      DX=DX/CL
      WRITE(5,100)
100   FORMAT(/' MAXIMUM X VALUE IN MM= ',$)
      READ(5,120)XMAX
      XMAX=XMAX/CL
      WRITE(5,110)
110   FORMAT(/' NUMBER OF STEPS PER PRINTOUT= ',$)
      READ(5,130)I
120   FORMAT(F)
130   FORMAT(I)
      WRITE(5,140)
140   FORMAT(///'  HEAD/GREEN METHOD FOR TUBULENT BOUNDARY LAYERS'/
     2'   X-MM        TH-MM     DSTR-MM      H
     3          CF'/)
150   J=0
160   KSUM=0
      J=J+1
170   KSUM=KSUM+1
      U=A+B*X+C*X**2+D*X**3
      DUDX=B+2.0*C*X+3.0*D*X**2
      F=TH/U*DUDX
      RTH=RE*U*TH
      CF=0.246*EXP(-1.561*H)*RTH**(-0.268)
      EF=(H-1.0)*(0.025*H-0.022)
      F1=-(H*(H**2-1.0)*F+0.5*(H-1.0)*(EF-H*CF))/TH
      F2=0.5*CF-F*(2.0+H)
      IF (KSUM.EQ.1) GOTO 180
      IF (KSUM.EQ.2) GOTO 190
      IF (KSUM.EQ.3) GOTO 200
      IF (KSUM.EQ.4) GOTO 205
180   AK1=DX*F1
      AL1=DX*F2
      X=X+0.5*DX
      H=H+0.5*AK1
      TH=TH+0.5*AL1
      GOTO 170
190   AK2=DX*F1
      AL2=DX*F2
      H=H-0.5*AK1+0.5*AK2
      TH=TH-0.5*AL1+0.5*AL2
      GOTO 170
200   AK3=DX*F1
      AL3=DX*F2
      X=X+0.5*DX
      H=H-0.5*AK2+AK3
      TH=TH-0.5*AL2+AL3
      GOTO 170
205   AK4=DX*F1
      AL4=DX*F2
      H=H-AK3+(AK1+2.0*AK2+2.0*AK3+AK4)/6.0
      TH=TH-AL3+(AL1+2.0*AL2+2.0*AL3+AL4)/6.0
      IF (J.EQ.I) GOTO 210
      GOTO 160
210   D1=H*TH
      XMM=X*CL
      DSTR=D1*CL
      THMM=TH*CL
      WRITE(5,220)XMM,THMM,DSTR,H,CF
220   FORMAT(F8.2,3X,F7.3,3X,F7.3,3X,F6.3,3X,F8.5)
      IF (H.GT.2.4) GOTO 230
      IF (X.GT.XMAX) GOTO 250
      GOTO 150
230   XMM=X*CL
      WRITE(5,240)XMM
240   FORMAT(///' SEPARATION OCCURS AT X-MM = ',F8.2)
      STOP
250   END
```

CALCULATION OF TURBULENT BOUNDARY LAYER

```
TY LAGENT.FOR
      COMMON X,XMAX,DX,E,P,A,B,C,D,ANU,RHO,UO
      WRITE(5,10)
10    FORMAT(//' THEORETICAL TURBULENT
     2 BOUNDARY LAYER DEVELOPMENT ',///' BY
     3 GREENS LAG ENTRAINMENT METHOD ' )
      WRITE(5,20)
20    FORMAT(//' AIR TEMP IN DEG. C = ',$)
      READ(5,180)T
      WRITE(5,30)
30    FORMAT(/' ATMOS. PRESS. IN MM. HG. = ',$)
      READ(5,180)Z
      WRITE(5,40)
40    FORMAT(/' FREESTREAM VELOCITY
     2 DISTRIBUTION :- ' )
      WRITE(5,50)
50    FORMAT(/' U/UO = E(Q)**P + A + B(Q) +
     2 C(Q)**2 + D(Q)**3 ',/ ' WITH Q = X/XMAX ' )
      WRITE(5,60)
60    FORMAT(/' WHERE E = ',$)
      READ(5,180)E
      WRITE(5,70)
70    FORMAT(/'         P = ',$)
      READ(5,180)P
      WRITE(5,80)
80    FORMAT(/'         A = ',$)
      READ(5,180)A
      WRITE(5,90)
90    FORMAT(/'         B = ',$)
      READ(5,180)B
      WRITE(5,100)
100   FORMAT(/'         C = ',$)
      READ(5,180)C
      WRITE(5,110)
110   FORMAT(/'         D = ',$)
      READ(5,180)D
      WRITE(5,120)
120   FORMAT(/' AND UO IN M/S = ',$)
      READ(5,180)UO
      WRITE(5,130)
130   FORMAT(///' STARTING POINT IN MM. = ',$)
      READ(5,180)X
      WRITE(5,140)
140   FORMAT(/' STEP LENGTH IN MM. = ',$)
      READ(5,180)DX
      WRITE(5,150)
150   FORMAT(/' LENGTH OF PLATE IN MM. = ',$)
      READ(5,180)XMAX
      WRITE(5,160)
160   FORMAT(///' INITIAL SHAPE FACTOR = ',$)
      READ(5,180)H
      WRITE(5,170)
170   FORMAT(/' INITIAL MOMENTUM TH. IN MM. = ',$)
      READ(5,180)THETA
180   FORMAT(F)
190   FORMAT(I)
      RHO=(0.46535*Z)/(T+273)
      VISC=(1.725+0.004375*T)/10.0**5
      ANU=VISC/RHO
      XS=X
      WRITE(5,200)
200   FORMAT(////'   X     DSTAR  THETA   H(12)
     2     CF      TO     BETA   ENT.      PI       G ',
     3 //'   (MM)    (MM)    (MM)
     4  (N/M^2) ' )
210   Q=X/XMAX
      U=UO*((E*(Q)**P)+A+B*Q+C*Q*Q+D*Q*Q*Q)
      DUDX=(UO*1000.0/XMAX)*
     2       ((P*E*(Q**(P-1.0)))+B+2.0*C*Q+3.0*D*Q*Q)
      RTHETA=U*THETA/(ANU*1000.0)
      DSTAR=THETA*H
      CFO=0.01013/(0.43429*(ALOG(RTHETA))-1.02)-0.00075
      IF(RTHETA.LE.1200.0) GOTO 211
      CF=CFO*(0.9/(H*(1.0-6.55*((CFO/2.0)**0.5))-
     2        0.4)-0.5)
      GOTO 212
211   B1=H*(H+1.0)/(H-1.0)
      AP1=2.0/(H-1.0)
      AP2=2.0*(H-1.0)/(H+1.0)
      B2=16.432**AP1
      B3=RTHETA*B2*B1/100.0
      CF1=2.0/(B3**AP2)
      CFF=0.01013/(0.43429*(ALOG(RTHETA))-1.02)-0.00075
      CF2=CFF*(0.9/(H*(1.0-6.55*((CFF/2.0)**0.5))-
     2         0.4)-0.5)
      IF(CF1.LE.CF2) GOTO 208
      CF=CF1
      GOTO 212
208   CF=CF2
212   IF(XS.LT.X) GOTO 215
      G=(H-1.0)*((2.0/CF)**0.5)/H
      TO=(CF*RHO/2.0)*U*U
      BET=-(DSTAR*RHO*U*DUDX)/(TO*1000.0)
      GEQ=6.432*(1.0+0.8*BET)**0.5
      CON=G/GEQ
      IF(CON.GE.1.2) GOTO 213
      IF(CON.LE.0.8) GOTO 213
      FS3=3.15+1.72/(H-1.0)-0.01*(H-1.0)**2.0
      FS7=1.25*((CF/2.0)-((H-1.0)/
     2          (6.432*H))**2.0)/H
      FE=FS3*((CF/2.0)-(H+1.0)*FS7)
      ALAM=1.0
      ALSQ=ALAM*ALAM
      ZED=(0.024*FE+1.2*FE*FE+0.32*CFO)/(1.2*ALSQ)-
     2    0.2667*CFO
      F=((0.0001+ZED)**0.5)-0.01
      GOTO 215
213   F=0.025*H-0.022
215   TO=(CF*RHO/2.0)*U*U
      BETA=-(DSTAR*RHO*U*DUDX)/(TO*1000.0)
      DEL=(H+3.15+1.72/(H-1.0)-0.01*(H-1.0)**2.0)*THETA
      G=(H-1.0)*((2.0/CF)**0.5)/H
      APIE=(DSTAR/DEL)*0.41*((2.0/CF)**0.5)-1.0
      IF(TO.LE.0.000001) GOTO 230
      XPR=(X-XS)/50.0
      IF(XPR.NE.INT(XPR)) GOTO 225
```

```
      WRITE(5,220)X,DSTAR,THETA,H,CF,TO,BETA,F,APIE,G
220   FORMAT(1X,F5.0,1X,F6.2,1X,F6.2,2X,F5.2,2X,
     2      F7.5,1X,F6.3,1X,F6.2,1X,F7.4,1X,F7.4,1X,F6.2)
225   IF(X.GT.XMAX) GOTO 250
      CALL RUNGE(F,H,THETA,FNX,HNX,THNX)
      THETA=THNX
      H=HNX
      F=FNX
      GOTO 210
230   WRITE(5,240)
240   FORMAT(//'   SEPARATION REGION ' )
250   STOP
      END
```


ANALYSIS OF PRESTON TUBE DATA

```
TY CFPT.FOR
      DIMENSION DPP(30),XST(30),YST(30),TAU(30),CF(30)
      WRITE(5,10)
10    FORMAT(//' ANALYSIS OF PRESTON TUBE DATA'//)
      WRITE(5,20)
20    FORMAT(//' ATMOS PRESS IN MM HG= ',$)
      READ(5,130)Z
      WRITE(5,30)
30    FORMAT(//' AIR TEMP IN DEG C= ',$)
      READ(5,130)T
      WRITE(5,40)
40    FORMAT(//' FREESTREAM VELOCITY IN M/S= ',$)
      READ(5,130)U
      WRITE(5,50)
50    FORMAT(//' PRESTON TUBE O.D. IN MM= ',$)
      READ(5,130)D
      WRITE(5,60)
60    FORMAT(//' NO. OF READINGS= ',$)
      READ(5,140)N
      WRITE(5,70)
70    FORMAT(//' NOW TYPE IN THE PRESS. READINGS IN MM WG'
     2//' (TAKE A NEW LINE TO EACH VALUE)')
      DO 80 K=1,N
      READ(5,130)DPP(K)
80    CONTINUE
      RHO=(0.46535*Z)/(T+273.)
      VNU=(1.725+0.004375*T)/(RHO*100000.)
      CONST=(D*D/1000000.0)/(4.0*RHO*VNU*VNU)
      DO 120 K=1,N
      XST(K)=ALOG(DPP(K)*9.81*CONST)*0.4343
      YST(K)=0.8287-0.1381*XST(K)+0.1437*XST(K)**2-0.006*XST(K)**
      IF (YST(K).LE.1.5) GOTO 100
      GOTO 110
100   YST(K)=0.5*XST(K)+0.037
110   TAU(K)=(10.0**YST(K))/CONST
      CF(K)=2.0*TAU(K)/(RHO*U*U)
      WRITE(5,150)DPP(K),YST(K),TAU(K),CF(K)
120   CONTINUE
130   FORMAT(F)
140   FORMAT(I)
150   FORMAT(4(3X,F))
      STOP
      END
```

Reduction of Turbulent Velocity Profile Data

```
TY CFTBL.FOR
      DIMENSION Y(40),U(40),UNOR(40),URMS(40),GAMA(40),
     2          PCT(40),YD(40)
      WRITE(5,10)
10    FORMAT(//' DATA FOR TURBULENT BOUNDARY LAYER
     2 VELOCITY PROFILE')
      WRITE(5,20)
20    FORMAT(///' AIR TEMPERATURE IN DEG. C= ',$)
      READ(5,70)T
      WRITE(5,30)
30    FORMAT(/' ATMOS. PRESSURE IN MM HG= ',$)
      READ(5,70)Z
      WRITE(5,40)
40    FORMAT(/' MAINSTREAM VELOCITY IN M/S= ',$)
      READ(5,70)UINF
      WRITE(5,50)
50    FORMAT(/' DISTANCE FROM L.E. IN MM= ',$)
      READ(5,70)X
      WRITE(5,51)
51    FORMAT(/' SPANWISE LOCATION IN MM= ',$)
      READ(5,70)SPAN
      WRITE(5,52)
52    FORMAT(/' REFERENCE Y-VALUE IN MM= ',$)
      READ(5,70)YD
      WRITE(5,54)
54    FORMAT(/' REFERENCE DISPLACEMENT VOLTAGE= ',$)
      READ(5,70)VD
      WRITE(5,60)
60    FORMAT(/' NUMBER OF DATA POINTS= ',$)
      READ(5,80)N
70    FORMAT(F)
80    FORMAT(I)
      WRITE(5,90)
90    FORMAT(///' NOW READ IN DISP. VOLTS, U-M/S, URMS
     2 AND THE INTERMITTENCY'//
     3' (START WITH THE VALUES CORRES. TO MINM. Y)')
      DO 100 K=1,N
      READ(5,110)Y(K),U(K),URMS(K),GAMA(K)
      Y(K)=YD+(VD-Y(K))*9.96
      PCT(K)=URMS(K)*100.0/UINF
      UNOR(K)=U(K)/UINF
100   CONTINUE
110   FORMAT(F,F,F,F)
      DELTA=AITKEN(UNOR,Y,0.995,N,2)
      RHO=(0.46535*Z)/(T+273.0)
      VISC=(1.725+0.004375*T)/10.0**5
      ANU=VISC/RHO
      RENOX=UINF*X/(ANU*1000.0)
      WRITE(5,120)X,SPAN,UINF,RENOX
120   FORMAT(////////
     2'            TURBULENT VELOCITY PROFILE'//
     3'            DISTANCE FROM LEADING EDGE=',F7.1,' MM'//
     4'            SPANWISE LOCATION=',F5.1,' MM'//
     5'            FREESTREAM VELOCITY=',F6.2,' M/S'//
     6'            PLATE REYNOLDS NUMBER=',F10.0,///
     7'                 Y-DIST (MM)    Y/DELTA    U/UINF
     8     PCT.       INTERMITTENCY'/)
      DO 150 K=1,N
      YD(K)=Y(K)/DELTA
      WRITE(5,160)Y(K),YD(K),UNOR(K),PCT(K),GAMA(K)
150   CONTINUE
160   FORMAT(16X,F6.2,8X,F6.3,4X,F6.3,3X,F6.2,8X,F6.3)
      WRITE(5,170)DELTA
170   FORMAT(///                  APPROX EDGE OF BOUNDARY
     2 LAYER=',F6.2,' MM'////////)
      DO 5 K=1,N
      IF (Y(K).GT.DELTA) GOTO 15
      NPTS=K
5     CONTINUE
15    CALL LOGLAW(UTAU,UT1,YT1,UINF,NPTS,UNOR,Y,ANU)
      IF (YT1.LE.50.0) GOTO 180
      GOTO 200
180   WRITE(5,190)
190   FORMAT(///        YT1 IS LESS THAN 50'/
     2'        DELETE FIRST READING AT WALL AND RERUN')
      GOTO 220
200   CALL WALINT(YT1,ANU,UTAU,UINF,S1,S2,S3,S4)
      CALL PARINT(UNOR,Y,N,SUM1,SUM2,SUM3,SUM4)
      SUM1=SUM1+S1
      SUM2=SUM2+S2
      SUM3=SUM3+S3
      SUM4=SUM4+S4
      DSTAR=SUM2
      THETA=SUM1-SUM3
      D2STR=SUM1-SUM4
      H12=DSTAR/THETA
      H32=D2STR/THETA
      RTHETA=(UINF*THETA)/(ANU*1000.0)
      RDSTAR=(UINF*DSTAR)/(ANU*1000.0)
      PI=(0.205*UINF/UTAU-0.5*ALOG(UTAU*DELTA/(ANU*1000.0))-
     2  1.066)
      CF1=0.246/(EXP(1.561*H12)*(RTHETA)**0.268)
      CF2=2.0*(UTAU/UINF)**2
      CF3=0.3/(EXP(1.33*H12)*(0.434294*ALOG(RTHETA))**
     2   (1.74+0.31*H12))
      TD=((CF1+CF2+CF3)/3)*RHO*UINF**2/2.0
      WRITE(5,210)DSTAR,THETA,D2STR,H12,H32,RTHETA,RDSTAR
     2,UTAU,CF1,CF2,CF3,TD,PI
210   FORMAT(///          BOUNDARY LAYER PARAMETERS'////
     2'          DISPLACEMENT TH.=',F8.4,' MM'//
     3'          MOMENTUM TH.=',F8.4,' MM'//
     4'          ENERGY TH.=',F8.4,' MM'//
     5'          SHAPE FACTOR H12=',F8.4,//
     6'          SHAPE FACTOR H32=',F8.4,//
     7'          MOM.TH.REYNOLDS NO.=',F8.0,//
     8'          DISP.TH.REYNOLDS NO.=',F8.0,//
     9'          WALL FRICTION VELOCITY=',F7.4,' M/S'//
     2'          CF(LUD/TILL)=',F,//
     3'          CF(LOG-PLOT)=',F,//
     4'          CF(COLES-FORM)=',F,//
     5'          WALL SHEAR STRESS=',F6.3,' N/M^2'//
     6'          WAKE PARAMETER PI=',F9.5)
      STOP
220   END
```

TY LOGLAW.FOR

```
      SUBROUTINE LOGLAW(UTAU1,UT1,YT1,UIF,NPTS,UN,WYE,GNU)
      DIMENSION UN(NPTS),WYE(NPTS),RESID(40),U(40),UTAU(40)
      DIMENSION YPLUS(40),UPLUS(40),E(40),AIUT(40)
      DIMENSION YP(40),UDEF(40)
      WRITE(5,10)
10    FORMAT(/////'              VELOCITY PROFILE IN TERMS OF Y+
     2 AND U+'//'             FROM WALL UP TO DELTA'//
     3'                  YPLUS          LOGYP          UPLUS
     4       RESIDUAL        UDEF '//)
      L=0
      SUM=0.0
      DO 50 K=1,NPTS
      UTAU(K)=1.0
      GOTO 30
20    UTAU(K)=AIUT(K)
30    U(K)=UN(K)*UIF
      YPLUS(K)=UTAU(K)*WYE(K)/(GNU*1000.0)
      UPLUS(K)=U(K)/UTAU(K)
      AIUT(K)=U(K)/(2.439*ALOG(YPLUS(K))+5.2)
      E(K)=UTAU(K)-AIUT(K)
      IF (ABS(E(K)).LE.0.00001) GOTO 40
      GOTO 20
40    IF (YPLUS(K).LE.60.0.OR.YPLUS(K).GE.220.0) GOTO 50
      L=L+1
      SUM=SUM+UTAU(K)
50    CONTINUE
      UTAU1=SUM/FLOAT(L)
      DO 60 K=1,NPTS
      UPLUS(K)=U(K)/UTAU1
      UDEF(K)=UIF/UTAU1-UPLUS(K)
      YPLUS(K)=UTAU1*WYE(K)/(GNU*1000.0)
      YP(K)=0.4343*(ALOG(YPLUS(K)))
      RESID(K)=UPLUS(K)-(2.439*ALOG(YPLUS(K))+5.2)
      WRITE(5,70)YPLUS(K),YP(K),UPLUS(K),RESID(K),UDEF(K)
60    CONTINUE
70    FORMAT(14X,F7.2,6X,F6.2,6X,F7.2,6X,F8.4,6X,F6.2)
      YT1=YPLUS(3)
      UT1=UPLUS(3)
      RETURN
      END
```

TY WALINT.FOR

```
      SUBROUTINE WALINT(YPL,VNU,UTAU,UINF,S1,S2,S3,S4)
      D1=540.6
      D2=6546.0
      D3=82770.0
      A=2.439
      B=5.2
      F11=A*(YPL*(ALOG(YPL)-1.0)-50.0*(ALOG(50.0)-1.0))
      F12=B*(YPL-50.0)
      F1=F11+F12
      F21=YPL*(ALOG(YPL))**2-50.0*(ALOG(50.0))**2
      F22=-2*(YPL*(ALOG(YPL)-1.0)-50.0*(ALOG(50.0)-1.0))
      F23=2*A*B*(YPL*(ALOG(YPL)-1.0)-50.0*(ALOG(50.0)-1.0))
      F24=B**2*(YPL-50.0)
      F2=A**2*(F21+F22)+F23+F24
      F31=YPL*(ALOG(YPL))**3-3.0*YPL*(ALOG(YPL))**2+
     2    6.0*YPL*(ALOG(YPL)-1.0)
      F32=-50.0*(ALOG(50.0))**3+150.0*(ALOG(50.0))**2-
     2    300.0*(ALOG(50.0)-1.0)
      F33=YPL*(ALOG(YPL))**2-50.0*(ALOG(50.0))**2
      F34=-2.0*(YPL*(ALOG(YPL)-1.0)-50.0*(ALOG(50.0)-1.0))
      F35=3.0*A*B**2*(YPL*(ALOG(YPL)-1.0)-
     2    50.0*(ALOG(50.0)-1.0))
      F36=B**3*(YPL-50.0)
      F3=A**3*(F31+F32)+3.0*B*A**2*(F33+F34)+F35+F36
      S1=(D1+F1)*(VNU/UINF)*1000.0
      S2=(YPL*(VNU/UTAU)*1000.0)-S1
      S3=(D2+F2)*(VNU/UINF)*(UTAU/UINF)*1000.0
      S4=(D3+F3)*(VNU/UINF)*(UTAU/UINF)**2*1000.0
      RETURN
      END
```

TY_PARINT.FOR

```
      SUBROUTINE PARINT(U,Y,N,SUM1,SUM2,SUM3,SUM4)
      DIMENSIONU(N),Y(N),A(40),B(40),C(40),DET(40)
      DIMENSION AINT1(40),AINT2(40),AINT3(40),AINT4(40)
      DIMENSION AINT5(40),AINT6(40),AINT7(40),AINT8(40)
      SUM1=0.0
      SUM2=0.0
      SUM3=0.0
      SUM4=0.0
      N2=N-2
      DO 60 K=3,N2
      DET(K)=(Y(K+1)*Y(K+2)**2-Y(K+2)*Y(K+1)**2)-
     2       Y(K)*(Y(K+2)**2-Y(K+1)**2)+Y(K)**2*(Y(K+2)-
     3       Y(K+1))
      A(K)=(U(K)*(Y(K+1)*Y(K+2)**2-Y(K+2)*Y(K+1)**2)-
     2     Y(K)*(U(K+1)*Y(K+2)**2-U(K+2)*Y(K+1)**2)+
     3     Y(K)**2*(U(K+1)*Y(K+2)-U(K+2)*Y(K+1)))/DET(K)
      B(K)=((U(K+1)*Y(K+2)**2-U(K+2)*Y(K+1)**2)-
     2      U(K)*(Y(K+2)**2-Y(K+1)**2)+Y(K)**2*(U(K+2)-
     3     U(K+1)))/DET(K)
      C(K)=((Y(K+1)*U(K+2)-Y(K+2)*U(K+1))-
     2     Y(K)*(U(K+2)-U(K+1))+U(K)*(Y(K+2)-Y(K+1)))/DET(K)
      AINT1(K)=A(K)*(Y(K+1)-Y(K))+B(K)*0.5*(Y(K+1)**2-
     2         Y(K)**2)+C(K)*(Y(K+1)**3-Y(K)**3)/3.0
      AINT2(K)=A(K)*(Y(K+2)-Y(K+1))+B(K)*0.5*(Y(K+2)**2-
     2         Y(K+1)**2)+C(K)*(Y(K+2)**3-Y(K+1)**3)/3.0
      AINT3(K)=(1.0-A(K))*(Y(K+1)-Y(K))-B(K)*0.5*(Y(K+1)**2-
     2         Y(K)**2)-C(K)*(Y(K+1)**3-Y(K)**3)/3.0
      AINT4(K)=(1.0-A(K))*(Y(K+2)-Y(K+1))-B(K)*0.5*(Y(K+2)**2-
     2         Y(K+1)**2)-C(K)*(Y(K+2)**3-Y(K+1)**3)/3.0
      A51=A(K)*A(K)*(Y(K+1)-Y(K))
      A52=A(K)*B(K)*(Y(K+1)**2-Y(K)**2)
      A53=(2.0*A(K)*C(K)+B(K)*B(K))*(Y(K+1)**3-Y(K)**3)/3.0
      A54=B(K)*C(K)*(Y(K+1)**4-Y(K)**4)/2.0
      A55=C(K)*C(K)*(Y(K+1)**5-Y(K)**5)/5.0
      AINT5(K)=A51+A52+A53+A54+A55
      A61=A(K)*A(K)*(Y(K+2)-Y(K+1))
      A62=A(K)*B(K)*(Y(K+2)**2-Y(K+1)**2)
      A63=(2.0*A(K)*C(K)+B(K)*B(K))*(Y(K+2)**3-Y(K+1)**3)/3.0
      A64=B(K)*C(K)*(Y(K+2)**4-Y(K+1)**4)/2.0
      A65=C(K)*C(K)*(Y(K+2)**5-Y(K+1)**5)/5.0
      AINT6(K)=A61+A62+A63+A64+A65
      A71=A(K)*A(K)*A(K)*(Y(K+1)-Y(K))
      A72=3.0*A(K)*A(K)*B(K)*(Y(K+1)**2-Y(K)**2)/2.0
      A73=A(K)*(A(K)*C(K)+B(K)*B(K))*(Y(K+1)**3-Y(K)**3)
      A74=B(K)*(6.0*A(K)*C(K)+B(K)*B(K))*(Y(K+1)**4-Y(K)**4)/4.0
      A75=0.6*C(K)*(A(K)*C(K)+B(K)*B(K))*(Y(K+1)**5-Y(K)**5)
      A76=B(K)*C(K)*C(K)*(Y(K+1)**6-Y(K)**6)/2.0
      A77=C(K)*C(K)*C(K)*(Y(K+1)**7-Y(K)**7)/7.0
      AINT7(K)=A71+A72+A73+A74+A75+A76+A77
      A81=A(K)*A(K)*A(K)*(Y(K+2)-Y(K+1))
      A82=3.0*A(K)*A(K)*B(K)*(Y(K+2)**2-Y(K+1)**2)/2.0
      A83=A(K)*(A(K)*C(K)+B(K)*B(K))*(Y(K+2)**3-Y(K+1)**3)
      A84=B(K)*(6.0*A(K)*C(K)+B(K)*B(K))*(Y(K+2)**4-Y(K+1)**4)/4.0
      A85=0.6*C(K)*(A(K)*C(K)+B(K)*B(K))*(Y(K+2)**5-Y(K+1)**5)
      A86=B(K)*C(K)*C(K)*(Y(K+2)**6-Y(K+1)**6)/2.0
      A87=C(K)*C(K)*C(K)*(Y(K+2)**7-Y(K+1)**7)/7.0
      AINT8(K)=A81+A82+A83+A84+A85+A86+A87
      IF (K.EQ.3) GOTO 10
      GOTO 20
   10 SUM1=SUM1+AINT1(K)
      SUM2=SUM2+AINT3(K)
      SUM3=SUM3+AINT5(K)
      SUM4=SUM4+AINT7(K)
   20 IF (K.LT.N2.AND.K.GT.3) GOTO 30
      GOTO 40
   30 SUM1=SUM1+0.5*(AINT1(K)+AINT2(K-1))
      SUM2=SUM2+0.5*(AINT3(K)+AINT4(K-1))
      SUM3=SUM3+0.5*(AINT5(K)+AINT6(K-1))
      SUM4=SUM4+0.5*(AINT7(K)+AINT8(K-1))
   40 IF (K.EQ.N2) GOTO 50
      GOTO 60
   50 SUM1=SUM1+0.5*(AINT1(K)+AINT2(K-1))+AINT2(K)
      SUM2=SUM2+0.5*(AINT3(K)+AINT4(K-1))+AINT4(K)
      SUM3=SUM3+0.5*(AINT5(K)+AINT6(K-1))+AINT6(K)
      SUM4=SUM4+0.5*(AINT7(K)+AINT8(K-1))+AINT8(K)
   60 CONTINUE
      RETURN
      END
```

```
TY AITKEN.FOR
C       AITKEN
C       X AND Y ARE ONE DIMENSIONAL ARRAYS OF LENGTH N CONTAINING THE
C       ARG, IE. THE VALUE OF X FOR WHICH THE INTERPOLATED VALUE OF Y
C         IS TO BE OBTAINED.THE CORRESPONDING Y IS OBTAINED FROM THE
C         POLYNOMIAL OF DEGREE M.
C
        FUNCTION AITKEN(X,Y,ARG,N,M)
        DIMENSION X(1),Y(1),Z(10),F(10)
        IF (M.GT.N) M=N
        IF (M.GT.9) M=9
        M1=M+1
C
CC      SETMIN LOOP
C
        DO 4 I=1,N
        IF (ARG-X(I)) 5,5,4
 4      CONTINUE
        I=N
 5      IF (ARG-X(I)) 6,51,6
 51     F(M1)=Y(I)
        GOTO 14
 6      I=I-M/2-1
        IF (I) 7,80,80
 7      J=0
        GOTO 10
 80     IF (I+M-N) 8,8,9
 8      J=I
        GOTO 10
 9      J=N-M
CC      END OF SETMIN LOOP
C
 10     DO 11 I=1,M1
        Z(I)=ARG-X(J)
        F(I)=Y(J)
        J=J+1
 11     CONTINUE
D       WRITE(5,100)(Z(L), L=1,10),(F(L), L=1,10)
D       WRITE(5,100)(X(L),L=1,10),(Y(L),L=1,10)
D100    FORMAT((2F10.4))
        DO 13 I=1,M
        FI=F(I)
        ZI=Z(I)
        K=I+1
        DO 12 J=K,M1
        F(J)=FI+ZI*(F(J)-FI)/(ZI-Z(J))
 12     CONTINUE
 13     CONTINUE
 14     AITKEN=F(M1)
        RETURN
        END
```


MOMENTUM BALANCE ANALYSIS

```
TY MOBAL.FOR
        DIMENSION X(40),U(40),TH(40),DS(40),UTA(40),T(40)
        DIMENSION S(40),F(40),Q(40),AL(40),PL(40),PR(40)
        WRITE(5,10)
10      FORMAT(/' DATA FOR MOMENTUM BALANCE')
        WRITE(5,20)
20      FORMAT(//' NO. OF DATA STATIONS= ',$)
        READ(5,50)N
        WRITE(5,30)
30      FORMAT(/' FLOW IDENTIFIER FOR FLAT PLATE'/
        2' (NO PRESS.GRAD.=1,PRESS.GRAD.=0) VALUE= ',$)
        READ(5,50)JFPO
        WRITE(5,40)
40      FORMAT(/' FLOW IDENTIFIER(INTEGER VALUE)= ',$)
        READ(5,50)IDENT
50      FORMAT(I)
        WRITE(5,60)
60      FORMAT(/' NOW READ IN THE FOLLOWING PARAMETERS
        2 FOR EACH STATION'/' (SEPARATE BY COMMAS OR SPACES)'/
        3' (X-MM),(THETA-MM),(D1-MM),(U-M/S),(UTAU-M/S)'/)
        DO 70 K=1,N
        READ(5,80)X(K),TH(K),DS(K),U(K),UTA(K)
70      CONTINUE
80      FORMAT(5F)
        DO 90 K=1,N
        XI=X(1)
        THI=TH(1)
        UI=U(1)
        T(K)=U(K)**2*TH(K)/(UI**2*THI)
        S(K)=DS(K)/THI
        F(K)=(U(K)/UI)**2
        Q(K)=(UTA(K)/UI)**2
        AL(K)=X(K)/THI
90      CONTINUE
        CALL MOINT(T,S,F,Q,AL,N,PL,PR,JFPO)
        WRITE(5,100)IDENT
100     FORMAT(/'            MOMENTUM BALANCE'//
        2'          FLOW-    ',I2,////
        3'          LEFT HAND SIDE    RIGHT HAND SIDE'//)
        DO 110 K=1,N
        WRITE(5,120)PL(K),PR(K)
110     CONTINUE
120     FORMAT(13X,F8.4,10X,F8.4)
        STOP
        END
```

```
TY MOINT.FOR
      SUBROUTINE MOINT(T,S,F,Q,AL,N,PL,PR,I)
      DIMENSION T(N),S(N),F(N),Q(N),AL(N),PL(N),PR(N)
      DIMENSION AINT1(40),AINT2(40),AINT3(40),AINT4(40)
      DIMENSION A1(40),B1(40),C1(40),A2(40),B2(40),C2(40)
      DIMENSION DET1(40),DET2(40)
      N2=N-2
      SUM1=0.0
      SUM2=0.0
      PL(1)=0.0
      PR(1)=0.0
      DO 110 K=1,N2
      IF (I.EQ.1) GOTO 10
      DET1(K)=((F(K+1)*F(K+2)**2)-(F(K+2)*F(K+1)**2))-
     2(F(K)*(F(K+2)**2-F(K+1)**2))+F(K)*F(K)*(F(K+2)-F(K+1))
      A1(K)=(S(K)*(F(K+1)*F(K+2)**2-F(K+2)*F(K+1)**2)-
     2      F(K)*(S(K+1)*F(K+2)**2-S(K+2)*F(K+1)**2)+
     3      F(K)**2*(S(K+1)*F(K+2)-S(K+2)*F(K+1)))/DET1(K)
      B1(K)=((S(K+1)*F(K+2)**2-S(K+2)*F(K+1)**2)-
     2      S(K)*(F(K+2)**2-F(K+1)**2)+
     3      F(K)**2*(S(K+2)-S(K+1)))/DET1(K)
      C1(K)=((F(K+1)*S(K+2)-F(K+2)*S(K+1))-
     2      F(K)*(S(K+2)-S(K+1))+
     3      S(K)*(F(K+2)-F(K+1)))/DET1(K)
      AINT1(K)=(A1(K)*(F(K+1)-F(K))+B1(K)*(F(K+1)**2-F(K)**2)/2.0+
     2         C1(K)*(F(K+1)**3-F(K)**3)/3.0)
      AINT2(K)=(A1(K)*(F(K+2)-F(K+1))+
     2         B1(K)*(F(K+2)**2-F(K+1)**2)/2.0+
     3         C1(K)*(F(K+2)**3-F(K+1)**3)/3.0)
10    DET2(K)=(AL(K+1)*AL(K+2)**2-AL(K+2)*AL(K+1)**2)-
     2         AL(K)*(AL(K+2)**2-AL(K+1)**2)+
     3         AL(K)**2*(AL(K+2)-AL(K+1))
      A2(K)=(Q(K)*(AL(K+1)*AL(K+2)**2-AL(K+2)*AL(K+1)**2)-
     2      AL(K)*(Q(K+1)*AL(K+2)**2-Q(K+2)*AL(K+1)**2)+
     3      AL(K)**2*(Q(K+1)*AL(K+2)-Q(K+2)*AL(K+1)))/DET2(K)
      B2(K)=((Q(K+1)*AL(K+2)**2-Q(K+2)*AL(K+1)**2)-
     2      Q(K)*(AL(K+2)**2-AL(K+1)**2)+
     3      AL(K)**2*(Q(K+2)-Q(K+1)))/DET2(K)
      C2(K)=((AL(K+1)*Q(K+2)-AL(K+2)*Q(K+1))-
     2      AL(K)*(Q(K+2)-Q(K+1))+
     3      Q(K)*(AL(K+2)-AL(K+1)))/DET2(K)
      AINT3(K)=(A2(K)*(AL(K+1)-AL(K))+
     2         B2(K)*(AL(K+1)**2-AL(K)**2)/2.0+
     3         C2(K)*(AL(K+1)**3-AL(K)**3)/3.0)
      AINT4(K)=(A2(K)*(AL(K+2)-AL(K+1))+
     2         B2(K)*(AL(K+2)**2-AL(K+1)**2)/2.0+
     3         C2(K)*(AL(K+2)**3-AL(K+1)**3)/3.0)
      IF (K.EQ.1) GOTO 20
      GOTO 40
20    IF (I.EQ.1) GOTO 30
      SUM1=SUM1+AINT1(K)
30    SUM2=SUM2+AINT3(K)
      PL(K+1)=T(K+1)-1.0+SUM1/2.0
      PR(K+1)=SUM2
40    IF (K.LT.N2.AND.K.GT.1) GOTO 50
      GOTO 70
50    IF (I.EQ.1) GOTO 60
      SUM1=SUM1+0.5*(AINT1(K)+AINT2(K-1))
60    SUM2=SUM2+0.5*(AINT3(K)+AINT4(K-1))
      PL(K+1)=T(K+1)-1.0+SUM1/2.0
      PR(K+1)=SUM2
70    IF (K.EQ.N2) GOTO 80
      GOTO 110
80    IF (I.EQ.1) GOTO 90
      SUM1=SUM1+0.5*(AINT1(K)+AINT2(K-1))
      GOTO 100
90    AINT2(N2)=0.0
100   SUM2=SUM2+0.5*(AINT3(K)+AINT4(K-1))
      PL(K+1)=T(K+1)-1.0+SUM1/2.0
      PR(K+1)=SUM2
      PL(N)=T(N)-1.0+(SUM1+AINT2(N2))/2.0
      PR(N)=SUM2+AINT4(N2)
110   CONTINUE
      RETURN
      END
```

Reduction of Laminar Velocity Profile Data

```
TY CFLBL.FOR
      DIMENSION Y(30),U(30),UNOR(30),URMS(30),GAMA(30),
     2          PCT(30),YD(30)
      WRITE(5,10)
   10 FORMAT(/' DATA FOR LAMINAR BOUNDARY LAYER VELOCITY PROFILE')
      WRITE(5,20)
   20 FORMAT(/' AIR TEMPERATURE IN DEG C= ',$)
      READ(5,15)T
      WRITE(5,30)
   30 FORMAT(/' ATMOS PRESSURE IN MM HG= ',$)
      READ(5,15)Z
      WRITE(5,40)
   40 FORMAT(/' MAINSTREAM VELOCITY IN M/S= ',$)
      READ(5,15)UINF
      WRITE(5,50)
   50 FORMAT(/' DISTANCE FROM L.E. IN MM= ',$)
      READ(5,15)X
        WRITE(5,51)
   51   FORMAT(/' SPANWISE LOCATION IN MM= ',$)
        READ(5,15)SPAN
        WRITE(5,52)
   52   FORMAT(/' REFERENCE Y-VALUE IN MM= ',$)
        READ(5,15)YO
        WRITE(5,54)
   54   FORMAT(/' REFERENCE DISPLACEMENT VOLTAGE= ',$)
        READ(5,15)VO
      WRITE(5,60)
   60   FORMAT(/' NUMBER OF DATA POINTS= ',$)
      READ(5,25)N
   15 FORMAT(F)
   25 FORMAT(I)
      WRITE(5,70)
   70   FORMAT(/' NOW READ IN DISP. VOLTS, U-M/S, URMS
        2 AND THE INTERMITTENCY'/
        3' (START WITH THE VALUES CORRES. TO MINM. Y)')
      DO 80 K=1,N
      READ(5,35)Y(K),U(K),URMS(K),GAMA(K)
        Y(K)=YO+(VO-Y(K))*9.96
        UNOR(K)=U(K)/UINF
        PCT(K)=URMS(K)*100.0/UINF
   80 CONTINUE
   35   FORMAT(F,F,F,F)
      DELTA=AITKEN(UNOR,Y,0.995,N,2)
      RHO=(0.46535*Z)/(T+273.)
      VISC=(1.725+0.004375*T)/10.0**5
      ANU=VISC/RHO
      RENOX=UINF*X/(ANU*1000.0)
      WRITE(5,90)X,SPAN,UINF,RENOX
   90 FORMAT(/////////'           LAMINAR VELOCITY PROFILE'//
     2'           DISTANCE FROM LEADING EDGE= ',F7.1,' MM'//
     3'           SPANWISE LOCATION= ',F5.1,' MM'//
     4'           FREESTREAM VELOCITY= ',F6.2,' M/S'//
     5'           PLATE REYNOLDS NO= ',F7.0,////'                ',
     6'Y-DIST(MM)   Y/DELTA   U/UINF    PCT.    INTERMITTENCY'/)
        SUMS=0.0
        L=0
      DO 100 K=1,N
        YD(K)=Y(K)/DELTA
        IF (UNOR(K).GT.0.45) GOTO 92
        L=L+1
        SUMS=SUMS+UNOR(K)/Y(K)
   92   WRITE(5,130)Y(K),YD(K),UNOR(K),PCT(K),GAMA(K)
  100 CONTINUE
  130 FORMAT(15X,F6.2,8X,F6.3,4X,F6.3,2X,F6.2,8X,F6.3)
      YMAX=Y(N)
      WRITE(5,140)DELTA
  140 FORMAT(///                  APPROX EDGE OF BOUNDARY LAYER= ',
     2F6.2,' MM'/////////)
      CALL PLYINT(UNOR,Y,N,YMAX,AINT1,AINT2,AINT3,AINT4,A,B,C,D)
      DSTAR=AINT2
      THETA=AINT1-AINT3
      D2STR=AINT1-AINT4
      H12=DSTAR/THETA
      H32=D2STR/THETA
      RTHETA=(UINF*THETA)/(ANU*1000.0)
      RDSTAR=(UINF*DSTAR)/(ANU*1000.0)
      SL=SUMS/L*UINF*1000.0
      TO=VISC*SL
      CF=2.0*TO/(RHO*UINF**2)
      WRITE(5,150)DSTAR,THETA,D2STR,H12,H32,RTHETA,RDSTAR,CF,TO
  150 FORMAT(///          BOUNDARY LAYER PARAMETERS'/////       ',
     2'DISPLACEMENT TH.= ',F8.4,'MM'///          MOMENTUM TH.= '
     3,F8.4,'MM'///          ENERGY TH.= ',F8.4,'MM'//
     4'          SHAPE FACTOR H12= ',F8.4,///          SHAPE
     5 FACTOR H32= ',F8.4,///          MOM.TH.REYNOLDS NO.= ',F,//
     6'          DISP.TH.REYNOLDS NO.= ',F,//
     7'          SKIN FRICTION COEFF.= ',F,//
     8'          WALL SHEAR STRESS= ',F7.4,'N/M^2')
      STOP
      END
```

```
TY PLYINT.FOR
      SUBROUTINE PLYINT(U,Y,N,YT,AI1,AI2,AI3,AI4,G,AL,AM,F)
      DIMENSION U(N),Y(N),E(30),UP(30)
      SY2=0.0
      SY3=0.0
      SY4=0.0
      SY5=0.0
      SY6=0.0
      SY7=0.0
      SY8=0.0
      SYU=0.0
      SY2U=0.0
      SY3U=0.0
      SY4U=0.0
      DO 10 K=1,N
      SY2=SY2+Y(K)**2
      SY3=SY3+Y(K)**3
      SY4=SY4+Y(K)**4
      SY5=SY5+Y(K)**5
      SY6=SY6+Y(K)**6
      SY7=SY7+Y(K)**7
      SY8=SY8+Y(K)**8
      SYU=SYU+Y(K)*U(K)
      SY2U=SY2U+Y(K)**2*U(K)
      SY3U=SY3U+Y(K)**3*U(K)
      SY4U=SY4U+Y(K)**4*U(K)
10    CONTINUE
      DET=SY2*(SY4*(SY6*SY8-SY7*SY7)-SY5*(SY5*SY8-SY6*SY7)+
     2    SY6*(SY5*SY7-SY6*SY6))-
     3    SY3*(SY3*(SY6*SY8-SY7*SY7)-SY5*(SY4*SY8-SY5*SY7)+
     4    SY6*(SY4*SY7-SY5*SY6))+
     5    SY4*(SY3*(SY5*SY8-SY6*SY7)-SY4*(SY4*SY8-SY5*SY7)+
     6    SY6*(SY4*SY6-SY5*SY5))-
     7    SY5*(SY3*(SY5*SY7-SY6*SY6)-SY4*(SY4*SY7-SY5*SY6)+
     8    SY5*(SY4*SY6-SY5*SY5))
      G=(SYU*(SY4*(SY6*SY8-SY7*SY7)-SY5*(SY5*SY8-SY6*SY7)+
     2  SY6*(SY5*SY7-SY6*SY6))-
     3  SY3*(SY2U*(SY6*SY8-SY7*SY7)-SY5*(SY3U*SY8-SY4U*SY7)+
     4  SY6*(SY3U*SY7-SY4U*SY6))+
     5  SY4*(SY2U*(SY5*SY8-SY6*SY7)-SY4*(SY3U*SY8-SY4U*SY7)+
     6  SY6*(SY3U*SY6-SY4U*SY5))-
     7  SY5*(SY2U*(SY5*SY7-SY6*SY6)-SY4*(SY3U*SY7-SY4U*SY6)+
     8  SY5*(SY3U*SY6-SY4U*SY5)))/DET
      AL=(SY2*(SY2U*(SY6*SY8-SY7*SY7)-SY5*(SY3U*SY8-SY4U*SY7)+
     2  SY6*(SY3U*SY7-SY4U*SY6))-
     3  SYU*(SY3*(SY6*SY8-SY7*SY7)-SY5*(SY4*SY8-SY5*SY7)+
     4  SY6*(SY4*SY7-SY5*SY6))+
     5  SY4*(SY3*(SY3U*SY8-SY4U*SY7)-SY2U*(SY4*SY8-SY5*SY7)+
     6  SY6*(SY4*SY4U-SY5*SY3U))-
     7  SY5*(SY3*(SY3U*SY7-SY4U*SY6)-SY2U*(SY4*SY7-SY5*SY6)+
     8  SY5*(SY4*SY4U-SY5*SY3U)))/DET
      AM=(SY2*(SY4*(SY3U*SY8-SY4U*SY7)-SY2U*(SY5*SY8-SY6*SY7)+
     2  SY6*(SY5*SY4U-SY6*SY3U))-
     3  SY3*(SY3*(SY3U*SY8-SY4U*SY7)-SY2U*(SY4*SY8-SY5*SY7)+
     4  SY6*(SY4*SY4U-SY5*SY3U))+
     5  SYU*(SY3*(SY5*SY8-SY6*SY7)-SY4*(SY4*SY8-SY5*SY7)+
     6  SY6*(SY4*SY6-SY5*SY5))-
     7  SY5*(SY3*(SY5*SY4U-SY6*SY3U)-SY4*(SY4*SY4U-SY5*SY3U)+
     8  SY2U*(SY4*SY6-SY5*SY5)))/DET
      F=(SY2*(SY4*(SY6*SY4U-SY7*SY3U)-SY5*(SY5*SY4U-SY6*SY3U)+
     2  SY2U*(SY5*SY7-SY6*SY6))-
     3  SY3*(SY3*(SY6*SY4U-SY7*SY3U)-SY5*(SY4*SY4U-SY5*SY3U)+
     4  SY2U*(SY4*SY7-SY5*SY6))+
     5  SY4*(SY3*(SY5*SY4U-SY6*SY3U)-SY4*(SY4*SY4U-SY5*SY3U)+
     6  SY2U*(SY4*SY6-SY5*SY5))-
     7  SYU*(SY3*(SY5*SY7-SY6*SY6)-SY4*(SY4*SY7-SY5*SY6)+
     8  SY5*(SY4*SY6-SY5*SY5)))/DET
      WRITE(5,20)G,AL,AM,F
20    FORMAT(///                  LEAST SQUARES POLYNOMIAL FIT
     2:-'///                          U/UINF=
     3 A(Y)+B(Y)^2+C(Y)^3+D(Y)^4'//
     4'                          WHERE-'///                    ',
     5'    A= ',F,///                              B= ',F,
     6///                            C= ',F,
     7///                            D= ',F,//
     8'                 YDATA       U/UINF-DATA       U/UINF
     9-POLY          ERROR')
      ERR=0.0
      DO 30 K=1,N
      UP(K)=(G*Y(K)+AL*Y(K)**2+AM*Y(K)**3+F*Y(K)**4)
      E(K)=UP(K)-U(K)
      ERR=ERR+E(K)**2
      WRITE(5,40)Y(K),U(K),UP(K),E(K)
30    CONTINUE
40    FORMAT(14X,F6.2,8X,F7.4,10X,F7.4,9X,F9.5)
      ERMS=SQRT(ERR/N)
      WRITE(5,50)ERMS
50    FORMAT(///                        RMS ERROR OF FIT = ',F)
      AI1=YT**2*(G/2.+AL*YT/3.+AM*YT**2/4.+F*YT**3/5.)
      AI2=YT-AI1
      AI3=YT**3*(G*G/3.+G*AL*YT/2.+(2.*G*AM+AL*AL)*YT**2/5.+
     2(G*F+AL*AM)*YT**3/3.+(2.*AL*F+AM*AM)*YT**4/7.+
     3AM*F*YT**5/4.+F*F*YT**6/9.)
      AI4=YT**4*(G*G*G/4.+3.*G*G*AL*YT/5.+G*(AL*AL+G*AM)*YT**2
     2/2.+(3.*G*G*F+6.*G*AL*AM+AL*AL*AL)*YT**3/7.+3.*(2.*G
     3*AL*F+G*AM*AM+AM*AL*AL)*YT**4/8.+
     4(2.*G*F*AM+AL*AL*F+AL*AM*AM)*YT**5/3.+
     5(3.*G*F*F+6.*AL*AM*F+AM*AM*AM)*YT**6/10.+
     63*F*(AL*F+AM*AM)*YT**7/11.+
     7AM*F*F*YT**8/4.+F*F*F*YT**9/13.)
      RETURN
      END
```

CALCULATION OF LAMINAR, TRANSITIONAL AND TURBULENT BOUNDARY LAYER (1)

MAIN PROGRAM. — LTBL

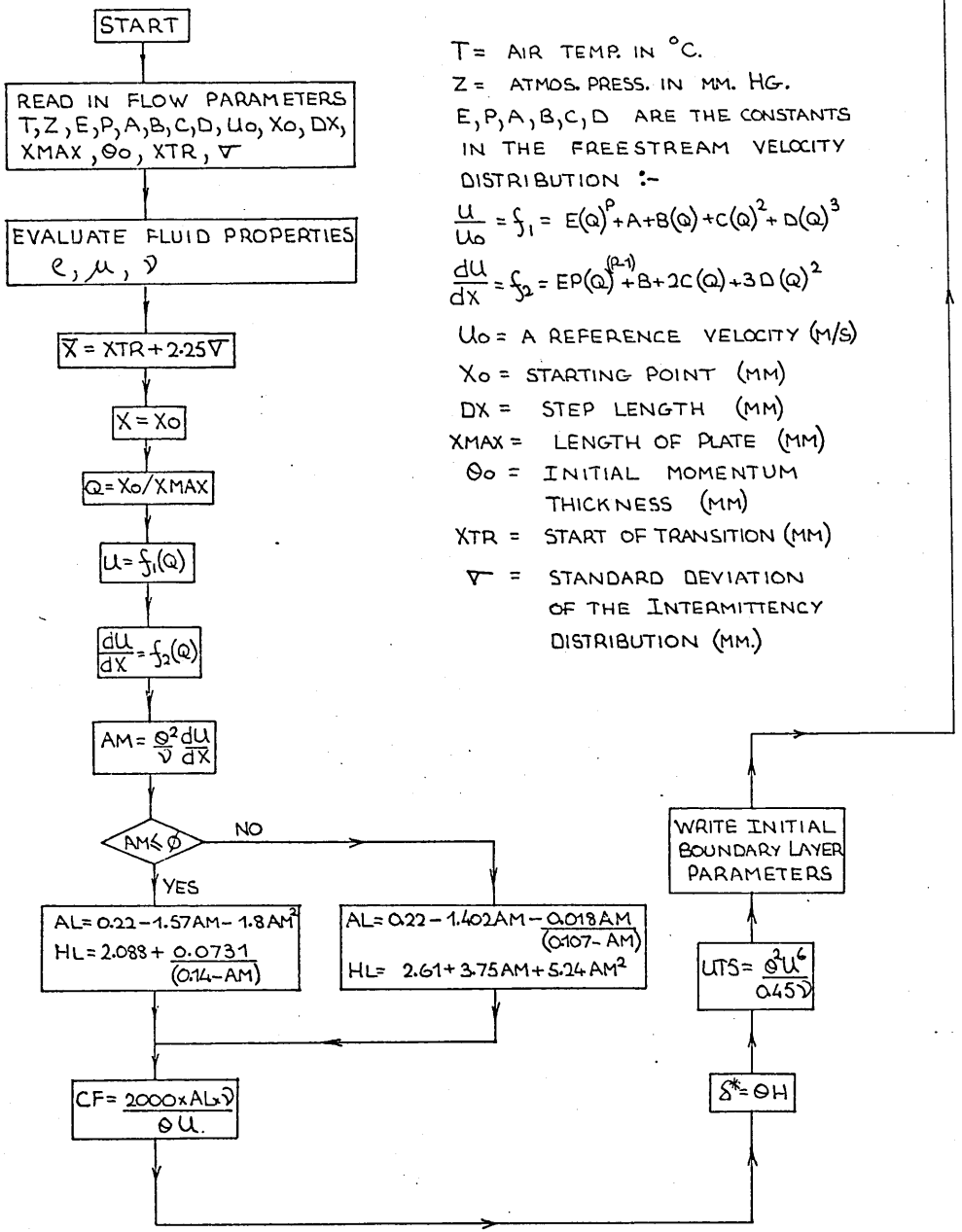

T = AIR TEMP. IN °C.

Z = ATMOS. PRESS. IN MM. HG.

E, P, A, B, C, D ARE THE CONSTANTS IN THE FREESTREAM VELOCITY DISTRIBUTION :-

$$\frac{u}{u_o} = f_1 = E(Q)^P + A + B(Q) + C(Q)^2 + D(Q)^3$$

$$\frac{du}{dx} = f_2 = EP(Q)^{(P-1)} + B + 2C(Q) + 3D(Q)^2$$

U_o = A REFERENCE VELOCITY (M/S)

X_o = STARTING POINT (MM)

DX = STEP LENGTH (MM)

XMAX = LENGTH OF PLATE (MM)

θ_o = INITIAL MOMENTUM THICKNESS (MM)

XTR = START OF TRANSITION (MM)

∇ = STANDARD DEVIATION OF THE INTERMITTENCY DISTRIBUTION (MM.)

CALCULATION OF LAMINAR, TRANSITIONAL AND TURBULENT BOUNDARY LAYER (2)

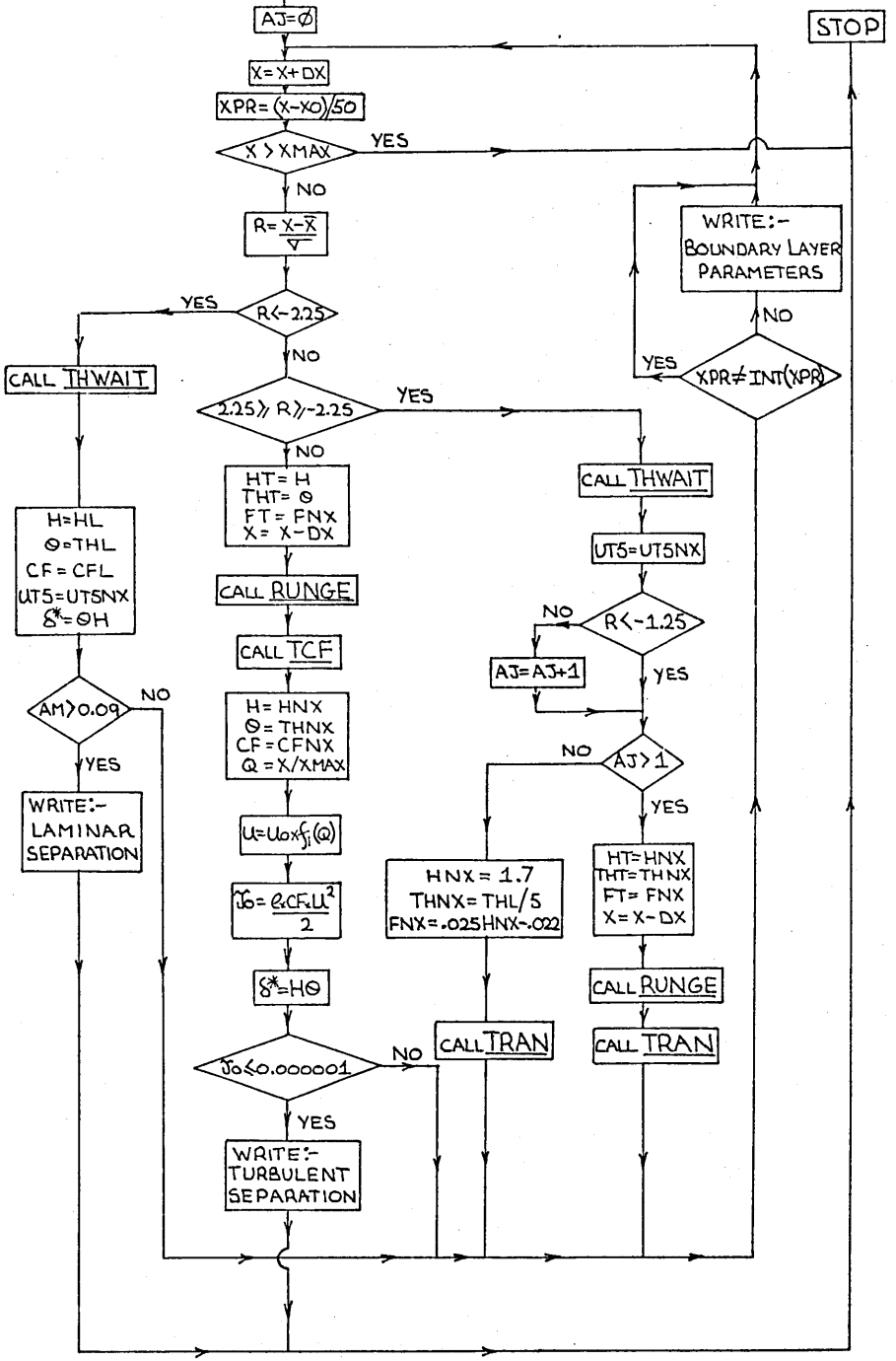

CALCULATION OF LAMINAR BOUNDARY LAYER
SUBROUTINE — THWAIT

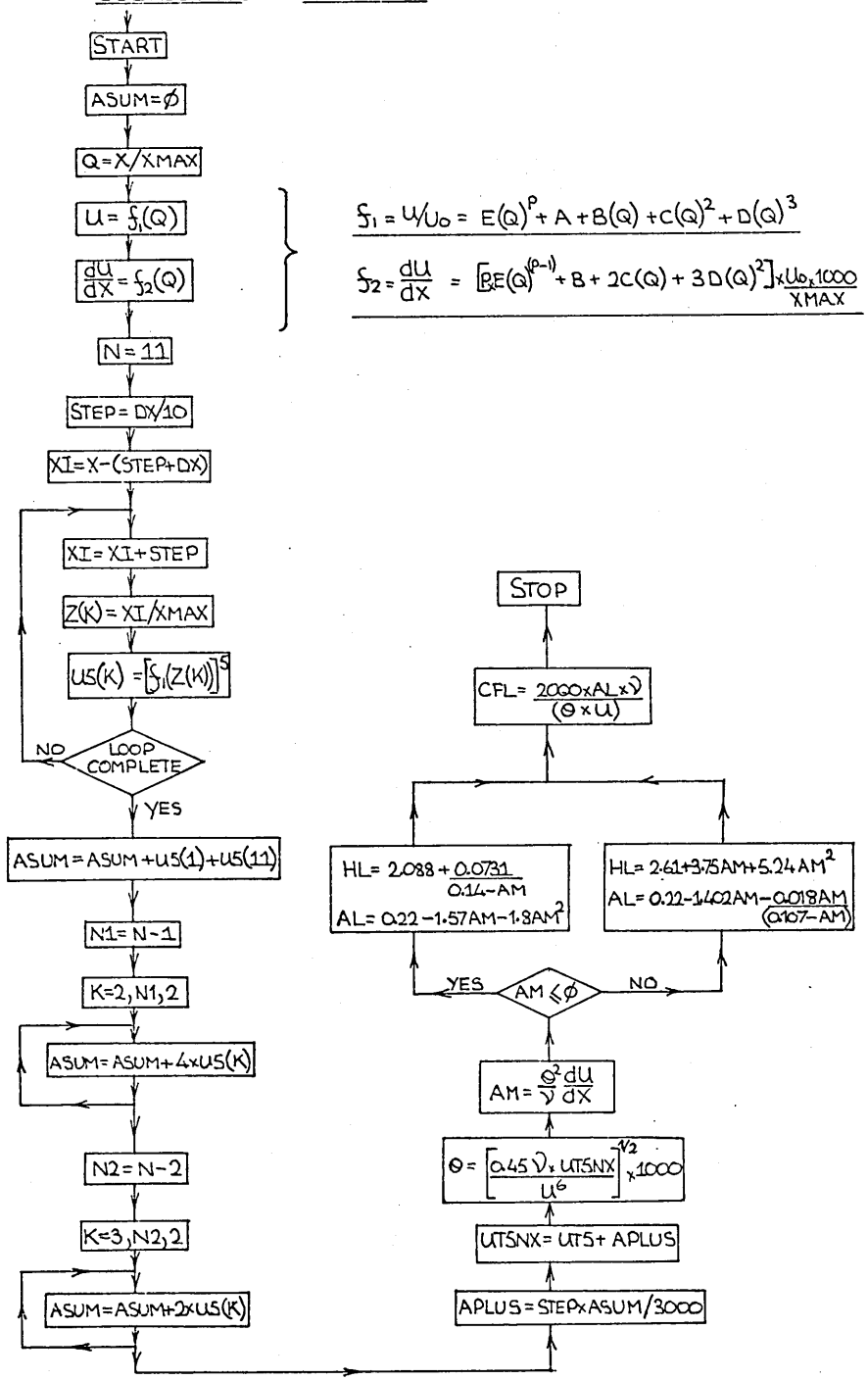

$$f_1 = U/U_0 = E(Q)^P + A + B(Q) + C(Q)^2 + D(Q)^3$$

$$f_2 = \frac{dU}{dX} = \left[BE(Q)^{(P-1)} + B + 2C(Q) + 3D(Q)^2\right] \times \frac{U_0 \times 1000}{XMAX}$$

CALCULATION OF TURBULENT BOUNDARY LAYER
SUBROUTINE — RUNGE

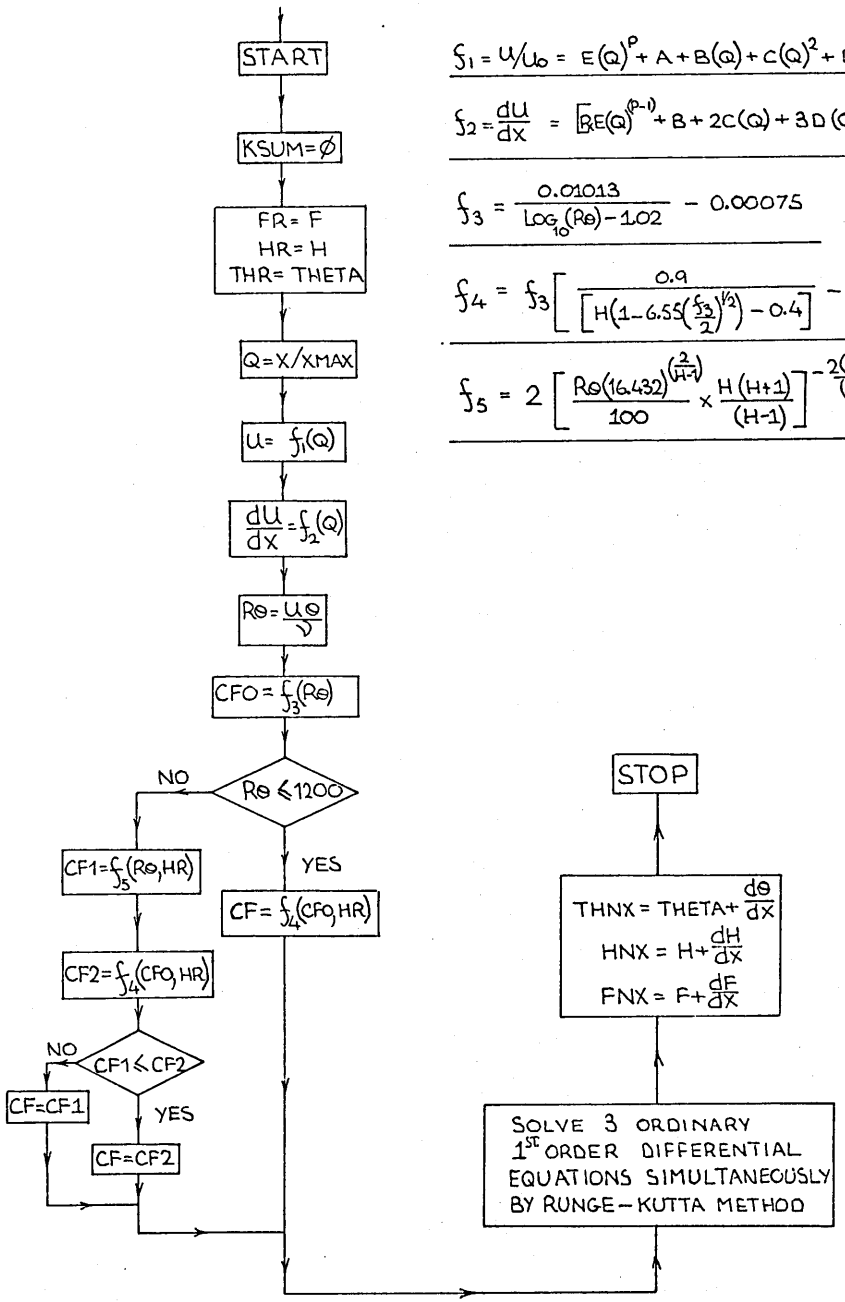

$$f_1 = U/U_0 = E(Q)^P + A + B(Q) + C(Q)^2 + D(Q)^3$$

$$f_2 = \frac{dU}{dX} = \left[BE(Q)^{(P-1)} + B + 2C(Q) + 3D(Q)^2\right] \times \frac{U_0 \times 1000}{XMAX}$$

$$f_3 = \frac{0.01013}{\log_{10}(R\Theta) - 1.02} - 0.00075$$

$$f_4 = f_3\left[\frac{0.9}{\left[H\left(1 - 6.55\left(\frac{f_3}{2}\right)^{1/2}\right) - 0.4\right]} - 0.5\right]$$

$$f_5 = 2\left[\frac{R\Theta(16.432)^{\left(\frac{2}{H-1}\right)}}{100} \times \frac{H(H+1)}{(H-1)}\right]^{-\frac{2(H-1)}{(H+1)}}$$

CALCULATION OF TRANSITIONAL BOUNDARY LAYER. (1)

SUBROUTINE — TRAN

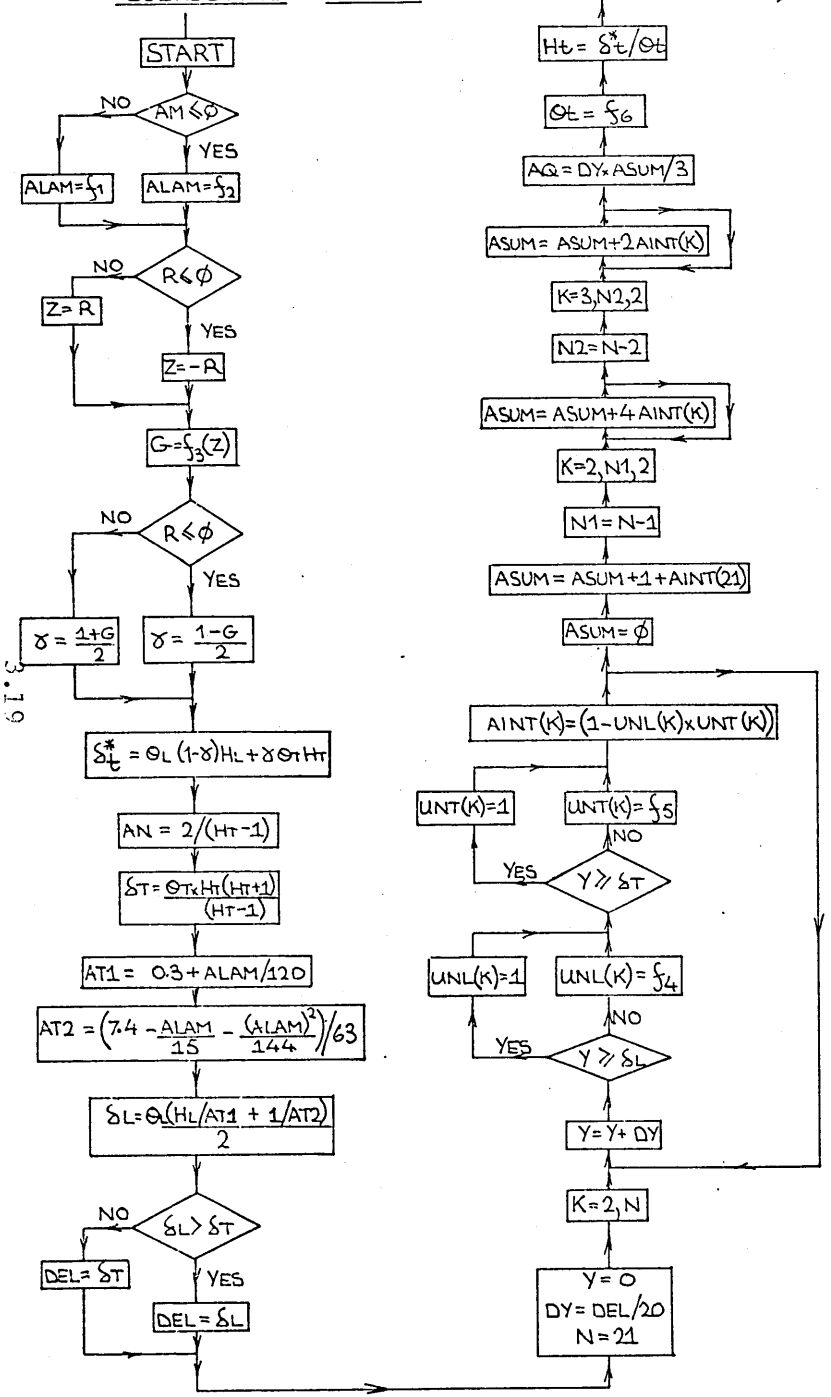

CALCULATION OF TRANSITIONAL BOUNDARY LAYER (2)

SUBROUTINE — TRAN

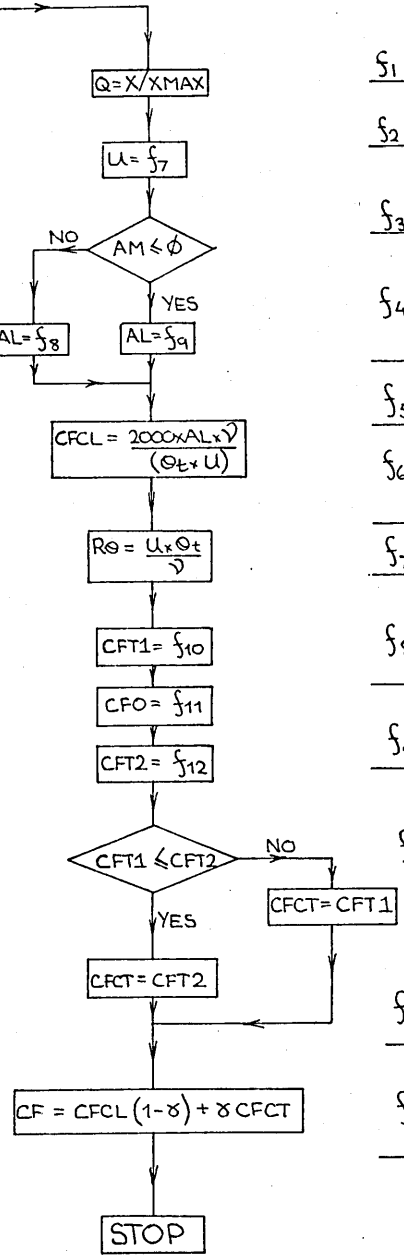

f_1 = ALAM = $-73AM + 109AM^2 - 790AM^3$

f_2 = ALAM = $-70AM + 310AM^2 + 5430AM^3 - 66000AM^4$

f_3 = $G = 0.8273Z - 0.094Z^2 - 0.073Z^3 + 0.0165Z^4$

f_4 = UNL = $\left(2(Y/\delta) - 2(Y/\delta)^3 + (Y/\delta)^4\right) + \frac{ALAM}{6}\left((Y/\delta) - 3(Y/\delta)^2 + 3(Y/\delta)^3 - (Y/\delta)^4\right)$

f_5 = UNT = $(Y/\delta T)^{1/AN}$

$f_6 = \Theta t = (1-\gamma)\left[(1-\gamma)\Theta L - \gamma\Theta LHL\right] + 2\gamma(1-\gamma)AG + \gamma\left[\gamma\Theta T - (1-\gamma)\Theta THT\right]$

f_7 = U = $U_0\left[E(Q)^P + A + B(Q) + C(Q)^2 + D(Q)^3\right]$

f_8 = AL = $0.22 - 1.402\,AM - \frac{0.18\,AM}{(0.107 - AM)}$

f_9 = AL = $0.22 - 1.57\,AM - 1.8\,AM^2$

$f_{10} = 2\left[\frac{R\Theta(16.432)^{\left(\frac{2}{H-1}\right)}}{100} \times \frac{H(H+1)}{(H-1)}\right]^{-\frac{2(H-1)}{(H+1)}}$

$f_{11} = \frac{0.01013}{\log_{10}(R\Theta) - 1.02} - 0.00075$

$f_{12} = f_{11}\left[\frac{0.9}{\left[H\left(1 - 6.55\left(\frac{f_{11}}{2}\right)^{1/2}\right) - 0.4\right]} - 0.5\right]$

Reduction of Turbulent Velocity Profile Data

Main Program — CFTBL.

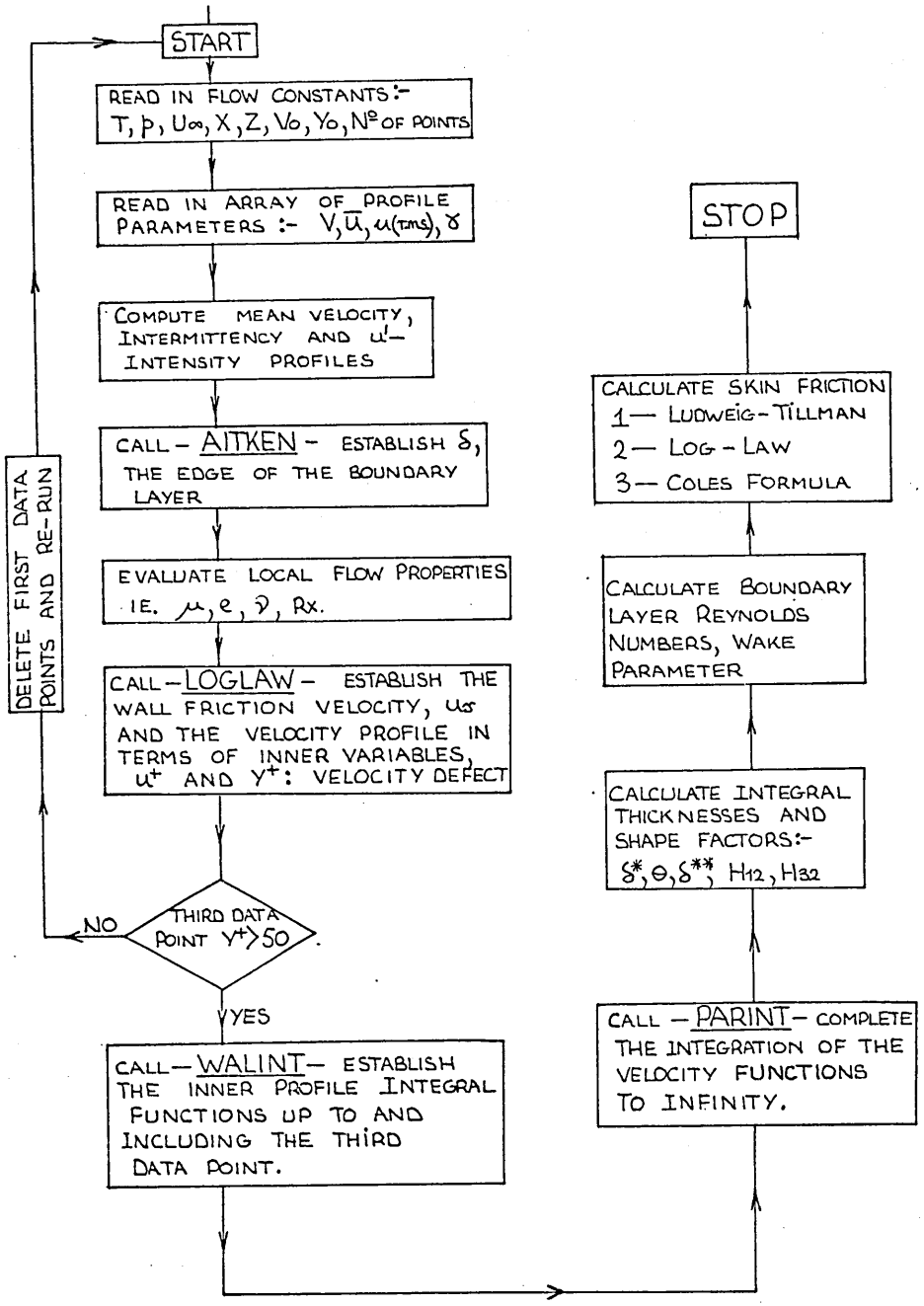

Calculation of Wall Friction Velocity

Sub-routine — LOG-LAW

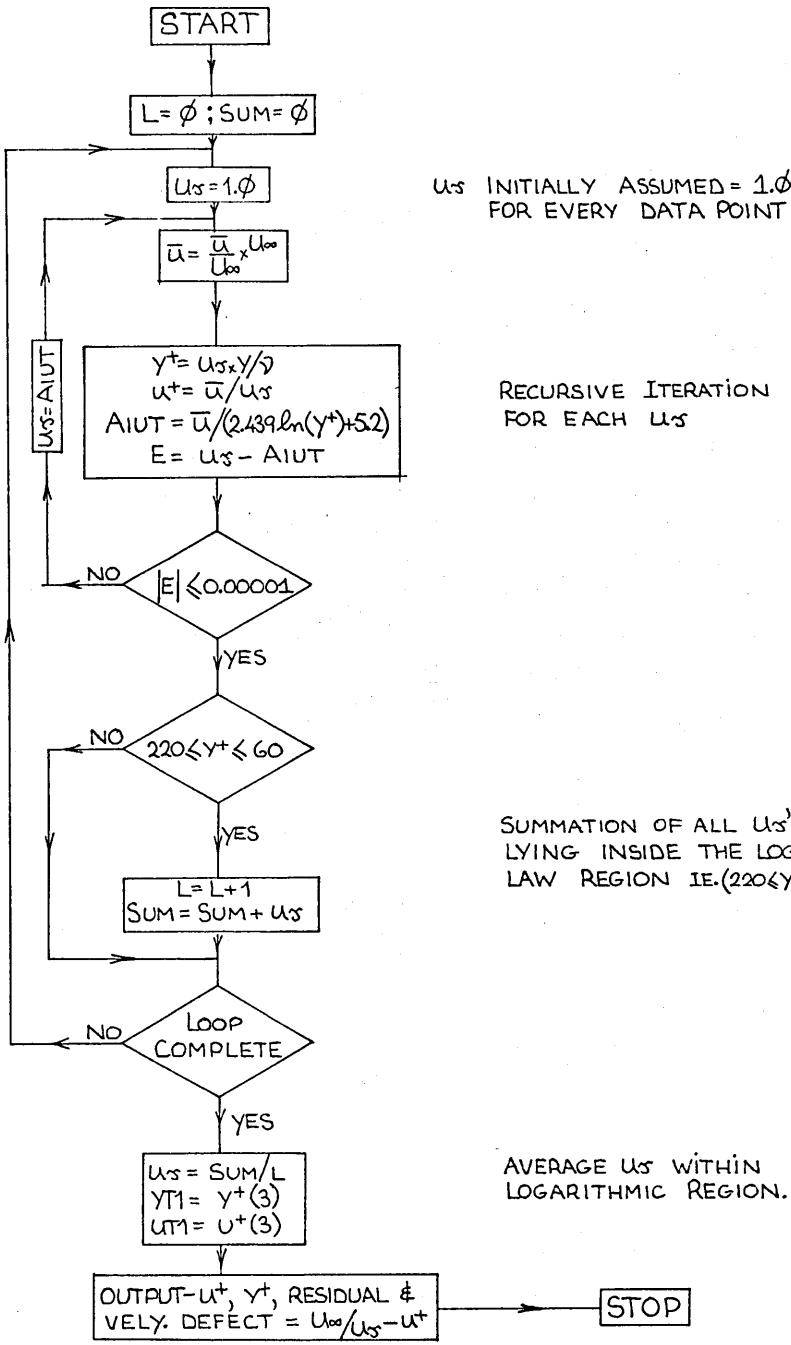

Calculation of Inner Profile Integrals

Sub-routine — WALINT

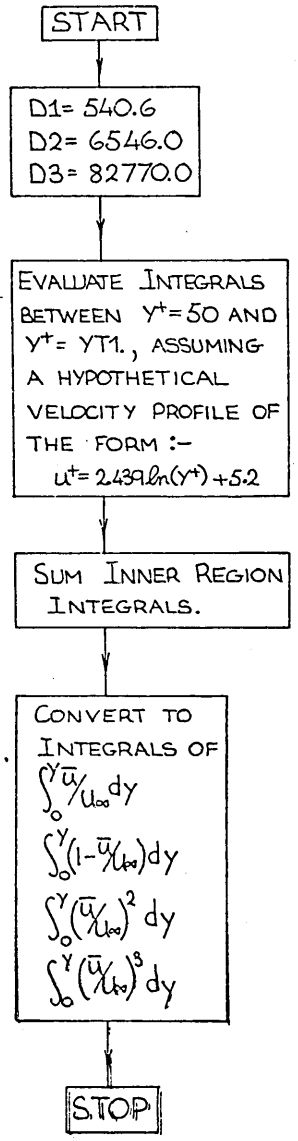

Coles Standard Integrals

IE. $\int_0^{50} u^+ dy^+$; $\int_0^{50} u^{+2} dy^+$; $\int_0^{50} u^{+3} dy^+$

WITH $Y = \dfrac{(YT1).\nu}{u_\tau}$

Calculation of Outer Profile Integrals

Sub-routine — PARINT

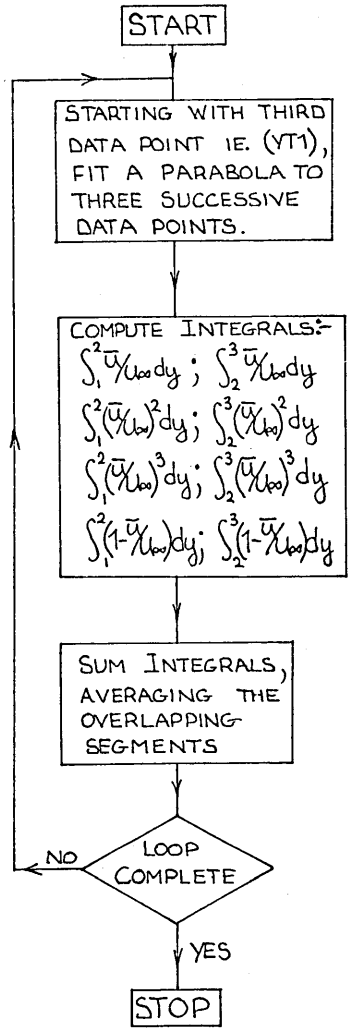

Least squares method

} Modified Simpson's Rule.

REDUCTION OF LAMINAR VELOCITY PROFILE DATA

MAIN PROGRAM — CFLBL.

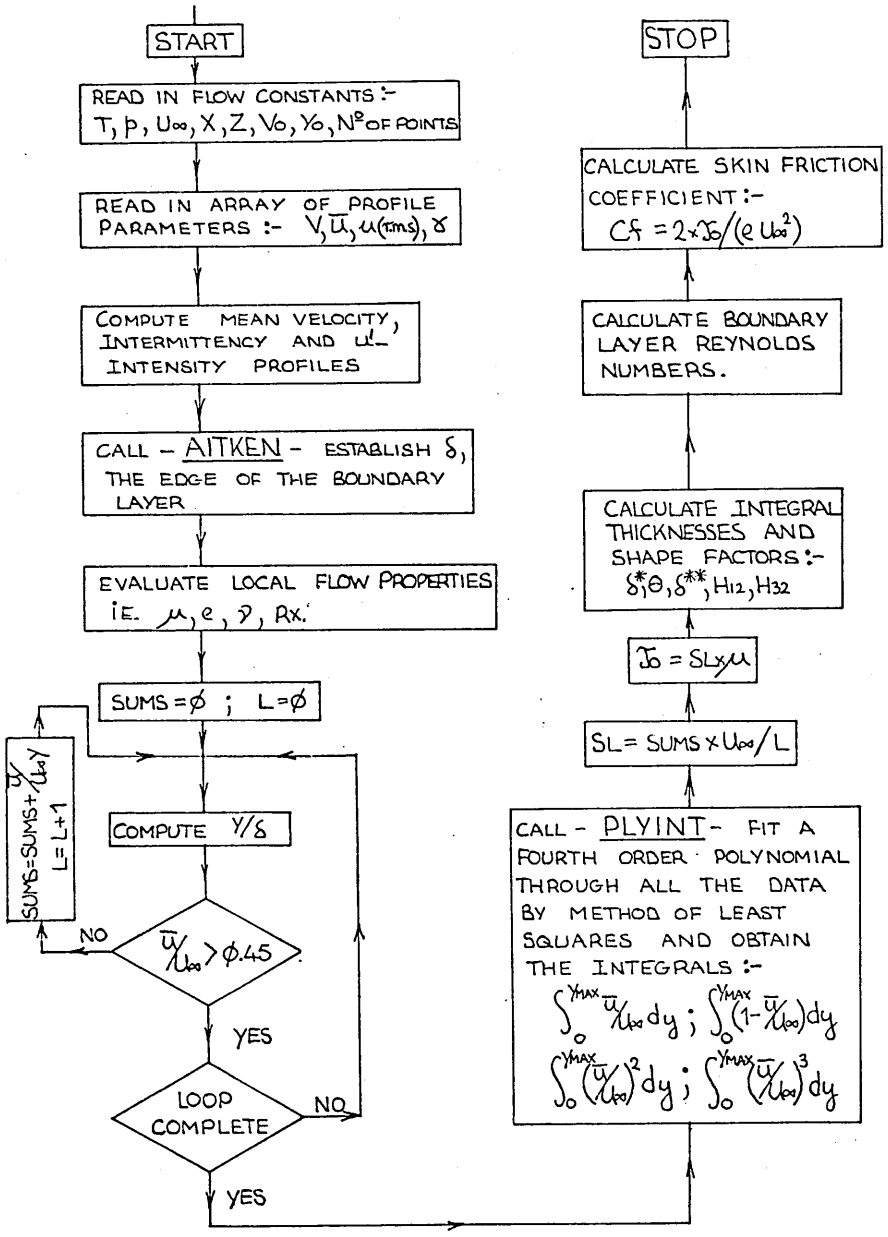

ESTIMATION OF EDGE OF BOUNDARY LAYER

SUB-ROUTINE — AITKEN

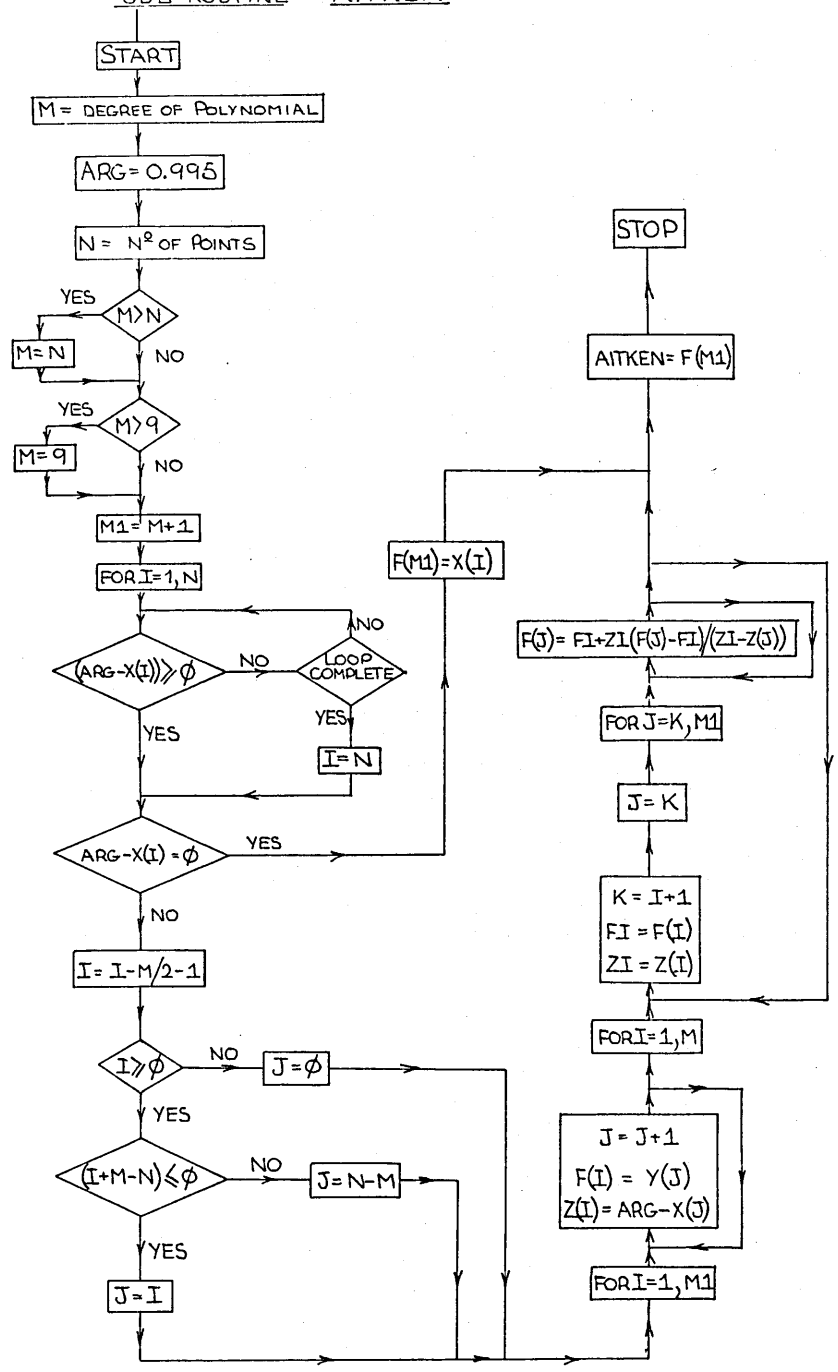

APPENDIX 4.

Development of a general relationship for estimating the transitional boundary layer skin friction coefficient.

A formula for estimating the transitional local skin friction coefficient is developed in the form :- $C_{f_t} = f(R_\theta, H, \bar{\delta})$. Thwaites' method is used as a basis for the calculation of the laminar contribution and a function, $f_2(R_\theta, H)$, is developed for the estimation of the turbulent contribution.

Development of a general relationship for estimating the transitional boundary layer skin friction coefficient.

A. 4.1 Introduction.

Section 3.5 outlines the difficulty in obtaining a representative skin friction coefficient from a measured transitional mean velocity profile. A general relationship was therefore developed in order to make, at least, an approximate estimate of the transitional values. The idea that the transitional skin friction coefficient could be expressed by the intermittency weighted average of the respective laminar and turbulent contributions, was originally proposed by Emmons and Bryson (1950). They gave a functional relationship in the form :-

$$C_{f_t} = (1 - \overline{\gamma})\, C_{f_L} + \overline{\gamma} C_{f_T} \qquad \text{A. 4.1}$$

where the suffixes t,L and T refer to transitional, laminar and turbulent skin friction coefficients respectively and $\overline{\gamma}$ is the mean value of intermittency near the wall.

Emmons and Bryson and also Dhawan and Narasimha, then used standard flat plate skin friction formulae to estimate the laminar and turbulent contributions to the overall skin friction coefficient. The above forms were however, restricted to the case of zero pressure gradient flows. Some doubt must also be cast as to the validity of the turbulent skin friction relations at such extremely low Reynolds numbers. Assuming the validity of eqn. A. 4.1, the problem thus resolves to one of specifying general functions for C_{f_L} and C_{f_T}.

A. 4.2 The laminar component.

Thwaites' method of solution for laminar boundary layers in arbitrary pressure gradients, see Appendix 5, utilises a parameter l_1, which is a sole function of the pressure gradient parameter M and is related to the wall shear stress by :-

$$\tau_{o_L} = \frac{\mu . U_\infty}{\theta_L} . l_1(M) \qquad \text{A. 4.2}$$

where $$M = \frac{\theta^2}{\nu} . \frac{dU_\infty}{dx}$$

The relations between l_1 and M are conveniently curve-fitted by Cebeci and Bradshaw (1976) as :-

$$l_1 = 0.22 + 1.57\ M - 1.8\ M^2 \qquad (0 \leq M \leq 0.10) \qquad \text{A. 4.3}$$

$$l_1 = 0.22 + 1.402\ M + \frac{0.018\ M}{0.107 + M} \qquad (-0.10 \leq M \leq 0) \qquad \text{A. 4.4}$$

From eqn. A. 4.2, the laminar skin friction coefficient then becomes :-

$$C_{f_L} = \frac{2 \times l_1(M)}{(R\theta)_L} \qquad \text{A. 4.5}$$

A. 4.3 The turbulent component.

Immediately after transition is complete, the resulting turbulent boundary layer has a very low momentum thickness Reynolds number coupled with an unusually high value of shape factor H. In a zero pressure gradient flow, the initial shape factor decreases rapidly over a short axial length and goes on decreasing at an ever slower rate towards an asymptotic value. The effect is associated with the approach to self-preserving conditions of the developing turbulent boundary layer, see section 3.7. The initial sharp decrease

however, indicates a substantial change in the velocity profile shape. It is assumed here that the profile in this region of rapid change can be described by a simple power law, with the exponent n a free parameter.

ie. $$\left(\bar{u}/U_\infty\right) = \left(y/\delta_T\right)^{1/n} \qquad \text{A. 4.6}$$

It is further assumed that a logarithmic wall region also exists and that the inner profile is also described by eqn. 3.4.

ie. $$\bar{u}/u_\tau = 1/k \ln.\left(\frac{y.u_\tau}{\nu}\right) + C \qquad \text{A. 4.7}$$

with k and C, as before, equal to 0.41 and 5.2, respectively.

Substituting eqn. A. 4.6 for $\bar{u}$ in eqn. A. 4.7 gives :-

$$\frac{U_\infty \left(y/\delta_T\right)^{1/n}}{u_\tau} = 1/k \ln.\left(\frac{y.u_\tau}{\nu}\right) + C \qquad \text{A. 4.8}$$

Bradshaw's method for calculating the turbulent skin friction, (see Winter (1975)), depends on the assumption that eqn. A. 4.7 is always valid when $\frac{y.u_\tau}{\nu} = 100$.

Substitution in eqn. A. 4.8 then gives :-

$$\frac{U_\infty \left[\frac{100\nu}{u_\tau.\delta_T}\right]^{1/n}}{u_\tau} = K = 16.432 \qquad \text{A. 4.9}$$

Writing the skin friction coefficient as :-

$$\sqrt{2/C_{f_T}} = U_\infty/u_\tau \qquad \text{A. 4.10}$$

Substituting A. 4.10 into A. 4.9 to eliminate u_τ gives :-

$$C_{f_T} = 2\left[\frac{R\delta_T.K^n}{100}\right]^{-\frac{2}{(n+1)}} \qquad \text{A. 4.11}$$

For a power law profile, it can be shown that :-

$$n = \frac{2}{H_T - 1}, \quad \delta_T/\theta_T = \frac{H_T(H_T + 1)}{(H_T - 1)} \quad \text{and} \quad \frac{2}{n+1} = \frac{2(H_T - 1)}{(H_T + 1)}$$

Replacing R_{δ_T} with $R_{\theta_T}.\delta_T/\theta_T$ and substituting into eqn. A. 4.11 ultimately results in :-

$$C_{f_T} = 2\times\left[\frac{R_{\theta_T}\, K^{\frac{2}{(H_T-1)}}}{100}\times H_T\frac{(H_T+1)}{(H_T-1)}\right]^{\frac{-2(H_T-1)}{(H_T+1)}} \qquad \text{A. 4.12}$$

A. 4.4 The composite transitional skin friction relation.

It is assumed that eqns. A. 4.6 and A. 4.7 are also applicable to the turbulent portion of an intermittently turbulent transition region. For simplicity however, the transitional values of H and R_θ are used for both the laminar and the turbulent skin friction components . This means that at low values of intermittency, ie. when the flow is dominantly laminar, C_{f_T} will be overestimated and similarly at higher intermittencies, the laminar skin friction component will be underestimated. Fortunately however, the intermittency function modulates the two components in a suitable manner to reduce the erroneous components. It is also unlikely that the laminar/turbulent switching process is exactly the step function with time as suggested by eqn. A. 4.1. The averaging effect of using transitional parameters therefore has some justification. The transition skin friction relation is therefore given by :-

$$C_{f_t} = \frac{2\times l_1(M)(1-\overline{\gamma})}{R_{\theta_t}} + 2\overline{\gamma}\times\left[\frac{R_{\theta_t}.K^{\frac{2}{(Ht-1)}}}{100}\times H_t\frac{(H_t+1)}{(Ht-1)}\right]^{\frac{-2(H_t-1)}{(Ht+1)}} \qquad \text{A. 4.13}$$

For the case of a zero pressure gradient, $l_1(M) = 0.22$ and the laminar skin friction component reduces to :-

$$C_{f_L} = \frac{0.44(1-\overline{\gamma})}{R_{\theta_t}} \qquad \text{A. 4.14}$$

Alternatively, the relation may be expressed in terms of the energy shape factor $H32_t$.

Writing $H32_t = \overline{H}_t$

$$C_{f_t} = \frac{2\, l_1(M)(1 - \overline{\delta})}{R\theta_t} + 2\overline{\delta}\left[\frac{R\theta_t \cdot K^{\frac{(3\overline{H}_t - 4)}{(2 - \overline{H}_t)}}}{100} \times \frac{2\overline{H}_t(\overline{H}_t - 1)}{(3\overline{H}_t - 4)(2 - \overline{H}_t)}\right]^{\frac{-2(\overline{H}_t - 1)}{(\overline{H}_t + 1)}} \qquad \text{A. 4.15}$$

The assumptions made in the derivation of eqns. A. 4.13 and A. 4.15 imply that the conglomeration of turbulent spots, which constitute the turbulent component, is equivalent to a ficticious portion of a fully developed turbulent boundary layer. While this is rather speculative, the conditionally-sampled data of Arnal et al. (1977), suggests that the mean velocity profile associated with a turbulent spot does have certain "turbulent-like" characteristics and lends some support to the assumptions made here.

A. 4.5 Comparisons with data.

As a means of comparison, the turbulent skin friction relation, ie. eqn. A. 4.12, was judged along with a relation due to Green et al. (1977), (see Appendix 5.), against the lowest Reynolds number data from the Stanford Conference, vol. II, see Coles and Hirst (1968). In all cases except one, ie. in an accelerating flow, the present formula gave a higher valued C_f., in closer agreement with the quoted C_f's as obtained from the log-law method. For $R_\theta > 1600$ however, the expression A. 4.12, tended to increasingly underestimate the C_f. value, such that $R_\theta = 1600$ should be regarded as an upper limit for the validity of eqn. A. 4.12.

To test eqn. A. 4.13 in the situation for which it was designed, the transitional velocity profile data of Schubauer and Klebanoff (1956) was re-analysed using the computer programs which were developed to analyse the present data. The resulting profile parameters were then inserted into eqn. A. 4.13 to obtain the local skin friction coefficients. A subsequent momentum balance analysis indicated a reasonable agreement between the left and right hand sides. Conclusions are subject to the provision that the flow was in fact two-dimensional, the results however suggest that eqn. A. 4.13 gives, at least, a representative transitional skin friction value.

APPENDIX 5.

Integral prediction methods for laminar and turbulent boundary layers.

The method of Thwaites (1949) for the prediction of laminar boundary layers, a simple entrainment method due to Green (1968) and a more sophisticated, lag-entrainment, method due to Green et.al. (1977) for turbulent boundary layer prediction are briefly described. The numerical methods of solution of the various equations are also outlined.

Integral prediction methods for laminar and turbulent boundary layers.

A. 5.1. Thwaites' (1949) method for laminar boundary layers.

The von Kármán momentum integral equation is expressed in the form :-

$$\tau_o/\rho = \frac{U_\infty^2}{2}\frac{d(\theta^2)}{dx} + (2\theta + \delta^*)U_\infty\frac{dU_\infty}{dx} \qquad \text{A. 5.1}$$

Multiplying through by $\theta/\nu U_\infty$ gives :-

$$\frac{\tau_o\theta}{\mu U_\infty} = \frac{U_\infty}{2\nu}\frac{d(\theta^2)}{dx} + \frac{\theta^2}{\nu}\frac{dU_\infty}{dx}(2 + \delta^*/\theta) \qquad \text{A. 5.2}$$

Defining the parameters :-

$$l_1 = \frac{\tau_o\theta}{\mu U_\infty} \qquad \text{A. 5.3}$$

$$M = -\frac{\theta^2}{\nu}\frac{dU_\infty}{dx} \qquad \text{A. 5.4}$$

and

$$H = \delta^*/\theta \qquad \text{A. 5.6}$$

Substitution into eqn. A. 5.2 gives :-

$$U_\infty\frac{d}{dx}(\theta^2/\nu) = 2(l_1 - M(2 + H)) = L \qquad \text{A. 5.7}$$

By examining a range of known solutions, Thwaites determined that L was a linear function of the pressure gradient parameter M alone.

ie.

$$L = 0.45 + 6.M \qquad \text{A. 5.8}$$

Substitution of eqn. A. 5.8 into eqn. A. 5.7 results in a first order differential equation in $(U_\infty\theta^2/\nu)$, which can be solved with the introduction of an integrating factor. The solution results

in the simple quadrature :-

$$\theta^2 = \frac{0.45\nu}{U_\infty^6}\int_0^x U_\infty^5 dx. \qquad \text{A. 5.9}$$

Thwaites then correlated one-parameter relations for l_1 and H. The functions have been conveniently approximated by Cebeci and Bradshaw (1977) in the forms :-

$$\left.\begin{aligned} l_1 &= 0.22 - 1.57M - 1.8M^2 \\ H &= 2.61 + 3.75M + 5.24M^2 \end{aligned}\right\} \quad (-0.075 \leq M \leq 0) \qquad \begin{matrix}\text{A. 5.10}\\ \text{A. 5.11}\end{matrix}$$

$$\left.\begin{aligned} l_1 &= 0.22 - 1.402M - \frac{0.018M}{0.107 - M} \\ H &= 2.088 + \frac{0.0731}{0.14 - M} \end{aligned}\right\} \quad (0 \leq M \leq 0.09) \qquad \begin{matrix}\text{A. 5.12}\\ \text{A. 5.13}\end{matrix}$$

Equations A. 5.9,10,11,12 and 13 and the definitions of M, l_1 and H then form a closed solution for the laminar boundary layer in arbitrary pressure gradients, with separation being denoted by :-

$$M > 0.09 \qquad \text{A. 5.14}$$

A. 5.2 Green's(1968) simple entrainment method for turbulent boundary layers.

The momentum integral equation is expressed in its more usual form :-

$$\text{ie.} \quad \frac{d\theta}{dx} = \frac{C_f}{2} - \frac{\theta}{U_\infty}\frac{dU_\infty}{dx}(H + 2) \qquad \text{A. 5.15}$$

and the entrainment equation is written non-dimensionally as :-

$$\frac{1}{U_\infty}\frac{d\left[U_\infty(\delta - \delta^*)\right]}{dx} = F \qquad \text{A. 5.16}$$

The shape factor Λ, is defined as $\Lambda = (\delta - \delta^*)/\theta$

For a one parameter family of velocity profiles, it can be shown that the shape factor Λ is related to the Kármán shape factor, H.

by the relationship :-

$$\mathcal{H} = \frac{2.H}{H - 1} \qquad \text{A. 5.17}$$

The entrainment function, eqn. A. 5.16, can then be expressed as a first order, ordinary differential equation for the streamwise rate of change of shape factor, H. The equation becomes, after some re-arranging :-

$$-\Theta.\frac{dH}{dx} = H(H^2 - 1)\frac{\Theta}{U_\infty}.\frac{dU_\infty}{dx} + \frac{(H - 1)}{2}\left[(H - 1).F - H.C_f\right] \qquad \text{A. 5.18}$$

Green correlated the entrainment parameter F, as a function of H alone, see section 3.9, in the form :-

$$F = 0.025_{\times}H - 0.022 \qquad \text{A. 5.19}$$

To close the solution, Green adopted the skin friction relation due to Ludwieg and Tillman (1950).

$$\text{ie.} \quad C_f = 0.246 \exp\left[-1.561_{\times} H\right] R_\Theta^{-0.268} \qquad \text{A. 5.20}$$

A. 5.3 Green et al's.(1977) lag-entrainment method for turbulent boundary layers.

The lag-entrainment method is an extension of the earlier simple entrainment method described in the previous section. The momentum integral equation, ie. eqn. A. 5.15 , and the entrainment equation, ie. eqn. A. 5.16, are supplemented by an equation for the streamwise rate of change of the entrainment parameter F, in the form :-

$$\Theta(\mathcal{H} + H).\frac{dF}{dx} = \left[\frac{F(F + 0.02) + 0.2667\, C_{f_o}}{(F + 0.01)}\right]\times$$
$$\left[2.8\times\left\{(0.32\, C_{f_o} + 0.024\, F_{eq.} + 1.2\, F_{eq.}^2)^{0.5} - (0.32\, C_{f_o} + 0.024\, F + 1.2\, F^2)^{0.5}\right\} + \left(\frac{\delta}{U_\infty}\frac{dU_\infty}{dx}\right)_{eq.} - \frac{\delta}{U_\infty}\frac{dU_\infty}{dx}\right] \qquad \text{A. 5.21}$$

The suffix eq. refers to equilibrium conditions and C_{f_o} is a flat plate skin friction relation.

Equation A. 5.21 is a development from an empirical, partial differential equation for the shear stress, which was originally derived by Bradshaw et al (1967) and is an approximation to the full turbulent energy equation.

Green et al. considered Bradshaw's equation at the height y corresponding to the position of maximum shear stress, thereby reducing the equation to an ordinary differential equation for the maximum shear stress. By then relating the maximum shear to the entrainment rate and the flat plate skin friction coefficient, Green converted the equation to one for the streamwise development of the entrainment parameter. Equilibrium considerations allowed Green to further simplify the equation to the form given above.

The flat plate skin friction relation is given by Green as :-

$$C_{f_o} = \frac{0.01013}{\log_{10} R\theta - 1.02} - 0.00075 \qquad \text{A. 5.22}$$

The local skin friction is then given by :-

$$C_f = C_{f_o} \times \left[\frac{0.9}{\left[H(1 - 6.55(\frac{C_{f_o}}{2})^{0.5}) - 0.4 \right]} - 0.5 \right] \qquad \text{A. 5.23}$$

Following Green et al., the characteristic parameters in an equilibrium boundary layer are considered to be the defect profile shape factor, G, eqn. 3.35 and the pressure gradient parameter, β, eqn. 3.30, see section 3.7. An empirical relation between G and β, used by Green is :-

$$G = 6.432(1 + 0.8\beta)^{0.5} \qquad \text{A. 5.24}$$

Substituting eqns. 3.35 and 3.30 into eqn. A. 5.24, results in , after some manipulation :-

$$\left(\frac{\Theta}{U_\infty}\frac{dU_\infty}{dx}\right)_{eq.} = \frac{1.25}{H}\left[\frac{C_f}{2} - \left(\frac{H-1}{6.432\,H}\right)^2\right] \qquad \text{A. 5.25}$$

and

$$\left(\frac{\delta}{U_\infty}\frac{dU_\infty}{dx}\right)_{eq.} = (H+\Lambda)\left(\frac{\Theta}{U_\infty}\frac{dU_\infty}{dx}\right)_{eq.} \qquad \text{A. 5.26}$$

The entrainment function, eqn. A. 5.16, is expressed in the form :-

$$\frac{d}{dx}\left[U_\infty \Theta \Lambda\right] = U_\infty F. \qquad \text{A. 5.27}$$

Eliminating $d\Theta/dx$ between eqns A. 5.27 and A. 5.15 and assuming that $d\Lambda/dx$ is approximately zero in an equilibrium boundary layer, results in :-

$$F_{eq.} = \Lambda\left[\frac{C_f}{2} - (H+1)\left(\frac{\Theta}{U_\infty}\frac{dU_\infty}{dx}\right)_{eq.}\right] \qquad \text{A. 5.28}$$

Green then proposed a correlation between the shape factors Λ and H, in the form :-

$$\Lambda = 3.15 + \frac{1.72}{H-1} - 0.01(H-1)^2 \qquad \text{A. 5.29}$$

Substitution of eqn. A. 5.29 into eqn. A. 5.27 ultimately results in an equation for the streamwise rate of change of shape factor H, with the form :-

$$\frac{dH}{dx} = \frac{-F + \left[3.15 + \frac{1.72}{H-1} - 0.01(H-1)^2\right]\left[\frac{C_f}{2} - (H+1)\frac{\Theta}{U_\infty}\frac{dU_\infty}{dx}\right]}{\Theta\left[\frac{1.72}{(H-1)^2} + 0.02(H-1)\right]} \qquad \text{A. 5.30}$$

Finally, the term $\frac{\delta}{U_\infty}\frac{dU_\infty}{dx}$, similar to eqn. A. 5.26, is recast as :-

$$\frac{\delta}{U_\infty}\frac{dU_\infty}{dx} = (H+\Lambda)\frac{\Theta}{U_\infty}\frac{dU_\infty}{dx} \qquad \text{A. 5.31}$$

The three ordinary differential equations, A. 5.15, A. 5.21 and A. 5.30 with the shape parameter relation, A. 5.29, the skin friction relation, eqns. A. 5.22 and A. 5.23 and the equilibrium functions, together form a closed solution for the turbulent boundary layer growth in arbitrary pressure gradients.

As eqn. A. 5.21 is derived from the turbulent energy equation, then the terms appearing in eqn. A. 5.21 explicitly represent the classic turbulent energy terms.

ie. $\left[\frac{\Theta(K+H)(F+0.01)}{(F(F+0.02)+0.2667\,C_{f_o})}\cdot\frac{dF}{dx}+\frac{\delta}{U_\infty}\frac{dU_\infty}{dx}\right]$ "advection"

$$\frac{}{2.8(0.32\,C_{f_o}+0.024\,F_{eq}+1.2\,F_{eq}^2)^{0.5}}$$ "production"

$$\frac{}{-2.8(0.32\,C_{f_o}+0.024\,F+1.2\,F^2)^{0.5}}$$ "dissipation"

$$\frac{}{\left(\frac{\delta}{U_\infty}\frac{dU_\infty}{dx}\right)_{eq.}}$$ "diffusion"

The method then has the considerable advantage of allowing for extraneous influences on the turbulence structure. Green et al. suggest, as a first order correction, to modulate the dissipation length scale, L/δ , by some overall scaling factor.

ie. $$\frac{L}{\delta} = \left(\frac{L}{\delta}\right)_o \alpha^{-1}$$ A. 5.32

The factor α is then carried through the analysis and appears as an operator on the term which represents the turbulence dissipation.

ie. $$\frac{}{-2.8\,\alpha(0.32\,C_{f_o}+0.024\,F+1.2\,F^2)^{0.5}}$$

The introduction of α however, necessitates the calculation to be carried out in a less direct manner, as the diffusion term must also

be modified. The calculation thus proceeds by determining F_{eq_o} from eqns. A. 5.25 and A. 5.28, where the double suffix eq_o denotes the equilibrium value in the absence of extraneous influences. F_{eq} can then be determined from :-

$$(0.024\, F_{eq} + 1.2\, F_{eq}^2 + 0.32\, C_{f_o})^{0.5} \alpha = (0.024\, F_{eq_o} + 1.2\, F_{eq_o} + 0.32\, C_{f_o})^{0.5} \qquad \text{A. 5.33}$$

taking the positive root of the resulting quadratic.

Eqn. A. 5.28 is then inverted to give :-

$$\left(\frac{\delta}{U_\infty}\frac{dU_\infty}{dx}\right)_{eq.} = \frac{H+1}{H+1}\left[\frac{C_f}{2} - \frac{F_{eq.}}{\alpha}\right] \qquad \text{A. 5.34}$$

and the calculation then continues as normally. The shear "production" term remains unchanged from its form in flows free from secondary influences and it is therefore written with the suffix eq_o replacing the suffix eq. The "advection" term remains unaltered.

A. 5.4 Numerical solution techniques.

The solution of the laminar boundary layer is carried out by employing a Simpsons rule integration, with 21 ordinates, of the quadrature given by eqn. A. 5.9. The boundary layer parameters H and C_f, or γ_o, immediately follow from the one-parameter relations. See subroutine THWAIT, listed in Appendix 3.

The simple entrainment method is solved by the simultaneous integration of eqns. A. 5.15 and A. 5.18 by the Runge-Kutta method. The computer program HEAD, see Appendix 3., performs the necessary calculations from an input data of θ_o and H_o.

The Runge-Kutta method is again utilised to solve, simultaneously, the three first order ordinary differential equations ie. A. 5.15, A. 5.21 and A. 5.30, appearing in the lag-entrainment method. The solution is formulated in the more general manner, which allows for extraneous influences, but with the scaling factor $\propto$ equal to 1.0. The computer program LAGENT and subroutine RUNGE, see Appendix 3., carry out the relevant calculations.

APPENDIX 6.

Experimental data.

The experimental data relating to flows 1,2,3 and 4 are shown in graphical and tabular form.

SUMMARY:-

The basic prime data, derived from an experimental study of four transitional boundary layers, is presented in tabular and graphical form.

Each flow includes a plot of the percentage variation in dynamic pressure about the mean value along the tunnel working section as an indication of the quality of the zero pressure gradient.

Mean velocity profiles are presented as functions of $(\overline{u}/U_\infty)$ vs. (y/δ) and are also compared, where applicable, with the Blasius profile, the semi-logarithmic turbulent velocity profile and the turbulent equilibrium velocity-defect profile in a zero pressure gradient.

The streamwise component of fluctuating velocity is shown as $(\sqrt{\overline{u'^2}}/U_\infty)\times 100\%$ vs. (y/δ) and as $(\sqrt{\overline{u'^2}}/U_y)^2$ vs. (y/δ) and the intermittency distribution through the boundary layer is plotted as γ vs. (y/δ) in all cases with the exception of FLOW 4, where they are plotted against the dimensional y- coordinate.

Velocity profiles analysed by the methods outlined in chapter 3. generate the secondary data including displacement, momentum and energy thicknesses, shape factors, skin friction coefficients, wake parameter, wake strength parameter and relevant boundary layer Reynolds numbers. These are tabulated and shown graphically to illustrate streamwise development and spanwise variation.

The development of wake parameter and wake strength parameter are plotted as functions of momentum thickness Reynolds number.

Stream-wise development of "near-wall" intermittency and entrainment function are included as are the the results of the momentum balance test for flow two-dimensionality.

FLOW 4 has an additional set of graphs indicating the development of the turbulent wakes formed behind two isolated spherical roughness elements, in terms of constant spanwise intermittency contours at each measuring station.

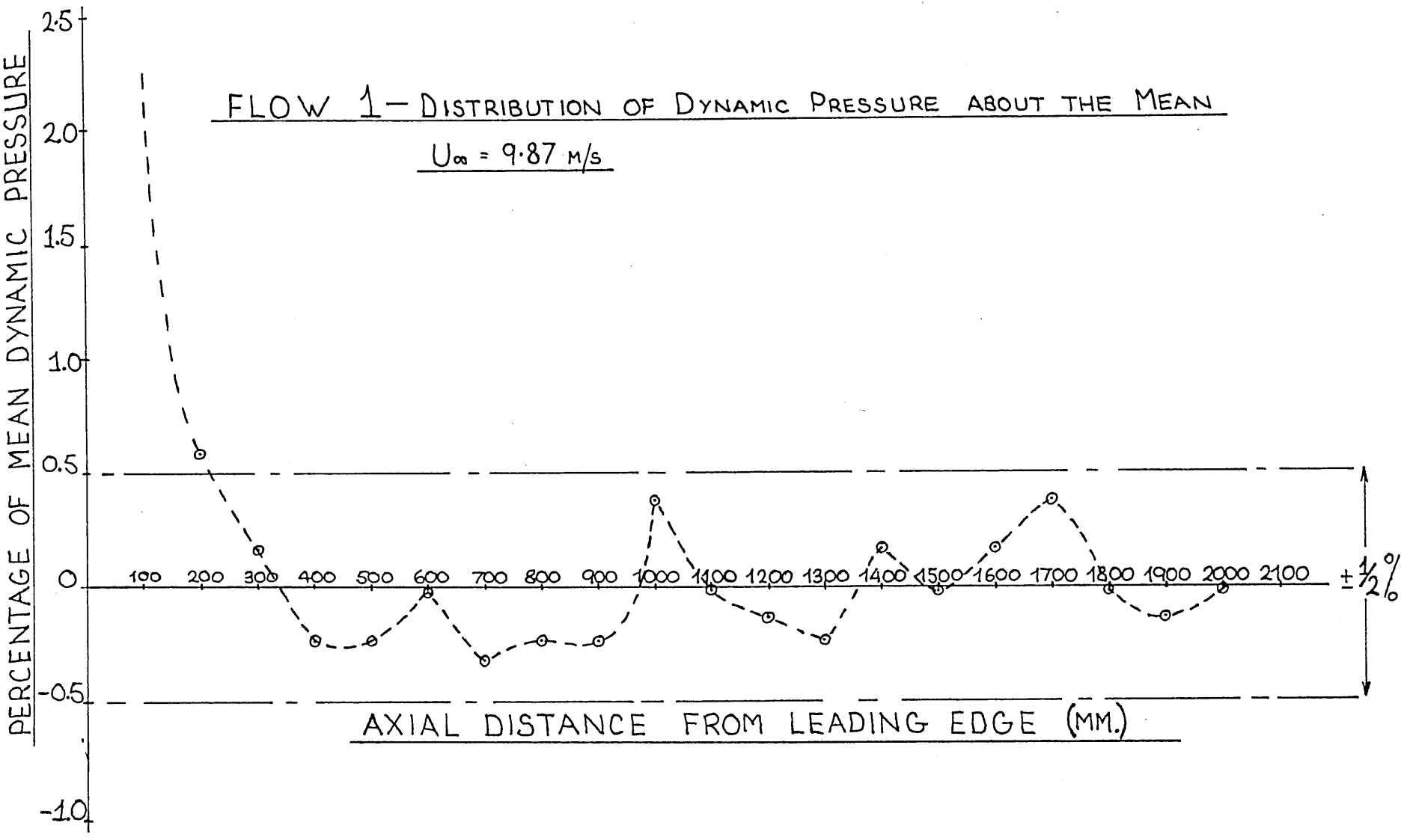
FLOW 1 – DISTRIBUTION OF DYNAMIC PRESSURE ABOUT THE MEAN
U∞ = 9·87 m/s
PERCENTAGE OF MEAN DYNAMIC PRESSURE
2·5
2·0
1·5
1·0
0·5
0
-0·5
-1·0
100 200 300 400 500 600 700 800 900 1000 1100 1200 1300 1400 1500 1600 1700 1800 1900 2000 2100
± ½ %
AXIAL DISTANCE FROM LEADING EDGE (MM.)

FIG. 1.1

FLOW 1 — DEVELOPMENT OF MEAN VELOCITY PROFILE ALONG Z = +145

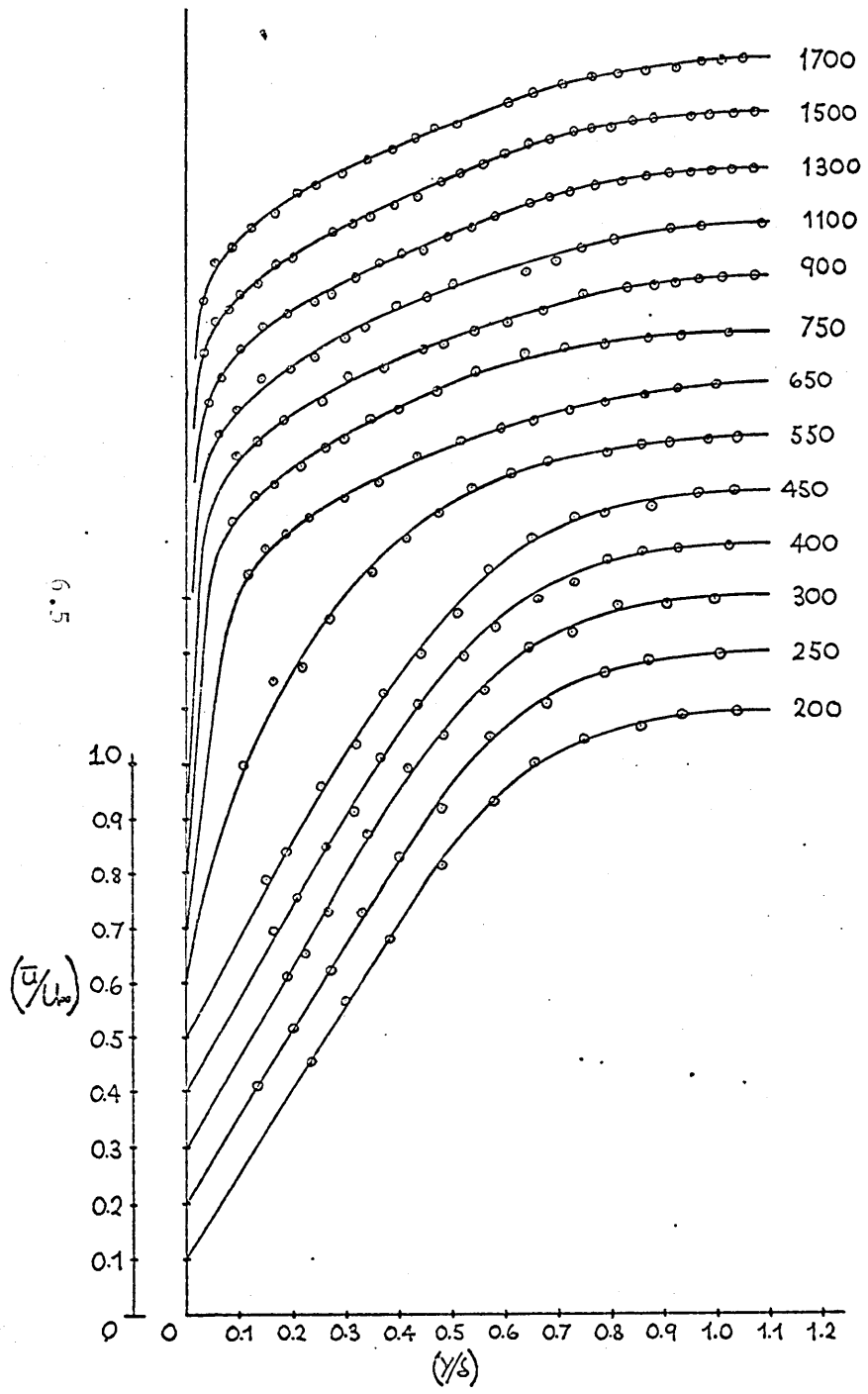

FLOW 1 — DEVELOPMENT OF MEAN VELOCITY PROFILE ALONG Z = +100

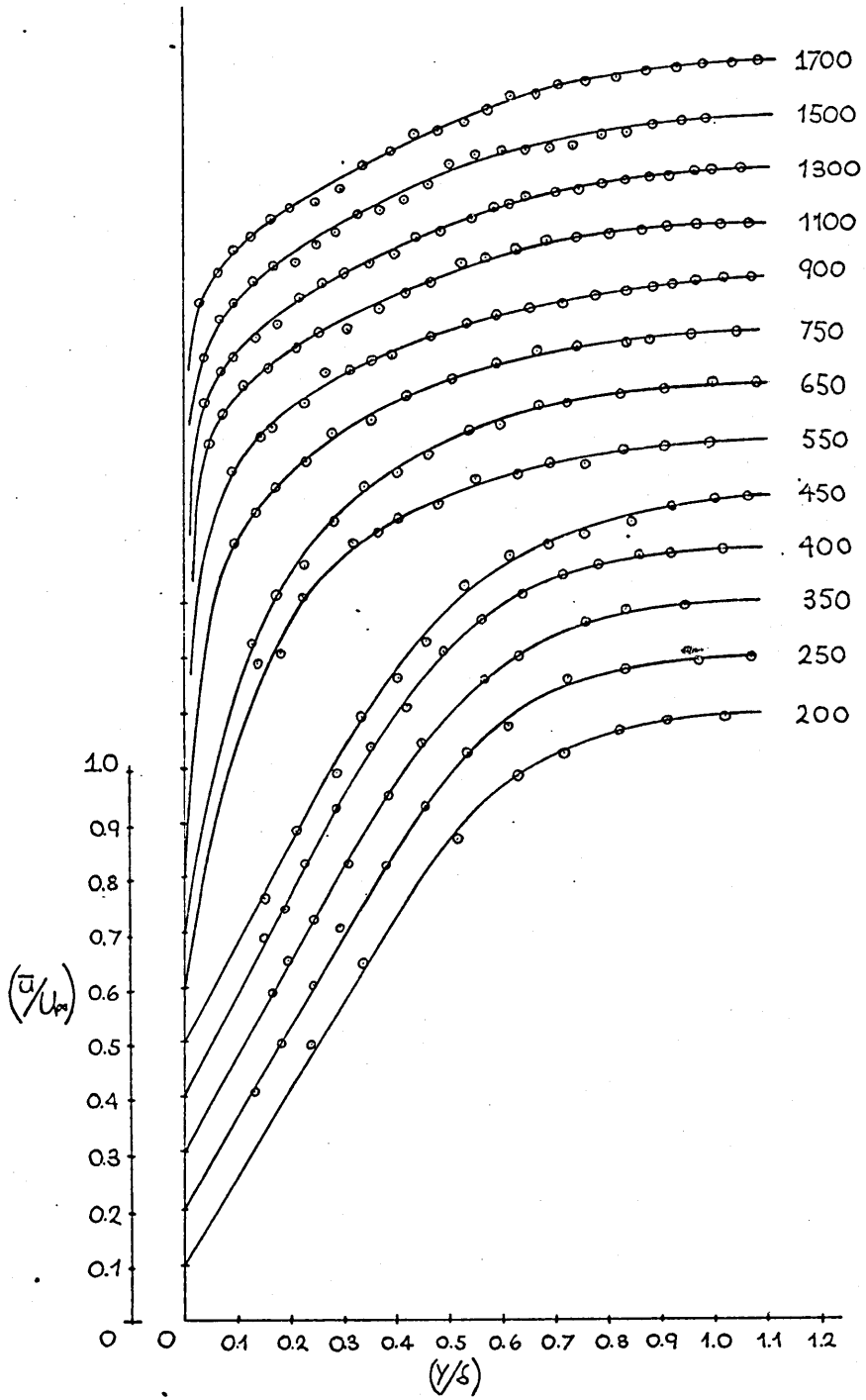

FIG. 1.2

FLOW 1 — DEVELOPMENT OF MEAN VELOCITY PROFILE ALONG Z = +50

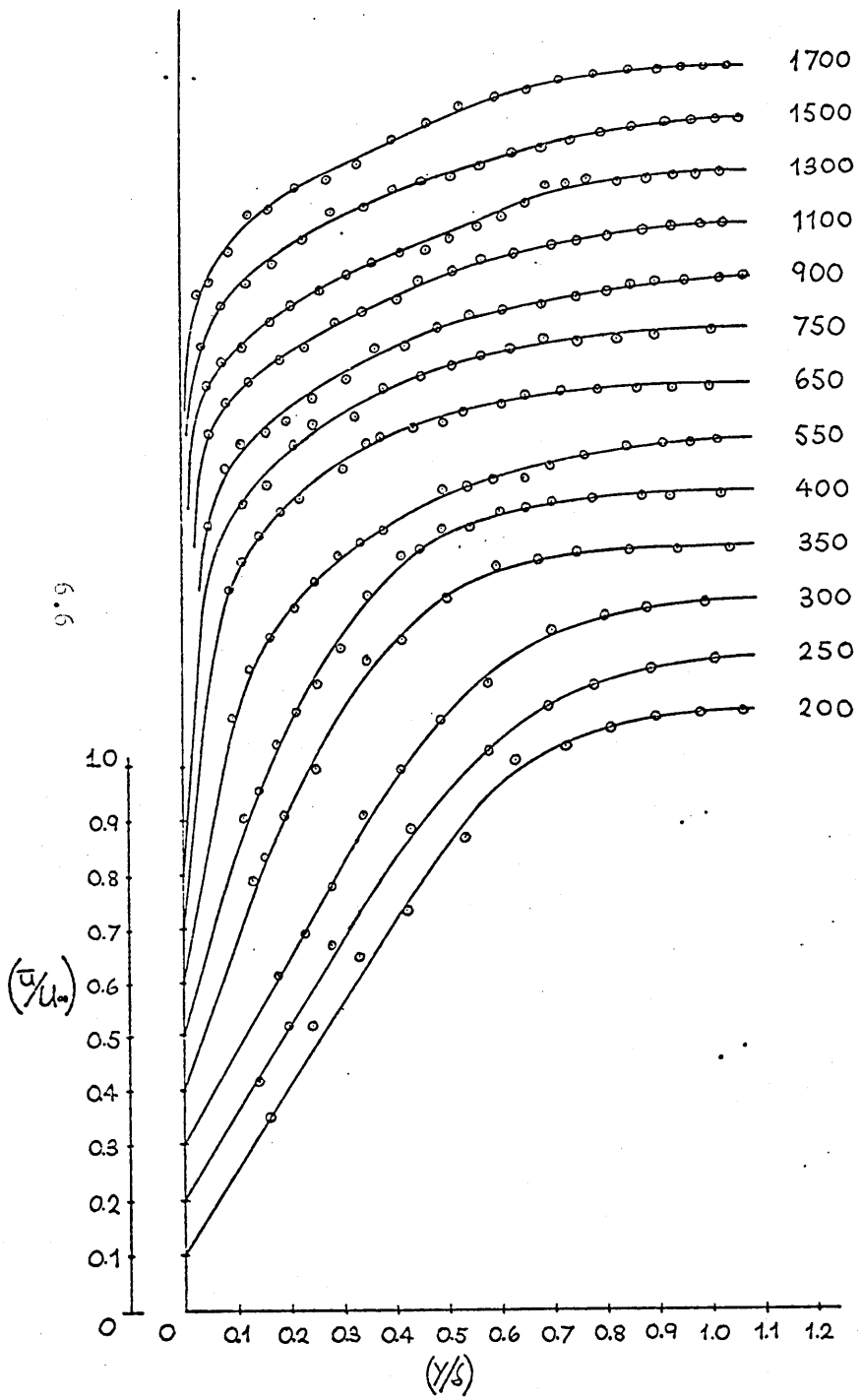

FLOW 1 — DEVELOPMENT OF MEAN VELOCITY PROFILE ALONG Z = 0

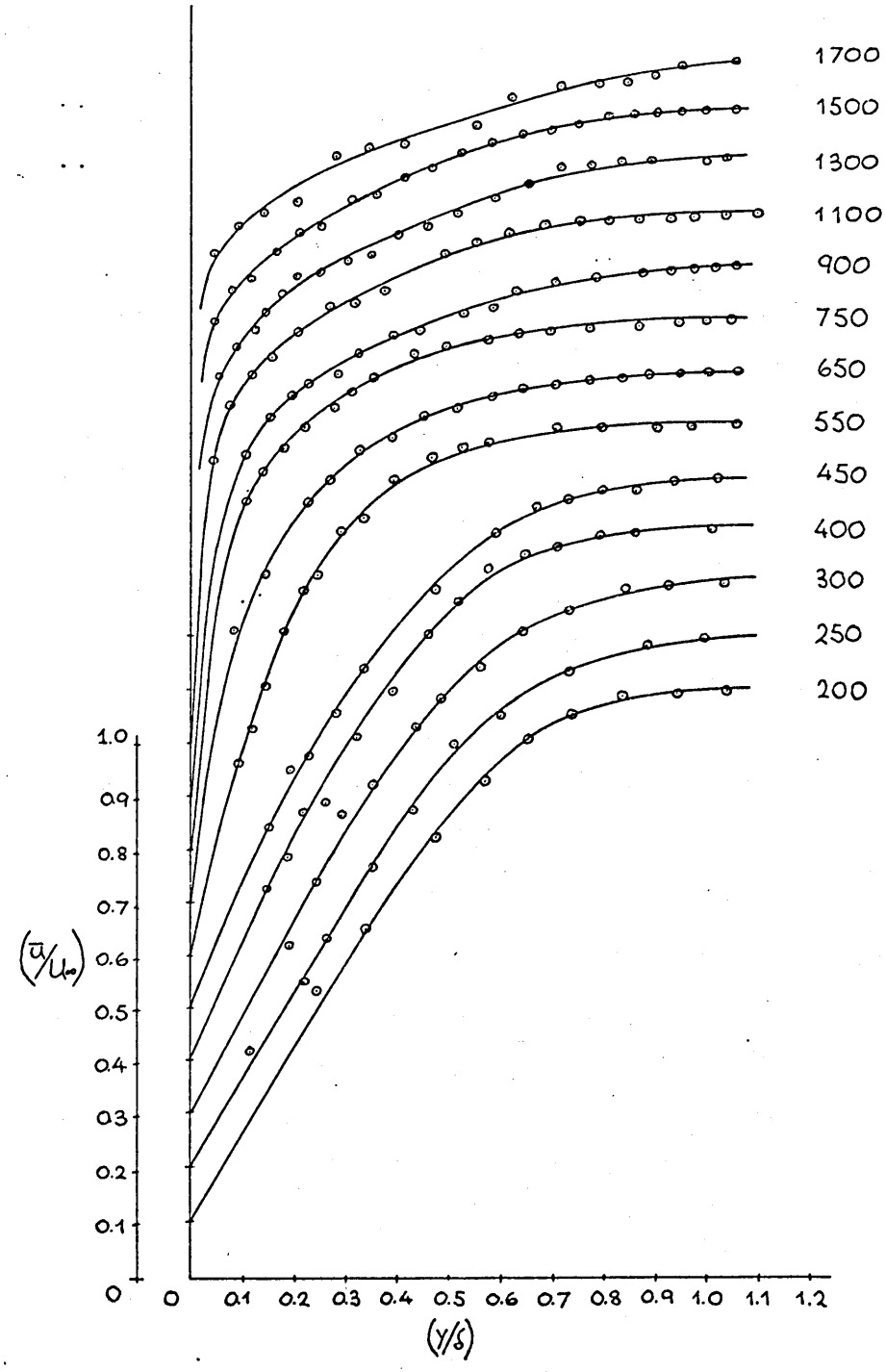

FIG. 1.3

FLOW 1 — DEVELOPMENT OF MEAN VELOCITY PROFILE ALONG Z = -50

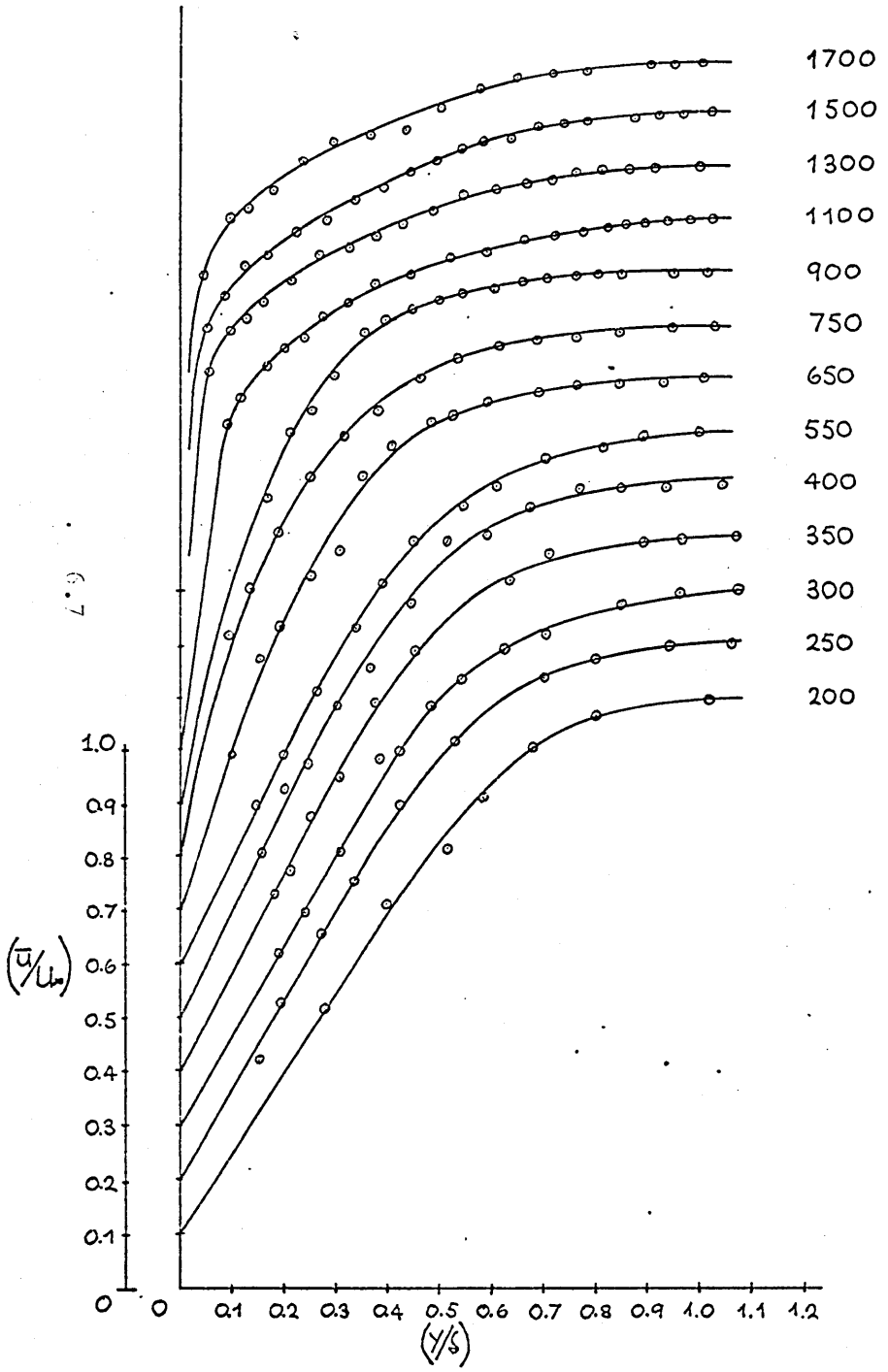

FLOW 1 — DEVELOPMENT OF MEAN VELOCITY PROFILE ALONG Z = -100

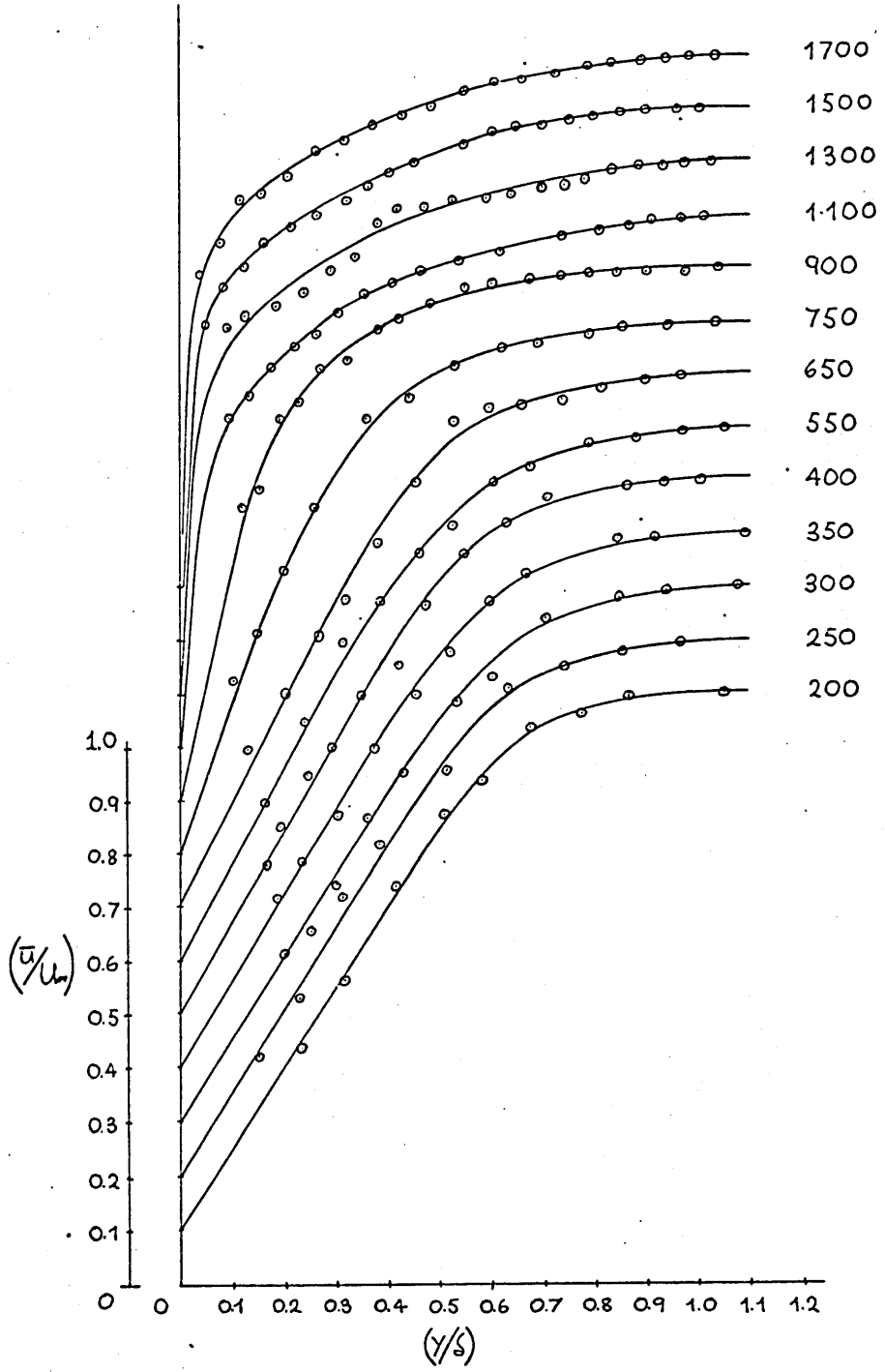

FIG. 1.4

FLOW 1 — DEVELOPMENT OF SEMI-LOGARITHMIC VELOCITY PROFILE ALONG Z = +145

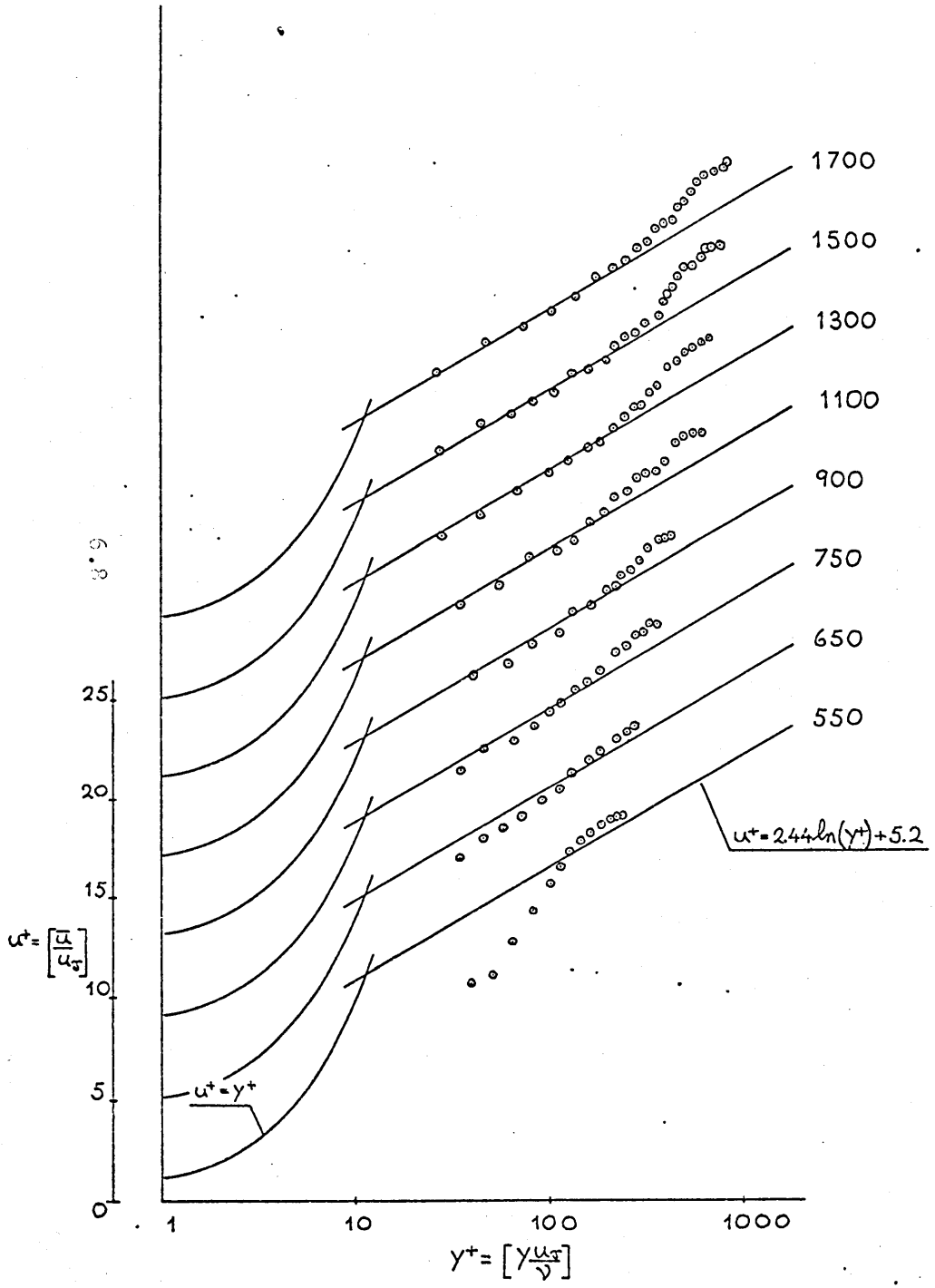

FLOW 1 — DEVELOPMENT OF VELOCITY-DEFECT PROFILE ALONG Z = +145

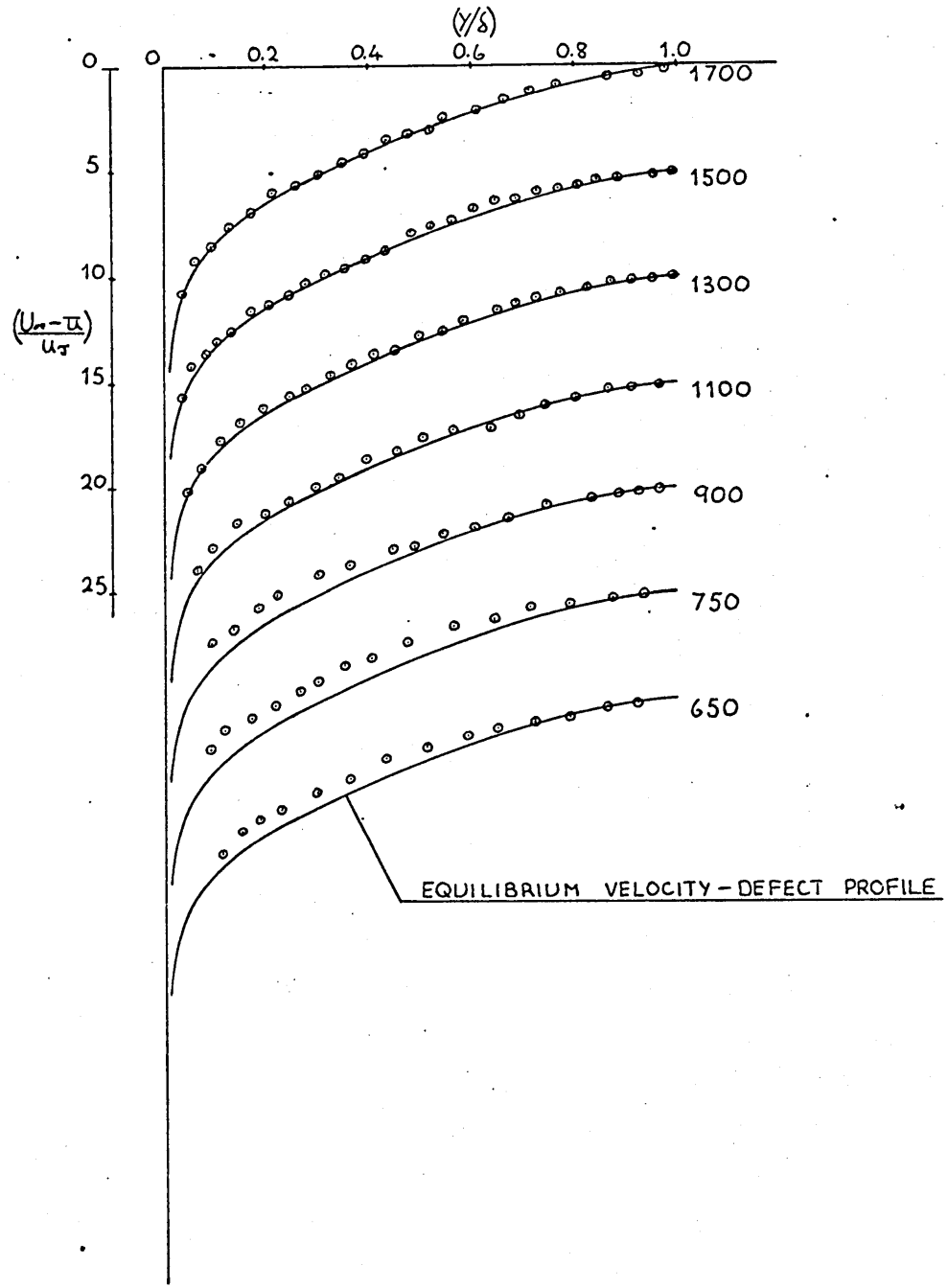

FIG. 1.5

FLOW 1 — DEVELOPMENT OF SEMI-LOGARITHMIC VELOCITY PROFILE ALONG Z = +100

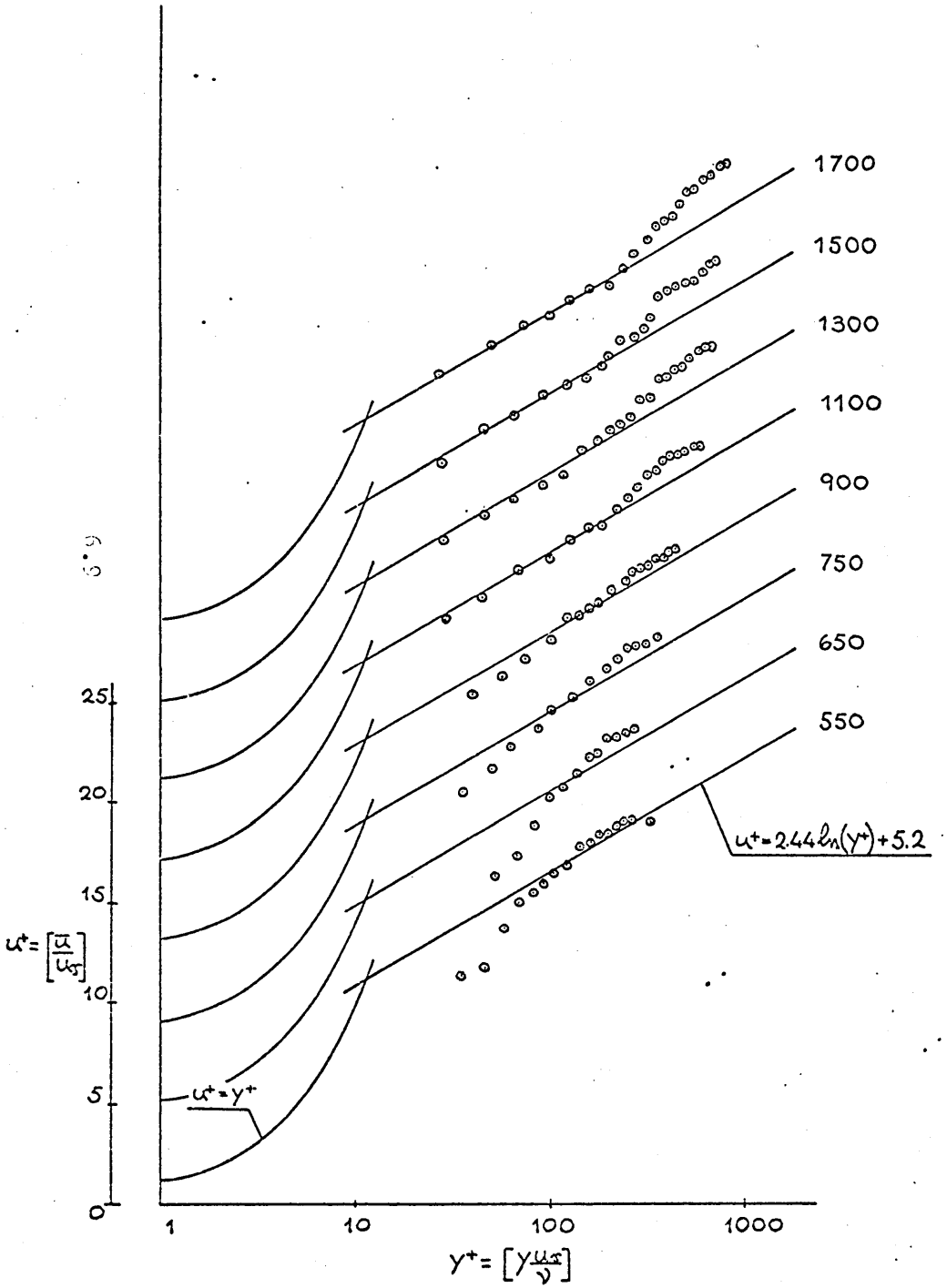

FLOW 1 — DEVELOPMENT OF VELOCITY-DEFECT PROFILE ALONG Z = +100

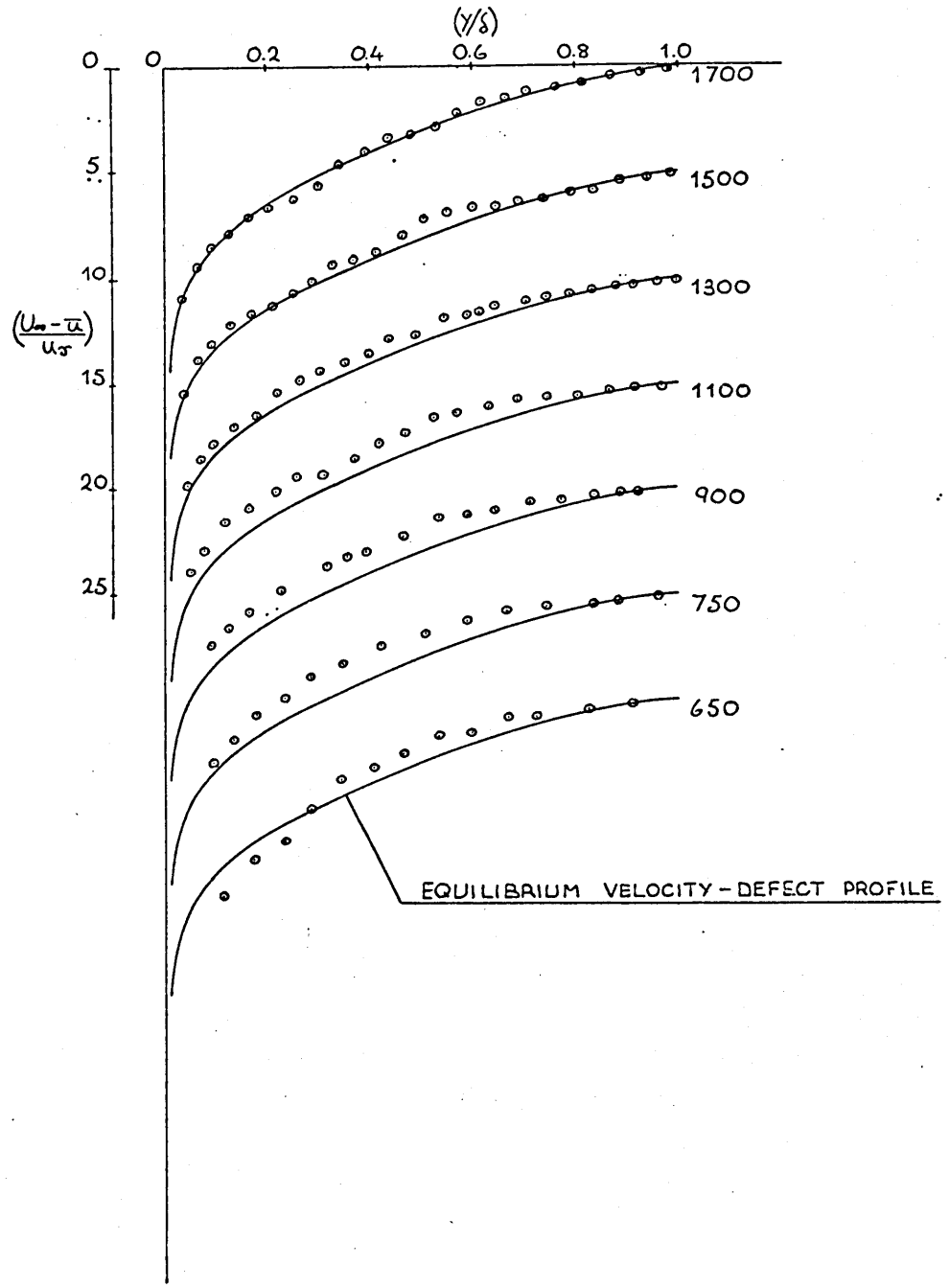

FIG. 1.6

FLOW 1 — DEVELOPMENT OF SEMI-LOGARITHMIC VELOCITY PROFILE ALONG Z = +50

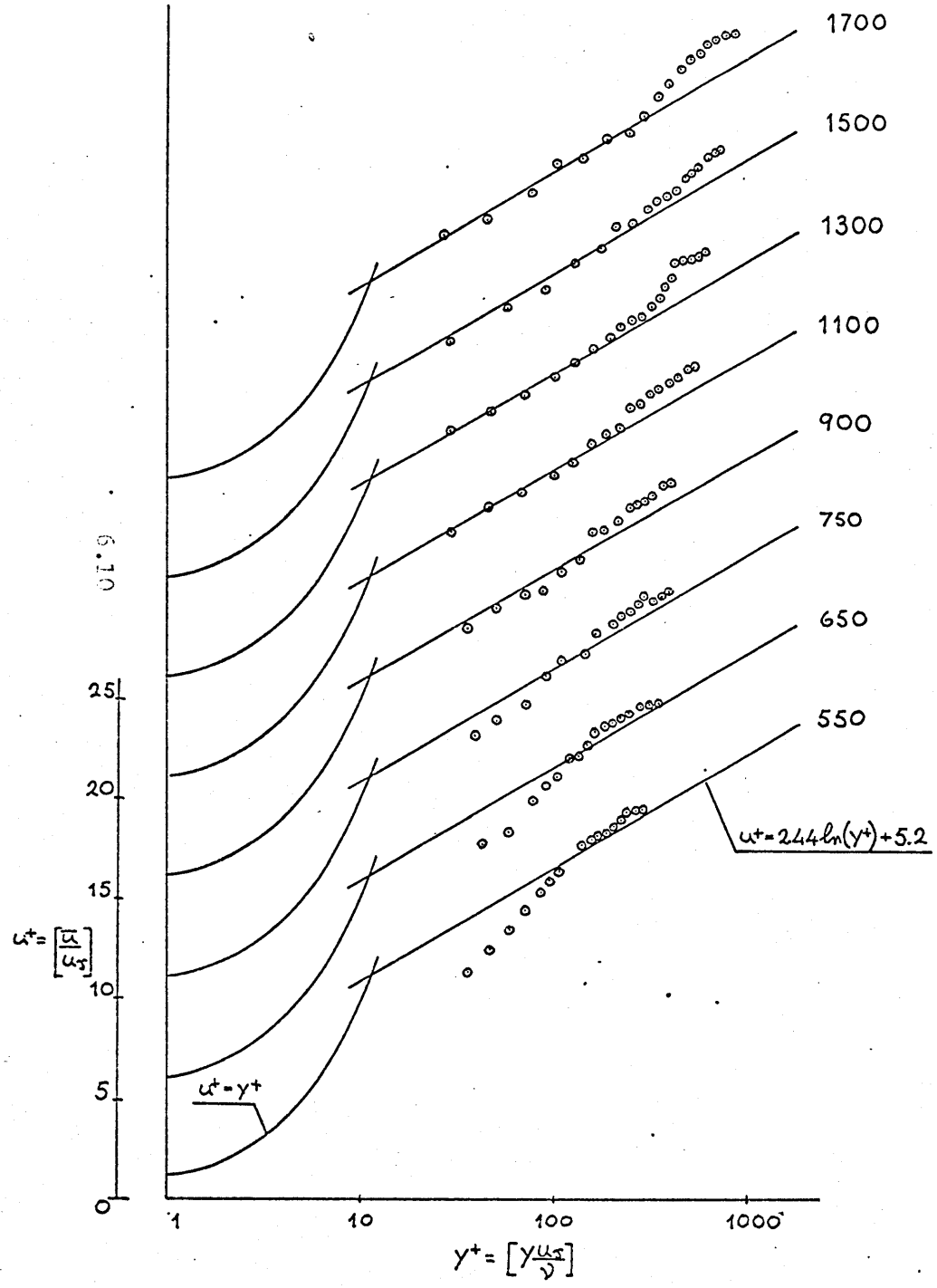

FLOW 1 — DEVELOPMENT OF VELOCITY-DEFECT PROFILE ALONG Z = +50

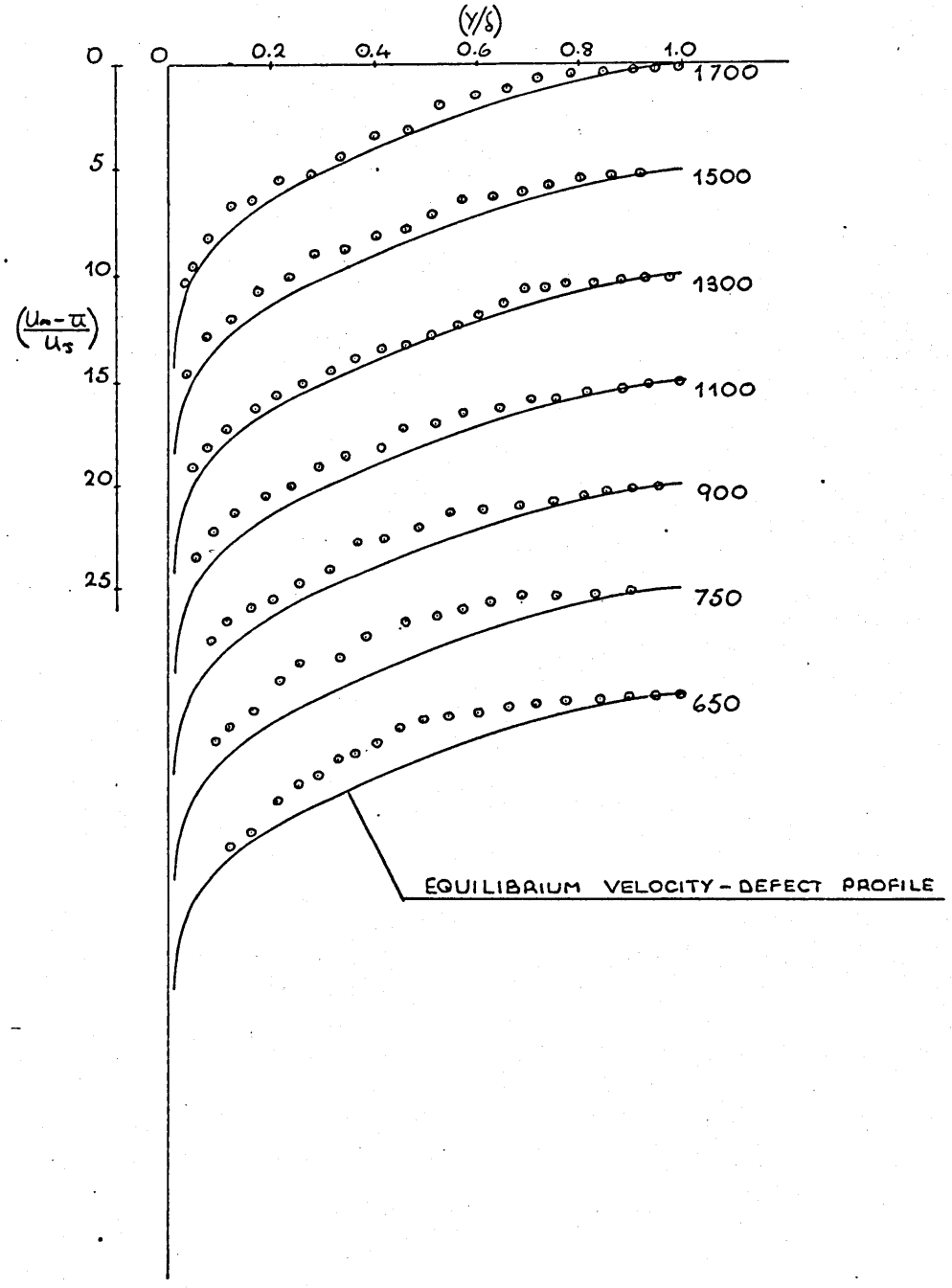

FIG. 1.7

FLOW 1 — DEVELOPMENT OF SEMI-LOGARITHMIC VELOCITY PROFILE ALONG Z = 0

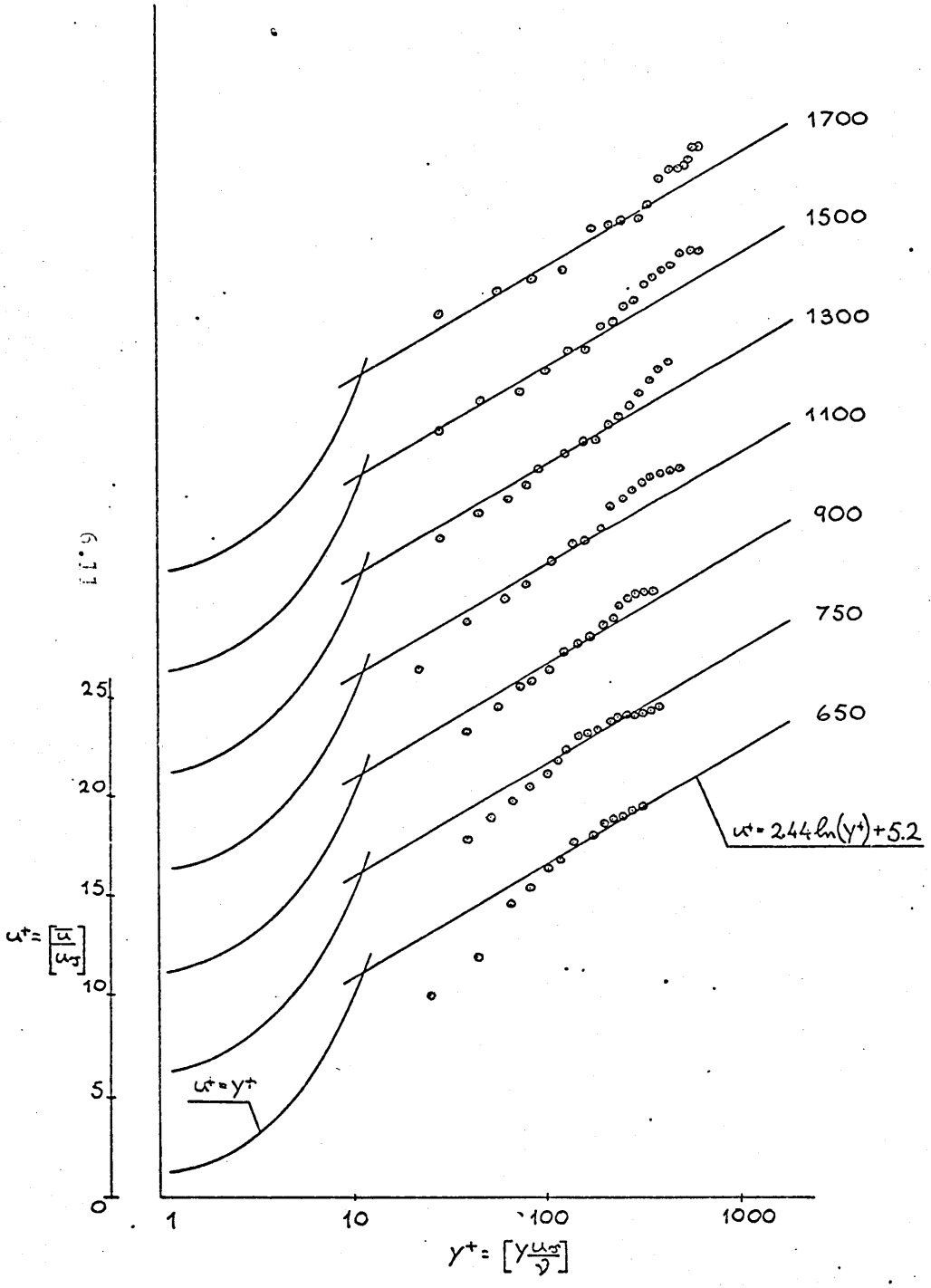

FLOW 1 — DEVELOPMENT OF VELOCITY-DEFECT PROFILE ALONG Z = 0

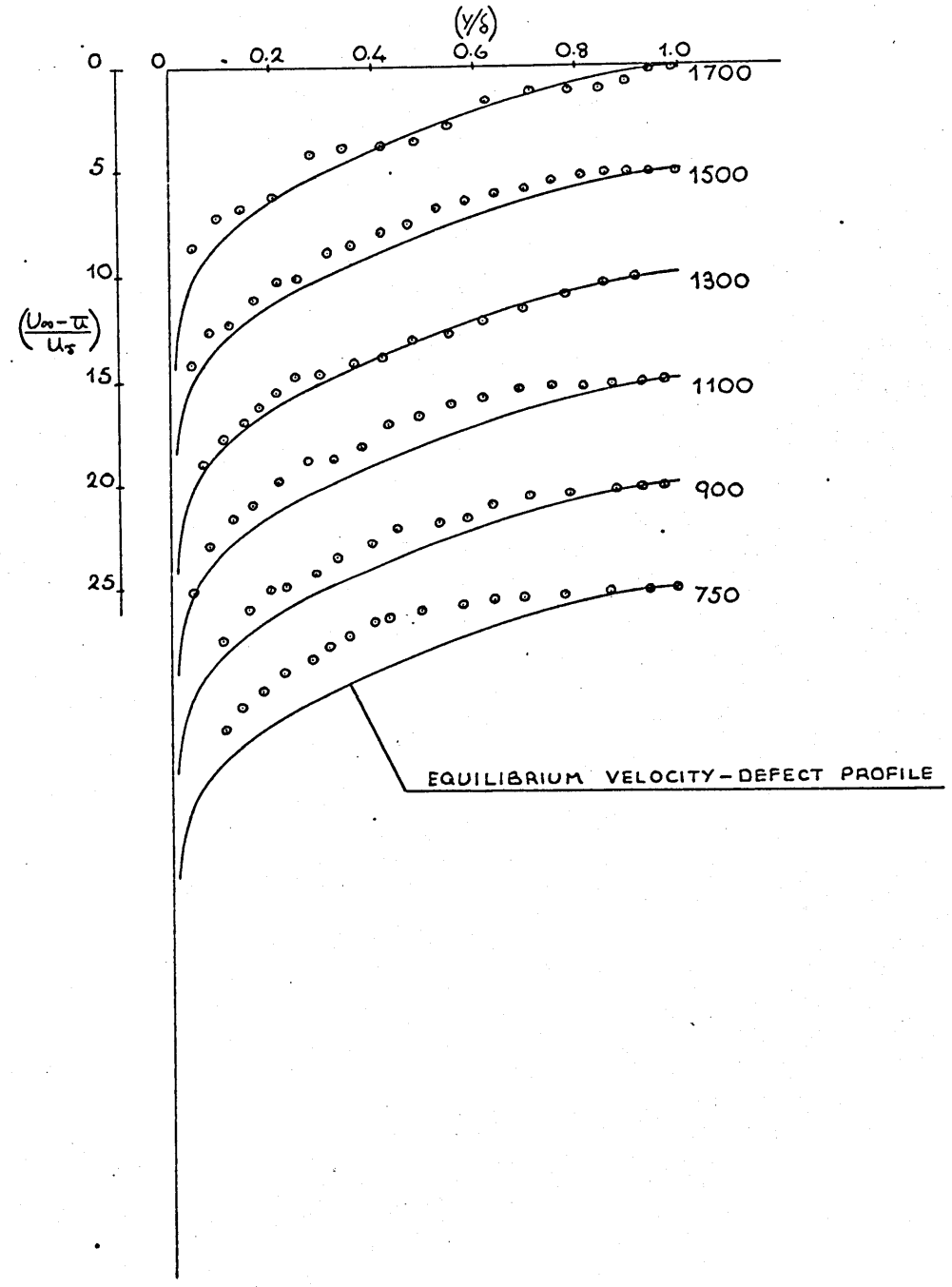

FIG. 1.8

FLOW 1 — DEVELOPMENT OF SEMI-LOGARITHMIC VELOCITY PROFILE ALONG Z = -50

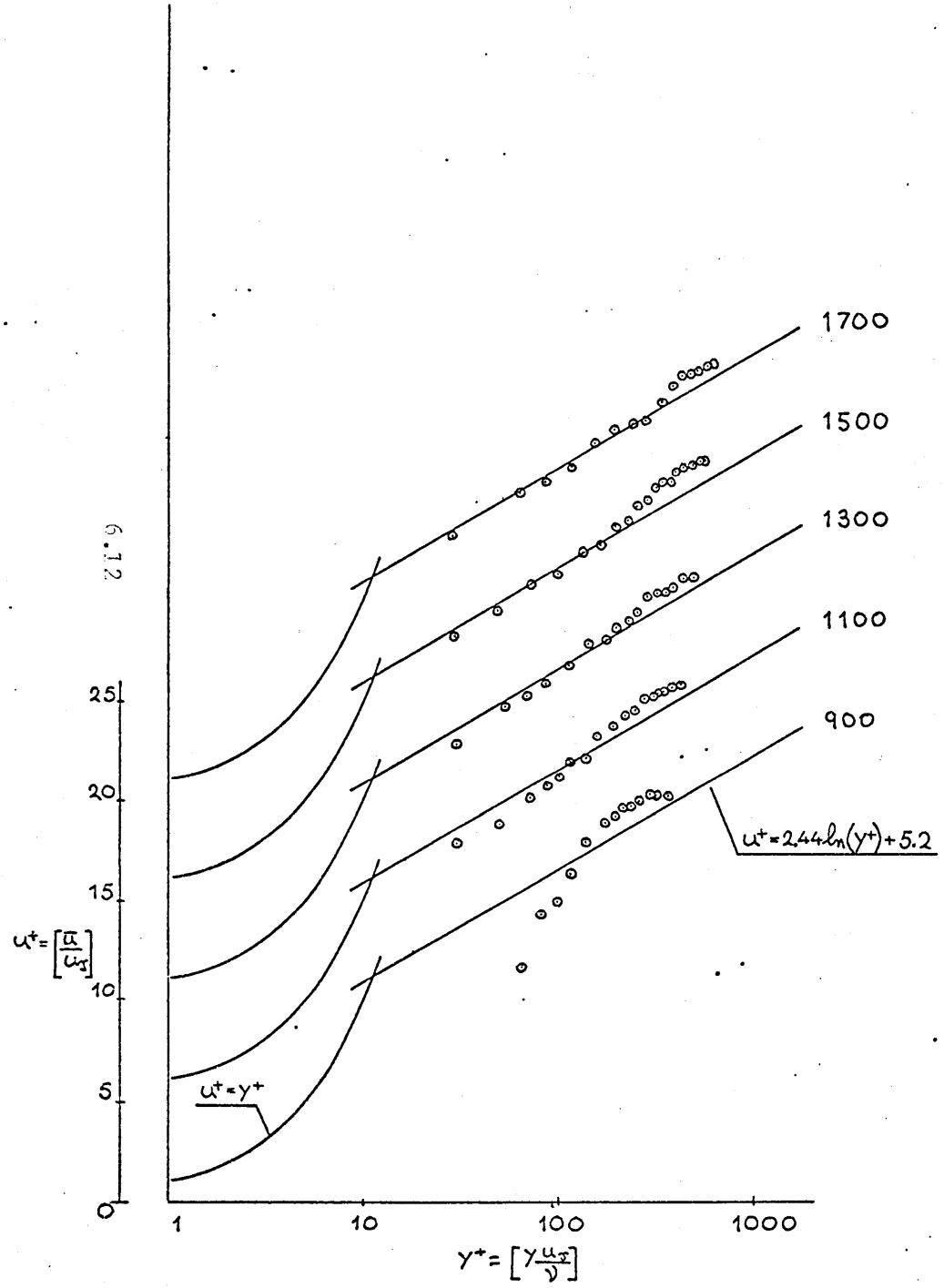

6.12

FLOW 1 — DEVELOPMENT OF VELOCITY-DEFECT PROFILE ALONG Z = -50

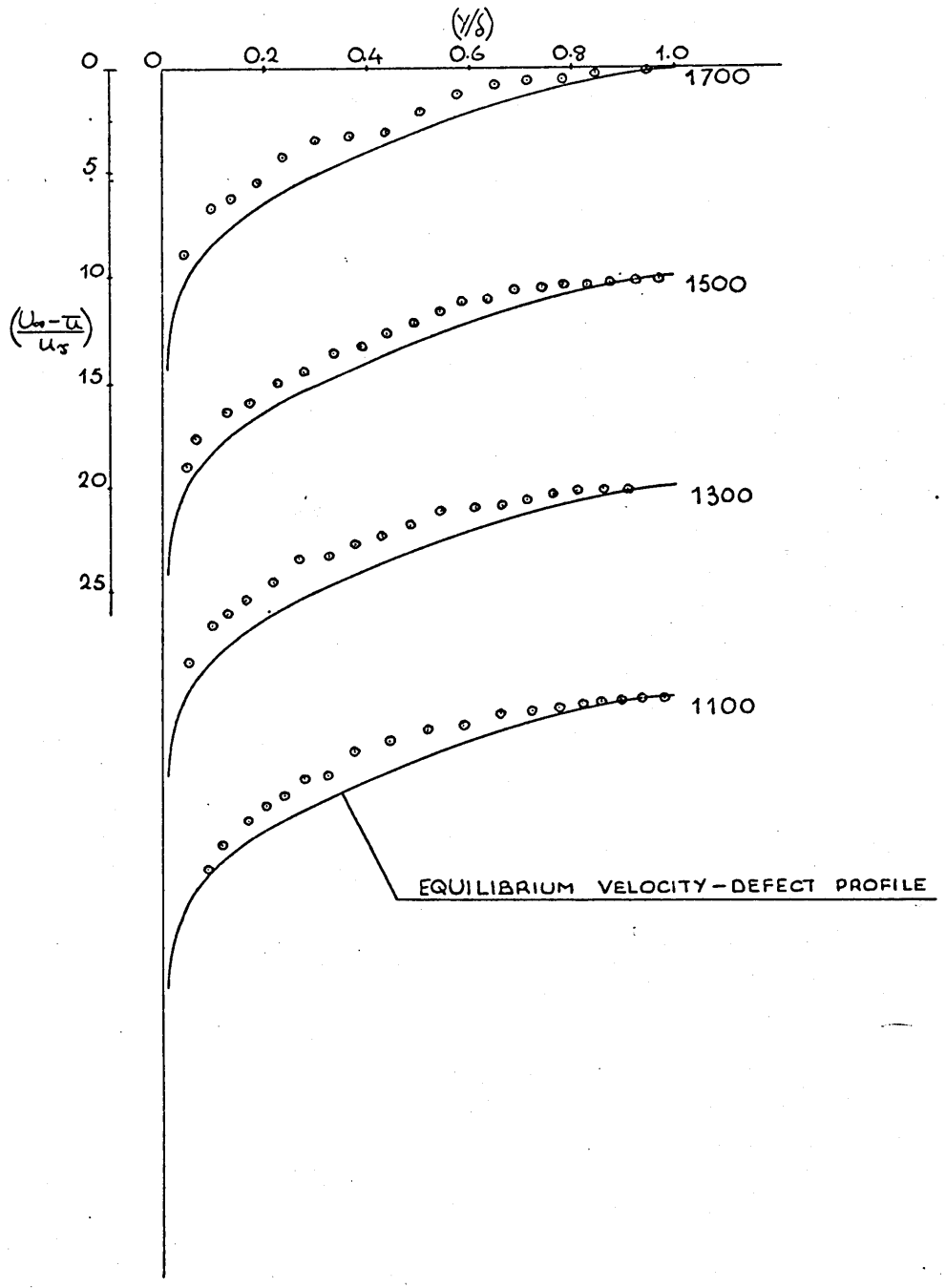

FIG. 1.9

FLOW 1 — DEVELOPMENT OF SEMI-LOGARITHMIC VELOCITY PROFILE ALONG Z = -100

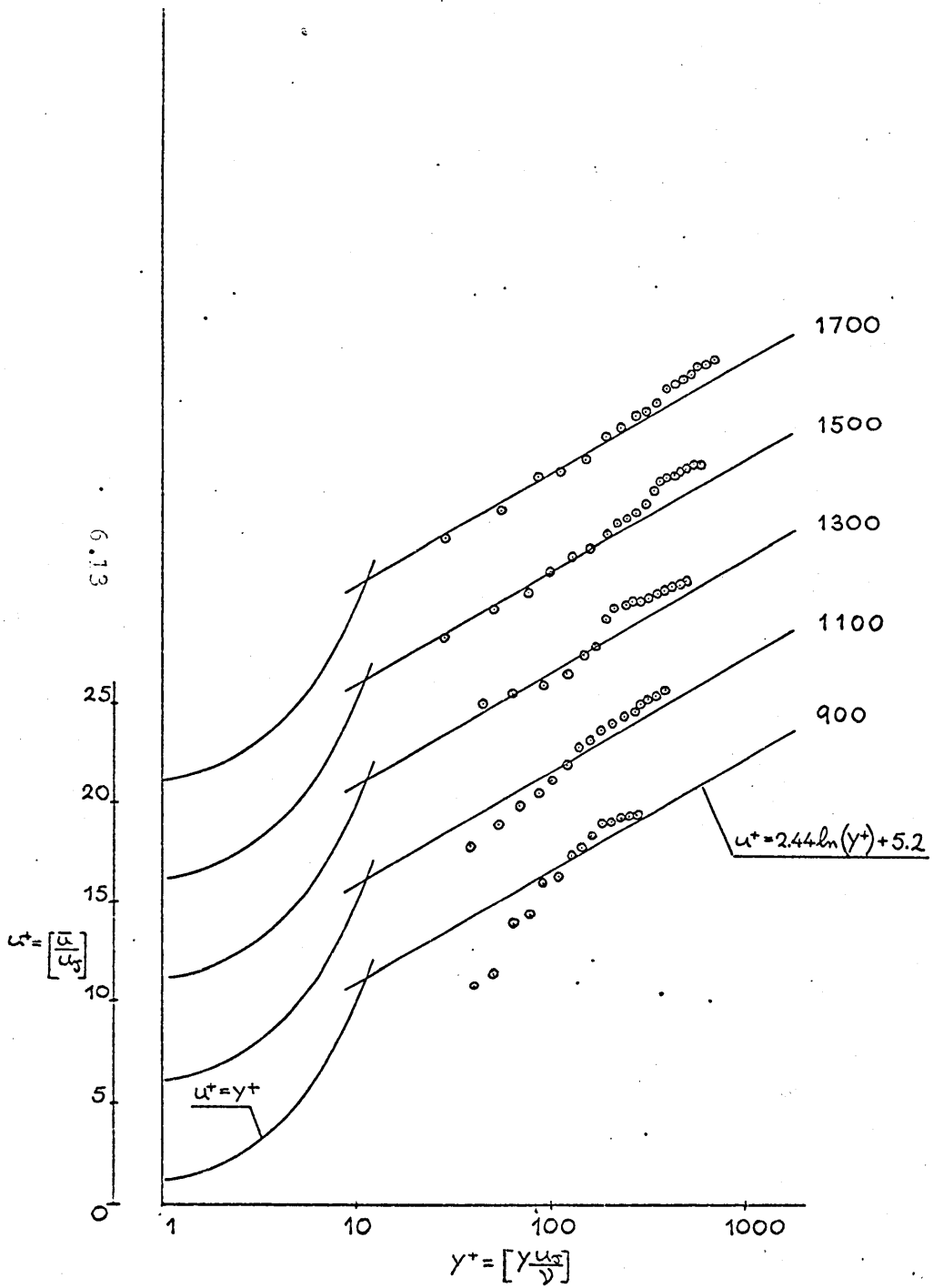

FLOW 1 — DEVELOPMENT OF VELOCITY-DEFECT PROFILE ALONG Z = -100

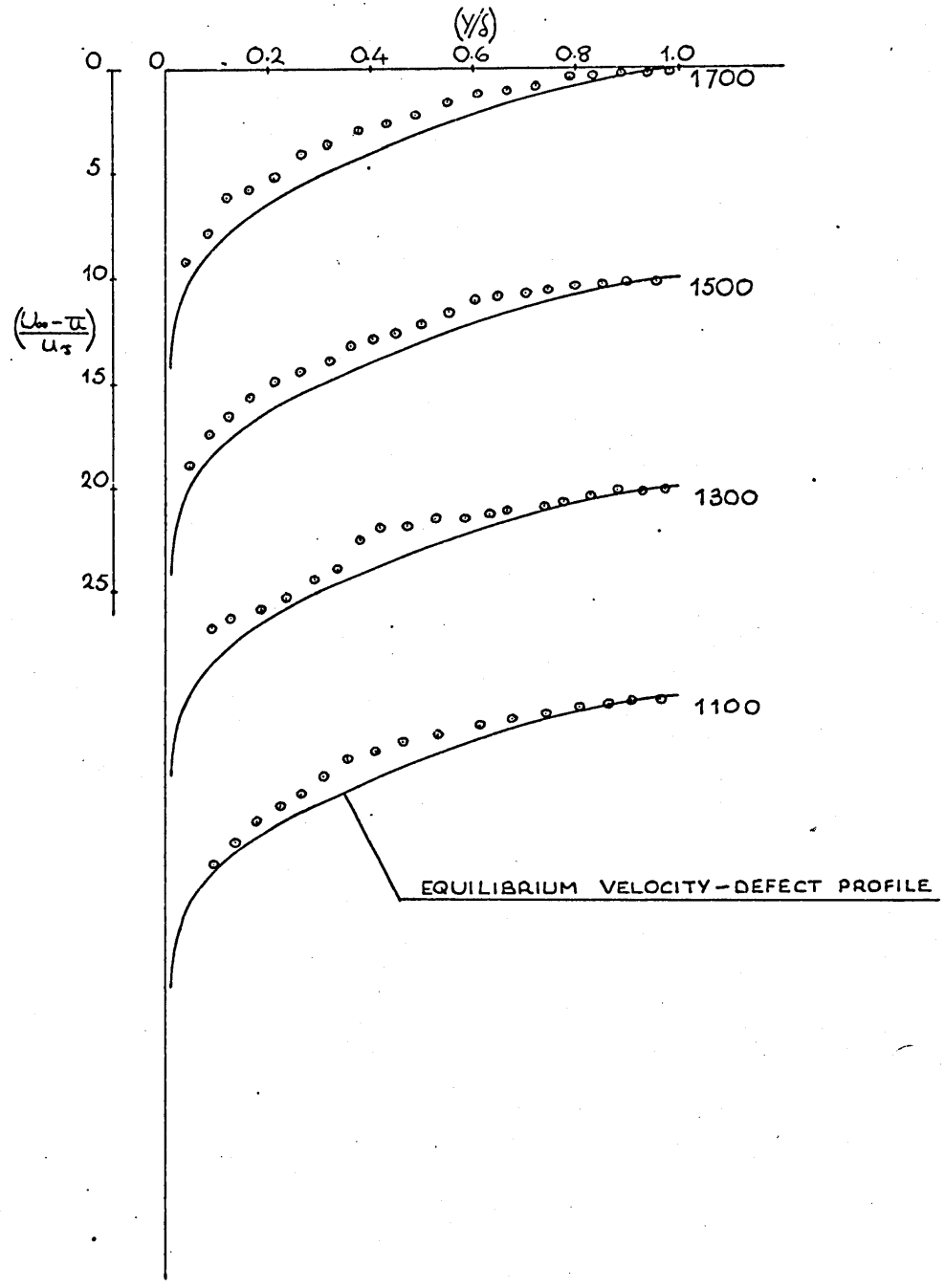

6.13

FIG. 1.10

FIG. 1.11

FLOW 1 DEVELOPMENT OF u' INTENSITY PROFILE ALONG Z = +145

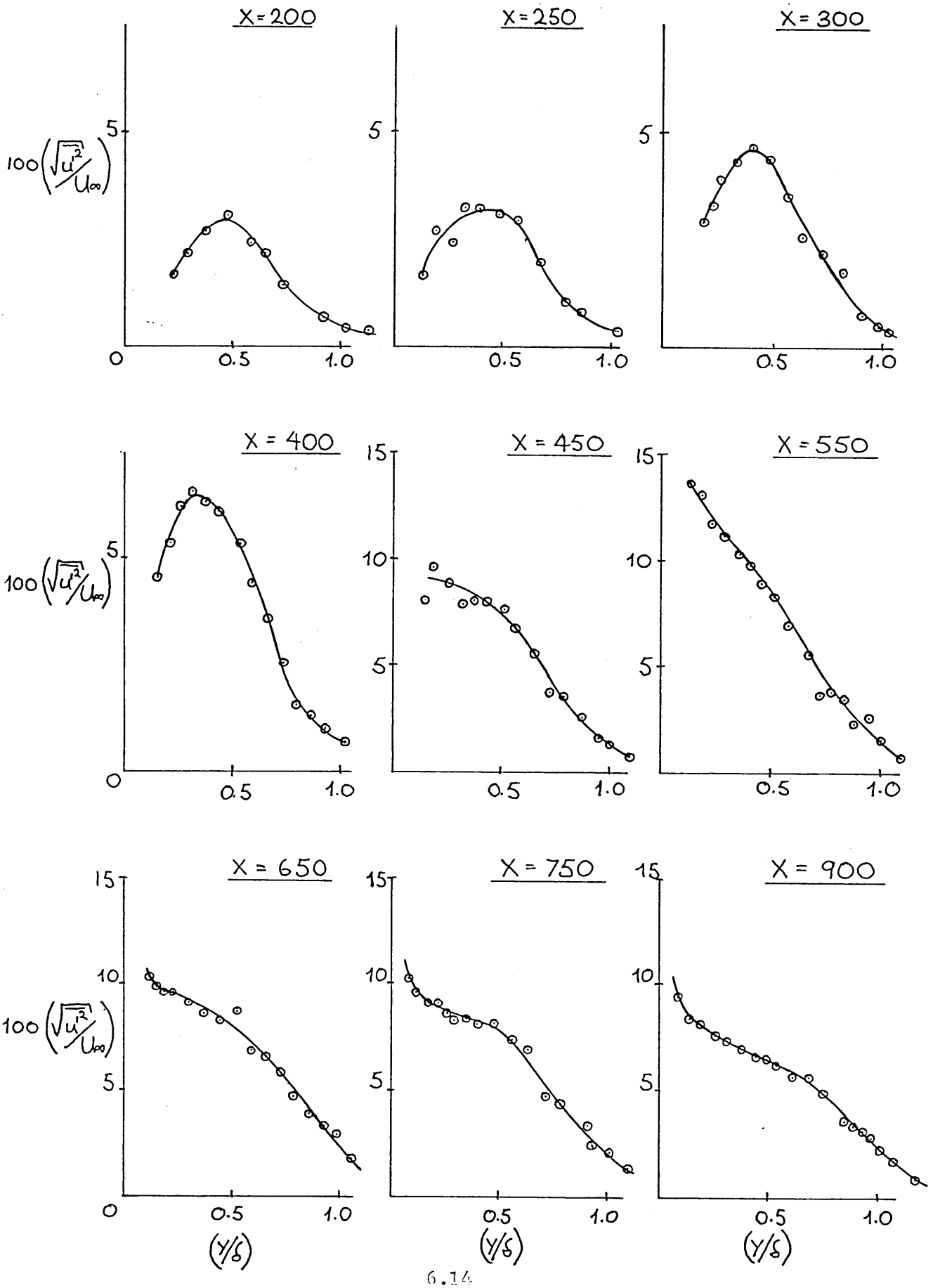

FLOW 1 DEVELOPMENT OF u' INTENSITY PROFILE ALONG Z = +145

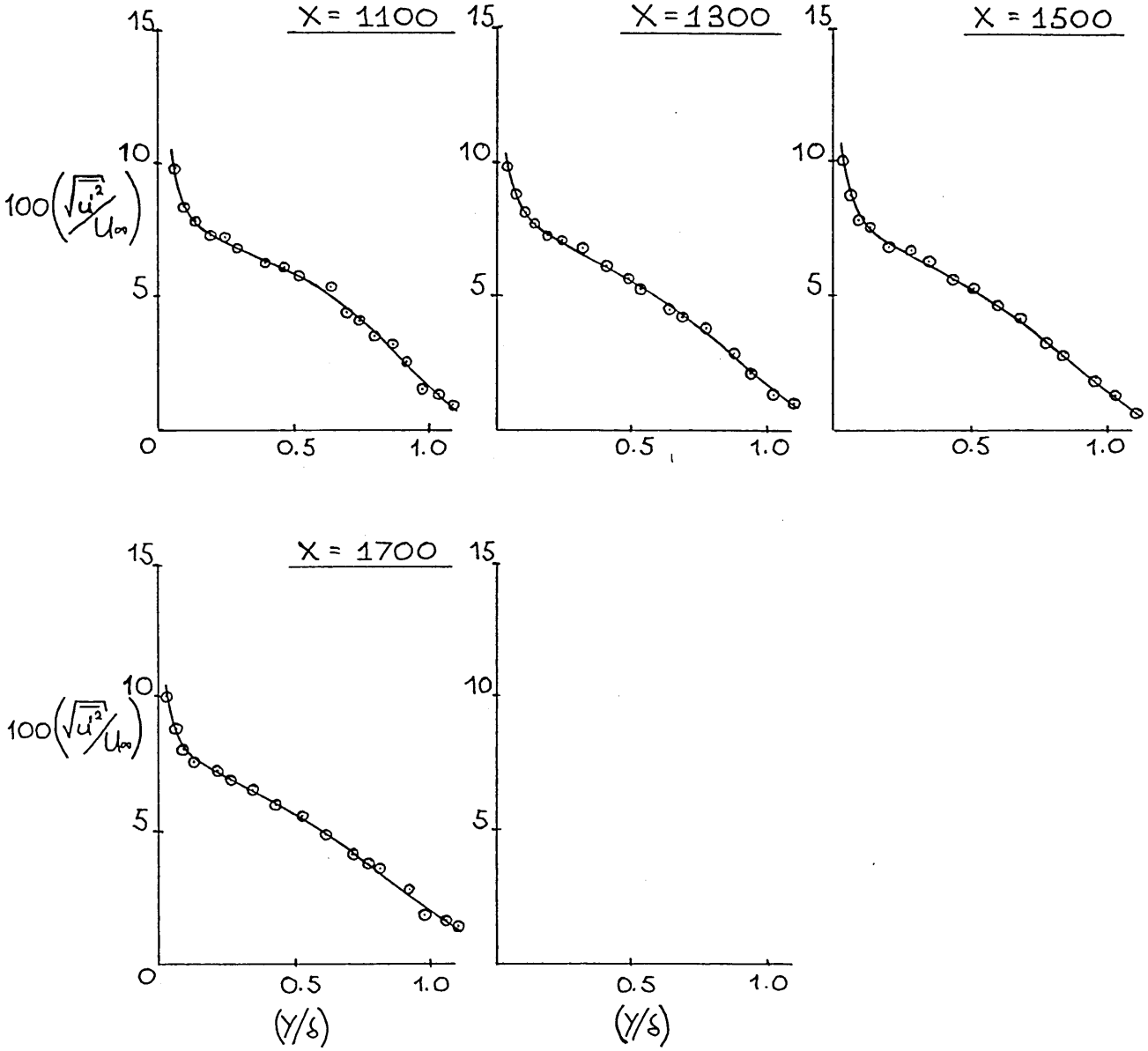

FIG. 1.13

FLOW 1 — DEVELOPMENT OF u' INTENSITY PROFILE ALONG Z = +100

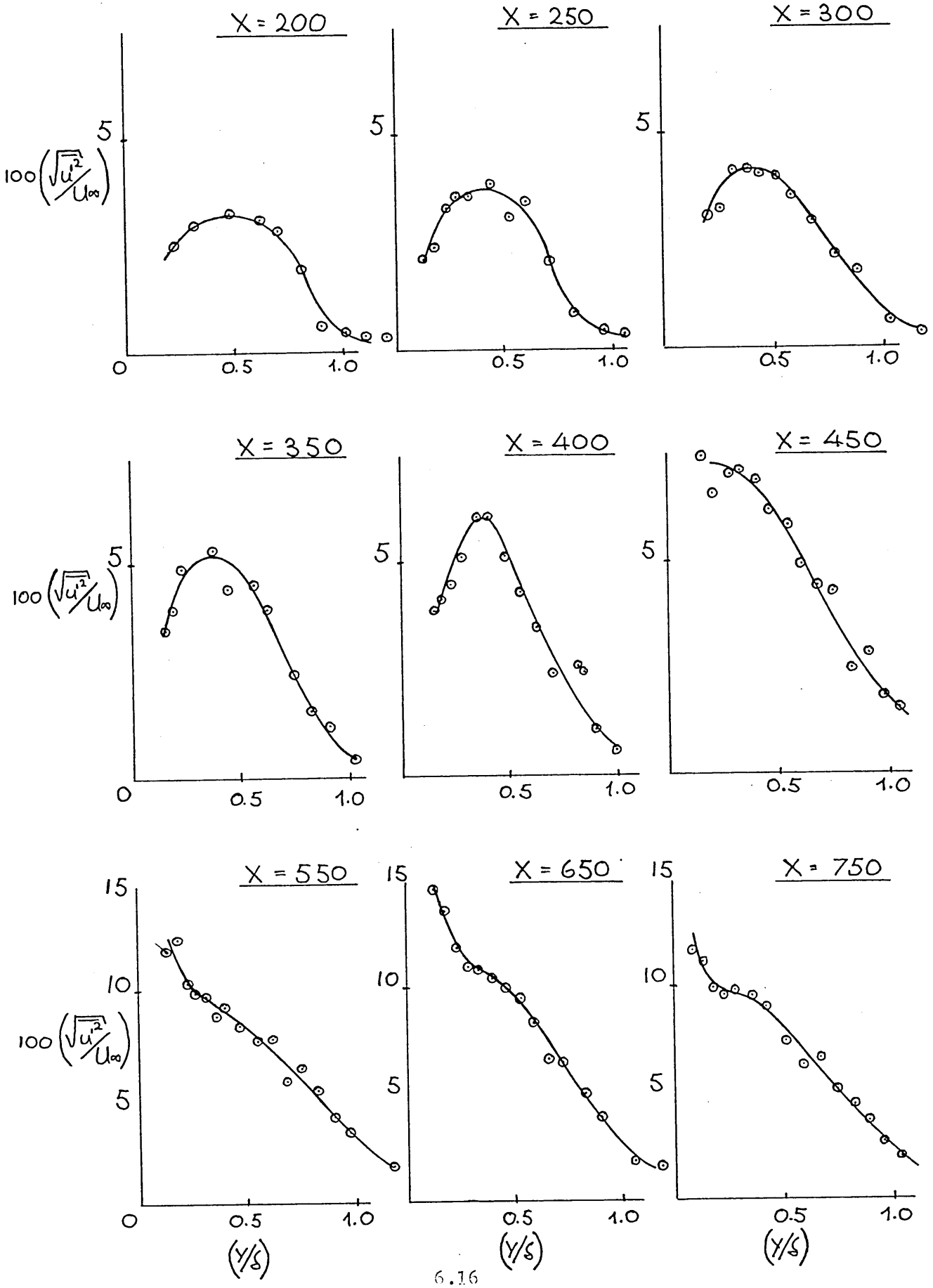

FIG. 1.14

FLOW 1 — DEVELOPMENT OF u' INTENSITY PROFILE ALONG $Z = +100$

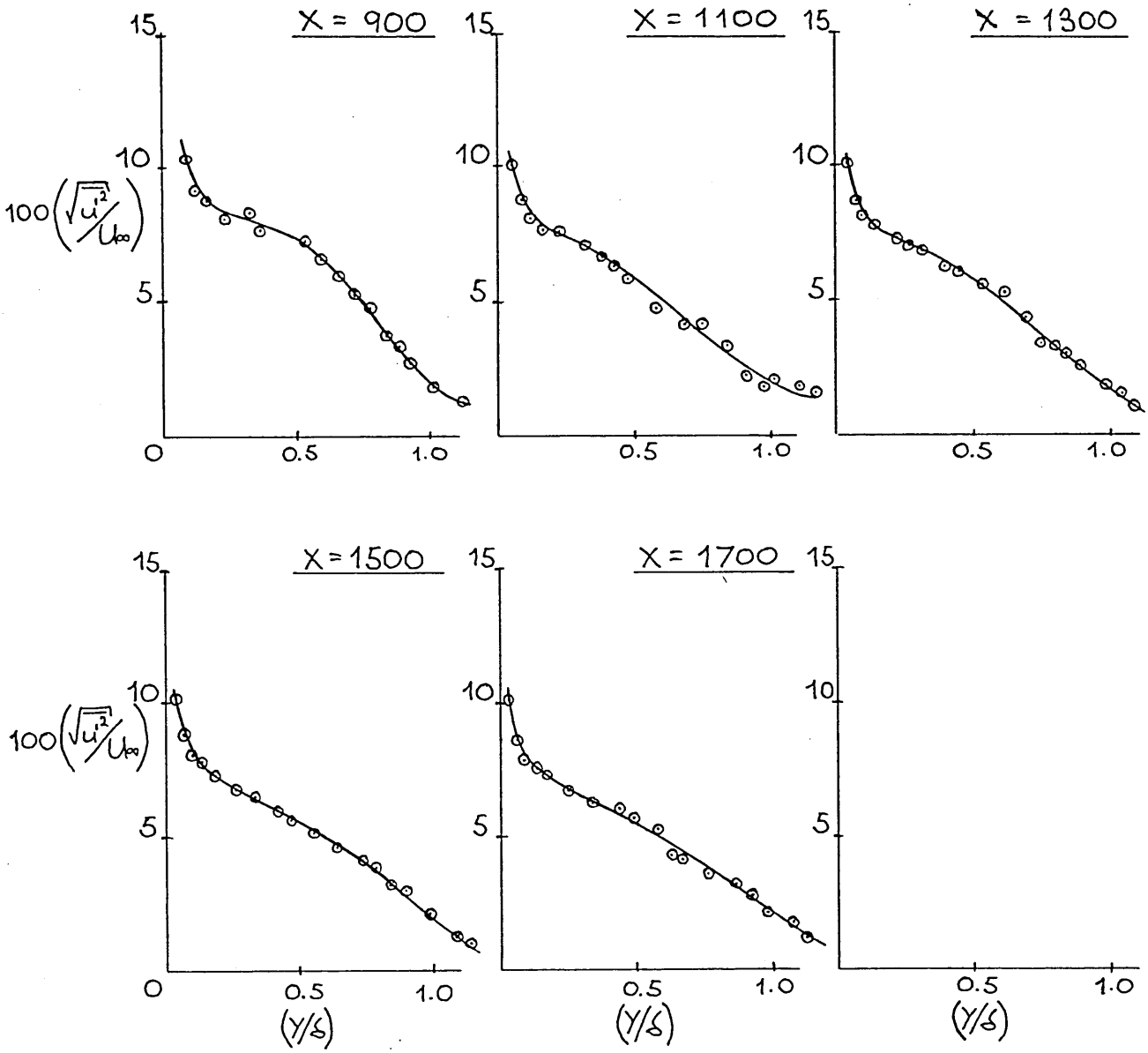

FIG. 1.15

FLOW 1 — DEVELOPMENT OF u' INTENSITY PROFILE ALONG Z = +50

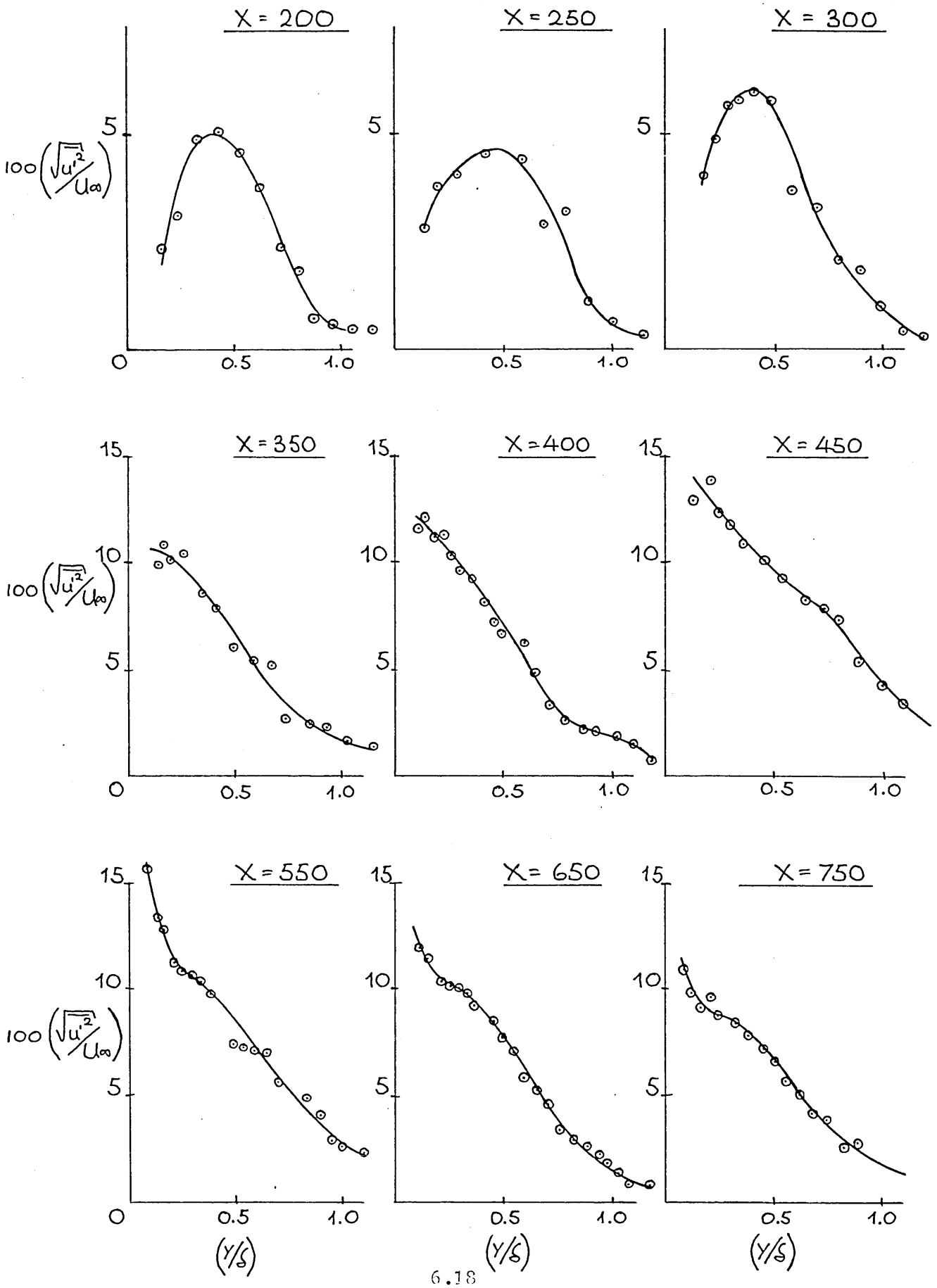

FIG. 1.16

FLOW 1 — DEVELOPMENT OF u' INTENSITY PROFILE ALONG Z = +50

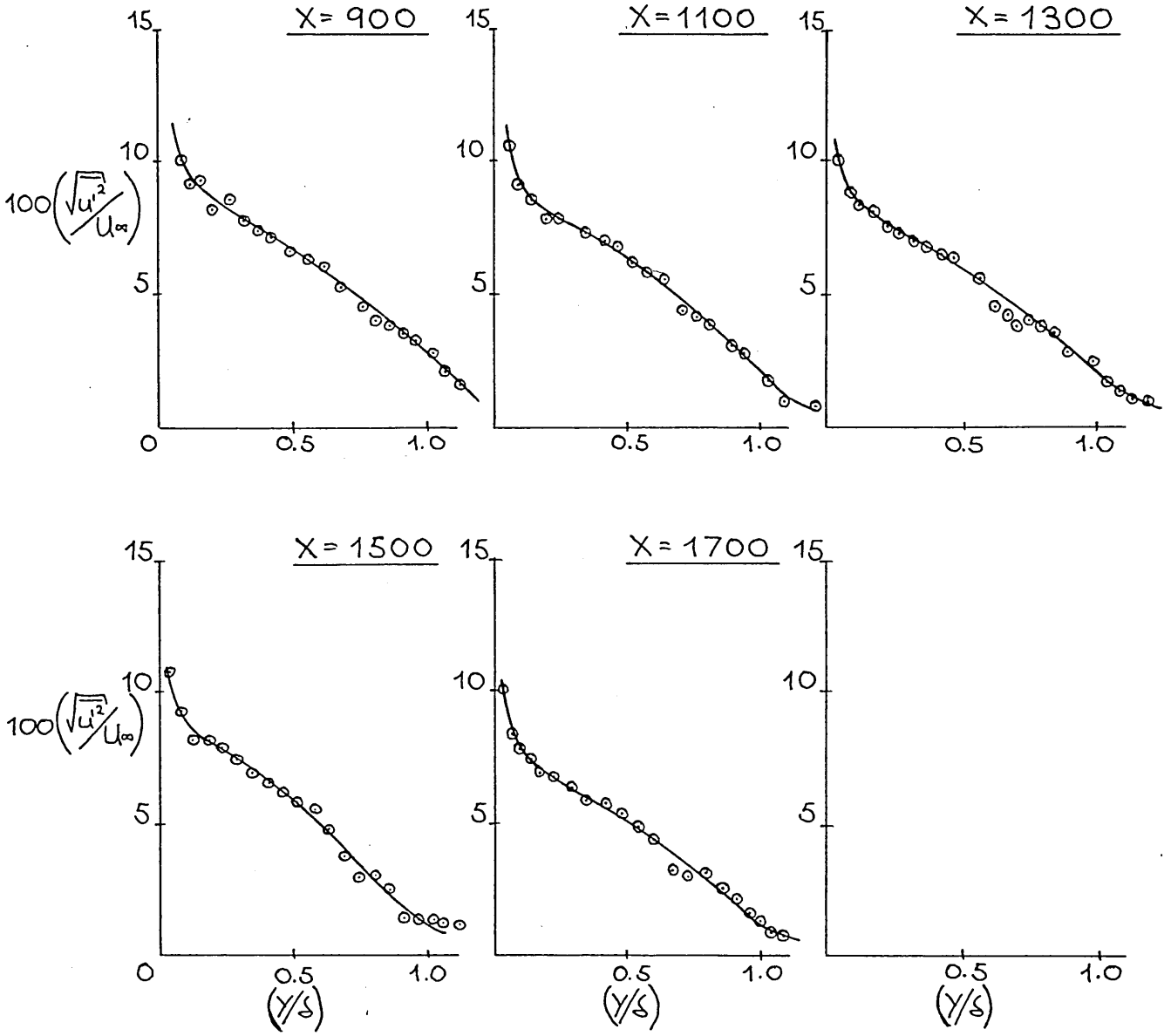

FIG. 1.17

FLOW 1 — DEVELOPMENT OF u' INTENSITY PROFILE ALONG Z = 0

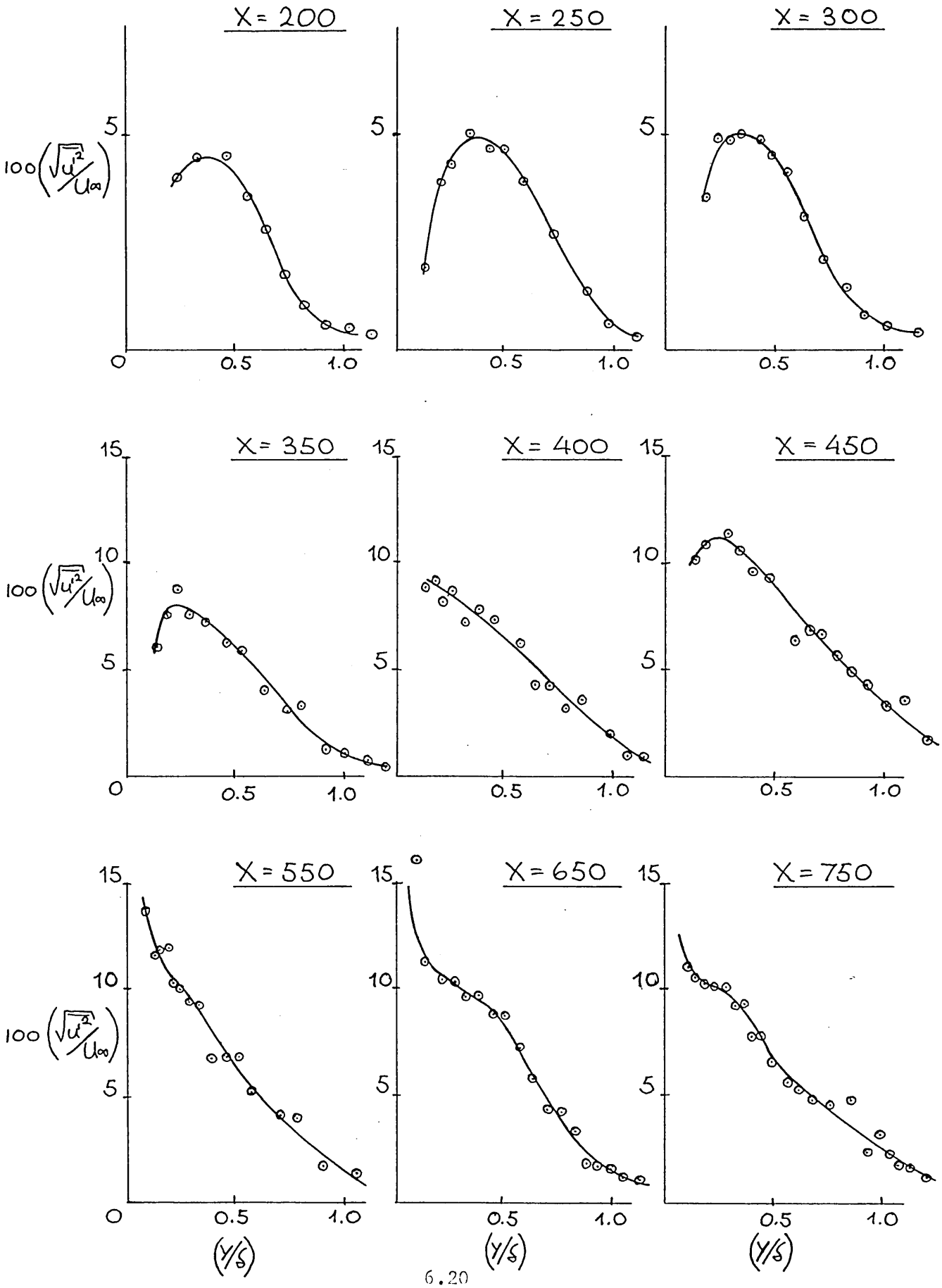

FLOW 1 — DEVELOPMENT OF u' INTENSITY PROFILE ALONG $Z = 0$

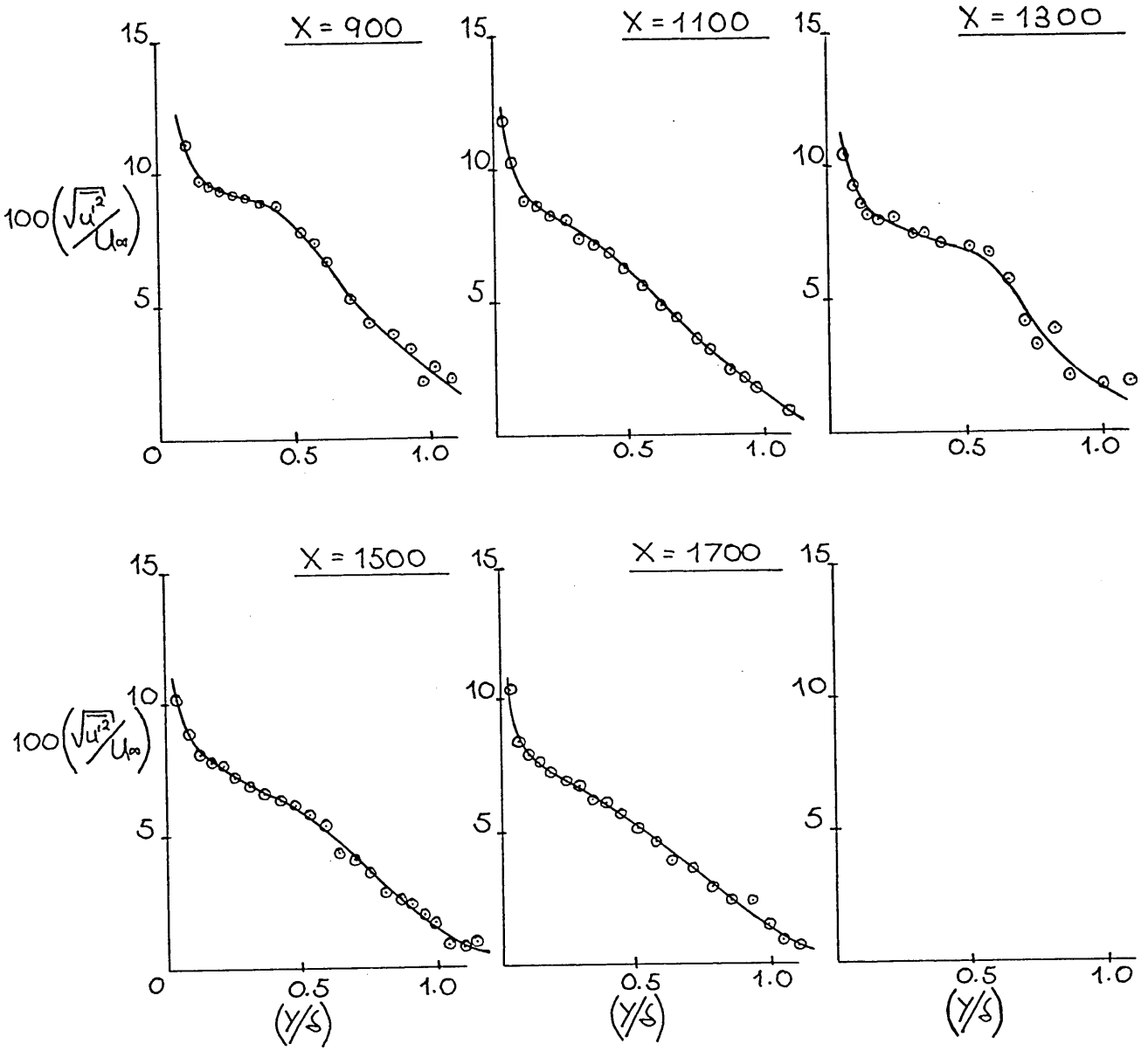

FIG. 1.14

FLOW 1 — DEVELOPMENT OF u' INTENSITY PROFILE ALONG Z = -50

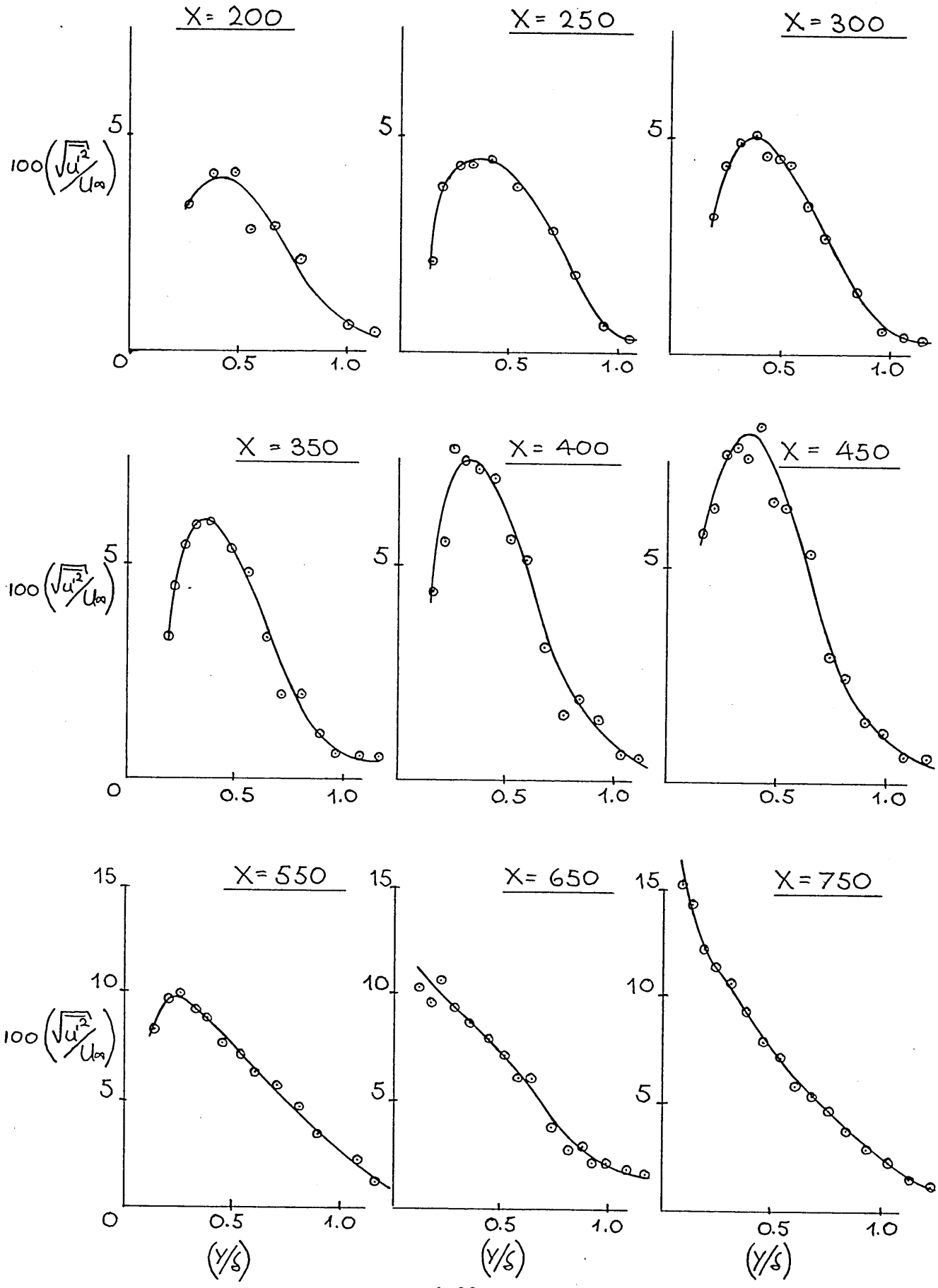

FIG. 1.20

FLOW 1 — DEVELOPMENT OF u' INTENSITY PROFILE ALONG Z = -50

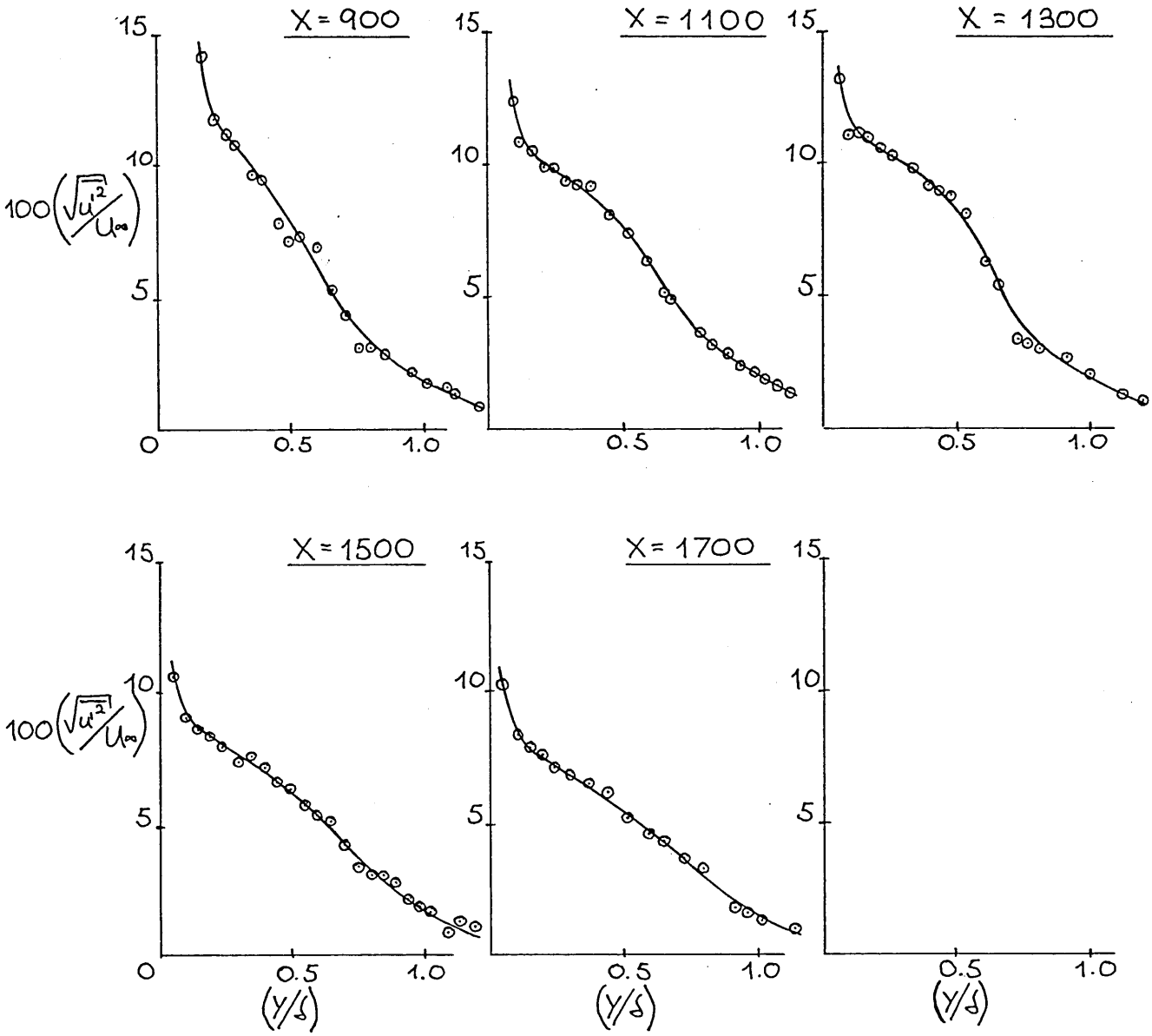

FIG. 1.21

FLOW 1 — DEVELOPMENT OF u' INTENSITY PROFILE ALONG Z = -100

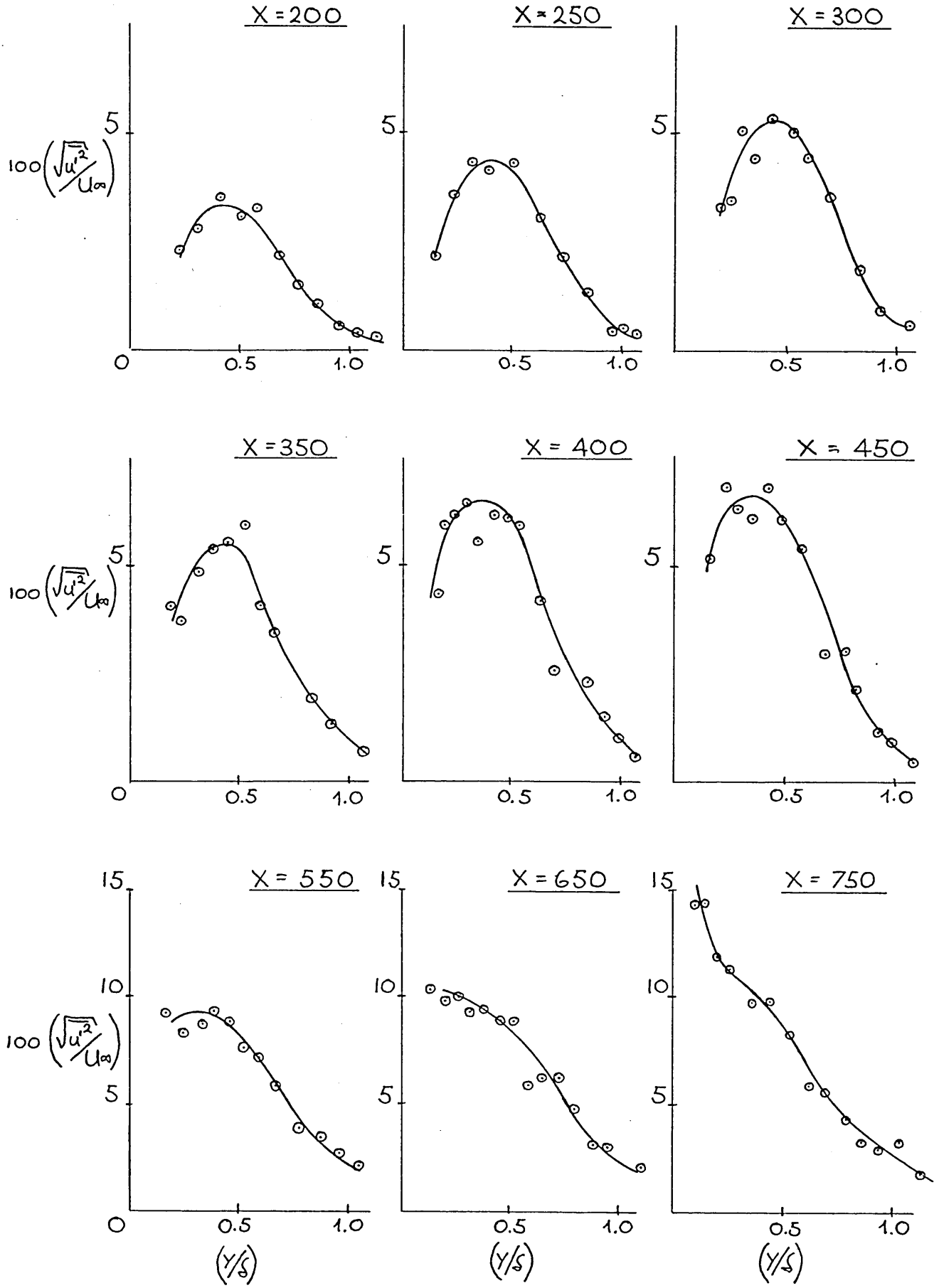

FIG. 1.22

FLOW 1 — DEVELOPMENT OF u' INTENSITY PROFILE ALONG Z = -100

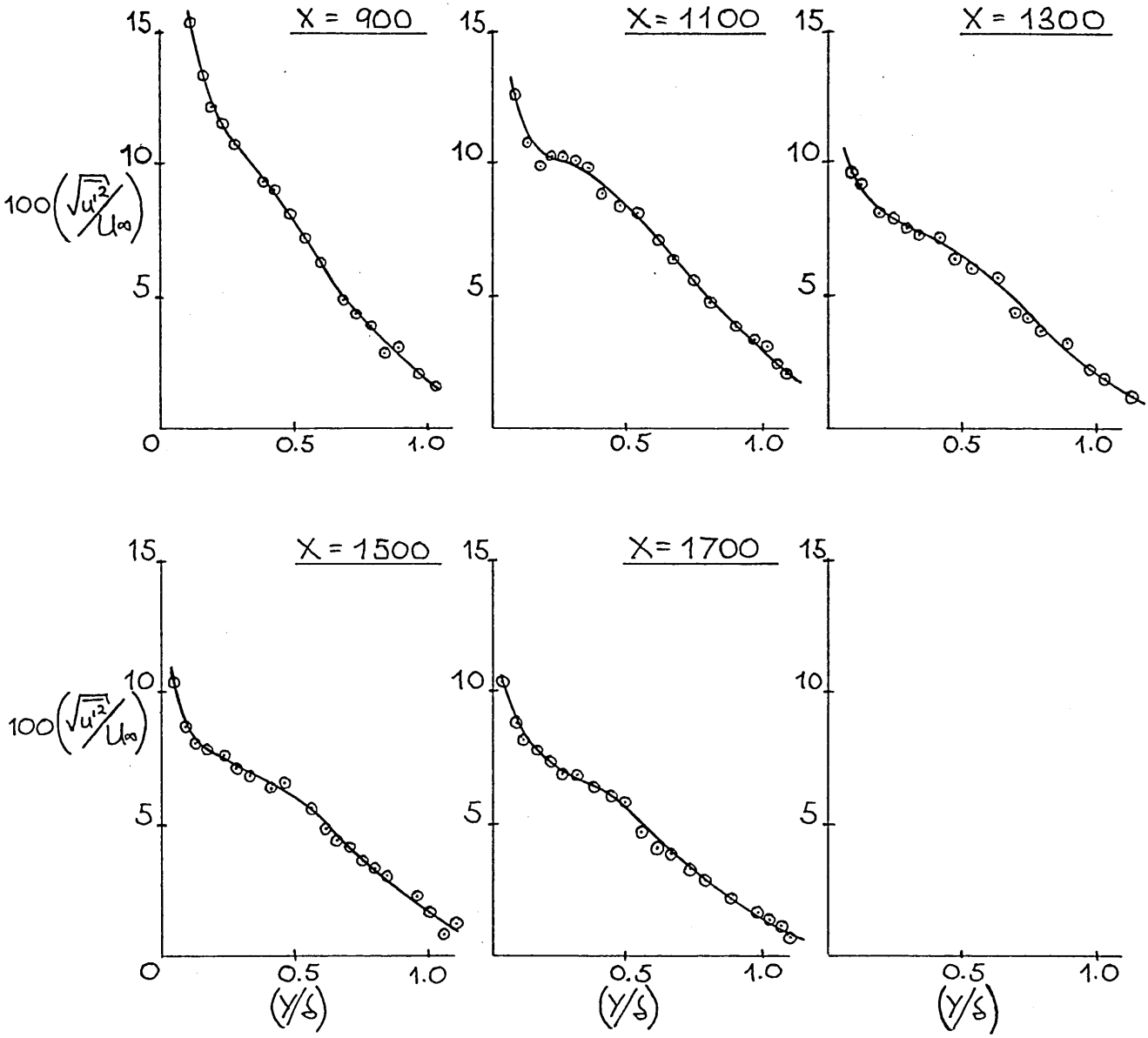

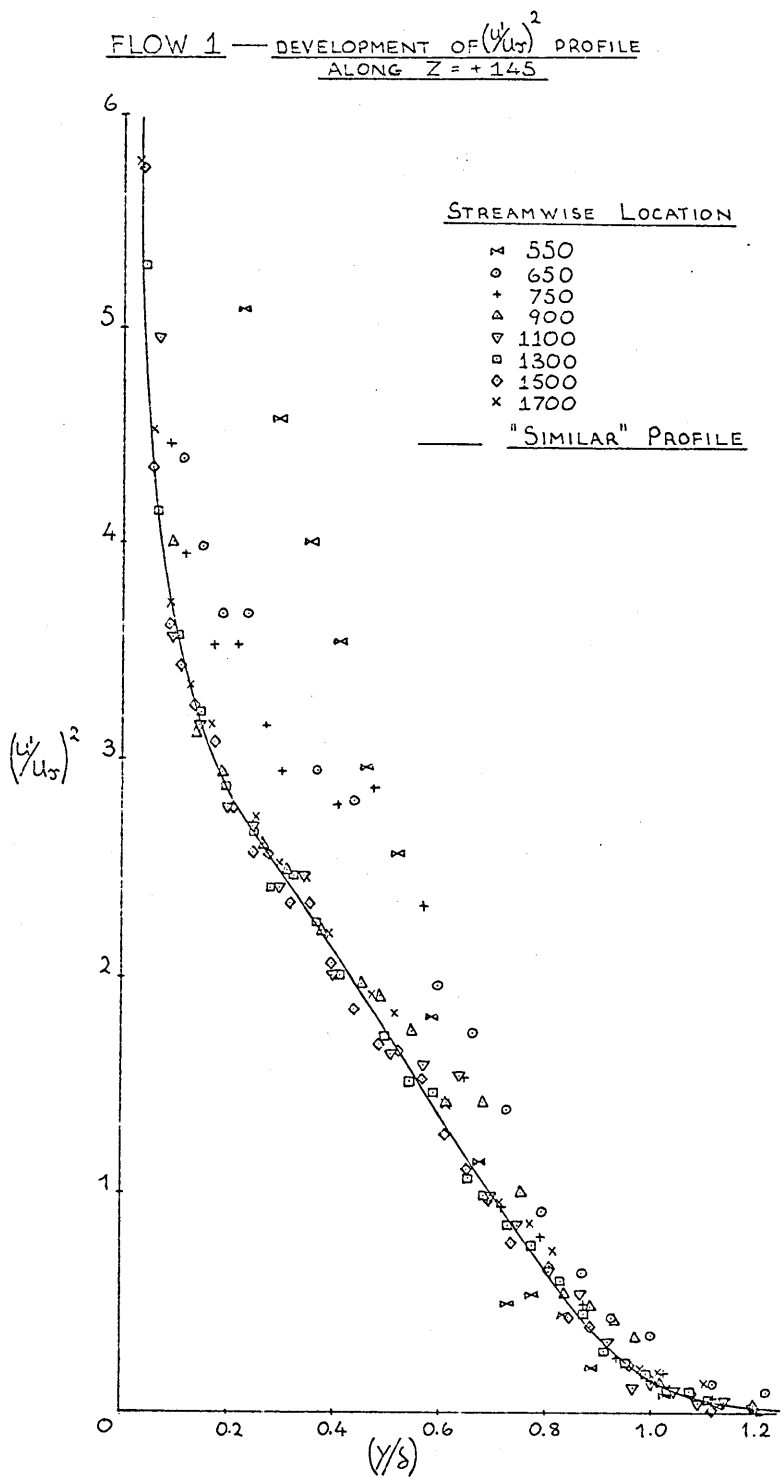
FLOW 1 — DEVELOPMENT OF $(u'/U_s)^2$ PROFILE
ALONG Z = +145
STREAMWISE LOCATION
550
650
750
900
1100
1300
1500
1700
"SIMILAR" PROFILE
$(u'/U_s)^2$
(y/δ)
0
1
2
3
4
5
6
0.2
0.4
0.6
0.8
1.0
1.2

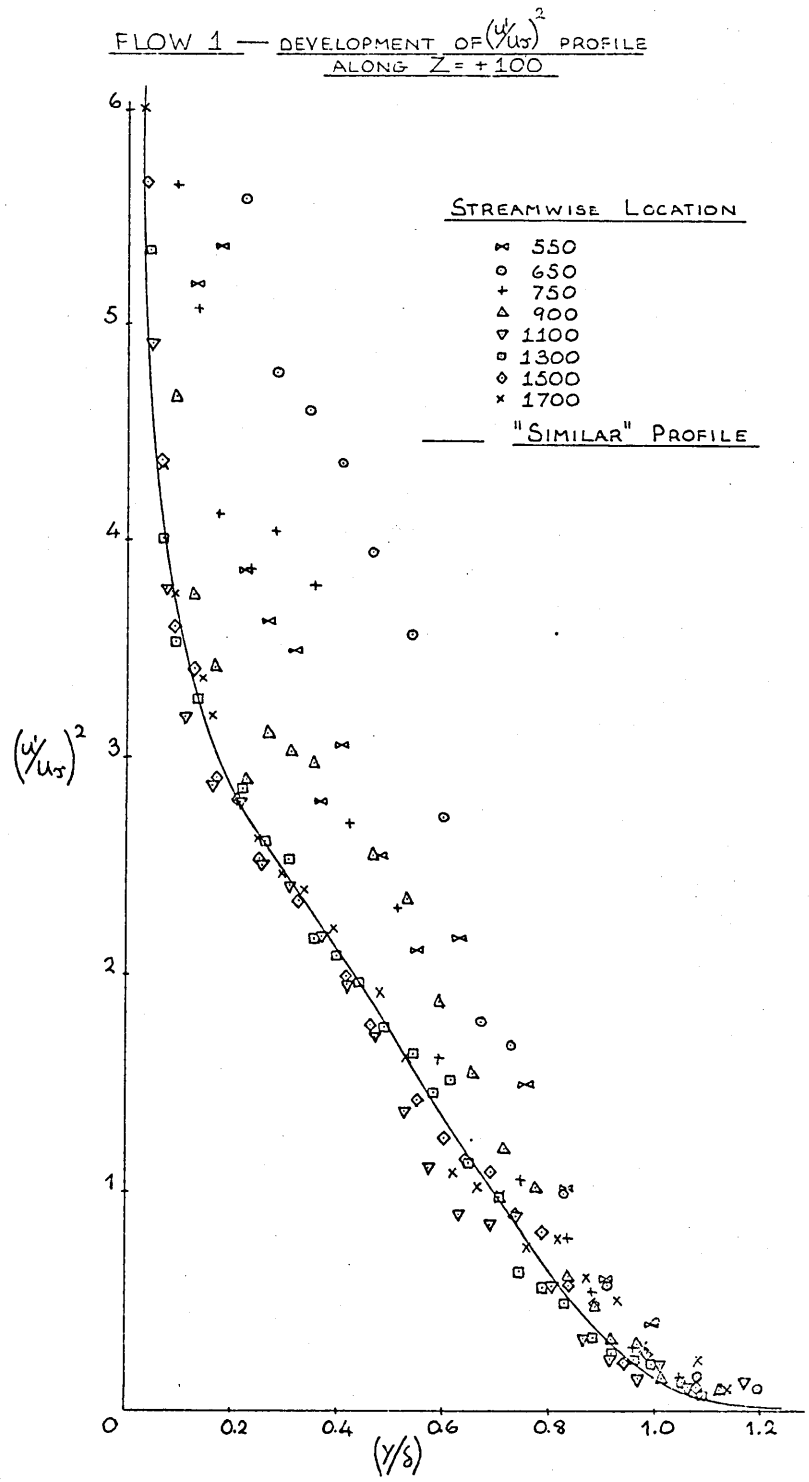
FLOW 1 — DEVELOPMENT OF $(u'/U_s)^2$ PROFILE
ALONG Z = +100
STREAMWISE LOCATION
550
650
750
900
1100
1300
1500
1700
"SIMILAR" PROFILE
$(u'/U_s)^2$
(y/δ)
0
1
2
3
4
5
6
0.2
0.4
0.6
0.8
1.0
1.2

FIG. 1.23

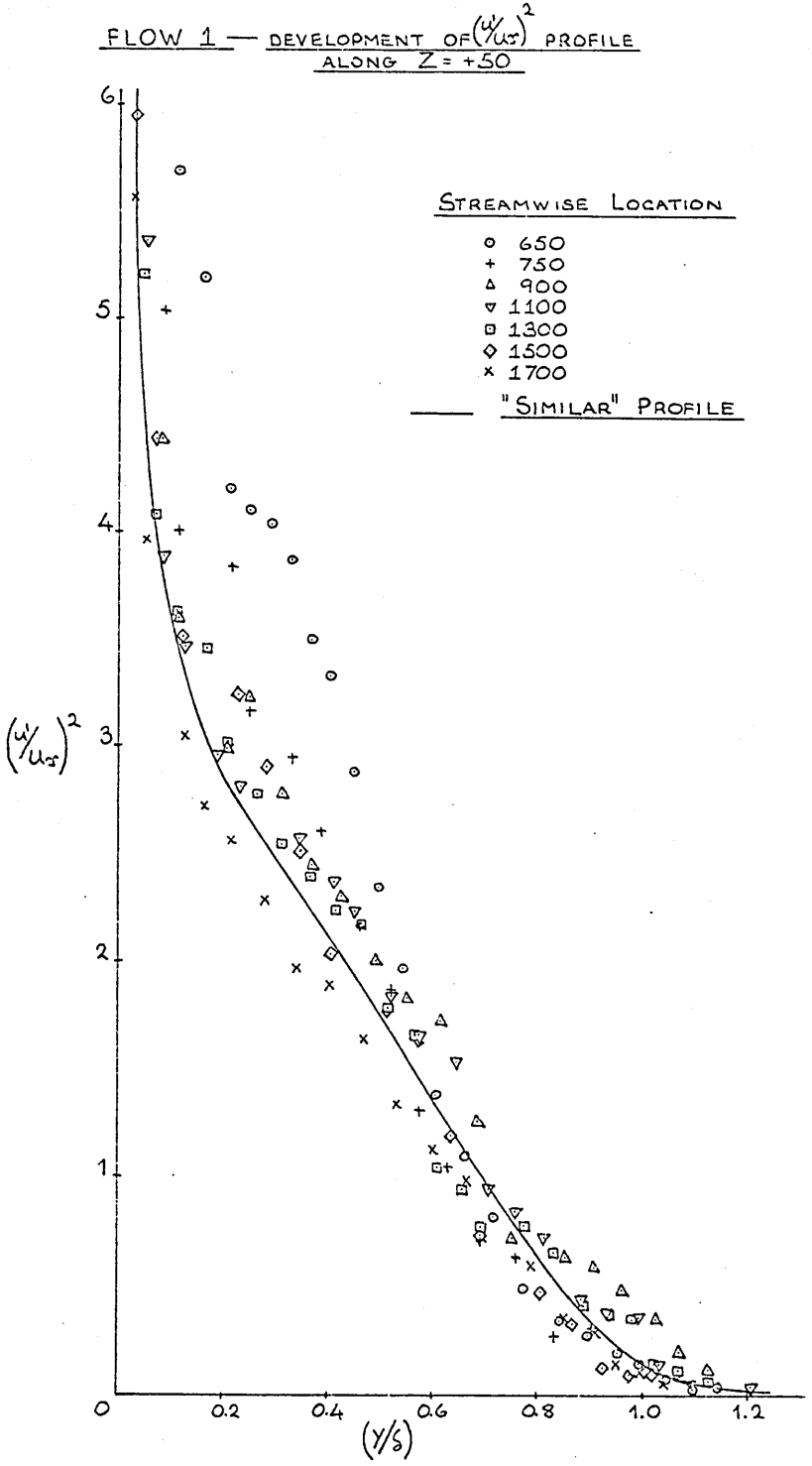
FLOW 1 — DEVELOPMENT OF $(u'/u_\tau)^2$ PROFILE ALONG Z = +50
STREAMWISE LOCATION
650
750
900
1100
1300
1500
1700
"SIMILAR" PROFILE
$(u'/u_\tau)^2$
(y/δ)
0
1
2
3
4
5
6
0.2
0.4
0.6
0.8
1.0
1.2

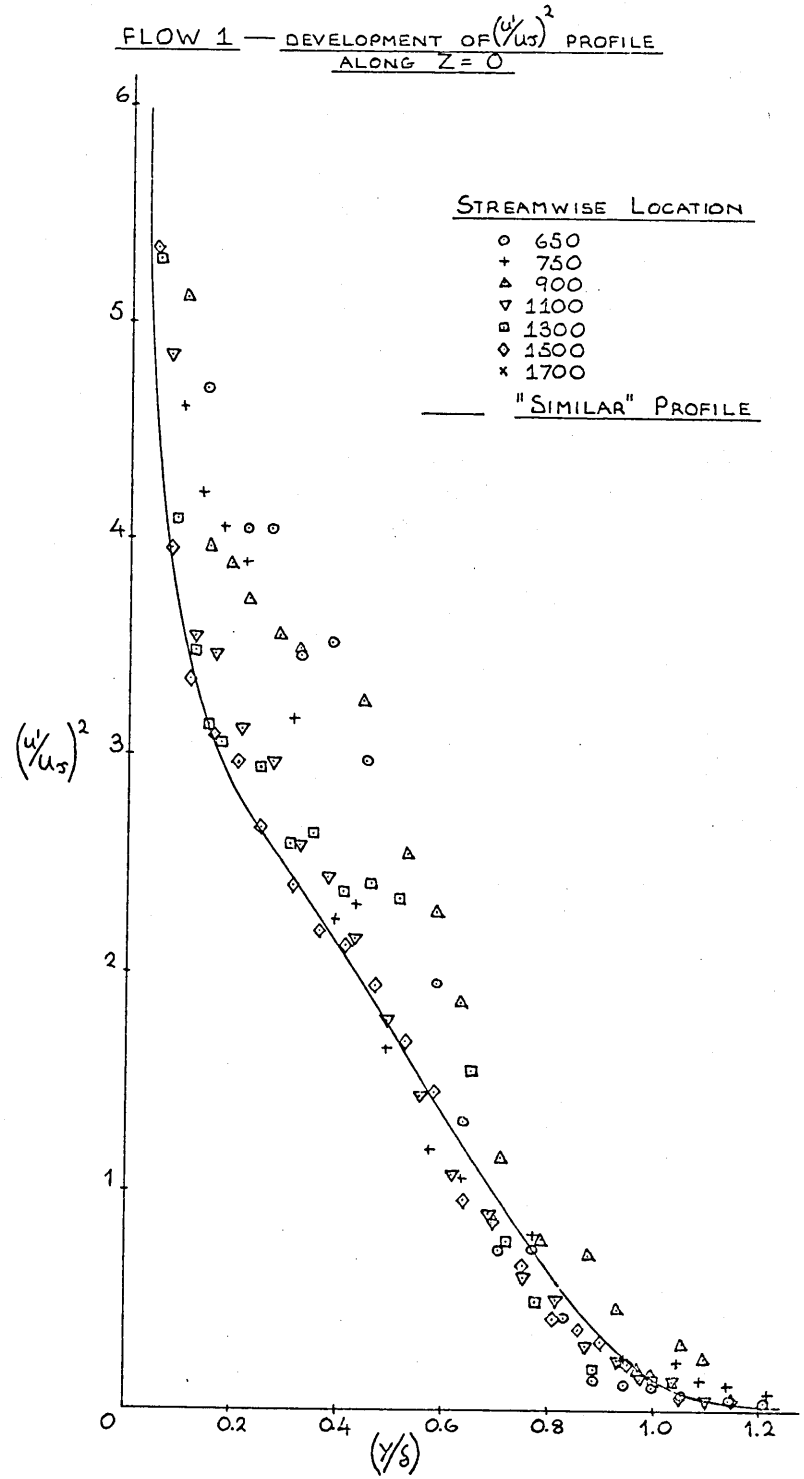
FLOW 1 — DEVELOPMENT OF $(u'/u_\tau)^2$ PROFILE ALONG Z = 0
STREAMWISE LOCATION
650
750
900
1100
1300
1500
1700
"SIMILAR" PROFILE
$(u'/u_\tau)^2$
(y/δ)
0
1
2
3
4
5
6
0.2
0.4
0.6
0.8
1.0
1.2

6.27

FIG 1.24

FLOW 1 — DEVELOPMENT OF $(u'/u_\sigma)^2$ PROFILE ALONG Z = -50

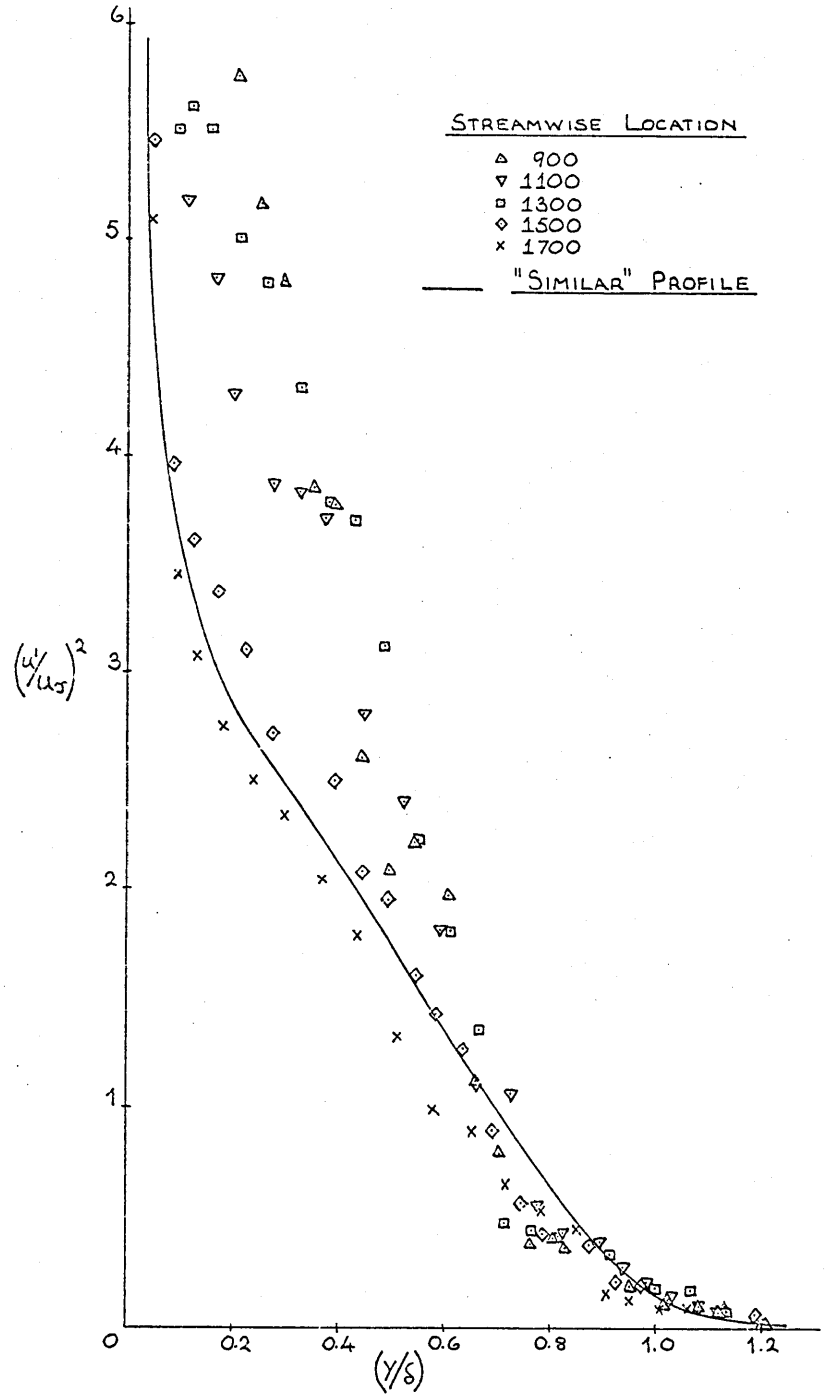

FLOW 1 — DEVELOPMENT OF $(u'/u_\sigma)^2$ PROFILE ALONG Z = -100

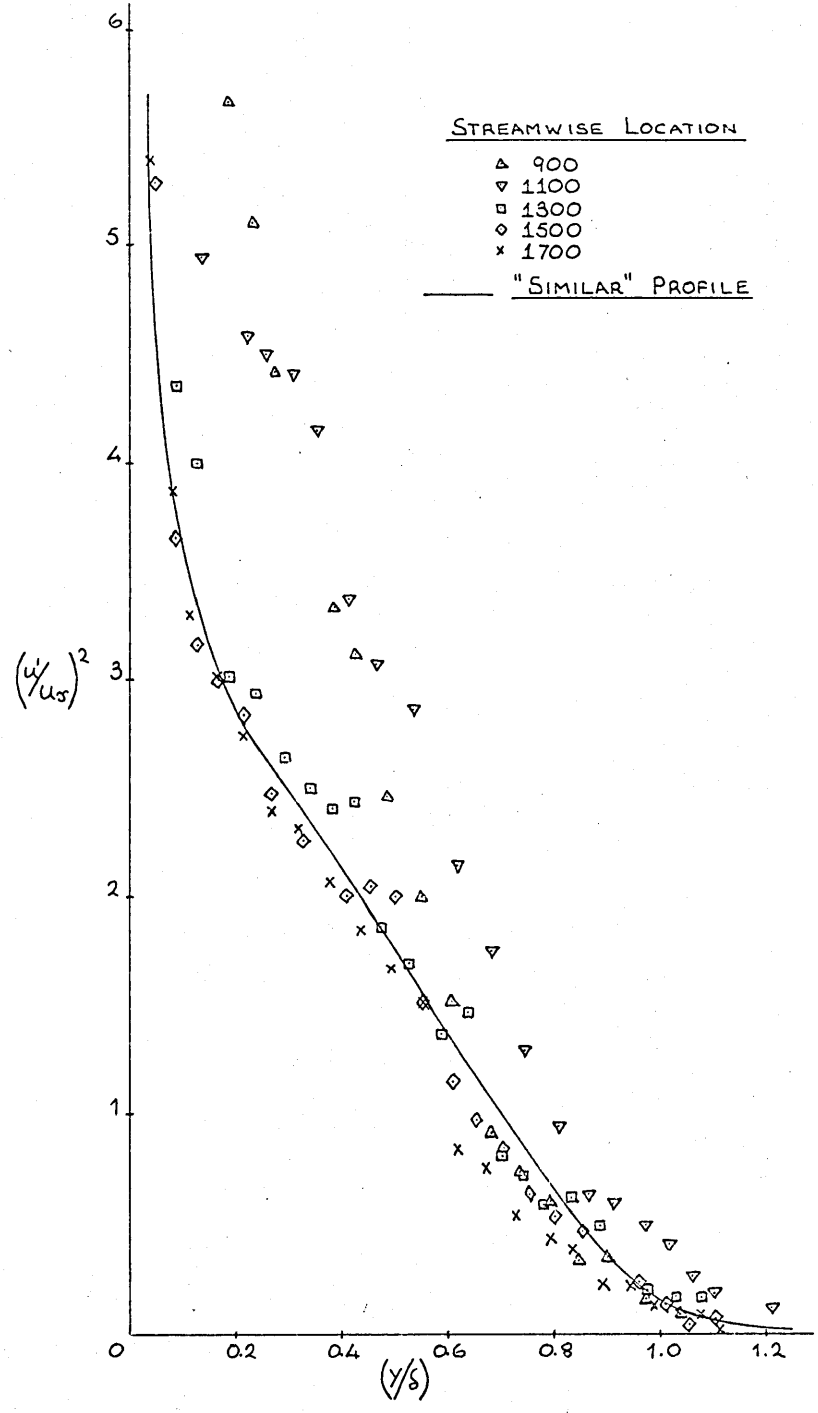

FIG 1.25

FLOW 1 — VELOCITY PROFILES AT WIRE POSITION WITH WIRE REMOVED

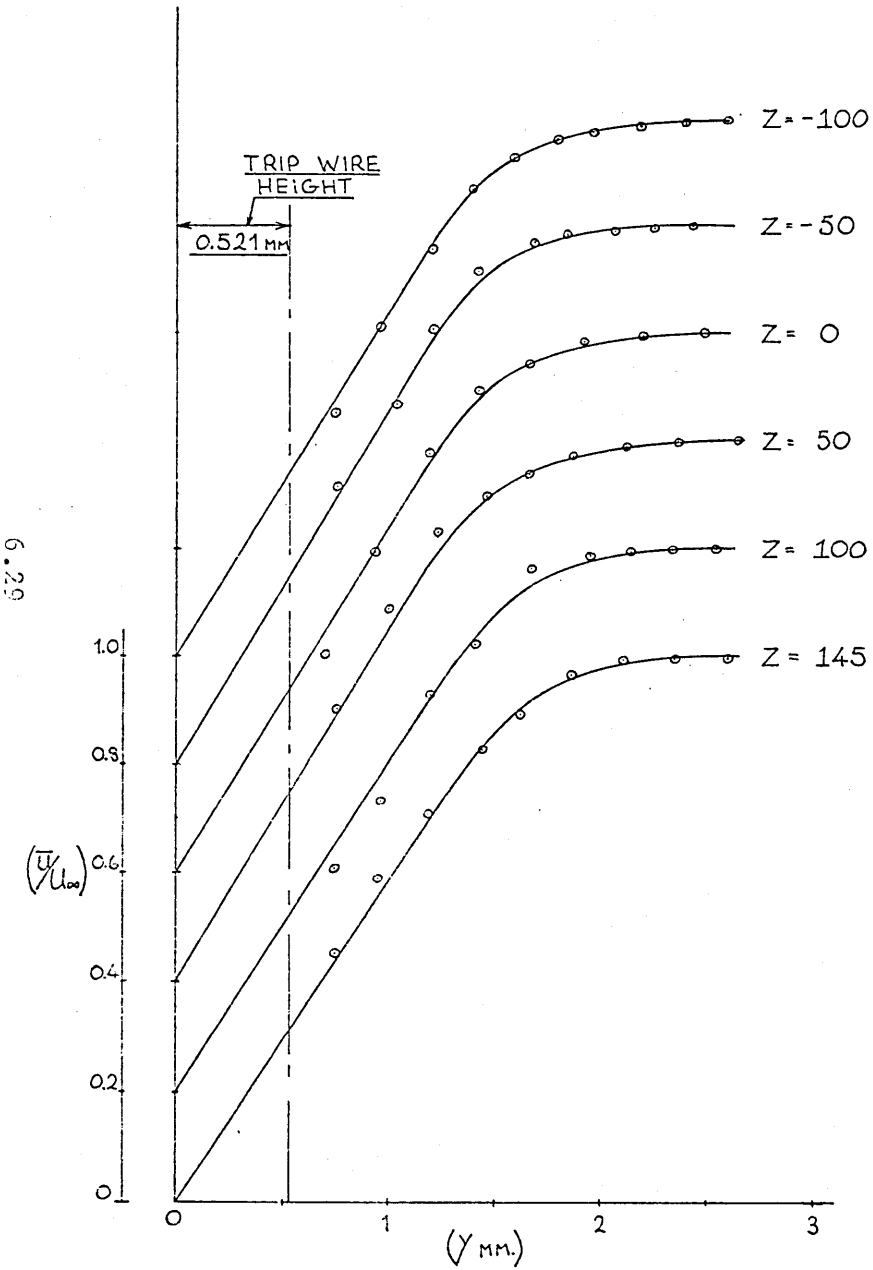

6.29

FLOW 1 — U' INTENSITY PROFILES AT WIRE POSITION WITH WIRE REMOVED

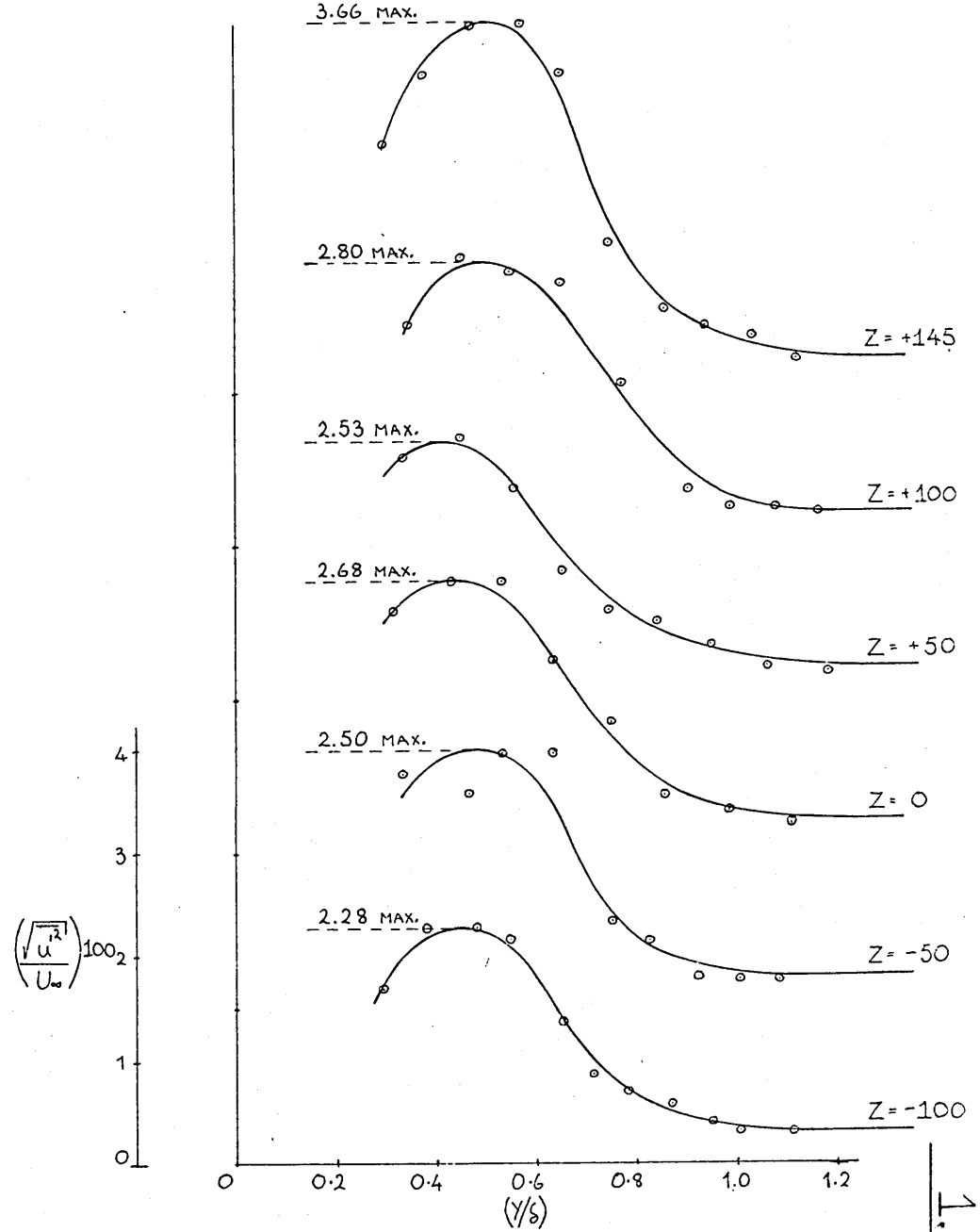

1.26

FIG. 1.27

FLOW 1 — DEVELOPMENT OF INTERMITTENCY PROFILE ALONG Z = +145

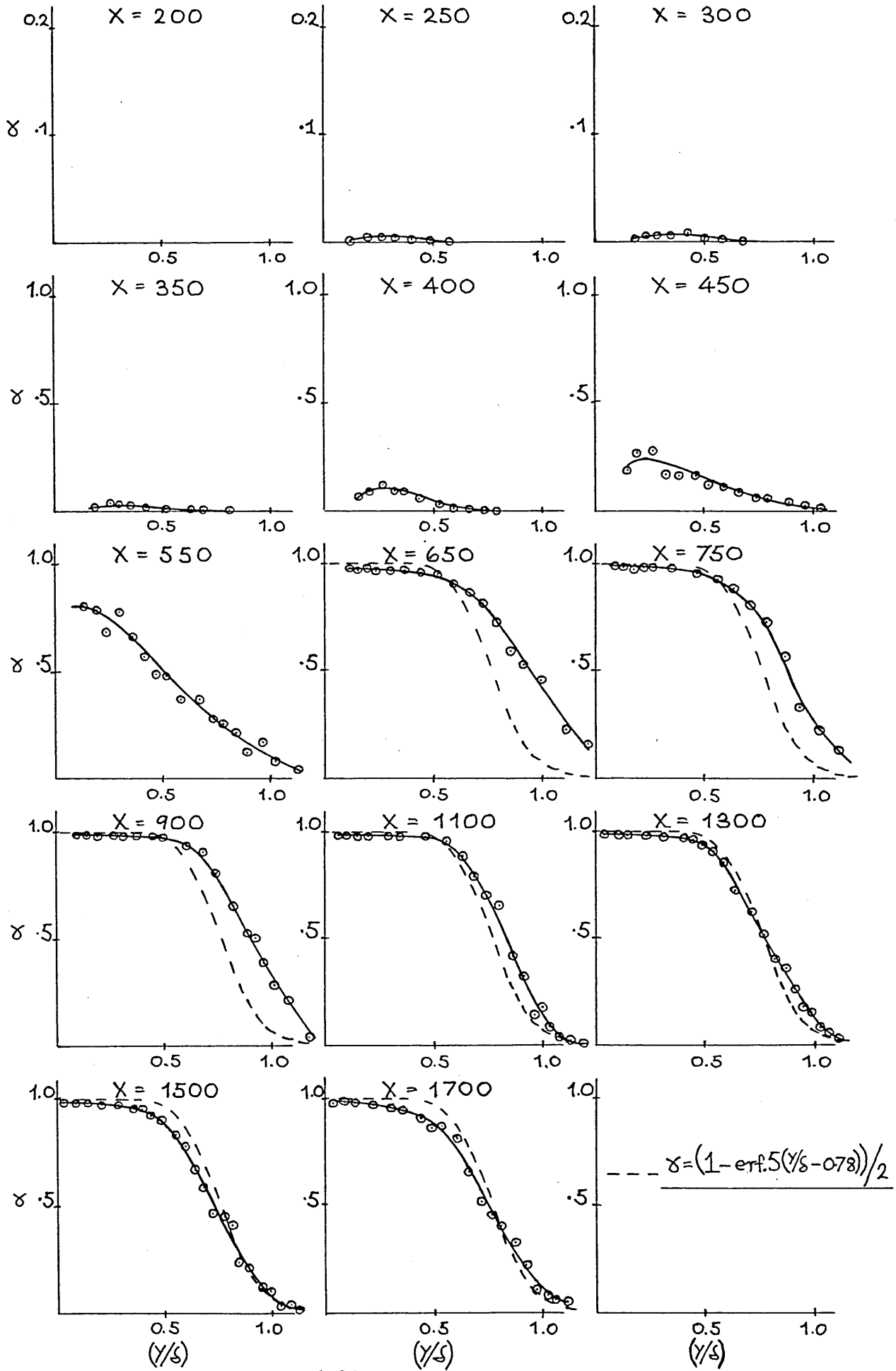

FLOW 1 — DEVELOPMENT OF INTERMITTENCY PROFILE ALONG Z = +100

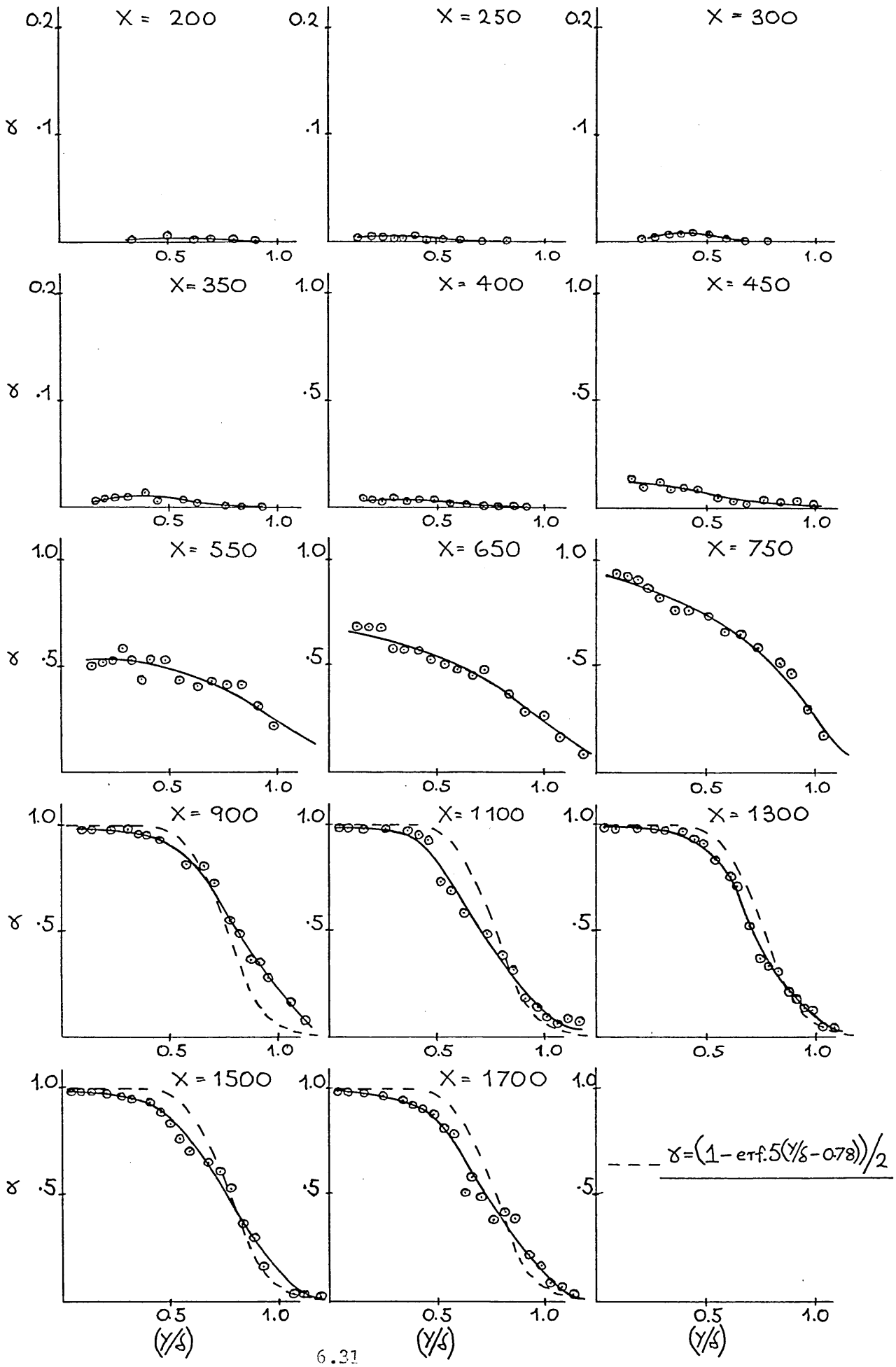

FIG. 1.29

FLOW 1 — DEVELOPMENT OF INTERMITTENCY PROFILE ALONG Z = +50

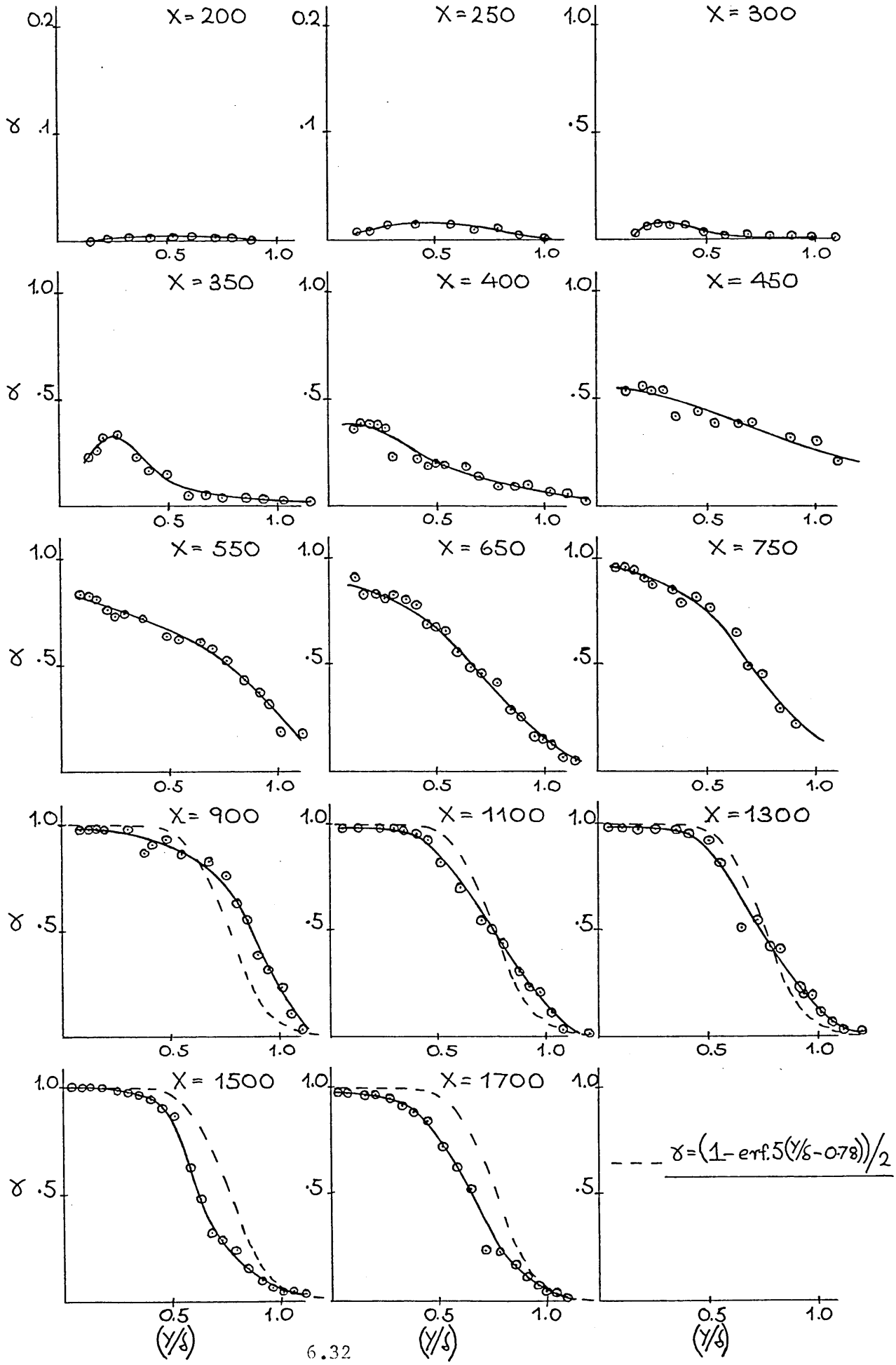

FLOW 1 — DEVELOPMENT OF INTERMITTENCY PROFILE ALONG Z = 0

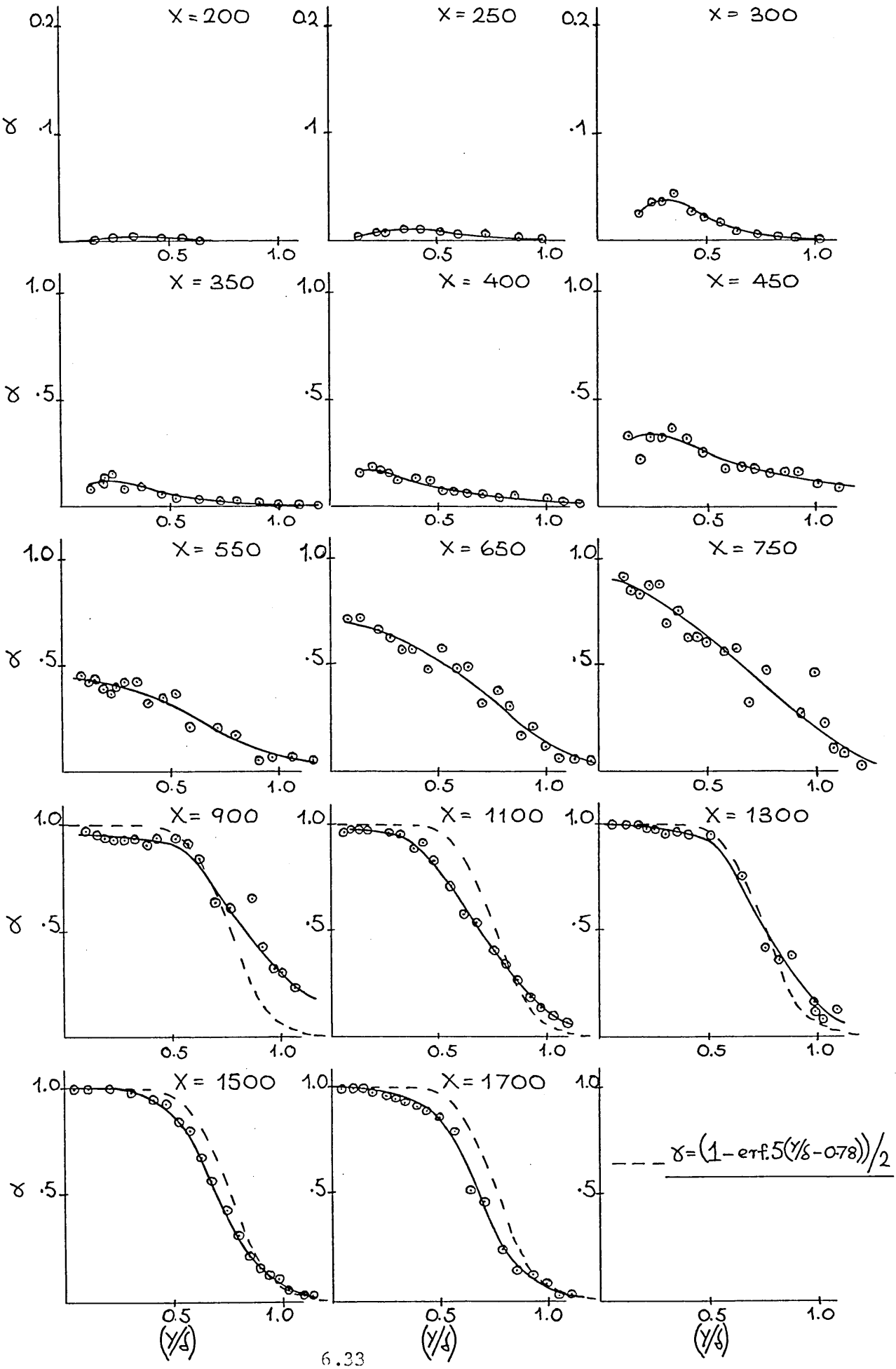

FLOW 1 — DEVELOPMENT OF INTERMITTENCY PROFILE ALONG Z = -50

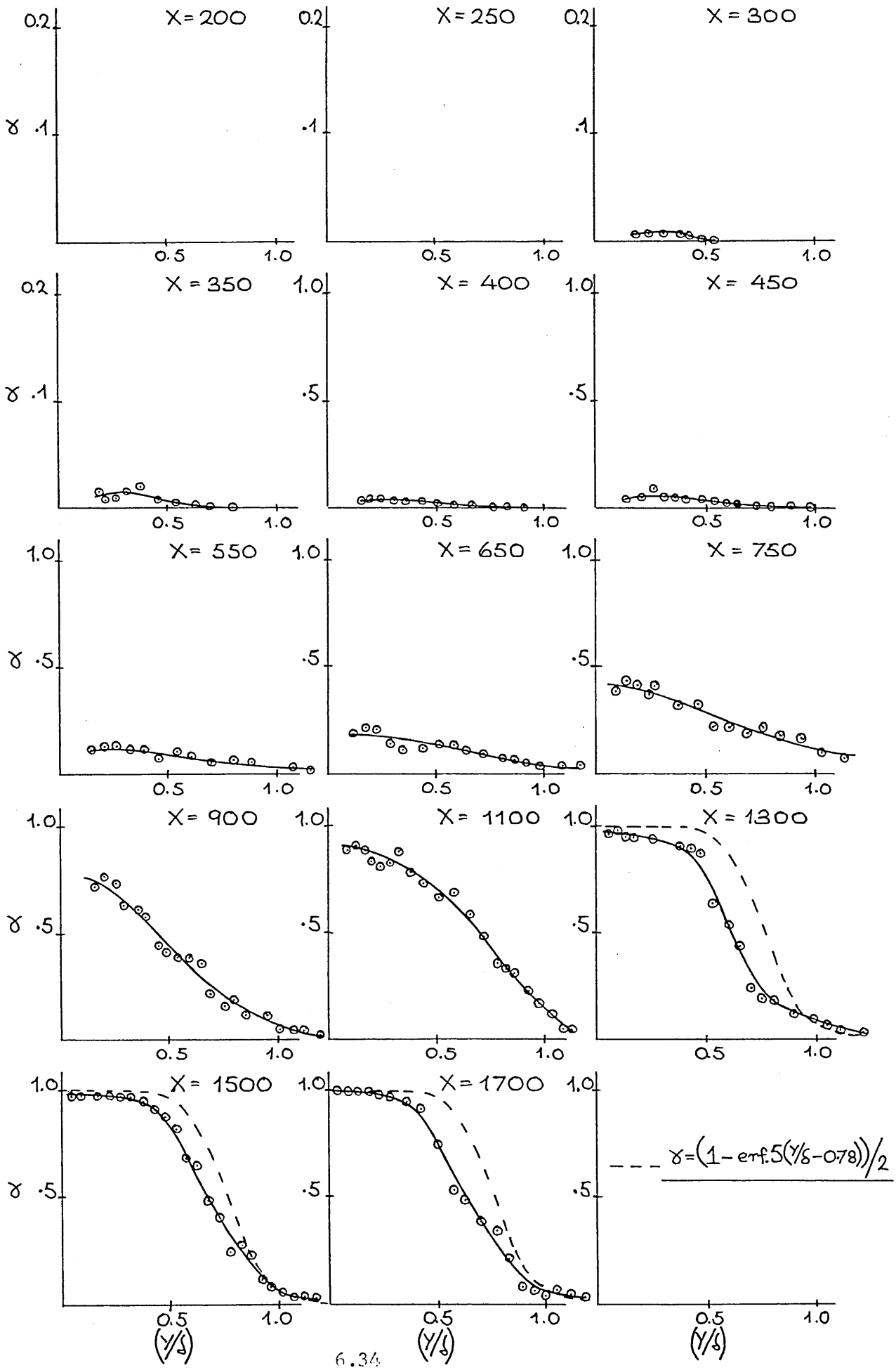

FLOW 1 — DEVELOPMENT OF INTERMITTENCY PROFILE ALONG Z = -100

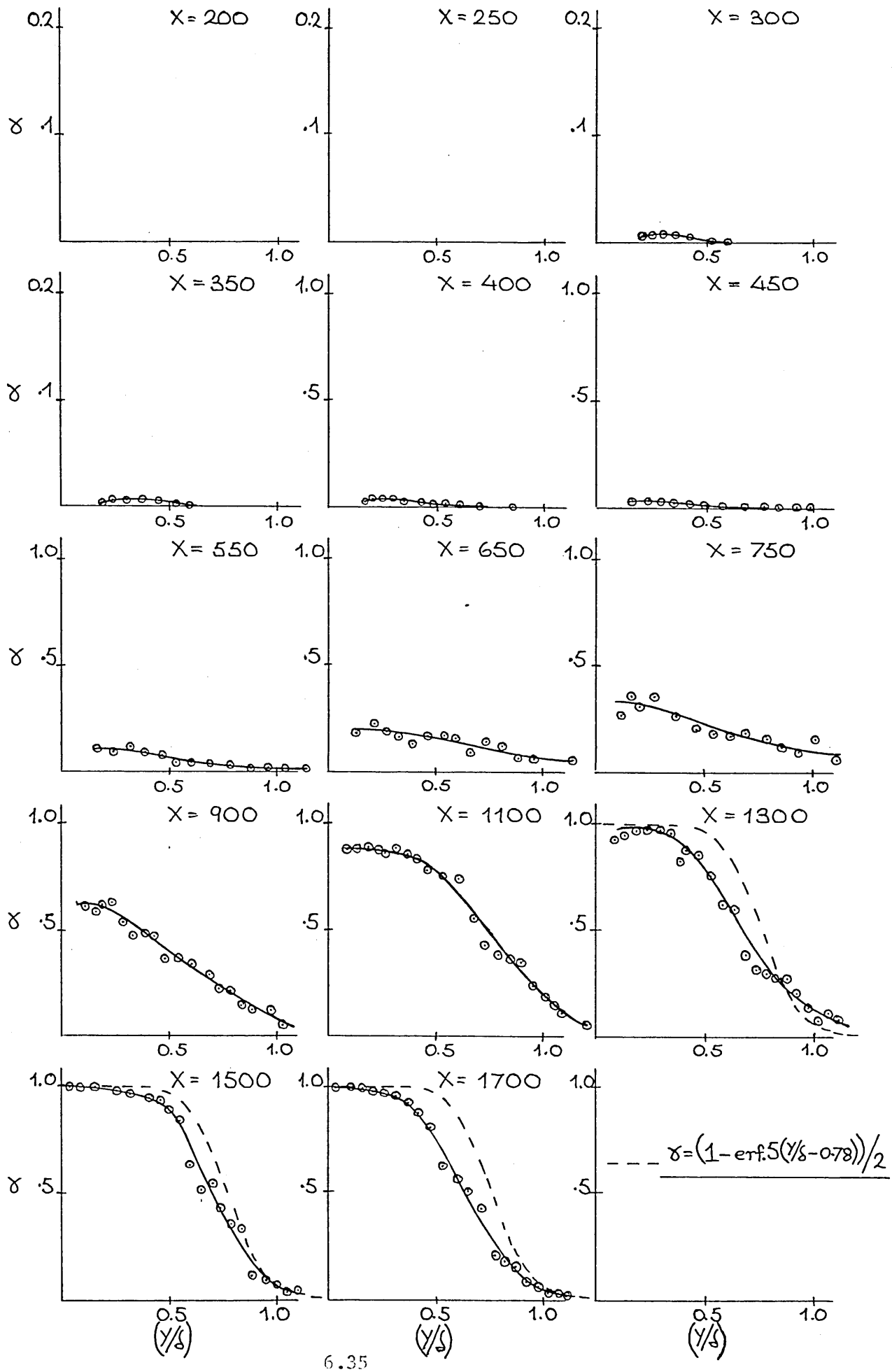

FLOW 1 - Secondary Data (Z = 145mm.)

Xmm	INTEGRAL PARAMETERS (mm.)				SHAPE FACTOR		SKIN FRICTION×1000			
	Delta	Displ	Mom	En	H12	H32	Cf.1	Cf.2	Cf.3	Cf.4
150	2.92	0.870	0.358	0.564	2.430	1.575	*****	1.864		
200	3.22	1.113	0.405	0.631	2.746	1.555	1.476	1.660		
250	3.73	1.274	0.471	0.734	2.707	1.560	1.312	1.458		
300	3.98	1.328	0.490	0.763	2.712	1.559	1.225	1.453		
350	3.79	1.471	0.543	0.848	2.709	1.562	1.142	1.378		
400	4.66	1.542	0.600	0.943	2.572	1.572	1.159	1.547		
450	4.96	1.644	0.675	1.072	2.436	1.589	1.134	1.921		
550	8.21	1.268	0.811	1.403	1.565	1.730	5.411	4.284		
650	9.48	1.598	1.060	1.855	1.507	1.750	4.958	4.615		
750	12.40	1.907	1.279	2.240	1.492	1.751	4.956	4.382	4.144	4.189
900	14.20	2.299	1.576	2.711	1.459	1.758	4.406	4.090	3.978	4.055
1100	19.10	3.153	2.185	3.839	1.443	1.757	3.914	3.662	3.689	3.682
1300	23.60	3.761	2.619	4.596	1.436	1.755	3.721	3.469	3.412	3.429
1500	28.51	4.495	3.135	5.494	1.434	1.752	3.501	3.259	3.255	3.314
1700	30.68	4.886	3.456	6.084	1.414	1.760	3.473	3.227	3.244	3.234

Xmm	Momentum Balance		Intermittency (mean value)	Rtheta	Wake Parameter	Wake Strength Parameter
	PL.	PR.	$\bar{\gamma}$	Re	∂G	$\Delta \bar{V} u_\sigma$
150	-	-	0.000	236	-	-
200	-	-	0.000	265	-	-
250	-	-	0.002	304	-	-
300	-	-	0.016	321	-	-
350	0.000	0.000	0.026	351	-	-
400	0.105	0.067	0.093	388	-	-
450	0.243	0.145	0.223	439	-	-
550	0.468	0.430	0.797	525	0.064	0.733
650	0.936	0.850	0.981	682	0.193	0.865
750	1.335	1.266	0.990	824	0.236	1.330
900	1.891	1.845	1.000	1022	0.267	1.231
1100	2.998	2.552	1.000	1440	0.407	1.887
1300	3.819	3.205	1.000	1705	0.439	2.164
1500	4.774	3.819	1.000	2042	0.506	2.535
1700	5.367	4.418	1.000	2246	0.492	2.305

Mean Entrainment Rate in Turbulent Region = F = 0.0175

Standard Deviation of Intermittency Distribution = $\bar{\nabla}$ = 75.27mm.

($X_{\bar{\gamma}=0.75}$ - $X_{\bar{\gamma}=0.25}$) = λ = 102mm.

$R_{\bar{\nabla}} = 4.893 \times 10^4$

$R_\lambda = 6.630 \times 10^4$

NB. Cf.1 - from velocity profile ie. average du/dy or Log-law
Cf.2 - equation
Cf.3 - by Preston tube 1.105mm. O.D.
Cf.4 - " " " 1.410mm. O.D.

FLOW 1 - Secondary Data (Z = 100mm.)

Xmm	INTEGRAL PARAMETERS (mm.)				SHAPE FACTOR		SKIN FRICTION×1000			
	Delta	Displ	Mom	En	H12	H32	Cf.1	Cf.2	Cf.3	Cf.4
150	2.97	0.988	0.350	0.537	2.827	1.537	*****	1.914		
200	3.05	1.025	0.399	0.627	2.568	1.571	1.713	1.692		
250	3.86	1.267	0.465	0.726	2.724	1.560	1.292	1.480		
300	3.65	1.326	0.505	0.790	2.625	1.565	1.309	1.393		
350	4.52	1.438	0.550	0.861	2.615	1.566	1.214	1.285		
400	4.85	1.498	0.570	0.897	2.628	1.573	1.133	1.368		
450	4.84	1.599	0.637	1.009	2.508	1.582	1.165	1.578		
550	7.50	1.204	0.788	1.382	1.527	1.754	5.498	3.156		
650	9.04	1.512	0.990	1.723	1.528	1.742	5.064	3.525		
750	11.72	1.734	1.162	2.041	1.492	1.756	4.779	4.193		
900	14.47	2.154	1.492	2.638	1.444	1.769	4.551	4.177	3.978	3.963
1100	20.19	2.879	2.005	3.534	1.436	1.763	4.082	3.779	3.825	3.776
1300	23.51	3.580	2.497	4.392	1.434	1.759	3.780	3.540	3.482	3.508
1500	26.11	4.067	2.859	5.036	1.423	1.762	3.636	3.409	3.308	3.393
1700	29.74	4.804	3.353	5.874	1.433	1.752	3.409	3.185	3.191	3.250

Xmm	Momentum Balance		Intermittency (mean value)	Rtheta	Wake Parameter	Wake Strength Parameter
	PL.	PR.	$\bar{\gamma}$	Re	∂G	$\Delta \bar{V} u_\sigma$
150	-	-	0.000	230	-	-
200	-	-	0.004	260	-	-
250	-	-	0.006	304	-	-
300	-	-	0.008	325	-	-
350	0.000	0.000	0.010	356	-	-
400	0.036	0.060	0.037	368	-	-
450	0.158	0.124	0.114	406	-	-
550	0.433	0.230	0.523	512	0.072	0.446
650	0.800	0.720	0.691	637	0.168	0.942
750	1.113	1.089	0.911	749	0.172	1.068
900	1.713	1.648	0.988	971	0.178	0.761
1100	2.646	2.375	0.990	1308	0.278	1.541
1300	3.540	3.036	1.000	1620	0.401	1.885
1500	4.198	3.656	1.000	1861	0.449	2.103
1700	5.096	4.253	1.000	2185	0.557	2.616

Mean Entrainment Rate in Turbulent Region = F = 0.0164

Standard Deviation of Intermittency Distribution = $\bar{\nabla}$ = 123.07mm.

($X_{\bar{\gamma}=0.75}$ - $X_{\bar{\gamma}=0.25}$) = λ = 157mm.

$R_{\bar{\nabla}} = 8.00 \times 10^4$

$R_\lambda = 1.0205 \times 10^5$

NB. Cf.1 - from velocity profile ie. average du/dy or Log-law
Cf.2 - equation
Cf.3 - by Preston tube 1.105mm. O.D.
Cf.4 - " " " 1.410mm. O.D.

FIG 1.33

FLOW 1 - Secondary Data (Z = 50mm.)

	INTEGRAL PARAMETERS (mm.)				SHAPE FACTOR		SKIN FRICTION×1000			
Xmm	Delta	Displ	Mom	En	H12	H32	Cf.1	Cf.2	Cf.3	Cf.4
150	2.95	0.964	0.357	0.556	2.697	1.557	*****	1.872		
200	3.12	1.042	0.393	0.613	2.651	1.559	1.649	1.723		
250	3.59	1.239	0.475	0.746	2.606	1.568	1.324	1.479		
300	4.10	1.315	0.510	0.802	2.579	1.573	1.291	1.677		
350	5.95	1.365	0.606	0.978	2.254	1.618	1.517	2.411		
400	6.70	1.415	0.638	1.035	2.219	1.623	1.660	2.686		
450	5.48	1.456	0.700	1.153	2.079	1.646	1.525	3.312		
550	8.43	1.380	0.900	1.569	1.533	1.743	5.216	4.172		
650	11.06	1.503	1.003	1.763	1.498	1.757	5.059	4.462		
750	13.63	1.718	1.149	2.014	1.495	1.753	4.798	4.418		
900	13.98	2.086	1.421	2.498	1.468	1.758	4.533	4.167	3.842	3.916
1100	17.91	2.653	1.841	3.247	1.441	1.764	4.202	3.898	3.808	3.760
1300	21.05	3.281	2.271	3.981	1.445	1.754	3.890	3.625	3.550	3.572
1500	25.92	3.804	2.728	4.844	1.394	1.776	3.864	3.574	3.395	3.456
1700	30.89	4.400	3.114	5.488	1.413	1.762	3.612	3.347	3.226	3.345

Xmm	Momentum Balance		Intermittency (mean value)	Rtheta	Wake Parameter	Wake Strength Parameter
	PL.	PR.	$\bar{\gamma}$	Rθ	$\mathcal{G}$	$\Delta U/U_\tau$
150	-	-	0.002	235	-	-
200	-	-	0.005	255	-	-
250	0.000	0.000	0.012	311	-	-
300	0.074	0.081	0.065	327	-	-
350	0.256	0.188	0.280	392	-	-
400	0.343	0.322	0.366	415	-	-
450	0.474	0.480	0.546	452	-	-
550	0.895	0.878	0.809	580	0.135	0.766
650	1.112	1.336	0.920	652	0.065	0.673
750	1.419	1.805	0.965	742	0.086	0.933
900	1.992	2.484	0.980	923	0.206	1.062
1100	2.876	3.319	1.000	1193	0.269	1.288
1300	3.781	4.089	1.000	1474	0.382	2.175
1500	4.743	4.825	1.000	1774	0.294	1.374
1700	5.556	5.532	1.000	2027	0.383	1.998

Mean Entrainment Rate in Turbulent Region = F = 0.0144

Standard Deviation of Intermittency Distribution = ∇ = 117.4mm.

$(X_{\bar{\gamma}=0.75} - X_{\bar{\gamma}=0.25}) = \lambda$ = 165mm.

$R_\nabla = 7.631 \times 10^4$

$R_\lambda = 1.0725 \times 10^5$

NB. Cf.1 - from velocity profile ie. average du/dy or Log-law
Cf.2 - equation
Cf.3 - by Preston tube 1.105mm. O.D.
Cf.4 - " " " 1.410mm. O.D.

FLOW 1 - Secondary Data (Z = 0mm.)

	INTEGRAL PARAMETERS (mm.)				SHAPE FACTOR		SKIN FRICTION×1000			
Xmm	Delta	Displ	Mom	En	H12	H32	Cf.1	Cf.2	Cf.3	Cf.4
150	2.79	0.946	0.338	0.509	2.799	1.506	*****	1.975		
200	3.12	0.980	0.401	0.629	2.443	1.568	2.093	1.686		
250	3.53	1.211	0.455	0.712	2.665	1.567	1.363	1.522		
300	4.01	1.262	0.501	0.788	2.519	1.575	1.337	1.528		
350	5.17	1.332	0.534	0.841	2.494	1.574	1.269	1.901		
400	5.14	1.452	0.572	0.900	2.537	1.573	1.274	1.952		
450	5.09	1.500	0.640	1.022	2.344	1.579	1.394	2.439		
550	8.43	1.580	0.749	1.237	2.109	1.652	1.401	2.606		
650	8.96	1.269	0.836	1.468	1.518	1.756	5.389	3.886		
750	11.00	1.364	0.917	1.621	1.487	1.768	5.307	4.299		
900	11.67	1.758	1.185	2.082	1.484	1.756	4.781	4.374	3.774	3.994
1100	17.03	2.301	1.569	2.757	1.466	1.757	4.336	4.028	3.825	3.932
1300	17.64	2.598	1.779	3.119	1.460	1.753	4.174	3.913	3.666	3.785
1500	21.59	3.116	2.165	3.809	1.440	1.759	3.939	3.694	3.464	3.456
1700	21.56	3.560	2.514	4.436	1.416	1.765	3.585	3.592	3.298	3.329

Xmm	Momentum Balance		Intermittency (mean value)	Rtheta	Wake Parameter	Wake Strength Parameter
	PL.	PR.	$\bar{\gamma}$	Rθ	$\mathcal{G}$	$\Delta U/U_\tau$
150	-	-	0.000	223	-	-
200	-	-	0.004	261	-	-
250	0.000	0.000	0.009	299	-	-
300	0.101	0.082	0.034	326	-	-
350	0.174	0.176	0.131	350	-	-
400	0.257	0.282	0.167	373	-	-
450	0.407	0.402	0.317	416	-	-
550	0.646	0.679	0.418	486	-	-
650	0.837	1.035	0.710	541	0.029	0.537
750	1.015	1.490	0.840	597	-0.042	0.553
900	1.604	2.211	0.965	770	0.169	1.048
1100	2.448	3.121	0.980	1012	0.218	1.557
1300	2.910	3.945	1.000	1159	0.331	1.806
1500	3.758	4.725	1.000	1416	0.333	1.802
1700	4.525	5.465	1.000	1634	0.348	1.690

Mean Entrainment Rate in Turbulent Region = F = 0.0107

Standard Deviation of Intermittency Distribution = ∇ = 158.4mm.

$(X_{\bar{\gamma}=0.75} - X_{\bar{\gamma}=0.25}) = \lambda$ = 230mm.

$R_\nabla = 1.0296 \times 10^5$

$R_\lambda = 1.4950 \times 10^5$

NB. Cf.1 - from velocity profile ie. average du/dy or Loglaw
Cf.2 - equation
Cf.3 - by Preston tube 1.105mm. O.D.
Cf.4 - " " " 1.410mm. O.D.

FIG 1.34

FLOW 1 - Secondary Data (Z = -50mm.)

	INTEGRAL PARAMETERS (mm.)				SHAPE FACTOR		SKIN FRICTION×1000			
Xmm	Delta	Displ	Mom	En	H12	H32	Cf.1	Cf.2	Cf.3	Cf.4
150	2.89	0.894	0.362	0.569	2.469	1.573	*****	1.846		
200	2.82	1.004	0.379	0.593	2.653	1.567	1.638	1.785		
250	3.42	1.128	0.419	0.657	2.696	1.571	1.415	1.616		
300	3.93	1.284	0.488	0.768	2.633	1.574	1.285	1.413		
350	4.22	1.261	0.488	0.768	2.587	1.575	1.312	1.456		
400	4.74	1.367	0.523	0.819	2.616	1.566	1.299	1.475		
450	4.91	1.419	0.534	0.834	2.659	1.563	1.140	1.536		
550	5.08	1.526	0.625	0.991	2.442	1.586	1.179	1.637		
650	6.45	1.699	0.719	1.149	2.362	1.598	1.194	1.732		
750	8.05	1.572	0.754	1.246	2.086	1.654	1.683	2.529		
900	12.17	1.577	1.040	1.819	1.516	1.749	4.827	3.540		
1100	13.81	1.959	1.331	2.342	1.472	1.760	4.592	3.930	3.637	3.729
1300	17.93	2.339	1.625	2.875	1.439	1.769	4.422	4.042	3.789	3.963
1500	20.35	2.887	2.009	3.541	1.437	1.763	4.088	3.777	3.671	3.800
1700	22.66	3.028	2.150	3.814	1.409	1.774	4.146	3.815	3.492	3.722

Xmm	Momentum Balance		Intermittency (mean value)	Rtheta	Wake Parameter	Wake Strength Parameter
	PL.	PR.	$\overline{\gamma}$	Rθ	$\mathcal{G}$	$\Delta U_\sigma / U_\sigma$
150	-	-	0.000	238	-	-
200	-	-	0.000	247	-	-
250	-	-	0.002	274	-	-
300	-	-	0.005	317	-	-
350	0.000	0.000	0.014	316	-	-
400	0.072	0.075	0.037	341	-	-
450	0.094	0.152	0.052	343	-	-
550	0.281	0.315	0.126	405	-	-
650	0.473	0.485	0.200	469	-	-
750	0.545	0.701	0.403	492	-	-
900	1.131	1.172	0.717	680	0.122	1.032
1100	1.728	1.951	0.893	864	0.181	1.064
1300	2.330	2.754	0.980	1051	0.143	1.067
1500	3.117	3.534	0.990	1307	0.272	1.525
1700	3.406	4.286	1.000	1397	0.183	1.188

Mean Entrainment Rate in Turbulent Region = F = 0.0117

Standard Deviation of Intermittency Distribution = ∇ = 208mm.

$(X_{\overline{\gamma}=0.75} - X_{\overline{\gamma}=0.25}) = \lambda$ = 300mm.

$R_\nabla = 1.3520 \times 10^5$

$R_\lambda = 1.9500 \times 10^5$

NB. Cf.1 - from velocity profile ie. average du/dy or Loglaw
Cf.2 - equation
Cf.3 - by Preston tube 1.105mm. O.D.
Cf.4 - " " " 1.410mm. O.D.

FLOW 1 - Secondary Data (Z = -100mm.)

	INTEGRAL PARAMETERS (mm.)				SHAPE FACTOR		SKIN FRICTION×1000			
Xmm	Delta	Displ	Mom	En	H12	H32	Cf.1	Cf.2	Cf.3	Cf.4
150	3.13	0.976	0.360	0.555	2.710	1.543	*****	1.858		
200	3.13	1.104	0.387	0.602	2.851	1.556	1.425	1.752		
250	3.44	1.179	0.428	0.667	2.752	1.557	1.303	1.579		
300	3.71	1.319	0.465	0.723	2.834	1.553	1.226	1.488		
350	4.07	1.357	0.500	0.776	2.714	1.552	1.293	1.391		
400	4.56	1.437	0.538	0.840	2.672	1.562	1.201	1.405		
450	4.77	1.534	0.536	0.835	2.861	1.556	1.022	1.426		
550	4.66	1.436	0.580	0.919	2.475	1.583	1.233	1.646		
650	5.81	1.703	0.687	1.094	2.479	1.593	1.139	1.830		
750	7.15	1.654	0.755	1.232	2.190	1.631	1.267	2.156		
900	10.20	1.376	0.898	1.565	1.533	1.743	5.240	3.345		
1100	12.54	1.912	1.297	2.281	1.474	1.759	4.671	3.928	3.876	3.869
1300	16.82	2.465	1.696	2.986	1.454	1.761	4.263	3.911	3.755	3.838
1500	20.86	2.866	2.017	3.560	1.431	1.765	4.099	3.822	3.602	3.722
1700	24.75	3.351	2.394	4.253	1.400	1.777	4.020	3.712	3.333	3.644

Xmm	Momentum Balance		Intermittency (mean value)	Rtheta	Wake Parameter	Wake Strength Parameter
	PL.	PR.	$\overline{\gamma}$	Rθ	$\mathcal{G}$	$\Delta U_\sigma / U_\sigma$
150	-	-	0.000	237	-	-
200	-	-	0.000	251	-	-
250	-	-	0.002	281	-	-
300	-	-	0.004	300	-	-
350	0.000	0.000	0.005	322	-	-
400	0.076	0.070	0.030	349	-	-
450	0.072	0.140	0.032	345	-	-
550	0.160	0.293	0.102	375	-	-
650	0.374	0.466	0.206	442	-	-
750	0.510	0.663	0.314	488	-	-
900	0.796	1.073	0.613	580	0.070	0.888
1100	1.594	1.816	0.882	840	0.190	0.948
1300	2.392	2.595	0.974	1102	0.263	1.366
1500	3.034	3.342	1.000	1316	0.250	1.448
1700	3.788	4.058	1.000	1554	0.217	1.208

Mean Entrainment Rate in Turbulent Region = F = 0.0164

Standard Deviation of Intermittency Distribution = ∇ = 216.6mm.

$(X_{\overline{\gamma}=0.75} - X_{\overline{\gamma}=0.25}) = \lambda$ = 302mm.

$R_\nabla = 1.4080 \times 10^5$

$R_\lambda = 1.9630 \times 10^5$

NB. Cf.1 - from velocity profile ie. average du/dy or Log-law
Cf.2 - equation
Cf.3 - by Preston tube 1.105mm. O.D.
Cf.4 - " " " 1.410mm. O.D.

FIG 1.35

FLOW 1 — STREAMWISE DEVELOPMENT OF INTEGRAL PARAMETERS ALONG Z = +145

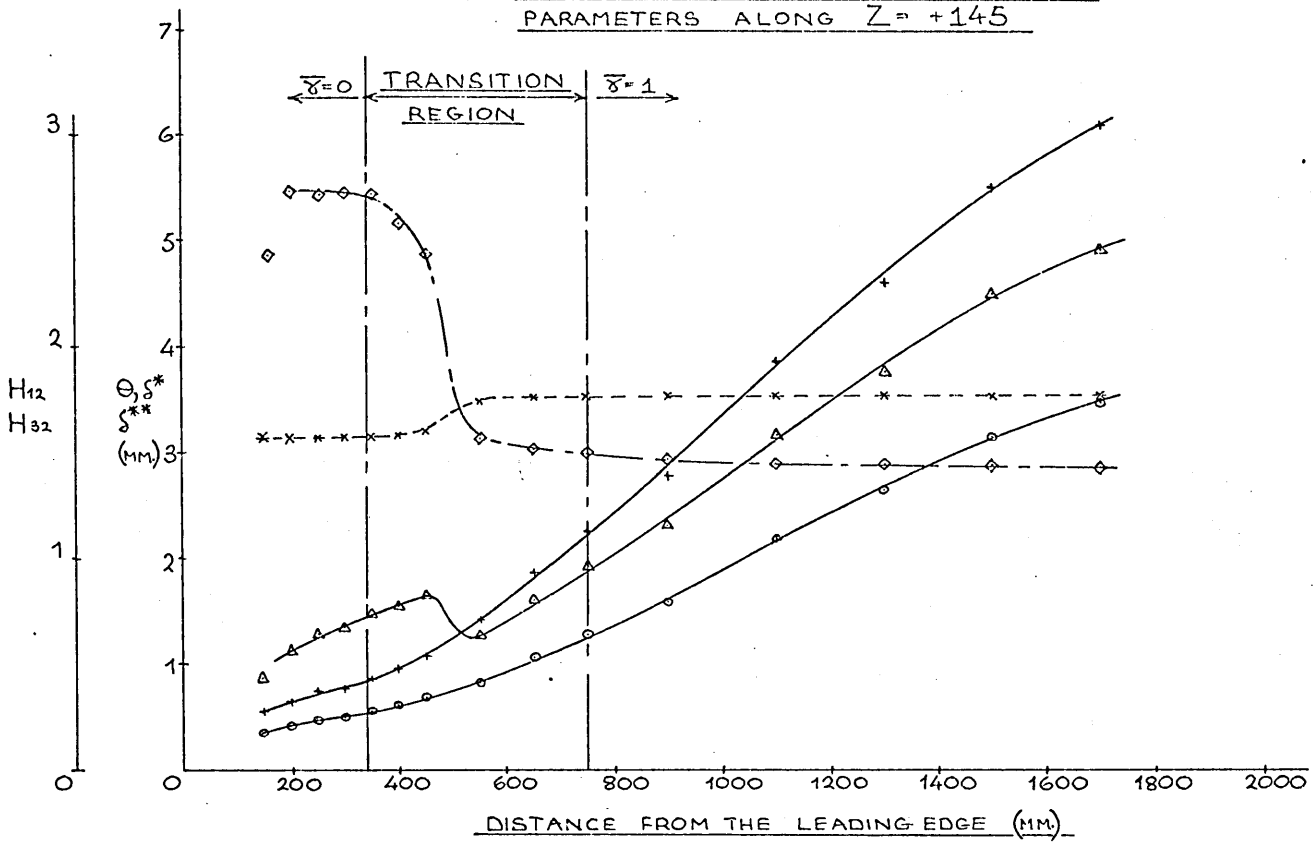

FIG.

FLOW 1 — VARIATION OF SKIN FRICTION CO-EFFICIENT ALONG Z = +145

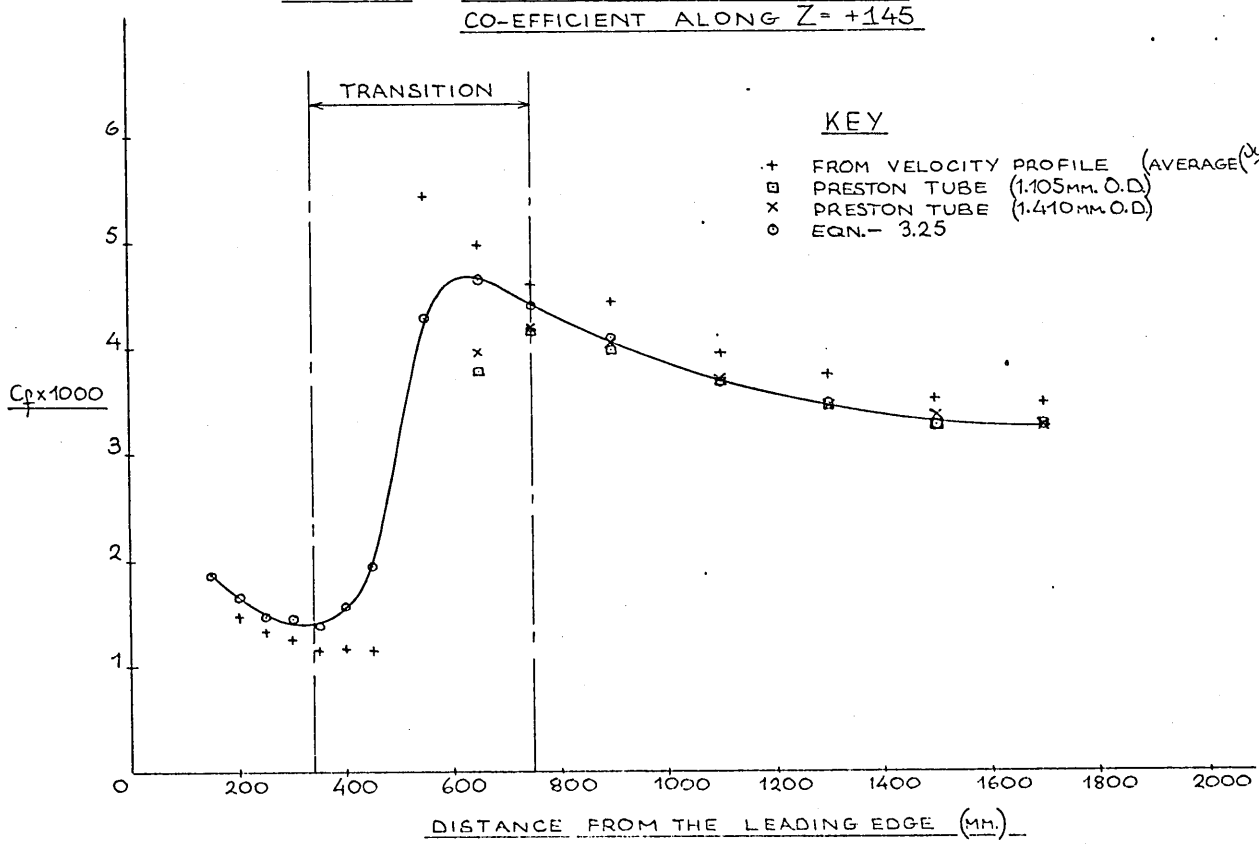

FIG.

FLOW 1 — STREAMWISE DEVELOPMENT OF INTEGRAL PARAMETERS ALONG Z = +100

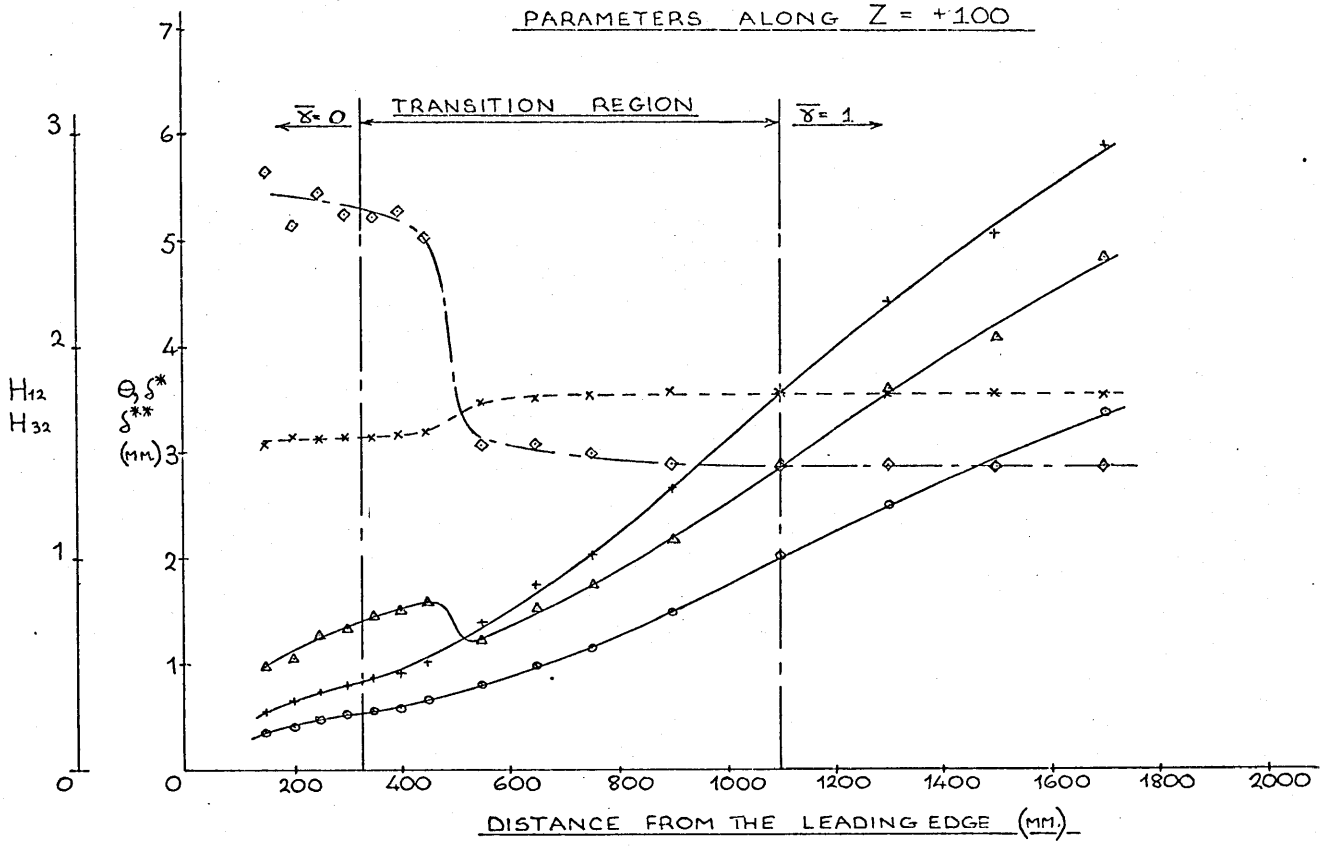

FIG.

FLOW 1 — VARIATION OF SKIN FRICTION CO-EFFICIENT ALONG Z = +100

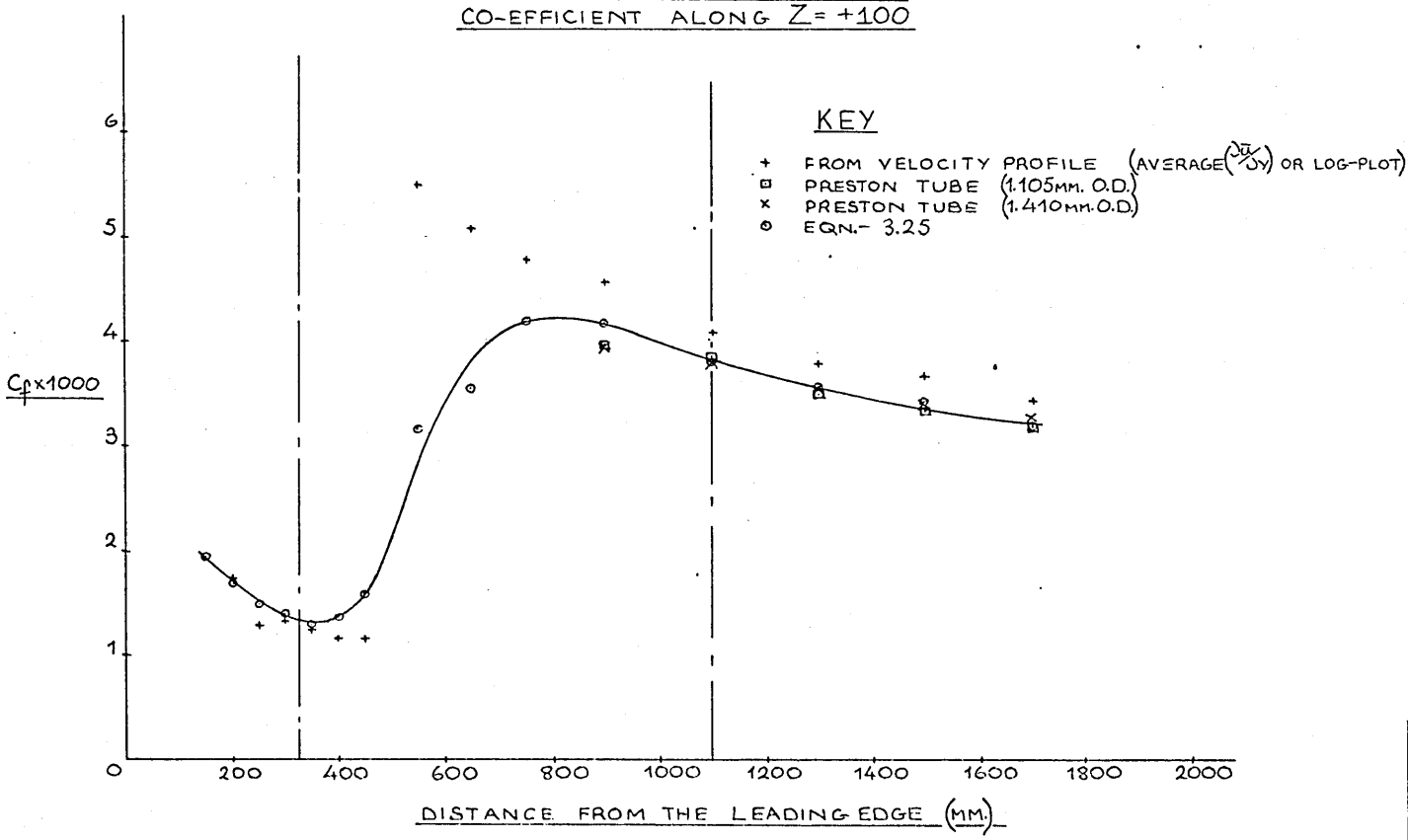

FIG.

FLOW 1 — STREAMWISE DEVELOPMENT OF INTEGRAL PARAMETERS ALONG Z = +50

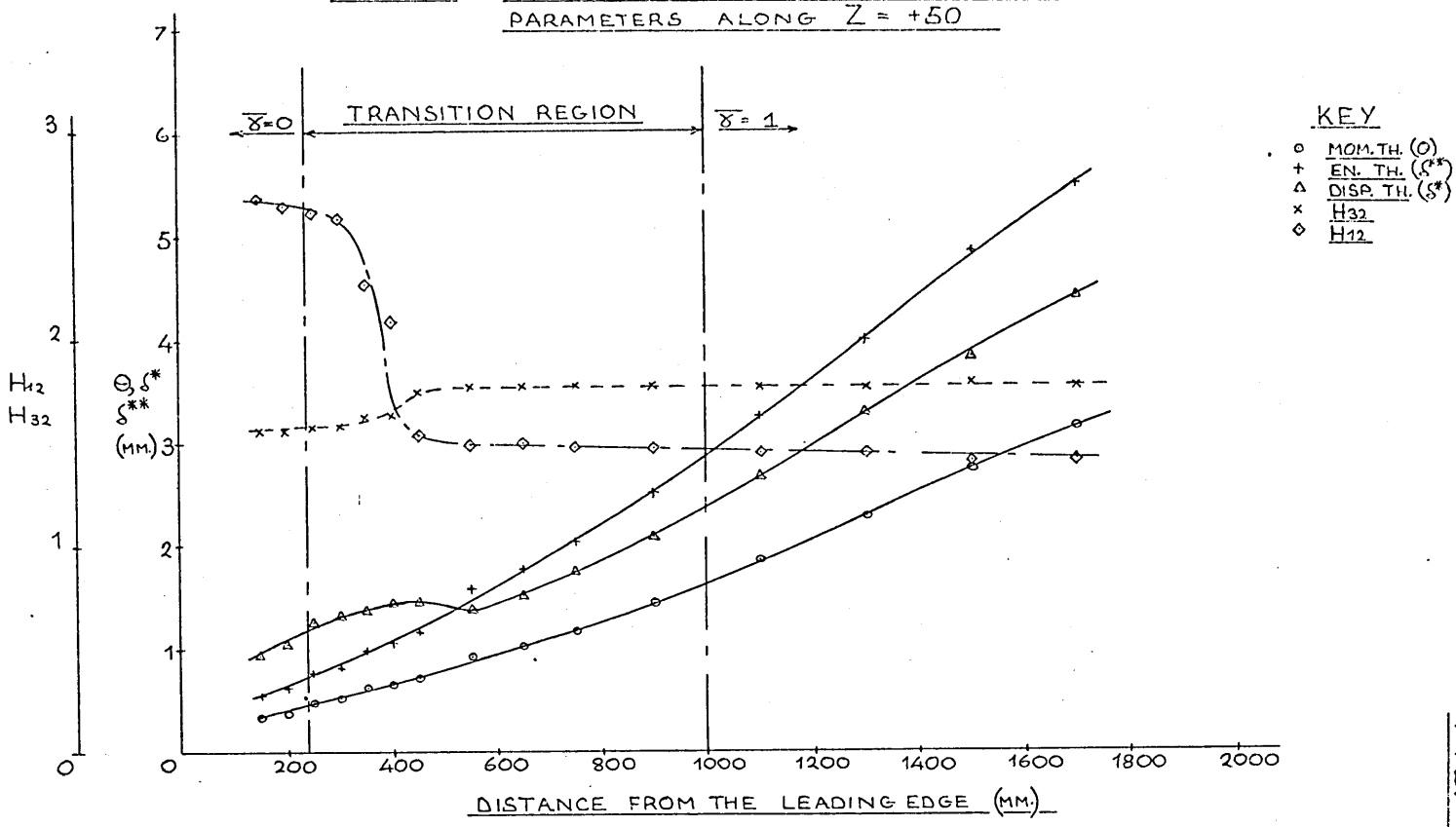

FIG.

FLOW 1 — VARIATION OF SKIN FRICTION CO-EFFICIENT ALONG Z = +50

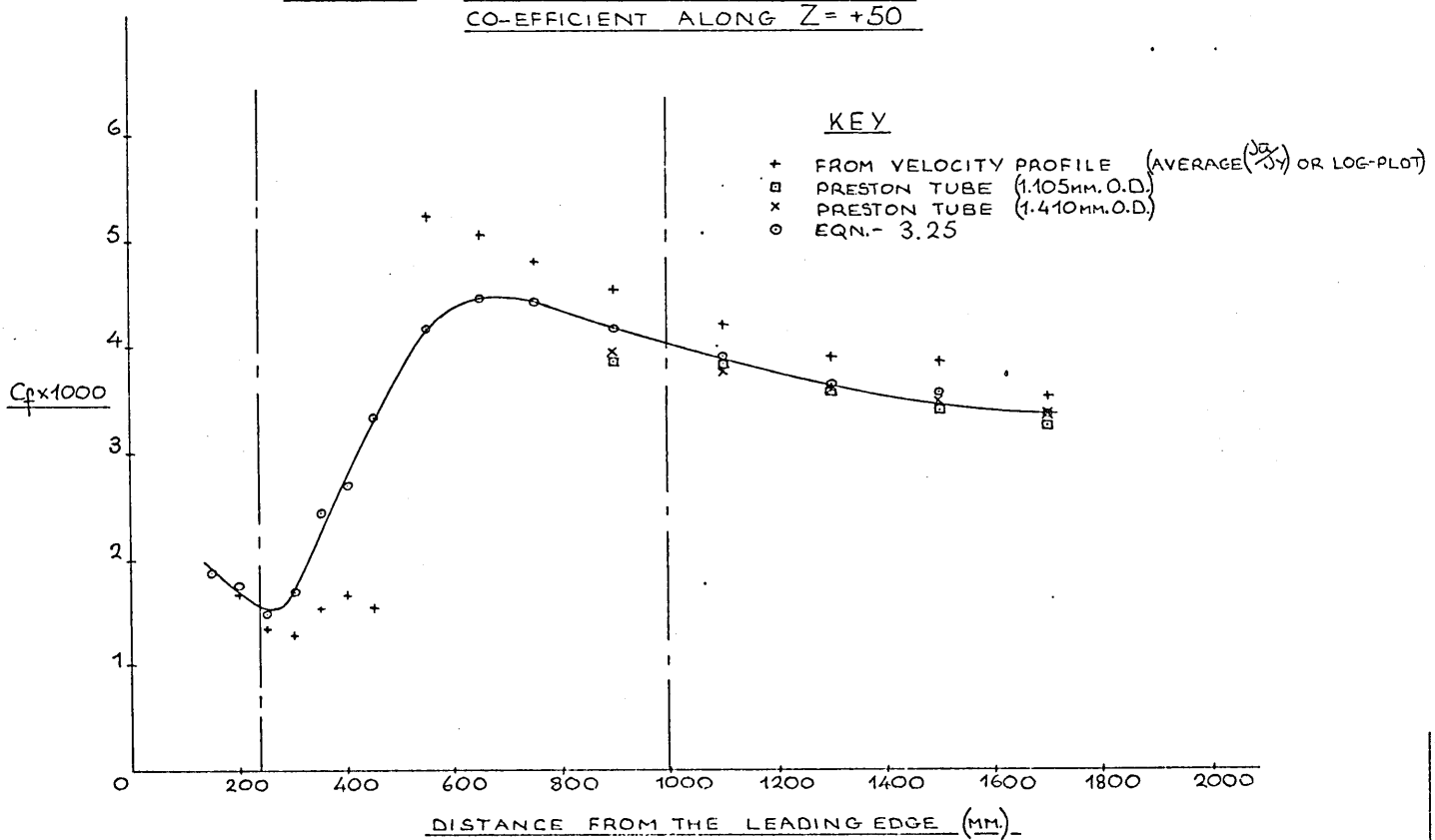

FIG.

FLOW 1 — STREAMWISE DEVELOPMENT OF INTEGRAL PARAMETERS ALONG Z = 0

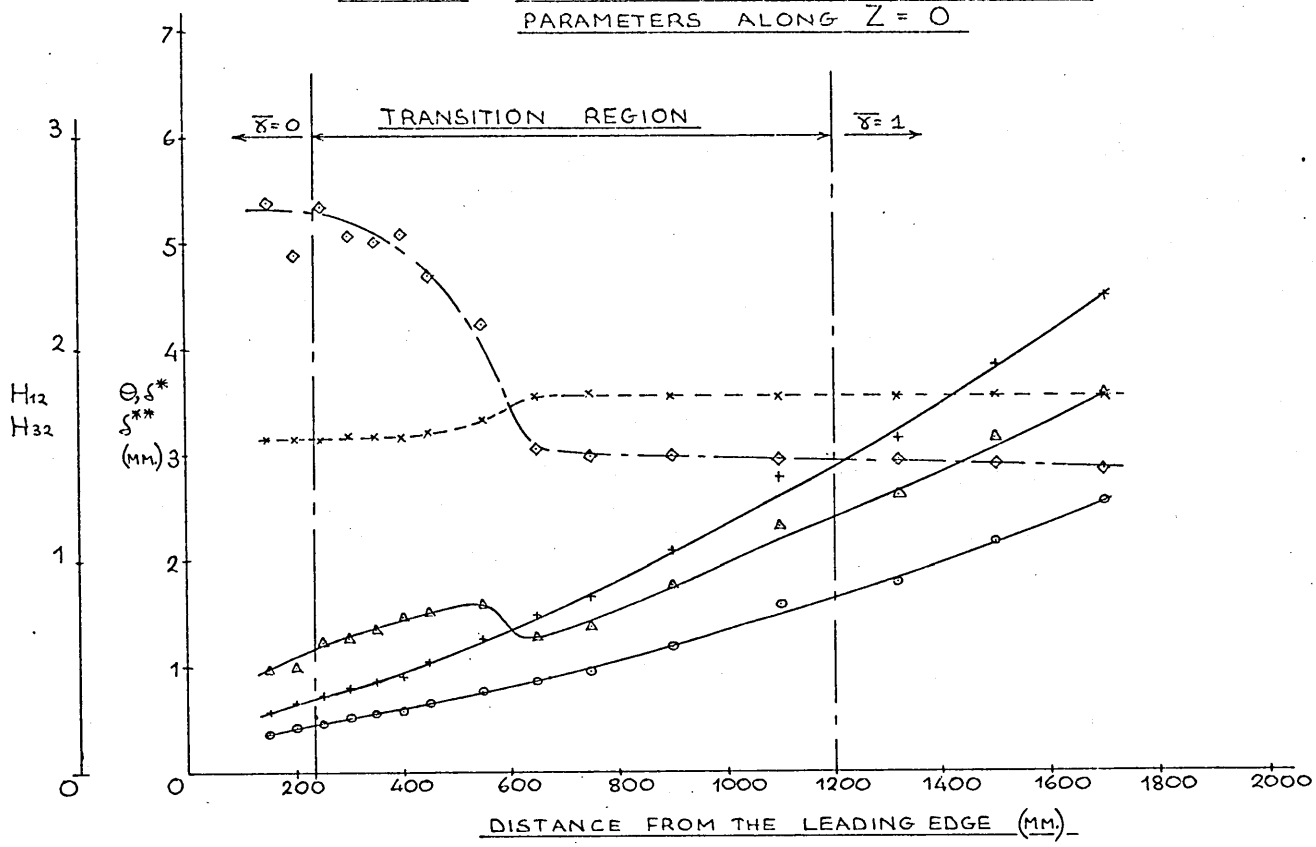

FIG.

FLOW 1 — VARIATION OF SKIN FRICTION CO-EFFICIENT ALONG Z = 0

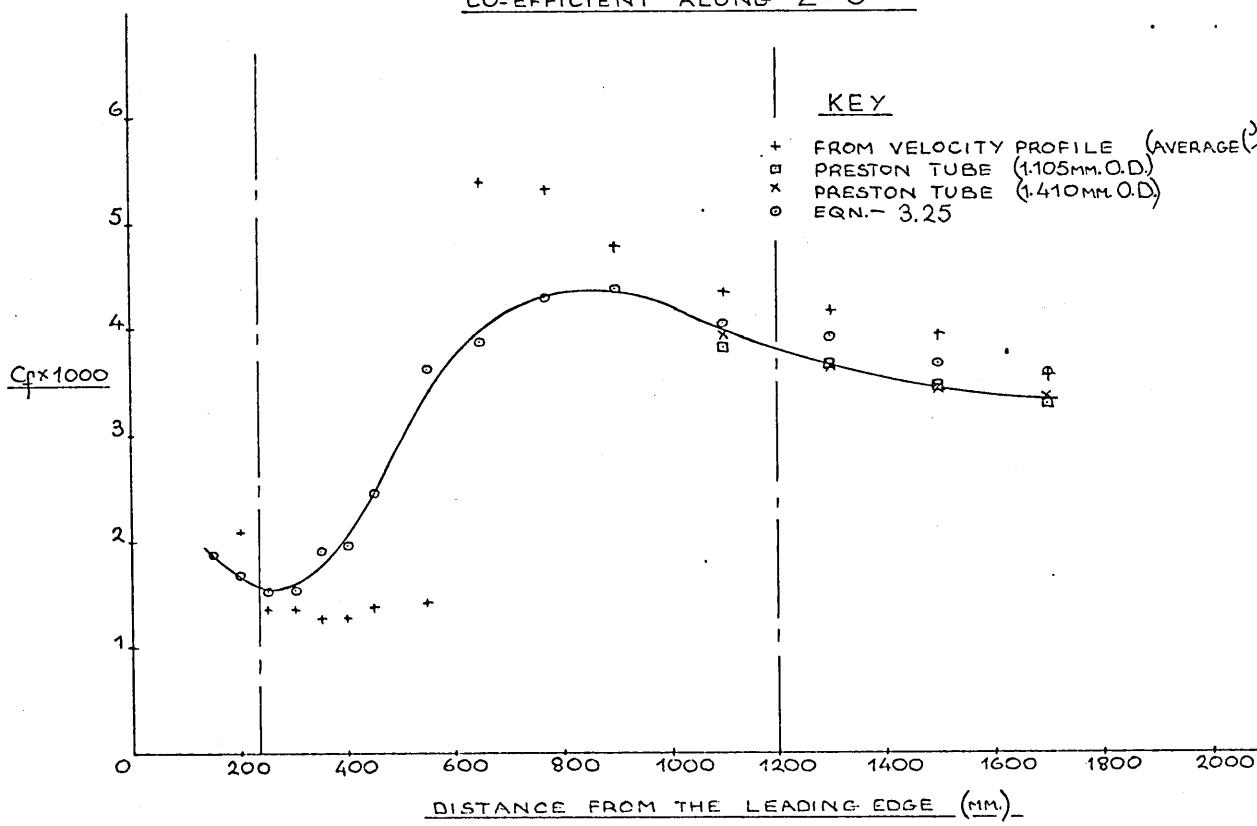

FIG.

FLOW 1 — STREAMWISE DEVELOPMENT OF INTEGRAL PARAMETERS ALONG Z = -50

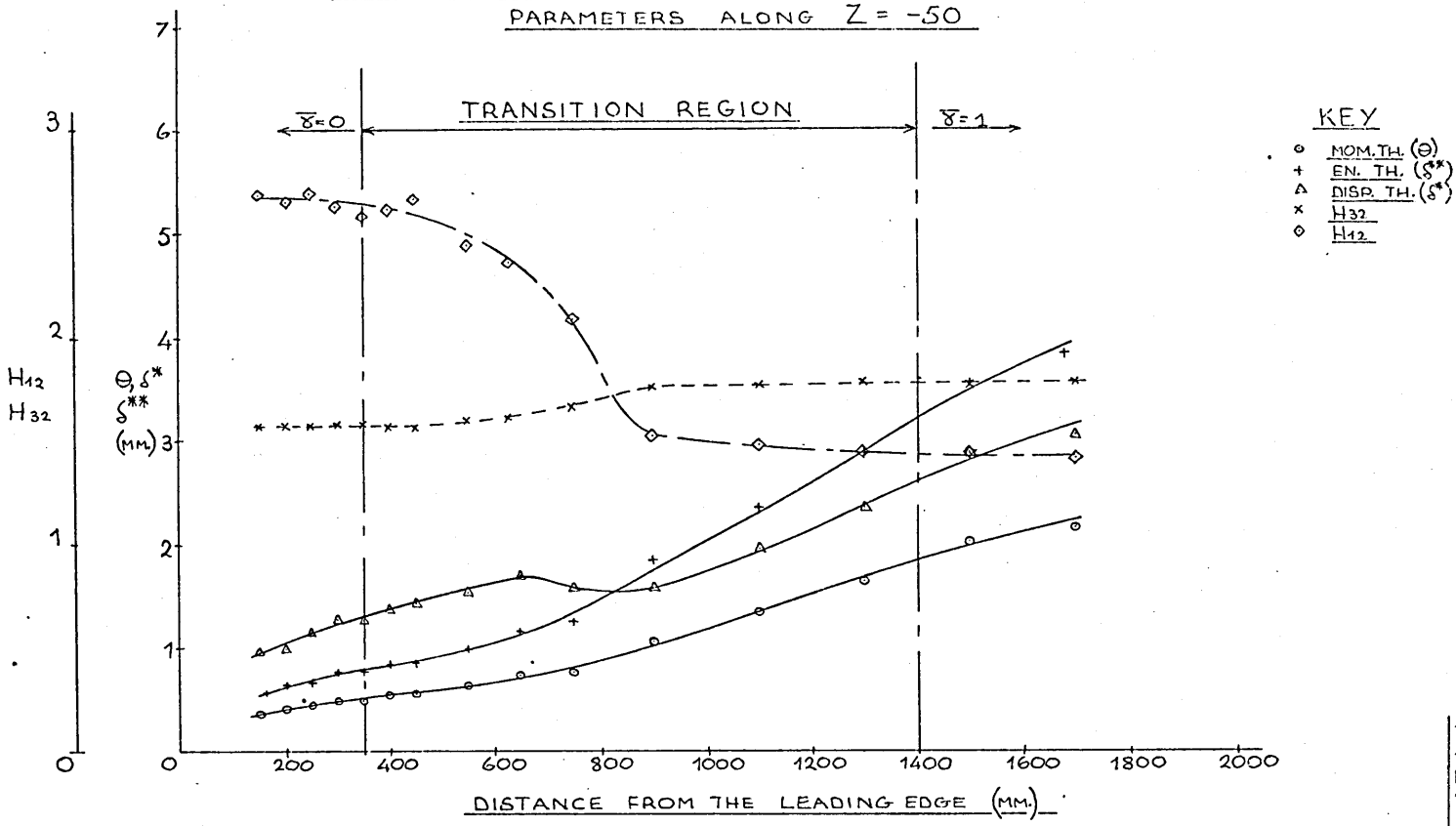

FIG.

FLOW 1 — VARIATION OF SKIN FRICTION CO-EFFICIENT ALONG Z = -50

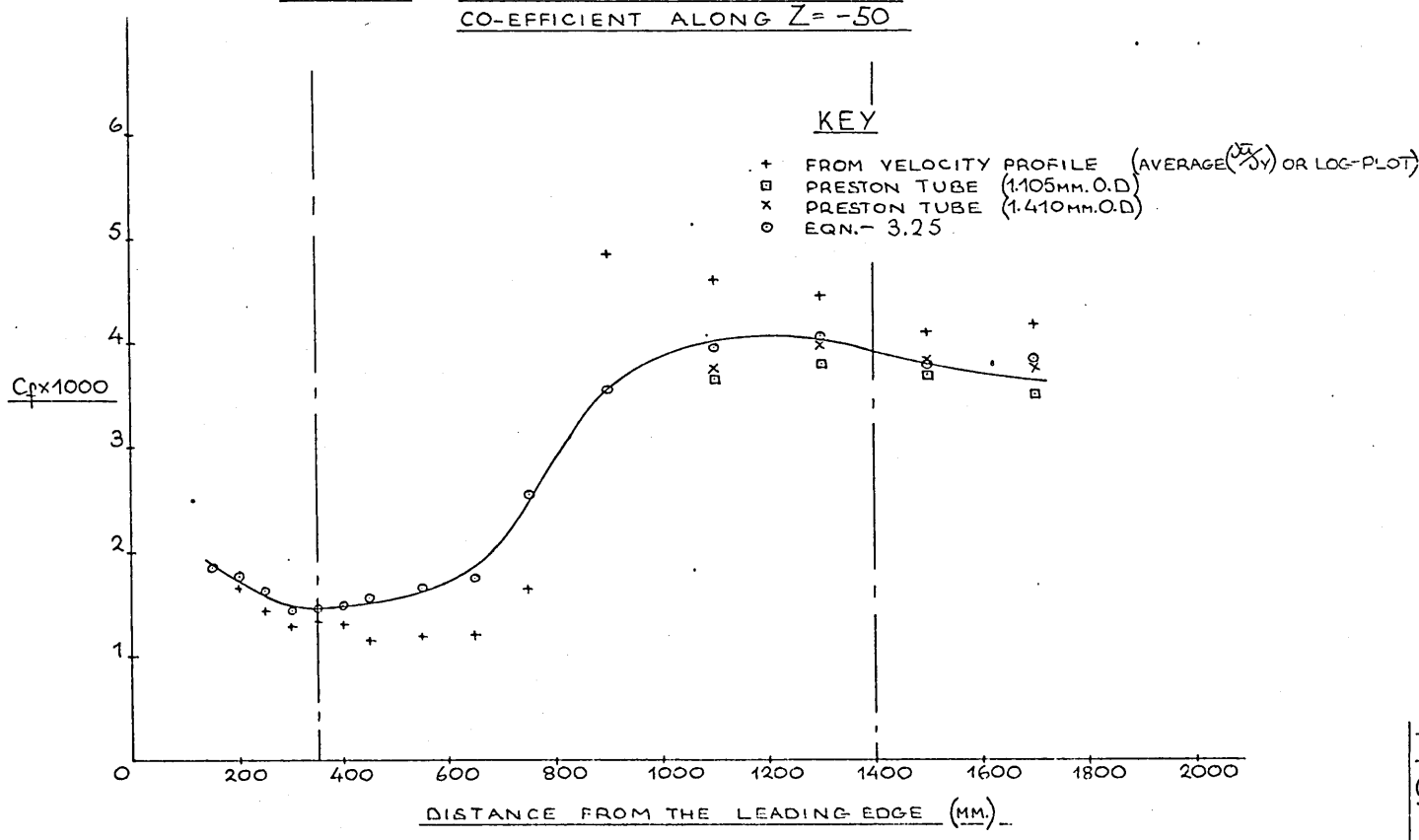

FIG.

FLOW 1 — STREAMWISE DEVELOPMENT OF INTEGRAL PARAMETERS ALONG Z = -100

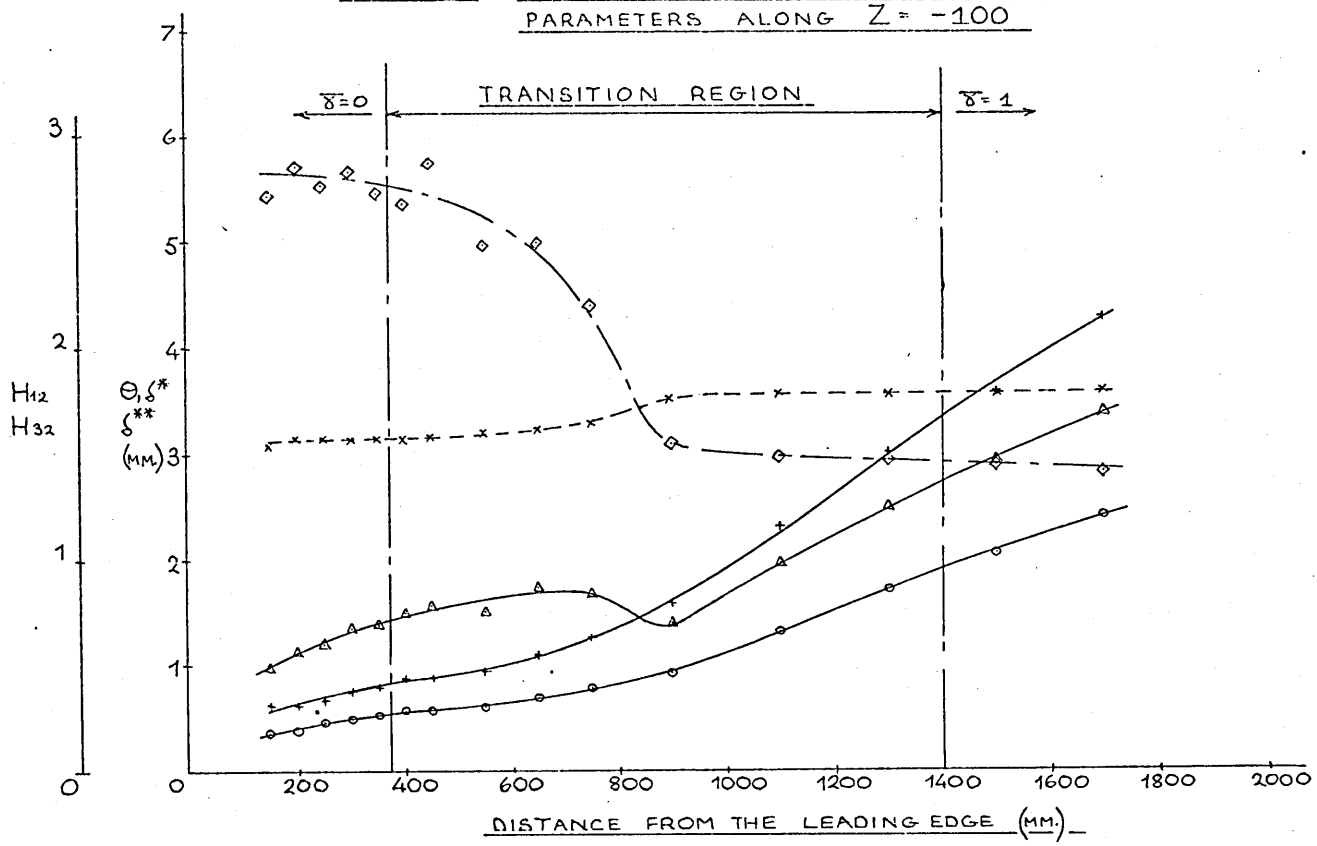

FIG.

FLOW 1 — VARIATION OF SKIN FRICTION CO-EFFICIENT ALONG Z = -100

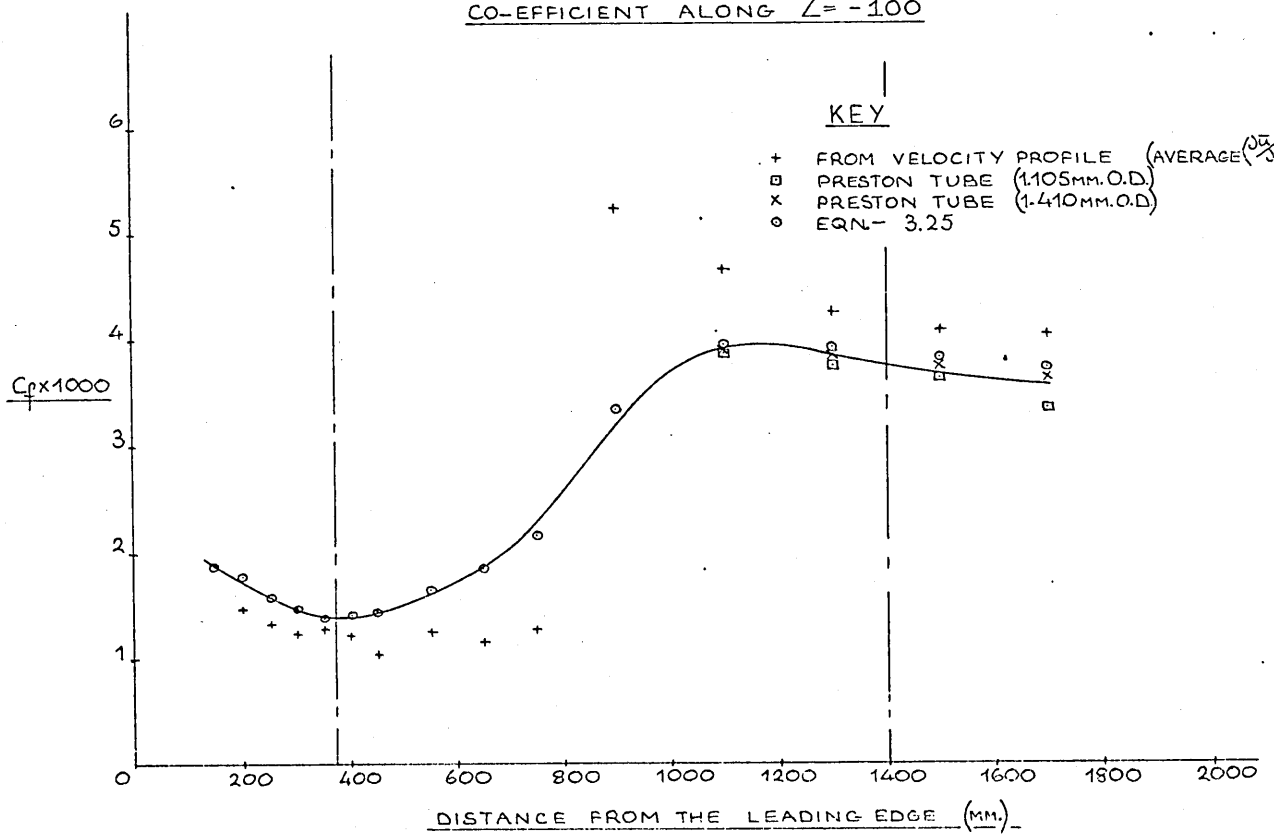

FIG.

FLOW 1 — ENTRAINMENT RATE ALONG Z = +145

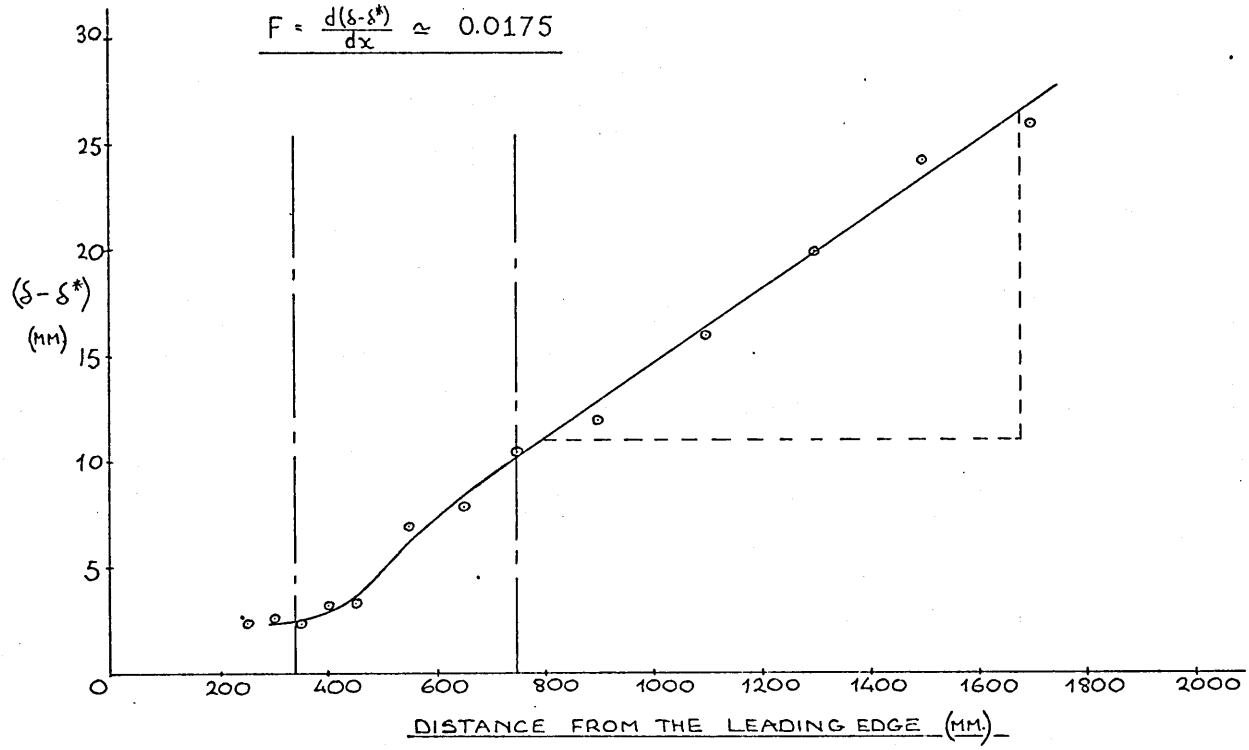

FIG.

FLOW 1 — ENTRAINMENT RATE ALONG Z = +100

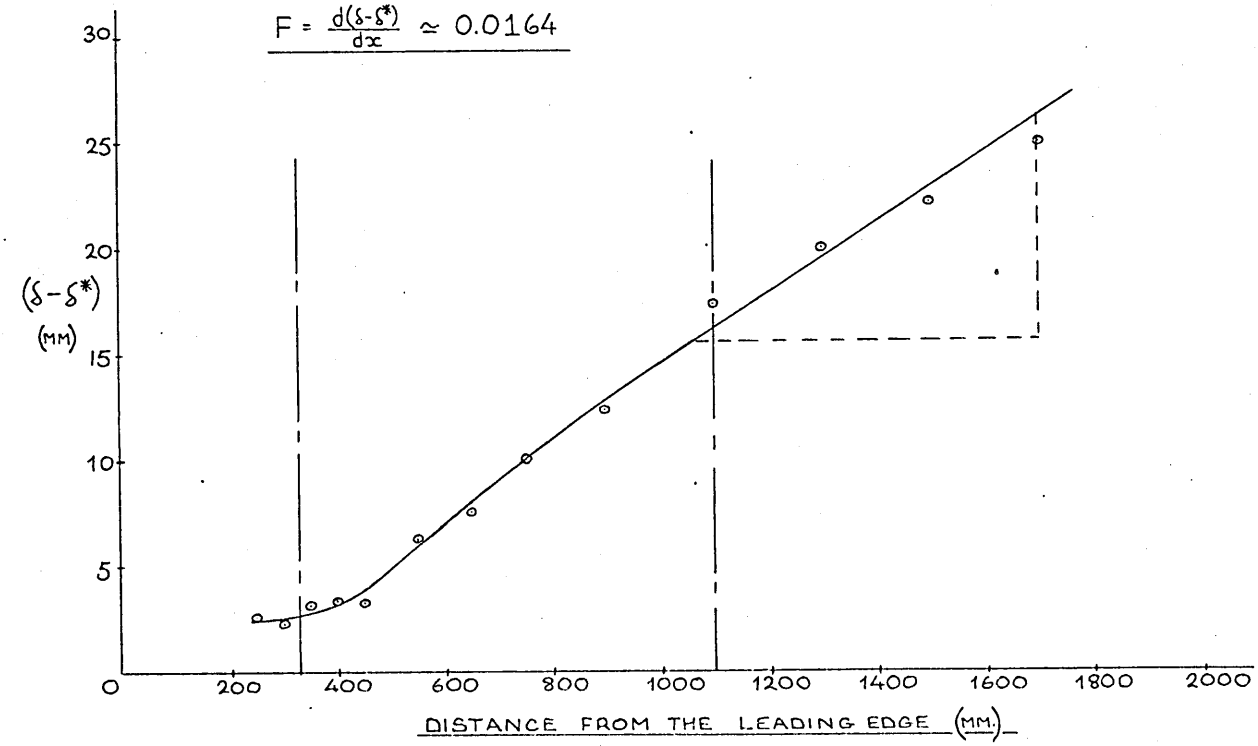

FIG.

FLOW 1 — ENTRAINMENT RATE ALONG Z = +50

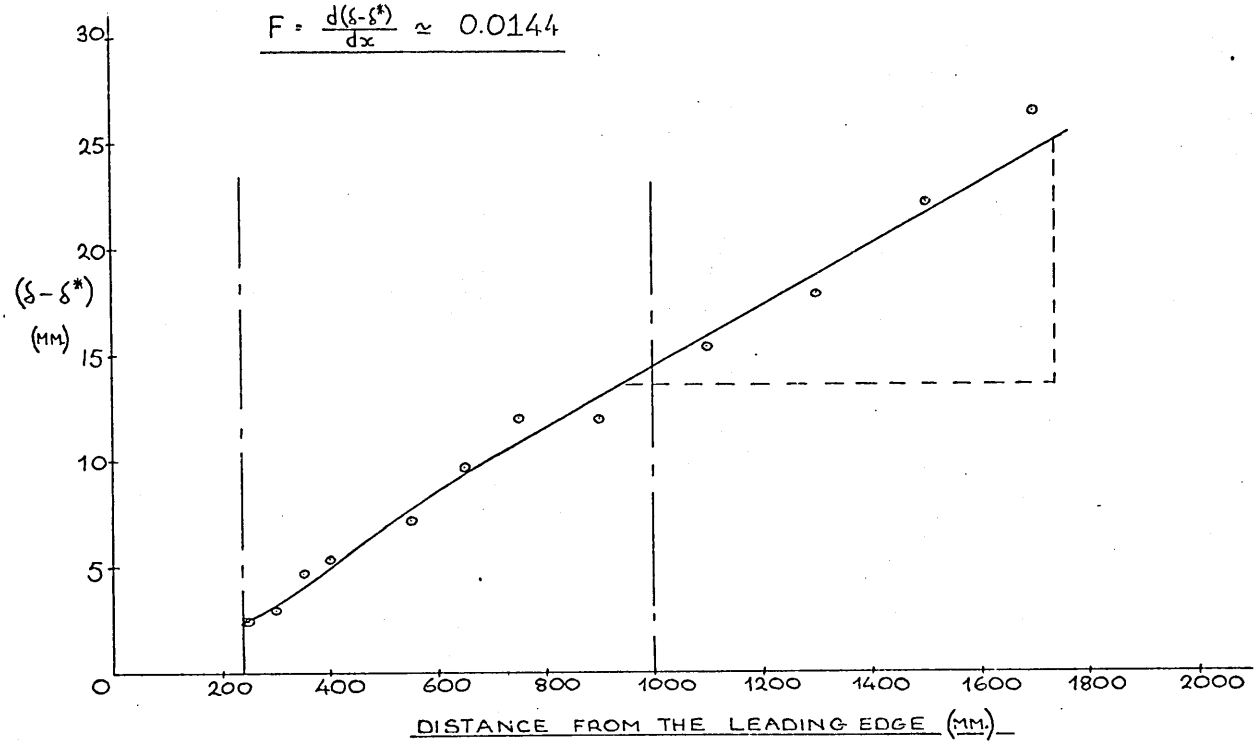

FIG.

FLOW 1 — ENTRAINMENT RATE ALONG Z = 0

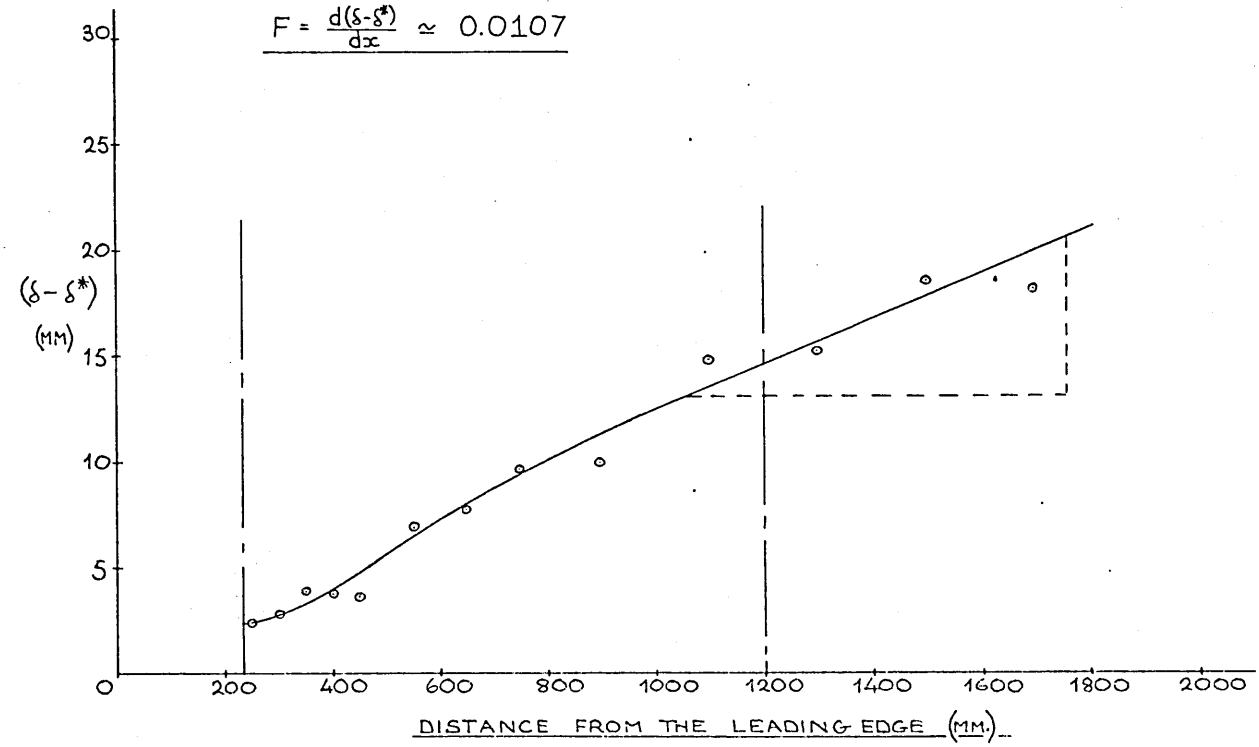

FIG.

FLOW 1 — ENTRAINMENT RATE ALONG Z = -50

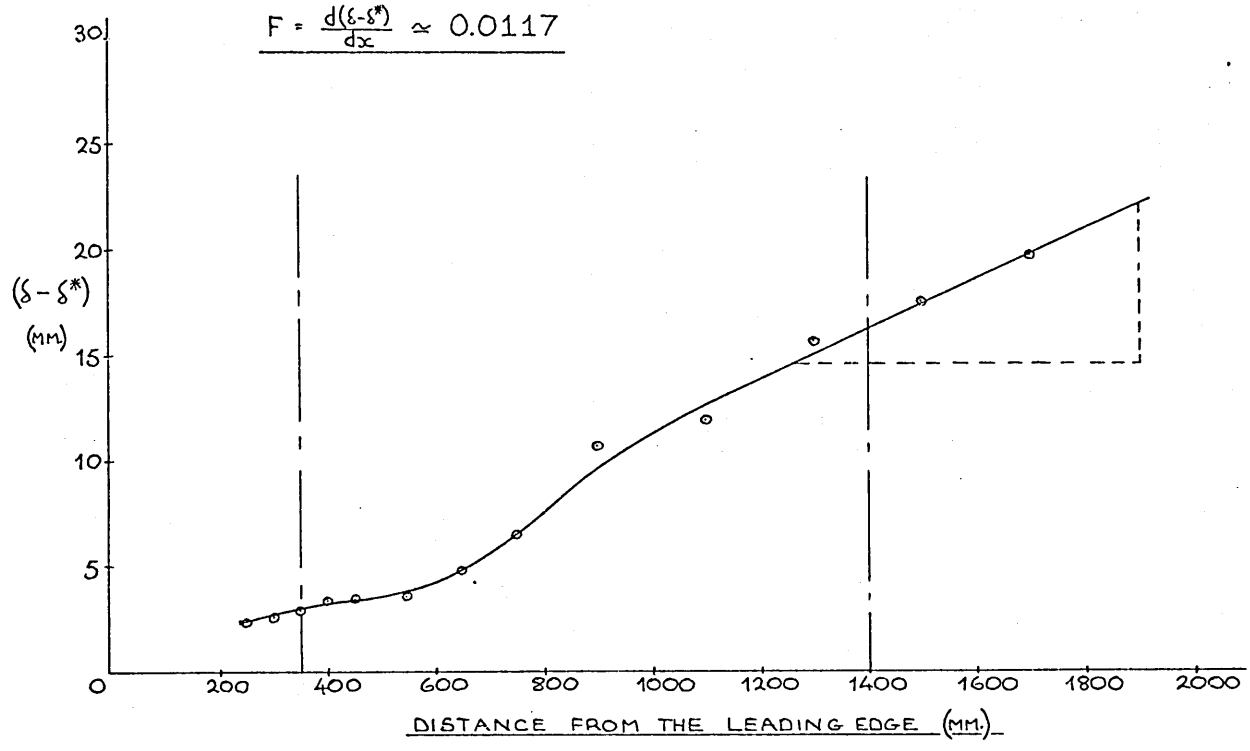

FIG.

FLOW 1 — ENTRAINMENT RATE ALONG Z = -100

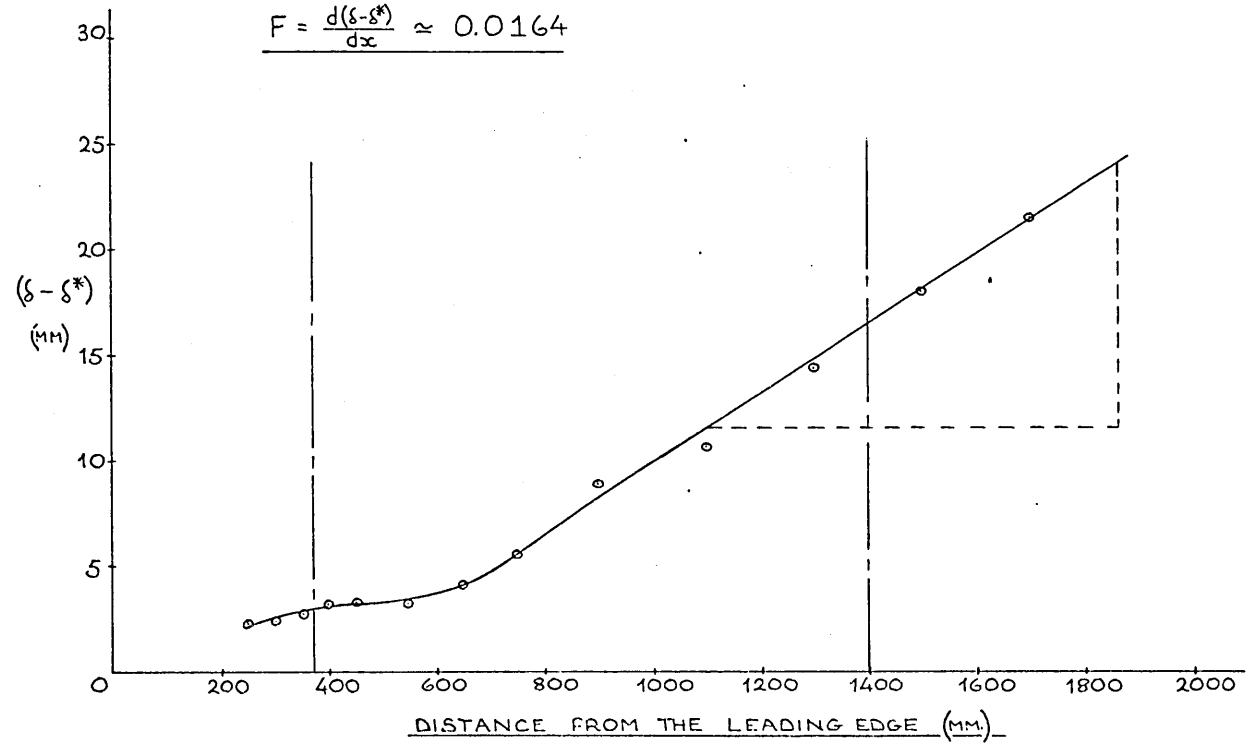

FIG.

STREAMWISE DEVELOPMENT OF "NEAR" WALL INTERMITTENCY

FLOW 1 — Z = +145

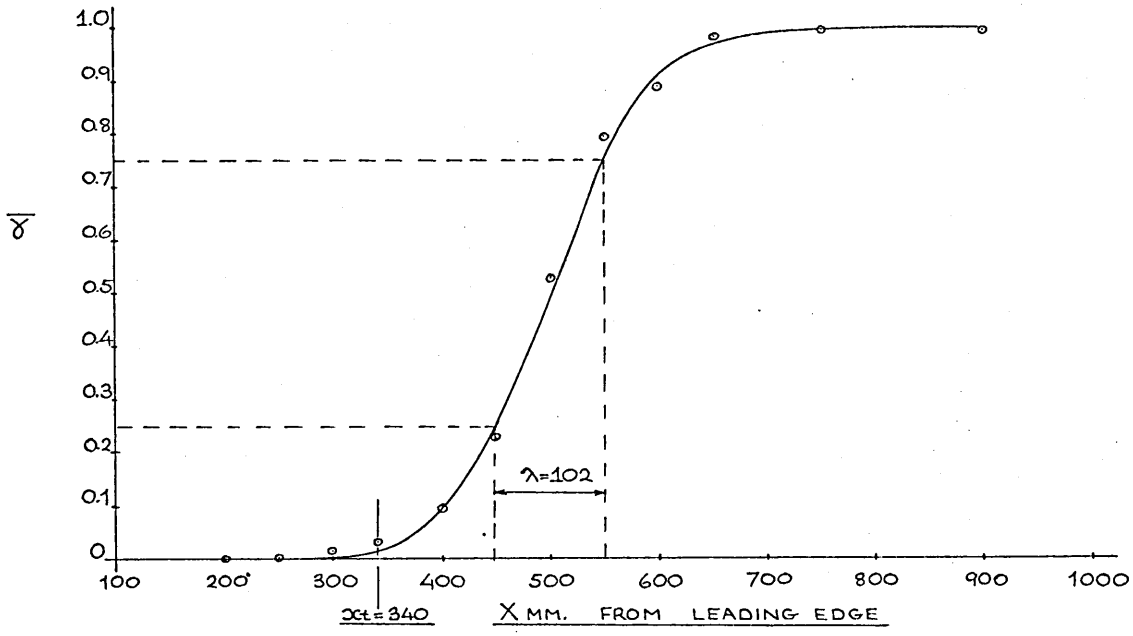

FIG.

STREAMWISE DEVELOPMENT OF "NEAR" WALL INTERMITTENCY

FLOW 1 — Z = +100

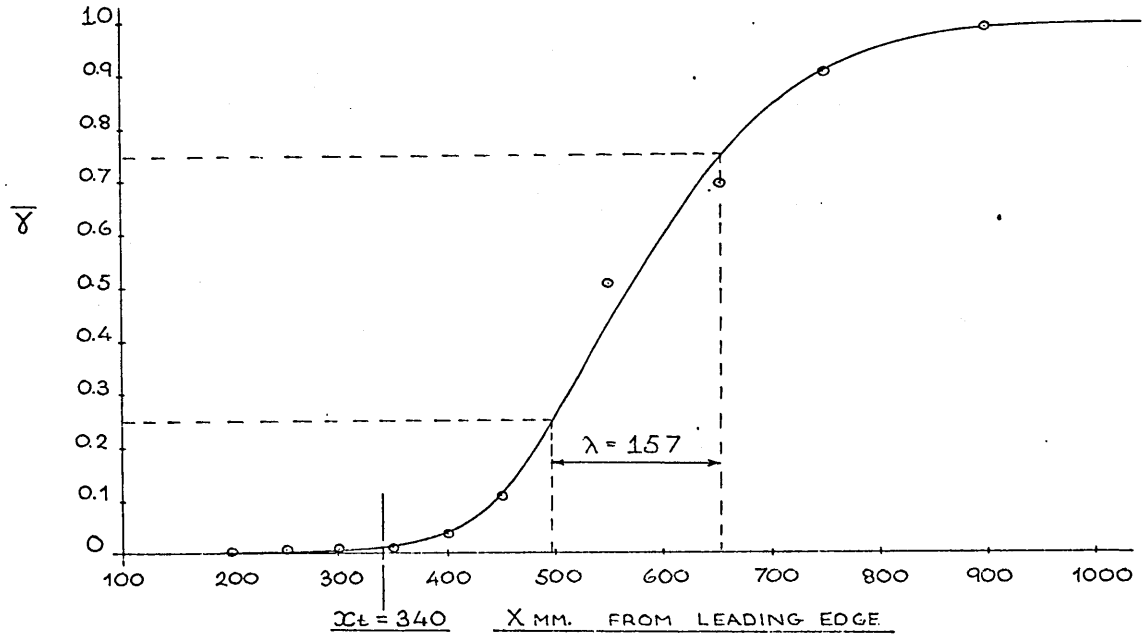

FIG.

STREAMWISE DEVELOPMENT OF "NEAR" WALL INTERMITTENCY

FLOW 1 — Z = +50

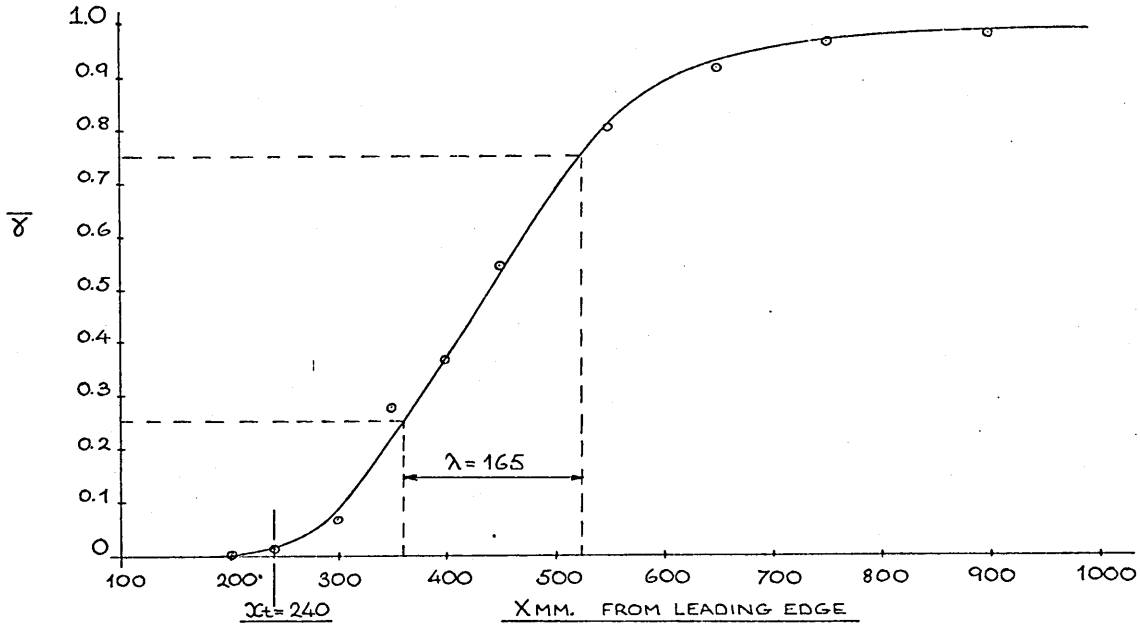

FIG.

STREAMWISE DEVELOPMENT OF "NEAR" WALL INTERMITTENCY

FLOW 1 — Z = 0

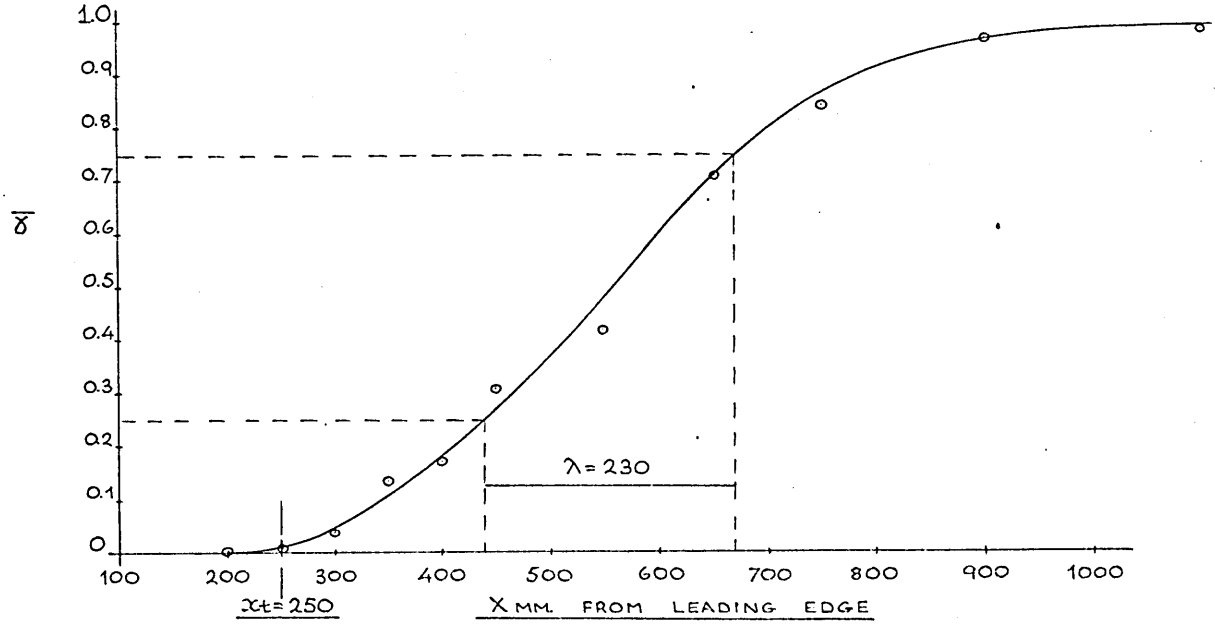

FIG.

STREAMWISE DEVELOPMENT OF "NEAR" WALL INTERMITTENCY

FLOW 1 — Z=-50

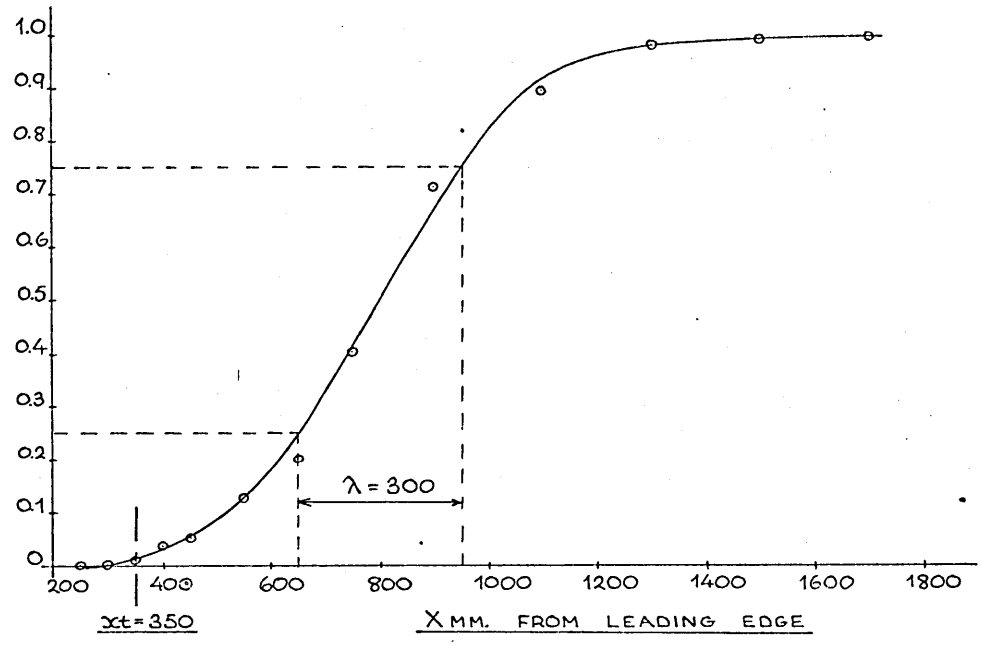

FIG

STREAMWISE DEVELOPMENT OF "NEAR" WALL INTERMITTENCY

FLOW 1 — Z=-100

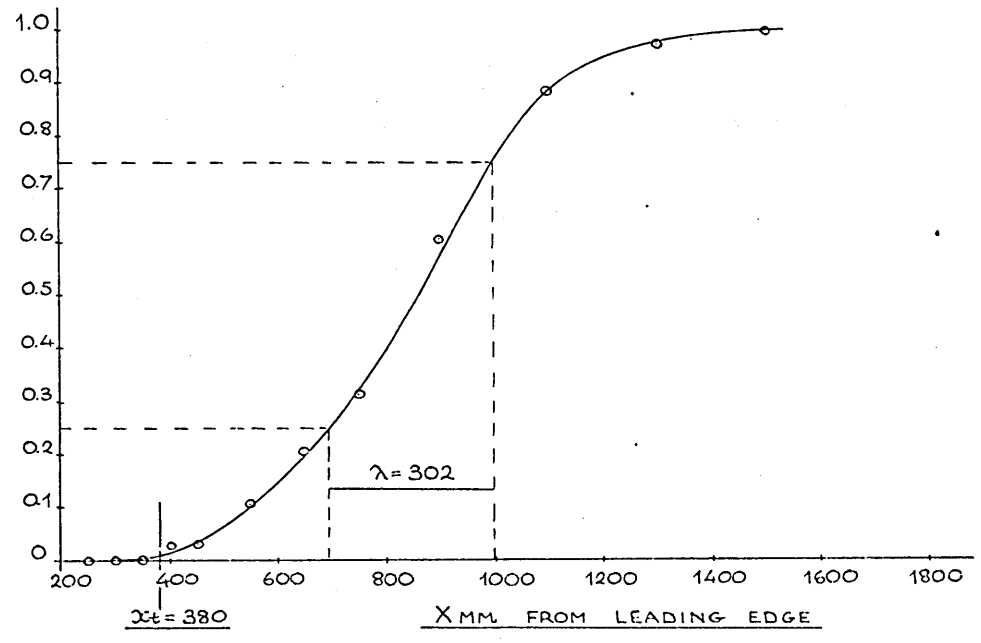

FIG

FLOW 1 — TWO PIN WAKE TRAVERSE

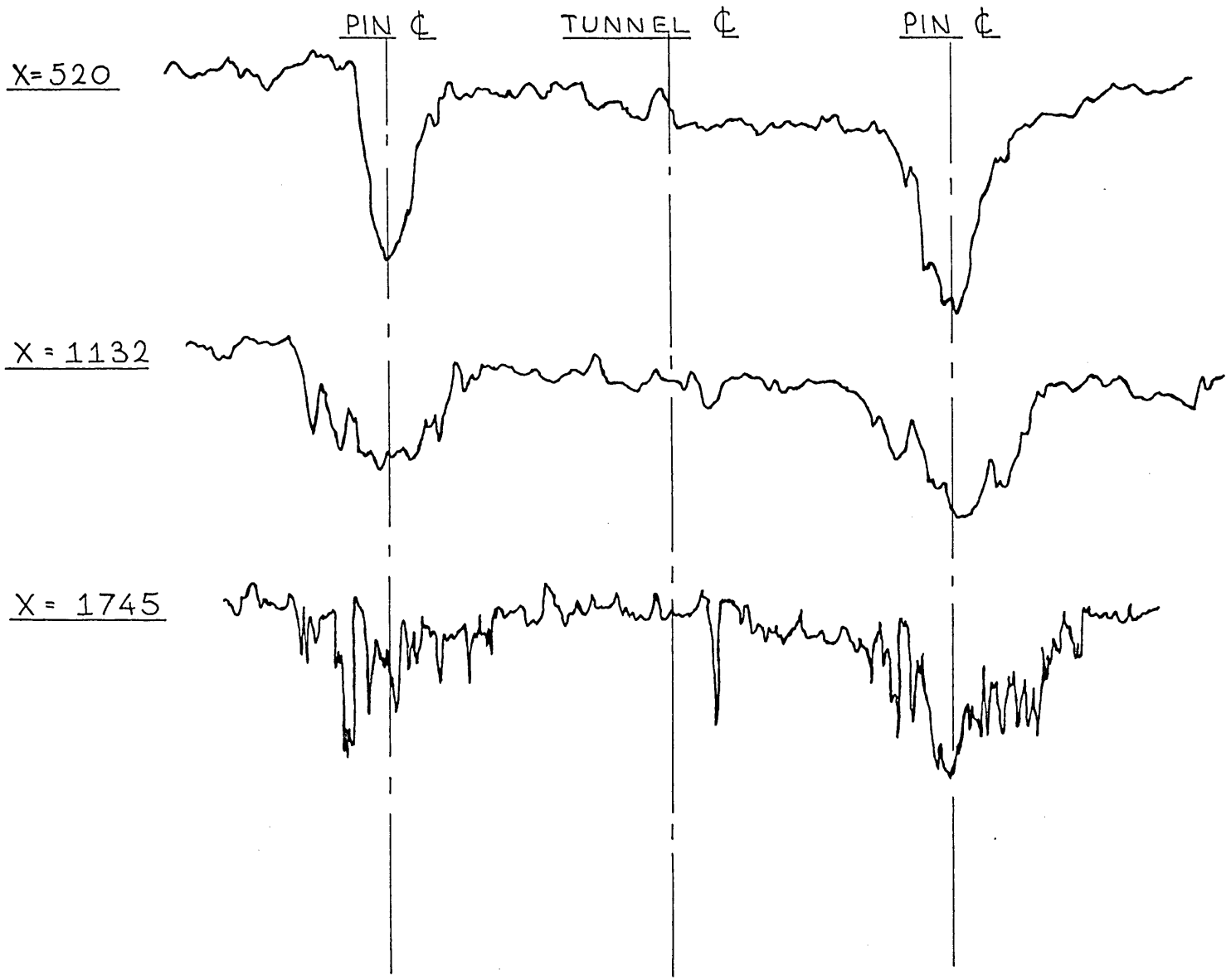

FIG. 1.48

FIG. 1.49

FLOW 1 — MOMENTUM BALANCE

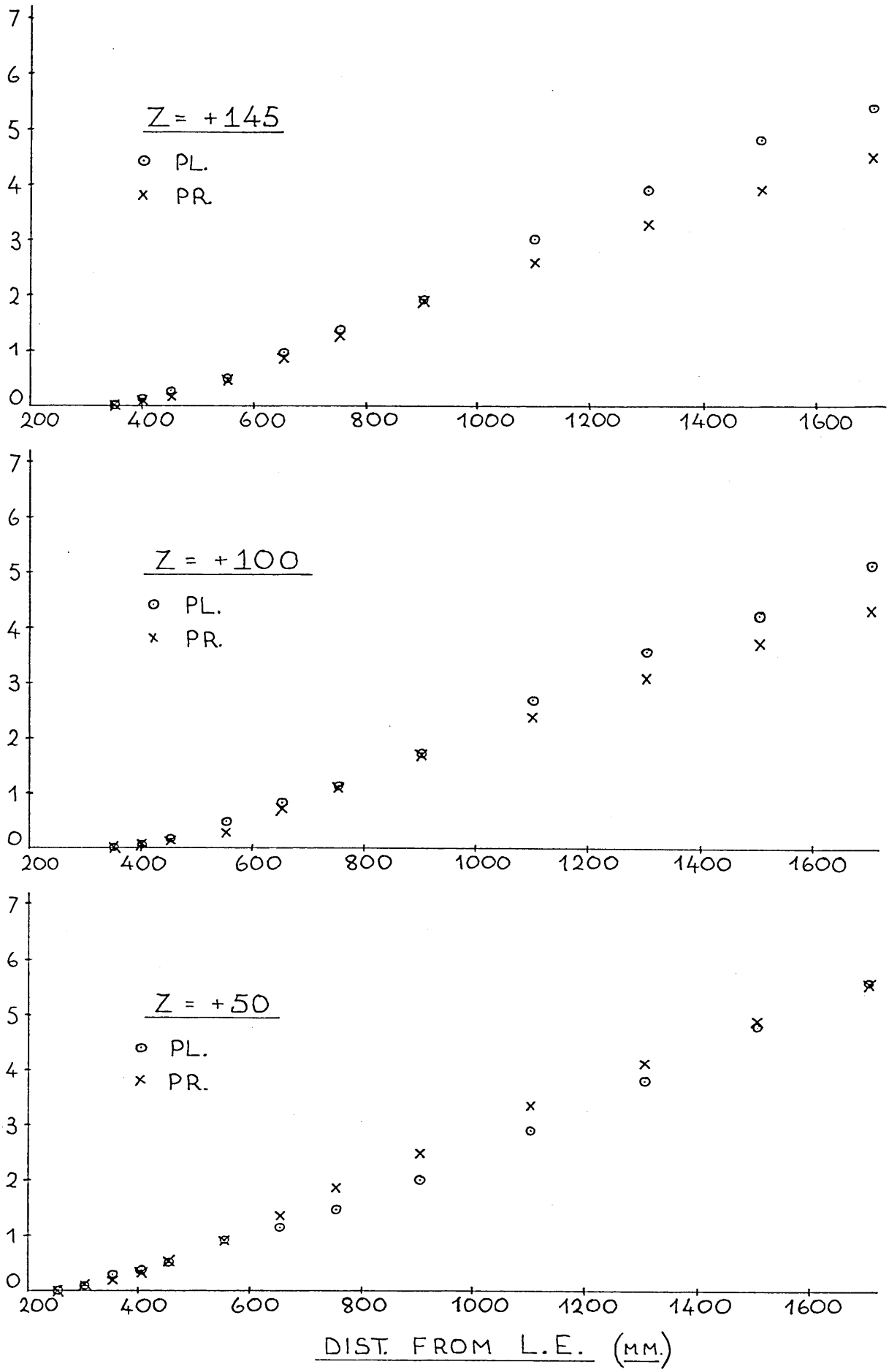

FIG. 1.50

FLOW 1 — MOMENTUM BALANCE

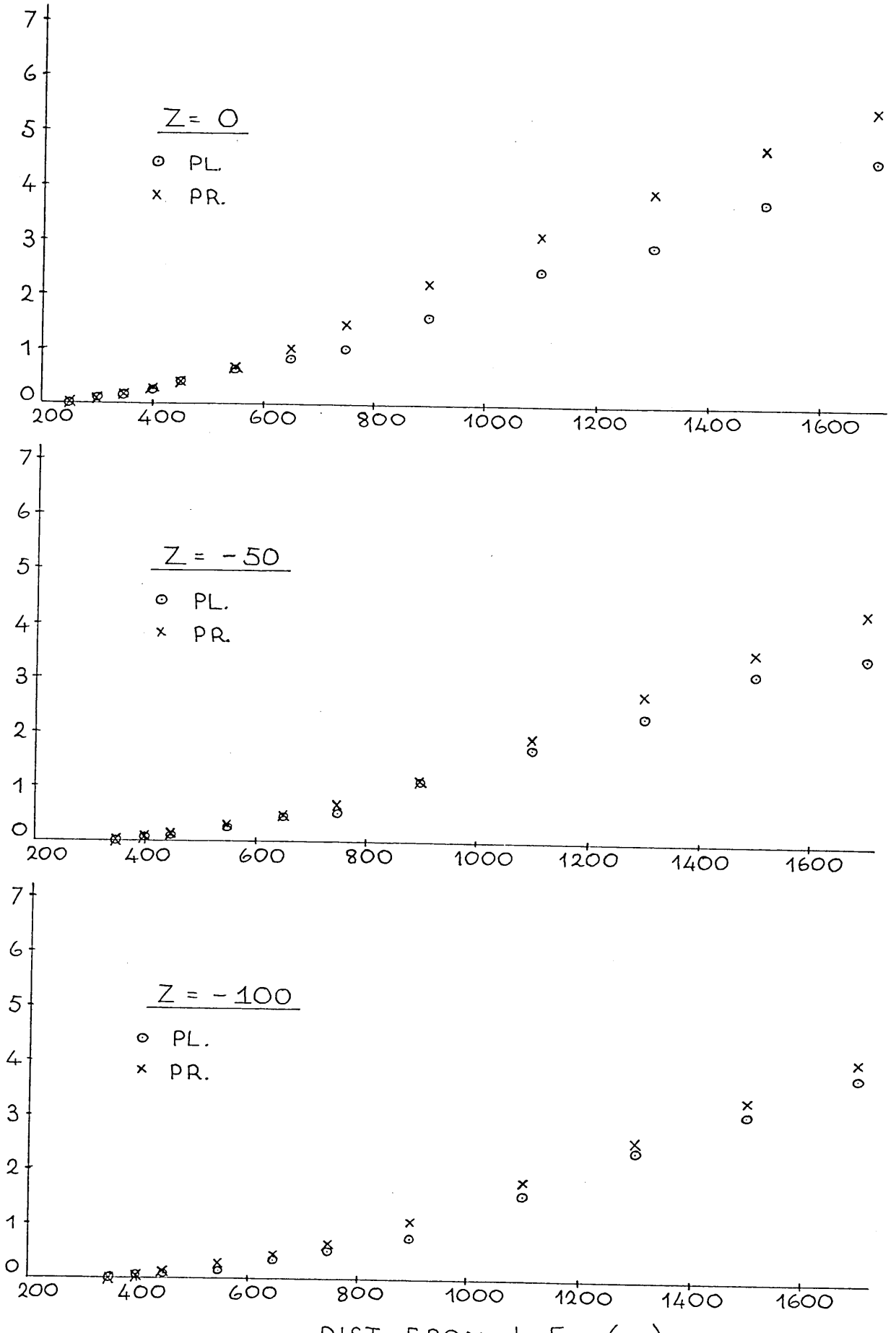

FIG. 1.51

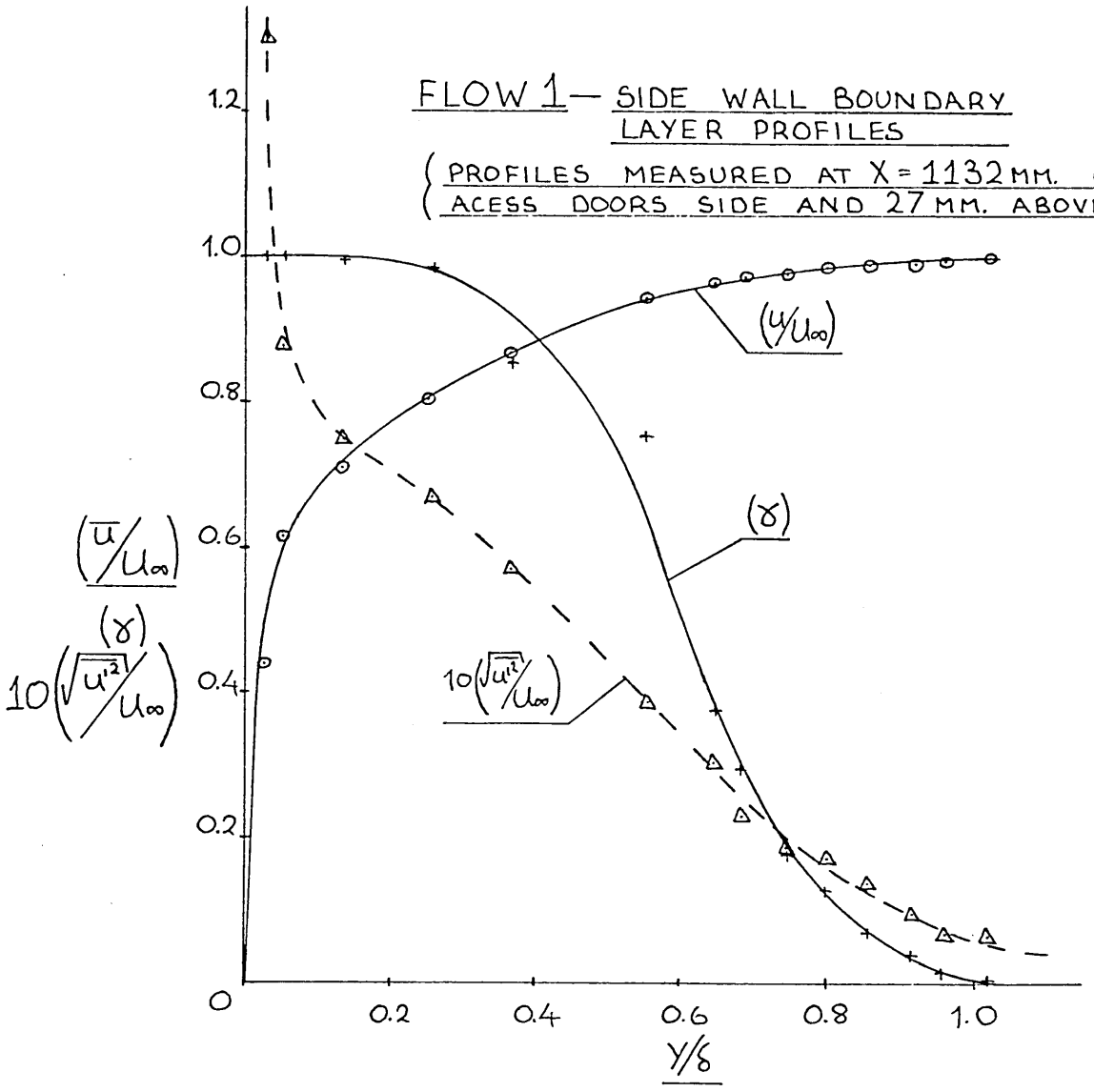
FLOW 1 — SIDE WALL BOUNDARY LAYER PROFILES
(PROFILES MEASURED AT X = 1132 MM. ON THE ACESS DOORS SIDE AND 27 MM. ABOVE THE PLATE)
(u/U∞)
(γ)
10(√u'²/U∞)
(u/U∞)
(γ) 10(√u'²/U∞)
1.2
1.0
0.8
0.6
0.4
0.2
0
0.2
0.4
0.6
0.8
1.0
y/δ

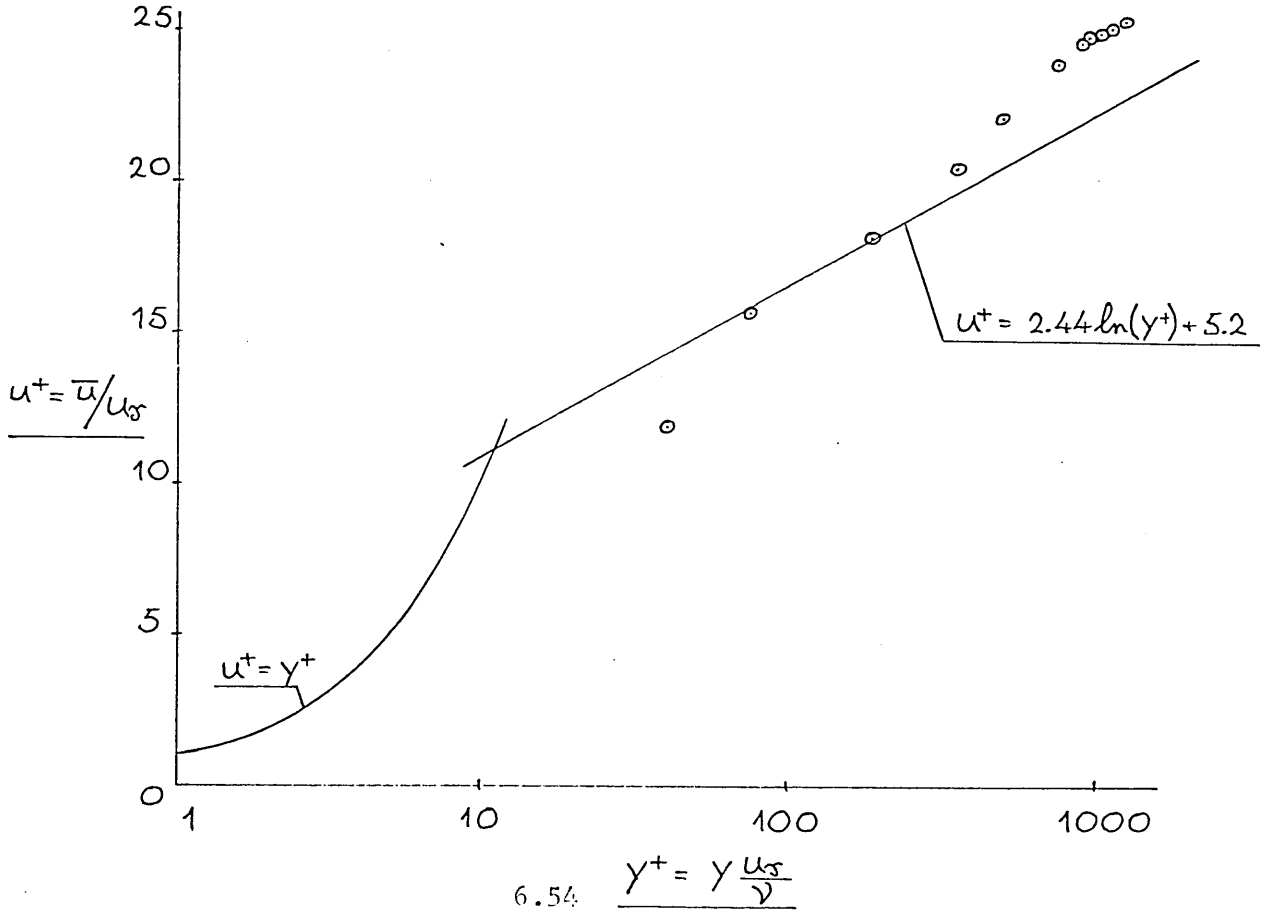
u⁺ = 2.44 ln(y⁺) + 5.2
u⁺ = y⁺
u⁺ = u/u_τ
25
20
15
10
5
0
1
10
100
1000
y⁺ = y u_τ/ν

FLOW 1 — APPROACH TO EQUILIBRIUM

KEY

⊙ Z = 145 , △ Z = 0
\+ Z = 100, ⊡ Z = -50
▽ Z = 50 , × Z = -100

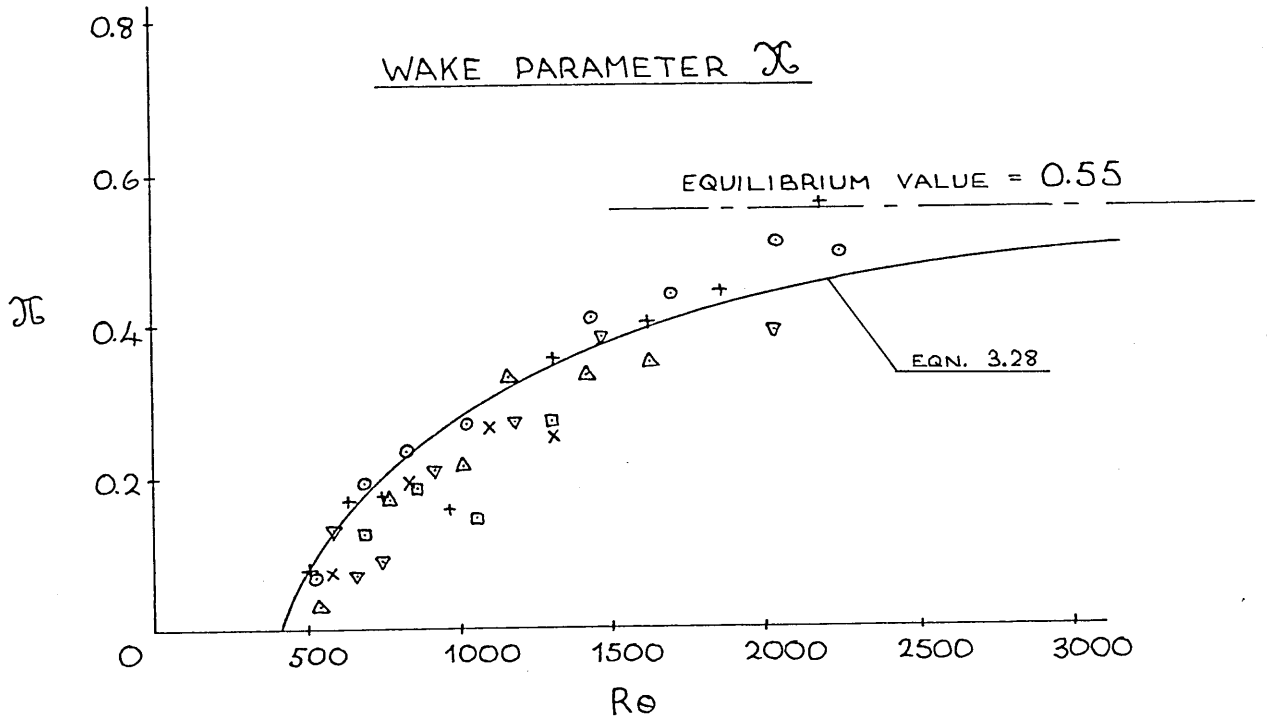

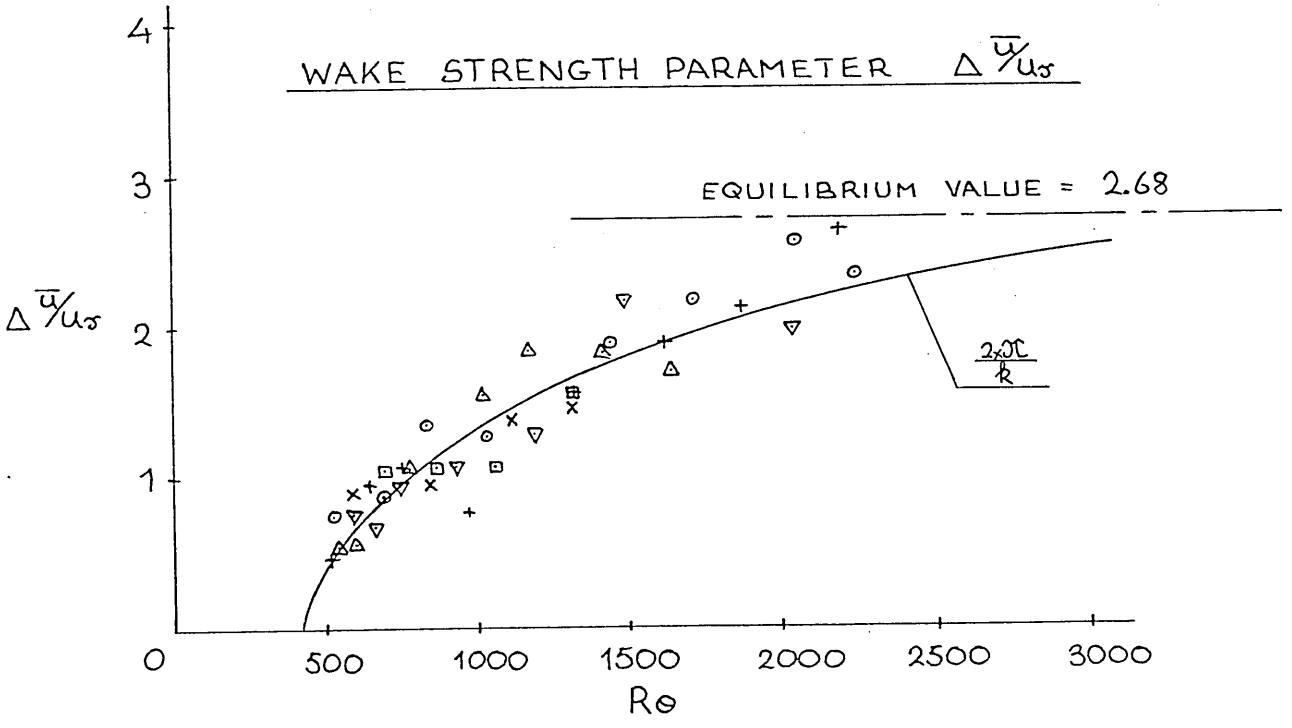

FIG 1.53

FLOW 1 — DEVELOPMENT OF SPANWISE VARIATION IN MOMENTUM THICKNESS (MM.)

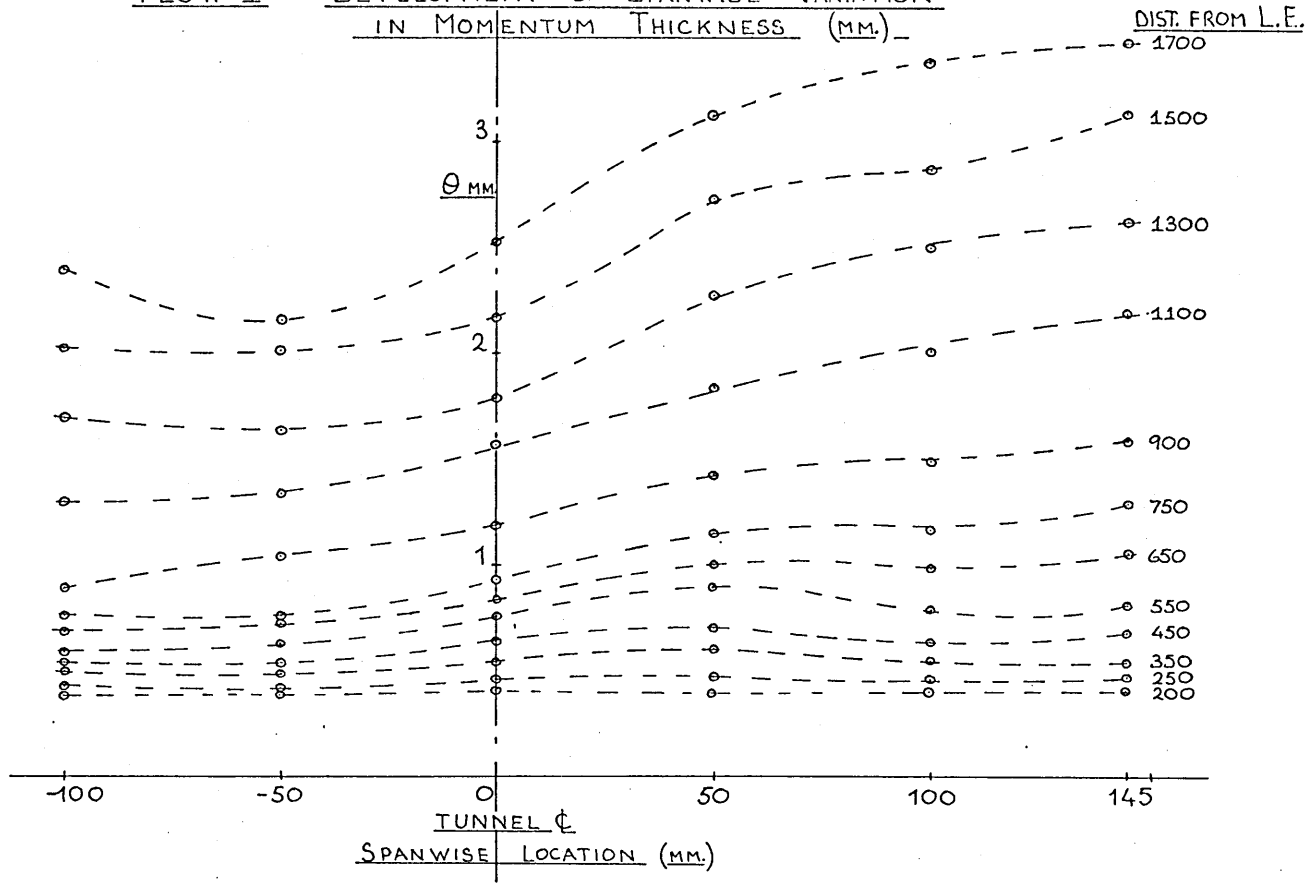

FIG.

FLOW 1 — DEVELOPMENT OF SPANWISE VARIATION IN ENERGY THICKNESS (MM.)

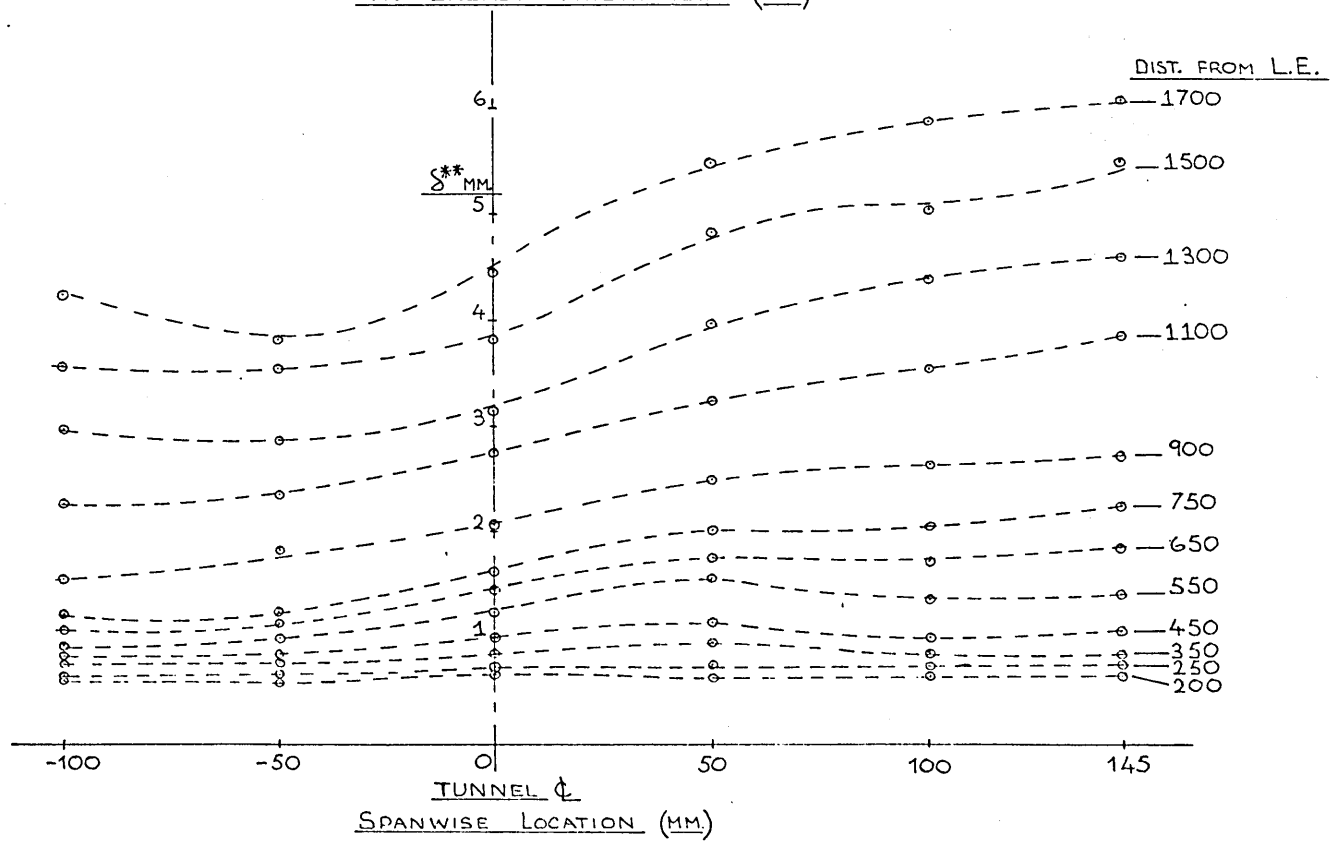

FLOW 1

BOUNDARY LAYER PROFILES AT X = 250 MM.

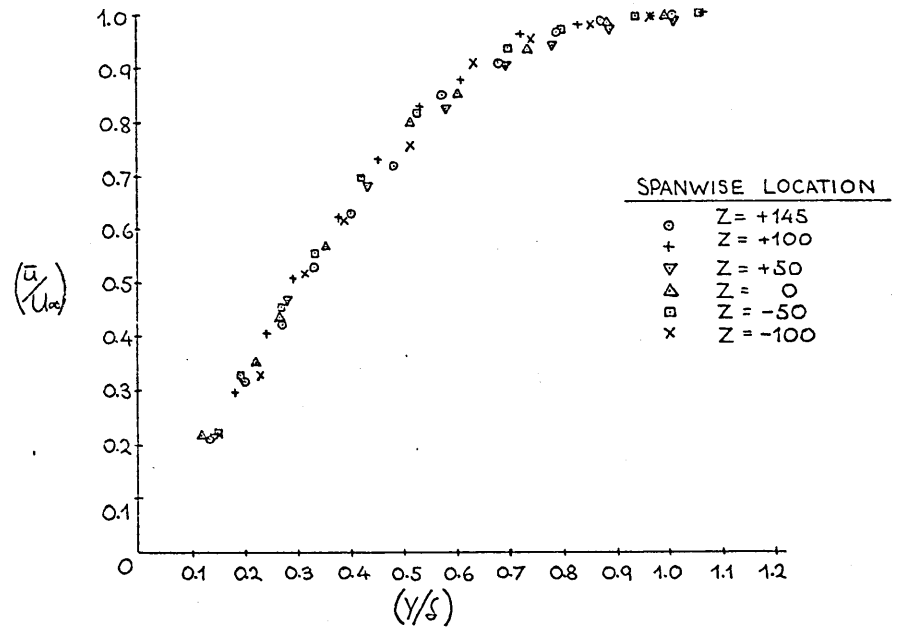

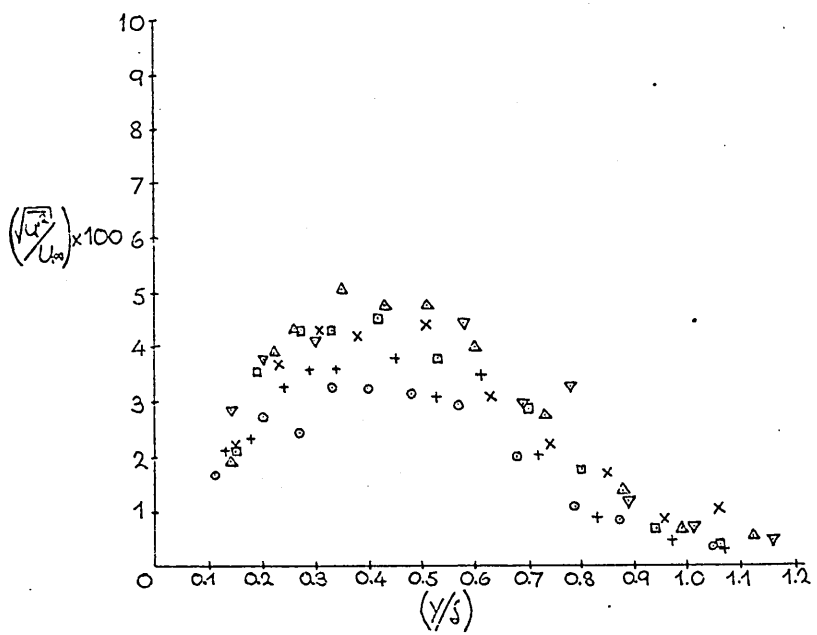

FLOW 1

BOUNDARY LAYER PROFILES AT X = 300 MM.

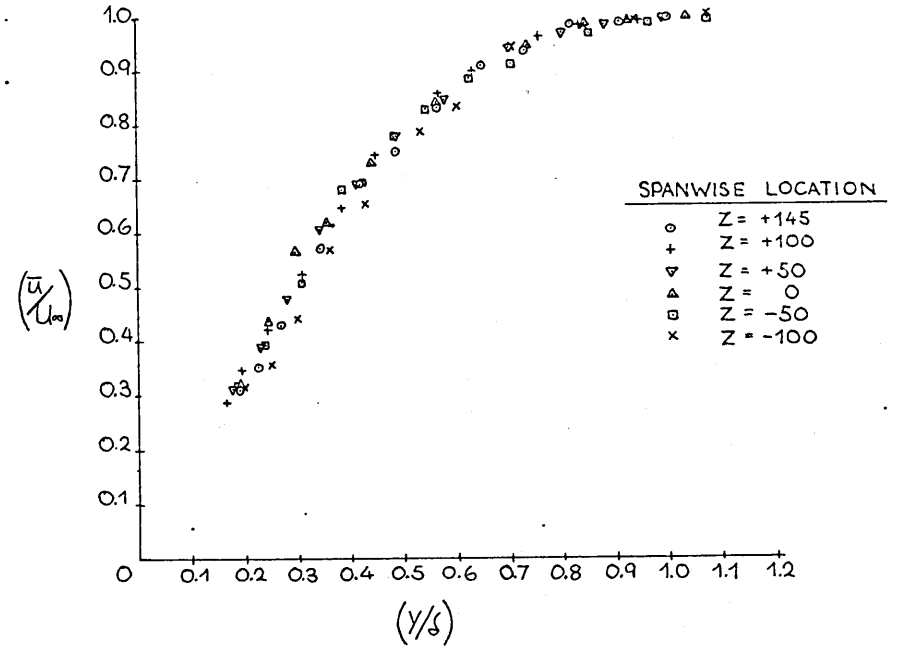

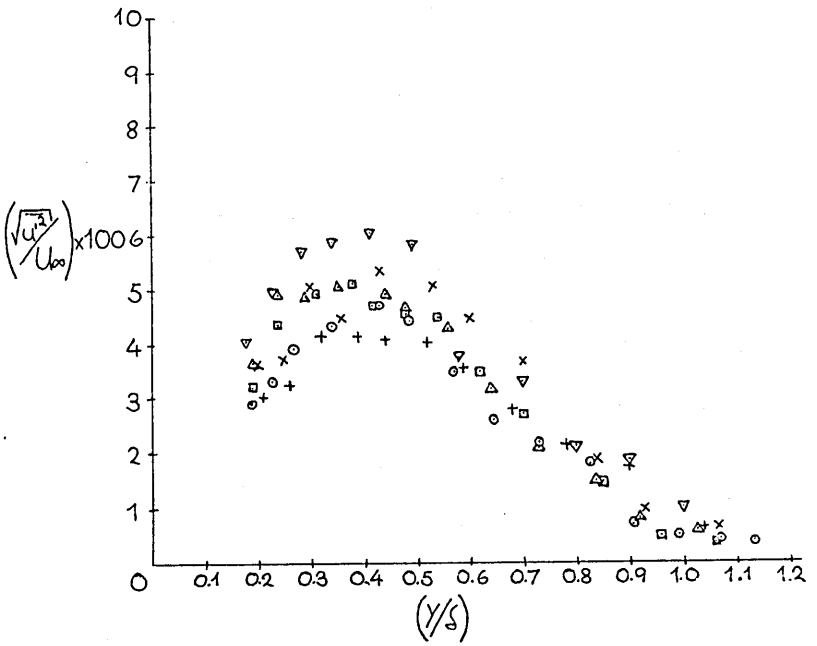

FIG 1.54

FLOW 1

BOUNDARY LAYER PROFILES AT X = 350 MM.

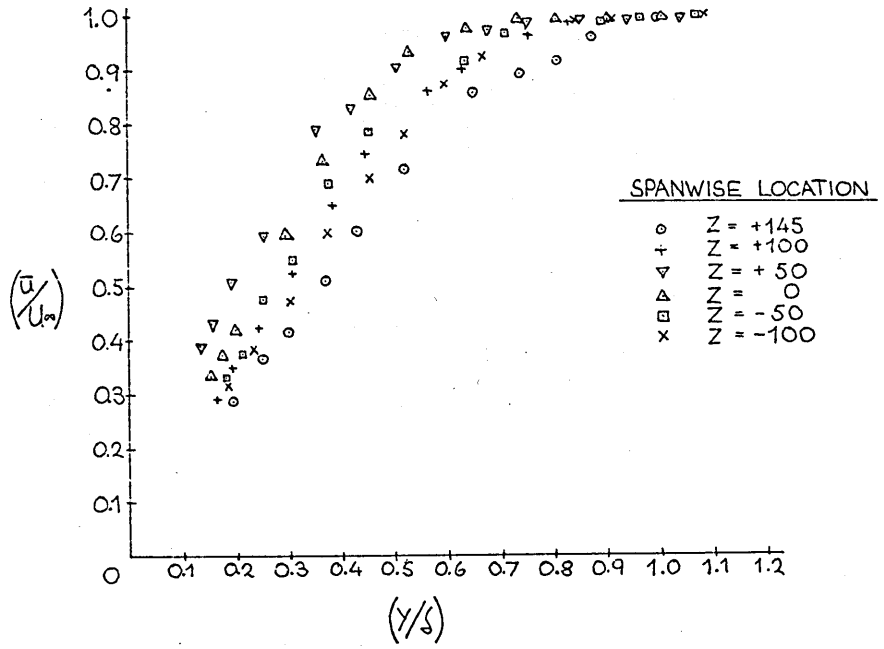

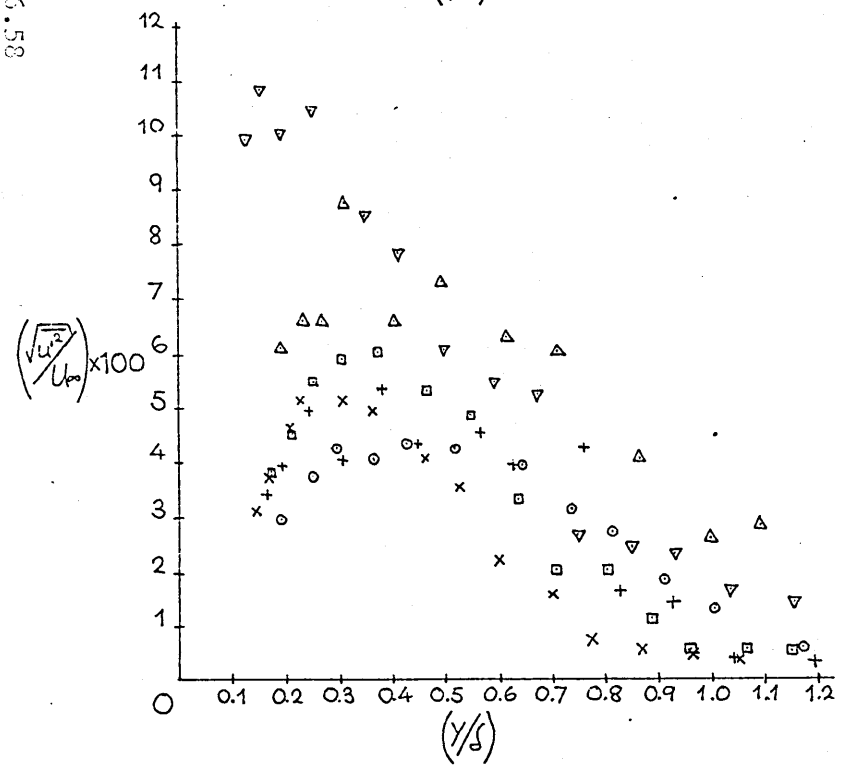

FLOW 1

BOUNDARY LAYER PROFILES AT X = 400 MM.

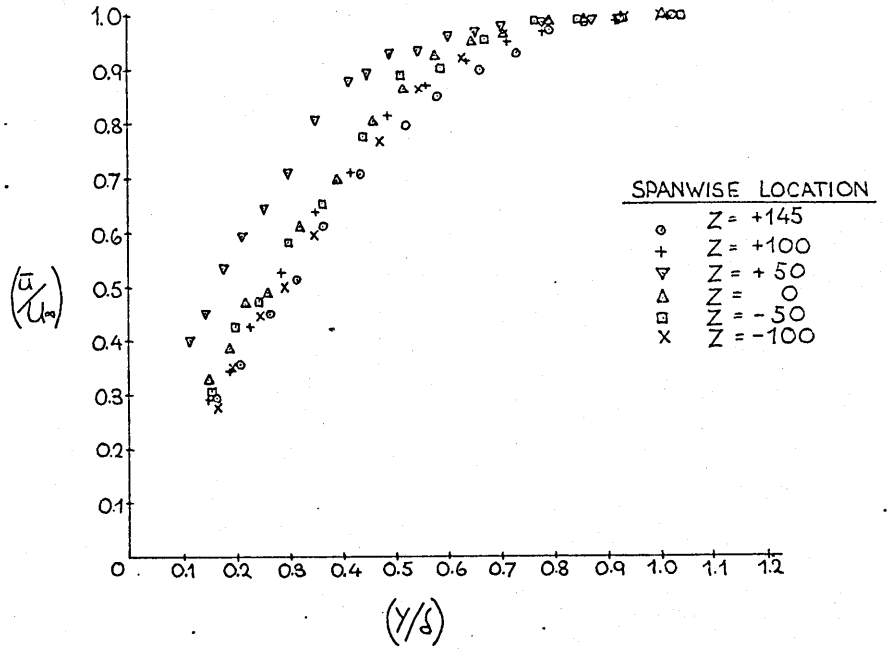

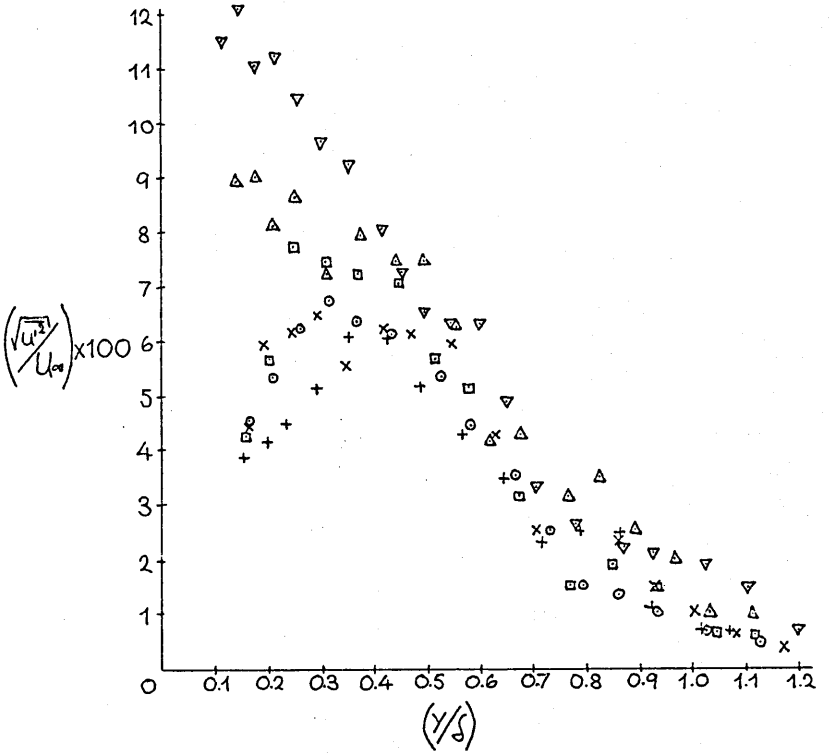

FIG 1.55

FLOW 1

BOUNDARY LAYER PROFILES AT X = 450 MM.

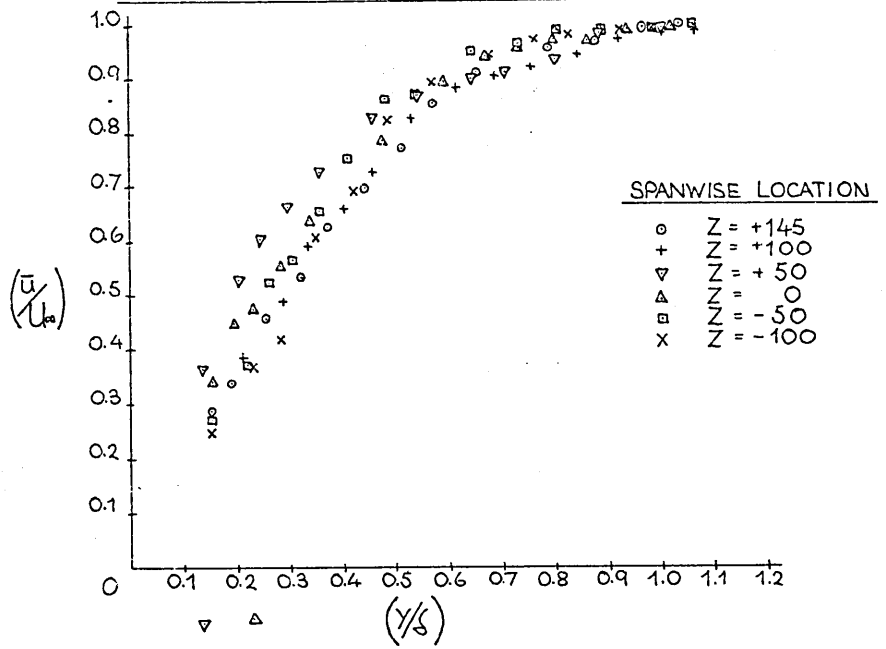

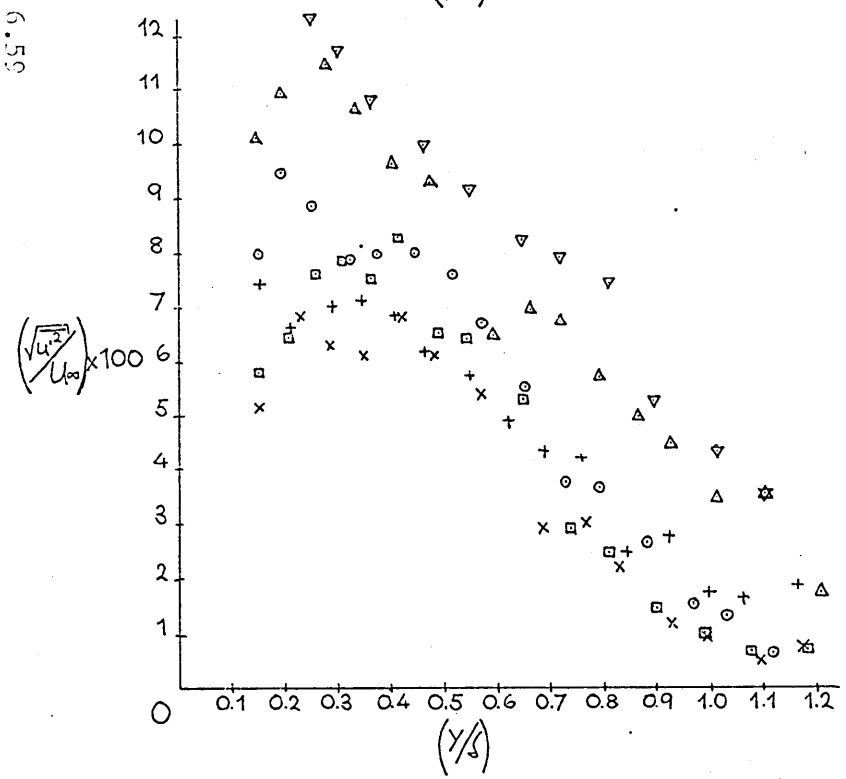

FLOW 1

BOUNDARY LAYER PROFILES AT X = 550 MM.

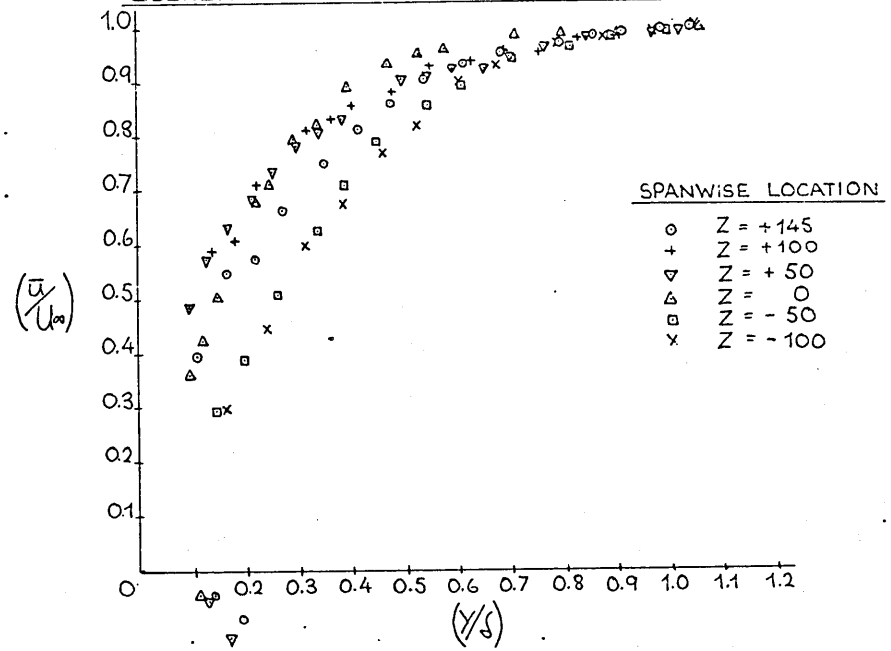

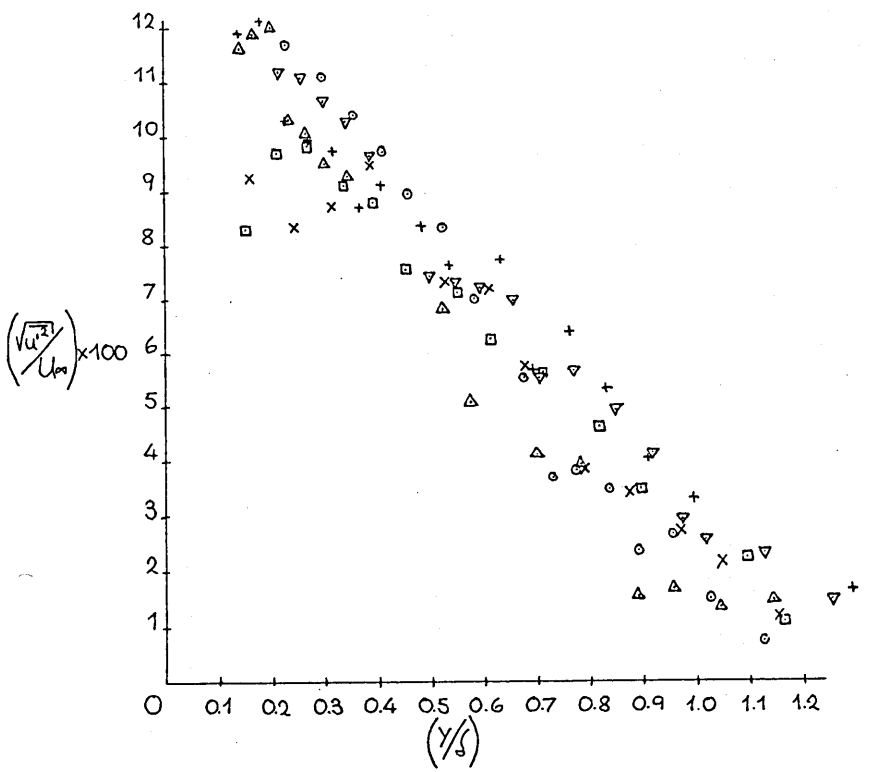

FIG 1.56

FLOW 1

BOUNDARY LAYER PROFILES AT X = 650 MM.

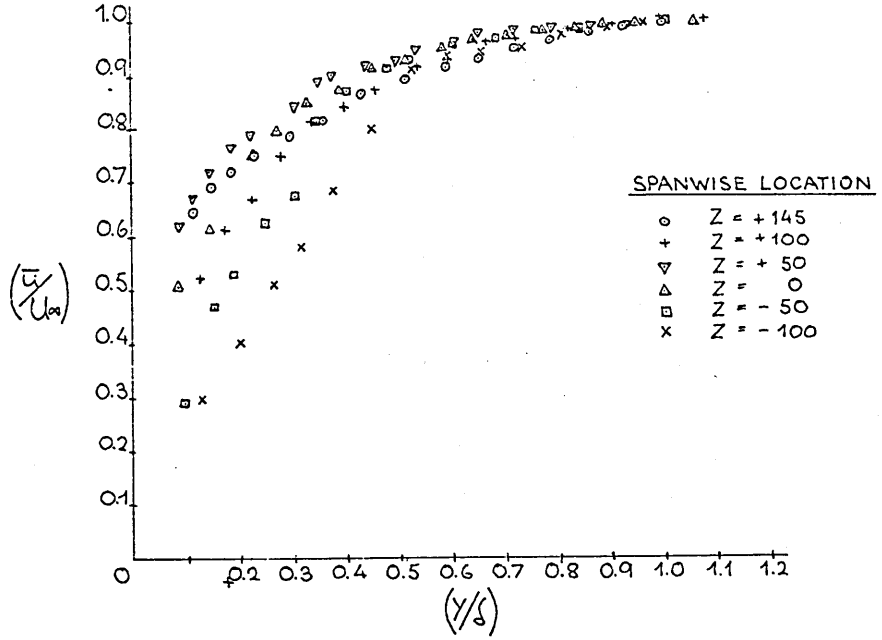

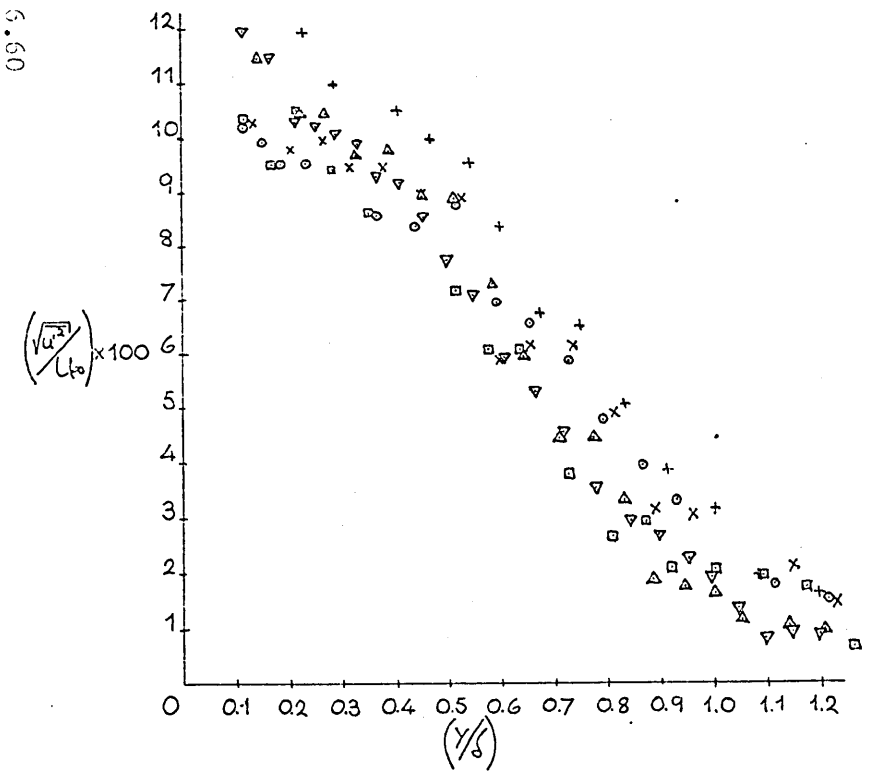

FLOW 1

BOUNDARY LAYER PROFILES AT X = 750 MM.

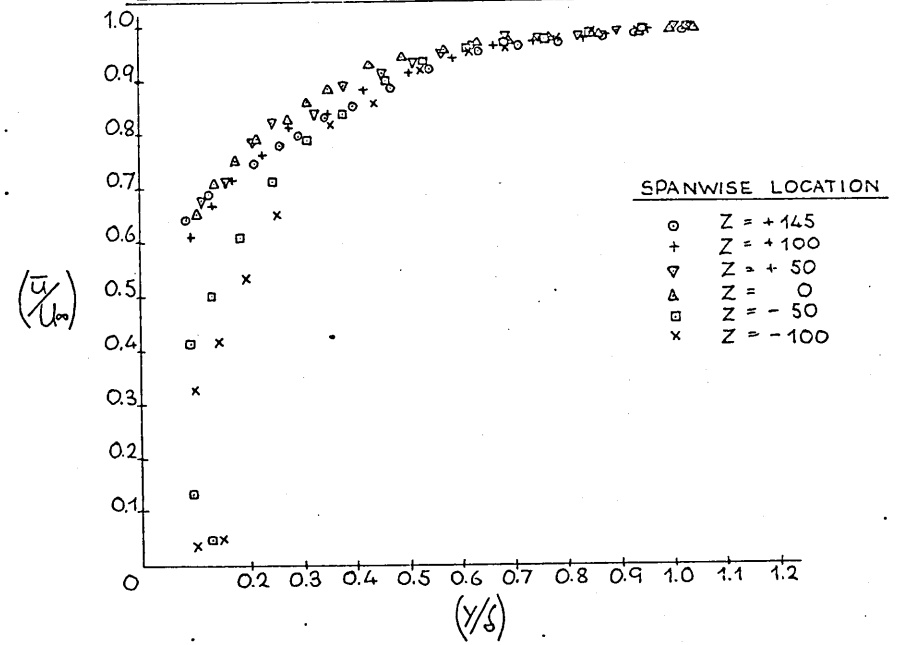

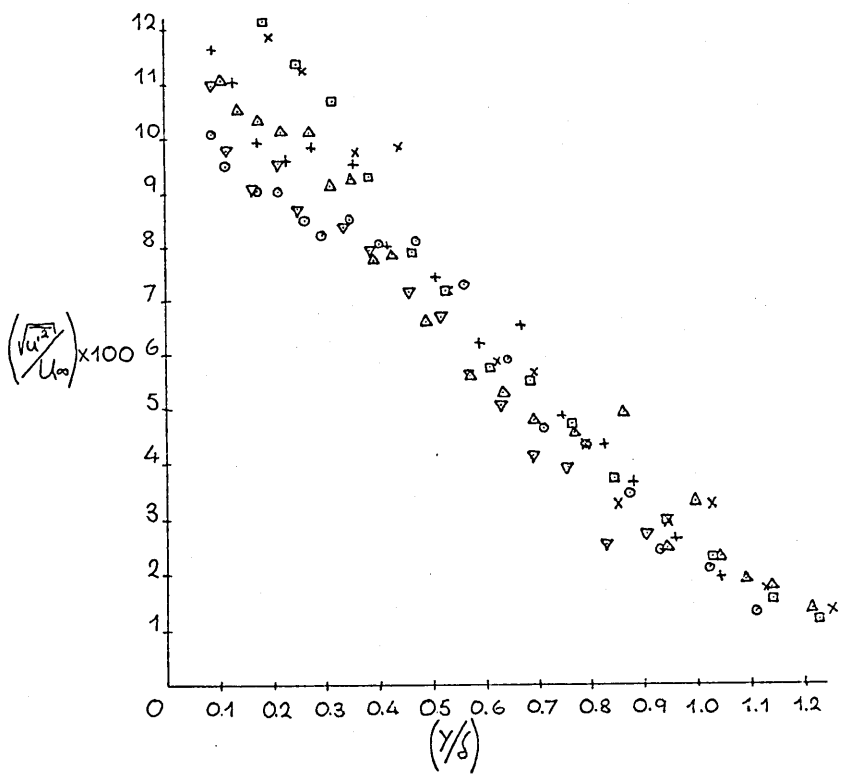

FIG 1.57

FLOW 1

BOUNDARY LAYER PROFILES AT X= 900 MM.

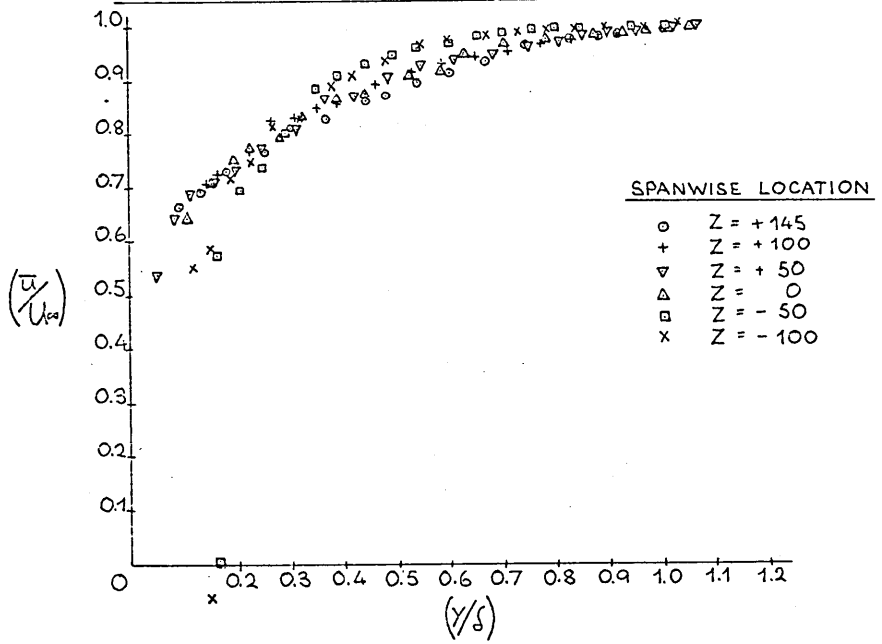

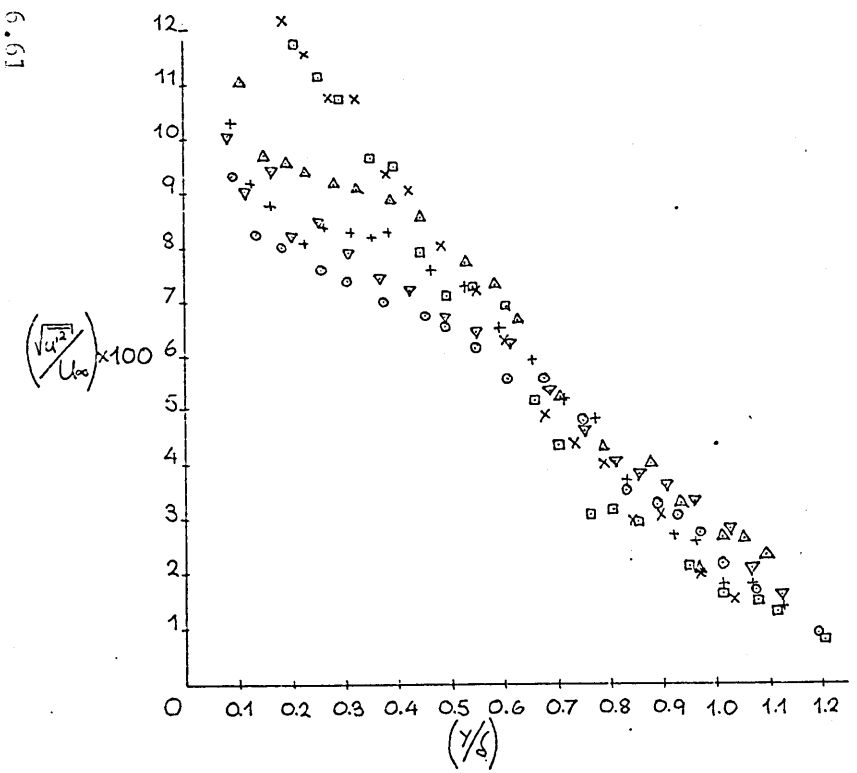

FLOW 1

BOUNDARY LAYER PROFILES AT X= 1100 MM.

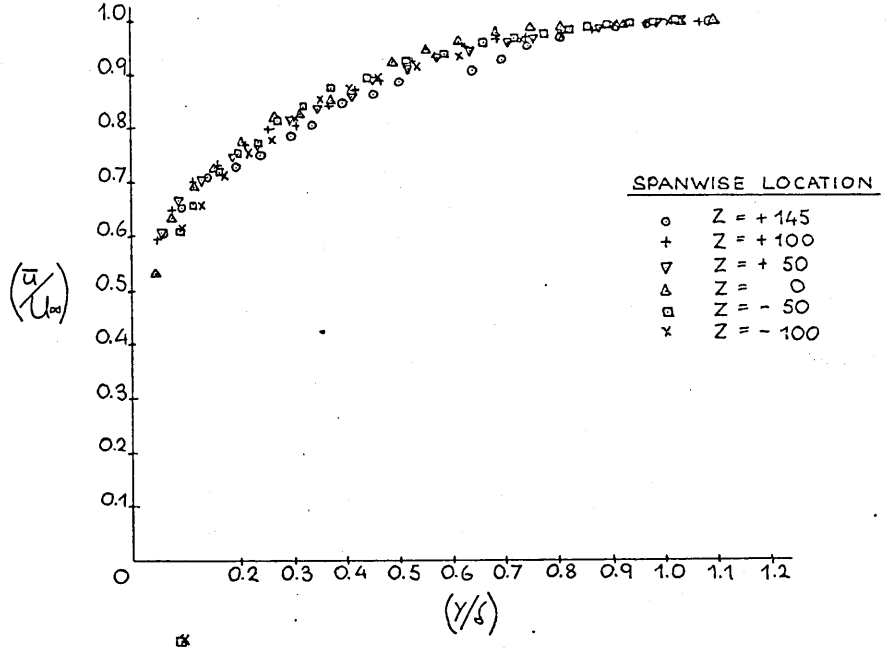

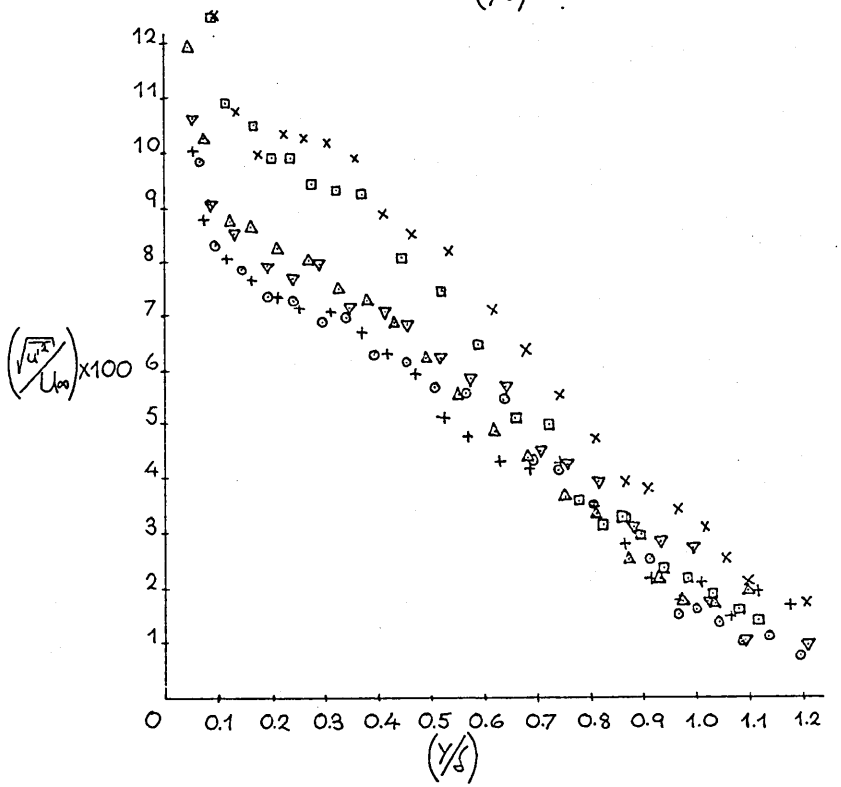

FIG 1.58

FLOW 1

BOUNDARY LAYER PROFILES AT X = 1300 mm.

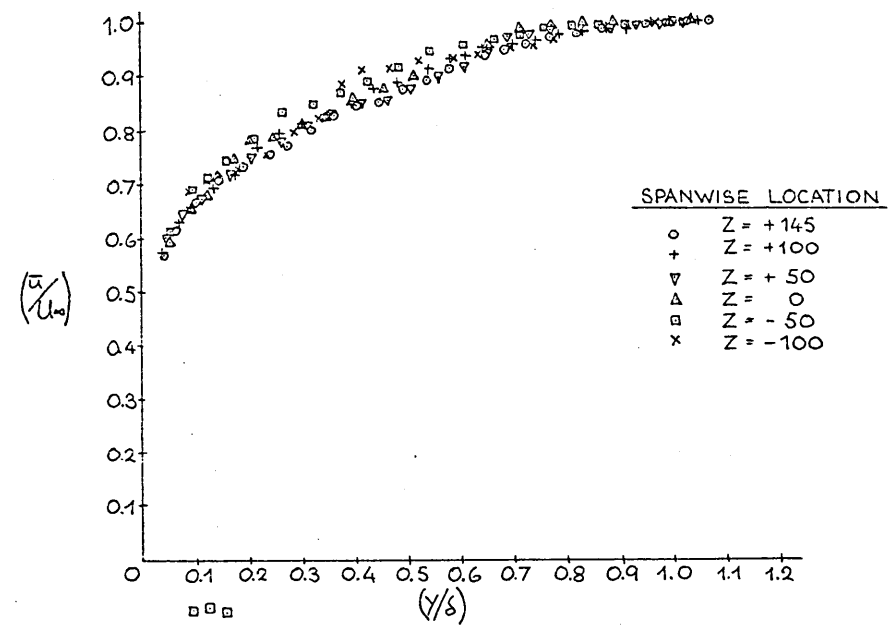

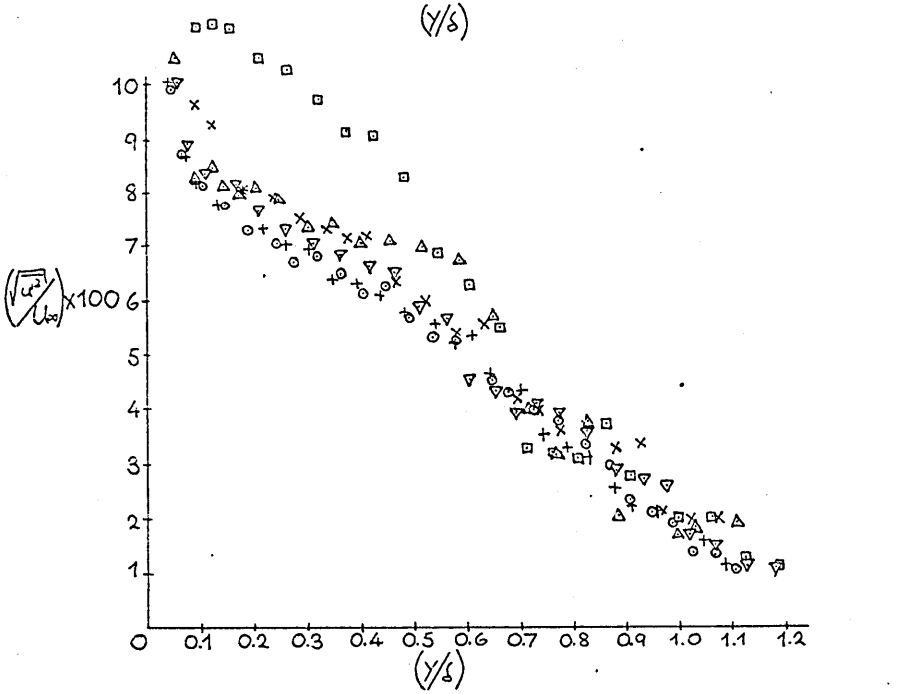

FLOW 1

BOUNDARY LAYER PROFILES AT X = 1500 mm.

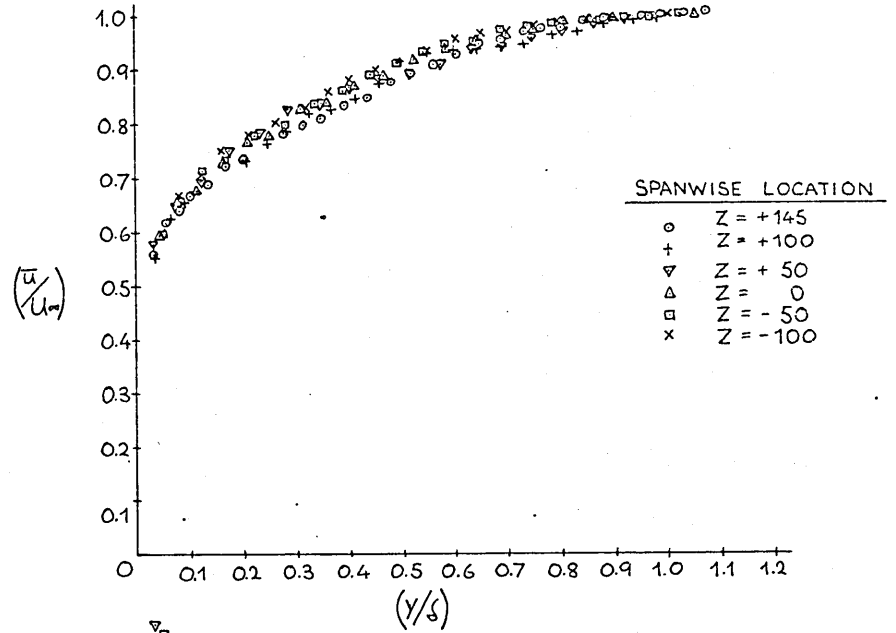

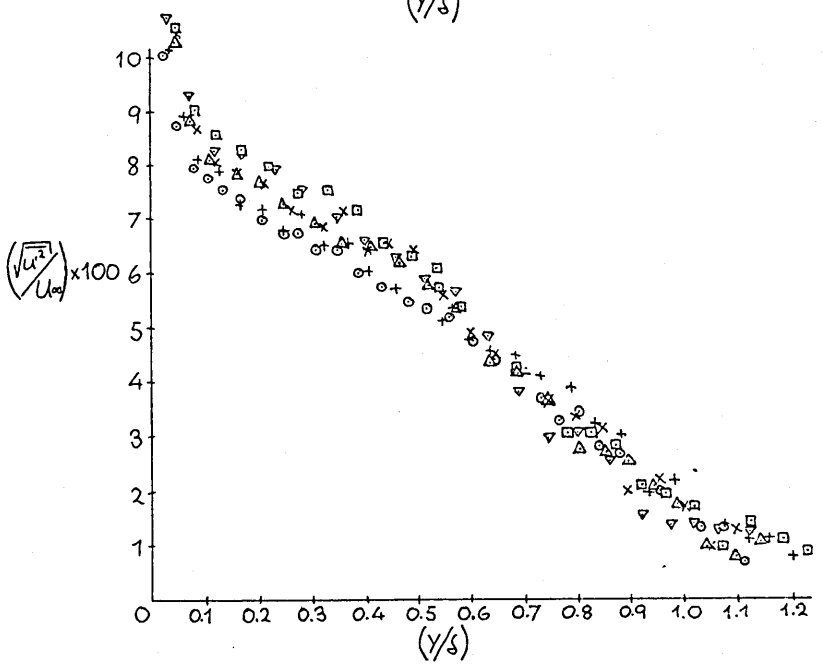

FIG 1.59

6.62

FLOW 1

BOUNDARY LAYER PROFILES AT X= 1700MM.

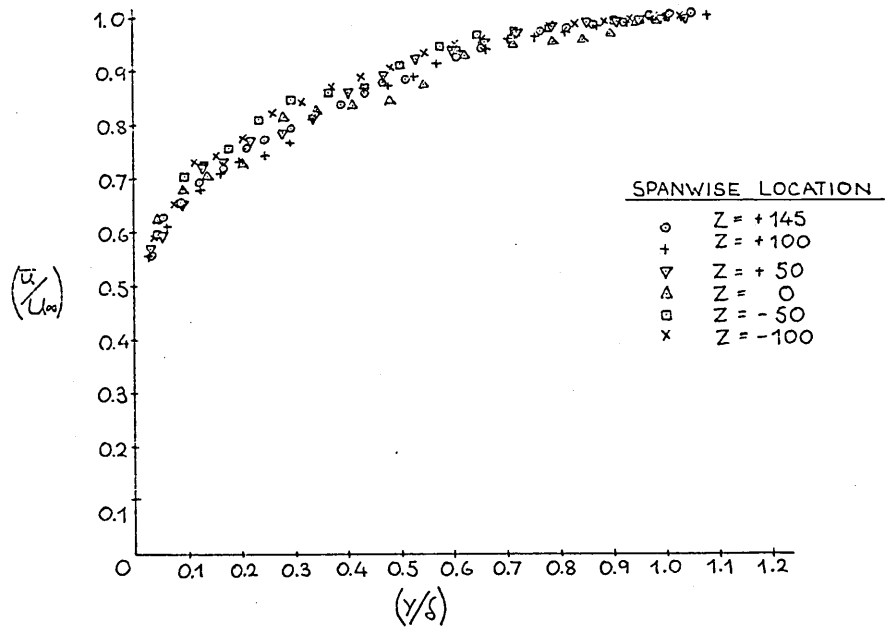

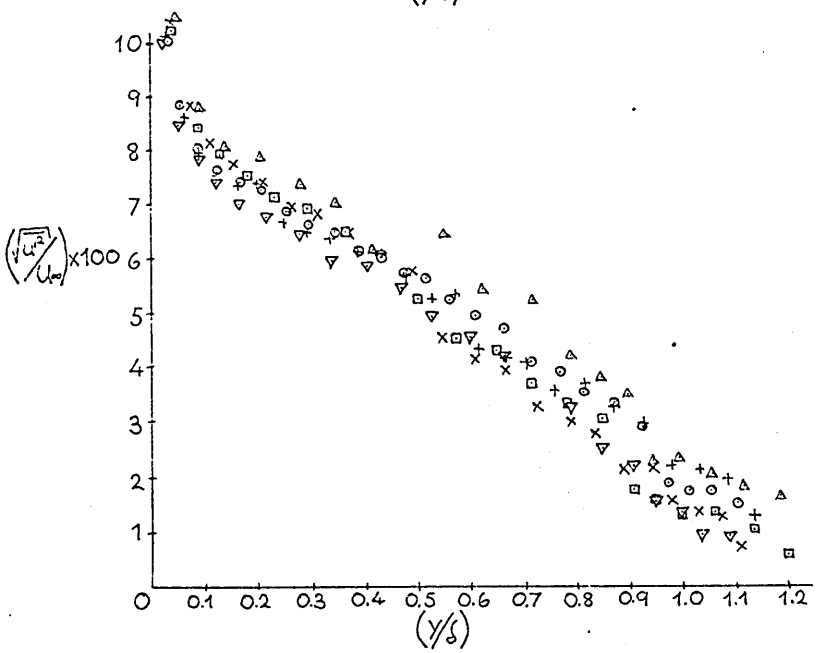

FIG 1.60

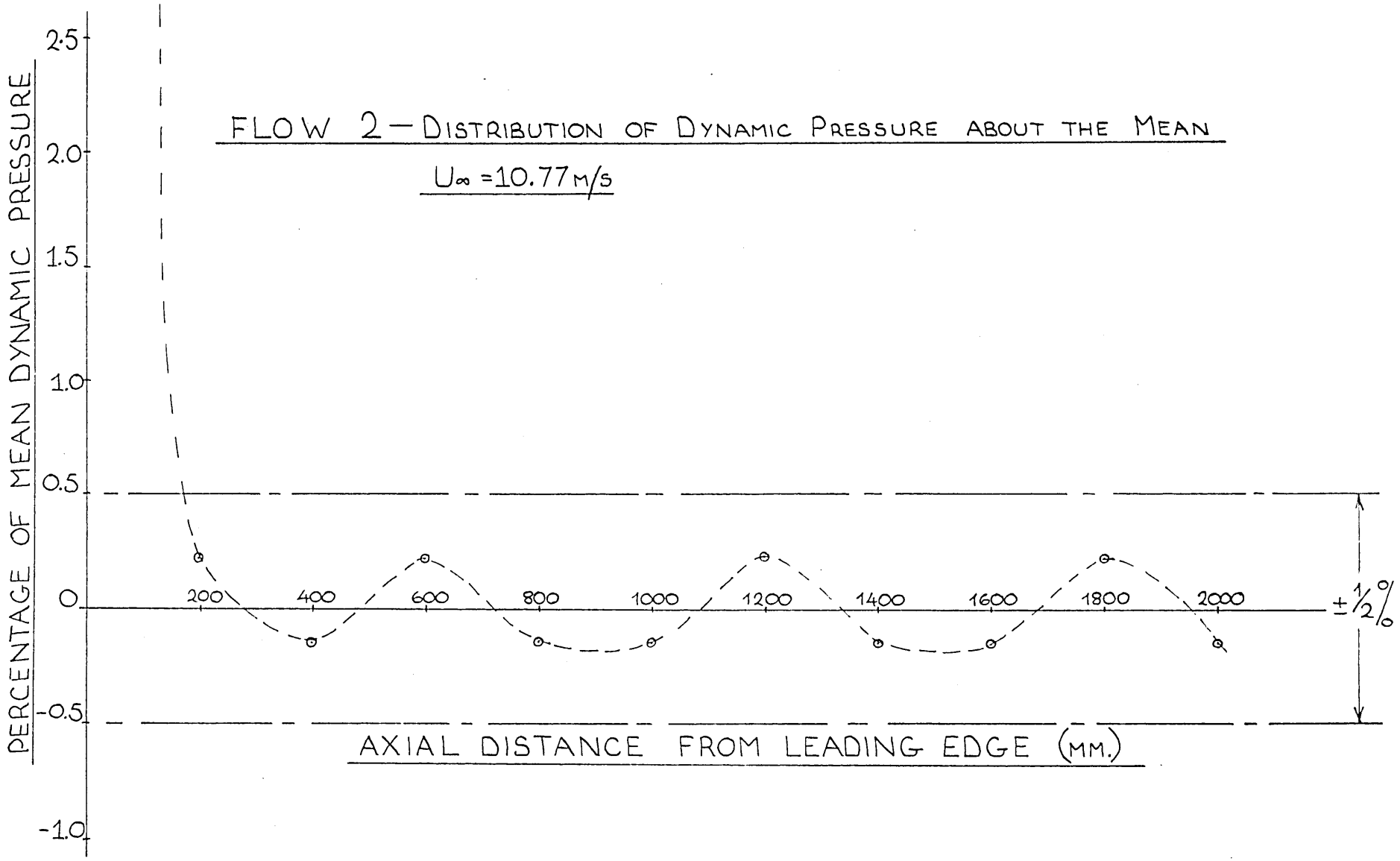
FLOW 2 — DISTRIBUTION OF DYNAMIC PRESSURE ABOUT THE MEAN
U_∞ = 10.77 m/s
PERCENTAGE OF MEAN DYNAMIC PRESSURE
2·5
2.0
1.5
1.0
0.5
0
-0.5
-1.0
200
400
600
800
1000
1200
1400
1600
1800
2000
± ½ %
AXIAL DISTANCE FROM LEADING EDGE (MM.)

FIG. 2.1

FLOW 2 — DEVELOPMENT OF MEAN VELOCITY PROFILE ALONG Z = +50

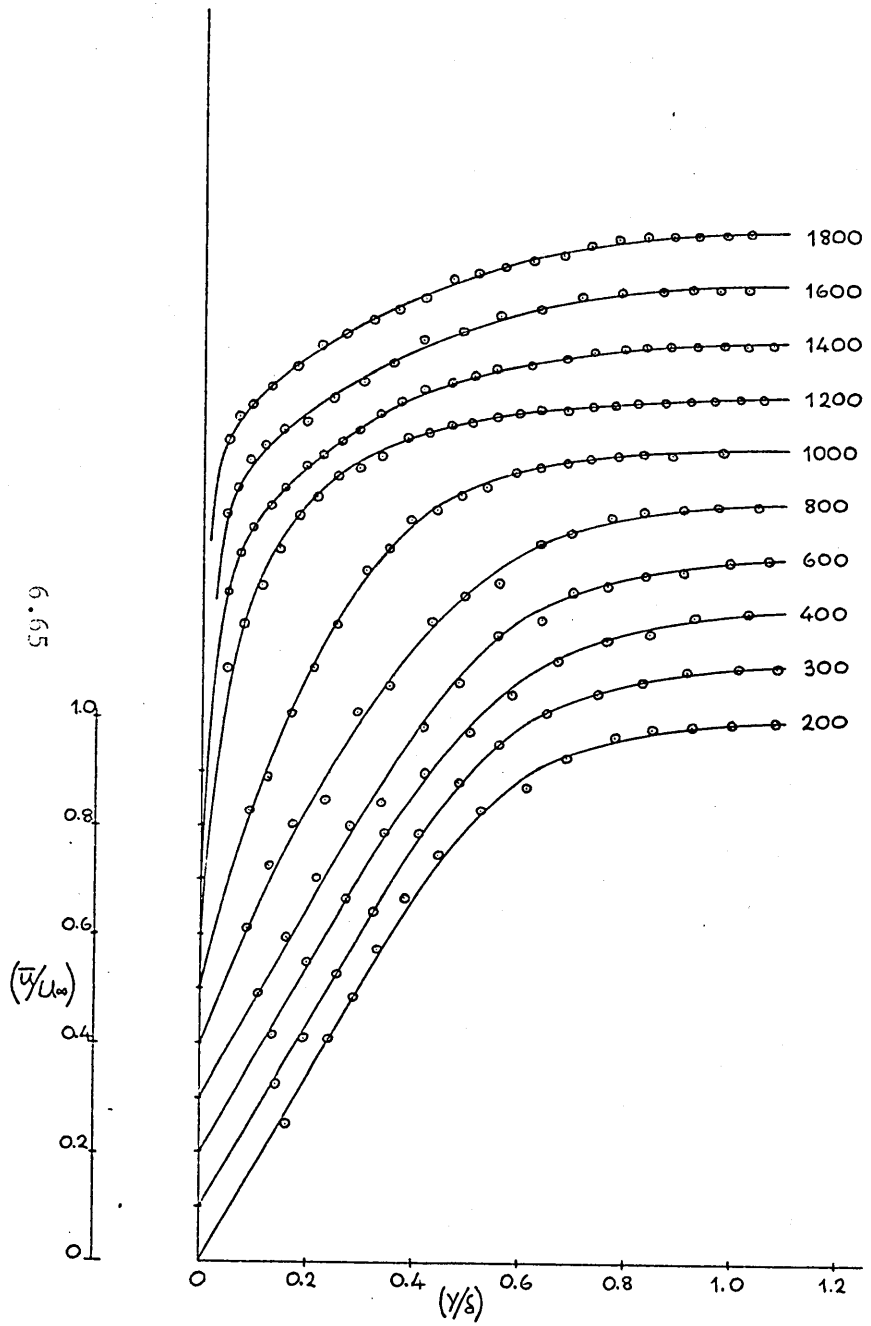

59.9

FLOW 2 — DEVELOPMENT OF MEAN VELOCITY PROFILE ALONG Z = -50

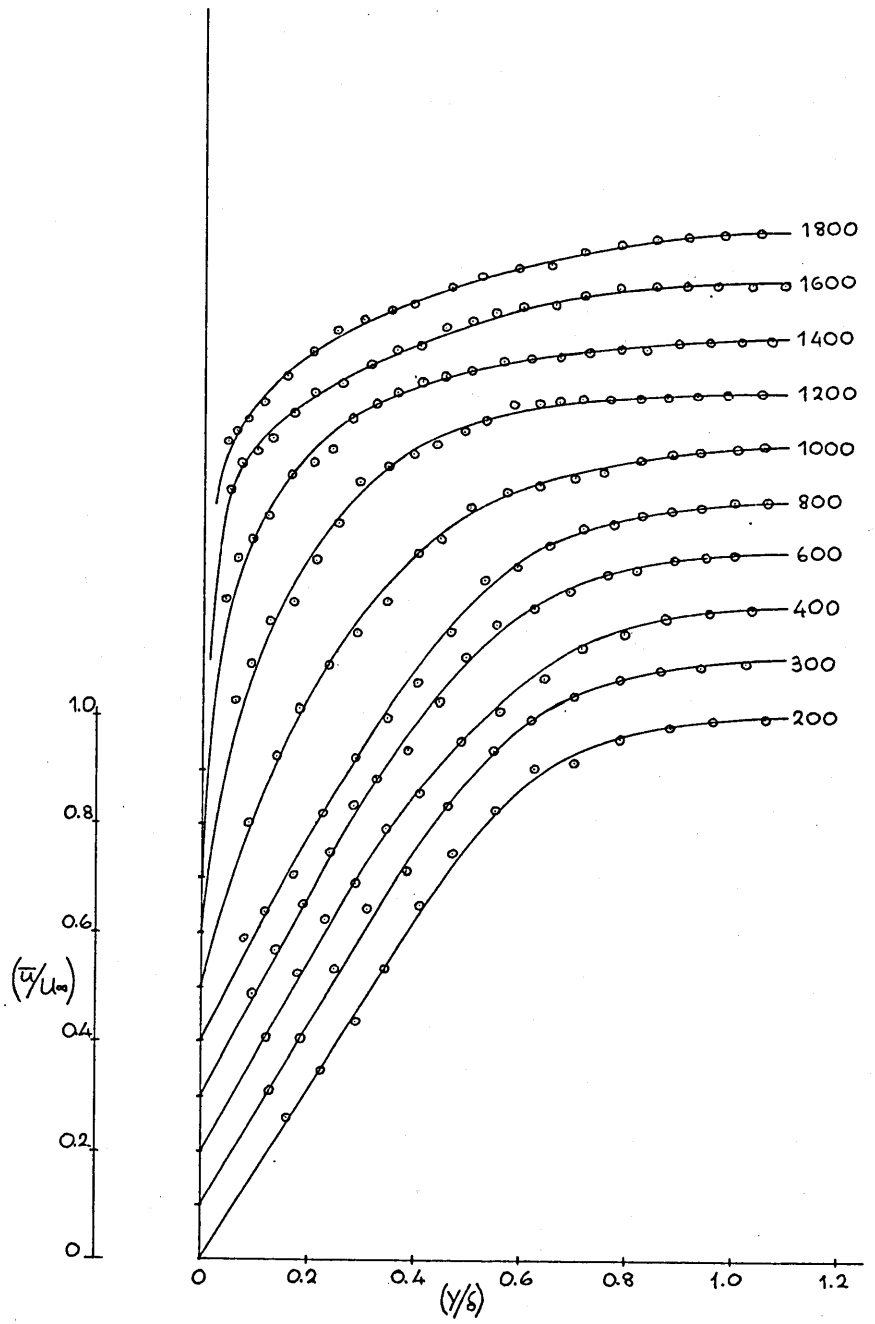

FIG 2.2

FLOW 2 — COMPARISON OF MEAN VELOCITY WITH BLASIUS PROFILE ALONG Z = +50

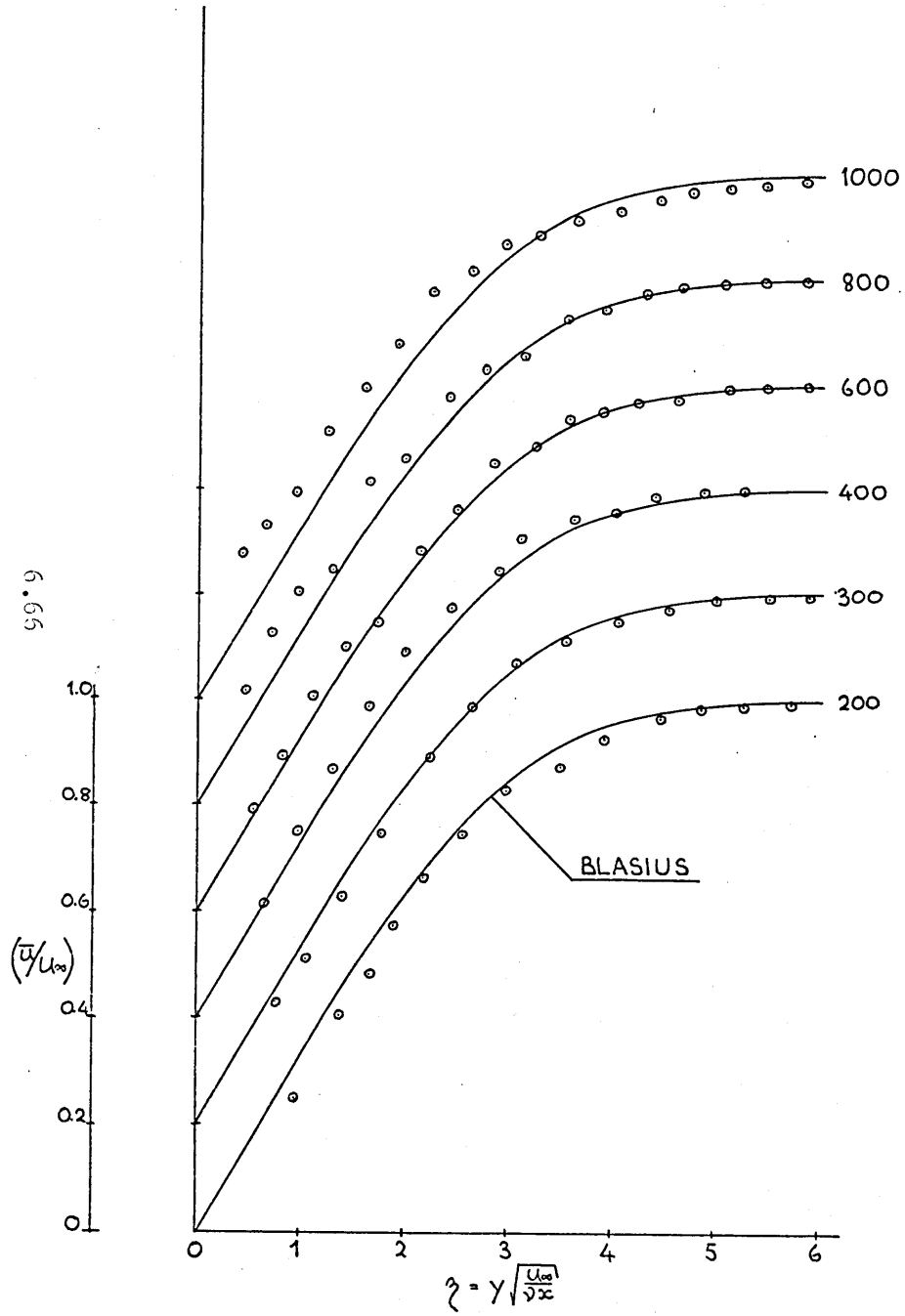

FLOW 2 — COMPARISON OF MEAN VELOCITY WITH BLASIUS PROFILE ALONG Z = -50

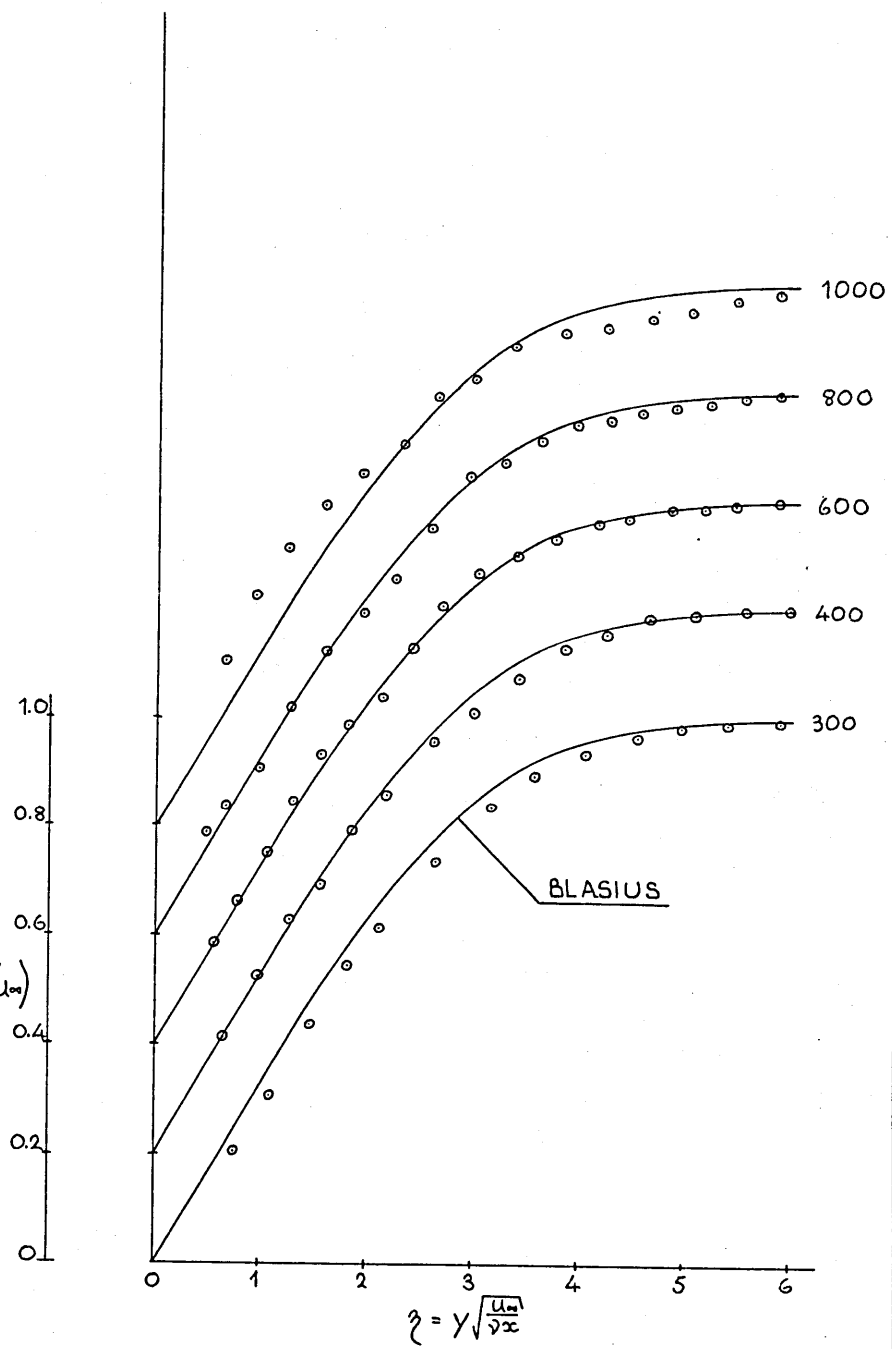

99.9

FIG 2.3

FLOW 2 — DEVELOPMENT OF SEMI-LOGARITHMIC VELOCITY PROFILE ALONG Z=+50

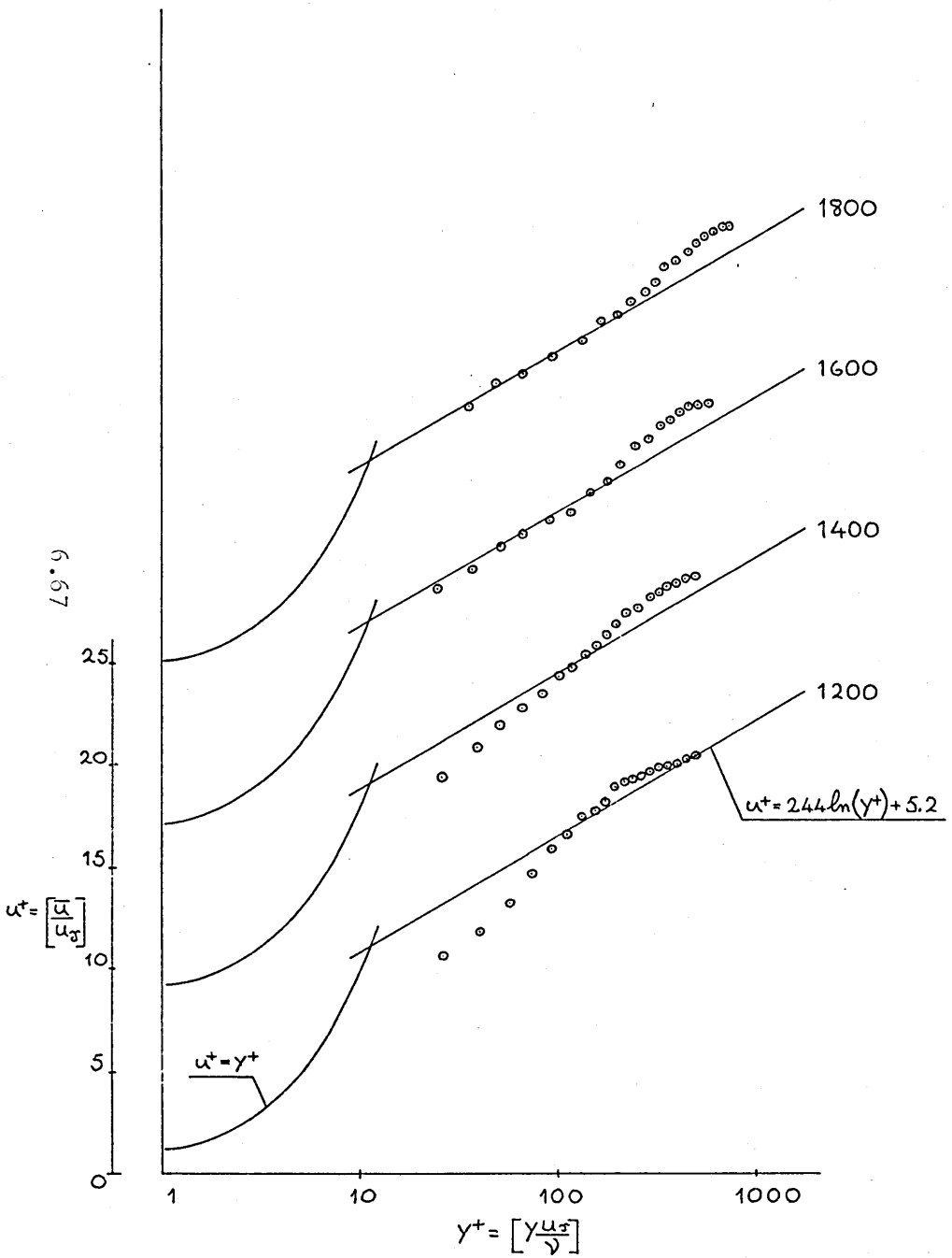

6.67

FLOW 2 — DEVELOPMENT OF VELOCITY-DEFECT PROFILE ALONG Z=+50

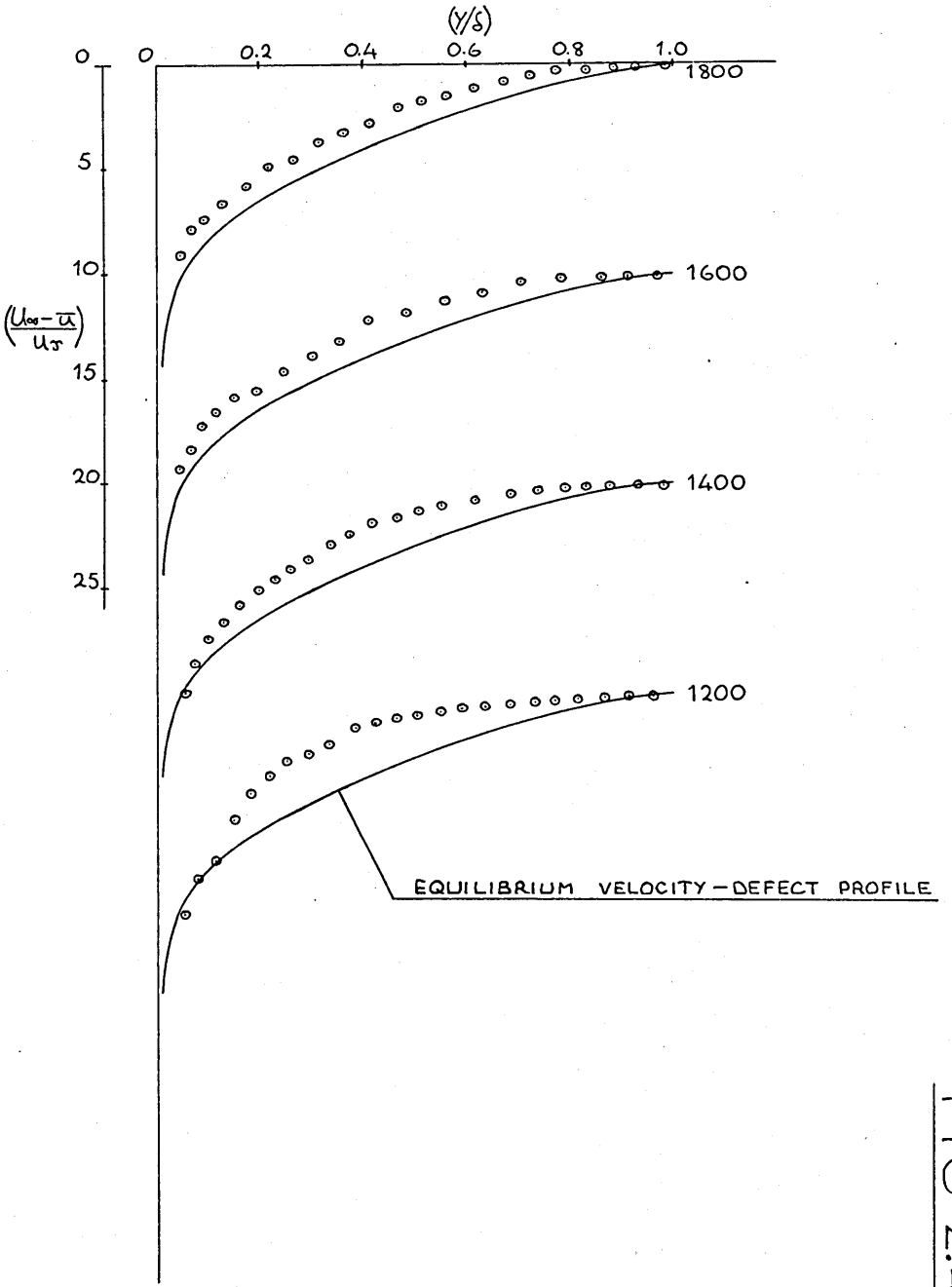

FIG 2.4

FLOW 2 — DEVELOPMENT OF SEMI-LOGARITHMIC VELOCITY PROFILE ALONG Z = -50

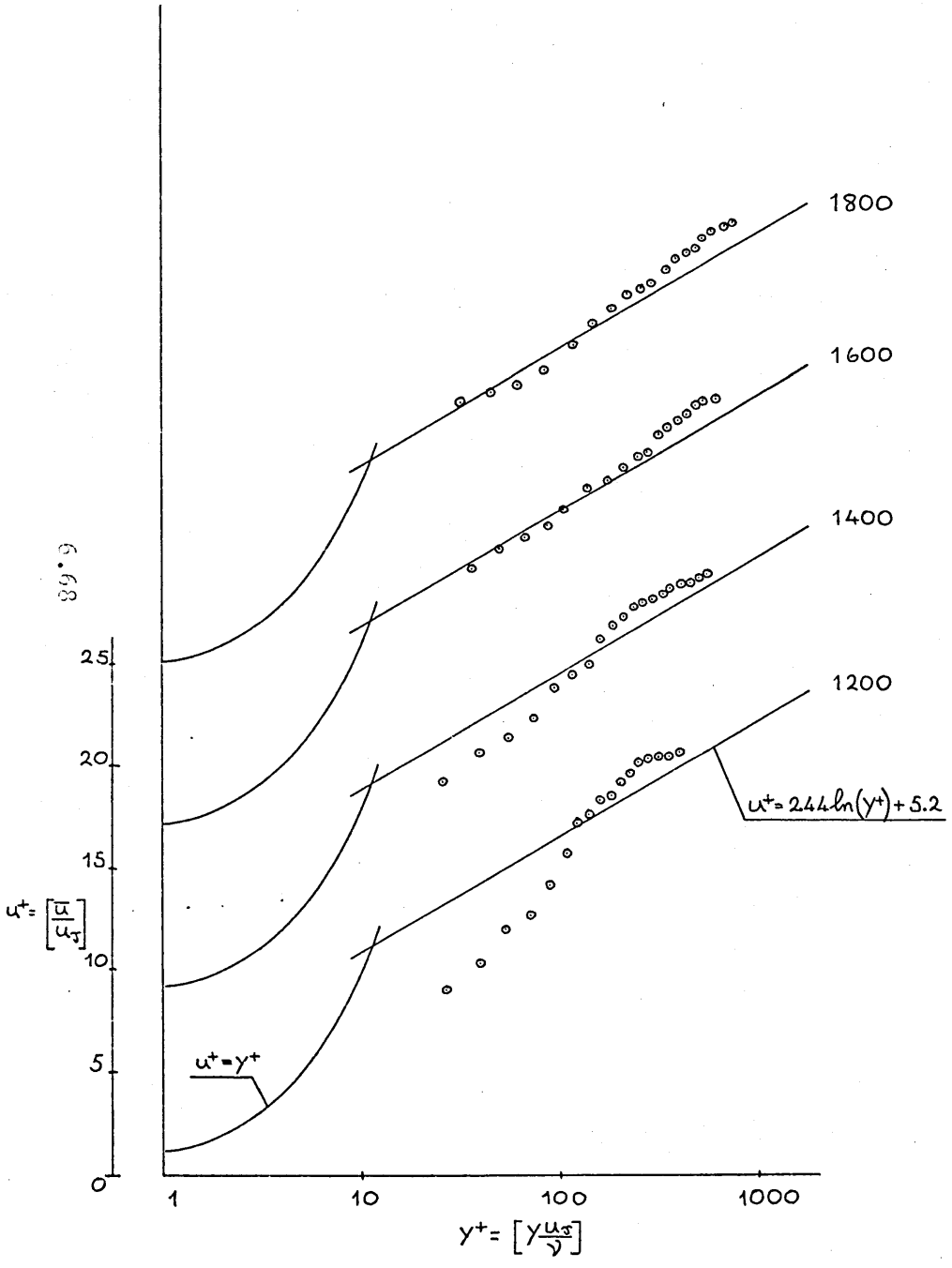

FLOW 2 — DEVELOPMENT OF VELOCITY-DEFECT PROFILE ALONG Z = -50

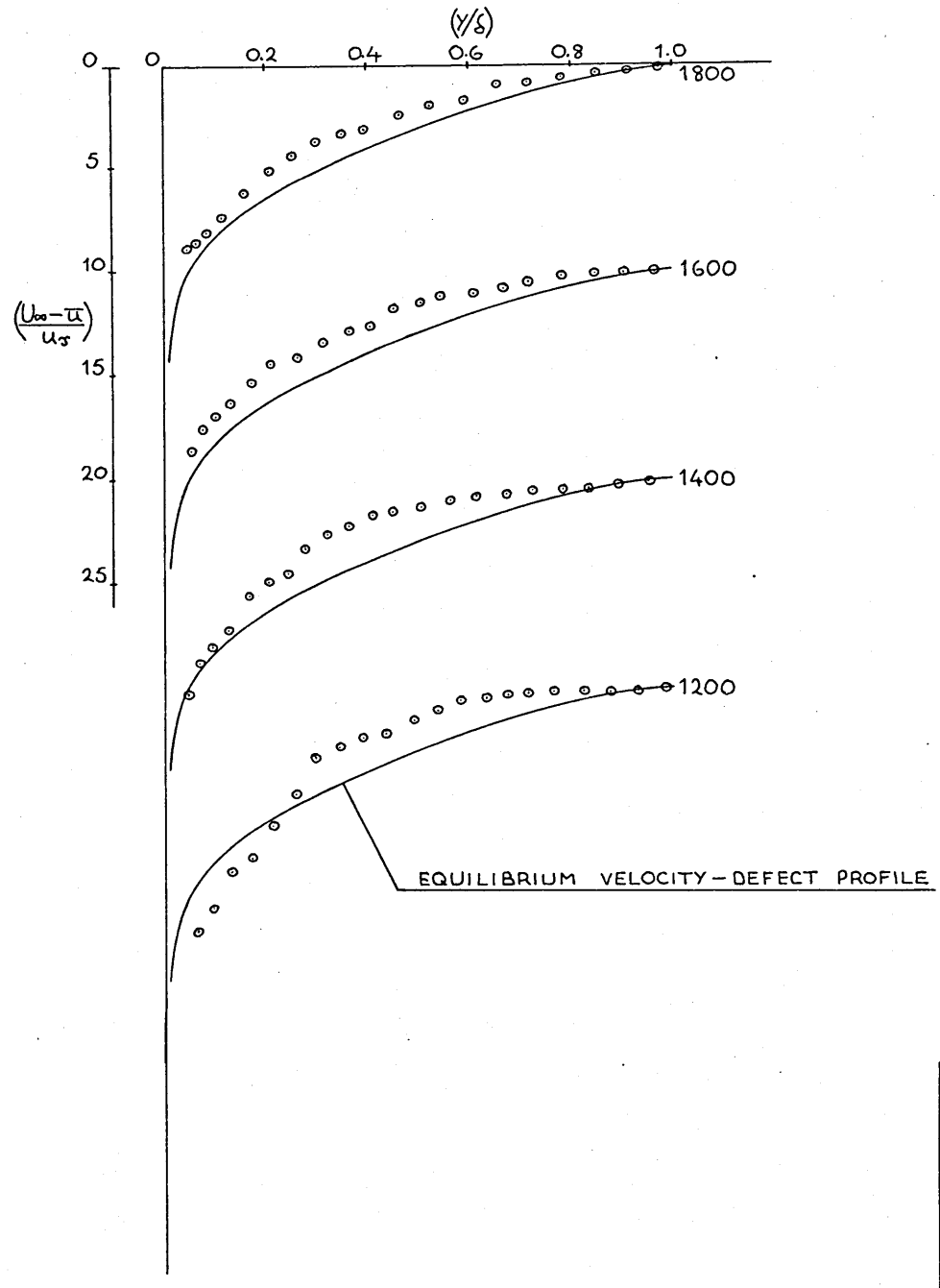

FIG 2.5

89·9

FIG. 2.6

FLOW 2 — DEVELOPMENT OF u' INTENSITY PROFILE ALONG Z = +50

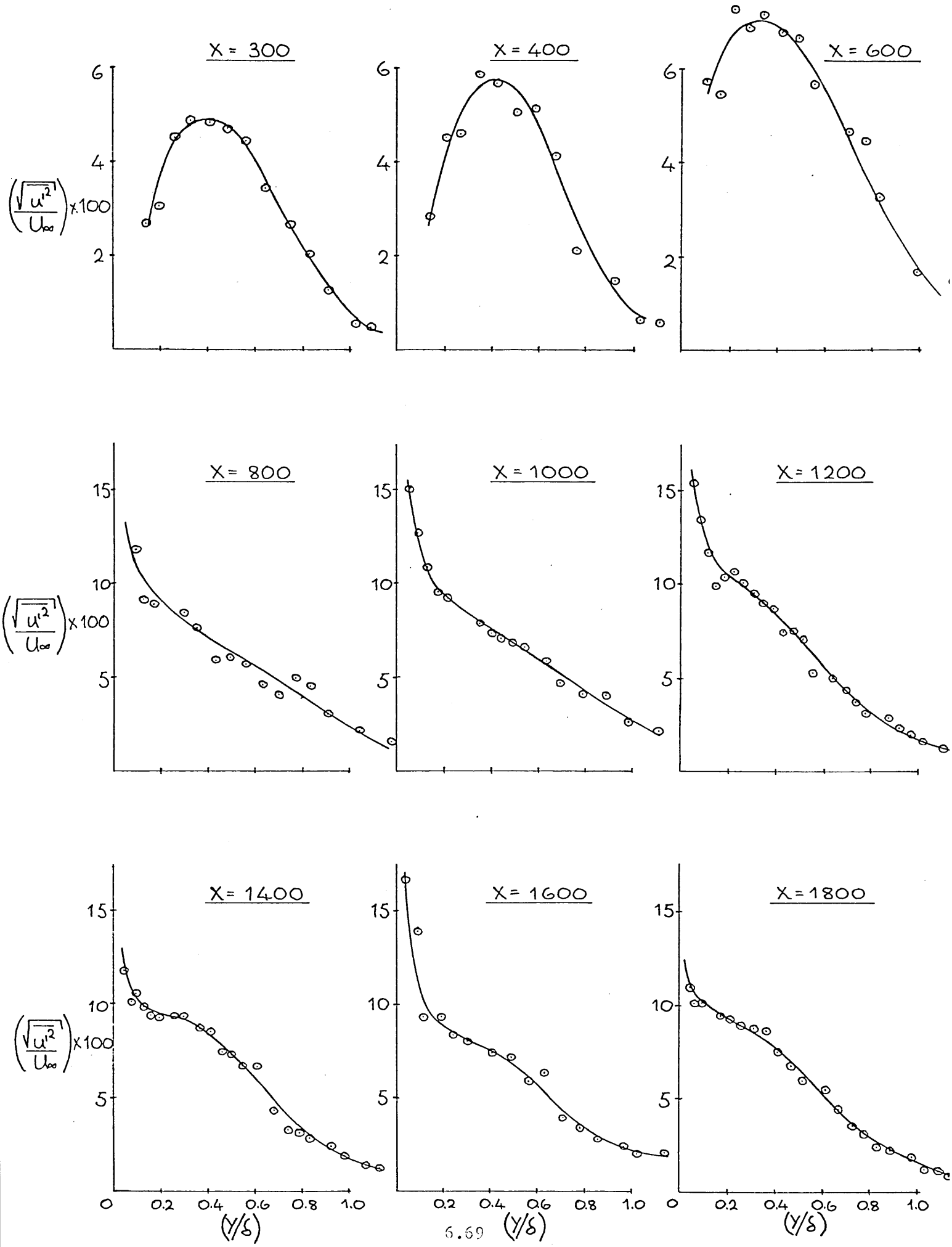

FIG. 2.7

FLOW 2 — DEVELOPMENT OF u' INTENSITY PROFILE ALONG Z = -50

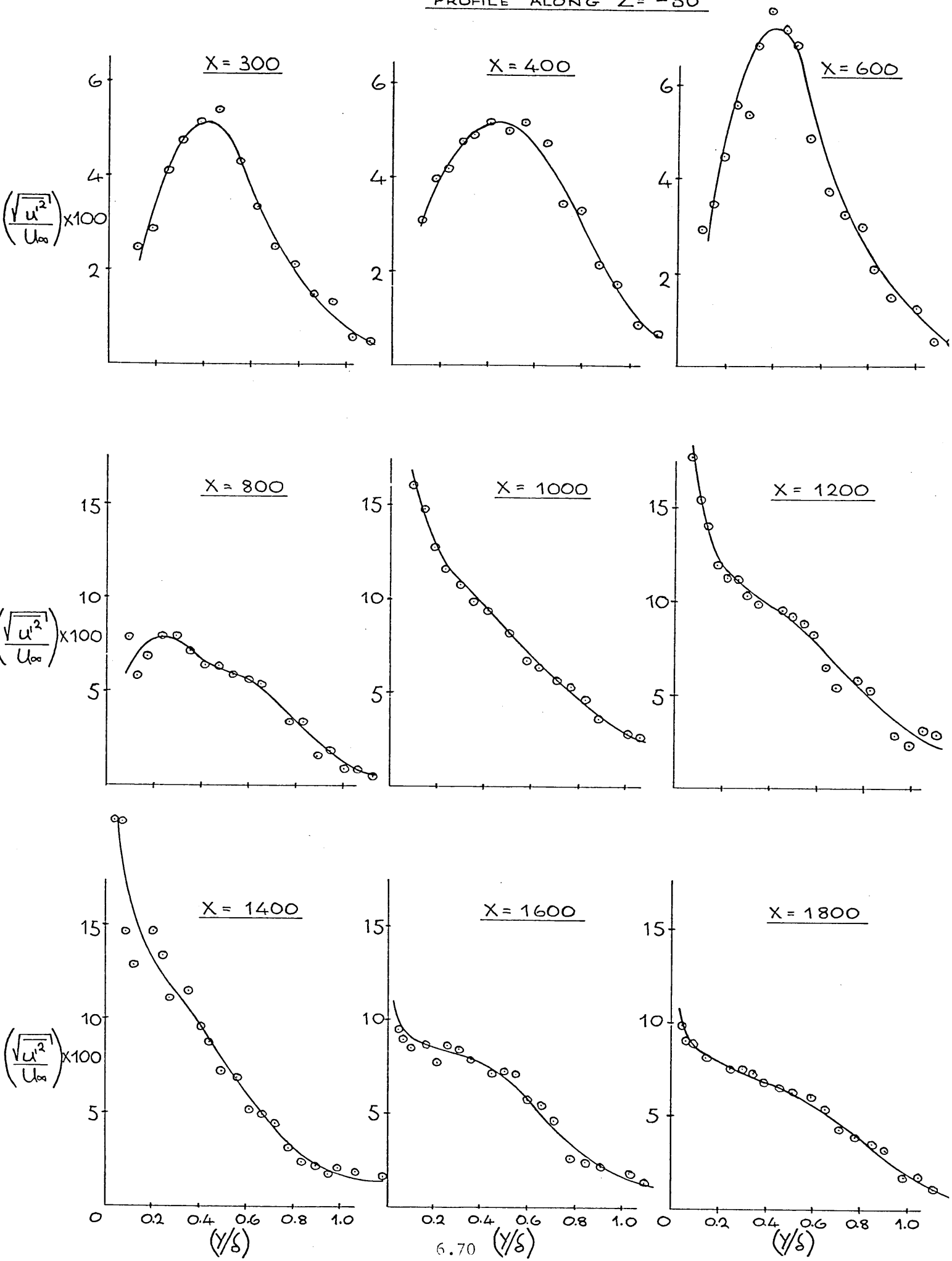

FIG. 2.8

FLOW 2 — DEVELOPMENT OF INTERMITTENCY PROFILE ALONG Z = +50

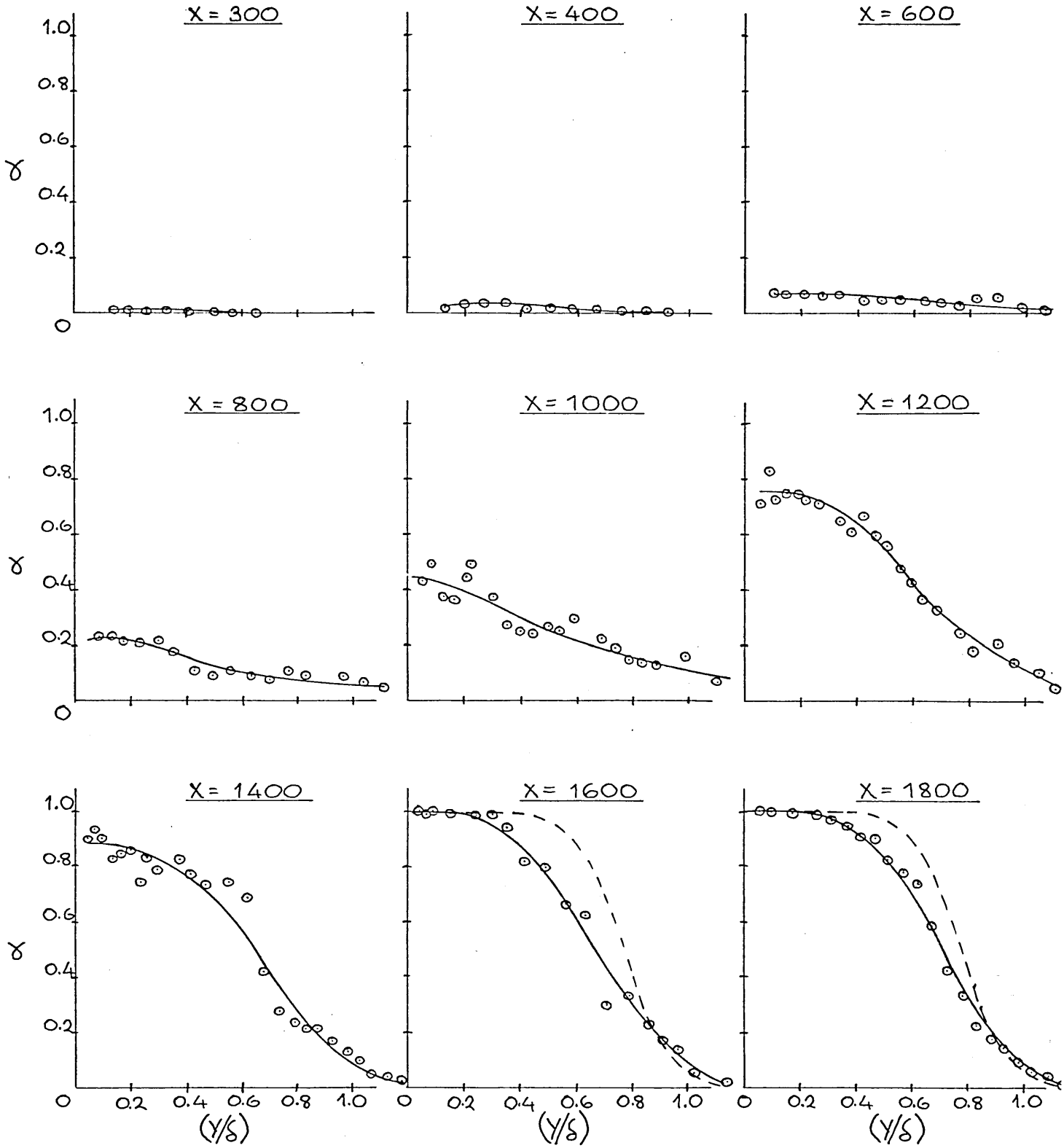

– – – – – $\gamma = \frac{1}{2}[1 - \text{erf}\, 5(Y/\delta - 0.78)]$

FIG. 2.9

FLOW 2 — DEVELOPMENT OF INTERMITTENCY PROFILE ALONG Z = −50

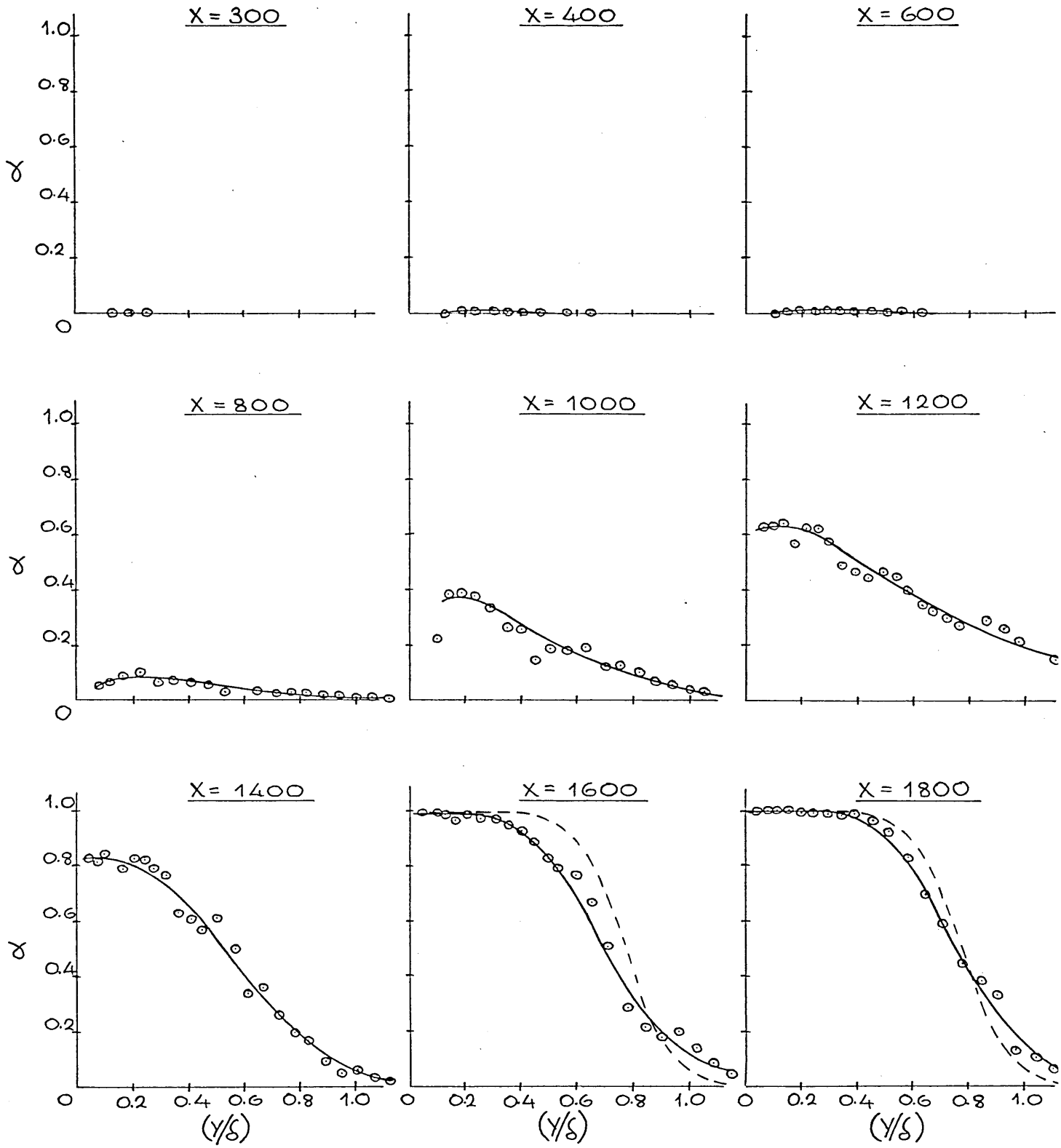

– – – – – $\gamma = \frac{1}{2}\left[1 - \text{erf}\, 5(Y/\delta - 0.78)\right]$

FLOW 2 - Secondary Data (Z = 50mm.)

	INTEGRAL PARAMETERS (mm.)				SHAPE FACTOR		SKIN FRICTION×1000			
Xmm	Delta	Displ	Mom	En	H12	H32	Cf.1	Cf.2	Cf.3	Cf.4
200	3.00	0.976	0.359	0.561	2.721	1.565	1.460	1.692		
300	3.52	1.176	0.437	0.685	2.693	1.569	1.271	1.514		
400	3.55	1.195	0.461	0.727	2.592	1.578	1.270	1.492		
600	4.67	1.523	0.603	0.951	2.527	1.579	1.094	1.291		
800	5.91	1.662	0.701	1.116	2.370	1.592	1.088	1.658		
1000	8.80	1.834	0.844	1.380	2.170	1.634	1.216	2.194		
1200	14.40	1.689	1.153	2.036	1.465	1.766	4.784	3.399		
1400	15.41	2.016	1.374	2.416	1.467	1.758	4.406	3.802		
1600	17.89	2.394	1.651	2.905	1.450	1.760	4.162	3.898		
1800	23.51	3.161	2.233	3.949	1.415	1.768	3.878	3.616		

Xmm	Momentum Balance		Intermittency (mean value)	Rtheta	Wake Parameter	Wake Strength Parameter
	PL.	PR.	$\bar{\gamma}$	Re	∂G	$\Delta\, u/u_\delta$
200	0.000	0.000	0.000	260	-	-
300	0.217	0.222	0.011	314	-	-
400	0.284	0.431	0.032	331	-	-
600	0.680	0.812	0.068	434	-	-
800	0.953	1.215	0.212	507	-	-
1000	1.351	1.741	0.427	609	-	-
1200	2.212	2.520	0.737	830	0.011	0.681
1400	2.827	3.536	0.911	992	0.172	1.178
1600	3.600	4.618	0.998	1189	0.240	1.574
1800	5.220	5.675	1.000	1607	0.283	1.668

Standard Deviation of Intermittency Distribution = ∇ = 289mm.

$(X_{\bar{\gamma}=0.75} - X_{\bar{\gamma}=0.25}) = \lambda$ = 380mm.

$R_\nabla = 2.08\times10^5$

$R_\lambda = 2.736\times10^5$

NB. Cf.1 - from velocity profile ie. average du/dy or Log-law
Cf.2 - equation
No Preston tube readings are applicable for this flow.

FLOW 2 - Secondary Data (Z = -50mm.)

	INTEGRAL PARAMETERS (mm.)				SHAPE FACTOR		SKIN FRICTION×1000			
Xmm	Delta	Displ	Mom	En	H12	H32	Cf.1	Cf.2	Cf.3	Cf.4
200	3.03	1.056	0.374	0.580	2.826	1.553	1.380	1.630		
300	3.70	1.221	0.457	0.716	2.676	1.569	1.199	1.347		
400	3.97	1.337	0.524	0.822	2.554	1.570	1.198	1.197		
600	4.97	1.579	0.621	0.981	2.542	1.579	1.013	1.024		
800	5.82	1.859	0.738	1.168	2.521	1.584	0.900	1.070		
1000	7.85	1.938	0.905	1.477	2.142	1.632	1.083	1.812		
1200	11.46	1.696	1.083	1.860	1.567	1.718	4.699	2.885		
1400	17.05	2.228	1.533	2.704	1.453	1.763	4.334	3.333		
1600	20.45	2.639	1.853	3.280	1.424	1.770	4.101	3.790		
1800	23.29	3.272	2.326	4.143	1.407	1.773	3.864	3.595		

Xmm	Momentum Balance		Intermittency (mean value)	Rtheta	Wake Parameter	Wake Strength Parameter
	PL.	PR.	$\bar{\gamma}$	Re	∂G	$\Delta\, u/u_\delta$
200	0.000	0.000	0.000	270	-	-
300	0.222	0.197	0.002	329	-	-
400	0.401	0.366	0.006	377	-	-
600	0.660	0.659	0.010	447	-	-
800	0.973	0.928	0.071	533	-	-
1000	1.420	1.301	0.342	651	-	-
1200	1.896	1.933	0.617	782	0.166	1.568
1400	3.099	2.771	0.814	1105	0.163	1.161
1600	3.955	3.731	0.990	1335	0.210	1.356
1800	5.219	4.732	1.000	1674	0.297	1.488

Standard Deviation of Intermittency Distribution = ∇ = 274mm.

$(X_{\bar{\gamma}=0.75} - X_{\bar{\gamma}=0.25}) = \lambda$ = 365mm.

$R_\nabla = 1.973\times10^5$

$R_\lambda = 2.628\times10^5$

NB. Cf.1 - from velocity profile ie. average du/dy or Log-law
Cf.2 - equation
No Preston tube readings are applicable for this flow.

FIG 2.10

FLOW 2 — STREAMWISE DEVELOPMENT OF INTEGRAL PARAMETERS ALONG Z = +50

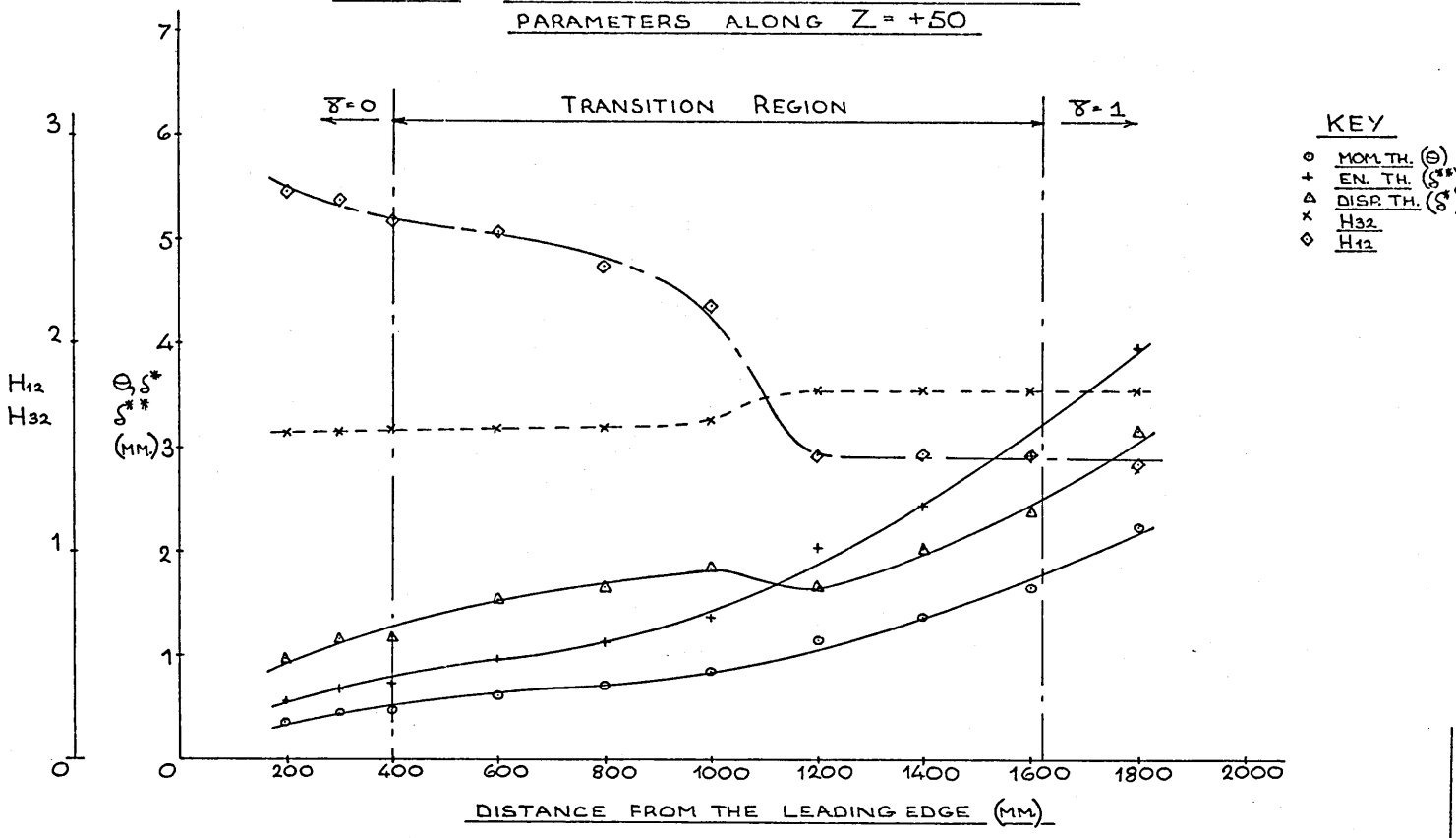

FIG.

FLOW 2 — VARIATION OF SKIN FRICTION CO-EFFICIENT ALONG Z = +50

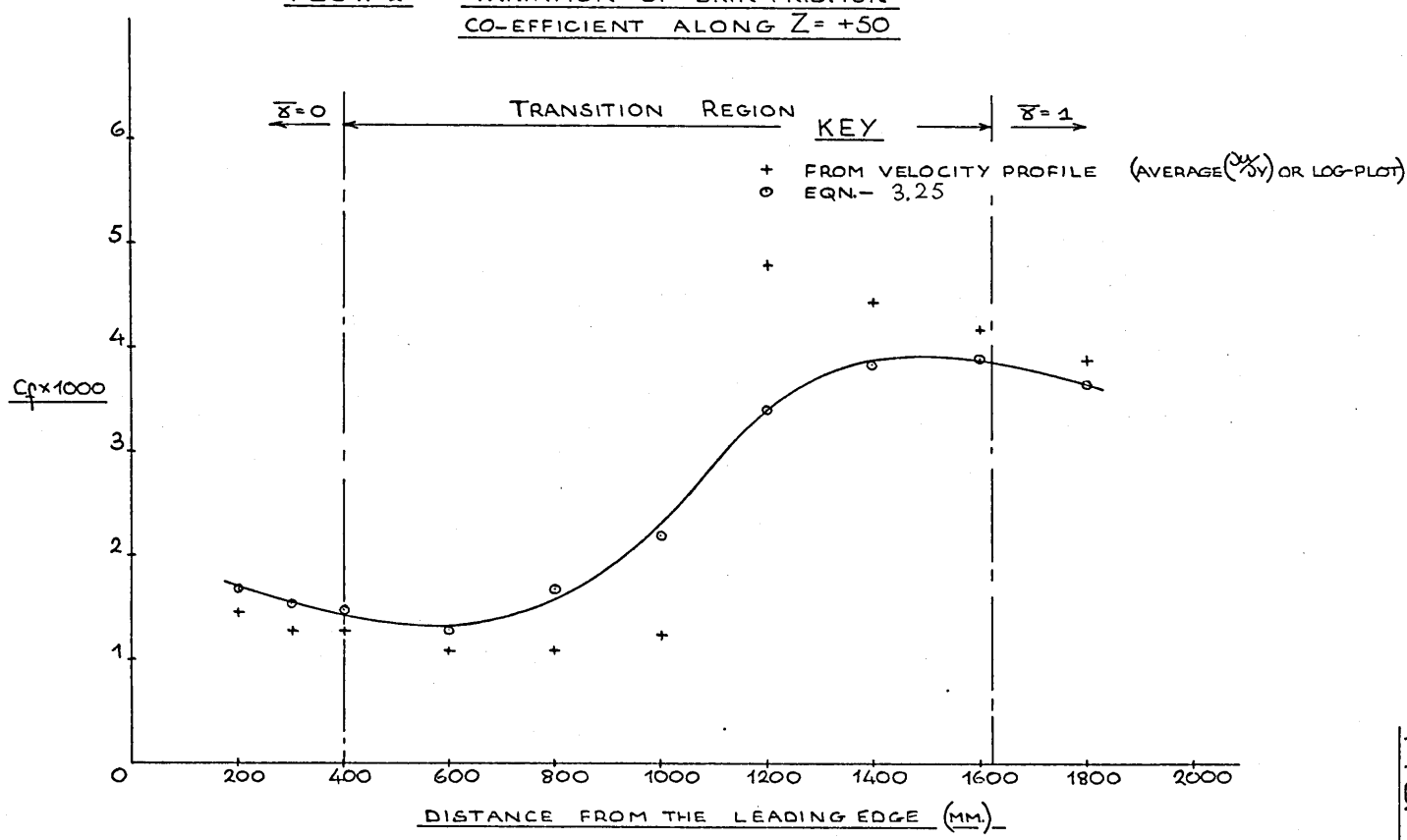

FIG.

FLOW 2 — STREAMWISE DEVELOPMENT OF INTEGRAL PARAMETERS ALONG Z = -50

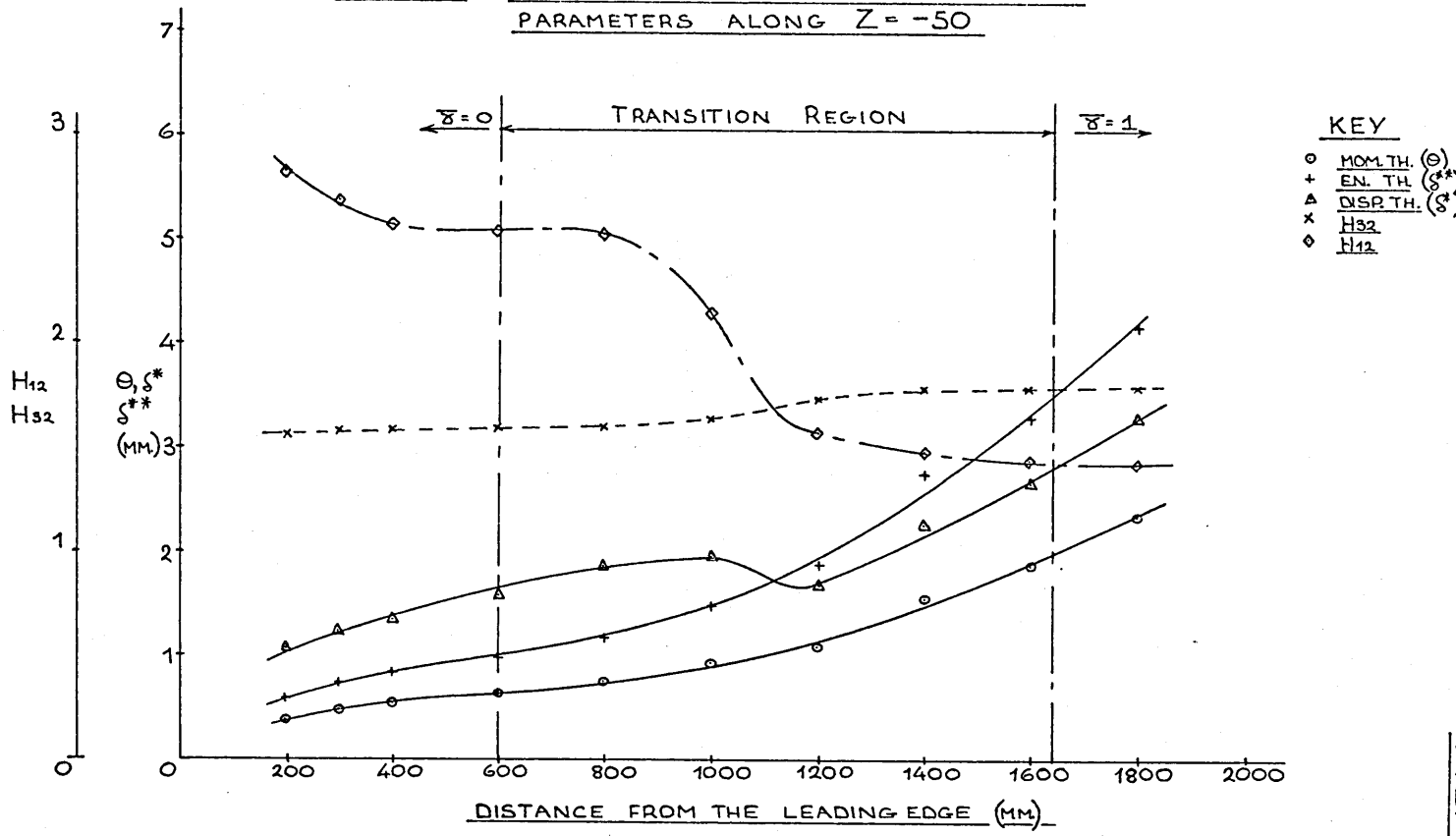

FIG.

FLOW 2 — VARIATION OF SKIN FRICTION CO-EFFICIENT ALONG Z = -50

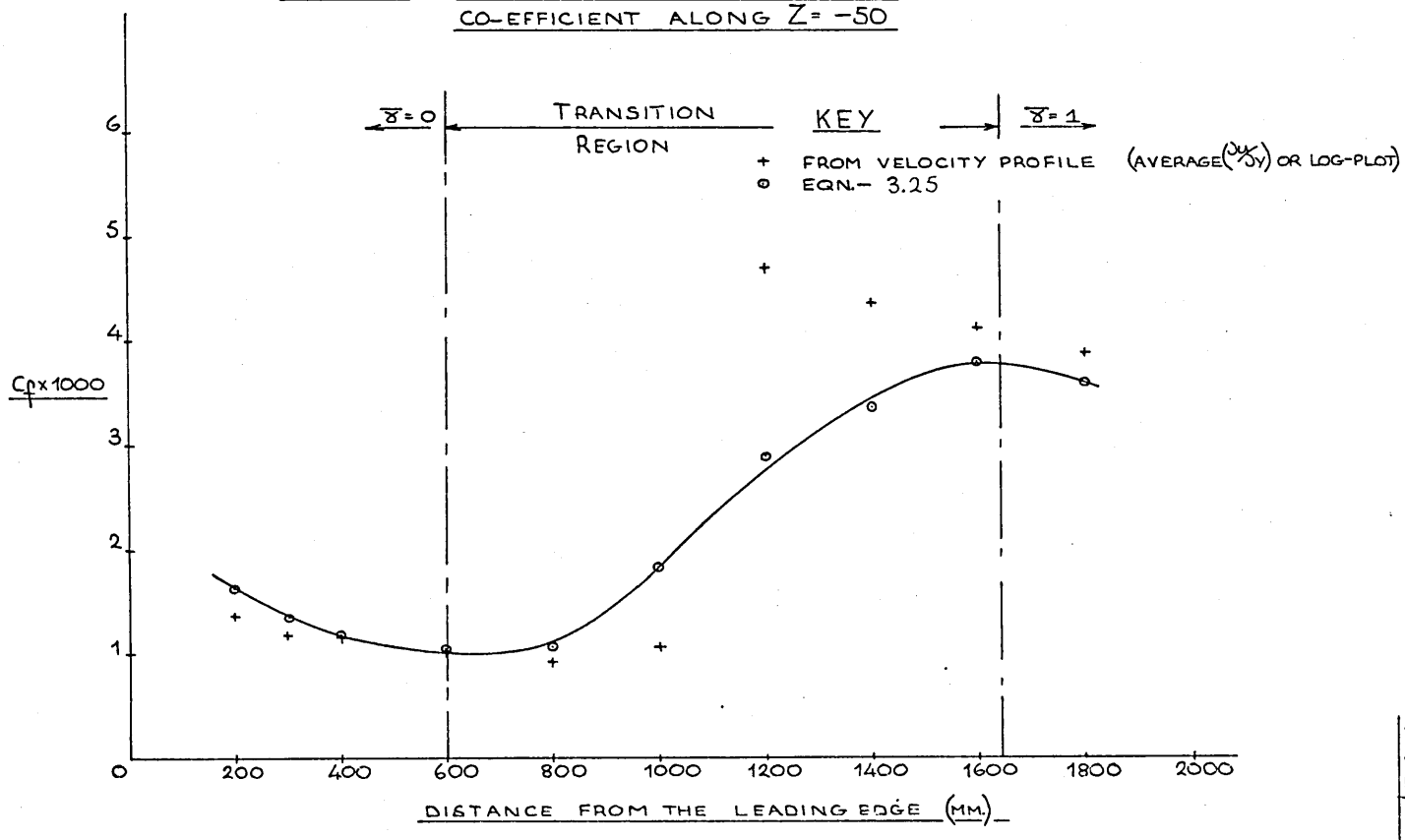

FIG.

FIG. 2.13

FLOW 2 — ENTRAINMENT RATE ALONG Z = +50

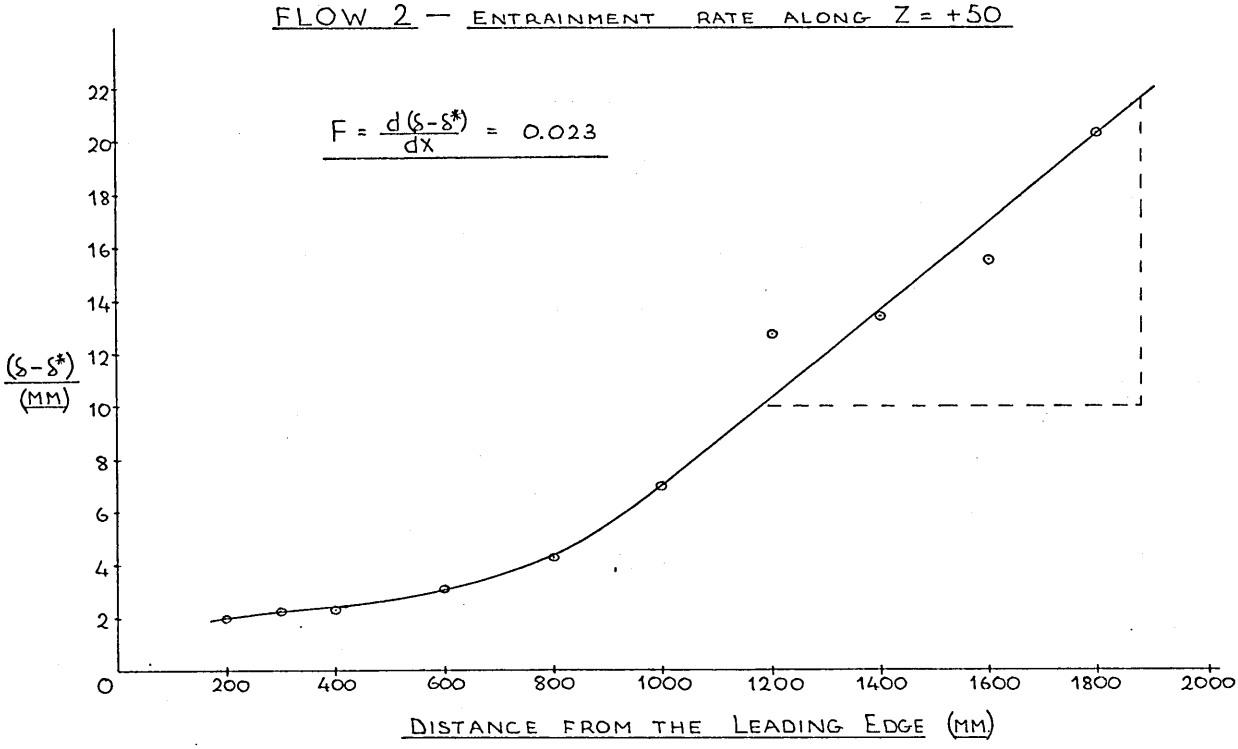

FLOW 2 — ENTRAINMENT RATE ALONG Z = -50

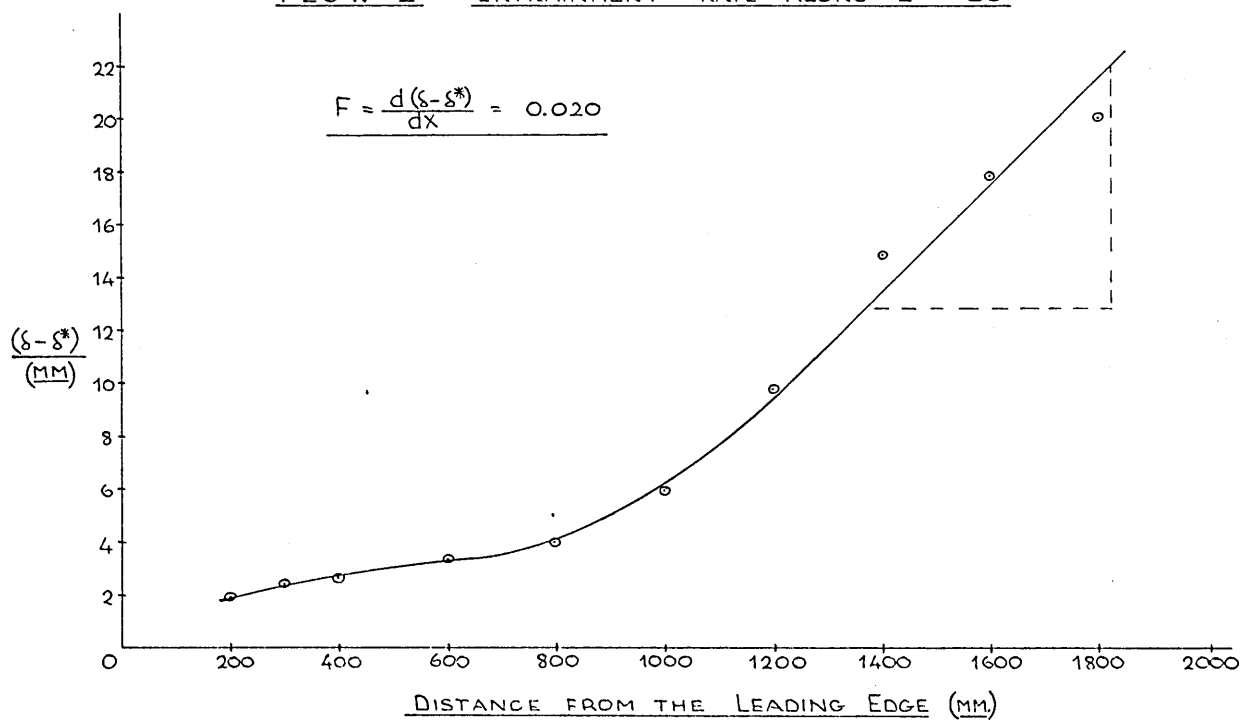

STREAMWISE DEVELOPMENT OF "NEAR" WALL INTERMITTENCY

FLOW 2 Z= +50

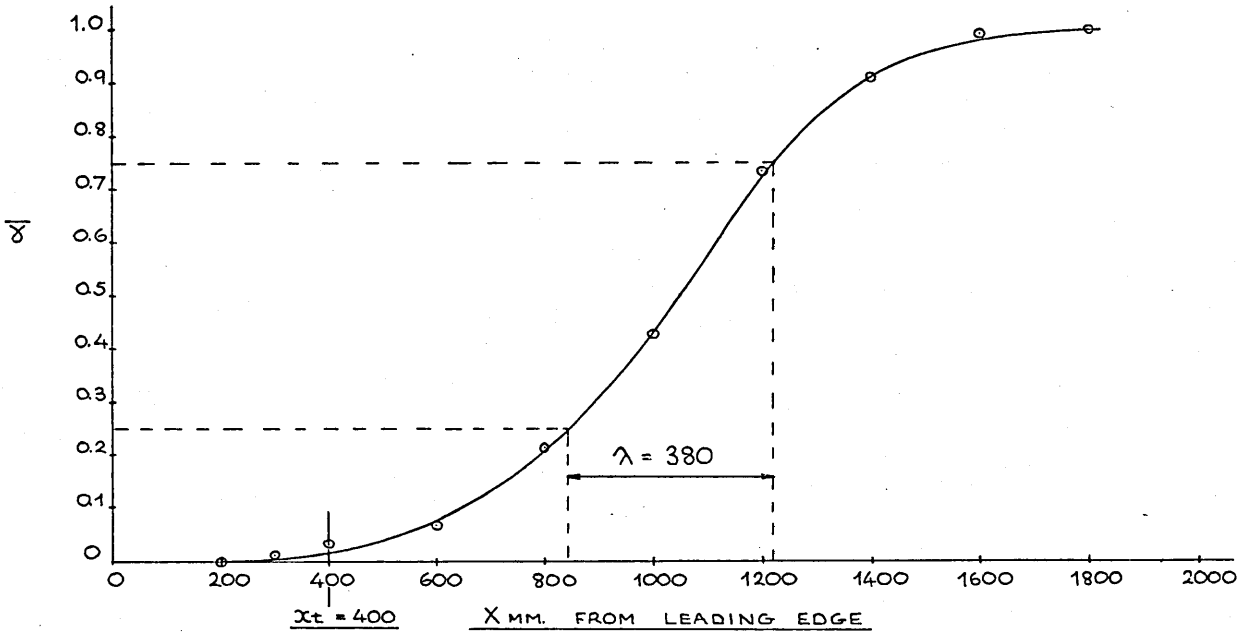

FIG.

STREAMWISE DEVELOPMENT OF "NEAR" WALL INTERMITTENCY

FLOW 2 Z= -50

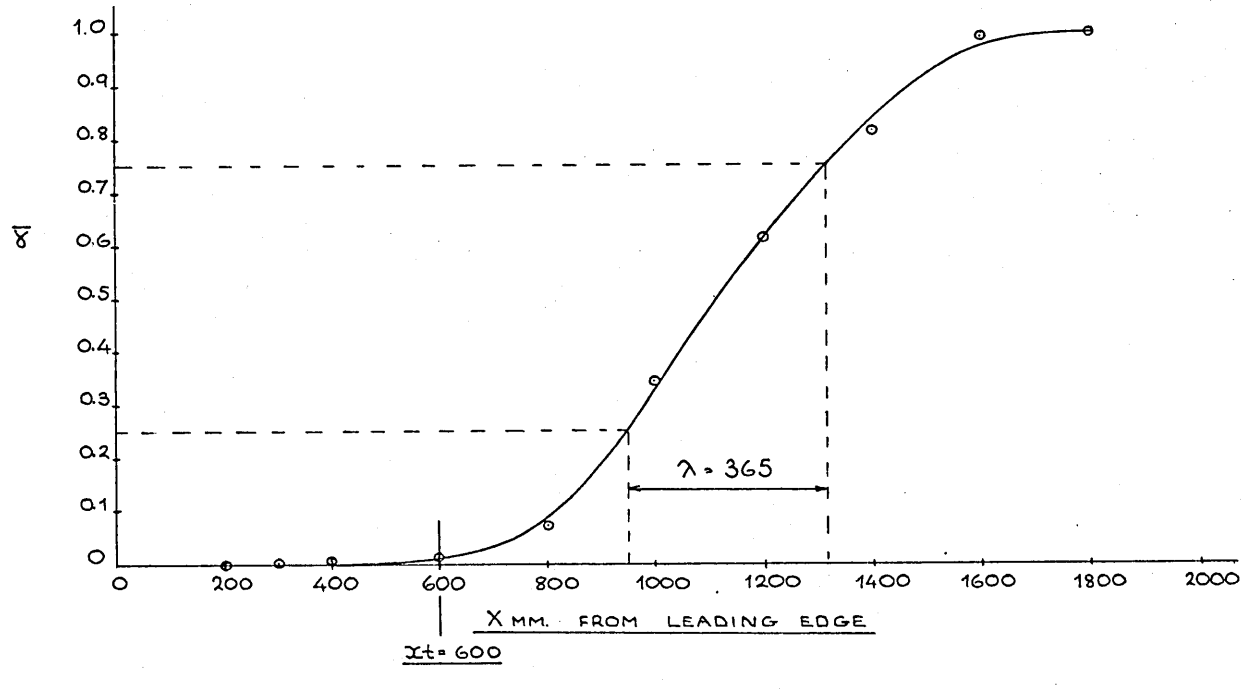

FIG.

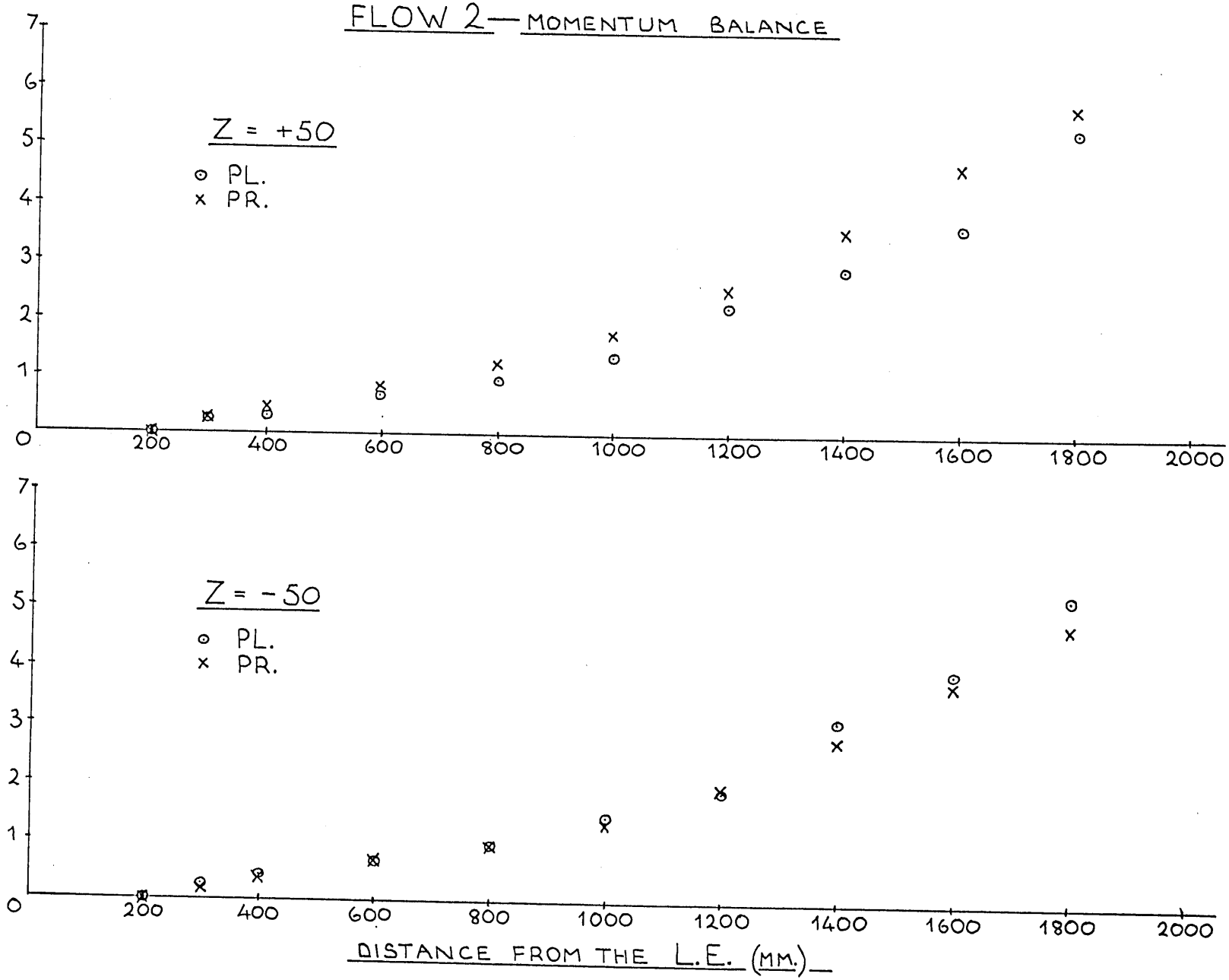
FLOW 2— MOMENTUM BALANCE
Z = +50
PL.
PR.
Z = -50
PL.
PR.
0
1
2
3
4
5
6
7
200
400
600
800
1000
1200
1400
1600
1800
2000
DISTANCE FROM THE L.E. (MM.)

FIG. 2.15

FIG. 2.16

FLOW 2— APPROACH TO EQUILIBRIUM

KEY
⊙ Z= 50
+ Z= -50

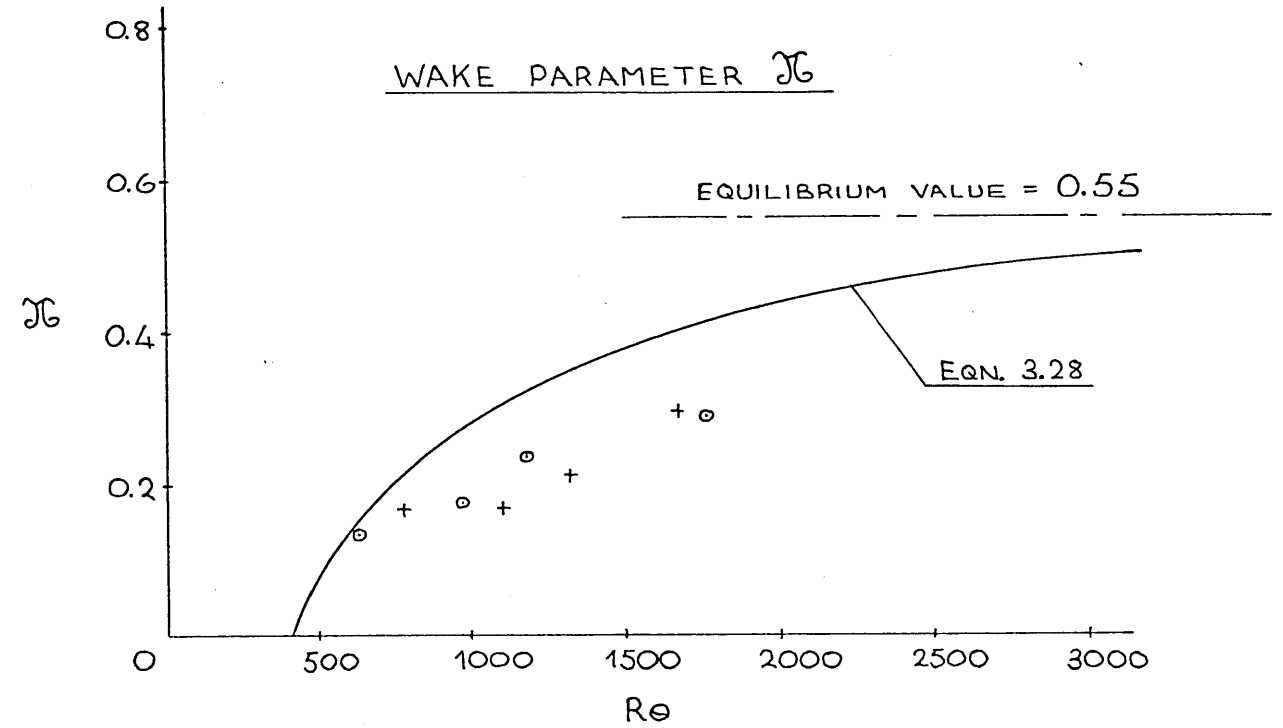

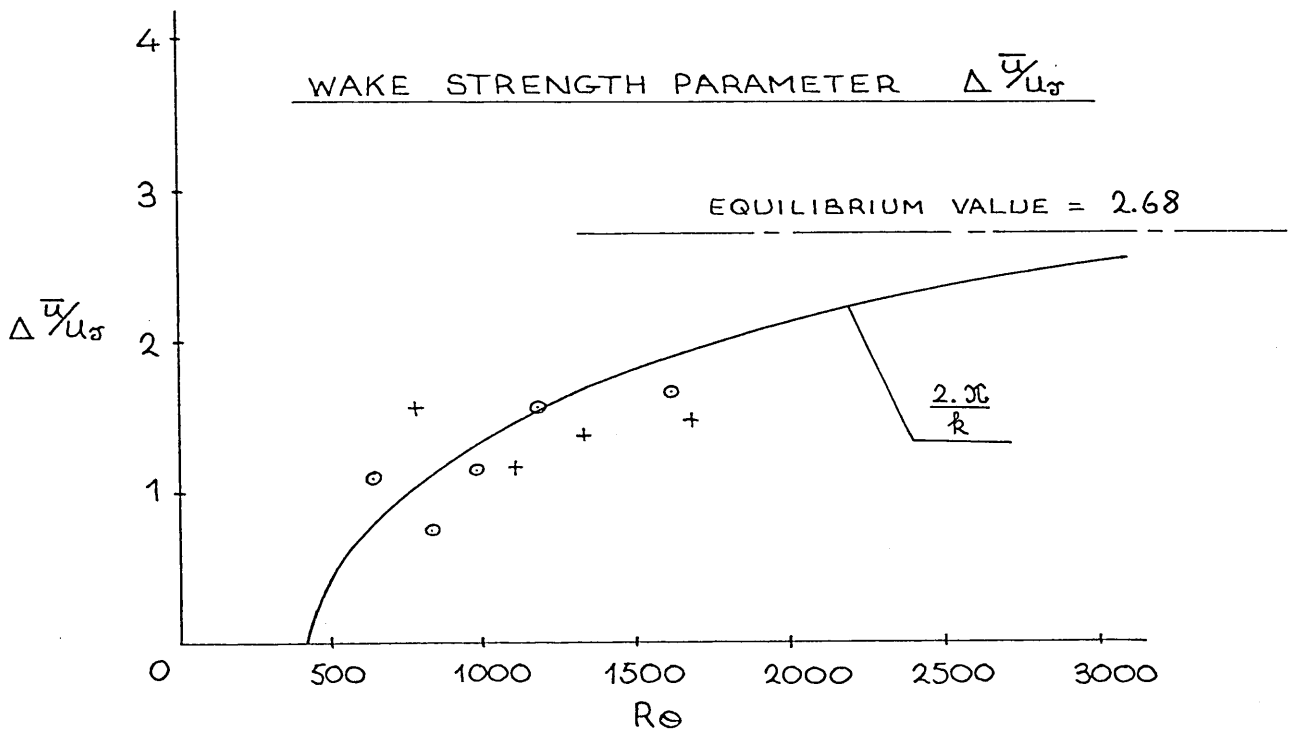

FIG. 2.17

FLOW 2 —

BOUNDARY LAYER PROFILES AT X= 200 MM.

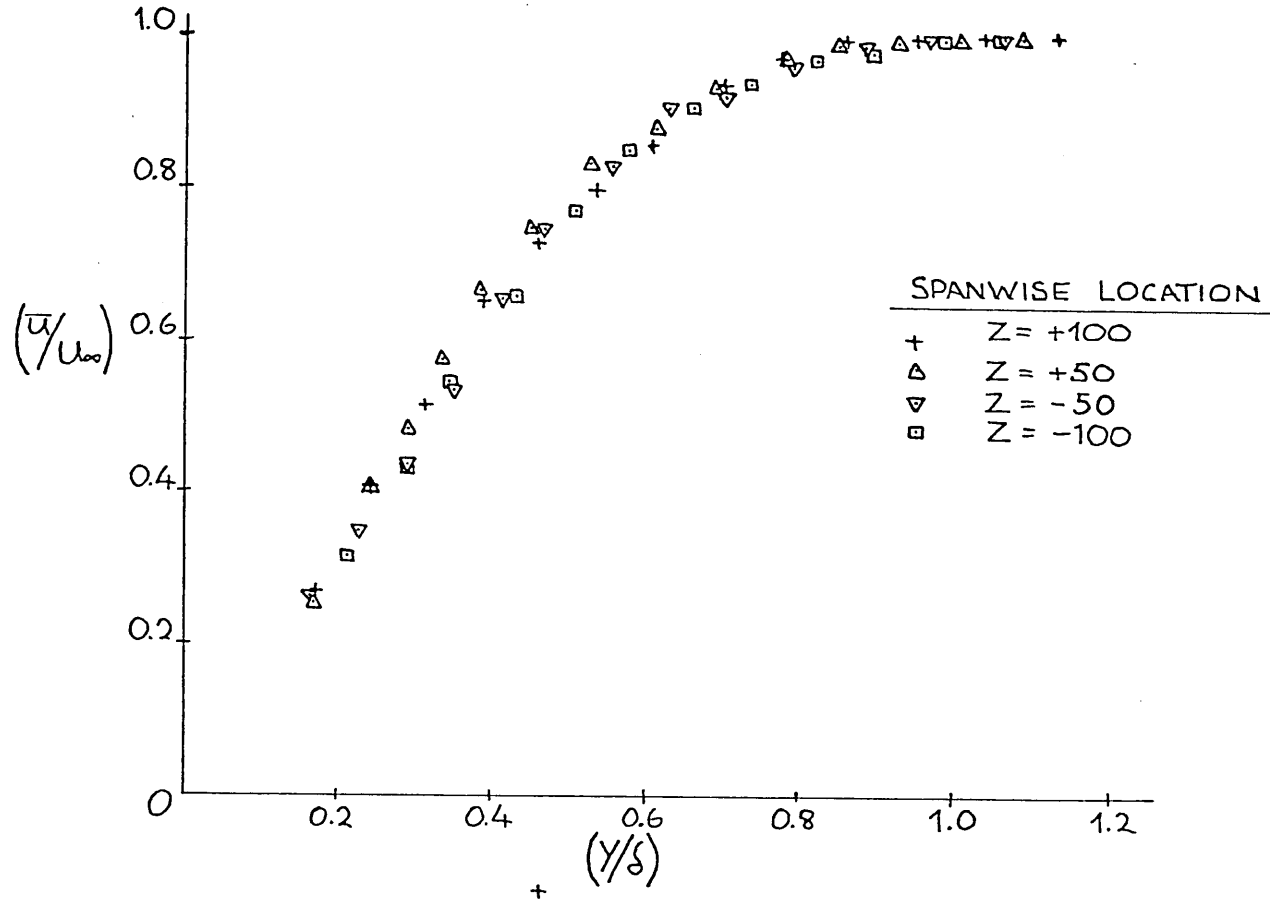

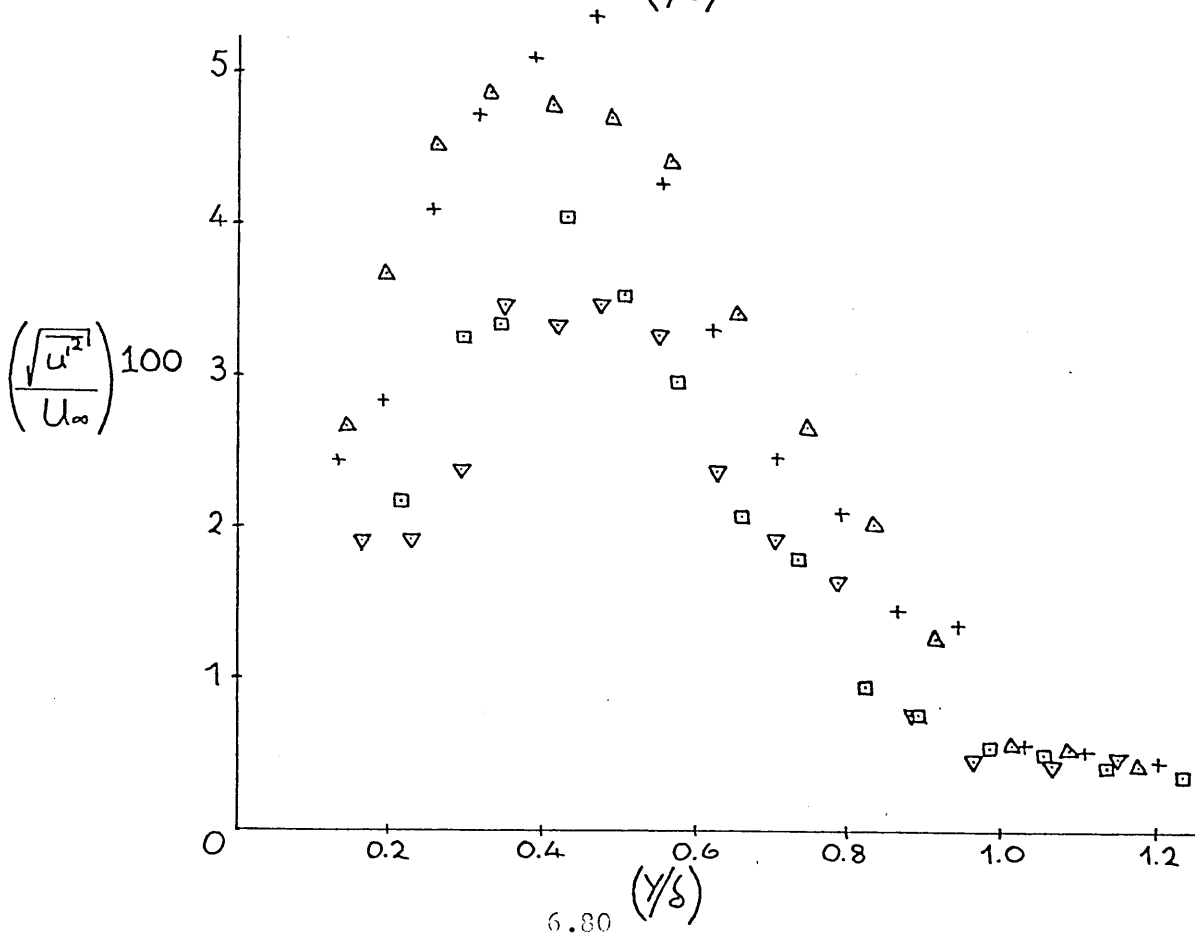

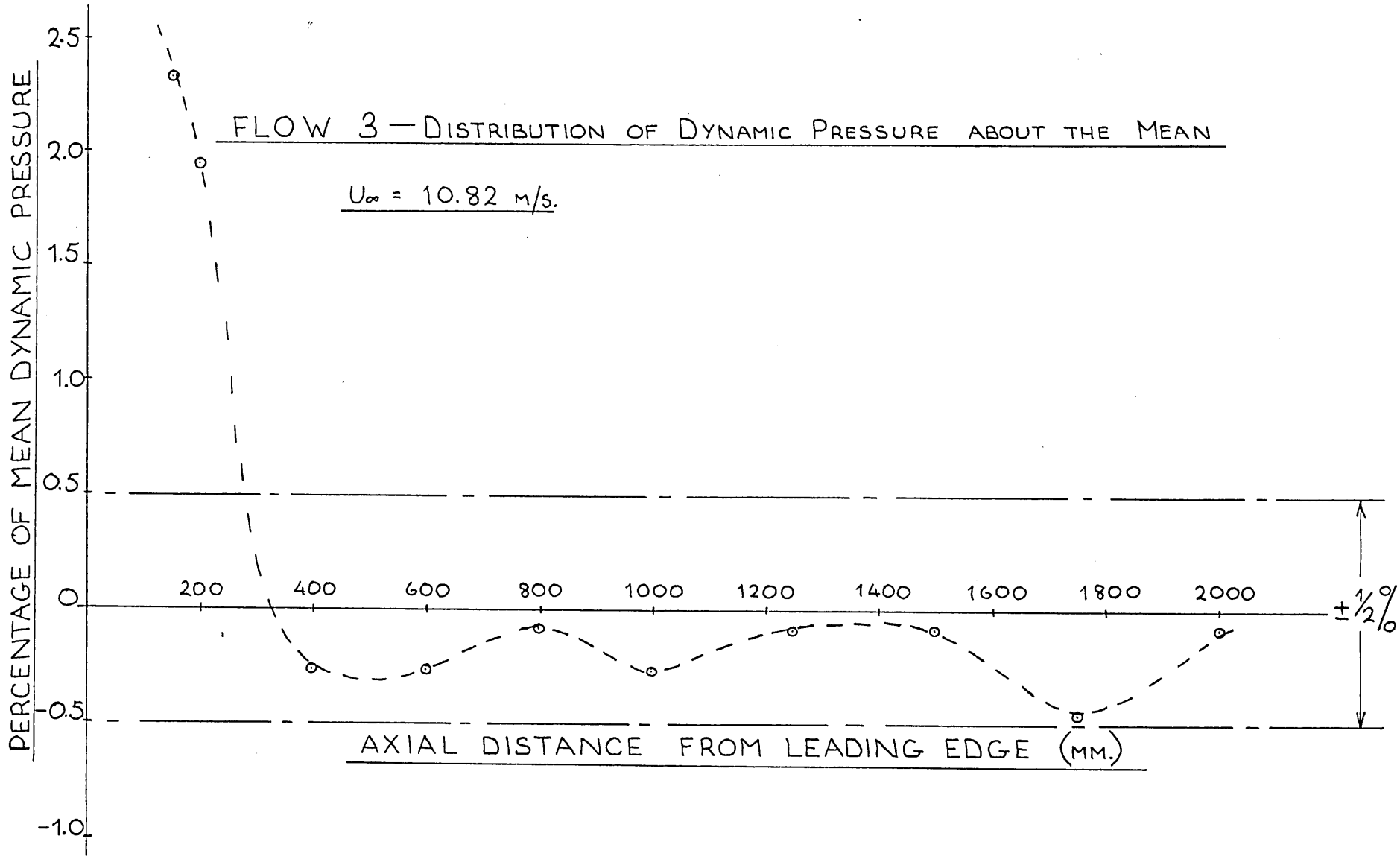
FLOW 3 — DISTRIBUTION OF DYNAMIC PRESSURE ABOUT THE MEAN
U_∞ = 10.82 m/s.
PERCENTAGE OF MEAN DYNAMIC PRESSURE
2·5
2·0
1·5
1·0
0·5
0
-0·5
-1·0
200
400
600
800
1000
1200
1400
1600
1800
2000
AXIAL DISTANCE FROM LEADING EDGE (MM.)
± ½%

FIG. 3.1

FLOW 3 — DEVELOPMENT OF MEAN VELOCITY PROFILE ALONG Z = -50

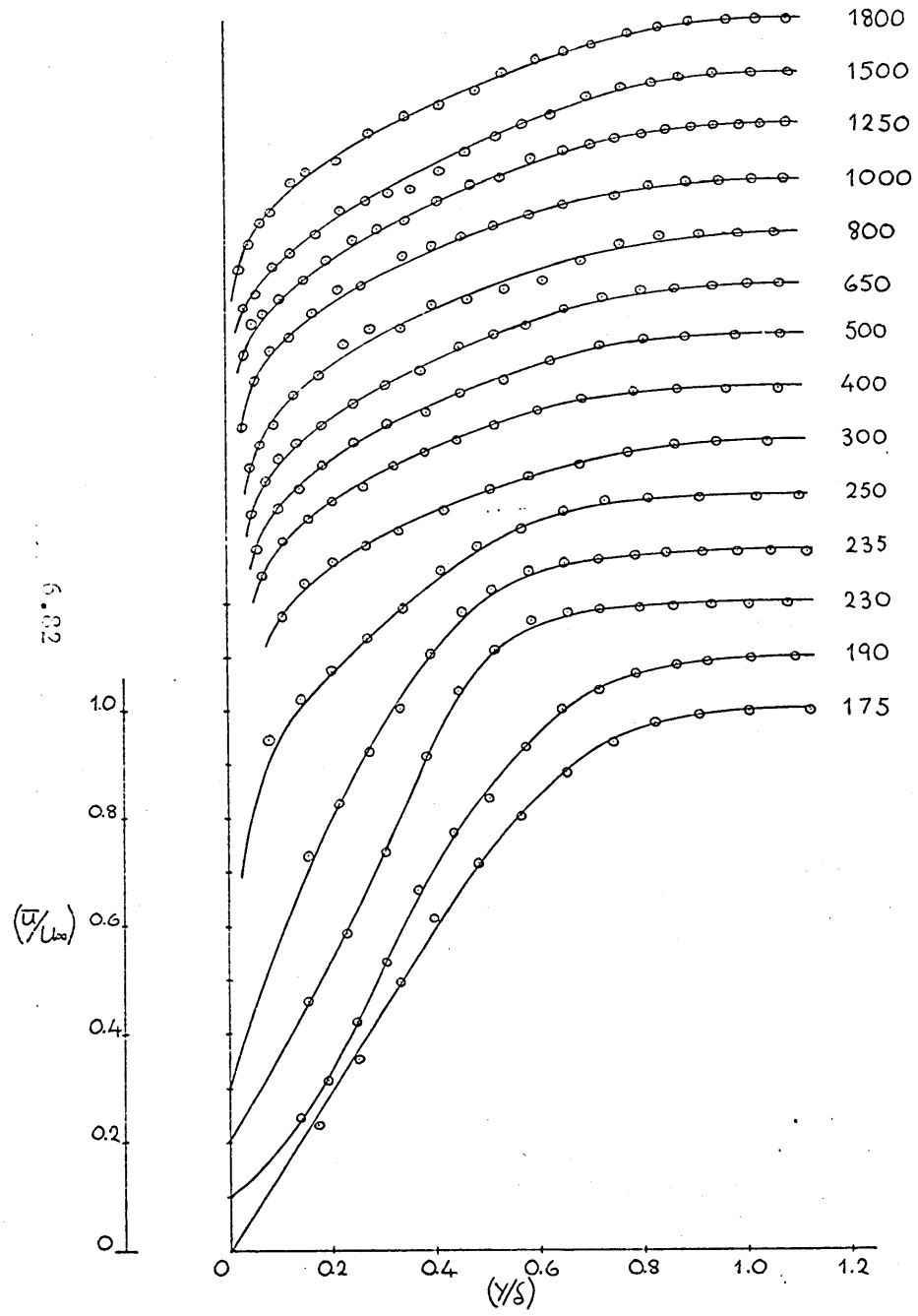

FLOW 3 — DEVELOPMENT OF (u'/U_∞) PROFILE ALONG Z = -50

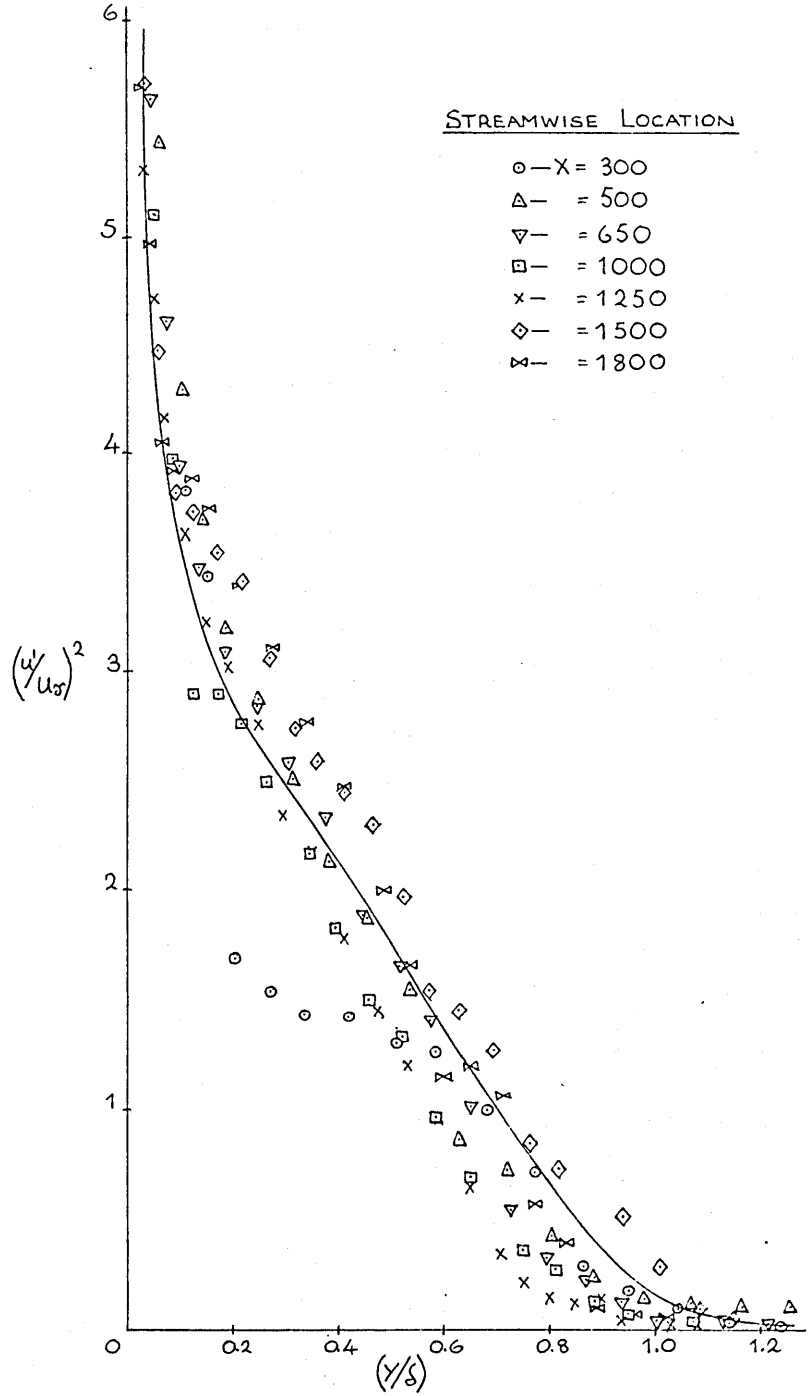

6.82

FIG 3.2

FLOW 3 — DEVELOPMENT OF SEMI-LOGARITHMIC VELOCITY PROFILE ALONG Z = -50

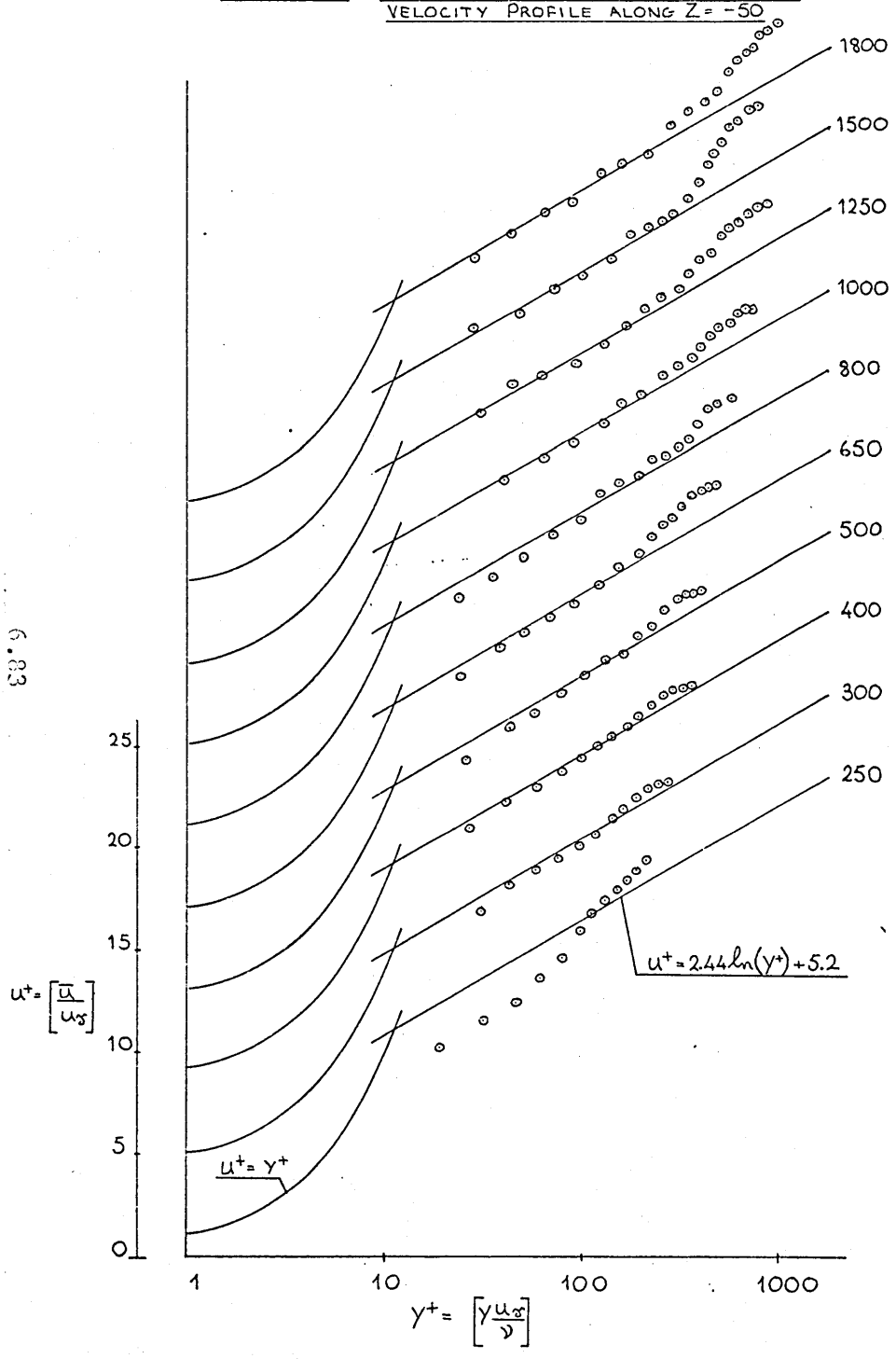

FLOW 3 — DEVELOPMENT OF VELOCITY DEFECT PROFILE ALONG Z = -50

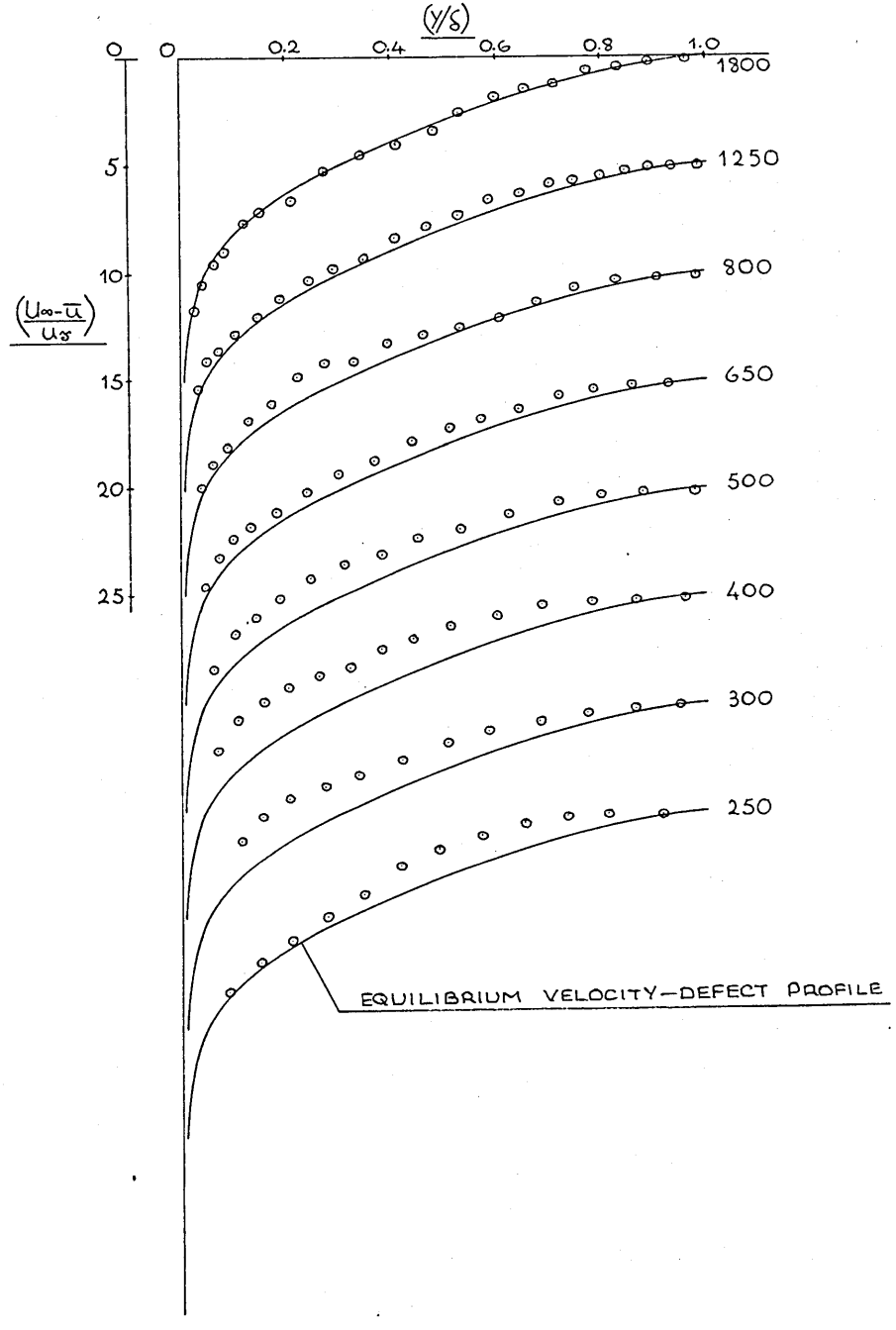

FIG 3.3

FIG. 3.4

FLOW 3 — DEVELOPMENT OF u' INTENSITY PROFILE ALONG Z = -50

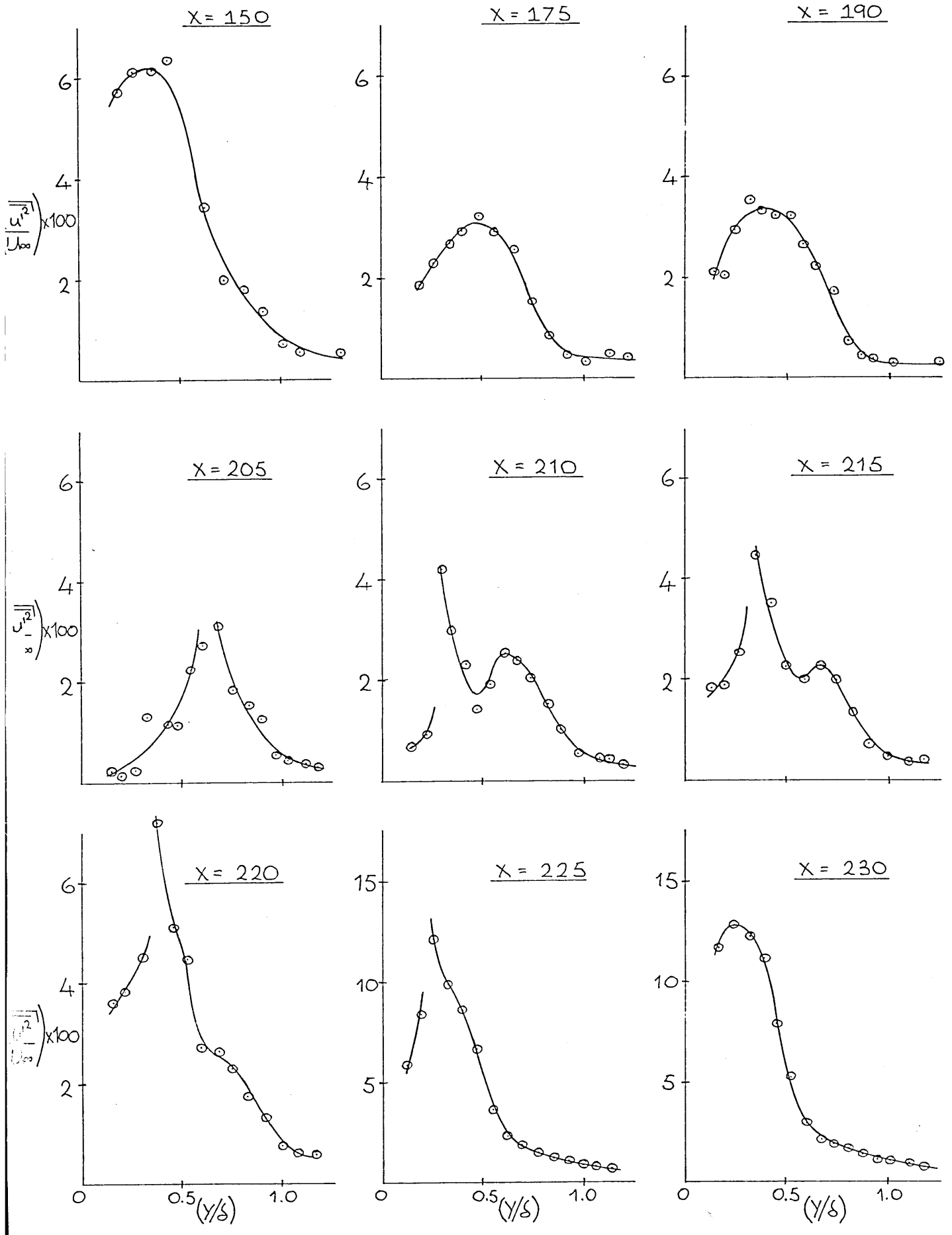

FIG. 3.5

FLOW 3 – DEVELOPMENT OF u' INTENSITY PROFILE ALONG Z = -50

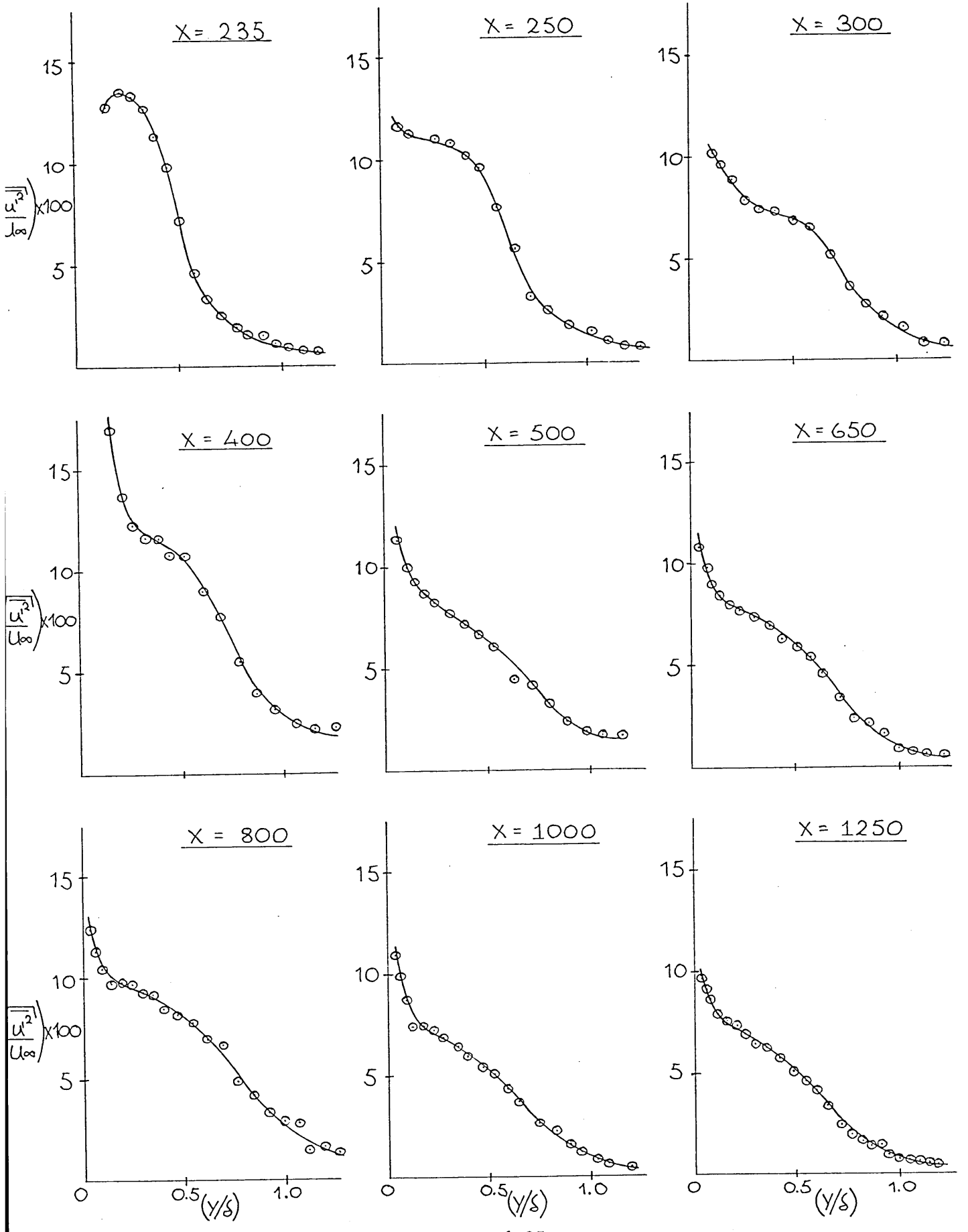

FIG. 3.6

FLOW 3 — DEVELOPMENT OF u' INTENSITY PROFILE ALONG Z = -50

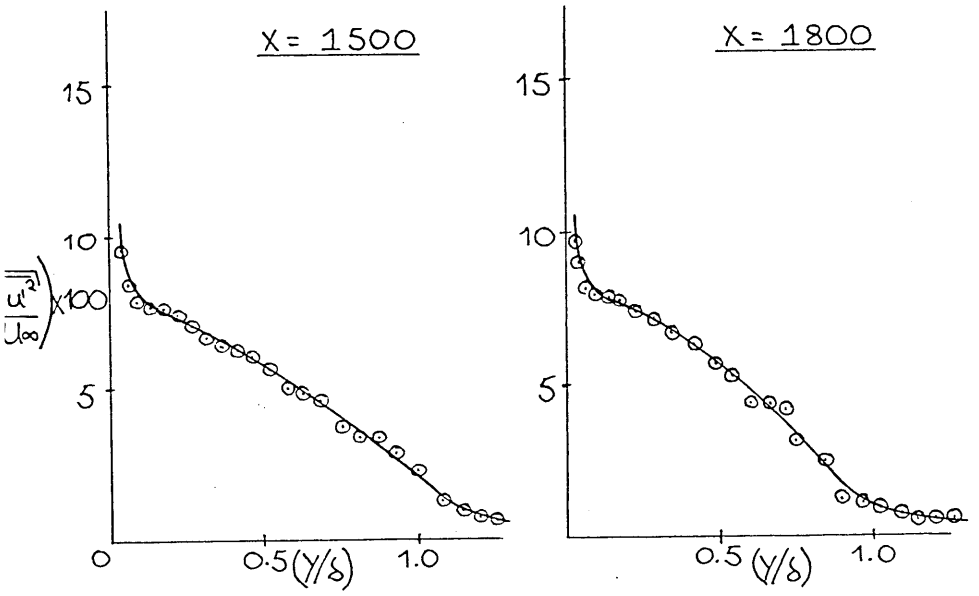

FIG. 3.7

FLOW 3 – DEVELOPMENT OF INTERMITTENCY PROFILE ALONG Z = -50

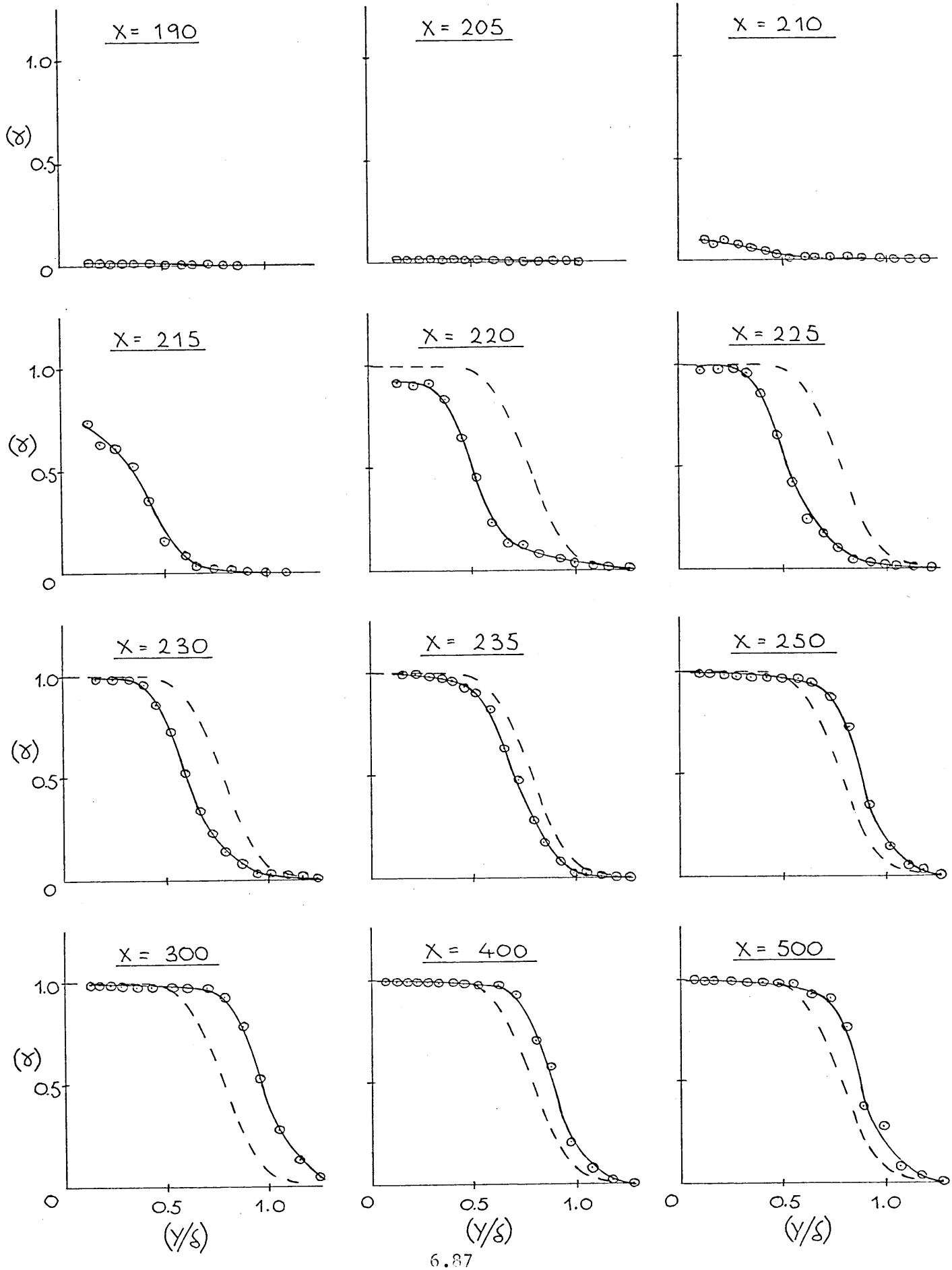

FLOW 3 — DEVELOPMENT OF INTERMITTENCY PROFILE ALONG Z = -50

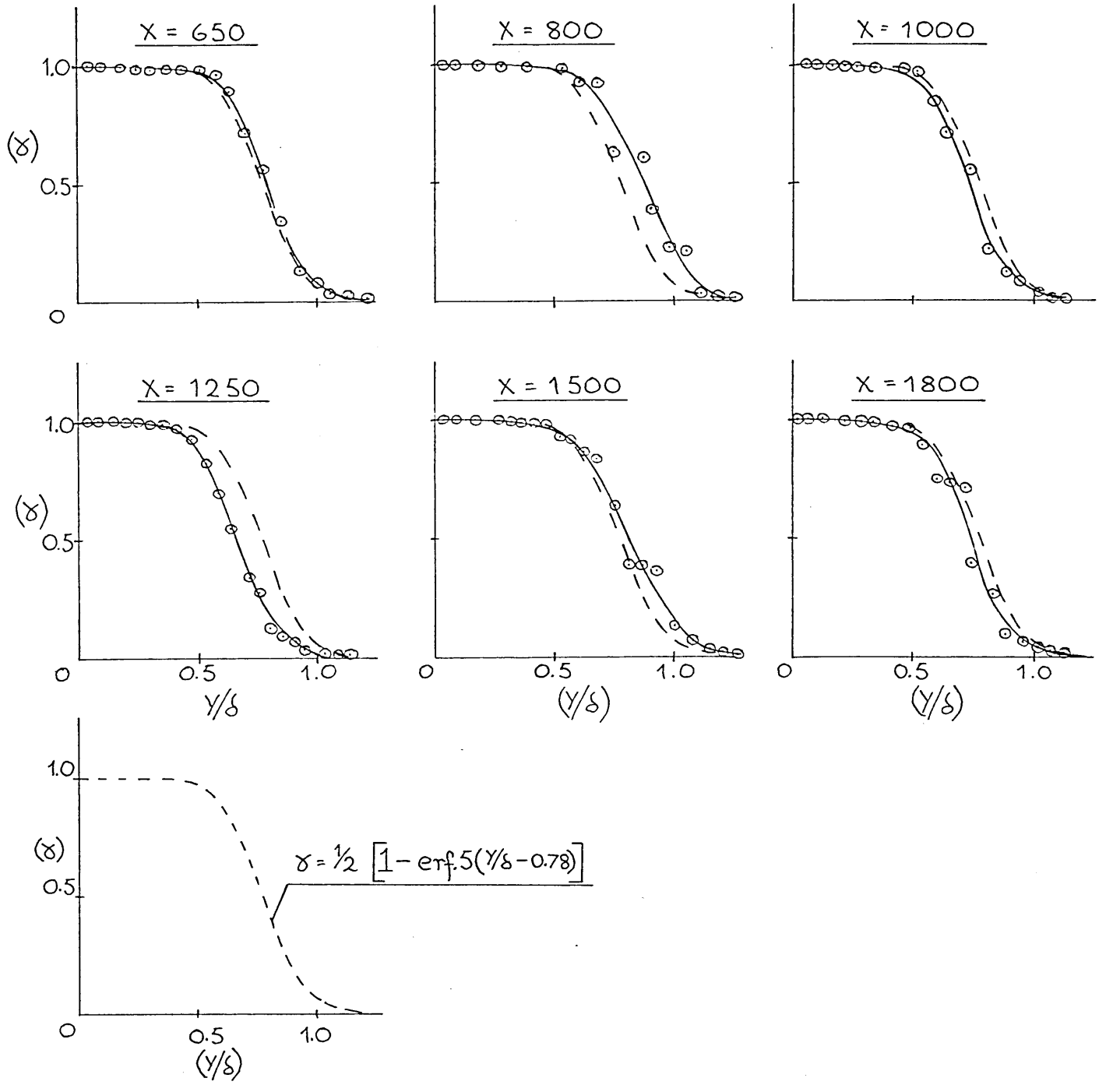

FLOW 3 - Secondary Data (Z = -50mm.)

	INTEGRAL PARAMETERS (mm.)				SHAPE FACTOR		SKIN FRICTION×1000			
Xmm	Delta	Displ	Mom	En	H12	H32	Cf.1	Cf.2	Cf.3	Cf.4
150	2.60	0.977	0.331	0.508	2.953	1.535	1.436	1.849		
175	2.89	1.044	0.364	0.564	2.865	1.547	1.300	1.679		
190	3.59	1.313	0.420	0.649	3.130	1.547	0.925	1.498		
205	3.73	1.934	0.291	0.487	6.645	1.675	0.173	2.038		
210	3.94	1.938	0.353	0.564	5.493	1.600	0.200	2.146		
215	4.05	1.231	0.617	0.990	1.997	1.605	5.575	3.727		
220	4.00	1.225	0.627	1.010	1.955	1.611	5.475	4.695		
225	4.75	1.040	0.597	0.994	1.742	1.665	5.786	5.384		
230	5.30	0.926	0.559	0.948	1.657	1.697	5.854	5.721		
235	5.62	0.927	0.568	0.971	1.632	1.711	5.812	5.761		
250	6.00	0.919	0.581	1.009	1.580	1.736	5.821	5.698	4.557	4.446
300	7.52	1.137	0.749	1.314	1.518	1.756	5.385	5.143	5.092	5.127
400	8.95	1.400	0.931	1.632	1.504	1.753	4.988	4.808	4.636	4.593
500	12.13	1.762	1.205	2.125	1.462	1.763	4.667	4.352	4.346	4.323
650	15.60	2.409	1.647	2.887	1.463	1.753	4.108	3.873	3.795	3.937
800	17.78	2.739	1.910	3.365	1.434	1.761	4.059	3.752	3.603	3.673
1000	24.07	3.362	2.400	4.256	1.401	1.774	3.835	3.575	3.561	3.647
1250	28.38	4.247	2.994	5.268	1.419	1.759	3.502	3.254	3.353	3.533
1500	28.10	4.864	3.348	5.823	1.453	1.739	3.235	3.001	3.199	3.328
1800	35.21	5.545	3.925	6.895	1.413	1.757	3.214	2.980	3.142	3.199

Xmm	Momentum Balance		Intermittency (mean value)	Rtheta	Wake Parameter	Wake Strength Parameter
	PL.	PR.	$\bar{\gamma}$	R_θ	Π	$\Delta \bar{u}/u_\sigma$
150	-	-	0.000	238	-	-
175	-	-	0.000	262	-	-
190	-	-	0.008	302	-	-
205	-	-	0.013	221	-	-
210	-	-	0.104	272	-	-
215	-	-	0.667	476	-	-
220	-	-	0.896	479	-	-
225	-	-	0.981	447	-	-
230	-	-	0.992	408	-	-
235	-	-	1.000	408	-	-
250	0.000	0.000	1.000	419	0.008	0.555
300	0.289	0.241	1.000	540	0.064	0.495
400	0.602	0.685	"	661	0.030	0.609
500	1.074	1.100	"	870	0.154	0.990
650	1.835	1.565	"	1185	0.342	1.756
800	2.287	2.190	"	1376	0.306	1,673
1000	3.131	2.870	"	1734	0.298	1.519
1250	4.153	3.659	"	2156	0.457	2.254
1500	4.763	4.380	"	2412	0.680	3.283
1800	5.756	5.204	"	2845	0.583	2.905

Standard Deviation of the Intermittency Distribution = ∇ = 3.50mm.

$(X_{\bar{\gamma}=0.75} - X_{\bar{\gamma}=0.25}) = \lambda = 4.10$mm.

$R_\nabla = 2520$

$R_\lambda = 2952$

NB, Cf.'s as before.

6.89

FLOW 3— APPROACH TO EQUILIBRIUM

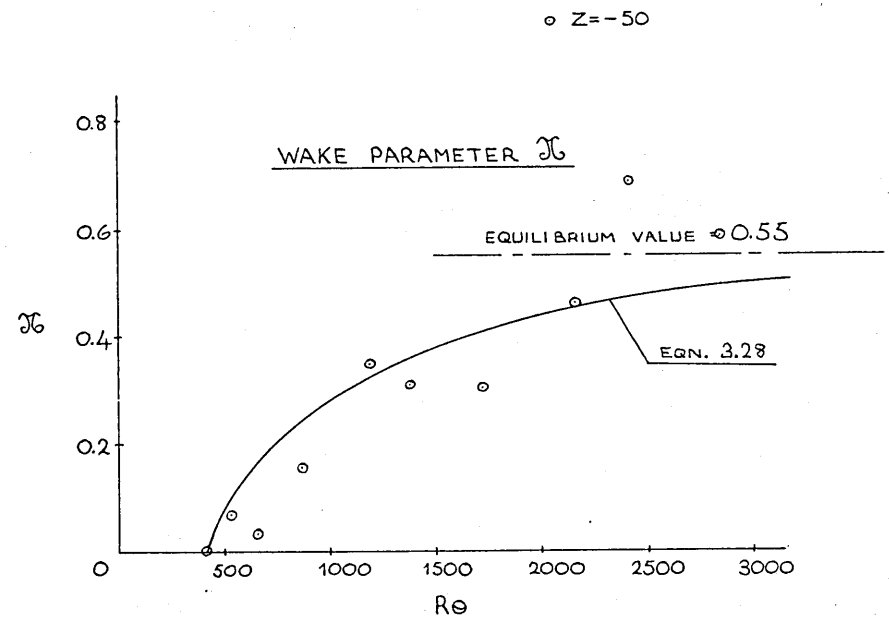

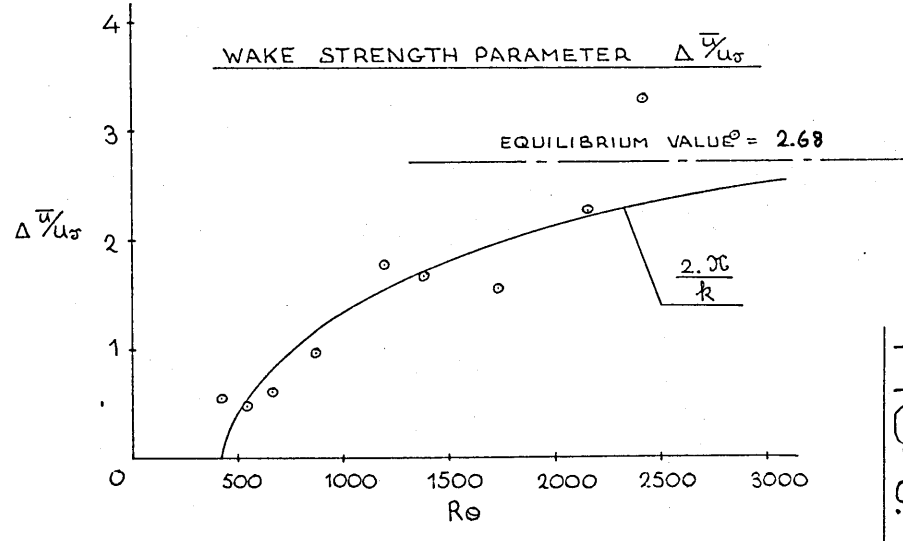

FIG 3.9

FLOW 3 — DEVELOPMENT OF INTEGRAL PARAMETERS IN VICINITY OF TRIP WIRE

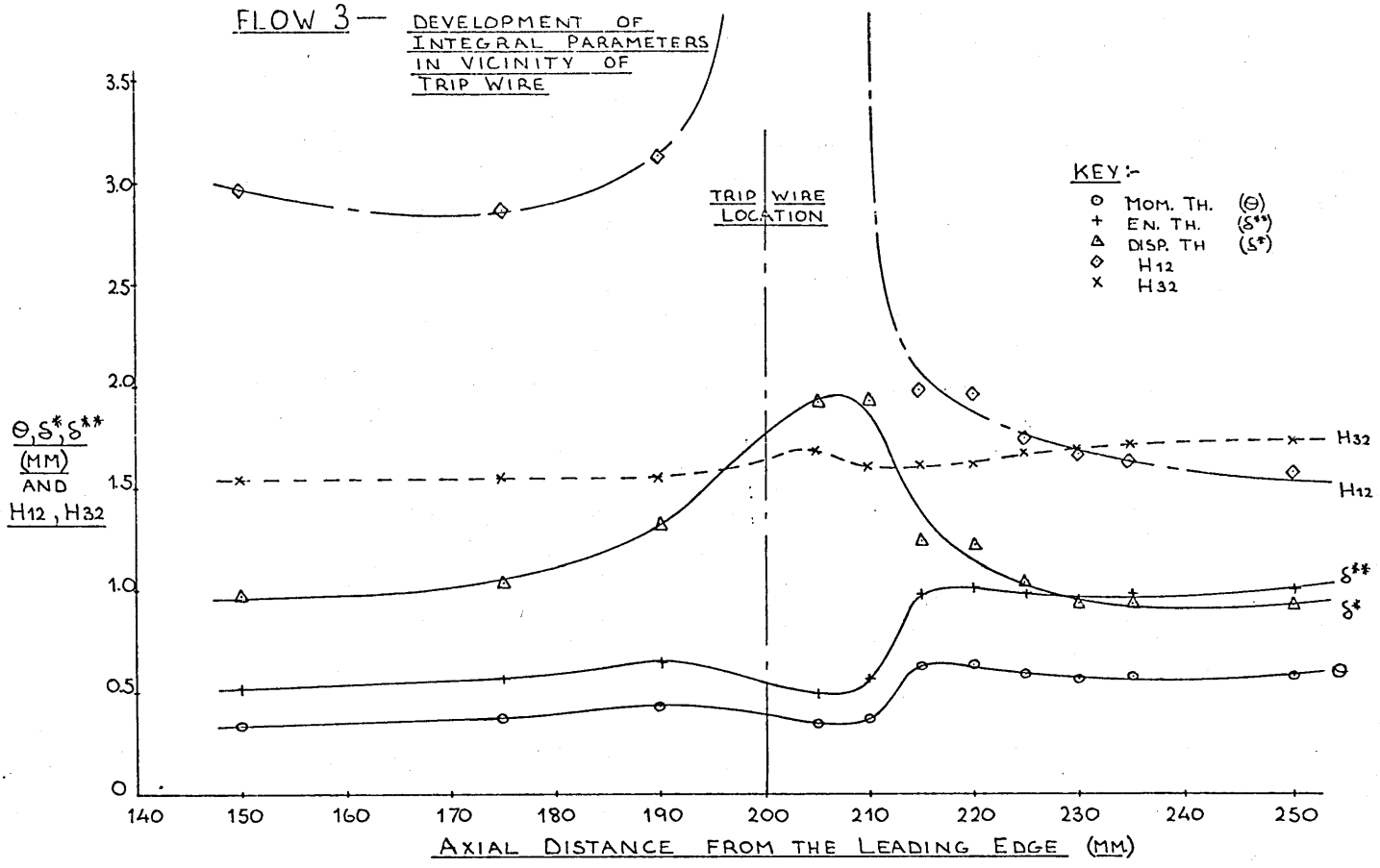

FIG.

FLOW 3 — VARIATION OF SKIN FRICTION CO-EFFICIENT IN VICINITY OF TRIP WIRE

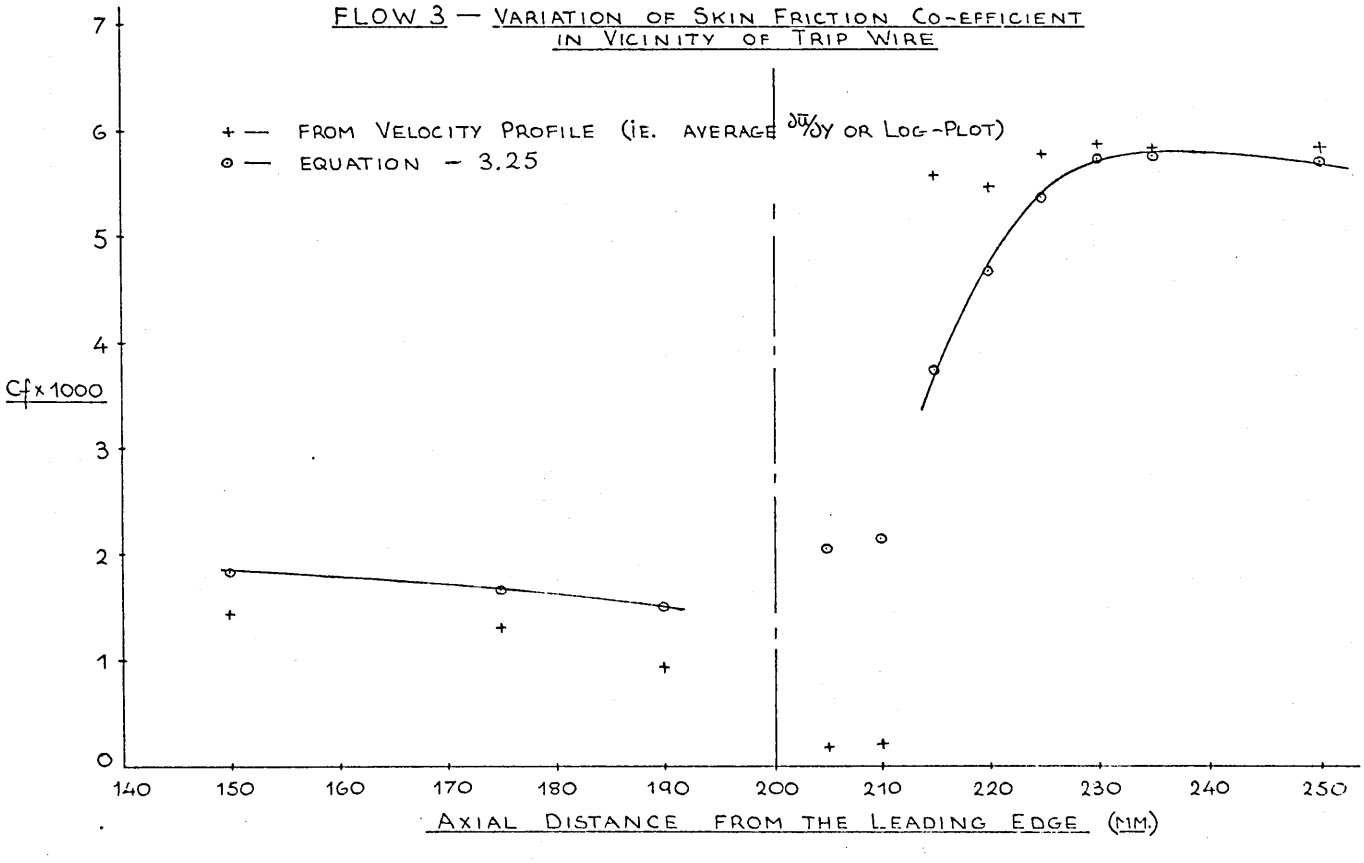

FIG.

FLOW 3 — DEVELOPMENT OF INTEGRAL PARAMETERS ALONG Z = -50

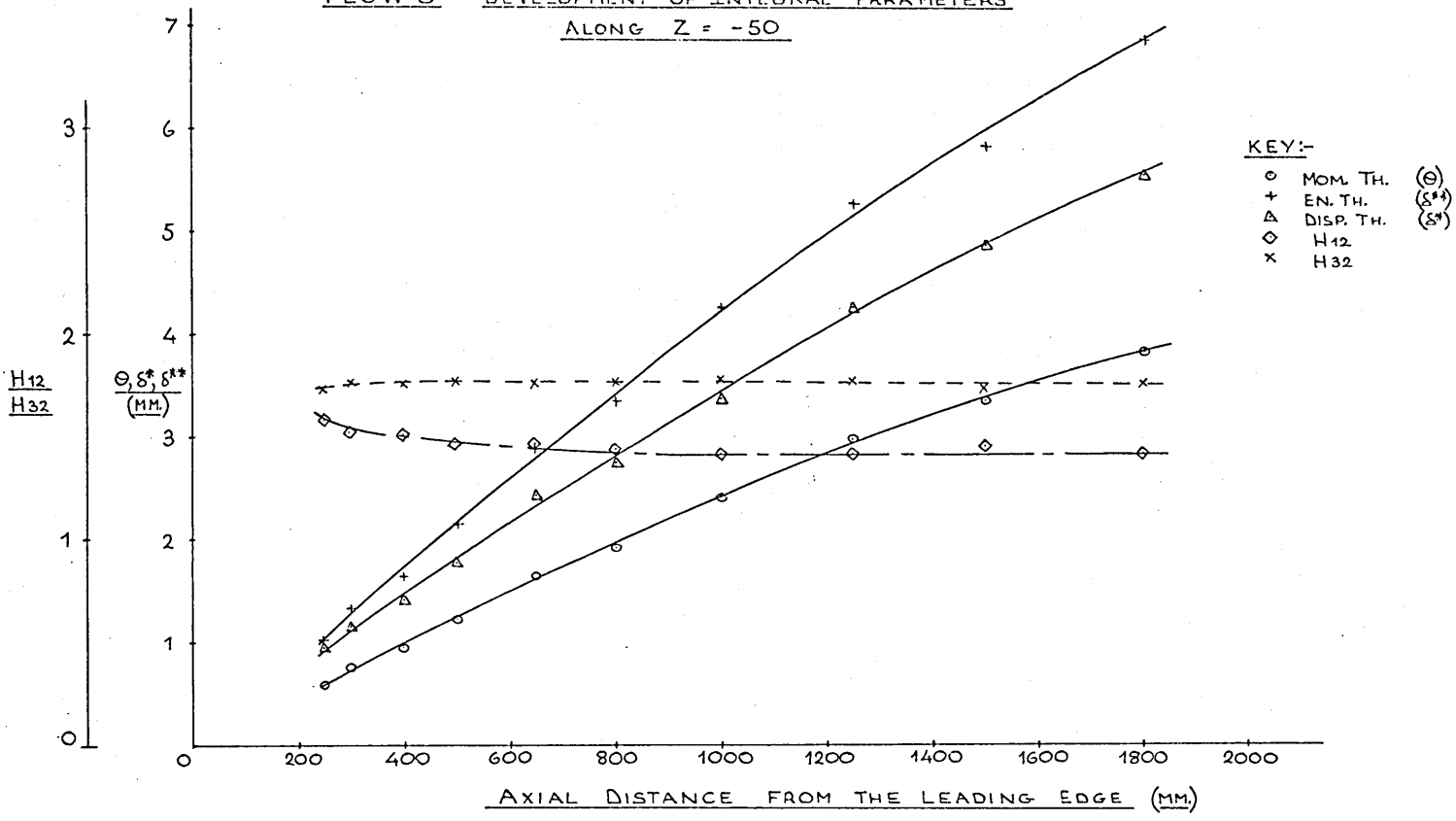

FIG.

FLOW 3 — VARIATION OF SKIN FRICTION CO-EFFICIENT ALONG Z = -50

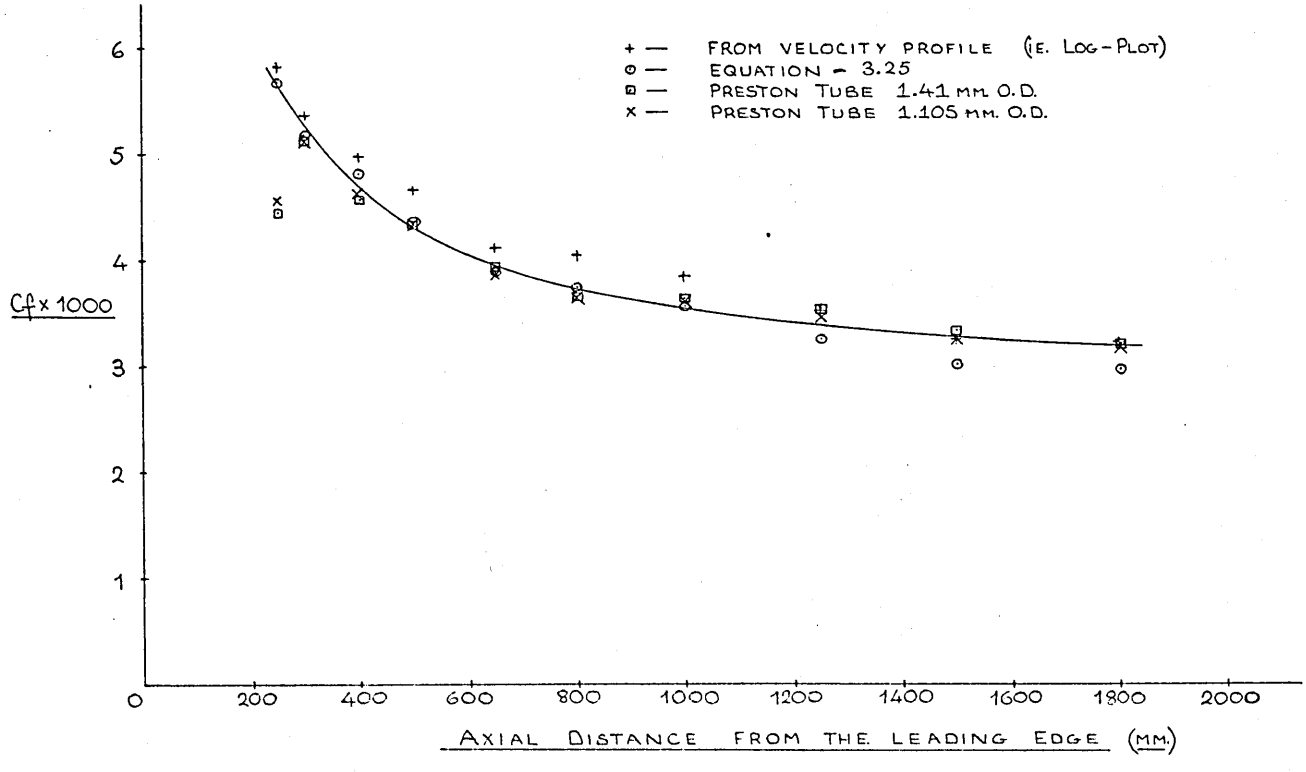

FIG.

FLOW 3 — MEAN ENTRAINMENT RATE ALONG Z = -50

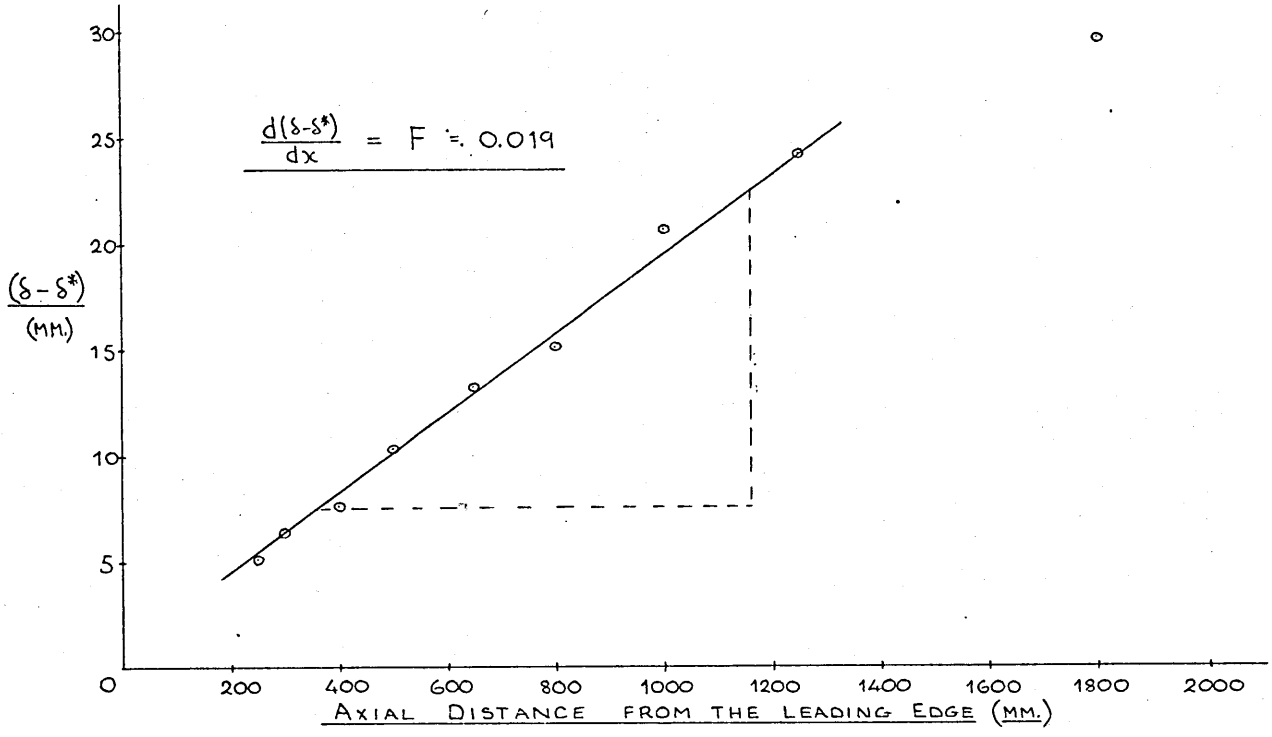

FIG.

FLOW 3 — MOMENTUM BALANCE

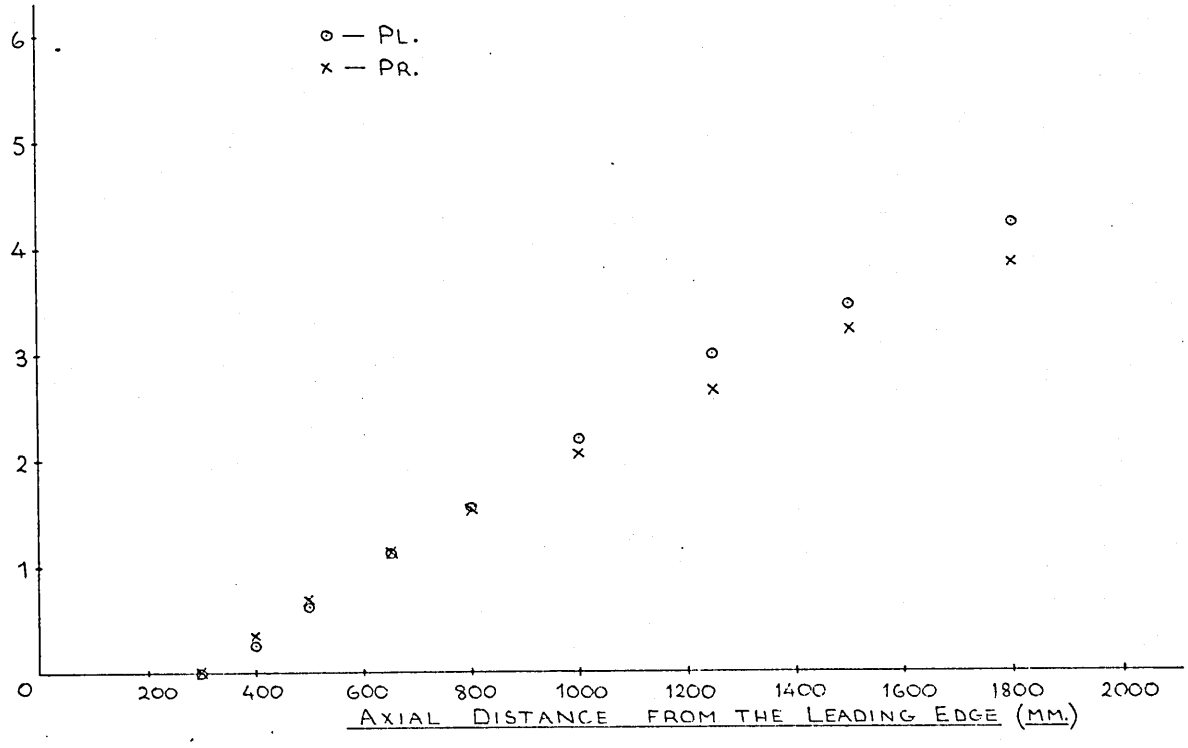

FIG.

STREAMWISE DEVELOPMENT OF "NEAR" WALL INTERMITTENCY

FLOW 3 — Z = -50

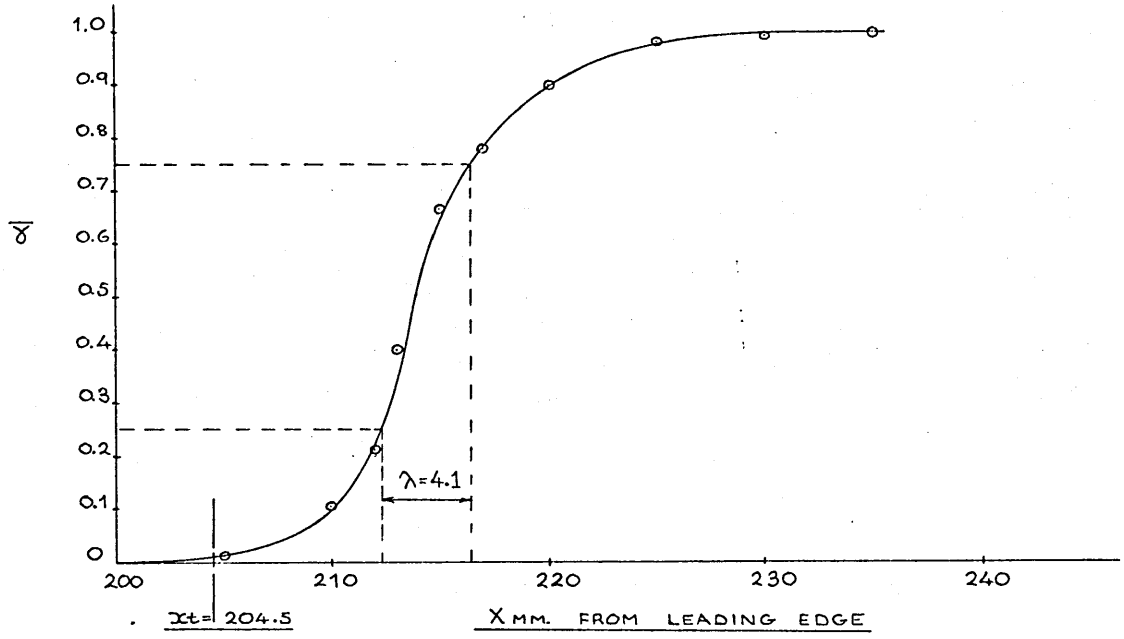

FIG.

FLOW 3 - MEAN VELOCITY PROFILES IN THE RECOVERY ZONE

EFFECTIVE TRIP WIRE HEIGHT = 1.20 MM

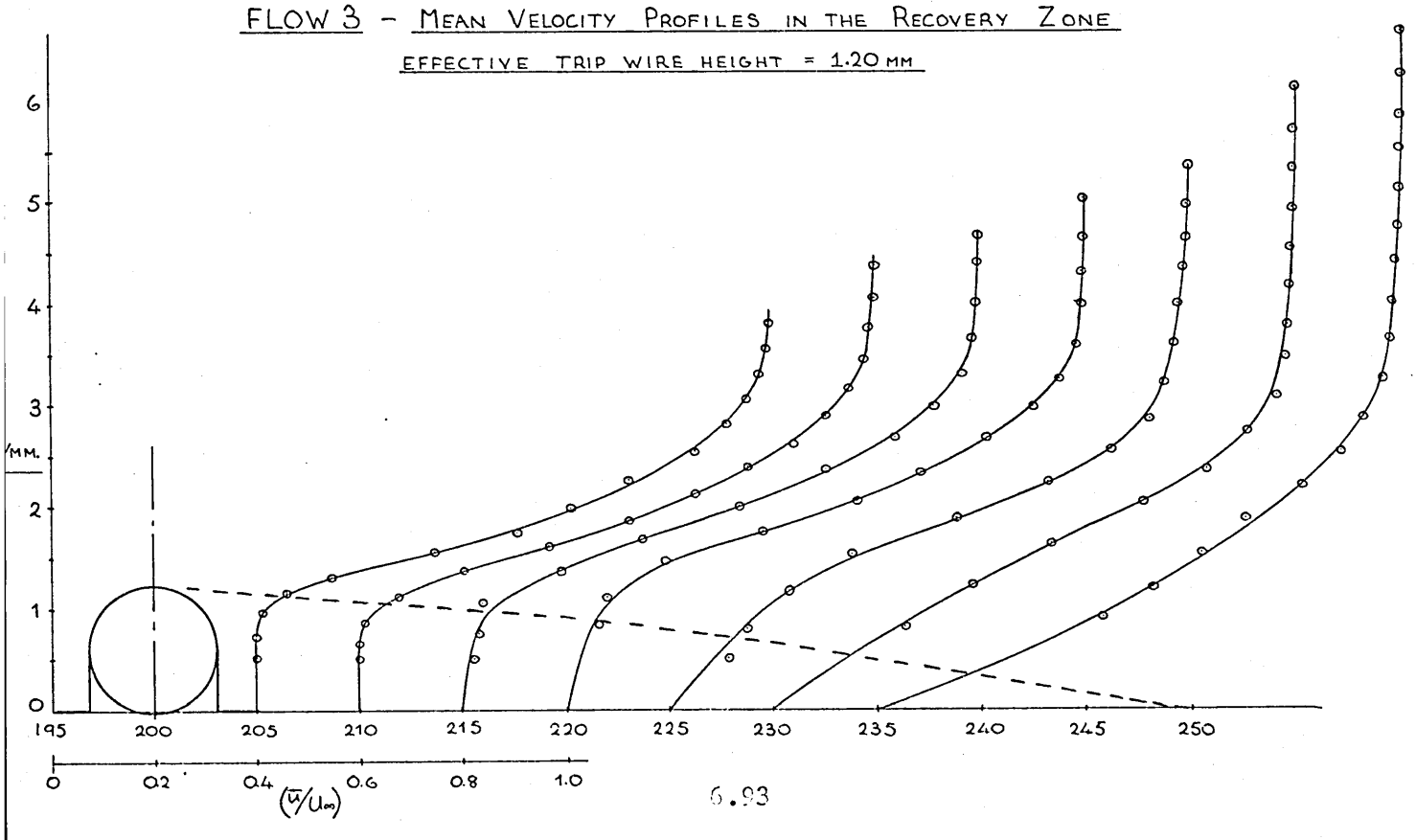

6.93

FIG.

FLOW 3 — BOUNDARY LAYER PROFILES AT X = 400 MM.

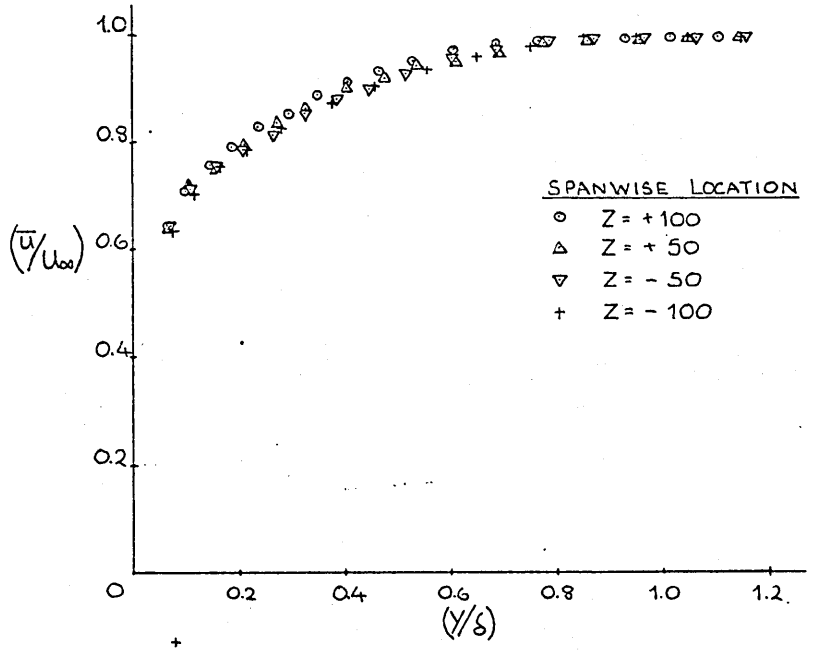

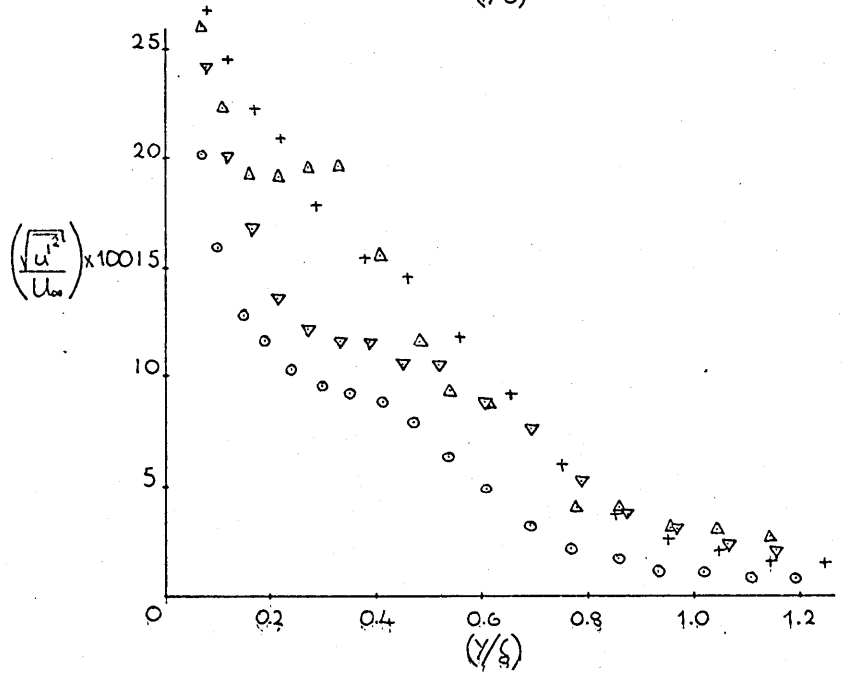

FIG 3.9

FLOW 3 — SPANWISE VARIATION OF LOCAL SKIN FRICTION CO-EFFICIENT (MEASUREMENT BY PRESTON TUBE)

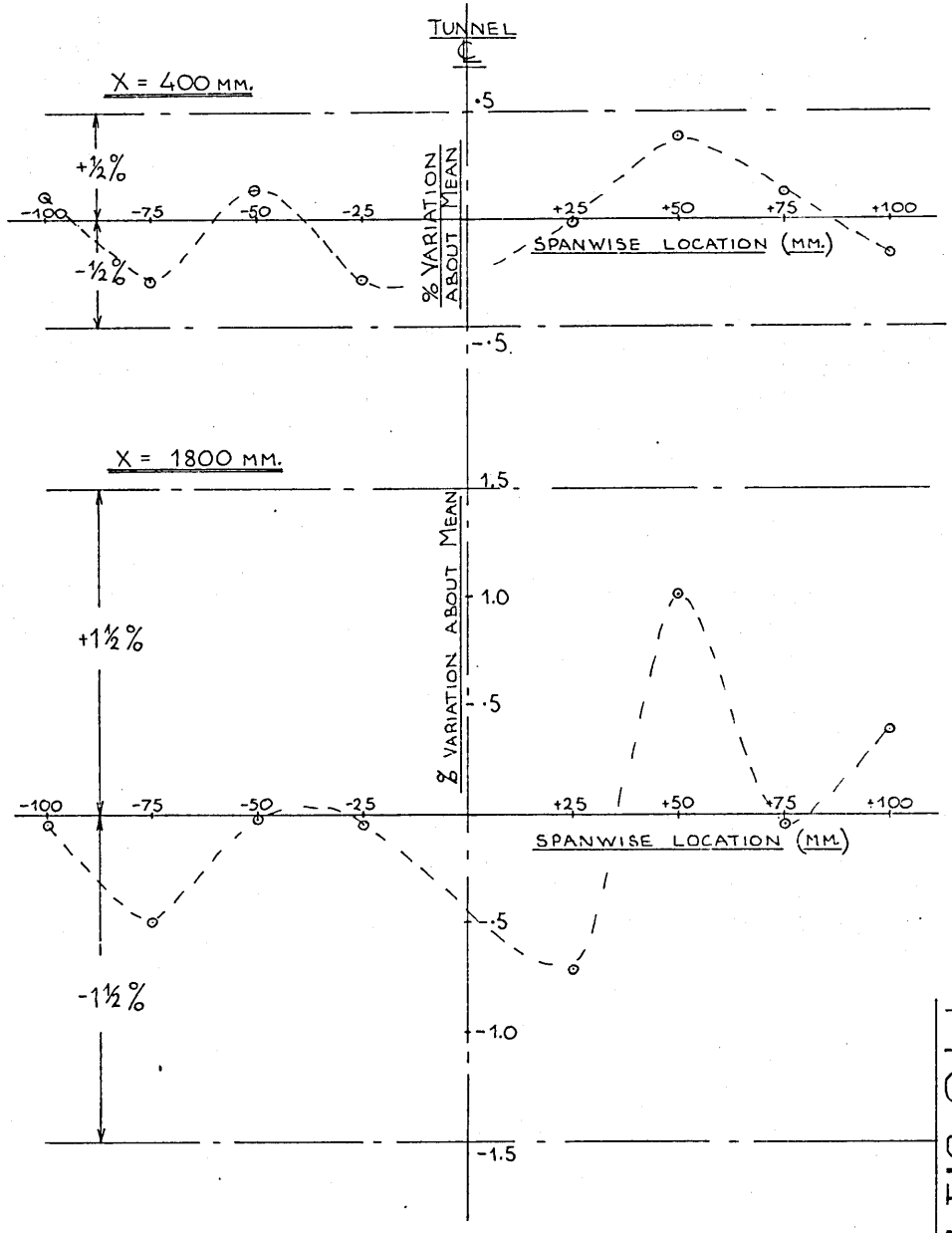

FIG 3.14

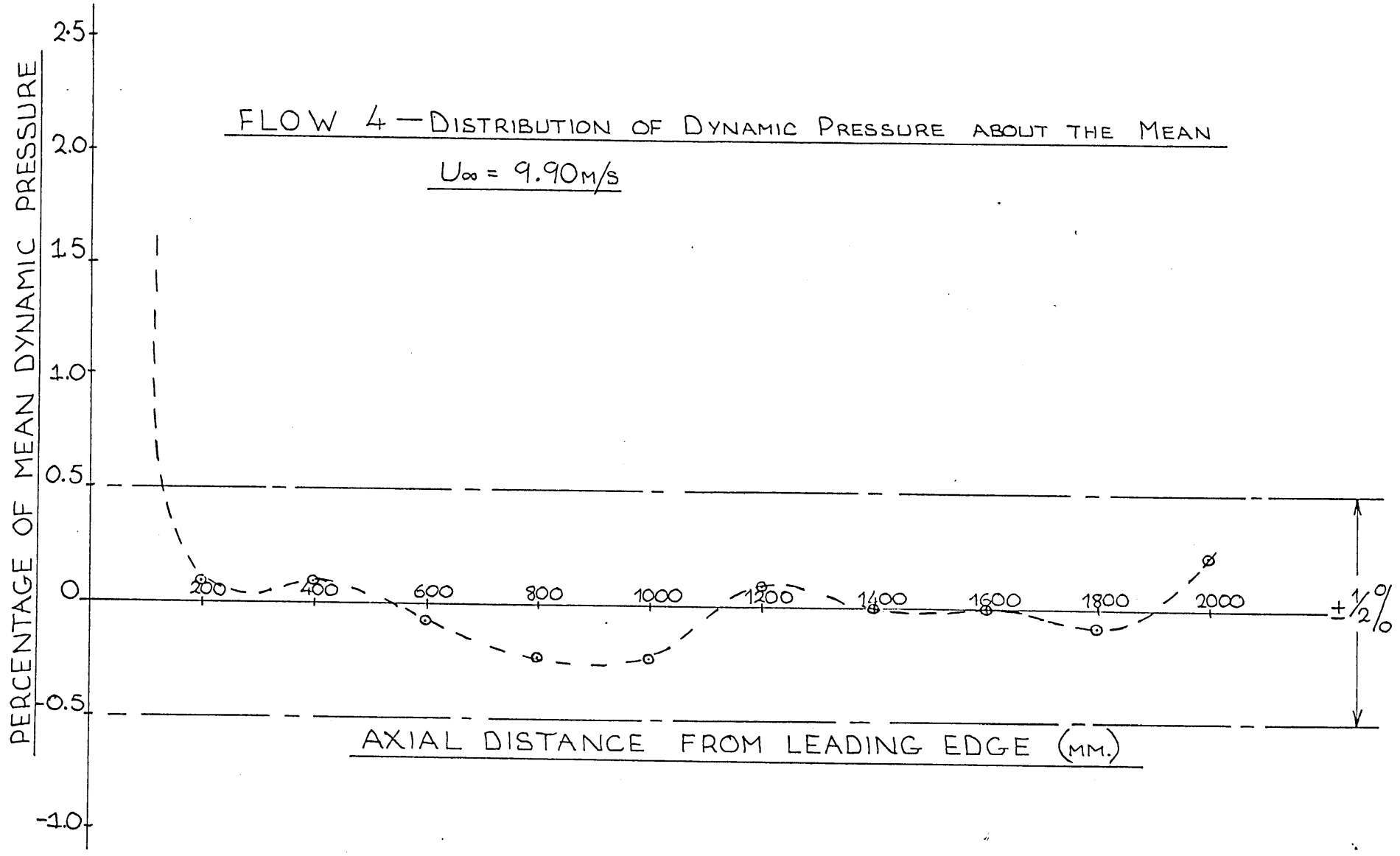
FLOW 4 — DISTRIBUTION OF DYNAMIC PRESSURE ABOUT THE MEAN
U_∞ = 9.90 M/S
PERCENTAGE OF MEAN DYNAMIC PRESSURE
2·5
2.0
1.5
1.0
0.5
0
-0.5
-1.0
200
400
600
800
1000
1200
1400
1600
1800
2000
± ½ %
AXIAL DISTANCE FROM LEADING EDGE (MM.)

FIG. 4.1

FIG 4.2

FLOW 4 — SPANWISE MEAN VELOCITY PROFILES AT X = 300 MM.

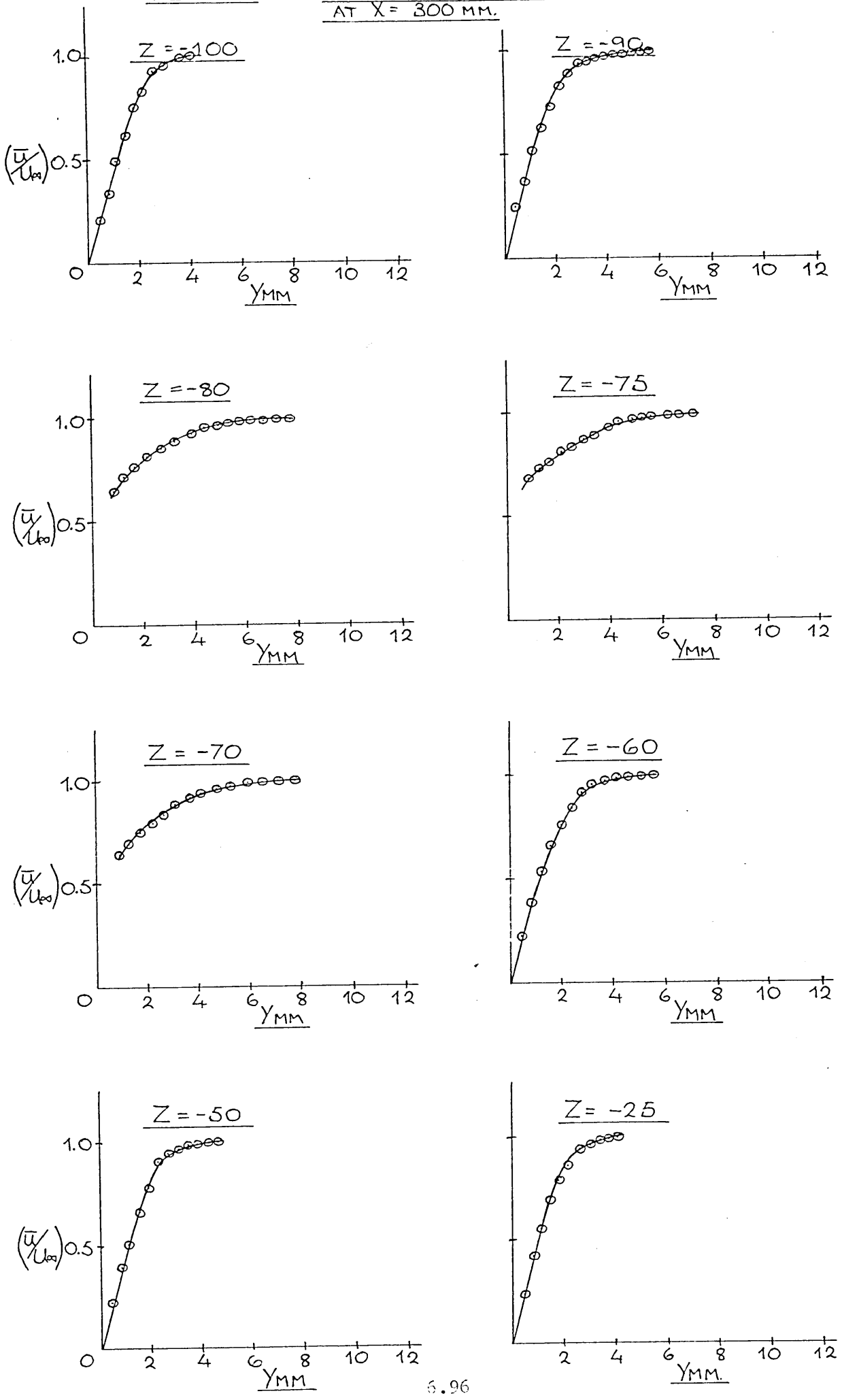

FIG 4.3

FLOW 4 — SPANWISE MEAN VELOCITY PROFILES AT X = 300 MM.

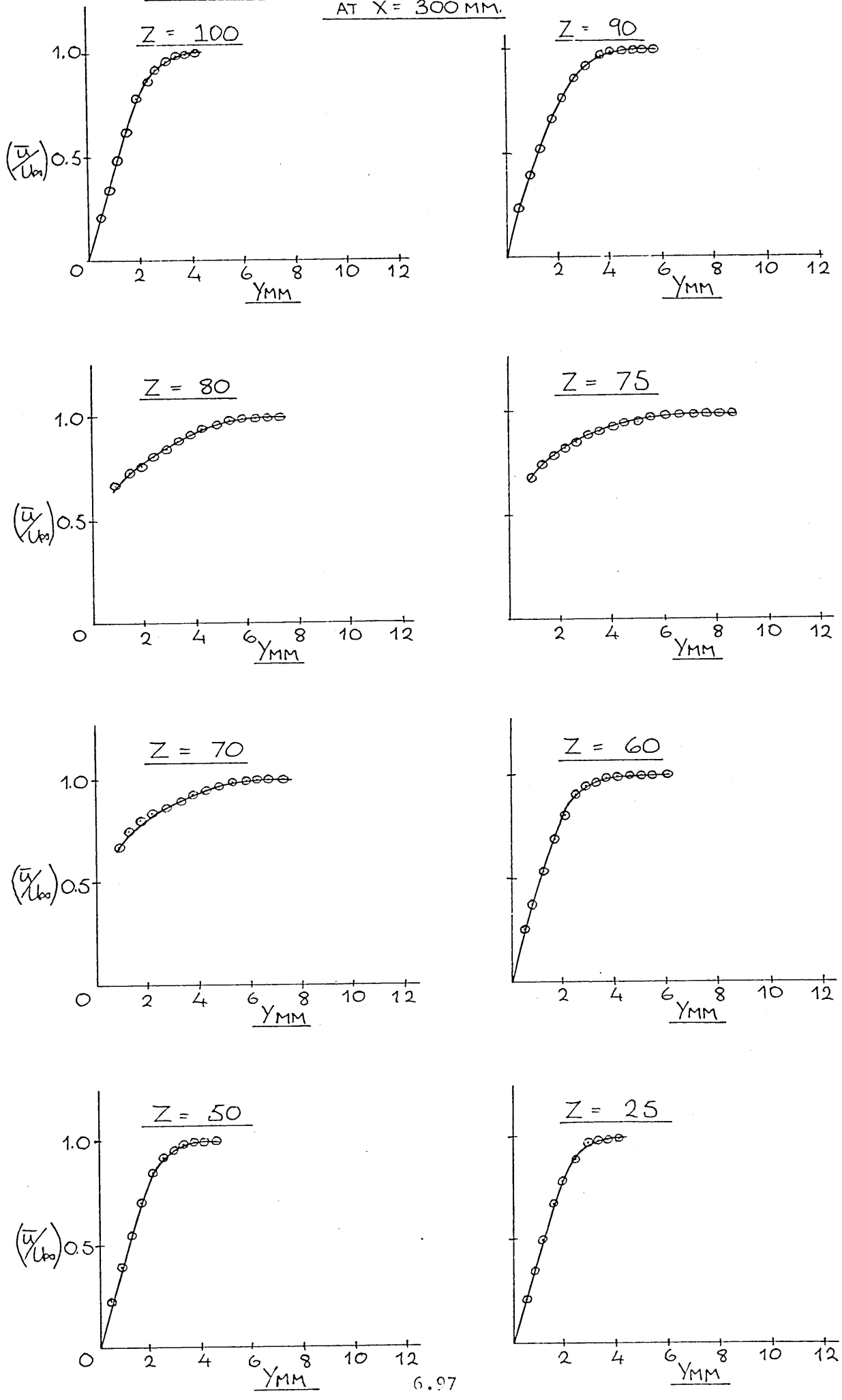

6.97

FIG 4.4

FLOW 4 — SPANWISE MEAN VELOCITY PROFILES AT X= 550 MM.

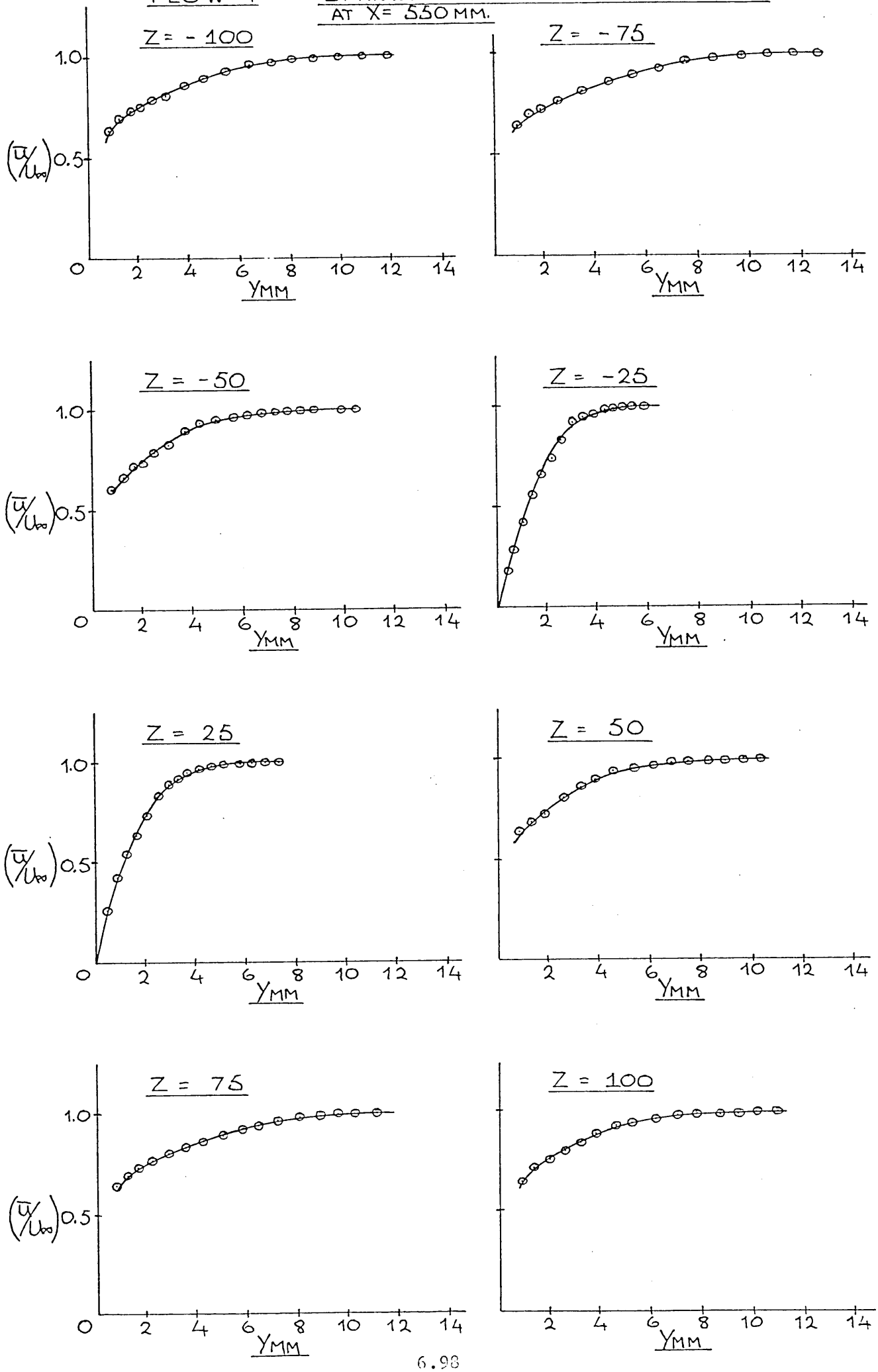

FLOW 4— MEAN VELOCITY PROFILES AT X = 750 MM.

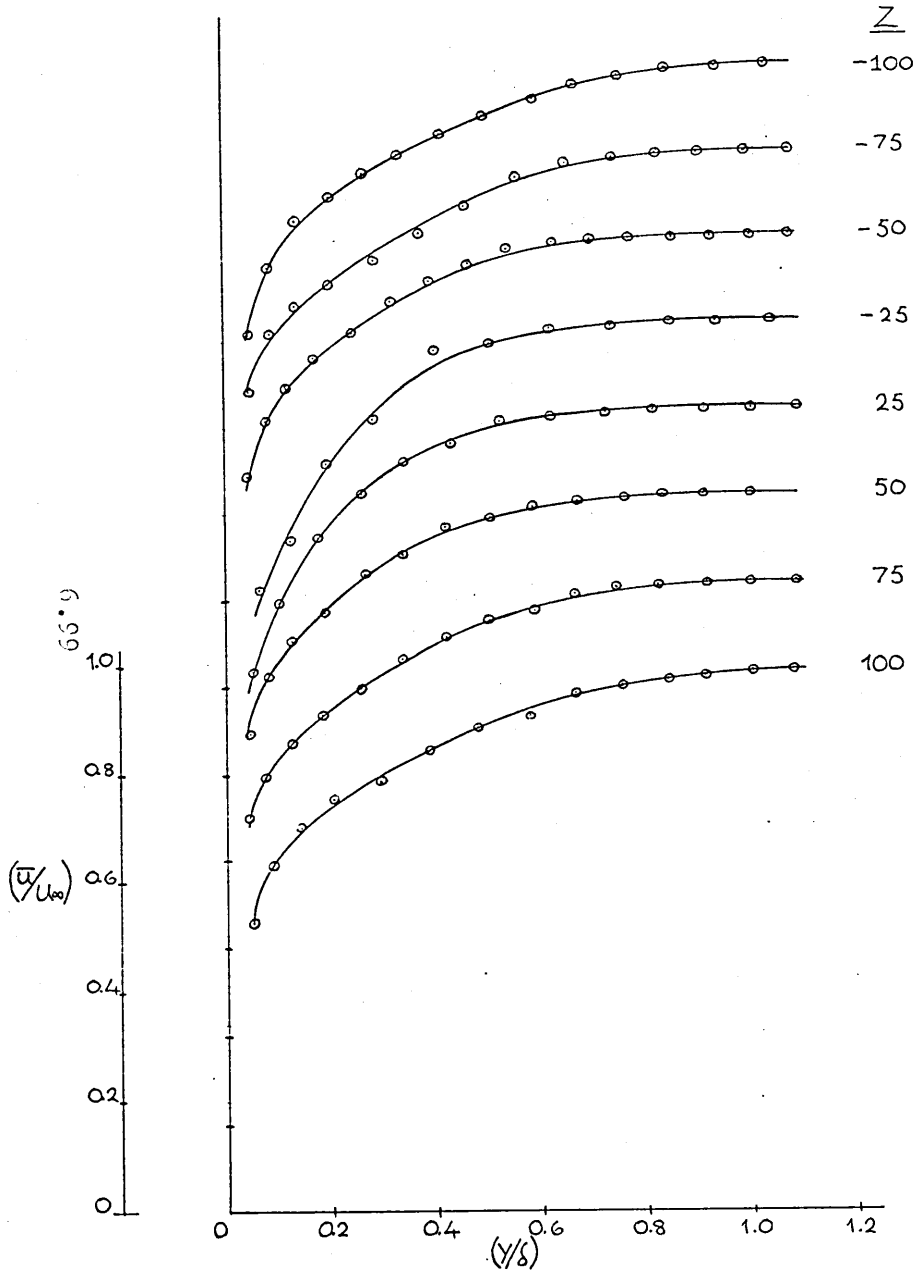

FIG 4.5

FLOW 4— MEAN VELOCITY PROFILES AT X = 1000 MM.

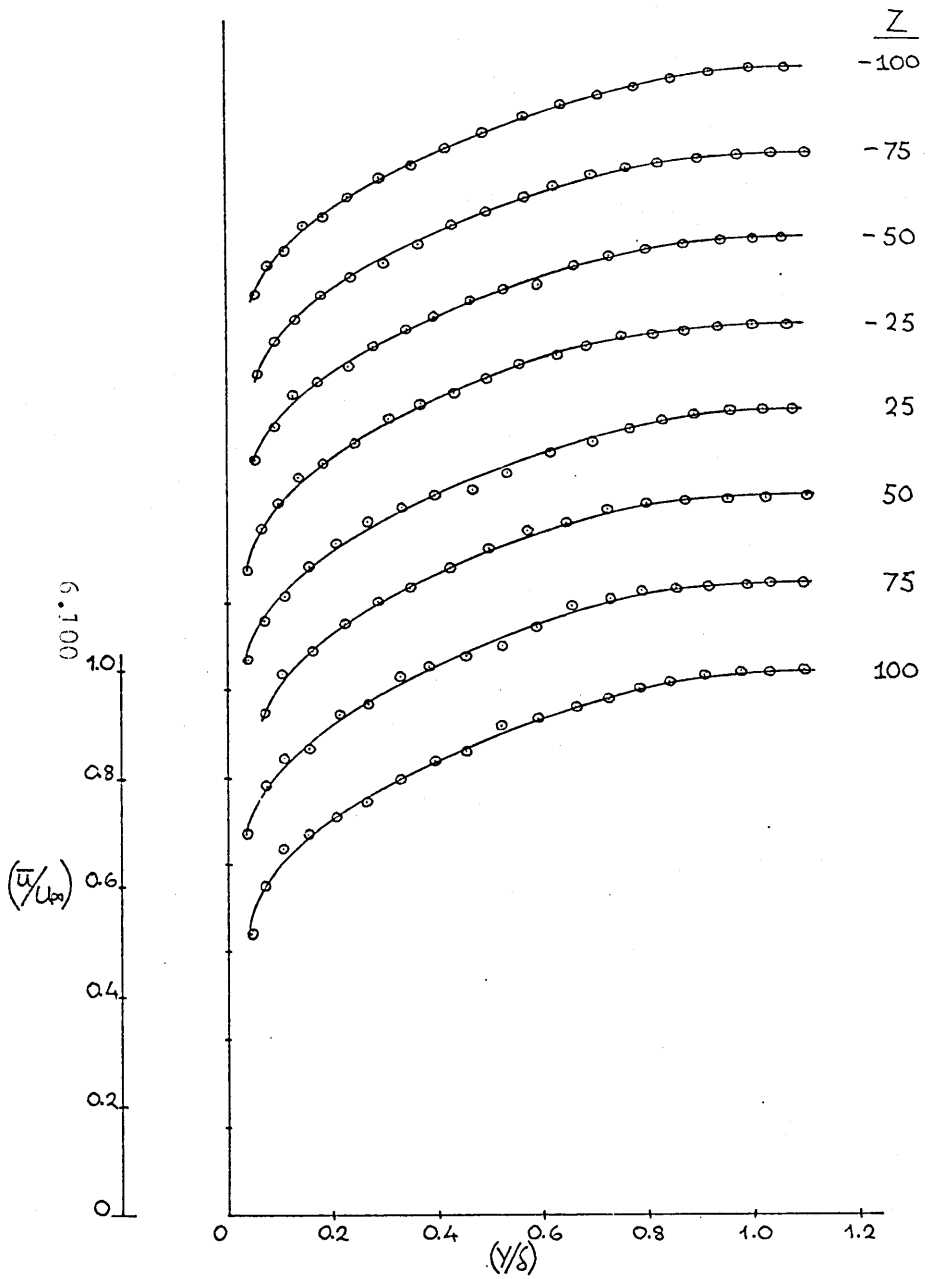

FLOW 4— MEAN VELOCITY PROFILES AT X = 1500 MM.

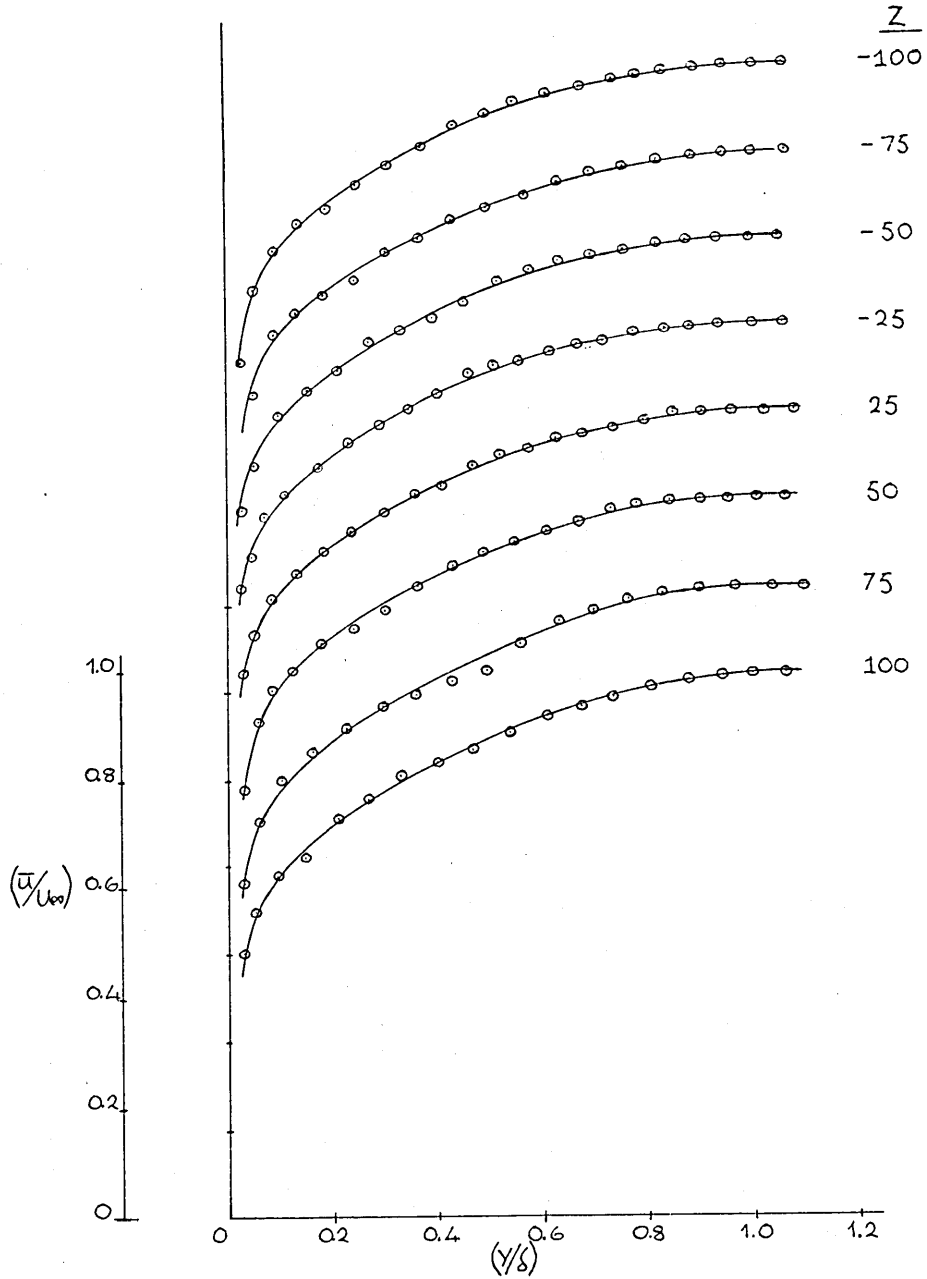

FIG 4.6

FLOW 4 — SEMI-LOGARITHMIC VELOCITY PROFILES AT X = 550 MM.

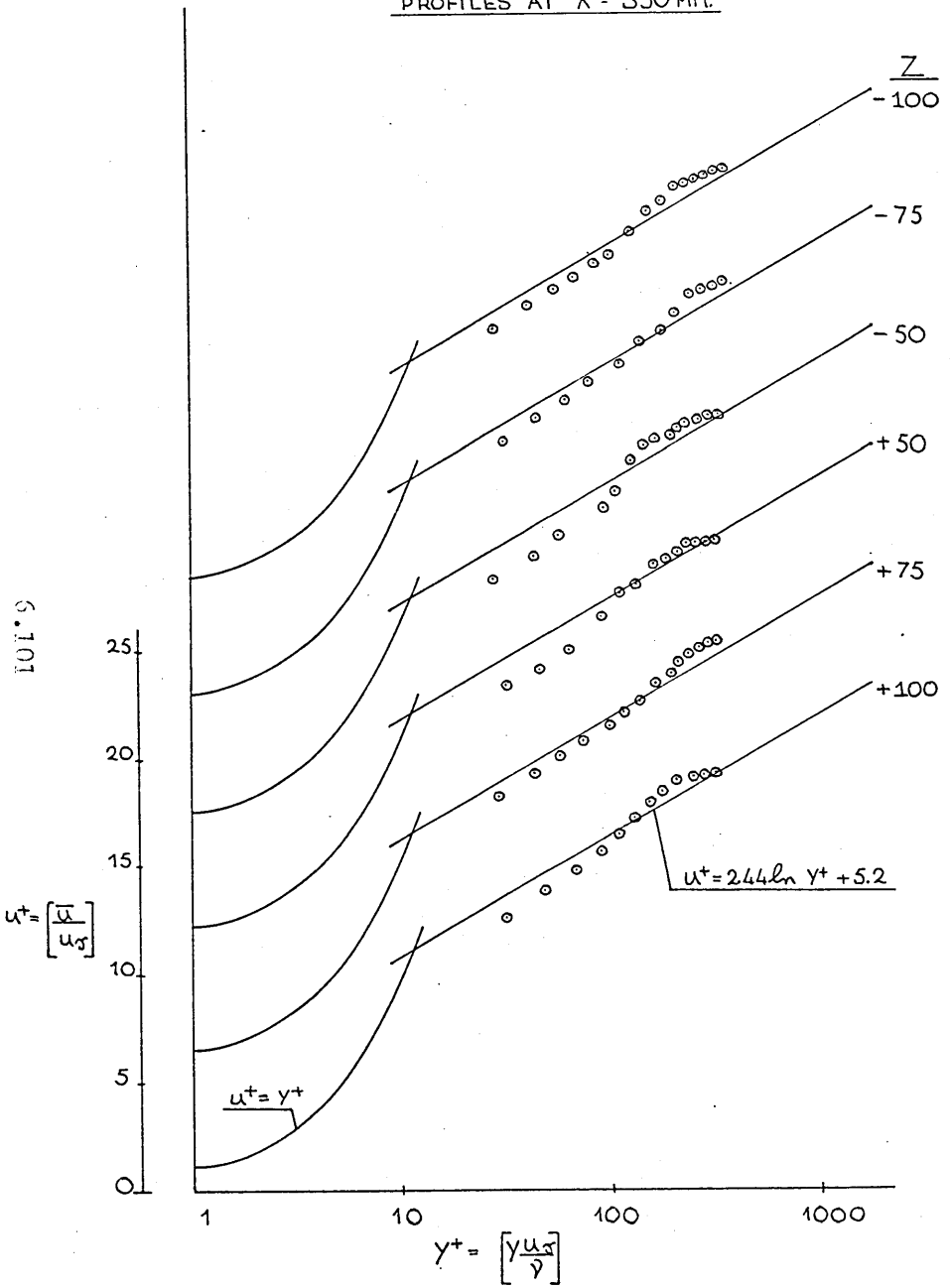

FLOW 4 — VELOCITY DEFECT PROFILES AT X = 550 MM.

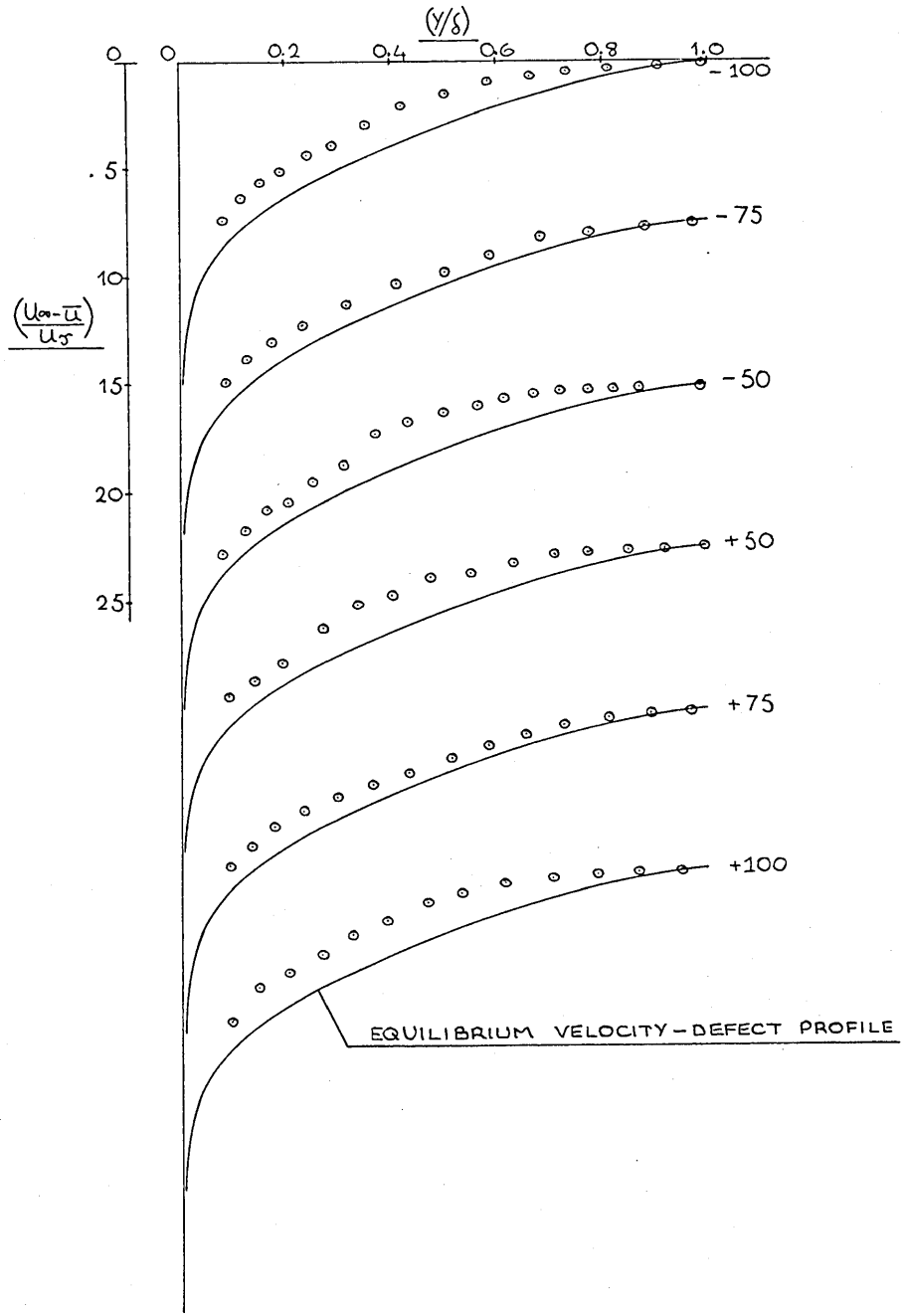

FIG 4.7

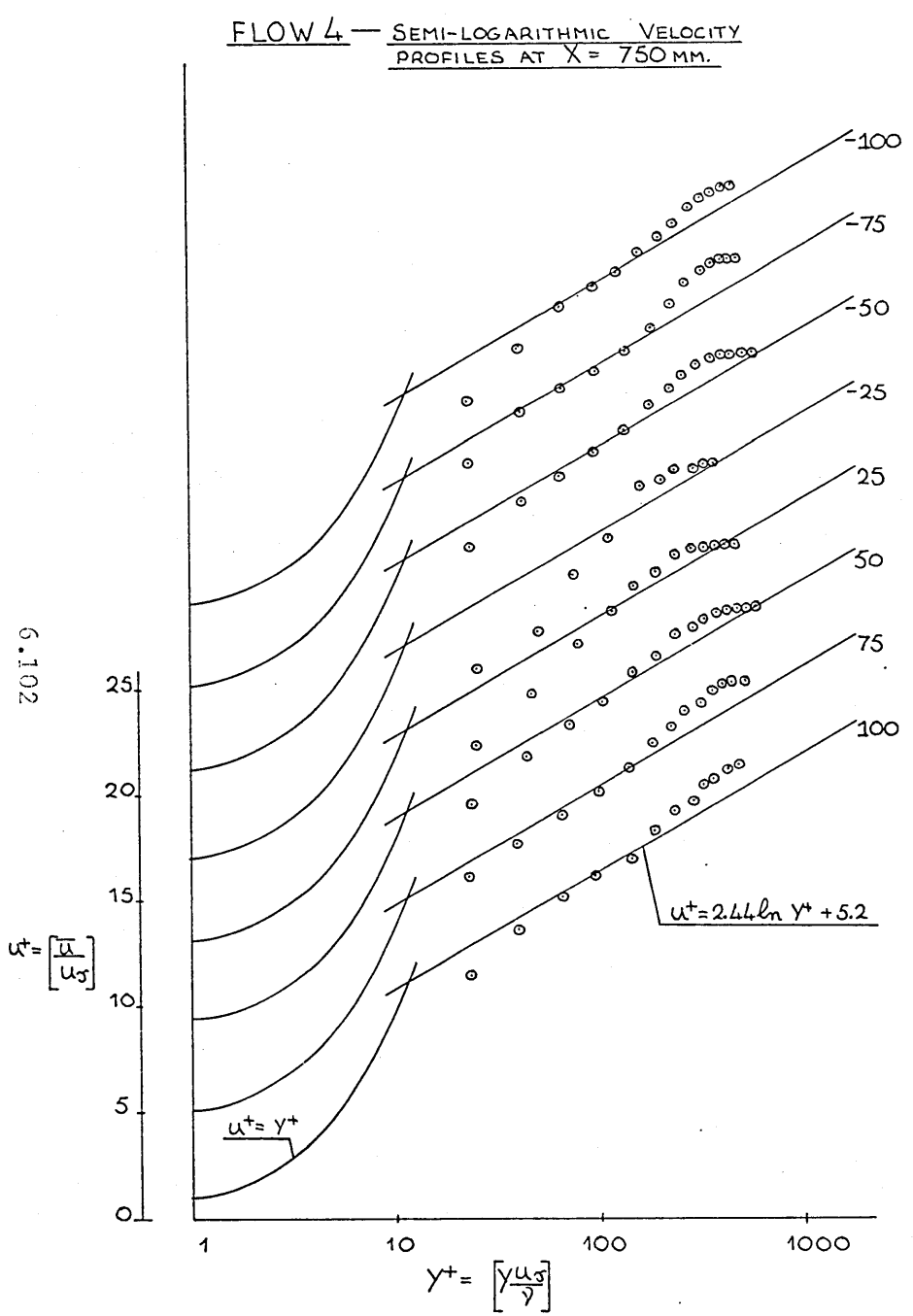
FLOW 4 — SEMI-LOGARITHMIC VELOCITY PROFILES AT X = 750 MM.
-100
-75
-50
-25
25
50
75
100
$u^+ = y^+$
$u^+ = 2.44 \ln y^+ + 5.2$
$u^+ = \left[\frac{\bar{u}}{u_\tau}\right]$
$y^+ = \left[\frac{y u_\tau}{\nu}\right]$
0
5
10
15
20
25
1
10
100
1000

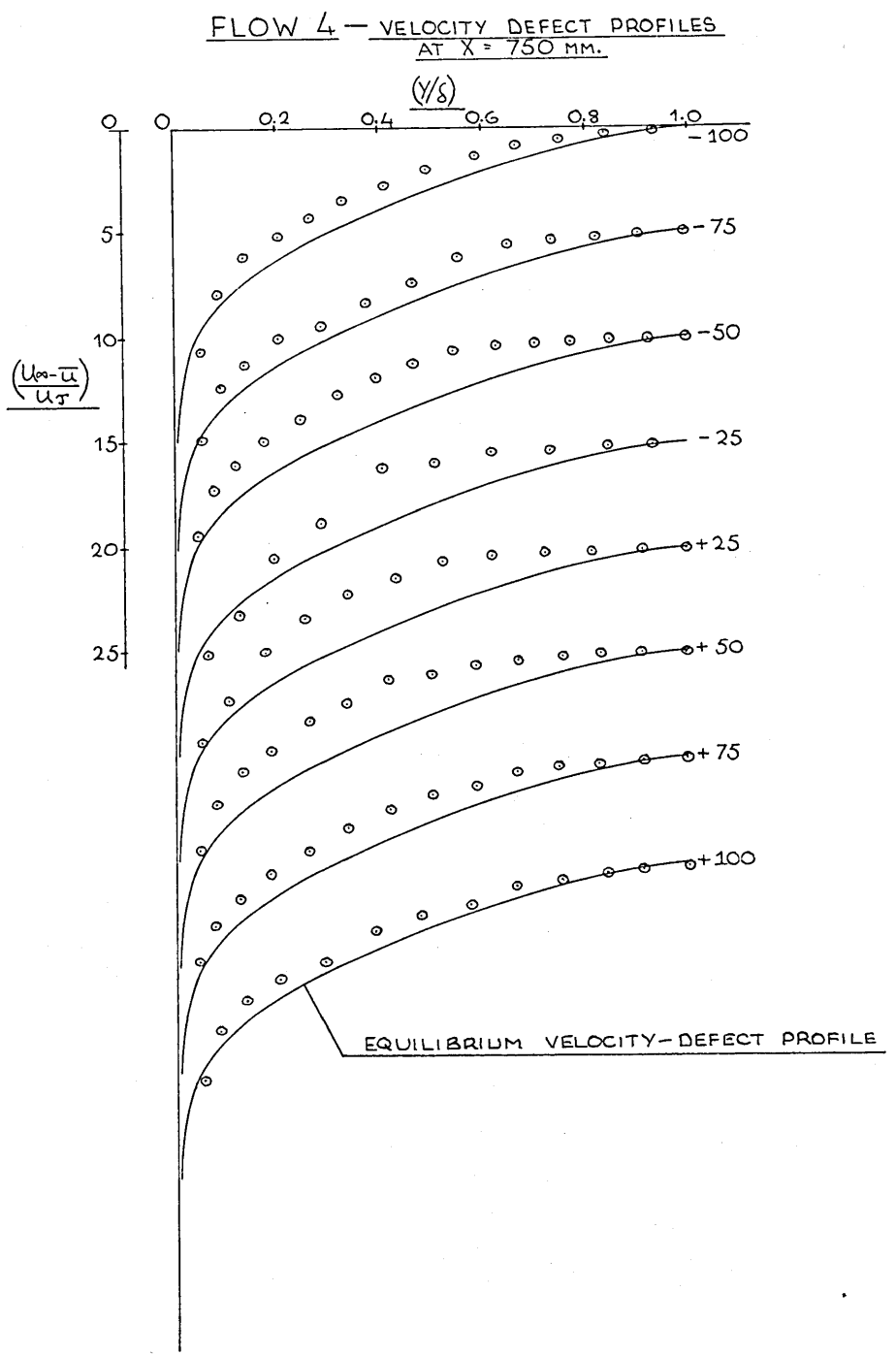
FLOW 4 — VELOCITY DEFECT PROFILES AT X = 750 MM.
$\left(\frac{y}{\delta}\right)$
0
0.2
0.4
0.6
0.8
1.0
$\left(\frac{U_\infty - \bar{u}}{u_\tau}\right)$
0
5
10
15
20
25
-100
-75
-50
-25
+25
+50
+75
+100
EQUILIBRIUM VELOCITY-DEFECT PROFILE

FIG 4.8

FLOW 4 — SEMI-LOGARITHMIC VELOCITY PROFILES AT X = 1000 MM.

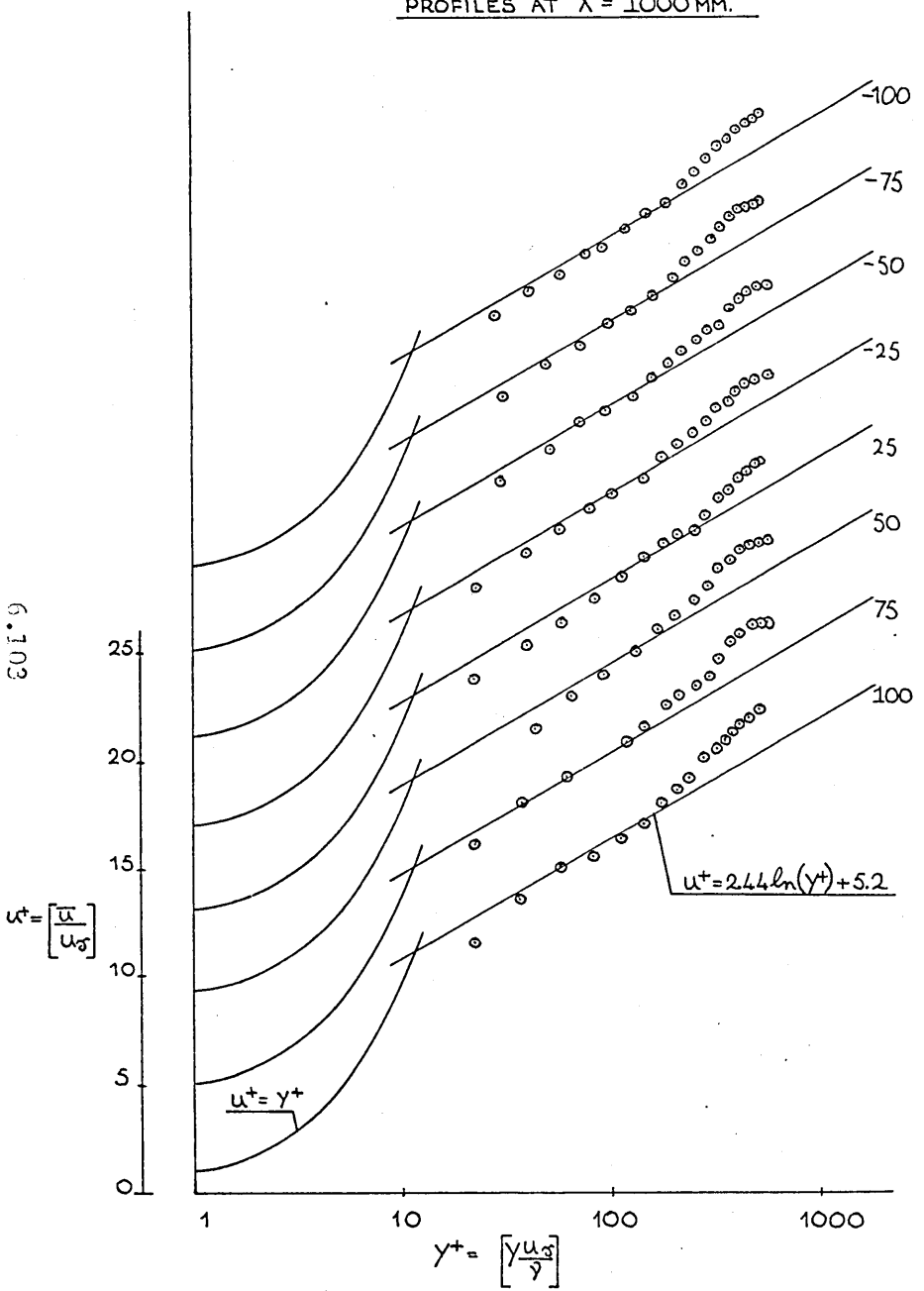

FLOW 4 — VELOCITY DEFECT PROFILES AT X = 1000 MM.

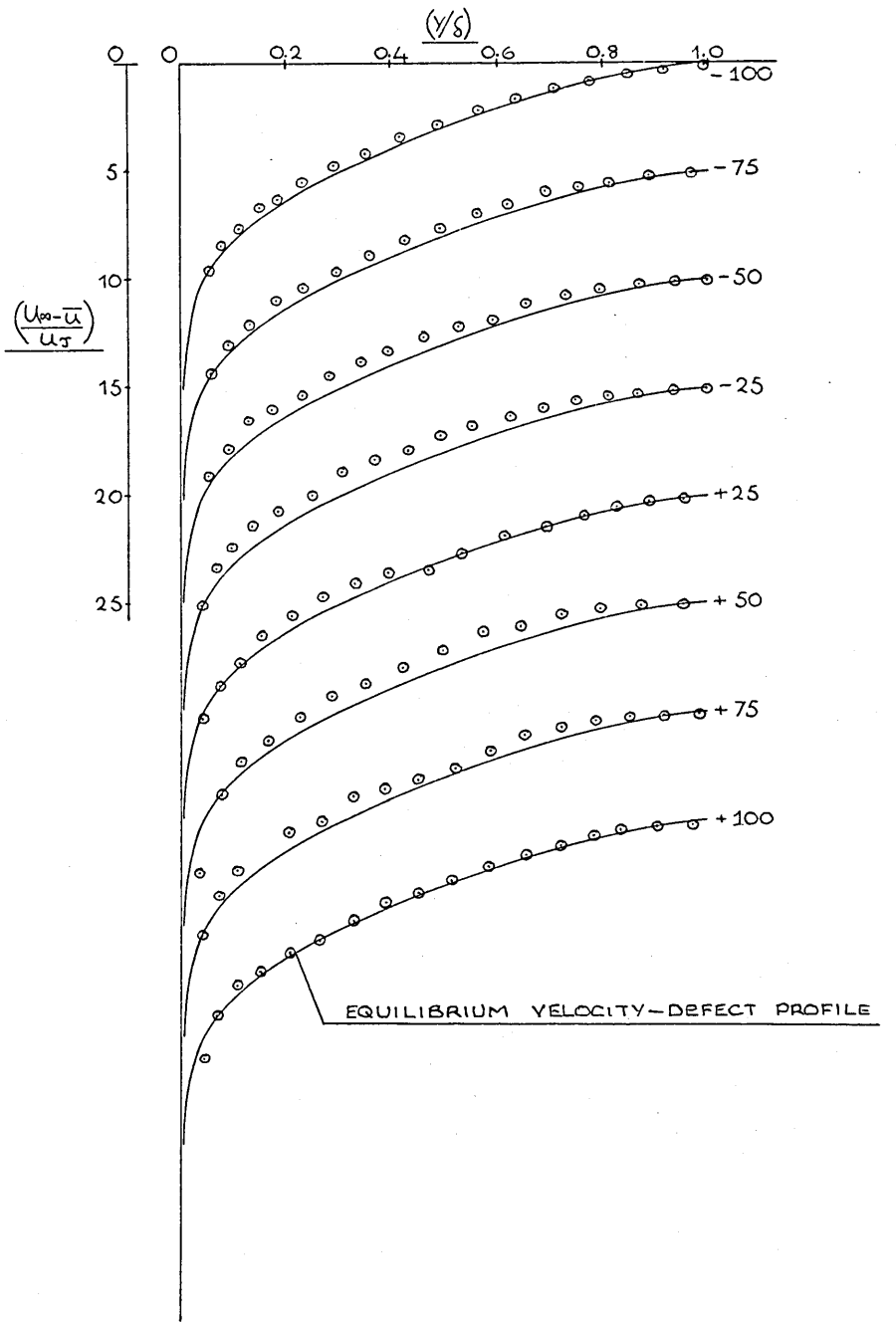

6103

FIG 4.9

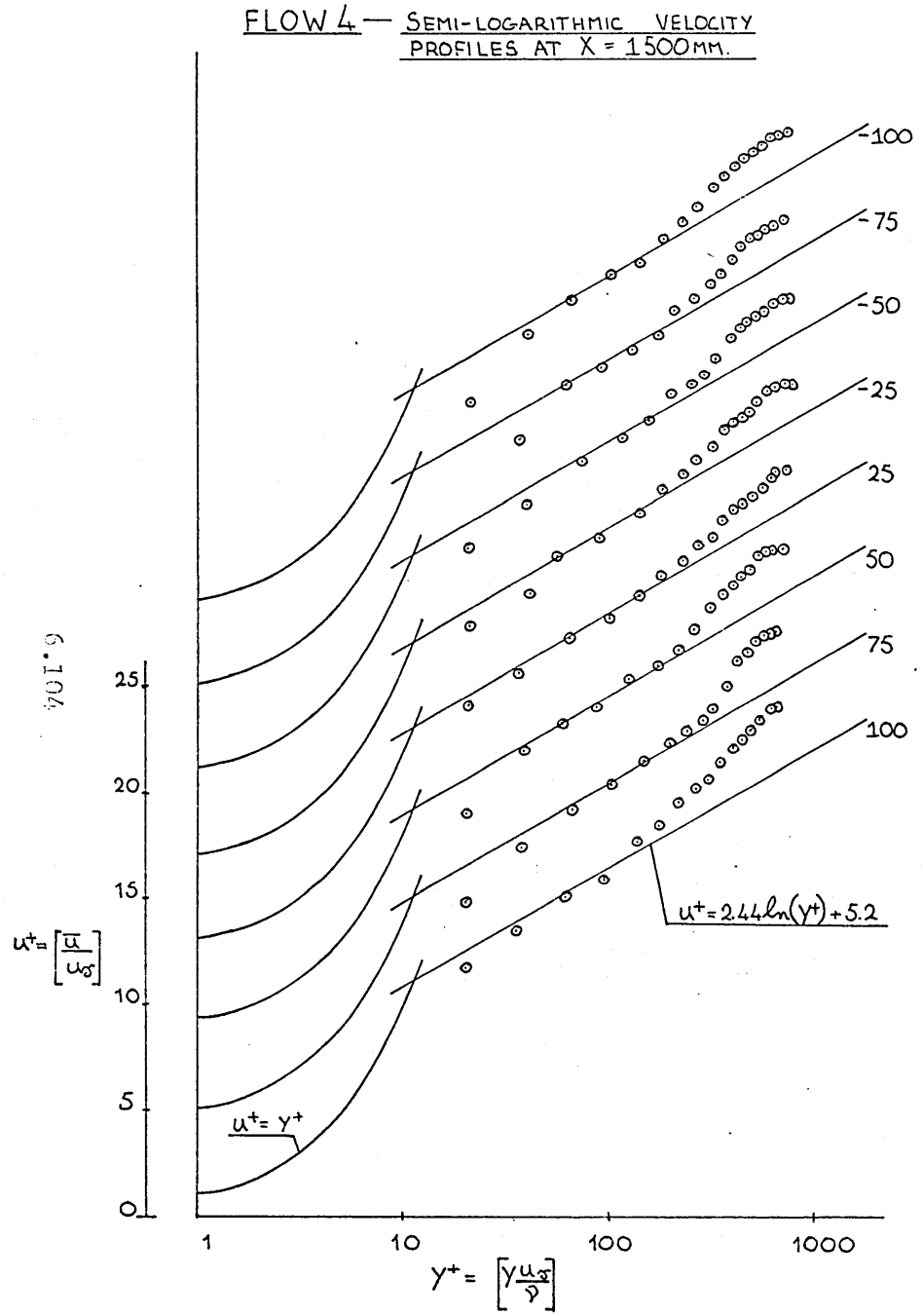
FLOW 4 — SEMI-LOGARITHMIC VELOCITY PROFILES AT X = 1500MM.
-100
-75
-50
-25
25
50
75
100
$u^+ = 2.44 \ln(y^+) + 5.2$
$u^+ = y^+$
$u^+ = \left[\frac{\bar{u}}{u_\tau}\right]$
$y^+ = \left[\frac{y u_\tau}{\nu}\right]$
0
5
10
15
20
25
1
10
100
1000

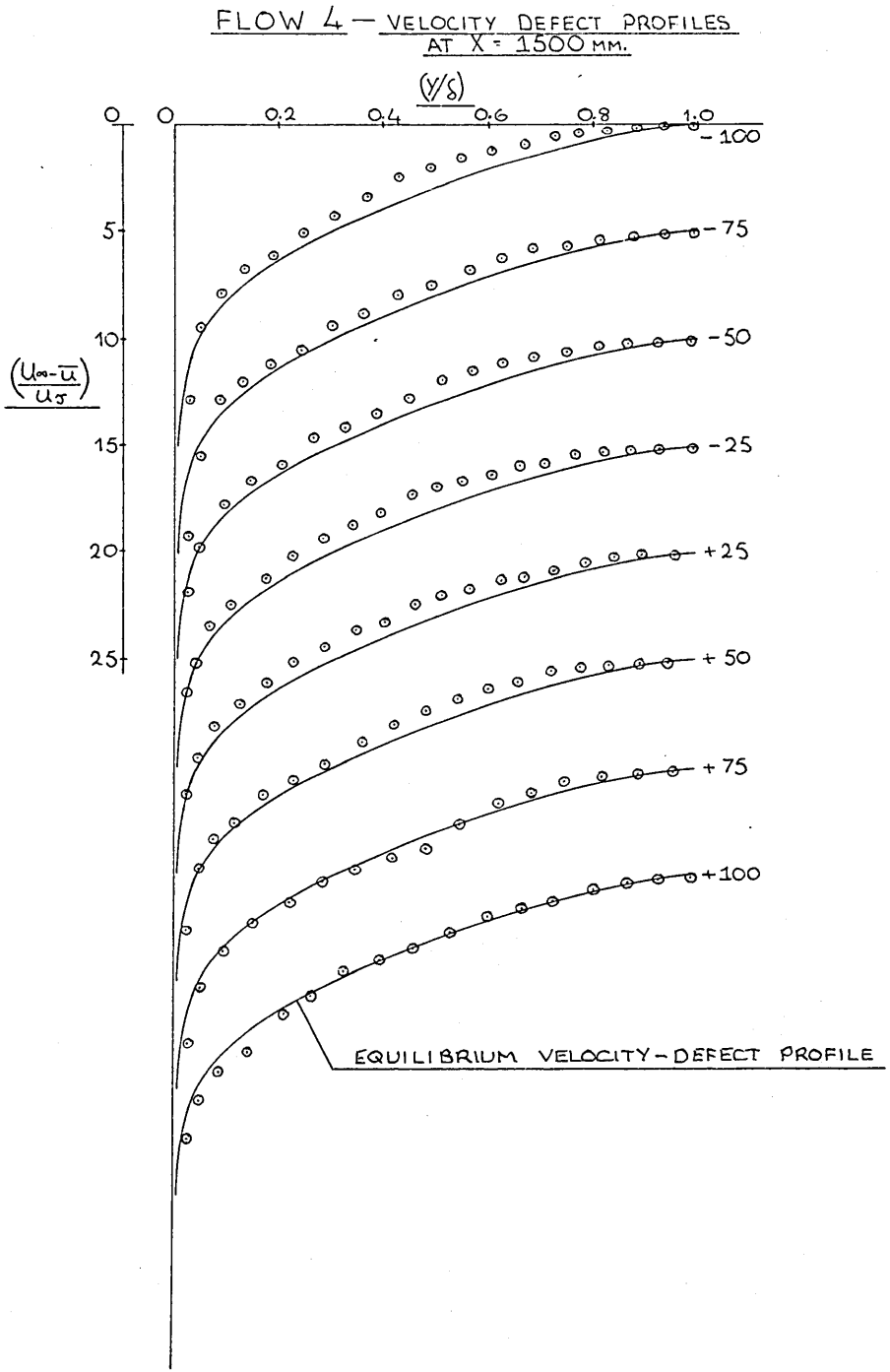
FLOW 4 — VELOCITY DEFECT PROFILES AT X = 1500 MM.
(y/δ)
0
0.2
0.4
0.6
0.8
1.0
$\left(\frac{U_\infty - \bar{u}}{u_\tau}\right)$
0
5
10
15
20
25
-100
-75
-50
-25
+25
+50
+75
+100
EQUILIBRIUM VELOCITY-DEFECT PROFILE

FIG 4.10

FIG 4.11

FLOW 4 — SPANWISE u'-INTENSITY PROFILES AT X = 300 MM.

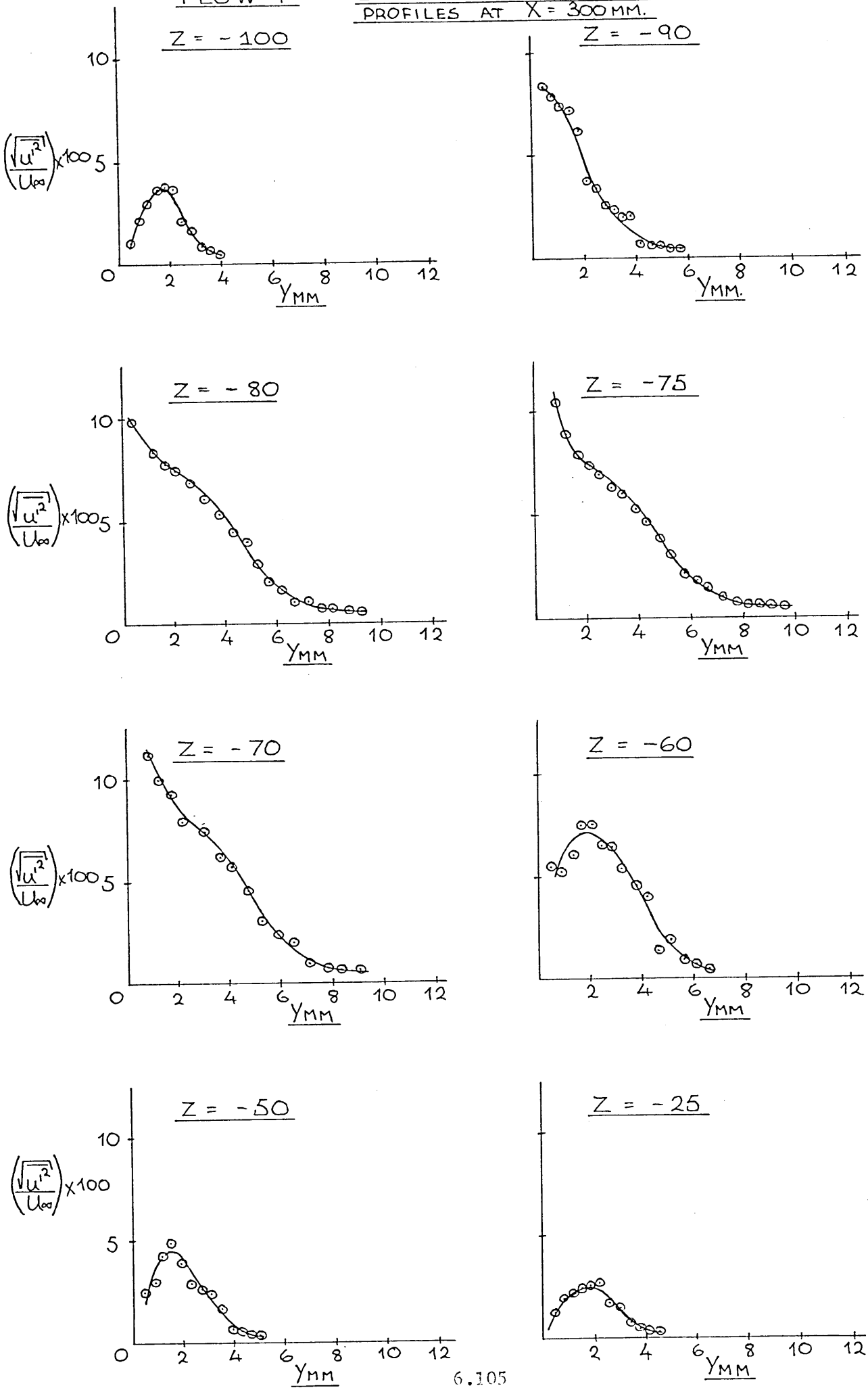

FLOW 4 — SPANWISE u'-INTENSITY PROFILES AT X = 300MM.

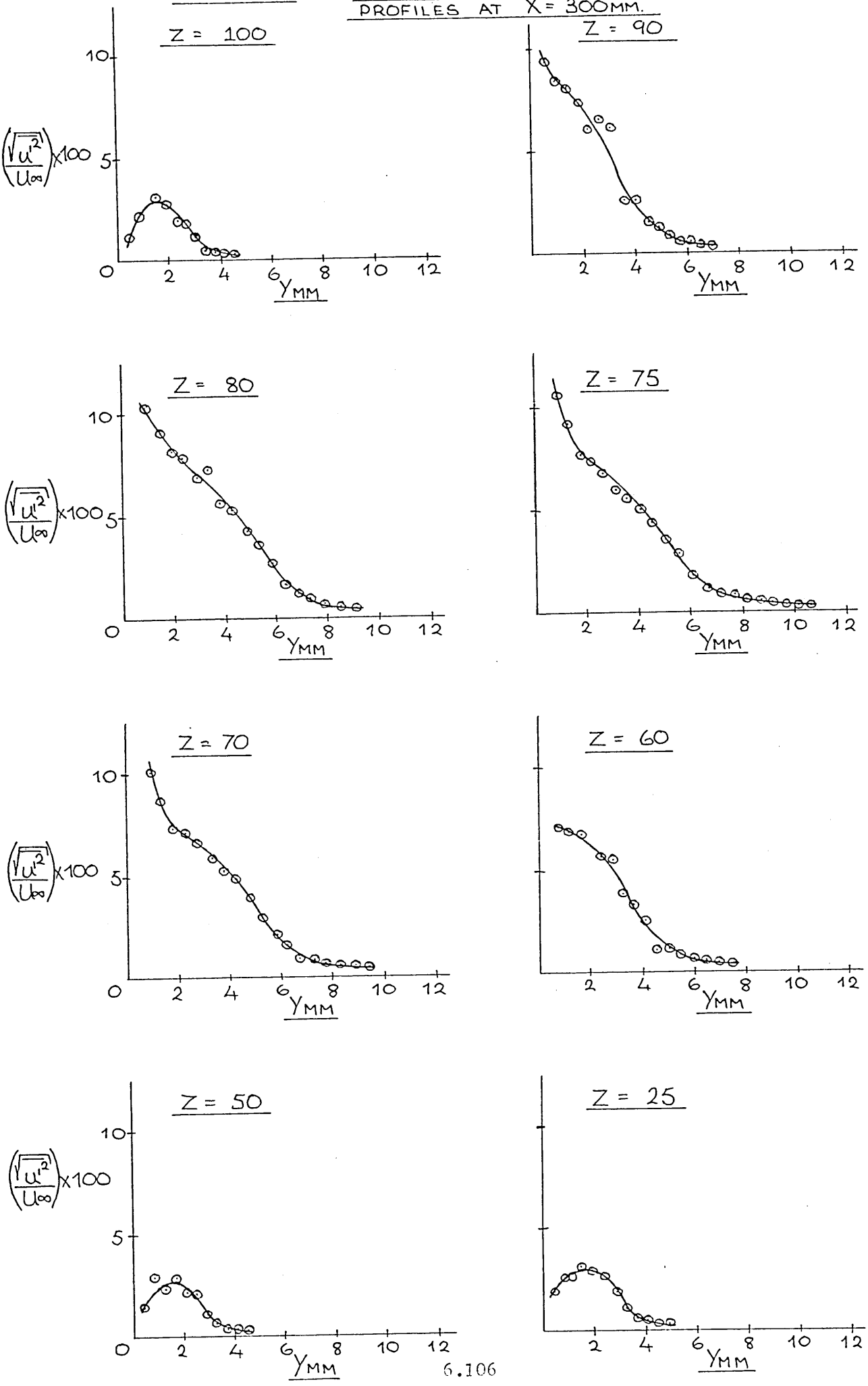

FIG 4.13

FLOW 4 — SPANWISE u'-INTENSITY PROFILES AT X = 550MM.

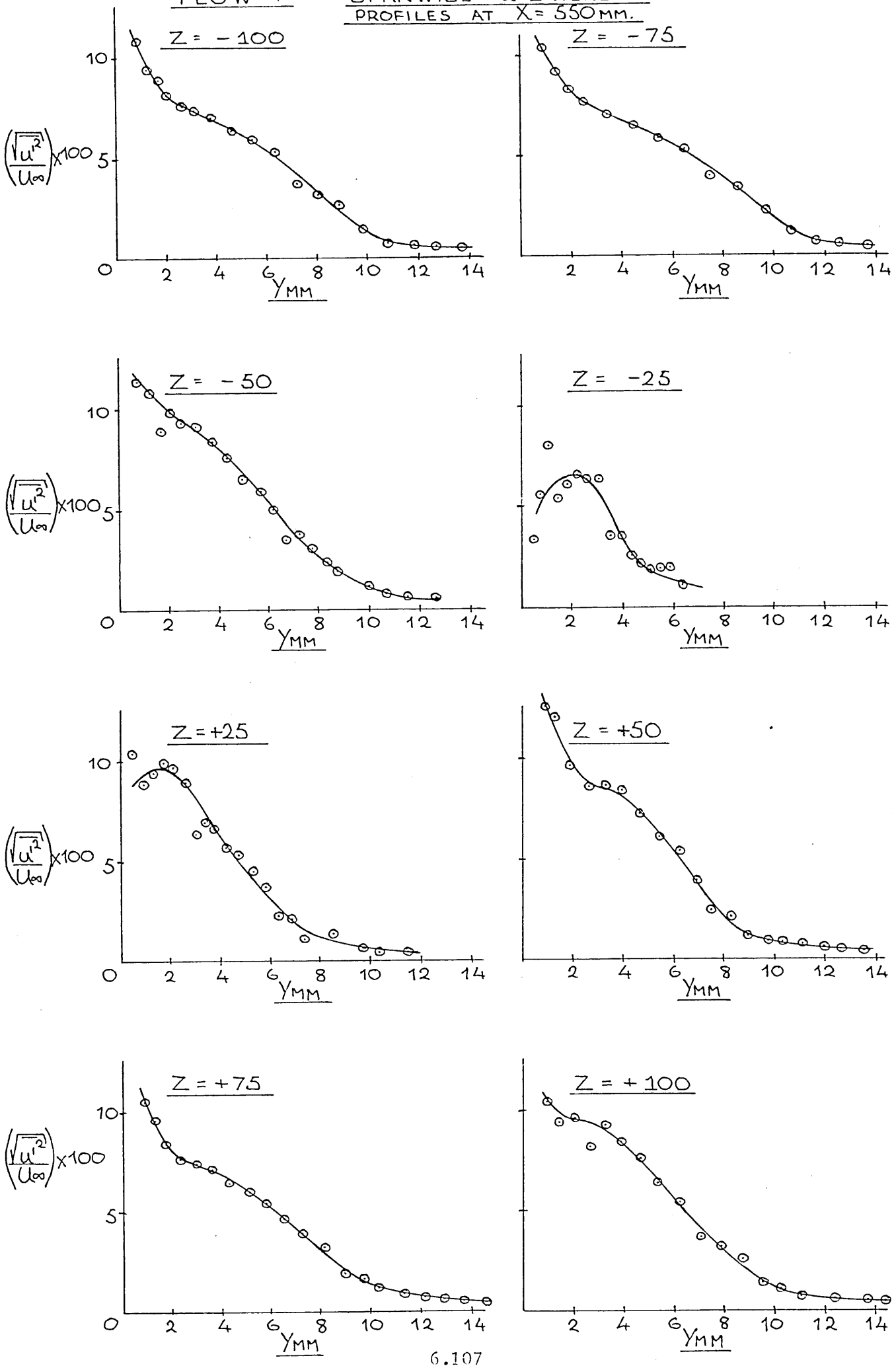

FIG 4.14

FLOW 4 — SPANWISE u'-INTENSITY PROFILES AT X = 750MM

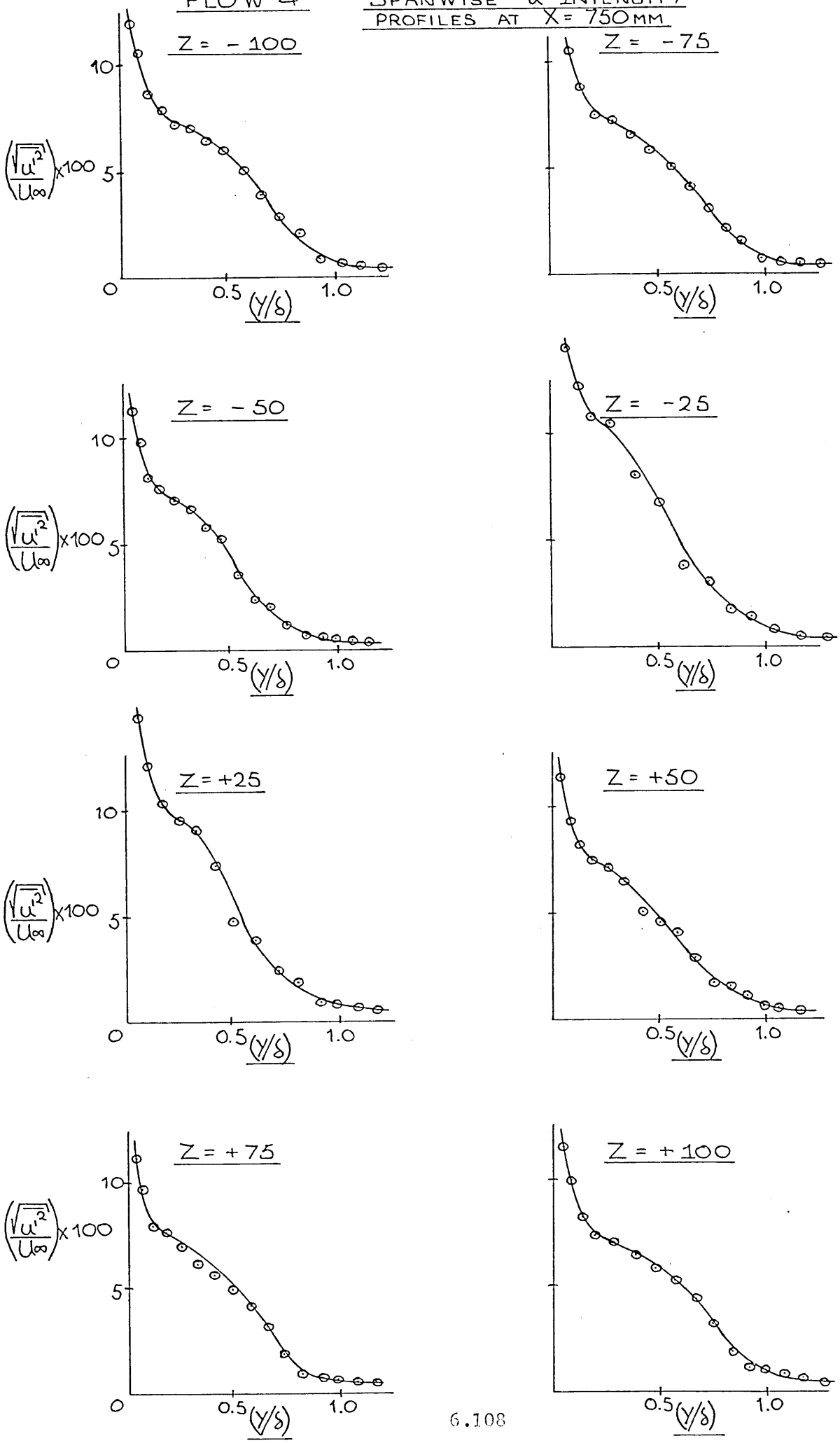

FLOW 4 — SPANWISE u'-INTENSITY PROFILES AT X = 1000 MM

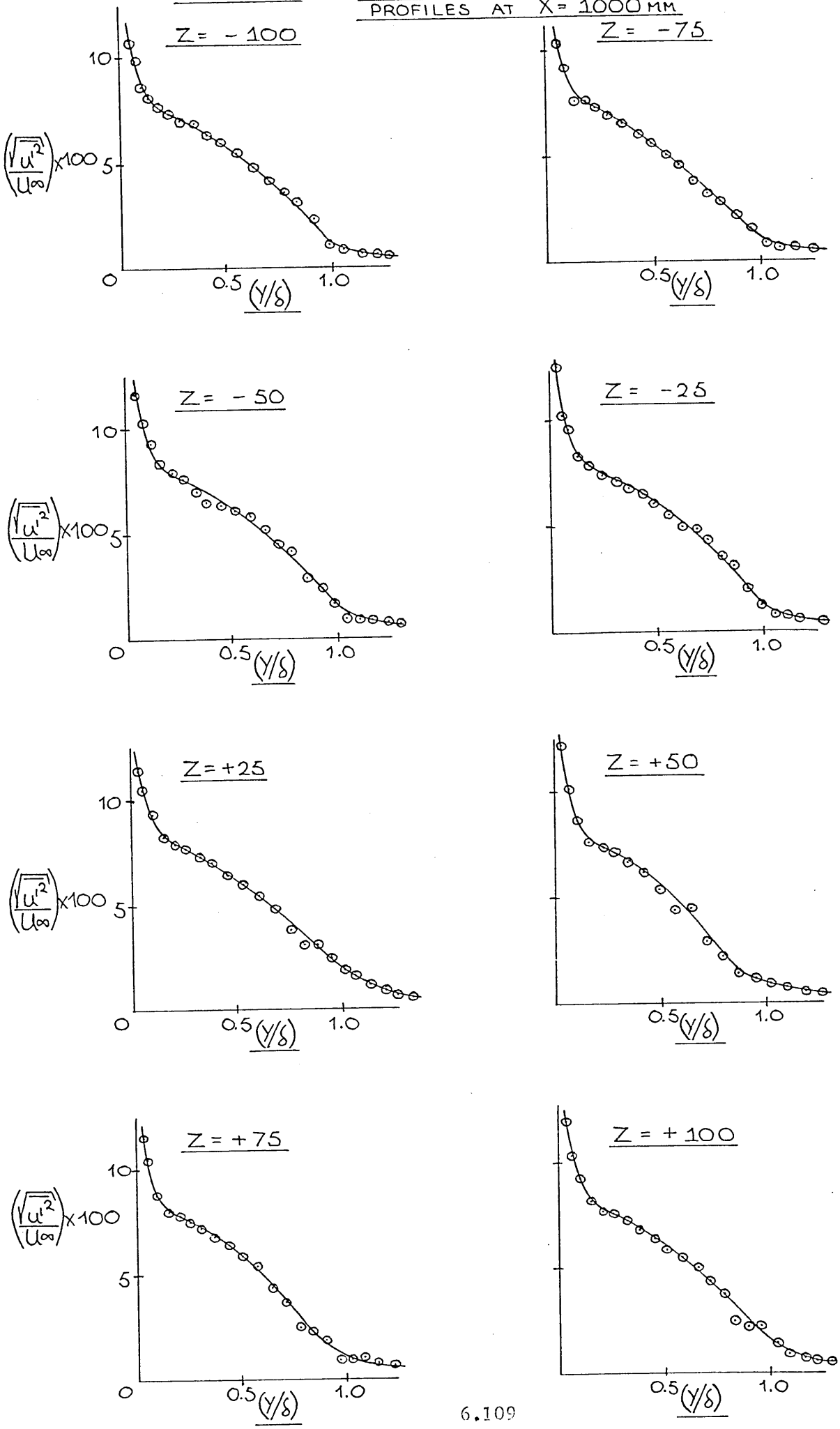

FIG 4.16

FLOW 4 — SPANWISE $\overline{u'}$-INTENSITY PROFILES AT X = 1500 MM.

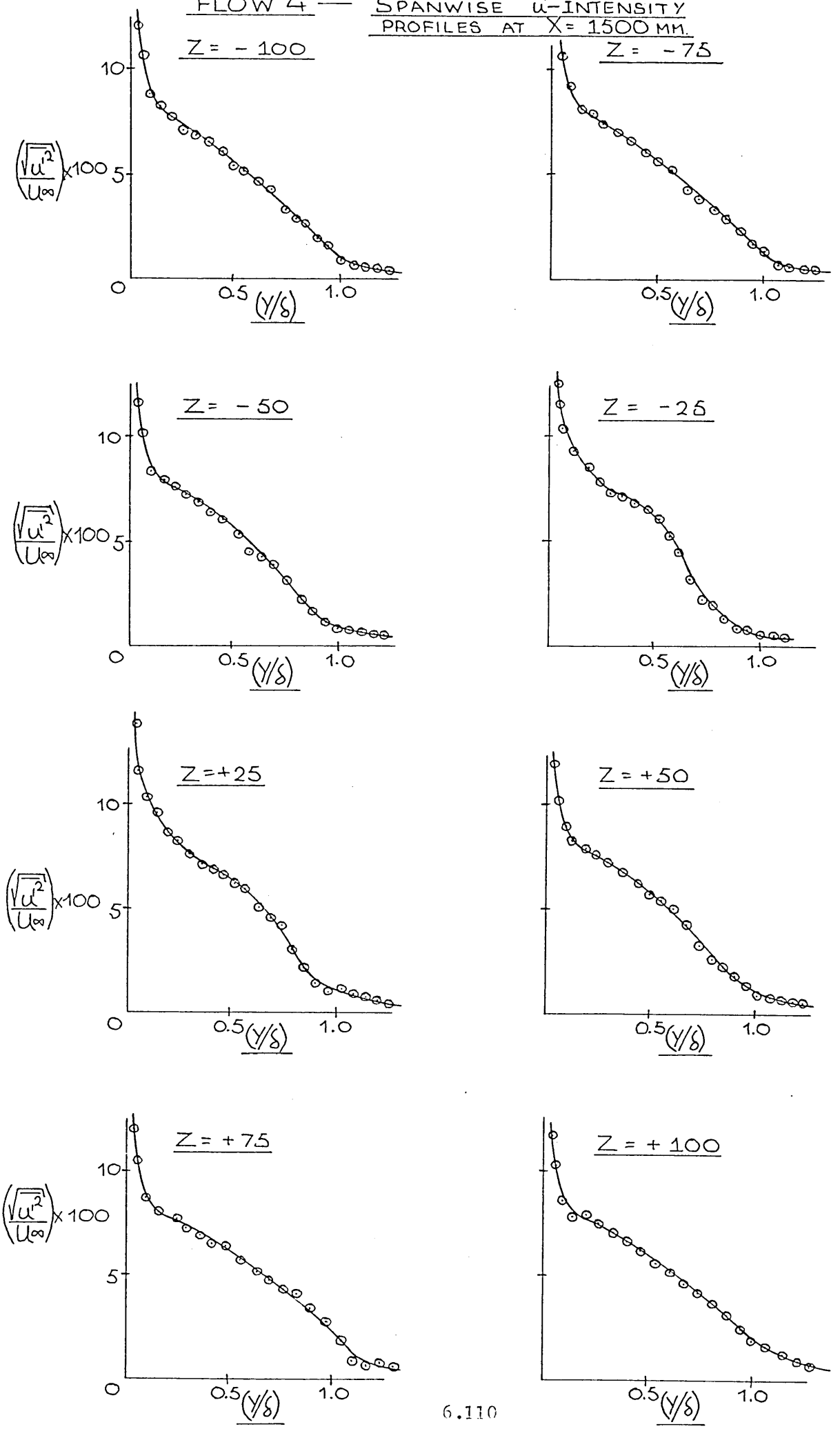

FLOW 4 – INTERMITTENCY DEVELOPMENT BEHIND ISOLATED ROUGHNESS ELEMENTS

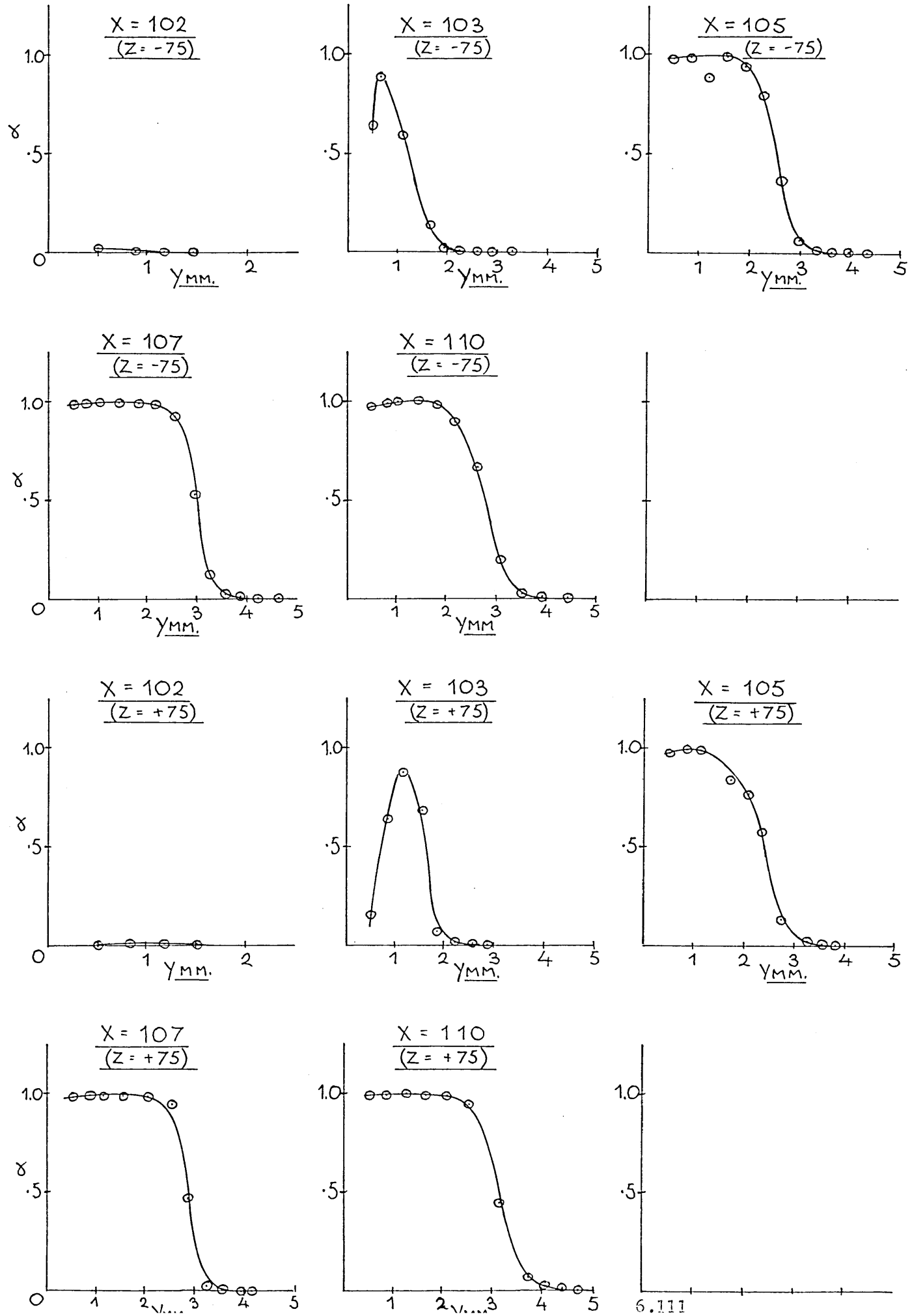

FIG 1.18

FLOW 4 — SPANWISE INTERMITTENCY PROFILES AT X = 200MM.

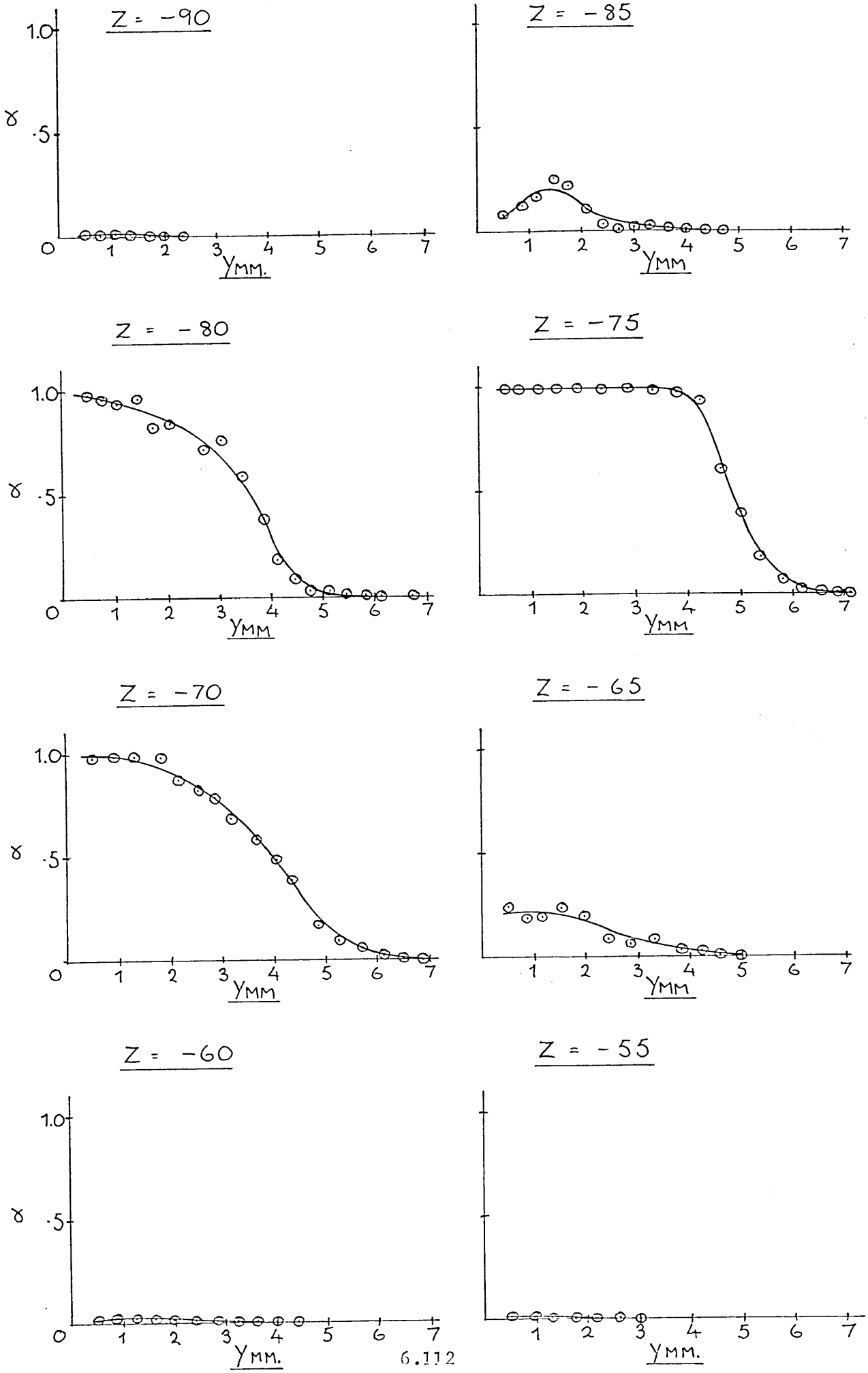

FLOW 4 — SPANWISE INTERMITTENCY PROFILES AT X = 200MM.

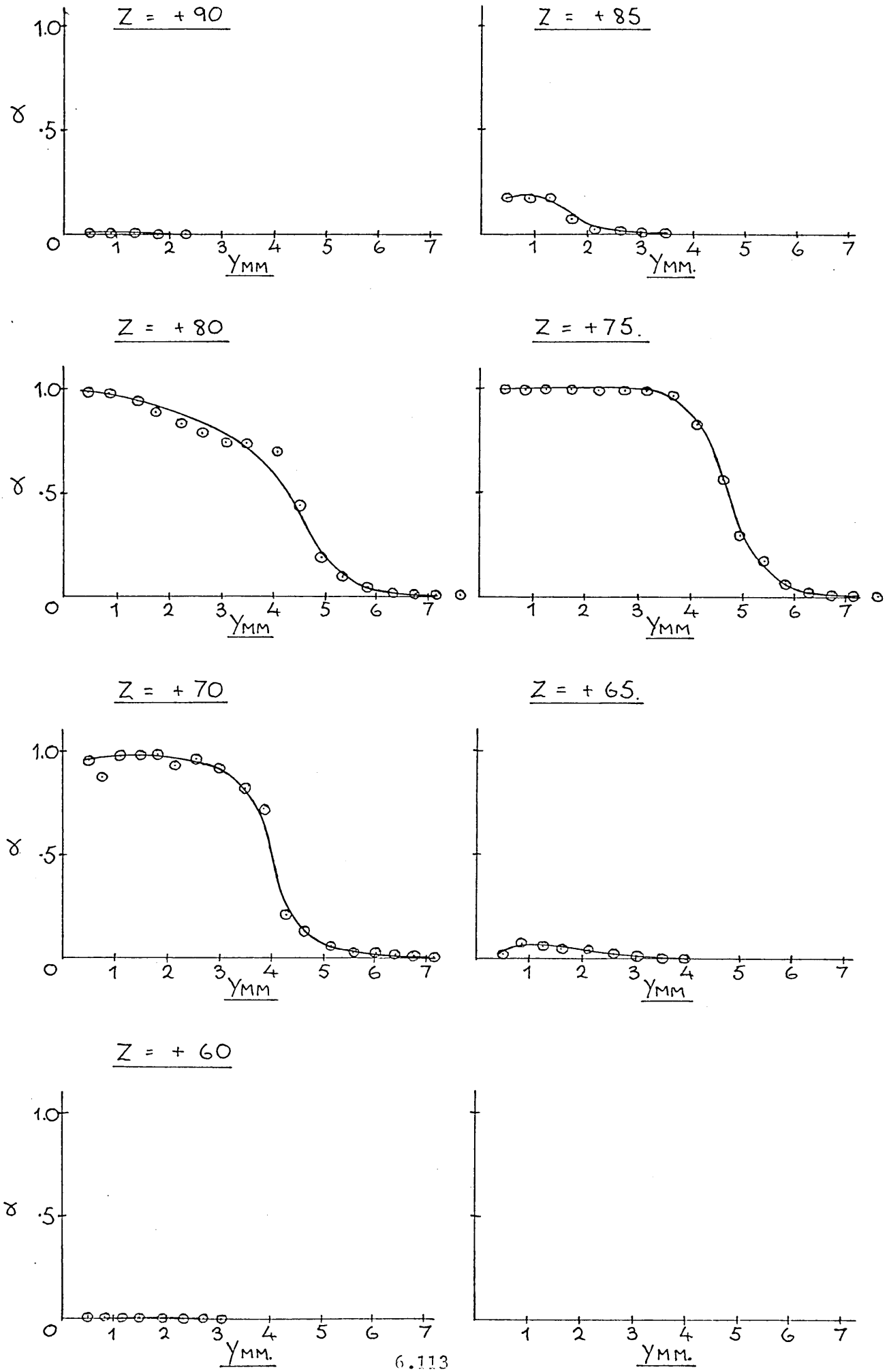

FIG 4.20

FLOW 4 — SPANWISE INTERMITTENCY PROFILES AT X = 300 MM.

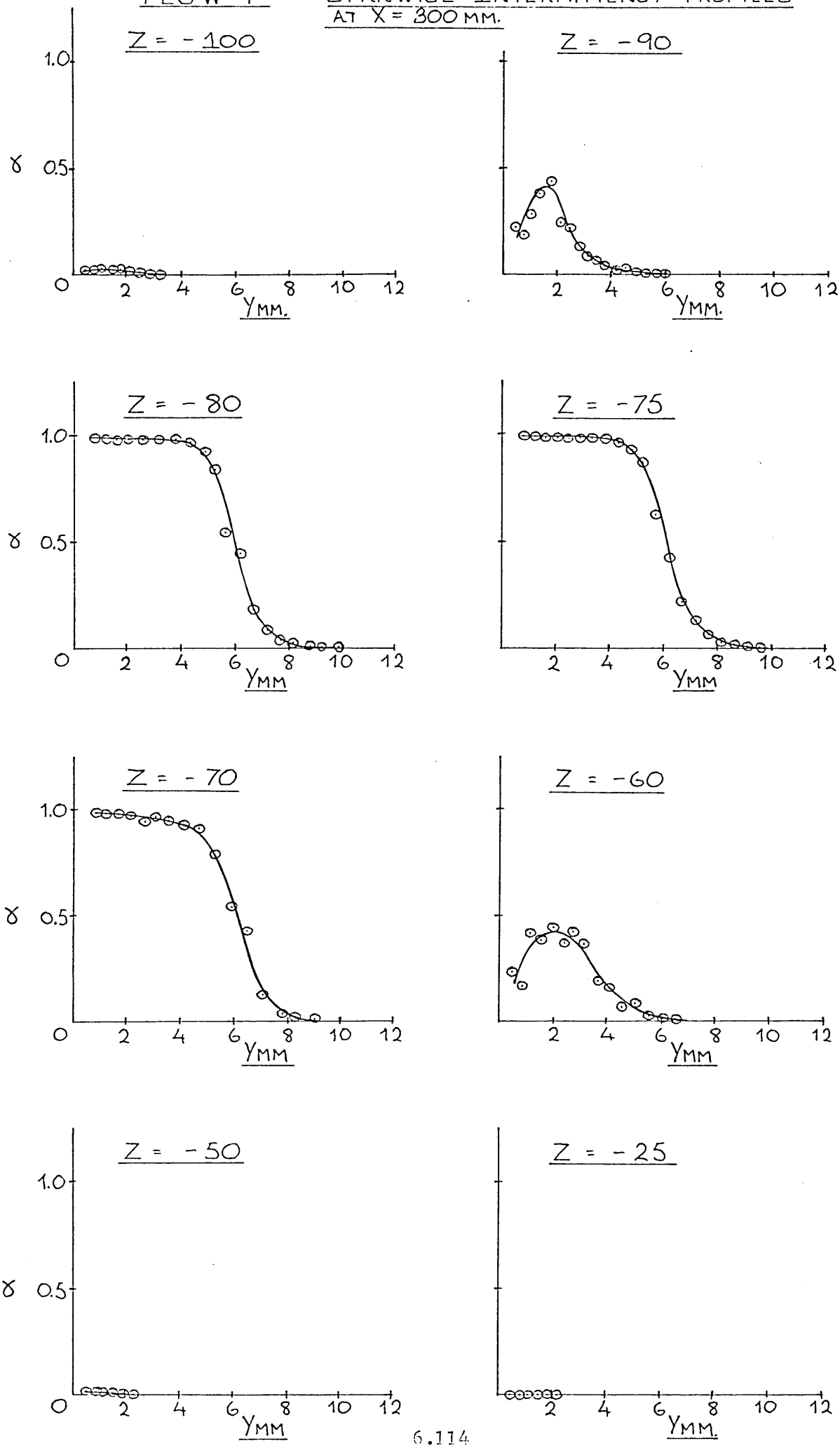

FIG 4.21

FLOW 4 — SPANWISE INTERMITTENCY PROFILES AT X = 300 MM.

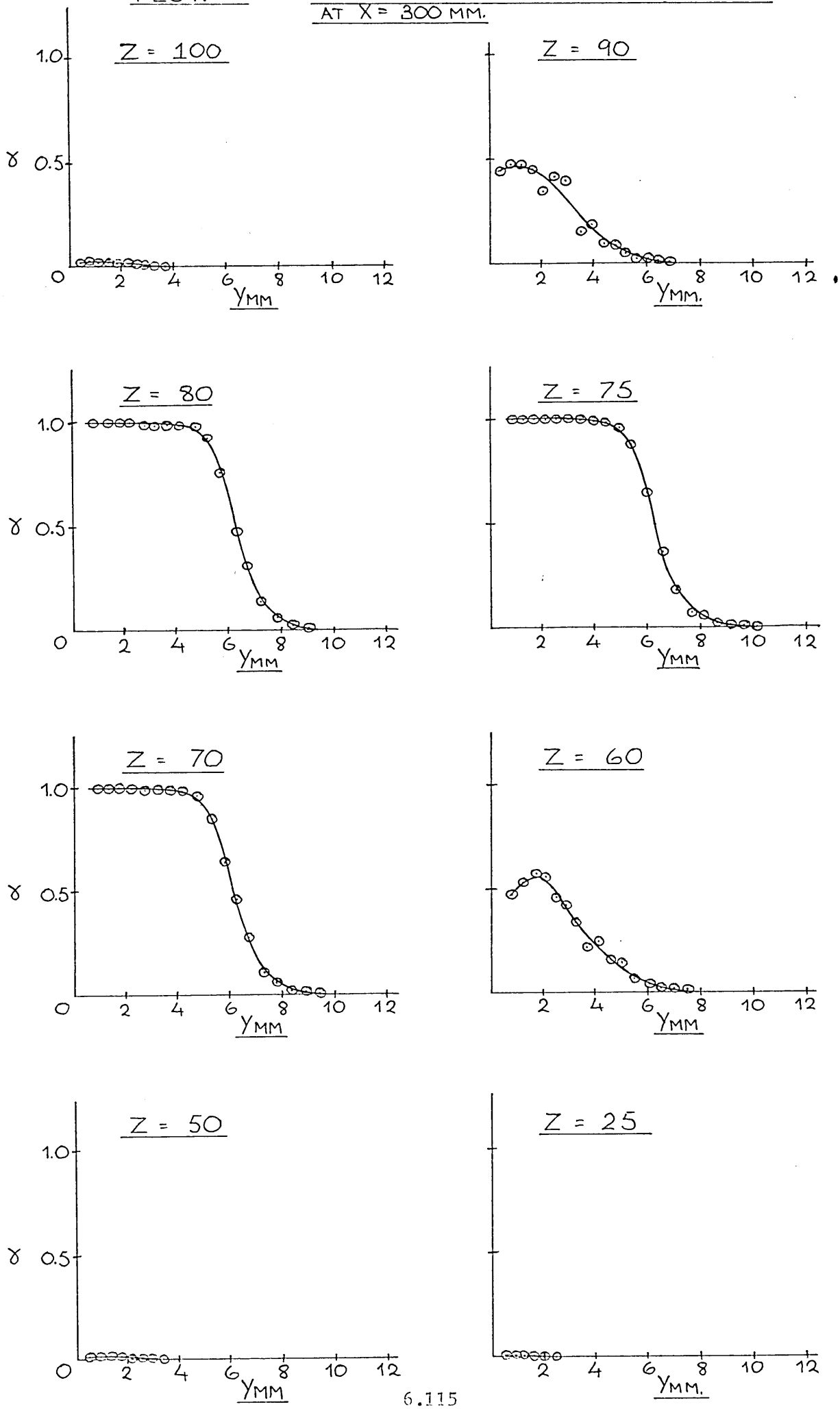

FIG 4.22

FLOW 4 — SPANWISE INTERMITTENCY PROFILES AT X = 550 MM.

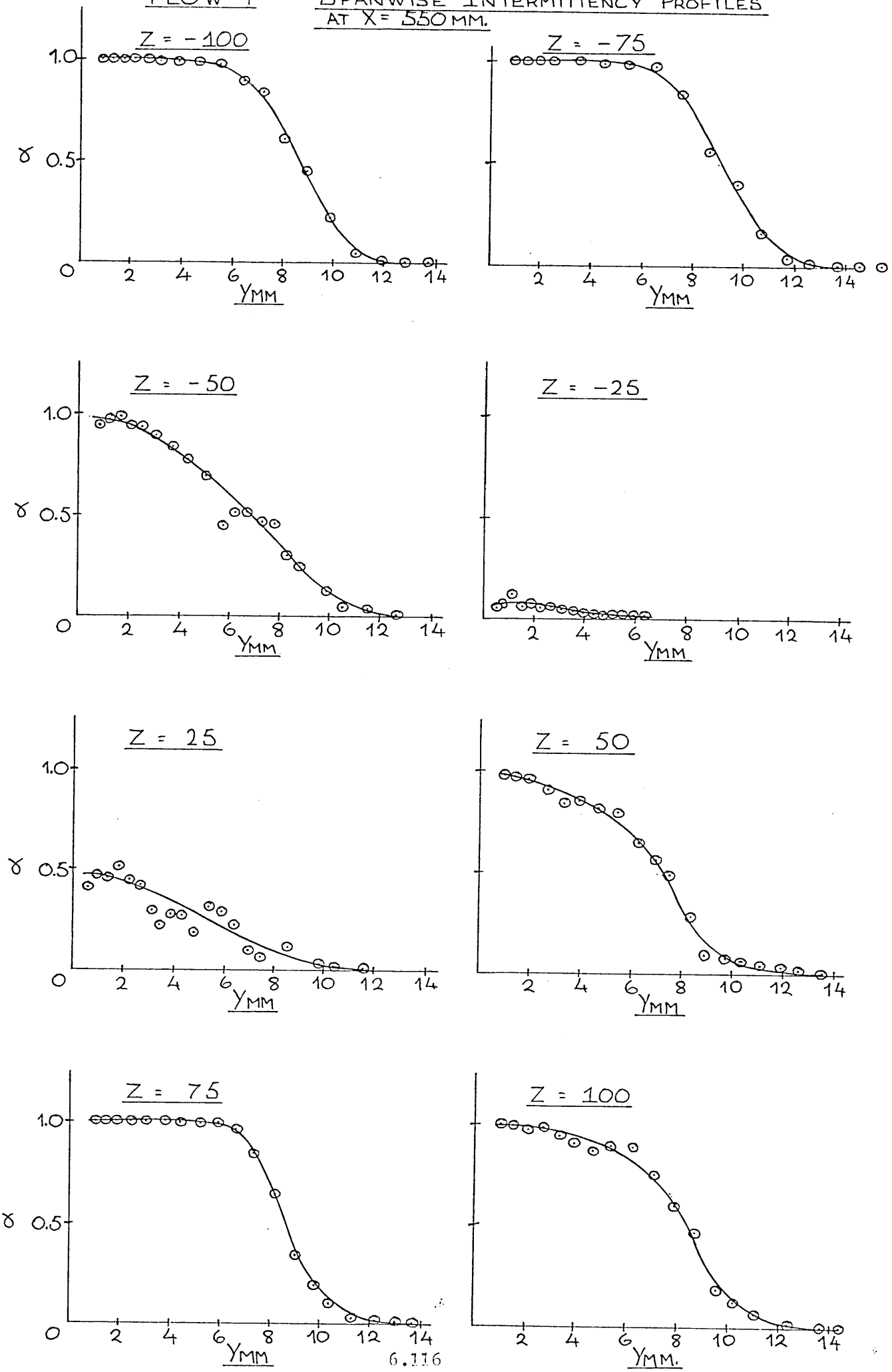

FIG 4.23

FLOW 4 — SPANWISE INTERMITTENCY PROFILES AT X= 750MM.

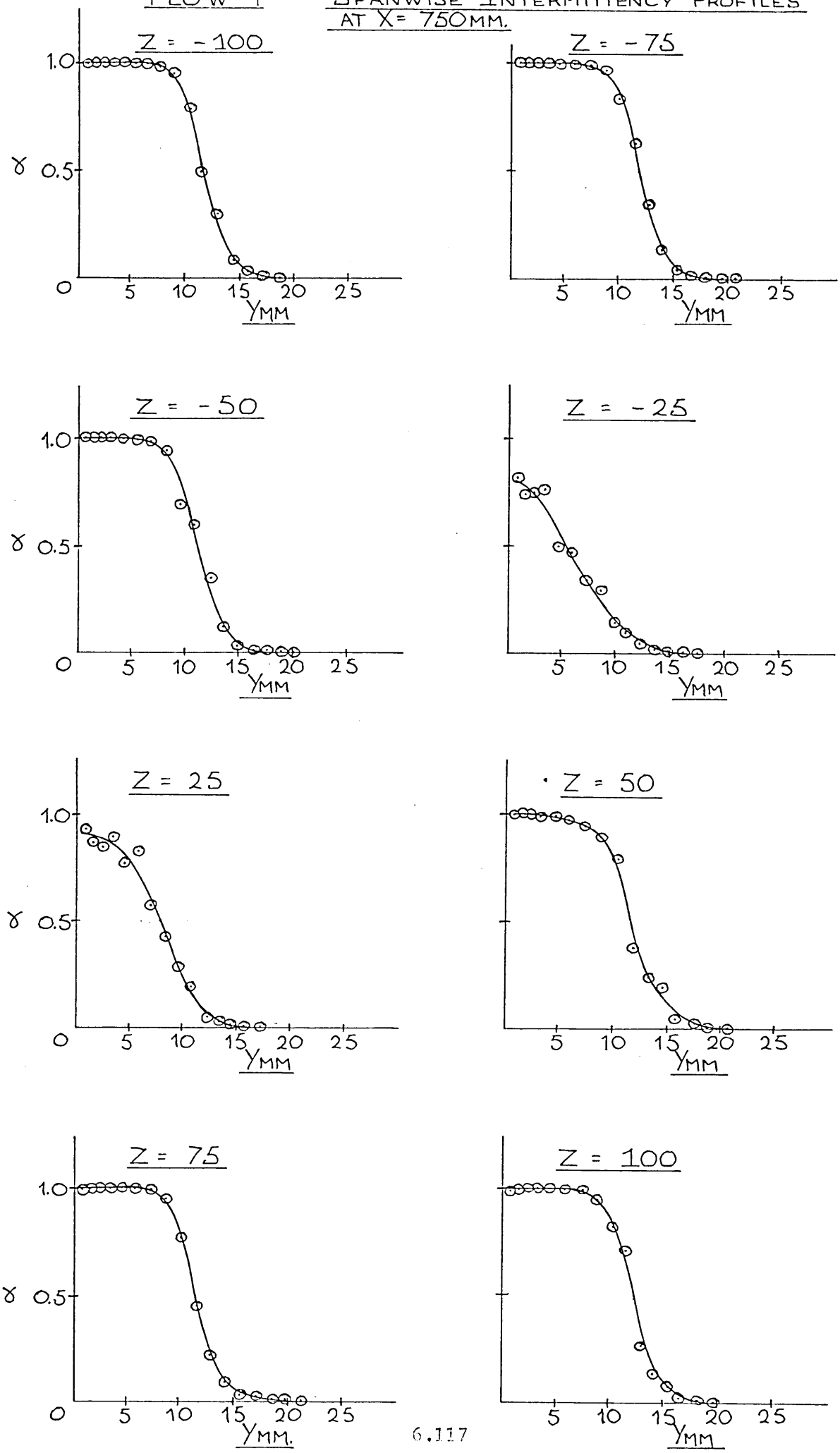

FIG 4.24

FLOW 4 — SPANWISE INTERMITTENCY PROFILES AT X = 1000 MM

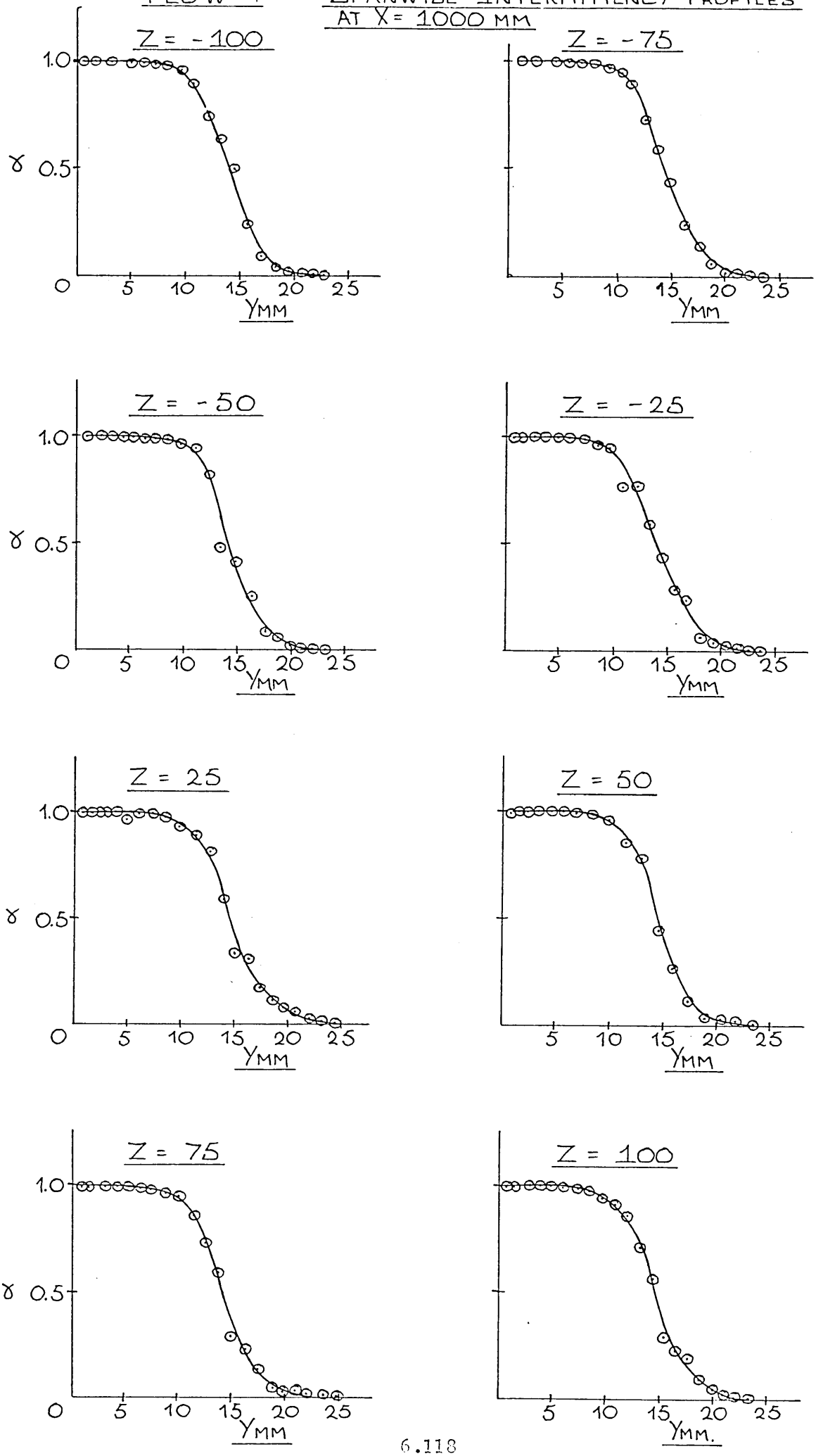

FIG 4.25

FLOW 4 — SPANWISE INTERMITTENCY PROFILES AT X= 1500 MM

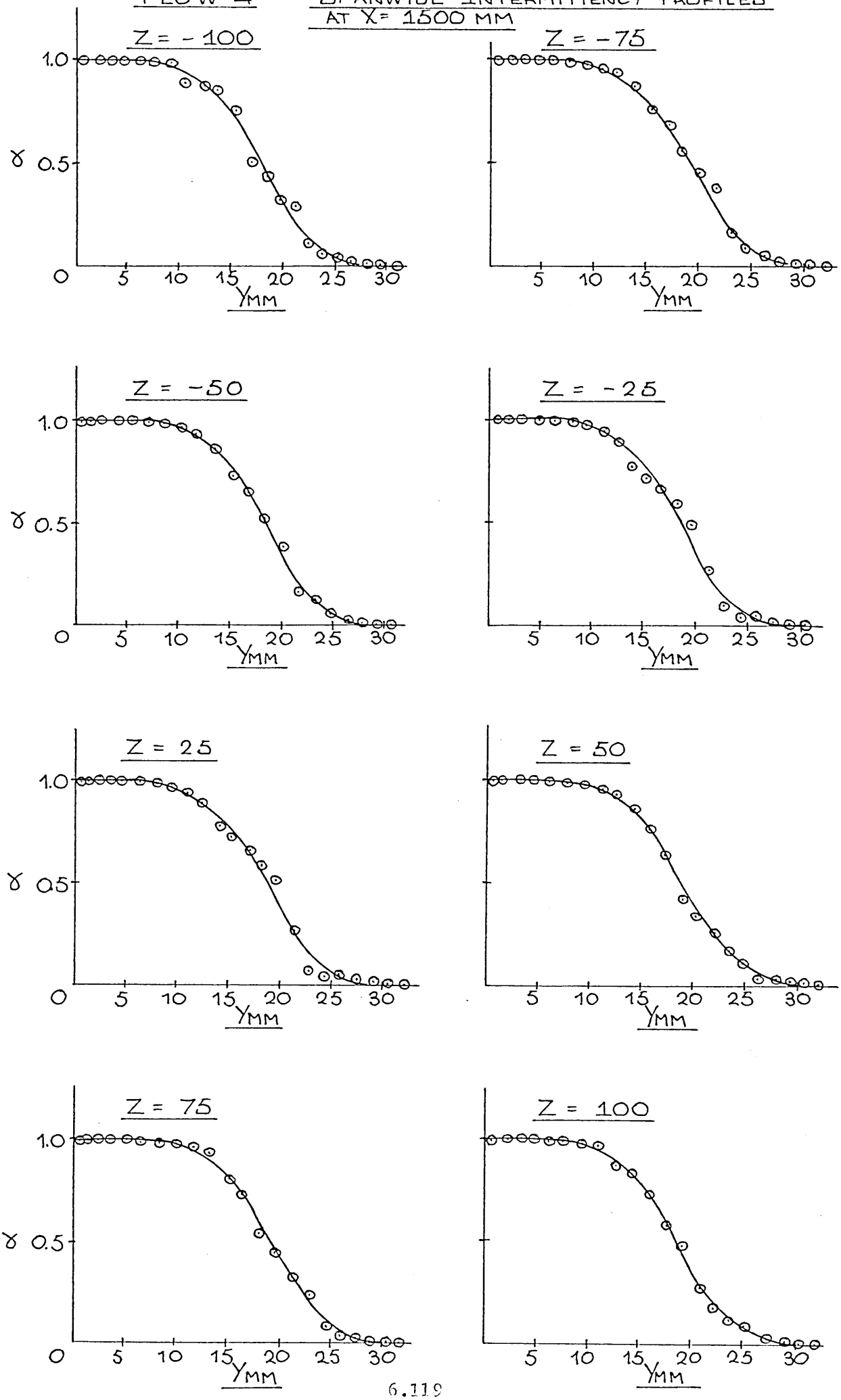

FLOW 4 - Secondary Data (X = 300mm.)

	INTEGRAL PARAMETERS (mm.)				SHAPE FACTOR		SKIN FRICTION×1000			
Zmm	Delta	Displ	Mom	En	H12	H32	Cf.1	Cf.2	Cf.3	Cf.4
100	3.73	1.282	0.476	0.741	2.69	1.56	1.286	1.530		
90	5.67	1.440	0.577	0.907	2.50	1.57	1.331	3.778		
80	7.16	1.109	0.712	1.241	1.56	1.74	5.585	5.458		
75	8.00	1.084	0.707	1.243	1.53	1.76	5.705	5.484		
70	6.74	1.043	0.673	1.177	1.55	1.75	5.768	5.596		
60	5.42	0.839	0.515	0.888	1.63	1.73	6.203	3.891		
50	4.11	1.296	0.484	0.758	2.68	1.57	1.318	1.445		
25	3.92	1.258	0.465	0.722	2.71	1.55	1.324	1.480		
-25	4.04	1.174	0.470	0.747	2.50	1.59	1.479	1.433		
-50	4.08	1.256	0.483	0.758	2.60	1.57	1.358	1.454		
-60	5.35	1.367	0.571	0.910	2.39	1.59	1.331	2.815		
-70	6.57	1.094	0.703	1.225	1.57	1.74	5.653	5.389		
-75	7.00	1.060	0.683	1.195	1.55	1.75	5.734	5.566		
-80	7.16	1.056	0.683	1.195	1.55	1.75	5.760	5.518		
-90	4.93	1.285	0.550	0.884	2.33	1.61	1.475	2.412		
-100	3.25	1.265	0.450	0.695	2.81	1.54	1.284	1.652		

Zmm	Intermittency (mean value)	Rtheta	Wake Parameter	Wake Strength Parameter
	$\bar{\gamma}$	R_θ	Π	$\Delta\frac{u}{u_\tau}$
100	0.020	309		
90	0.454	378		
80	1.000	463	0.06	0.606
75	1.000	461	-0.04	0.290
70	1.000	438	0.02	0.346
60	0.515	336	-0.03	0.506
50	0.010	316		
25	0.005	304		
-25	0.000	307		
-50	0.010	314		
-60	0.346	372		
-70	0.980	458	0.076	0.430
-75	0.998	445	0.013	0.474
-80	0.990	444	-0.007	0.420
-90	0.242	358		
-100	0.022	288		

NB. Cf.1 - from velocity profile ie. average du/dy or Log-law.
Cf.2 - equation
Cf.3 - by Preston tube 1.105mm. O.D.
Cf.4 - " " " 1.410mm. O.D.

021.6

FLOW 4 - Secondary Data (X = 550mm.)

	INTEGRAL PARAMETERS (mm.)				SHAPE FACTOR		SKIN FRICTION×1000			
Zmm	Delta	Displ	Mom	En	H12	H32	Cf.1	Cf.2	Cf.3	Cf.4
100	10.04	1.328	0.878	1.542	1.51	1.76	5.289	4.966		
75	10.00	1.568	1.046	1.833	1.50	1.75	4.998	4.706		
50	9.73	1.307	0.868	1.525	1.51	1.76	5.406	4.900		
25	7.48	1.528	0.687	1.117	2.22	1.63	1.525	2.888		
-25	5.23	1.537	0.617	0.976	2.50	1.58	1.110	1.355		
-50	10.07	1.369	0.894	1.556	1.53	1.74	5.240	4.770		
-75	11.06	1.706	1.146	2.010	1.49	1.76	4.853	4.559		
-100	10.93	1.516	1.008	1.767	1.51	1.75	5.050	4.764		

Zmm	Intermittency (mean value)	Rtheta	Wake Parameter	Wake Strength Parameter
	$\bar{\gamma}$	R_θ	Π	$\Delta\frac{u}{u_\tau}$
100	0.984	572	0.011	0.656
75	1.000	681	0.143	0.837
50	0.962	564	-0.021	0.384
25	0.450	446		
-25	0.059	401		
-50	0.950	580	0.032	0.686
-75	1.000	745	0.160	0.966
-100	1.000	655	0.074	0.805

Secondary Data (X = 750)

	INTEGRAL PARAMETERS (mm)				SHAPE FACTOR		SKIN FRICTION×1000			
Zmm	Delta	Displ	Mom	En	H12	H32	Cf.1	Cf.2	Cf.3	Cf.4
100	15.41	2.376	1.631	2.870	1.46	1.76	4.306	4.043		
75	17.09	2.317	1.587	2.793	1.46	1.76	4.322	4.087	4.090	4.109
50	17.59	1.979	1.360	2.404	1.46	1.77	4.629	4.300		
25	13.37	1.520	1.024	1.807	1.49	1.76	5.047	4.256		
-25	11.60	1.427	0.939	1.643	1.52	1.75	5.109	3.902		
-50	17.55	2.025	1.382	2.435	1.47	1.76	4.538	4.282		
-75	15.34	2.222	1.492	2.606	1.49	1.75	4.307	4.109	4.139	4.199
-100	15.15	2.153	1.470	2.587	1.46	1.76	4.468	4.211		

Zmm	Intermittency (mean value)	Rtheta	Wake Parameter	Wake Strength Parameter
	$\bar{\gamma}$	R_θ	Π	$\Delta\frac{u}{u_\tau}$
100	1.000	1062	0.281	1.319
75	1.000	1032	0.220	1.430
50	0.992	884	0.040	1.020
25	0.886	666	-0.025	0.861
-25	0.763	610	0.018	1.167
-50	1.000	898	0.089	1.292
-75	1.000	970	0.283	1.821
-100	1.000	953	0.201	1.185

FIG 4.26

FLOW 4 - Secondary Data (X = 1000mm)

	INTEGRAL PARAMETERS (mm)				SHAPE FACTOR		SKIN FRICTION×1000			
Zmm	Delta	Displ	Mom	En	H12	H32	Cf.1	Cf.2	Cf.3	Cf.4
100	18.07	3.014	2.056	3.593	1.47	1.75	3.924	3.679	3. 675	3.731
75	19.08	3.022	2.045	3.563	1.48	1.74	3.930	3.657	3.692	3.761
50	19.81	2.892	1.990	3.492	1.45	1.76	4.019	3.785	3.709	3.792
25	18.17	2.976	2.070	3.642	1.44	1.76	4.089	3.762	3.759	3.837
-25	19.31	2.852	1.983	3.495	1.44	1.76	4.118	3.820	3.776	3.822
-50	18.80	2.843	1.972	3.471	1.44	1.76	4.094	3.830	3.773	3.792
-75	18.28	2.835	1.950	3.424	1.45	1.76	4.034	3.812	3.742	3.822
-100	17.20	2.838	1.954	3.430	1.45	1.76	4.067	3.810	3.726	3.837

Zmm	Intermittency (mean value)	Rtheta	Wake Parameter	Wake Strength Parameter
100	1.000	1338	0.434	2.094
75	1.000	1331	0.403	2.149
50	1.000	1295	0.327	1.790
25	1.000	1347	0.327	1.549
-25	1.000	1291	0.278	1.458
-50	1.000	1281	0.307	1.538
-75	1.000	1270	0.358	1.722
-100	1.000	1272	0.368	1.704

Secondary Data (X = 1500mm)

	INTEGRAL PARAMETERS (mm)				SHAPE FACTOR		SKIN FRICTION×1000			
Zmm	Delta	Displ	Mom	En	H12	H32	Cf.1	Cf.2	Cf.3	Cf.4
100	24.10	4.074	2.782	4.851	1.47	1.74	3.449	3.277	3.422	3.422
75	24.19	4.033	2.764	4.814	1.46	1.74	3.564	3.321	3.405	3.423
50	26.53	3.924	2.715	4.755	1.45	1.75	3.604	3.379	3.439	3.438
25	27.11	3.921	2.758	4.862	1.42	1.76	3.692	3.464	3.456	3.454
-25	27.52	3.893	2.723	4.792	1.43	1.76	3.667	3.444	3.507	3.516
-50	26.71	3.875	2.698	4.737	1.44	1.76	3.667	3.419	3.490	3.485
-75	24.76	3.734	2.608	4.588	1.43	1.76	3.737	3.496	3.507	3.516
-100	25.41	3.674	2.560	4.503	1.44	1.76	3.705	3.484	3.473	3.485

Zmm	Intermittency (mean value)	Rtheta	Wake Parameter	Wake Strength Parameter
	$\bar{\gamma}$	Re_θ	$\mathcal{C}$	$\Delta U_s/U_s$
100	1.000	1813	0.630	2.986
75	1.000	1798	0.541	2.770
50	1.000	1763	0.466	2.557
25	1.000	1793	0.391	2.075
-25	1.000	1770	0.401	2.135
-50	1.000	1755	0.415	2.177
-75	1.000	1696	0.404	1.971
-100	1.000	1666	0.413	2.100

FIG 4.27

FLOW 4 — STREAMWISE DEVELOPMENT OF SKIN FRICTION COEFFICIENT ALONG Z = +75

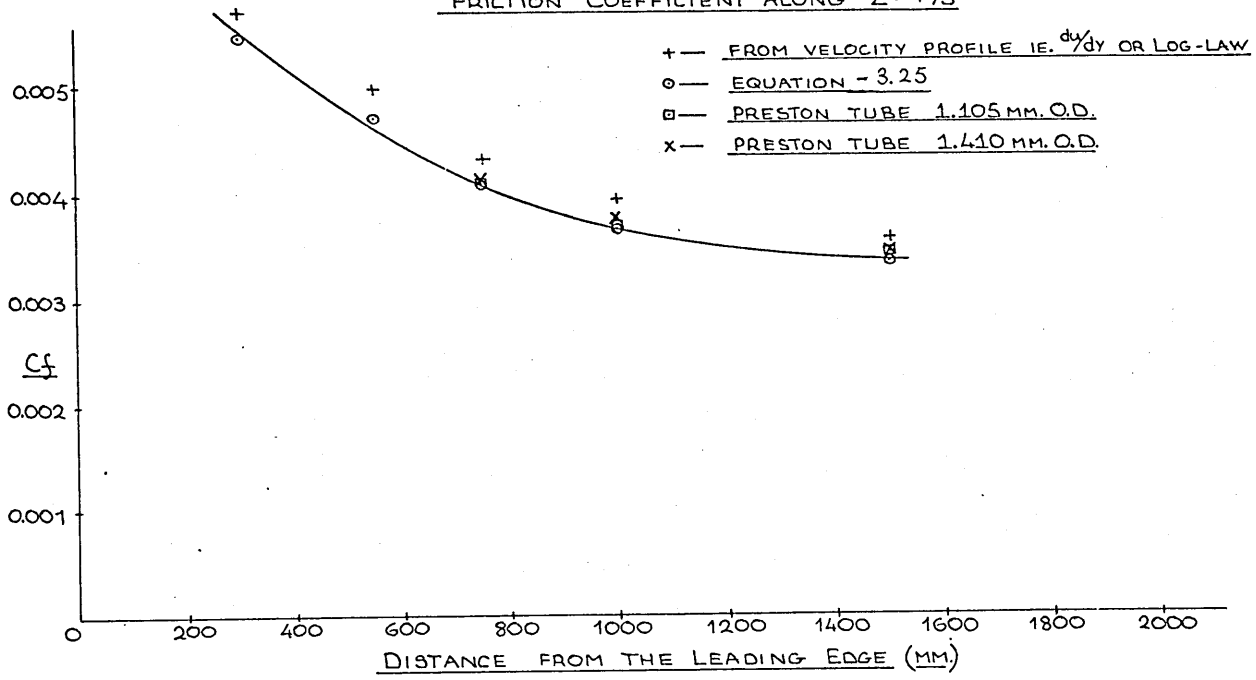

FLOW 4 — STREAMWISE DEVELOPMENT OF INTEGRAL PARAMETERS ALONG Z = +75 MM.

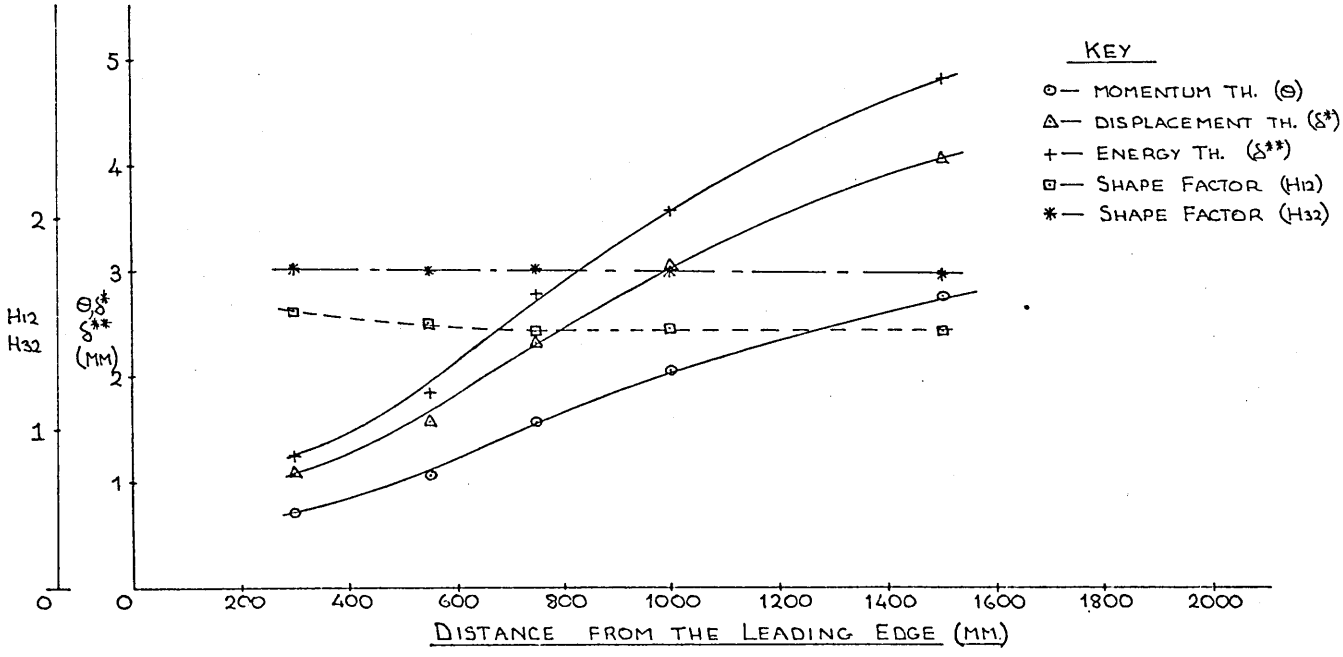

FLOW 4 — STREAMWISE DEVELOPMENT OF SKIN FRICTION COEFFICIENT ALONG Z = -75

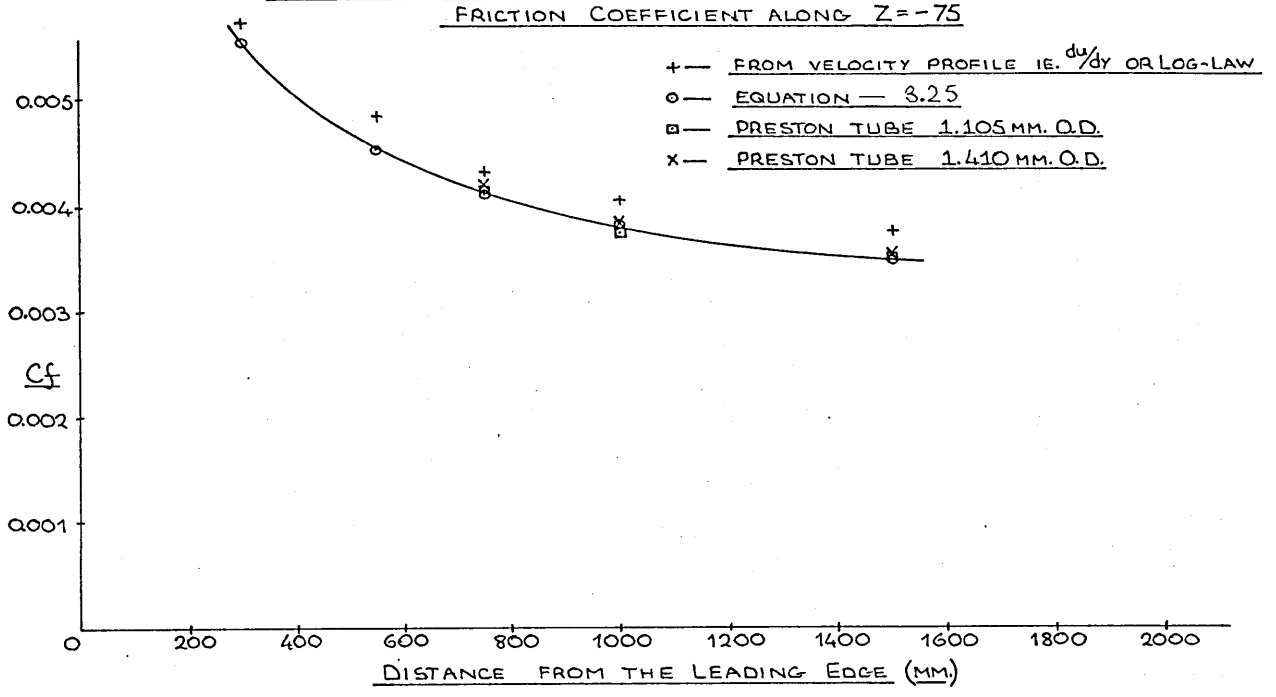

FLOW 4 — STREAMWISE DEVELOPMENT OF INTEGRAL PARAMETERS ALONG Z = -75 MM.

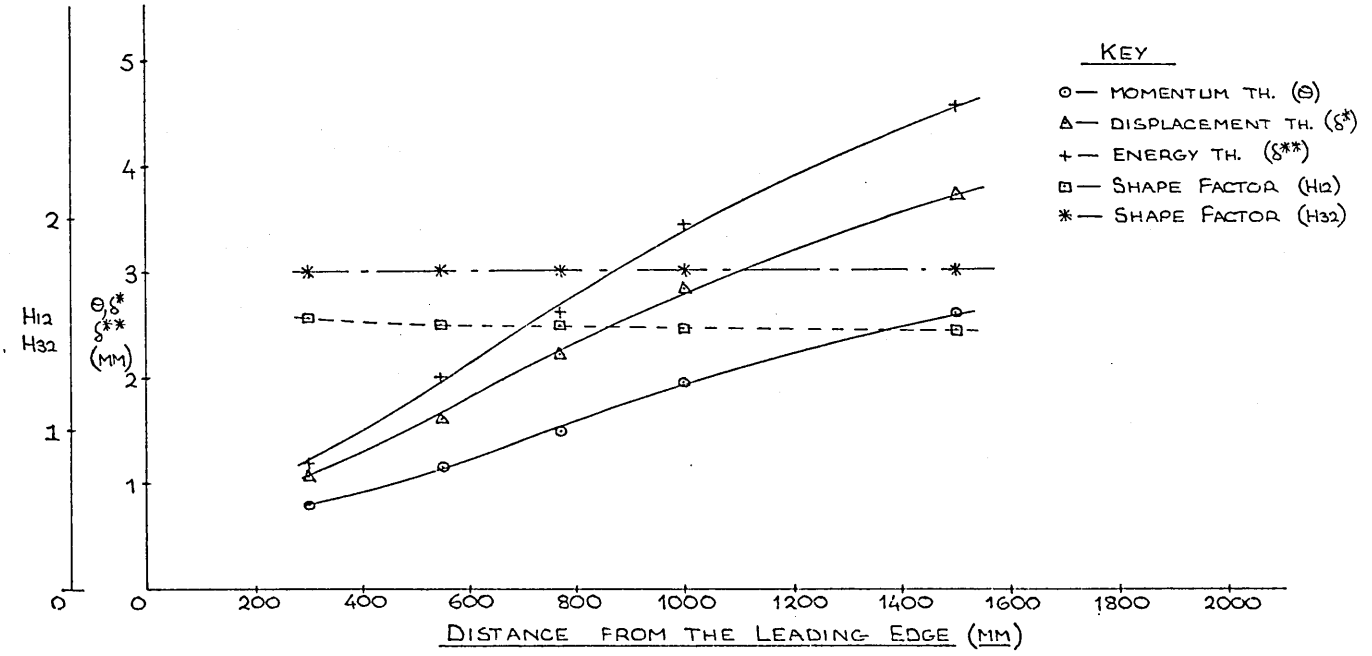

FLOW 4 — MOMENTUM BALANCE ALONG Z = ±75MM

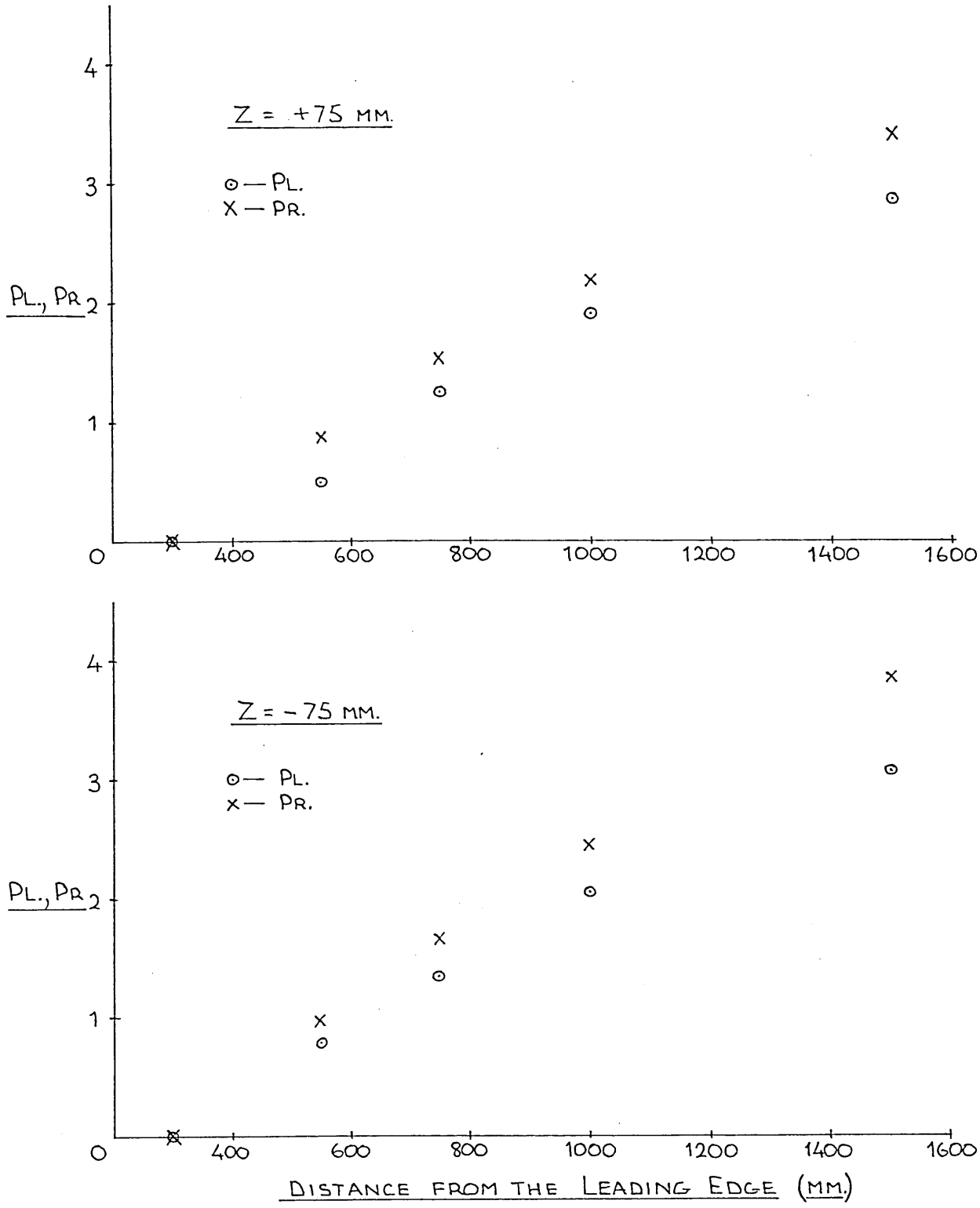

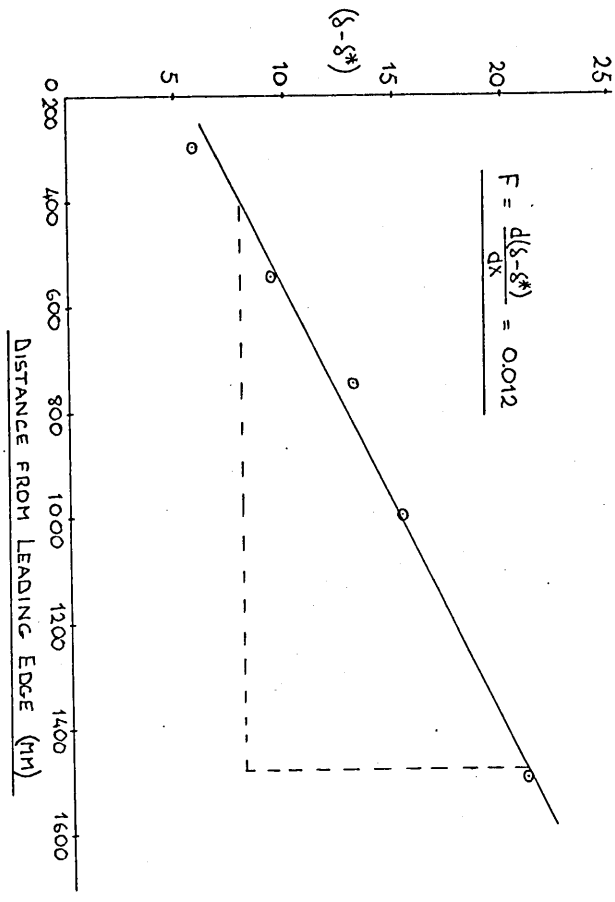

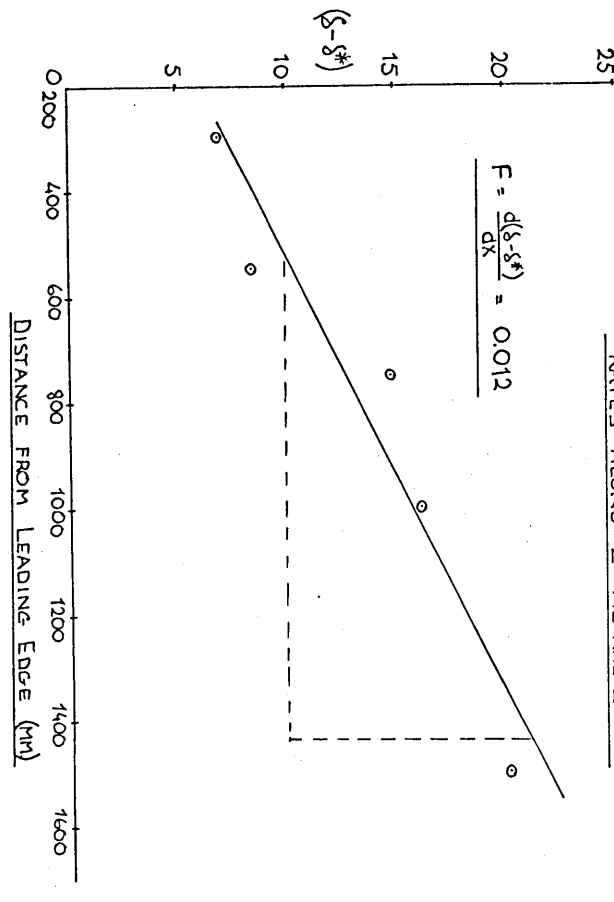

FLOW 4 — MEAN STREAMWISE ENTRAINMENT RATES ALONG Z = +75 AND Z = -75

FLOW 4 — SPANWISE ENTRAINMENT

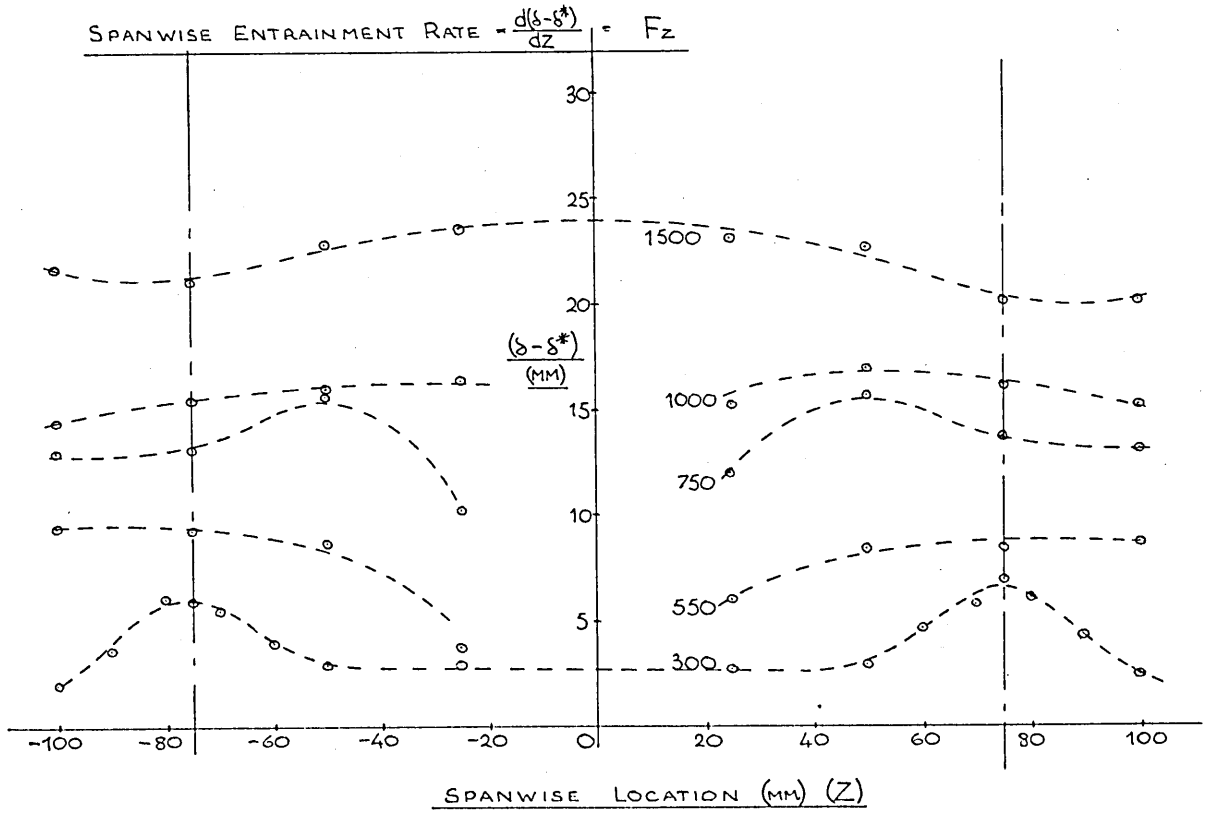

FLOW 4 — SPANWISE VARIATION IN MOMENTUM THICKNESS (MM)

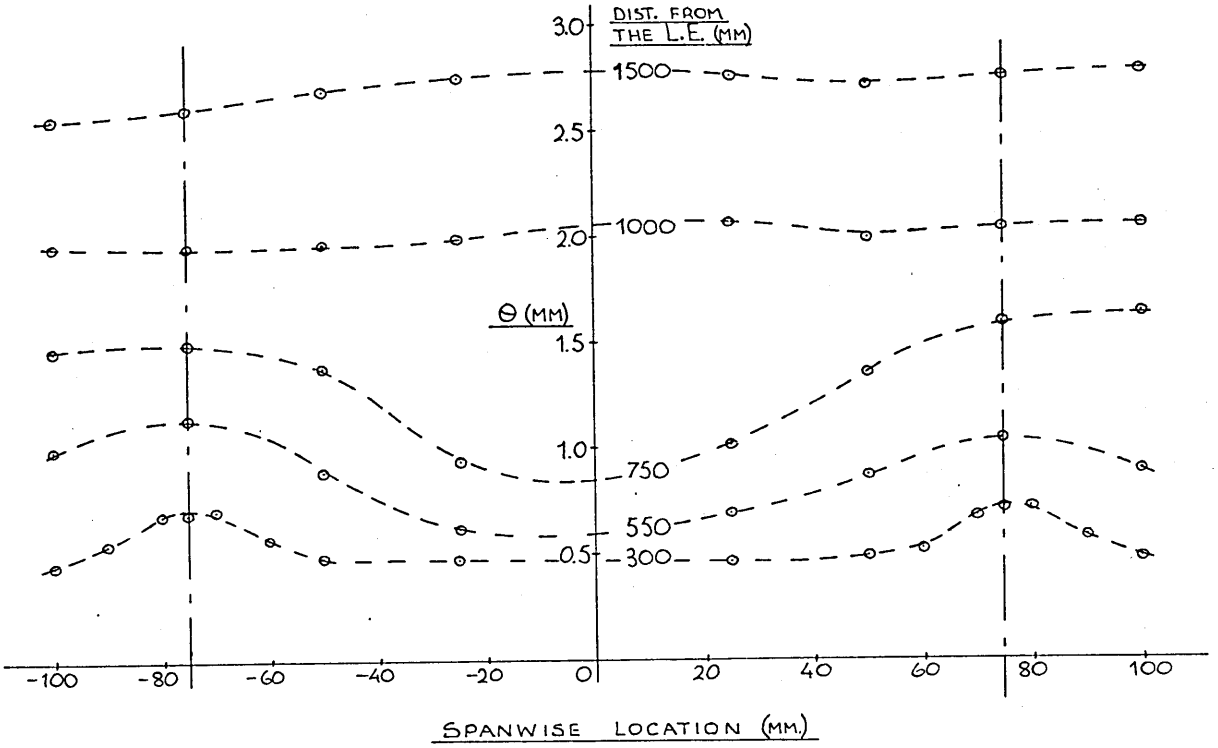

FLOW 4 — SPANWISE VARIATION IN ENERGY THICKNESS (MM)

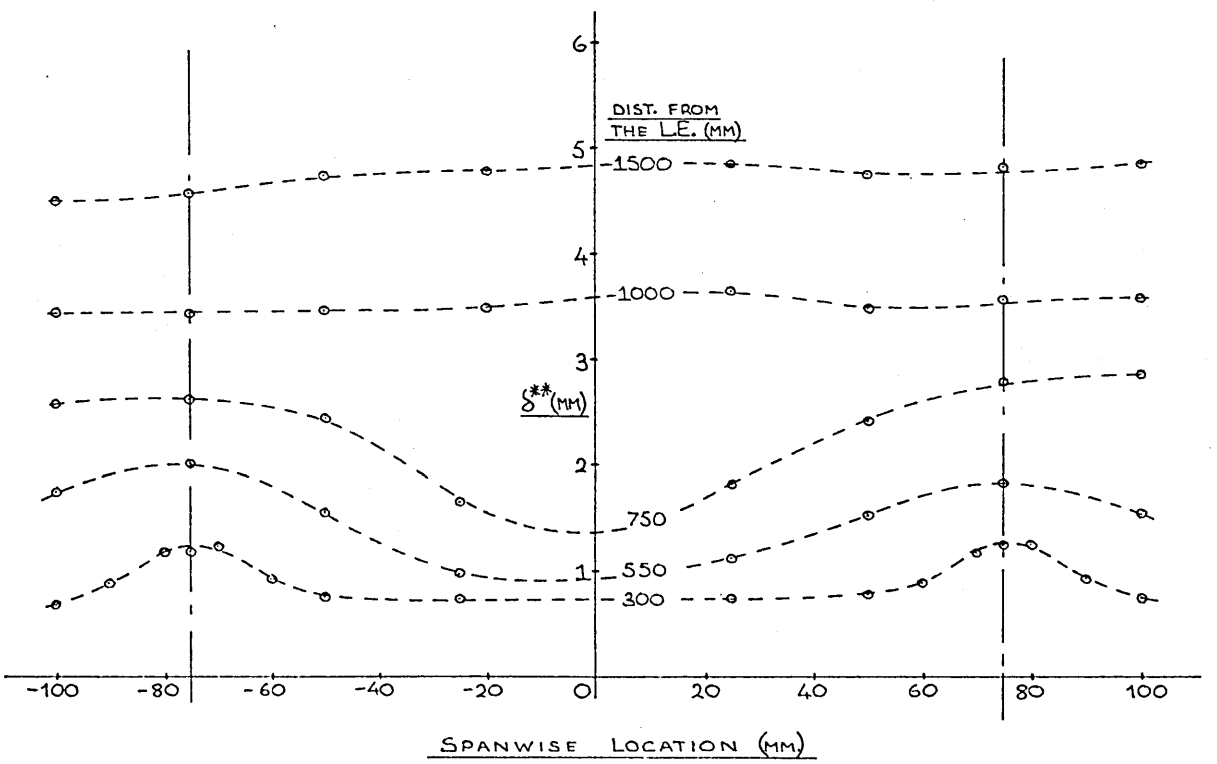

FIG 4.33

FLOW 4 — DEVELOPMENT OF WAKES BEHIND ROUGHNESS ELEMENTS

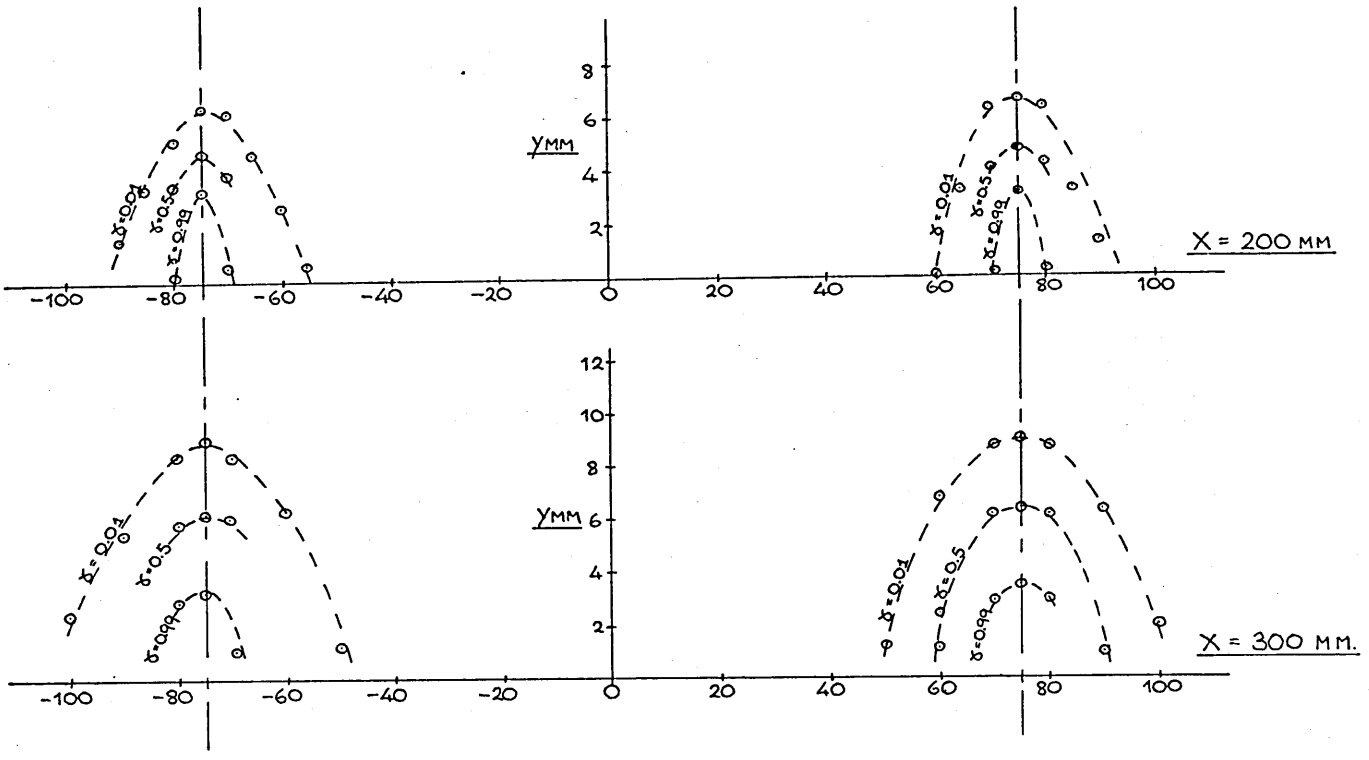

FLOW 4 — DEVELOPMENT OF WAKES BEHIND ROUGHNESS ELEMENTS

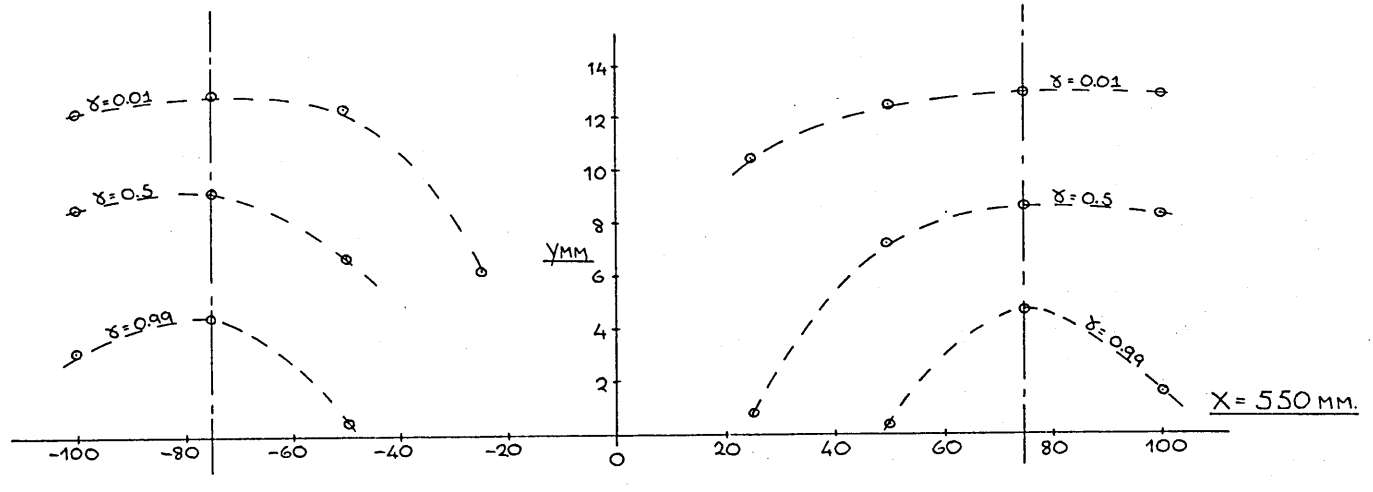

FIG 4.34

FLOW 4 — DEVELOPMENT OF WAKES BEHIND ROUGHNESS ELEMENTS

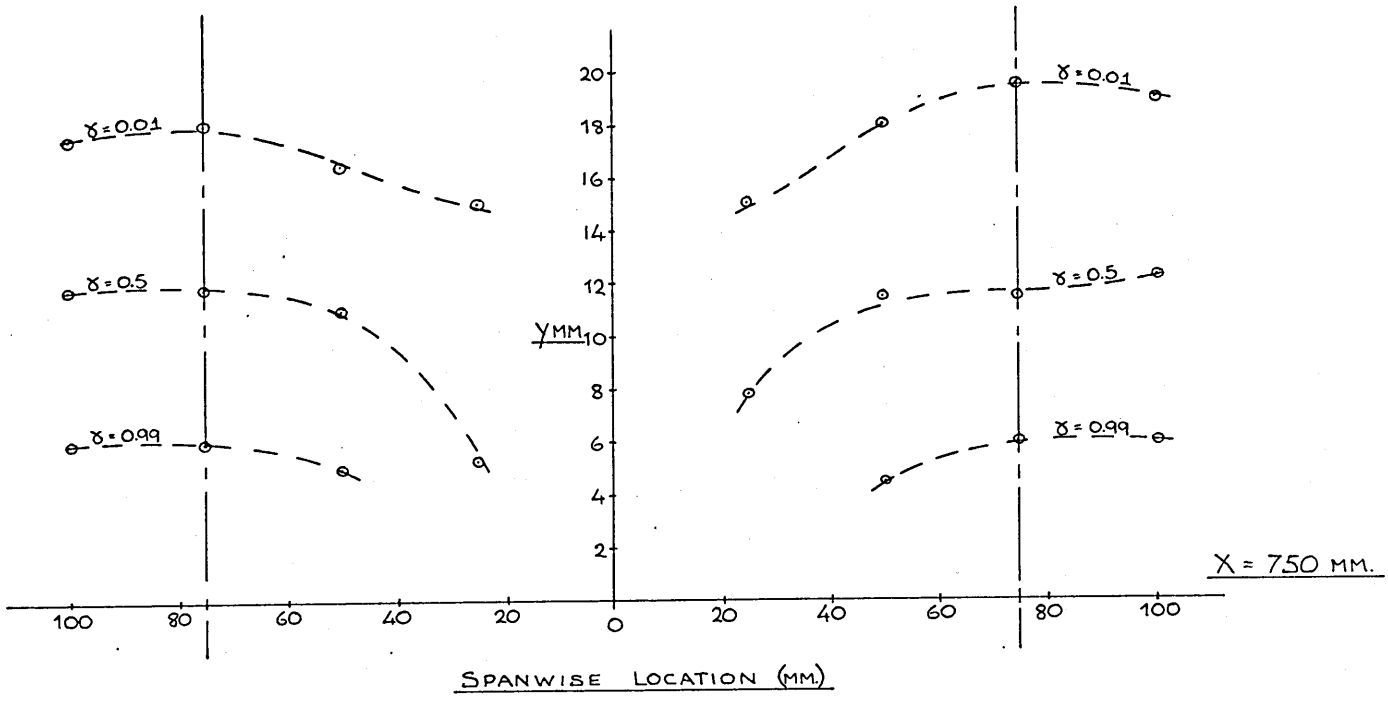

FLOW 4 — DEVELOPMENT OF WAKES BEHIND ROUGHNESS ELEMENTS

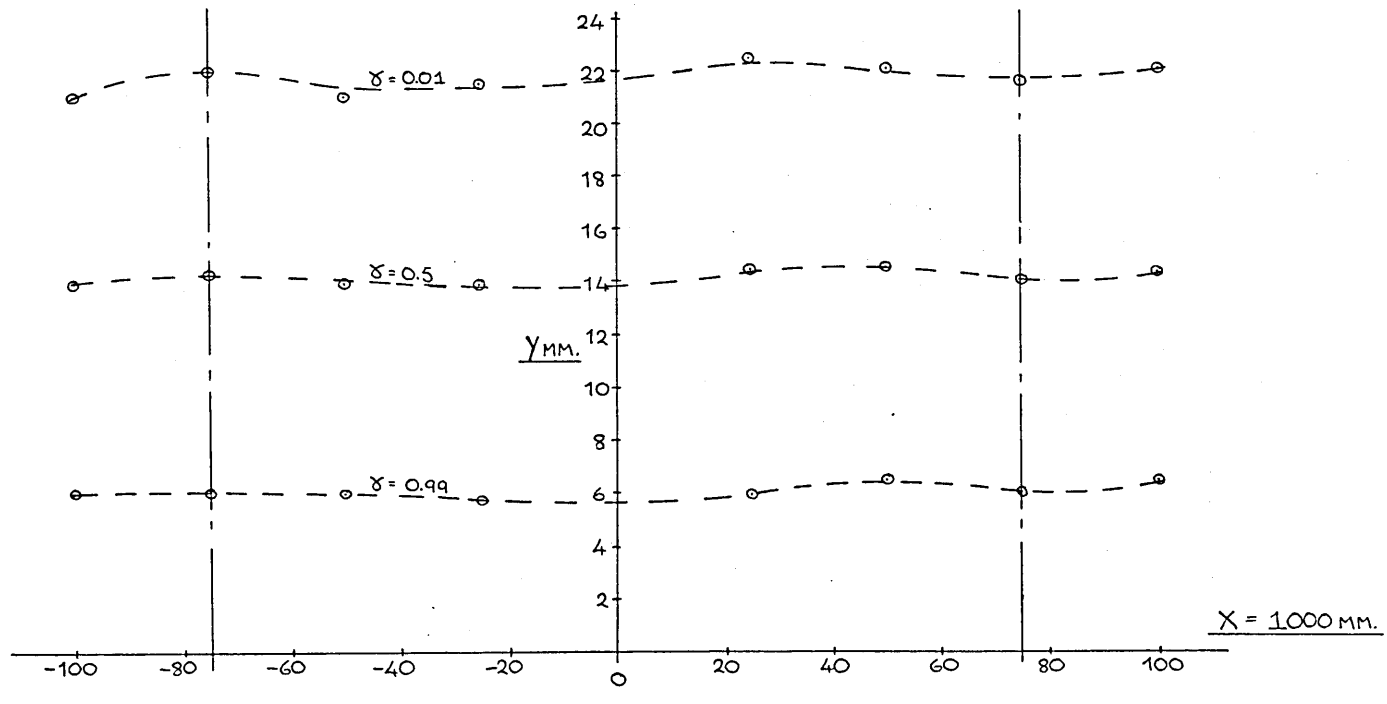

FIG 4.35

FLOW 4 — DEVELOPMENT OF WAKES BEHIND ROUGHNESS ELEMENTS

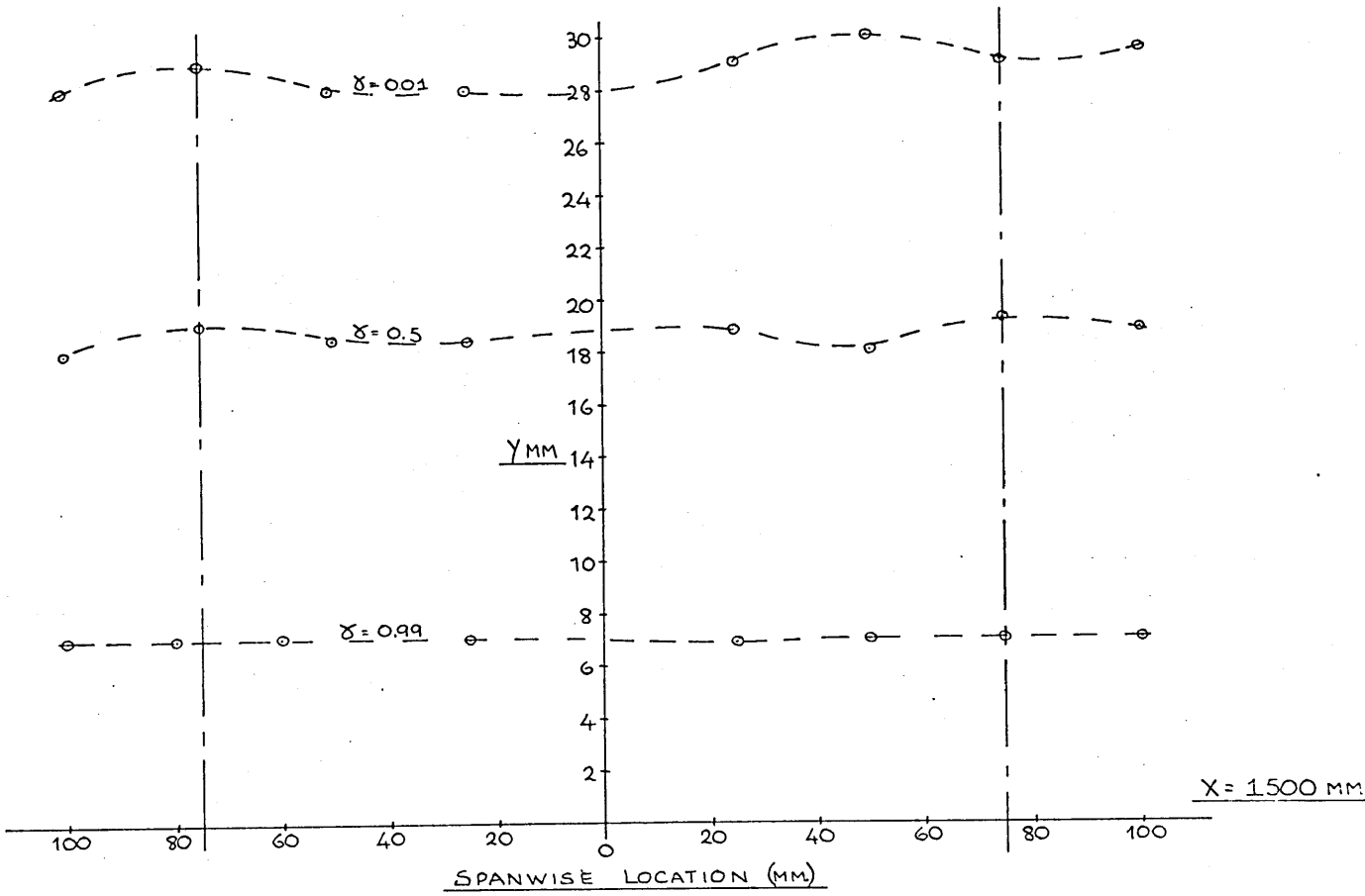

FLOW 4 — SPANWISE VARIATION IN SKIN FRICTION COEFFICIENT AT X = 300 MM

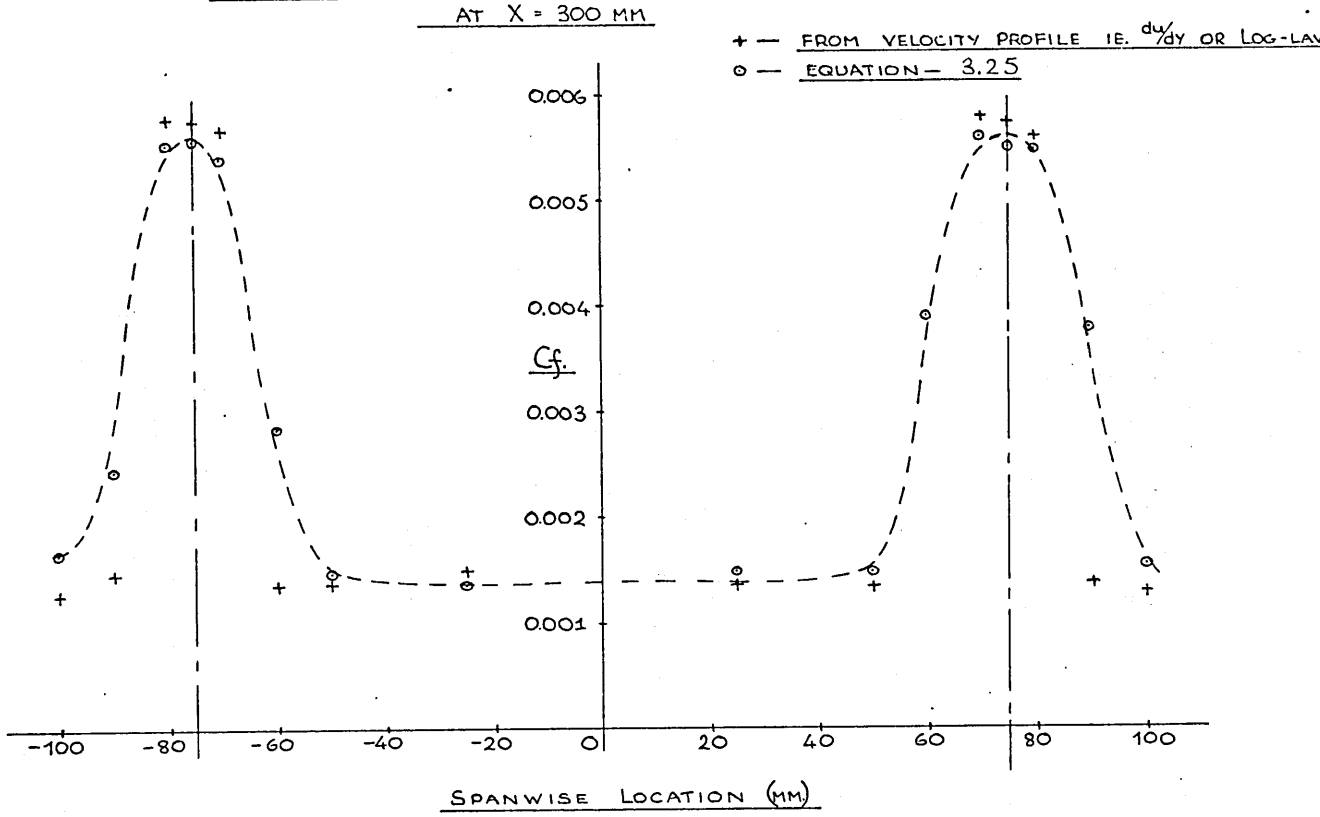

FLOW 4 — SPANWISE VARIATION IN SKIN FRICTION COEFFICIENT AT X = 550 MM.

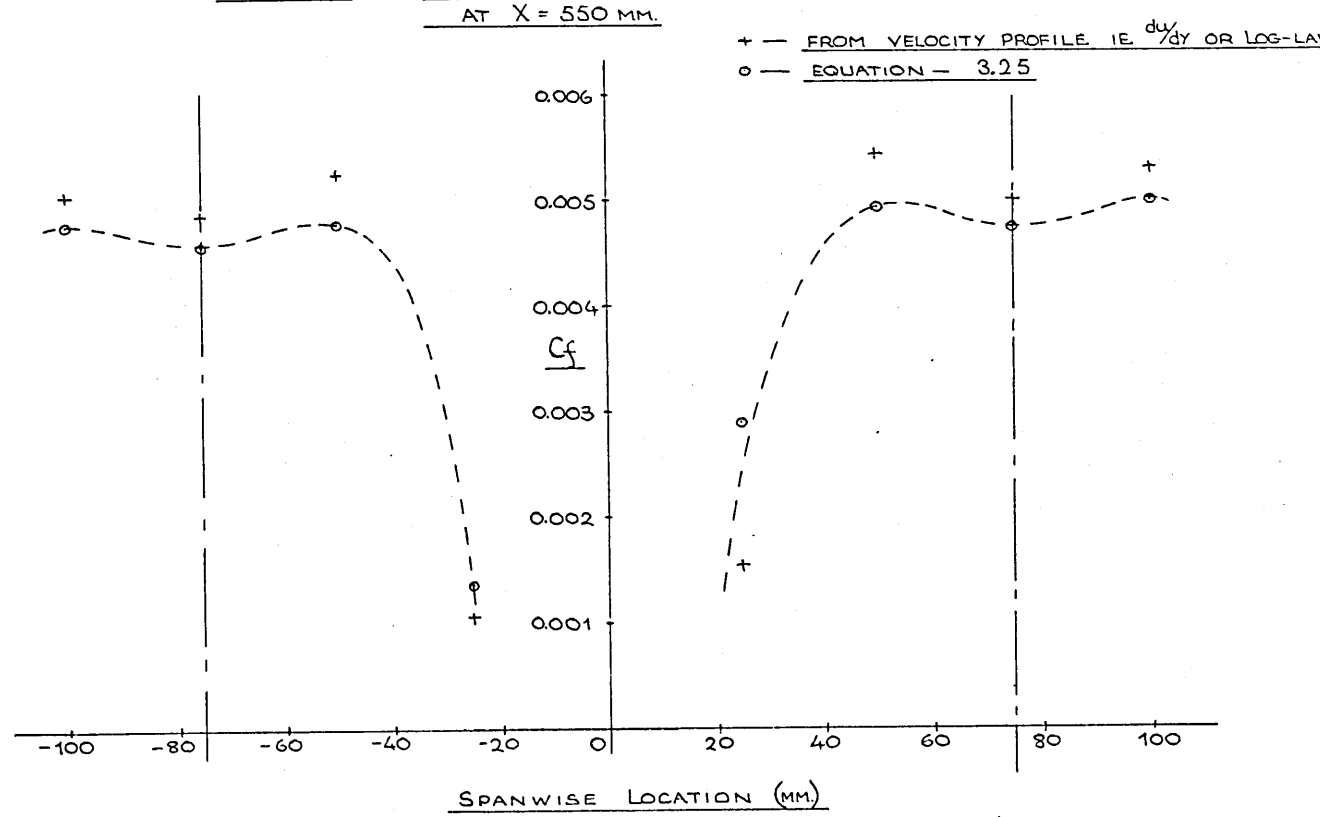

FLOW 4 — SPANWISE VARIATION IN SKIN FRICTION COEFFICIENT AT X = 750 MM.

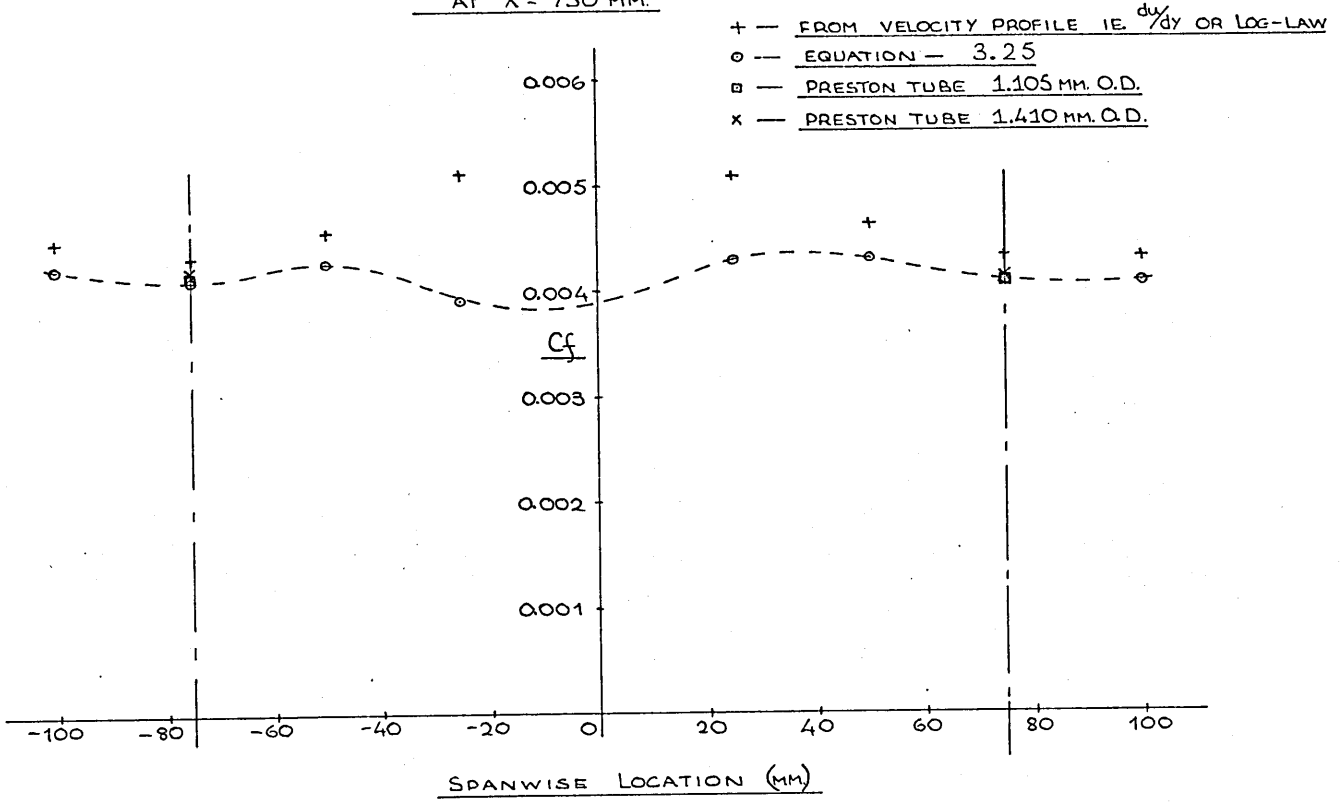

FLOW 4 — SPANWISE VARIATION IN SKIN FRICTION COEFFICIENT AT X = 1000 MM.

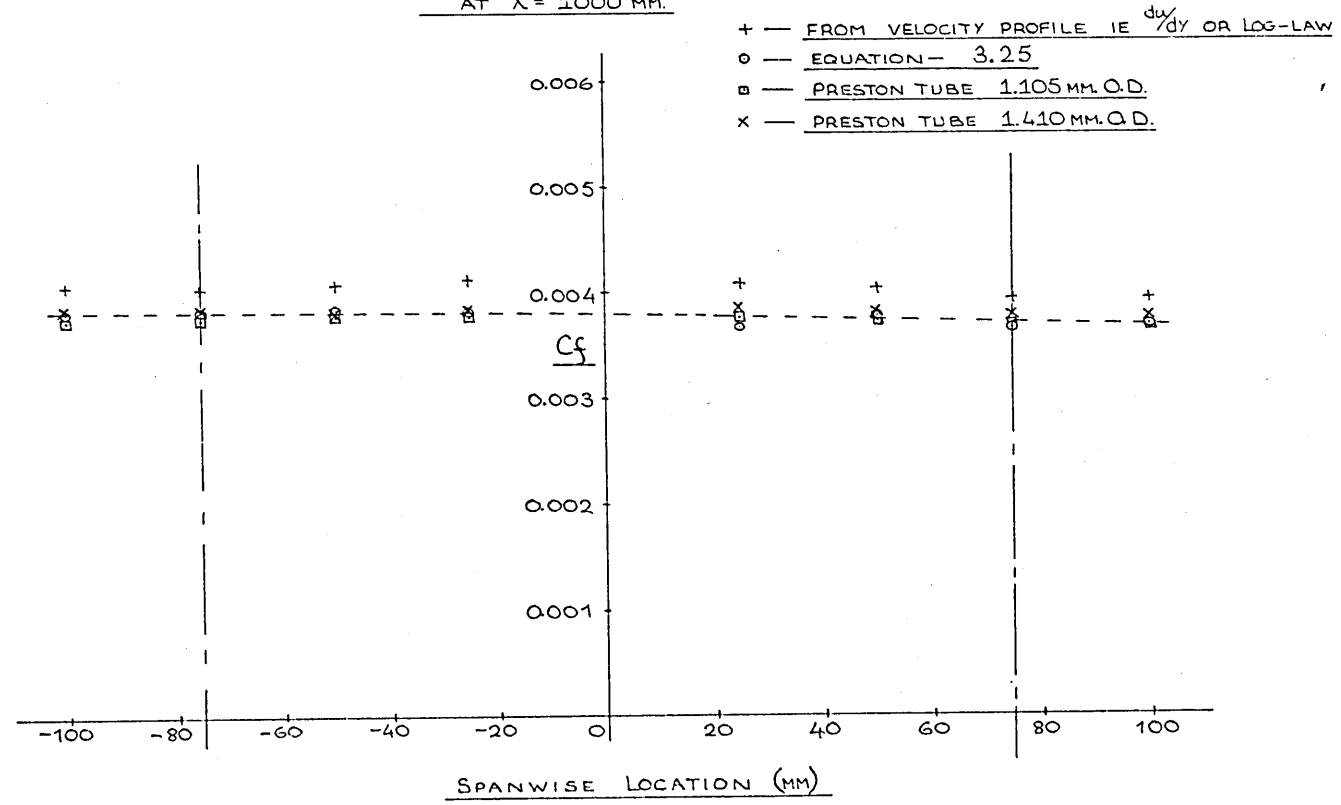

FLOW 4 — SPANWISE VARIATION IN SKIN FRICTION COEFFICIENT AT X = 1500 MM.

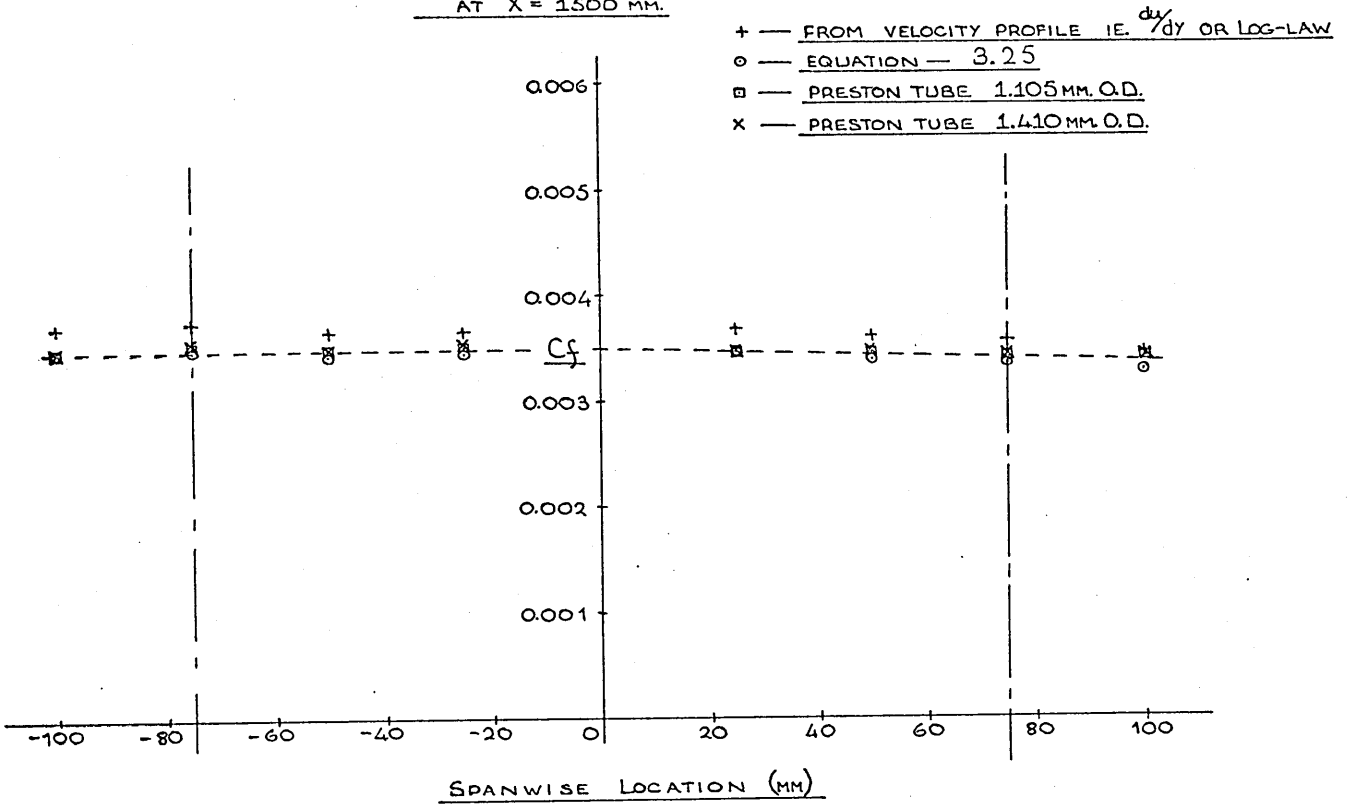

FLOW 4

BOUNDARY LAYER PROFILES AT X = 1500 MM.

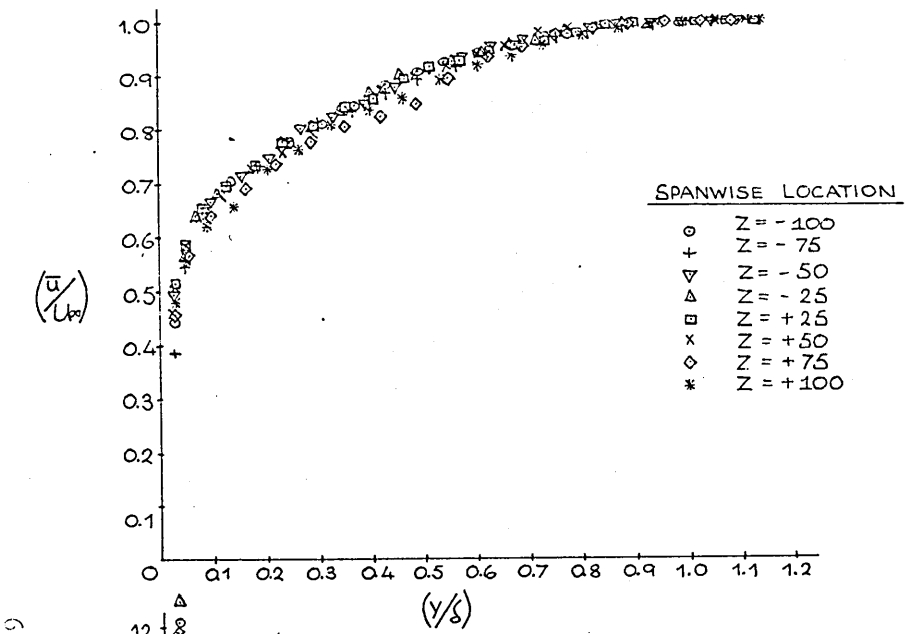

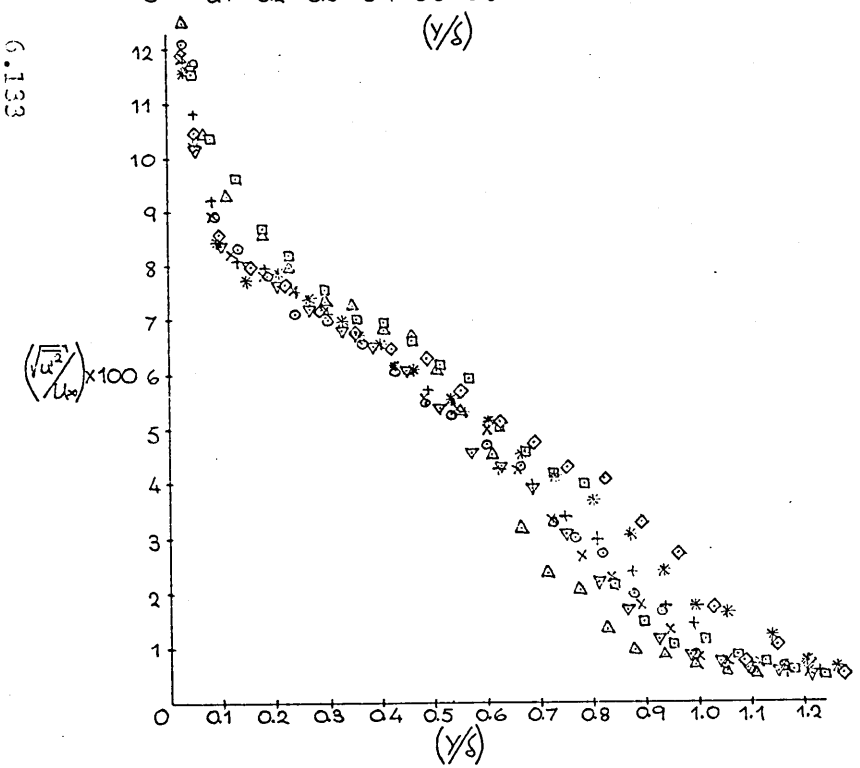

FLOW 4

BOUNDARY LAYER PROFILES AT X = 1000 MM.

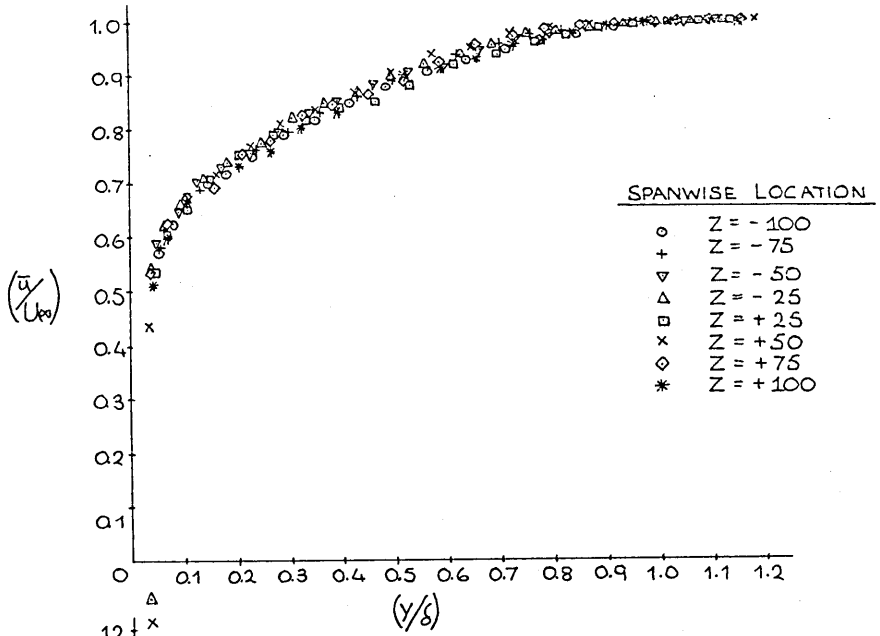

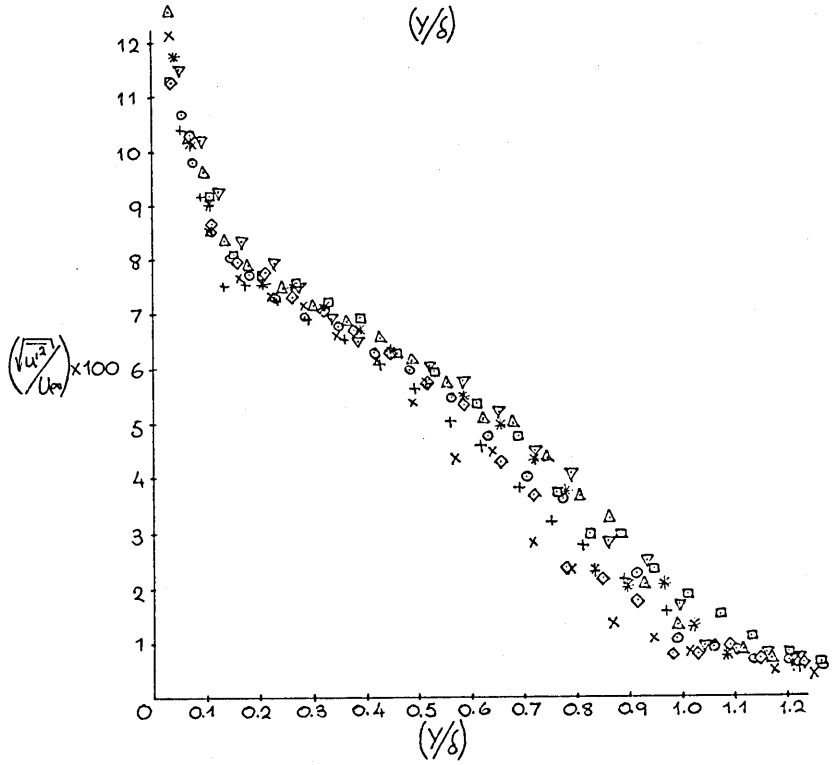

6.133

FIG 4.39